

FTD-MT-24-1450-71

AD 745470

FOREIGN TECHNOLOGY DIVISION



GAS DYNAMICS OF DIFFUSERS AND EXHAUST
DUCTS OF TURBOMACHINES

by

M. Ye. Deych and A. Ye. Zaryankin



DDC
RECEIVED
JUL 27 1972
RECEIVED

Approved for public release;
distribution unlimited.

Reproduced by
NATIONAL TECHNICAL
INFORMATION SERVICE

U.S. Department of Commerce
Springfield, VA 22151

UNCLASSIFIED
Security Classification

DOCUMENT CONTROL DATA - R & D

(Security classification of title, body of abstract and indexing annotation must be entered when the overall report is classified)

1. ORIGINATING ACTIVITY (Corporate author) Foreign Technology Division Air Force Systems Command U. S. Air Force		2A. REPORT SECURITY CLASSIFICATION UNCLASSIFIED	
		2B. GROUP	
3. REPORT TITLE GAS DYNAMICS OF DIFFUSERS AND EXHAUST DUCTS OF TURBOMACHINES			
4. DESCRIPTIVE NOTES (Type of report and inclusive dates) Translation			
5. AUTHOR(S) (First name, middle initial, last name) M. Ye. Deych and A. Ye. Zaryankin			
6. REPORT DATE 1970		7A. TOTAL NO. OF PAGES 467	7B. NO. OF REFS 169
8A. CONTRACT OR GRANT NO. A. PROJECT NO. G101		9A. ORIGINATOR'S REPORT NUMBER(S) FTD-MT-24-1450-71	
		9B. OTHER REPORT NO(S) (Any other numbers that may be assigned this report)	
10. DISTRIBUTION STATEMENT Approved for public release; distribution unlimited.			
11. SUPPLEMENTARY NOTES		12. SPONSORING MILITARY ACTIVITY Foreign Technology Division Wright-Patterson AFB, Ohio	
13. ABSTRACT Certain problems of the gas dynamics of diffusers and exhaust ducts from single positions of the boundary layer theory are given in the book. Methods of calculation, generalized experimental data and recommendations as to the choice of various parameters of diffusers are given. New effective designs of exhaust ducts, such as branch connections with cross-cut and elliptical diffusers are described. The book is intended for workers of design offices and research laboratories of turbine factories and also for students and post-graduate students. The book has many figures and tables.			

DD FORM 1 APR 68 73

UNCLASSIFIED
Security Classification

UNCLASSIFIED
Security Classification

14: KEY WORDS	LINK A		LINK B		LINK C	
	ROLE	WT	ROLE	WT	ROLE	WT
Laminar Boundary Layer Reynolds Numbers Diffuser Pressure Gradient Parameter Mach Number Gas Dynamics						

UNCLASSIFIED
Security Classification

EDITED MACHINE TRANSLATION

FTD-MT-24-1450-71

GAS DYNAMICS OF DIFFUSERS AND EXHAUST NOZZLES OF
TURBOMACHINES

By: M. Ye. Deych and A. Ye. Zaryankina

English pages: 467

Source: Gazodinamika Diffuzorov i Vkhlopnykh
Patrubkov Turbomashin, Energiya, Moscow,
1970, pp. 1-384.

Requester: AEDC

This document is a SYSTRAN machine aided translation,
post-edited for technical accuracy by:
Robert D. Hill.

Approved for public release;
distribution unlimited.

THIS TRANSLATION IS A RENDITION OF THE ORIGINAL FOREIGN TEXT WITHOUT ANY ANALYTICAL OR EDITORIAL COMMENT. STATEMENTS OR THEORIES ADVOCATED OR IMPLIED ARE THOSE OF THE SOURCE AND DO NOT NECESSARILY REFLECT THE POSITION OR OPINION OF THE FOREIGN TECHNOLOGY DIVISION.

PREPARED BY:

TRANSLATION DIVISION
FOREIGN TECHNOLOGY DIVISION
WP-AFB, OHIO.

TABLE OF CONTENTS

U. S. Board on Geographic Names Transliteration System.....	v
Designations of the Trigonometric Functions.....	vi
Preface.....	vii
CHAPTER ONE. ELEMENTS OF THE BOUNDARY LAYER THEORY.....	1
§ 1-1. Basic Definitions and Relations for the Boundary Layer.....	1
§ 1-2. Condition of the Transition of the Laminar Layer into the Turbulent Layer.....	3
§ 1-3. Calculation of the Turbulent Boundary Layer.....	10
§ 1-4. Some Results of the Investigation and Calculation of the Boundary Layer During Diffuser Flows.....	15
§ 1-5. The Effect of Compressibility on Characteristics of the Turbulent Boundary Layer.....	24
§ 1-6. Condition and Criteria of the Boundary Layer Separation.....	29
§ 1-7. Effect of the Initial Turbulence on the Boundary Layer Characteristics.....	37
§ 1-8. Boundary Layer Calculation on the Basis of the Semiempirical Theories of Turbulence.....	38
CHAPTER TWO. METHODS OF CALCULATION AND AERODYNAMIC CHARACTERISTICS OF DIFFUSERS.....	47

§ 2-1.	Types of Diffusers.....	47
§ 2-2.	Aerodynamic Characteristics of Diffusers.....	53
§ 2-3.	Procedure of the Experimental Determination of Aerodynamic Characteristics of Diffusers.....	64
§ 2-4.	Diffuser Losses and Their Calculation.....	78
§ 2-5.	The Influence of Conditions of the Inlet on the Gas Flow in Diffuser Elements.....	98
§ 2-6.	Selection of Optimum Expansion Ratios of Diffusers.....	110
CHAPTER THREE. RECTILINEAR PLANE AND AXISYMMETRIC DIFFUSERS.....		115
§ 3-1.	Flow Pattern in Plane and Axisymmetric Diffusers.....	115
§ 3-2.	Influence of Mode Parameters on Characteristics of Conical Diffusers.....	119
§ 3-3.	Influence of Geometric Parameters on the Aerodynamic Characteristics of Axisymmetric and Plane Diffusers.....	133
§ 3-4.	Calculation of Losses in Conical and Plane Diffusers According to Boundary Layer Characteristics.....	158
§ 3-5.	Compariso. of Calculated and Experimental Data..	171
§ 3-6.	Detached Flows in Flat and Conical Diffusers....	174
§ 3-7.	Procedure for Calculating Losses with the Sudden Flow Expansion.....	189
§ 3-8.	Change in the Flow Parameters Along the Axis of the Conical Diffuser.....	201
§ 3-9.	Example of the Calculation of a Diffuser with a Rectilinear Axis.....	206
CHAPTER FOUR. TRANSONIC AND SUPERSONIC DIFFUSERS.....		210
§ 4-1.	Effect of the Reynolds Number and Compressibility (Mach Number) on the Diffuser Performances at High Subsonic Speeds. Transonic Diffusers.....	210

§ 4-2.	Reverse Transition of the Turbulent Boundary Layer into Laminar.....	224
§ 4-3.	The Flow of Gas in Supersonic Diffusers.....	238
§ 4-4.	Characteristics of Transonic and Supersonic Diffusers.....	243
§ 4-5.	Variable Modes and Some Results of the Experimental Study of Supersonic Diffusers.....	249
CHAPTER FIVE. ANNUAL DIFFUSERS WITH LINEAR GENERATRICES.....		268
§ 5-1.	The Effect of Geometric and Mode Parameters on the Characteristics of Annular Diffusers with a Rectilinear Axis.....	268
§ 5-2.	Calculation of Annular Diffusers in an Equivalent Angle.....	284
§ 5-3.	Calculation of Losses in Annular Diffusers on the Basis of Characteristics of the Boundary Layer.....	289
§ 5-4.	Calculation of Annular Diffusers in Experimental Nomograms.....	292
§ 5-5.	Effect of Structural Elements and Shape of the Channel on the Efficiency of Annular Diffusers..	295
§ 5-6.	Example of the Calculation of an Annular Diffuser.....	299
CHAPTER SIX. CURVILINEAR DIFFUSERS. FLOW PATTERN IN CURVILINEAR CHANNELS.....		301
§ 6-1.	Secondary Flows in Curvilinear Channels.....	301
§ 6-2.	Effect of the Basic Geometric and Mode Parameters on the Effectiveness of Plane Curvilinear Diffusers.....	308
§ 6-3.	Effect of Basic Geometric and Mode Parameters on the Operation of Annular Curvilinear Diffusers.....	321
§ 6-4.	Some Problems in the Analytical Determination of Losses in Axiradial Diffusers.....	339

CHAPTER SEVEN. EXHAUST DUCTS OF TURBOMACHINES.....	345
§ 7-1. Fundamental Design of Exhaust Ducts and Their Effect on the Efficiency of Turbomachines.....	345
§ 7-2. Exhaust Ducts with Axial Annular Diffusers.....	361
§ 7-3. Exhaust Ducts with Obliquely Cut Diffusers.....	372
§ 7-4. Exhaust Ducts with Radial Diffusers..	384
§ 7-5. Exhaust Branch Connections with Axiradial Elliptical Diffusers.....	394
§ 7-6. Operation of Exhaust Ducts when the Stage of the Turbomachine Exists.....	400
APPENDICES.....	420
BIBLIOGRAPHY.....	458

U. S. BOARD ON GEOGRAPHIC NAMES TRANSLITERATION SYSTEM

Block	Italic	Transliteration	Block	Italic	Transliteration
А а	<i>А а</i>	A, a	Р р	<i>Р р</i>	R, r
Б б	<i>Б б</i>	B, b	С с	<i>С с</i>	S, s
В в	<i>В в</i>	V, v	Т т	<i>Т т</i>	T, t
Г г	<i>Г г</i>	G, g	У у	<i>У у</i>	U, u
Д д	<i>Д д</i>	D, d	Ф ф	<i>Ф ф</i>	F, f
Е е	<i>Е е</i>	Ye, ye; E, e*	Х х	<i>Х х</i>	Kh, kh
Ж ж	<i>Ж ж</i>	Zh, zh	Ц ц	<i>Ц ц</i>	Ts, ts
З з	<i>З з</i>	Z, z	Ч ч	<i>Ч ч</i>	Ch, ch
И и	<i>И и</i>	I, i	Ш ш	<i>Ш ш</i>	Sh, sh
Й й	<i>Й й</i>	Y, y	Щ щ	<i>Щ щ</i>	Shch, shch
К к	<i>К к</i>	K, k	Ъ ъ	<i>Ъ ъ</i>	"
Л л	<i>Л л</i>	L, l	Ы ы	<i>Ы ы</i>	Y, y
М м	<i>М м</i>	M, m	Ь ь	<i>Ь ь</i>	'
Н н	<i>Н н</i>	N, n	Э э	<i>Э э</i>	E, e
О о	<i>О о</i>	O, o	Ю ю	<i>Ю ю</i>	Yu, yu
П п	<i>П п</i>	P, p	Я я	<i>Я я</i>	Ya, ya

* ye initially, after vowels, and after ъ, Ъ; e elsewhere.
 When written as ѣ in Russian, transliterate as ye or e.
 The use of diacritical marks is preferred, but such marks
 may be omitted when expediency dictates.

FOLLOWING ARE THE CORRESPONDING RUSSIAN AND ENGLISH
 DESIGNATIONS OF THE TRIGONOMETRIC FUNCTIONS

Russian	English
sin	sin
cos	cos
tg	tan
ctg	cot
sec	sec
cosec	csc
sh	sinh
ch	cosh
th	tanh
cth	coth
sch	sech
csch	csch
arc sin	\sin^{-1}
arc cos	\cos^{-1}
arc tg	\tan^{-1}
arc ctg	\cot^{-1}
arc sec	\sec^{-1}
arc cosec	\csc^{-1}
arc sh	\sinh^{-1}
arc ch	\cosh^{-1}
arc th	\tanh^{-1}
arc cth	\coth^{-1}
arc sch	sech^{-1}
arc csch	csch^{-1}
rot	curl
lg	log

Preface

In recent years interest was noticeably raised in the research on diffusers and diffuser channels, which to a considerable degree is stimulated by the utilization of these elements in turbomachines, ejectors, aviation technology, MHD generators, etc.

The book proposed to the reader has been written from results of research on diffusers in the wind-tunnel laboratory of the department "Steam and Gas Turbines" [PGT] (ПГТ) of the Moscow Power Engineering Institute [MEI] (МЭИ), which were oriented in the first place on the solution to problems connected with the use of diffusers in turbomachines. At the same time in the examination of characteristics of various diffuser elements published experimental data obtained in other organizations were widely used.

The book consists of seven chapters. The first chapter is devoted to the general problems of the boundary layer theory and has a reference nature. The concepts discussed in this chapter are used in the following chapters. The reader who is familiar with the boundary layer theory can immediately pass over to the second chapter, where energy diffuser characteristics, existing methods of their calculation and coefficients used in the comparison of characteristics are examined.

The third chapter touches upon problems connected with the fluid flow in conical diffusers. On the basis of numerous test data, the role of geometric and mode parameters is investigated in detail. Detailed research on the flow in conical diffusers allowed explaining the nature of the

change in the integral boundary layer thicknesses along the generatrix of the surface and obtaining the base experimental values of internal losses. A detailed analysis of calculated methods of determining energy characteristics gives rise to conclusion that for nonseparable flows the most precise and physically substantiated are the methods based upon the boundary layer characteristics. For the maximum simplification of calculations nomograms which substantially decrease the volume of computational work are given. In this chapter some features of the calculation of losses with the sudden expansion of flow are noted.

The fourth chapter is devoted to research on flow in transonic and supersonic diffusers. Specific attention is given to transonic diffusers. The hypothesis which explains the crisis of diffuser losses at $M + 1$ by partial or complete degeneration of turbulence at the input has been advanced and experimentally confirmed.

Given in the fifth chapter are results of the experimental investigation of annular diffusers with rectilinear generatrices, and an analysis of the influence of the most important geometric parameters on their efficiency is given. Much space is used in the chapter for the theoretical calculation of diffusers according to the boundary layer characteristics and also the calculation according to equivalent angles and experimental nomograms.

Examined in the sixth chapter are problems connected with the flow in plane and circular curvilinear diffusers. Here the primary attention has been given to the examination of the physical picture of the flow in such channels.

The last, seventh, chapter is devoted to the flow in the exhaust ducts of turbomachines where an attempt has been made to generalize the work experience of the authors in the indicated direction. For this purpose, as a rule, initial variants are examined and the ways which allow with the observance of constructive requirements the lowering of the magnitude of losses of energy are shown. An important moment is the investigation on branch pipes together with the stage being rotated on overheated and moist steam.

For the facilitation of practical calculations, in the appendix to the book there are auxiliary nomograms which allow determining the integral boundary

layer characteristics in exit sections of conical, circular and axial-radial diffusers, and also great factual material on the diffusers tested.

Thus, in the book an attempt has been undertaken on the basis of experimental and theoretical investigations to sequentially describe the physical processes in simple and complex diffuser channels and to determine their characteristics over a wide range of mode and geometric parameters.

One should once again emphasize that the authors have attempted to solve the problems from the single positions based upon the theory and methods of the boundary layer and the physical apparatus of gas dynamics.

Chapter 4 and §§ 6-1 and 6-2 were written by M. Ye Deych. He accomplished the general editing of the monograph. A. Ye. Zaryankin wrote the remaining text of the book. The authors jointly wrote the preface and §§ 2-2, 3-2, 7-2 and 7-3. The § 4-5 was written by M. Ye. Deych together with G. G. Katsnel'son.

In conclusion let us note that the book touches upon only a number of particular problems and is one of a few attempts [16, 34, 55] to generalize the available experimental data on diffuser channels. In the examination of a number of the problems and the derivation of the calculated relations, the authors attempted to simplify maximally the final results, keeping in mind the applied directivity of the monograph.

It is natural that the treatment of some sections can be debatable, and the authors will accept the possible remarks with appreciation.

We consider it as our pleasant duty to indicate that in the book are used test data obtained under the guidance of the authors by colleagues of the laboratory of the department of "Steam and Gas Turbines" of MEI Candidates of Technical Sciences L. G. Golovina, M. F. Zatsepin, I. Ya. Lazarev, R. K. D. Shakh, engineer L. M. Dyskin and senior engineer V. V. Ett.

Furthermore, great practical help in the direct work on the book was given by the Candidate of Technical Sciences V. S. Yelizarov and Doctor of Technical Sciences A. N. Sherstyuk and A. S. Ginevskiy,

whose remarks significantly influenced the final editing of the book.

The authors offer their sincere appreciation to all the comrades mentioned and also the operating personnel of the department of PGT.

All figures, graphs, tables, equations, etc. merged into this translation were extracted from the best quality copy available.

CHAPTER ONE

ELEMENTS OF THE BOUNDARY LAYER THEORY

§ 1-1. Basic Definitions and Relations for the Boundary Layer

In the flow of viscous fluid near a solid surface, the whole region of flow in the case of the predominant influence of inertial forces over forces of viscosity (at large Reynolds numbers Re) is conditionally divided into two zones: the zone of the quasi-potential flow and the zone of the eddying motion of liquid where the action of the viscous forces is distinctly developed. The latter region can be called the boundary layer.

Within limits of the boundary layer two flow conditions - laminar and turbulent can take place. The boundary layer calculation in most cases is based on the utilization of the integral equation of momentum (the equation of Kármán). In the derivation of this equation it is usually considered that in the case of the turbulent flow conditions in the boundary layer in the external flow turbulent pulsations are small, and, consequently, the "turbulent" stresses induced by pulsations of velocity cannot be taken into consideration. However, if boundary layer is developed under conditions of great external turbulence, the magnitude of these additional stresses proves to be noticeable and, strictly speaking, must be considered.

The consideration of the influence of "turbulent" stresses in quasi-potential flow was realized by V. A. Vrublevskaya [13, 14]. The converted equation of the momentum of a turbulent boundary layer can be written in the following form:

$$(1 + b\varepsilon^2) \frac{d\delta^{**}}{dx} + \frac{dc_1}{dx} \cdot \frac{\delta^{**}}{u_i} (2 + H - M_1^2) = \frac{\tau_w}{\rho_1 c_1^2} \varepsilon^2, \quad (1.1)$$

where ε - the turbulence level of the external flow; c_1 , ρ_1 - the rate and density at the external edge of the boundary layer; τ_w - the frictional stress on the wall; ξ - the ratio of transverse and longitudinal pulsating amplitudes; δ^{**} - the momentum loss thickness; δ^* - the displacement thickness; $H = \delta^*/\delta^{**}$; $b = a\delta/\delta^{**}$; δ - the boundary layer thickness; a - the damping coefficient of longitudinal pulsations in the boundary layer; ψ - the correlation coefficient between longitudinal and transverse pulsations of velocity.

If we do not consider the turbulent stresses on the external edge of the boundary layer, expression (1-1) converts to the well-known momentum equation of Kármán:

$$\frac{d\delta^{**}}{dx} + \frac{dc_1}{dx} \cdot \frac{\delta^{**}}{c_1} (2 + H - M_1^2) = \frac{\tau_w}{\rho_1 c_1^2}, \quad (1-2)$$

which is valid both for the laminar and turbulent conditions of flow in the boundary layer.

The integral thicknesses of the boundary layer entering into equation (1-2) are easily determined at the known velocity profile from the following relations:

a) displacement thickness

$$\delta^* = \int_0^{\delta} \left(1 - \frac{pc}{\rho_1 c_1}\right) dy; \quad (1-3)$$

b) momentum thickness

$$\delta^{**} = \int_0^{\delta} \frac{\rho c}{\rho_1 c_1} \left(1 - \frac{c}{c_1}\right) dy; \quad (1-4)$$

c) energy thickness

$$\delta^{***} = \int_0^{\delta} \frac{\rho c}{\rho_1 c_1} \left(1 - \frac{c^2}{c_1^2}\right) dy. \quad (1-5)$$

Having multiplied δ^* by $\rho_1 c_1$, δ^{**} by $\rho_1 c_1^2$ and δ^{***} by $\rho_1 c_1^3$, we obtain the lost mass, lost momentum and lost energy in the boundary layer per unit of length of the profile, but with multiplication by the perimeter - the total loss of the indicated values in the given cross section of the boundary layer.

Before passing directly to the derivation of calculation equations, let us examine the conditions of the existence of the laminar and turbulent flow conditions in the boundary layer with a positive pressure gradient.

§ 1-2. Condition of the Transition of the Laminar Layer into the Turbulent Layer

It is well known that under specific conditions the laminar flow conditions go over into turbulent.

The basic method of the stability analysis of laminar flow consists in the fact that superimposed on the motion in question are additional slight disturbances, and when these disturbances exist the flow is analyzed. If the flow is stable, then the disturbances attenuate with time, and no qualitative changes are observed. On the other hand, with unstable flow the disturbances grow, and a transition to the new condition - turbulent, occurs.

The complexity of the indicated analysis as applied to the boundary layer flow is that the development of instability depends upon the nature of the superimposed disturbances, i.e., on their amplitude and frequency. If, for example, with a low frequency of disturbances the motion is stable, then with an increase in frequency the loss in stability can fully occur. The indicated circumstance led to the fact that until now the purely theoretical solutions to the problems of the stability of laminar flow in the boundary layer did not obtain noticeable distribution, and in most cases experimental data are used.

On the basis of these data it is considered that the beginning of the loss in stability is determined by the critical Reynolds number Re_{kp} , the magnitude of which depends upon a number of factors. The most important of them consist in following: the surface condition of body being streamlined, the turbulence level of the incoming flow, and the form of the boundary layer velocity profile.

The indicated factors are quite fully characterized by five parameters [72]:

1) by the turbulence level at the boundary layer edge ϵ ;

2) by the relative "scale" of turbulence l/δ^{**} , where $l =$

$$= \int_0^{\delta} \phi_y dy, \text{ and } \phi_y - \text{the correlation coefficient between}$$

pulsations at two points taken on one perpendicular to the direction of the velocity of the main flow;

3) by the relative surface roughness k/δ^{**} (k - the mean height of the prominences of the roughness);

4) by the relative wavelength of the roughness λ_1/δ^{**} (λ_1 - mean distance between the prominences of the roughness);

5) shape parameter $f = \frac{dc_1}{dx} \cdot \frac{\delta^{**2}}{\nu}$.

It is not difficult to see that the first two parameters characterize the turbulence, the next two - the surface condition, and last - the velocity gradient and shape of the boundary layer velocity profile dependent basically on the velocity gradient in the external flow.

Using for the determination of the Reynolds number the momentum loss thickness δ^{**} as a characteristic dimension, let us write the functional dependence for its critical value, which determines the loss in stability of the laminar boundary layer:

$$Re_{cr}^{**} = F\left(\frac{k}{\delta^{**}}, \frac{l}{\delta^{**}}, \frac{l_1}{\delta^{**}}, \epsilon, f\right). \quad (1-6)$$

If we assume that the reason for the instability of the laminar flow consists in some disturbances superimposed on the main flow, then as applied to the boundary layer one can indicate two sources of such disturbances and in accordance with this examine two cases of the formation of turbulence. Actually, acting on the layer of the liquid located directly at the wall are, on the one hand, disturbances connected with microseparations of the flow from prominences of the roughness and on the other - disturbances conditioned by the turbulence of the external flow.

For the case of the loss of stability only under the action of turbulence of the external flow or only under the action of the roughness, A. P. Mel'nikov [72] obtained the following formulas:

$$Re_{cr}^{**} = 0,3 \frac{(0,085 + f)^{2/3}}{\epsilon^{5/3}} + 225; \quad (1-7)$$

$$Re_{cr}^{**} = 6 \frac{(0,085 + f)^{2/3}}{(l, \delta^{**})^{5/3}} + 225, \quad (1-8)$$

the use of which makes it possible as a first approximation to estimate the order of the critical Reynolds number. For this, apparently, it is necessary on one graph to plot curves of the change in Re^{**} number along the length of the surface in question and curves determined by formulas (1-7) and (1-8). Then the intersection points of curve $Re^{**}=f_1(\bar{x})$ with curves $Re_{cr}^{**}=f_2(\bar{x})$ will determine the values of critical Reynolds numbers, the smallest of which corresponds to the position of the point of the loss in stability by the laminar boundary layer.

The nature of the change in the indicated curves along the diffuser channel with the drop in velocity in it, according to the law $\frac{c_1}{c_{stagn}} = \frac{1}{1+0,3x}$, is shown in Fig. 1-1. The points of

intersection a and b of curve 3 with curves 1 and 2 give values of the critical Reynolds numbers and coordinates of points of the loss in stability of the layer. The small value of Re_{cr}^{**} corresponds to the intersection of curve 3 with curve 1. Therefore, in this case the loss in stability is caused by disturbances connected with the turbulence of the external flow.

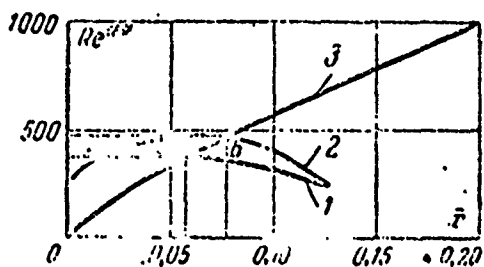


Fig. 1-1. On the calculation of the transition point of laminar flow into turbulent flow. 1 - calculation Re_{cr}^{**} according to formula (1-7); 2 - calculation Re_{cr}^{**} according to formula (1-8); 3 - the change in Re^{**} number in the diffuser channel.

Let us note that in most cases even with significant roughness the Re_{cr}^{**} in diffusers of outlet pipes of turbomachines is determined by formula (1-7), since for the flow which leaves the last stages of turbomachines a high turbulence level is characteristic.

Otherwise, with the use of diffusers for the recovery of the kinetic energy of the flow, one strives, as a rule, to have a minimum roughness, which also gives rise to the necessity during calculations for using formula (1-7).

The process of the transition of a laminar layer into a turbulent, as experiments show, occurs not instantly, and there is a certain transition region whose dimensions substantially depend upon the longitudinal velocity gradient, turbulence level of external flow and shape of the velocity profile in the beginning of the transition zone [25].

In the turbulence levels of 2-3% the dimensions of the transition region are usually small, and for its calculation it is sufficient to know the extent of this region $\bar{S} = S/L$ and the increase in it in the momentum thickness $r^{**} = \delta^{**}_H / \delta^{**}_H$, where L - the length of the surface in question; δ^{**}_H and δ^{**}_H - momentum thicknesses at the end and beginning of the transition.

Both introduced values depend basically upon the shape parameter f , which characterizes the shape of the velocity profile in the beginning of the transition. The indicated dependences given in Fig. 1-2 show that in the diffuser regions values \bar{S} and r^{**} noticeably drop.

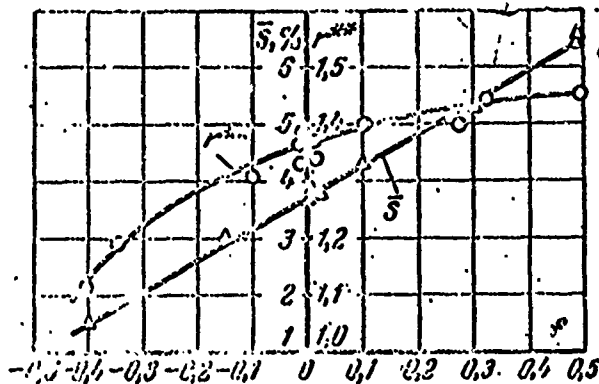


Fig. 1-2. Extent of the transition zone and magnitude of the relative increase in the displacement thickness in this zone depending on the shape parameter f .

For an illustration of the aforesaid, Fig. 1-3 gives curves of changes in the momentum loss thickness on the curvilinear wall with convergent and diffuser flows. The region of transition is quite clearly fixed according to the change in the angle of slope of the curves $\bar{\delta}^{**} = f(\bar{x})$.

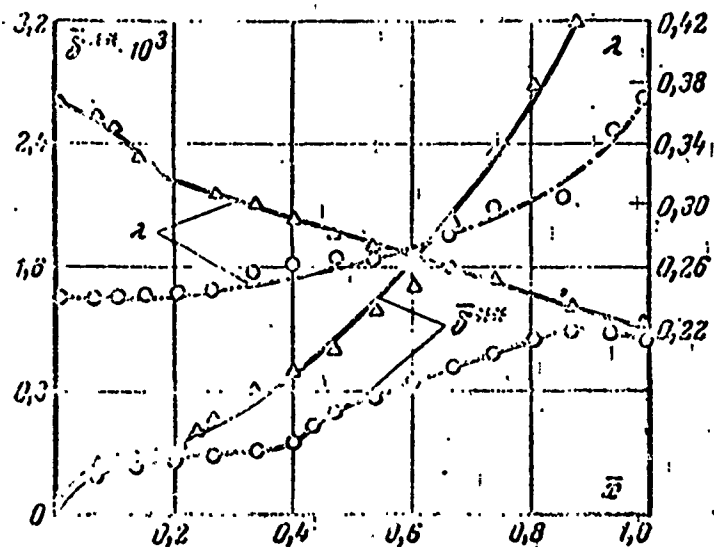


Fig. 1-3. Changes in the momentum loss thickness in the diffuser and convergent channels.

If with convergent flow the transition is begun when $\bar{x} = 0.4$, it occupies approximately 6% of the total length of the wall, and the magnitude of r^{**} in the transition region is about 1.45, then with diffuser flow the loss in stability approaches when $\bar{x} = 0.18$, and the region itself on curve $\bar{\delta}^{**} = f(\bar{x})$ occupies 1-2% of L . The absence in this case of the growth in magnitude r^{**} is explained by the fact that in the rearrangement of the profile in the transition zone there occurs, on the one hand, the growth in the physical thickness of layer δ , and on the other hand - its completeness is increased. If the first factor causes an increase in the momentum thickness $\bar{\delta}^{**}$, then the second, on the contrary, gives rise to its decrease. In diffuser regions, due to the small completeness of the initial velocity profile in the laminar layer,

there occurs so intense an increase in its completeness that the influence on δ^{**} of the increase in physical thickness δ is completely compensated, and magnitude r^{**} proves to be close to one. With convergent flow, as a result of the transition, an increase in thickness δ has the primary importance since the initial profile here is quite complete, and its deformation in this direction is insignificant, which also finally leads to a noticeable growth in magnitude r^{**} .

Thus, with the diffuser flow without great error, one can consider that the transition occurs in practice at the point, and with the boundary layer calculation one can be limited for the transition zone only to the definition of the position of the point of the loss in stability by the laminar layer.

With positive pressure gradients, as a first approximation for the estimate of the transition region, it is possible to recommend curves in Fig. 1-2 or the empirical formulas for the extent of the zone of transition and growth in it of the momentum loss thickness:

$$S = \left(\frac{10^3}{Re} \right)^{0.15} (3.7 \div 5.5) f, \% \quad (1-9)$$

$$r^{**} = [(7 + 100f)^{0.12+0.5f} + 0.12M], \% \quad (1-10)$$

Considering, however, that with large positive pressure gradients and the high degrees of external turbulence, the extent of the laminar section is insignificant (in Fig. 1-1, for example, with the turbulence level of the order of 1.5% and the moderate positive pressure gradient $\bar{E}_n = 0.06$), it is possible in most cases to consider the boundary layer flow of diffusers to be turbulent over entire length. Because of this we will discuss only the calculation of turbulent boundary layer.¹

¹Methods of calculation of the laminar boundary layer are presented in detail in L. G. Loytsyanskiy's monograph "Laminar Boundary Layer," Fizmatgiz, 1962.

§ 1-3. Calculation of the Turbulent Boundary Layer

The boundary layer calculation provides usually the determination of its thicknesses δ , δ^* , δ^{**} , δ^{***} and the resistance coefficient $c_f = \tau_w / \rho c_1^2$ along fairing. Consequently, for the calculation it is necessary to have a number of relations which connect the indicated magnitudes. In this case, used as a basic equation most frequently is the integral relation of Kármán (1-2), which for incompressible fluid is somewhat simplified:

$$\frac{d\delta^{**}}{dx} + \frac{dc_1}{dx} \cdot \frac{\delta^{**}}{c_1} (2 + H) = c_f. \quad (1-11)$$

Considering velocity at the external boundary layer edge to be assigned, we see that equation (1-11) connects the three unknown magnitudes, δ^{**} , H and c_f , and for its solution it is necessary to have two more equations. Used most frequently as such equations is a varying kind of empirical relations, which allow obtaining a closed system of equations. However, before using test data, let us establish, on the basis of the dimensional theory, the structural nature of the deficient dependences.

In general the frictional stress on the wall in an incompressible fluid τ_w is determined by velocity on the external boundary layer edge c_1 ; by its derivatives c'_1 , c''_1 , c'''_1 etc.; by the characteristic dimension which can be accepted as any boundary layer thickness (for instance, δ^{**}); and by the kinematic-viscosity coefficient ν and density ρ .

Consequently,

$$\tau_w = \varphi(c_1; c'_1; c''_2 \dots; \rho; \delta^{**}; \nu). \quad (1-12)$$

Using as the basic the dimensionalities of velocity, density and length, let us present (1-12) in the following dimensionless form:

$$c_f = \varphi \left(Re^{**}; \frac{c'_1 \delta^{**}}{c_1}; \frac{c''_1 \delta^{**2}}{c_1}; \dots \right). \quad (1-13)$$

Here

$$Re^{**} = c_1 \delta^{**} / \nu.$$

Let us be limited in expression (1-13) only to the first derivative of the velocity and let us expand it into series according to the parameter $c'_1 \delta^{**} / c_1$:

$$c_f = \psi_0(Re^{**}) + \psi_1(Re^{**}) \frac{c'_1 \delta^{**}}{c_1} + \psi_2(Re^{**}) \left(\frac{c'_1 \delta^{**}}{c_1} \right)^2 + \dots \quad (1-14)$$

When $dc_1/dx = 0$ equation (1-14) should determine the resistance coefficient of a flat plate. Hence

$$c_{f0} = \psi_0(Re^{**}). \quad (1-15)$$

According to the experimental data, irrespective of the flow conditions in boundary layer for the plate [25, 69, 71],

$$c_{f0} = \frac{\zeta_0}{Re^{**m}}, \quad (1-16)$$

where ζ_0 and exponent m are constants equal, respectively, to $\zeta_0 = 0.22$, $m = 1$ for the laminar flow and $\zeta_0 = 0.0125$ and $m = 0.25$ for the turbulent flow.

Having expanded function $\psi_1(Re^{**})$ in series according to parameter $1/Re^{**}$ and being limited to linear terms, let us present (1-14) in the following form:

$$c_f = \frac{\zeta_0}{Re^{**m}} \left(1 + a Re^{**m} \frac{c'_1 \delta^{**}}{c_1} \right). \quad (1-17)$$

Here the coefficient a is a certain constant, and complex $Re^{*+m} \frac{c_1' \delta^{**}}{c_1}$ is for the turbulent layer of parameter Buri [Translator's note: named not verified] Γ when $m = 1$, i.e., for laminar layer, into L. G. Loytsyansky's shape parameter.

Thus, for the turbulent boundary layer

$$c_1 = \frac{1}{Re^{*+m}} (\zeta_0 + a_0 \Gamma) = \frac{\zeta(\Gamma)}{Re^{*+m}}. \quad (1-18)$$

Similarly, it is possible to show that the magnitude H incoming into equation (1-11) is also the function of the parameter Γ , i.e.,

$$H = H(\Gamma). \quad (1-19)$$

The functional relations (1-18) and (1-19) allow the obtaining from equation (1-11) the differential relation relative to the parameter Γ in the following form:

$$\frac{d\Gamma}{dx} = \Gamma \frac{c_1''}{c_1'} + F(\Gamma) \frac{c_1'}{c_1}, \quad (1-20)$$

where

$$F(\Gamma) = (m+1)\zeta_0 + [1 + (m+1)(1,8 + H - a_0)]. \quad (1-21)$$

Equation (1-20) is an ordinary differential equation and permits integration in quadratures, if function $F(\Gamma)$ can be approximated by a straight line. From expression (1-21) it follows that such an approximation is possible only for the case $H = \text{const}$. Then the integration of equation (1-20) gives rise to the simple quadrature:

$$\Gamma = \frac{a_1}{c_1^b} \frac{dc_1}{dx} \int_{x_0}^x c_1^{b-1} dx + \Gamma_0, \quad (1-22)$$

where Γ_0 is the value of the parameter of Buri at $x = x_0$.

If the calculation is begun from $x = 0$, and at this point the thickness of the layer is equivalent to zero, then $\Gamma_0 = 0$:

$$a_1 = (m+1)\zeta_0; \quad b_1 = 1 + (m+1)(1,8+H-\beta_0). \quad (1-23)$$

The approximation nature of the examined solution is evident. However, for practical calculations in the region of small positive pressure gradients the accuracy of the calculations proves to be entirely acceptable. Moreover, using relations (1-18) and (1-19) as a basis, it is possible to construct sufficiently accurate solutions in diffuser ranges.

Actually, the dependence of the resistance coefficient upon the parameter Γ in a certain region of changes in magnitude Γ can always be approximated by the linear function of the form (1-18). Then, by taking in this region the mean value for magnitude H , it is possible to construct solutions analogous to solution (1-22).

Therefore, in the region of the high positive pressure gradients the continuous solution is replaced by piecewise smooth solutions, and the calculated correlation assumes the form:

$$\Gamma = \sum_{i=1}^z a_i \frac{c_1'}{c_1^{b_i}} \int_{x_i}^{x_{i+1}} c_1^{b_i-1} dx, \quad (1-24)$$

where z - the number of sections of the calculation into which the whole streamlined surface is divided; when $z = 1$ formula (1-24) turns into expression (1-22).

If coefficients a_1 and b_1 are known, the calculation according to formula (1-24) does not represent serious inconveniences, and for the assigned law of the velocity change $c_1 = c_1(x)$ can be conducted comparatively rapidly. In this case it is convenient to conduct all calculations of news in relative values, having selected as a scale of velocity its peak value $c_{1\text{МАКС}}$, and for the length of the scale - the length of streamlined surface L .

Then the calculation equation (1-24) takes the form:

$$\Gamma = \sum_{i=1}^z \frac{a_i}{\bar{c}_1^{b_i}} \cdot \frac{d\bar{c}_1}{d\bar{x}} \int_{\frac{x_i}{x_t}}^{\frac{x_{i+1}}{x_t}} \bar{c}_1^{b_i-1} d\bar{x} \quad (1-25)$$

By knowing the magnitude Γ , it is possible to obtain easily the value of the dimensionless momentum thickness, since

$$\bar{\delta}^{**} = \frac{\bar{\delta}^{**}}{L} = \left(\frac{\Gamma \bar{c}_1^{-m}}{\text{Re}_L^m \bar{c}_1} \right)^{\frac{1}{m+1}} \quad (1-26)$$

From formula (1-25) it follows that in the computation of the parameter of Γ , sufficient accuracy can be obtained only with the analytical assigned function $\bar{c}_1(\bar{x})$. With its graphic representation the accuracy of the computation of the velocity derivative is usually small. However, this fact does not affect the computation of the momentum thickness, since for its determination knowledge of the velocity derivative is not required.

Having substituted into (1-26) the value of the parameter Γ from (1-25), we obtain for the direct calculation of the momentum loss thickness the following expression:

$$\bar{\delta}^{**} = \left[\frac{1}{\text{Re}_L^m \bar{c}_1^m} \sum_{i=1}^z \frac{a_i}{\bar{c}_1^{b_i-1}} \int_{\frac{x_i}{x_t}}^{\frac{x_{i+1}}{x_t}} \bar{c}_1^{b_i-1} d\bar{x} \right]^{\frac{1}{m+1}} \quad (1-27)$$

Using further the dependence $H(\Gamma)$, it is possible to determine the displacement thickness, and according to the formula (1-18) in each section it is possible to calculate the local resistance coefficient.

Thus, at known values of coefficients a_1 , b_1 and m , it is possible in principle to conduct a complete theoretical calculation of the boundary layer. True, for the definition of these coefficients it is necessary to use experimental data.

§ 1-4. Some Results of the Investigation and Calculation of the Boundary Layer During Diffuser Flows.

In the preceding paragraph it is noted that the specific form of the dependences (1-18) and (1-19) placed as a basis for the calculation of the boundary layer is determined on the basis of experimental data. In this case boundary layer velocity profiles are used as the initial experimental material. If with convergent, gradient-free and weakly diffuser flows, these profiles can be adequately approximated by different kinds of polynomials, then at large positive pressure gradients such an approximation is extremely difficult. For example Fig. 1-4 gives six velocity profiles obtained on a flat wall at various external pressure gradients in a flat channel.

Profiles 1 and 2 correspond to convergent flow with angles $\alpha = -4^\circ$ and $1^\circ 30'$. Profile 3 corresponds to a gradient-free flow, and profiles 4, 5 and 6 are obtained in the diffuser channel with the angle of opening α equal, respectively, to 1° , $2^\circ 40'$ and $4^\circ 30'$.

If in the first four cases a smooth velocity change across the boundary layer takes place, then on curves 5 and 6 the appearance of characteristic bendings and the nonmonotonic nature of the entire velocity profile are distinctly noticeable.

For smoothly changing profiles with the appropriate selection of a variable scale along the y axis in most cases it is possible to obtain a certain universal or close to universal distribution. Used most frequently as a scale factor is the physical thickness of the layer δ , which allows presenting the family of profiles in the dependence of the form:

$$\frac{c}{c_1} = f\left(\frac{y}{\delta}\right). \quad (1-28)$$

However, in diffuser regions the universality of the dependence (1-28) is disturbed.

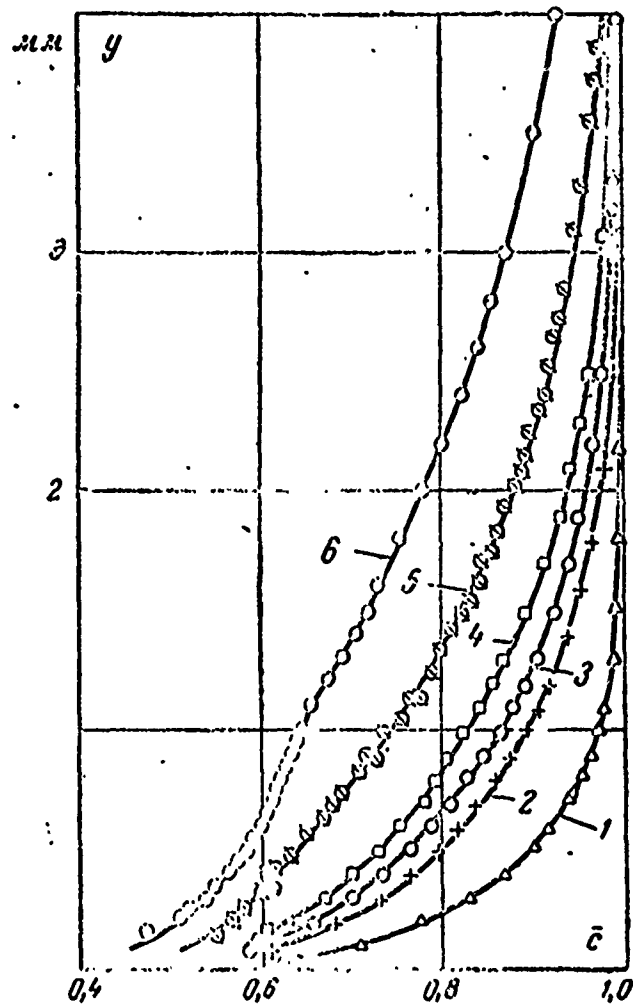


Fig. 1-4. Effect of the pressure gradient on the velocity profiles.

The aforesaid is visually confirmed by curves in Fig. 1-5, where the profiles examined above are reconstructed in coordinates

$\bar{c} = c/c_1$; $\bar{y} = y/\delta$. If the first four profiles lie approximately on one curve, then profiles 5 and 6 of the universal dependence are not subordinated. In this case the investigation on the boundary layer is substantially impeded.

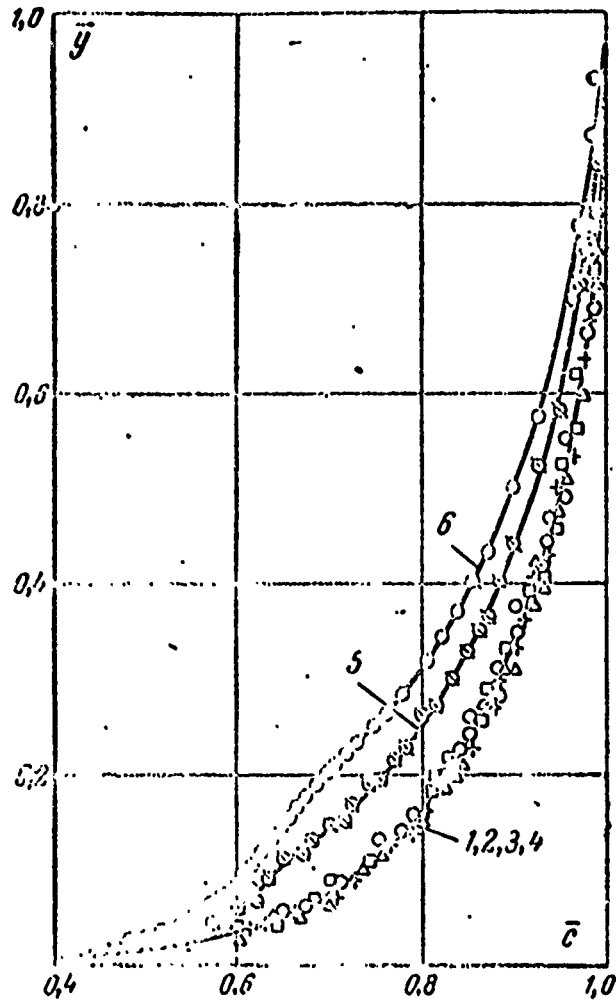


Fig. 1-5. Velocity profiles at various pressure gradients in relative coordinates.

By comparing the profiles given in Fig. 1-4, it should be noted that with the transition from convergent flow to diffuser flow, the physical thickness of the boundary layer increases, and the completeness of the profile is noticeably decreased. Both

these factors, as it is not difficult to see from expressions (1-3) and (1-4), give rise to an increase in the integral boundary layer thicknesses δ^* and δ^{**} , but the intensity of the growth at these magnitudes in the diffuser ranges is different.

By examining the integrand in the expression for the displacement thickness δ^* , it is easy to note that this function is continuously increased in proportion to the decrease in the completeness of the profile, and, consequently, in the diffuser region a noticeable increase in magnitude δ^* occurs.

The change in the integrand in the expression for the momentum thickness proves to be somewhat more complex:

$$\delta^{**} = \int_0^{\delta} \frac{\rho c}{\rho_1 c_1} \left(1 - \frac{c}{c_1}\right) dy = \int_0^{\delta} \frac{\rho c}{\rho_1 c_1} \varphi(y) dy.$$

Here with a decrease in the completeness of the profile, an increase in the function of $\phi(y)$ also takes place. However, this growth is slowed down by the factor $\rho c / \rho_1 c_1$ standing before the parenthesis, and with the great deformation of the profile it lowers the intensity of the growth of the momentum thickness in the diffuser region. In this respect the curve given in Fig. 1-6 is interesting, where depending on the parameter of Buri Γ values of the displacement thickness δ^{**} , referred to the corresponding thicknesses with gradient-free flow δ^{**}_0 , have been plotted. If in the zone of small gradients ($\Gamma = \pm 0.01$) the intensity of the increase in the displacement thickness is highly significant, then at $\Gamma > |0.01|$ this growth is slowed down, and at $\Gamma \leq -0.03$ and by $\Gamma \leq \pm 0.02$ the ratio $\delta^{**} / \delta^{**}_0$ approaches a certain limit close to 3 in the diffuser region and equal to 0.4 in the convergent region. These data are highly characteristic and indicate that in the diffuser regions the increase in the momentum loss thickness is limited. Subsequently we use this experimental fact which results from the very determination of the magnitude δ^{**} .

By analyzing the behavior of the energy thickness, it should be noted that the integrand in expression (1-5) is similar in structure to the function of $\phi(y)$ in the equation for the momentum thickness. However, since the ratio of the squares of velocities enters into this expression, the intensity of the increase in thickness δ^{***} with the decrease in the completeness of the profile will be still less than that for the thickness δ^{**} .

After the remarks made it is possible to predict sufficiently accurately the nature of the change in magnitudes $H = \delta^*/\delta^{**}$ and $H^* = \delta^{***}/\delta^{**}$ with the change in the pressure gradient.

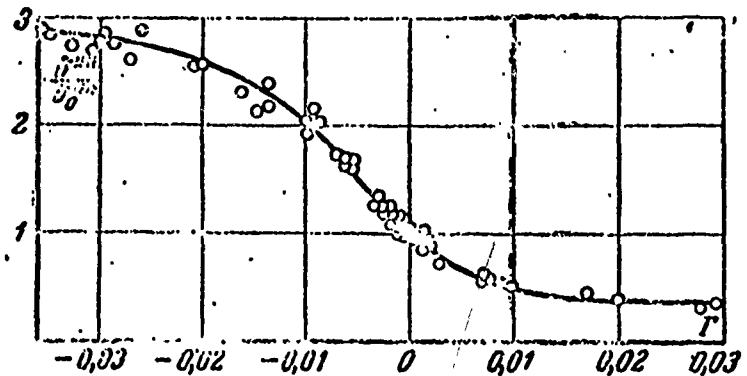


Fig. 1-6. Effect of pressure gradient on the relative momentum thickness.

Actually, at small pressure gradients, the intensity of the increase in thicknesses δ^* and δ^{**} is determined basically by the same term equal to $1 - \frac{c}{c_1}$. Therefore, here one should expect the insignificant increase in the parameter of H . In the region of large pressure gradients, as was already mentioned, the growth in the displacement thickness noticeably leads the growth of the momentum loss thickness, as a result of which the magnitude H should be changed most intensely. Such a nature of dependence $\bar{H}(\Gamma)$ is confirmed well by results of experiments of various authors (Fig. 1-7).

Thus, utilization with the integration of the differential boundary layer equation of condition $H = \text{const}$ in the zone of large positive pressure gradients is a very rough assumption, but on the basis of the experimental curve (Fig. 1-7) the error can be decreased.

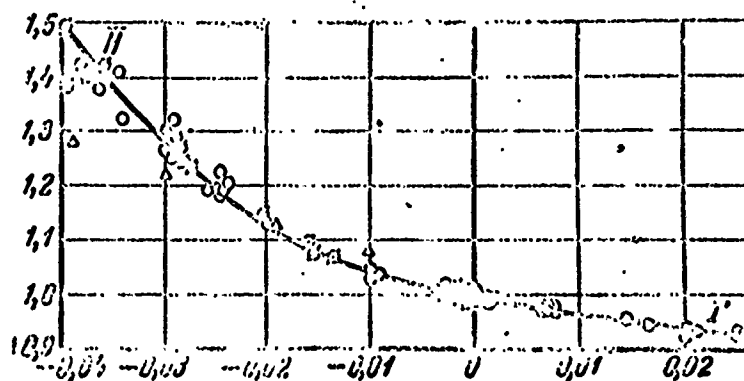


Fig. 1-7. Effect of pressure gradient on parameter \bar{H} . Δ - experiments of Nikuradze; \emptyset - experiments of N. M. Markov; \circ - experiments of the authors.

Subsequently, in the calculation of characteristics of the boundary layer, besides thicknesses δ^* and δ^{**} , for an evaluation of the energy losses it is necessary to determine the thickness δ^{***} . This problem at the known momentum thickness does not represent great difficulty, since the ratio $H^* = \delta^{***}/\delta^{**}$ both in the convergent and diffuser regions changes weakly and can be accepted for diffusers according to the experiments of N. M. Markov [71] equal to 1.6-1.75.

For the refinement of the approximation (1-18) which was used in the integration of equation (1-20), let us examine the dependence given in Fig. 1-8 of the normalized coefficient $\bar{\zeta}$ upon the normalized parameter $\bar{\Gamma}$, where accepted as normalizing values are values of the coefficient ζ_0 for the gradient-free flow and the parameter of Buri at the separation point Γ_s . The dependence in

question is plotted on the basis of experiments of Nikuradze, N. M. Markov and N. I. Konstantinov [61, 71, 111].

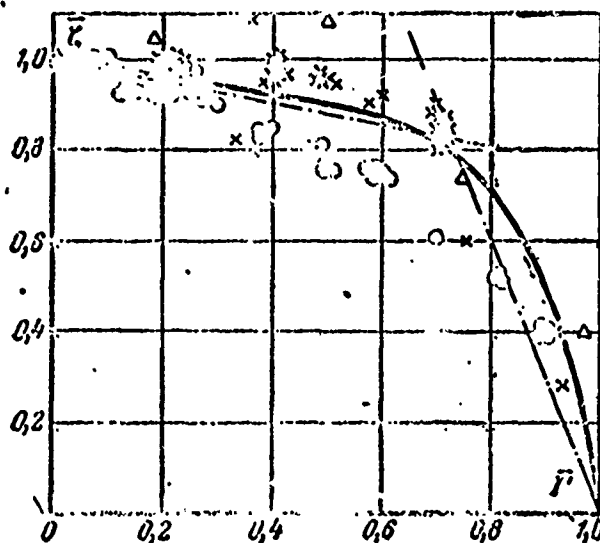


Fig. 1-8. Effect of the pressure gradient on coefficient $\bar{\zeta}$. ● — experiments of Konstantinov; Δ — experiments of Nikuradze; \times — experiments of N. M. Markov.

Here one should note the significant spread of experimental points, which is largely connected with the indirect method of determining the resistance coefficient. However, as a whole the nature of this dependence is quite clear. If in the beginning at $\bar{P} < 0.7$ the reduction in the resistance coefficient is comparatively small, then at $\bar{P} > 0.7$ its jump occurs. In connection with this it is advisable to examine these two regions separately, assuming in each of them its law of the change in the resistance coefficient.

As follows from test data, in the first region the actual curve can be approximated by the following equation:

$$\bar{\zeta} = 1 - 0,25\bar{P}. \quad (1-29)$$

In the second region at $\bar{\Gamma} > 0.7$ the linear approximation in the whole section is difficult. However, in order not to complicate greatly the practical calculations, we approximate the actual distribution by the equation of a straight line:

$$\bar{\zeta} = 3(1 - \bar{\Gamma}). \quad (1-30)$$

Having accepted for the normalization coefficient ζ_0 , which corresponds to the resistance coefficient with gradient-free flow most frequently encountering value $\zeta_0 = 0.0125$, we obtain:

$$\left. \begin{aligned} \zeta &= 0,0125 - \frac{0,00312}{\Gamma_s} \Gamma && \bar{\Gamma} < 0,7; \\ &&& \text{when} \\ \zeta &= 0,0375 - \frac{0,0375}{\Gamma_s} \Gamma && \bar{\Gamma} > 0,7. \end{aligned} \right\} \quad (1-31)$$

The magnitude of the parameter Γ_s incoming into expressions (1-31) at the separation point according to data of different authors changes in very wide limits from 0.028 to 0.12 and, consequently, is to a certain degree indefinite. Below this question is examined more in detail, and it is shown that for calculations the magnitude Γ_s can be accepted equal to 0.036. Then, by using expressions (1-23) and the experimental dependence $\bar{H}(\Gamma)$ given in Fig. 1-7, and considering $m = 0.25$, let us find the following values for coefficients a_1 and b_1 , which enter into formulas (1-25) and (1-26):

$$\left. \begin{aligned} a_1 &= 0,0157; \\ b_1 &= 4,92 \end{aligned} \right\} \text{when } \bar{\Gamma} < 0,7;$$

$$\left. \begin{aligned} a_2 &= 0,047; \\ b_2 &= 4,0 \end{aligned} \right\} \text{when } \bar{\Gamma} > 0,7.$$

As a result, for the calculation of the magnitudes Γ and $\bar{\delta}^{**}$ we will obtain:

I. At $\bar{\Gamma} < 0.7$;

$$\Gamma = \frac{\bar{c}'_1}{\bar{c}_1^{1.92}} \left[\frac{\bar{c}_0^{1.92}}{\bar{c}'_0} \Gamma_0 + 0.0157 \int_{\bar{x}_0}^{\bar{x}} \bar{c}_1^{3.92} d\bar{x} \right]; \quad (1-32)$$

$$\bar{\delta}^{**} = \frac{1}{\text{Re}_L^{0.2} \bar{c}_1^{3.34}} \left[\bar{\delta}_0^{**1.25} \text{Re}_L^{0.25} \bar{c}_0^{1.17} + 0.0157 \int_{\bar{x}_0}^{\bar{x}} \bar{c}_1^{3.92} d\bar{x} \right]^{0.8}.$$

II. At $\bar{\Gamma} > 0.7$

$$\Gamma = \frac{\bar{c}'_1}{\bar{c}_1} \left[\frac{\bar{c}_0^4}{\bar{c}'_0} \Gamma_0 + 0.047 \int_{\bar{x}_0}^{\bar{x}} \bar{c}_1^3 d\bar{x} \right]; \quad (1-33)$$

$$\bar{\delta}^{**} = \frac{1}{\text{Re}_L^{0.2} \bar{c}_1^{2.6}} \left[\bar{\delta}_0^{**1.25} \text{Re}_L^{0.25} \bar{c}_0^{3.25} + 0.047 \int_{\bar{x}_0}^{\bar{x}} \bar{c}_1^3 d\bar{x} \right]^{0.8}.$$

In formulas (1-32) \bar{c}_0 , \bar{c}'_0 , Γ_0 and $\bar{\delta}_0^{**}$ are the velocity, its derivative, the Buri parameter and momentum thickness in the beginning of the turbulent boundary layer. Correspondingly in formulas (1-33) \bar{c}_0 , \bar{c}'_0 , Γ_0 and $\bar{\delta}_0^{**}$ are the magnitudes in the cross section of the boundary layer, where $\bar{\Gamma} = 0.7$.

The obtained expressions based upon semiempirical relations allow conducting the boundary layer calculation in an incompressible fluid in the entire region of flow.

It must be noted that results of numerical computations according to formulas (1-32) and (1-33) in the zone of the large positive pressure gradients differ comparatively little (10-15%), and, consequently, for estimate calculations it is admissible to use only these formulas.

As an example let us examine the change in the momentum thickness and magnitude Γ in the diffuser channel with the linear law of the drop in velocity ($\bar{c}_1 = 1 - 0.5\bar{x}$). Results of the calculations for the given law of the velocity change are given in Fig. 1-9.

Here, besides the parameter Γ , values $\bar{\delta}^{**} = \delta^{**}/\delta^{**}_0$ are plotted, where $\bar{\delta}_0$ - the momentum thickness in the appropriate cross section with gradient-free flow. It is interesting to note that here, just as in Fig. 1-6, the value $\Gamma_s = 0.036$ corresponds to the ratio $\delta^{**}/\delta^{**}_0 = 3$.

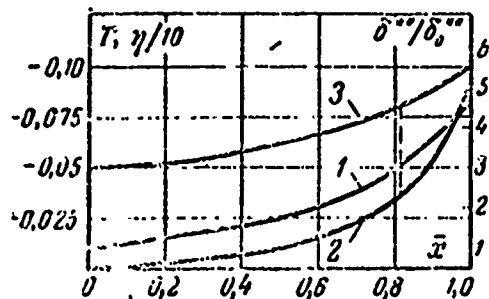


Fig. 1-9. Changes in magnitudes $\bar{\delta}^{**}$, Γ and η in the diffuser channel with the linear law of the velocity change. 1 - $\delta^{**}/\delta^{**}_0$; 2 - Γ ; 3 - η .

§ 1-5. The Effect of Compressibility on Characteristics of the Turbulent Boundary Layer

At high flow rates the method of calculation of the boundary layer examined above requires a certain refinement. In this case, it is necessary to use the more complex expression (1-2) and, furthermore, consider the dependence of magnitudes H and c_f not only on the Re number but also on the M number. According to experiments [25, 26], such a dependence proves to be noticeable.

At the same time one should emphasize that the compressibility of gas at subsonic speeds does not directly affect the velocity profile in practice. Thus, the six velocity profiles in the boundary layer given in Fig. 1-10, obtained at a constant Re number and M number changing from 0.3 to 1, lie on one experimental curve¹. However, despite the invariability of the velocity profiles, with an increase in the M number the integral thicknesses of the boundary layer are changed.

¹Let us note that with gradient flows, especially in the diffuser regions, with a speed gain there occurs an increase in the pressure gradients, which affects the velocity profile and can lead in the diffuser range to an earlier separation of the boundary layer.

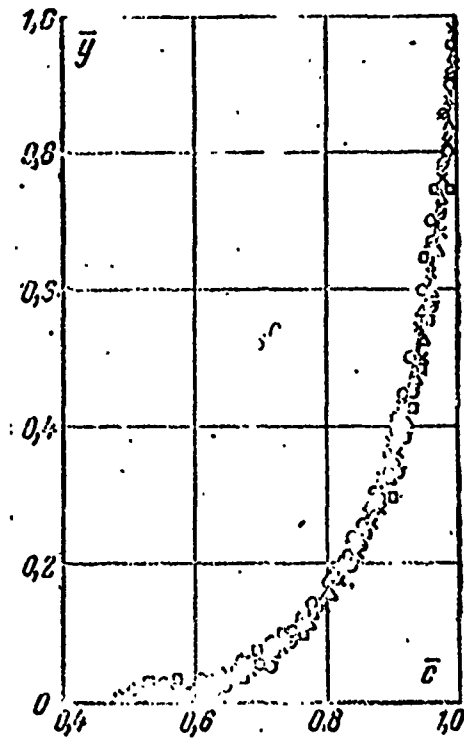


Fig. 1-10. Effect of Mach number on the boundary layer velocity profile. o - M = 0.31; Δ - M = 0.545; x - M = 0.610; \odot - M = 0.791; \square - M = 0.98.

Dependences $\bar{\delta}^{**} = f(M)$ and $\bar{\delta}^* = f_1(M)$ (Fig. 1-11), obtained with a gradient-free cross section on a flat plate, show that with an increase in the M number the displacement thickness grows, and the momentum thickness drops. Such a nature of change in these magnitudes is explained basically by the density change across the layer. Since within limits of the boundary layer $dp/dy = 0$, as a first approximation (not allowing for heat exchange, i.e., on the assumption that the wall temperature is equal to the stagnation temperature T_0) it is possible to present the law of the density change in the following form:

$$\frac{\rho}{\rho_1} = \frac{\rho}{\rho_w} \cdot \frac{\rho_w}{\rho_1} = \frac{T_1}{T_0} \cdot \frac{T_0}{T} = \frac{1 + \frac{k-1}{2} M^2}{1 + \frac{k-1}{2} M_1^2} < 1, \quad (1.34)$$

where ρ_w - density on the wall; M - dimensionless velocity within limits of the boundary layer; M_1 - dimensionless velocity at the outer edge of the layer.

The presence of heat exchange somewhat reduces the difference between the densities at the outer edge of the layer and inside it, and according to the test data of Wilson [112] it is expressed by relation

$$\frac{\rho}{\rho_1} = \left(\frac{1 + \frac{k-1}{2} M^2}{1 + \frac{k-1}{2} M_1^2} \right)^n \quad (1.35)$$

where

$$n = 0,35 \div 0,42.$$

From a qualitative side the indicated density change at the invariable velocity profile gives rise to the growth of the intergrand expression in formula (1-3) and to its reduction in formula (1-4).

Thus, theoretically the nature of the experimental dependences given in Fig. 1-11 proves to be entirely regular. Hence there follows the existence of the dependence of parameter H upon the M number. This dependence (Fig. 1-12) can be approximately approximated by the following formula:

$$H = H_0(1 + 0,3M). \quad (1.36)$$

Here H_0 - the value of parameter H in an incompressible fluid.

Besides parameter H , the compressibility of gas substantially affects the magnitude of the resistance coefficient c_f , which can be corrected by the successful selection of the determining temperature. Being limited to low supersonic velocities ($M_1 < 1.5$), for such temperature let us use the wall temperature T_w , and under these conditions let us introduce into the calculation the density

and kinematic-viscosity coefficient. Then the expression (1-17) takes the form:

$$c_f = \frac{\rho_0}{\rho_1} Re_0^{m-n} \zeta (1 + aF), \quad (1-37)$$

or

$$c_f = c_{f0} \frac{\rho_0}{\rho_1},$$

where c_{f0} - the resistance coefficient in the incompressible flow.

As a result, by using formula (1-35) when $M = 0$, we obtain:

$$c_f = \left(1 + \frac{k+1}{2} M_1\right)^{-n} c_{f0}.$$

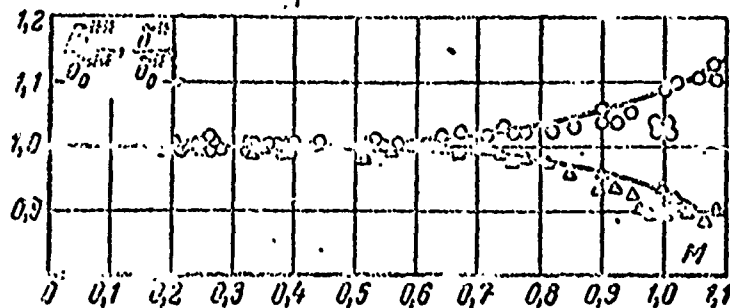


Fig. 1-11. The effect of Mach number on the momentum thickness and the displacement thickness. $o - \delta^*/\delta^*_0$; $\Delta - \delta^{**}/\delta^{**}_0$.

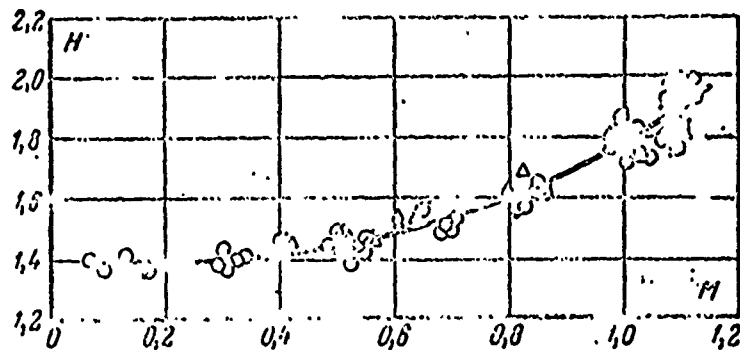


Fig. 1-12. The effect of the Mach number on parameter H. $o - Re = 10^5$; $\odot - Re = 10^6$; $\Delta - Re = (3-6) 10^5$.

Further solution to problem no longer represents serious difficulties, since the consideration of the compressibility does not change the type of the basic differential equation (1-2) but leads only to a certain complication of the final formulas.

The combined solution of equations (1-2), (1-36) and (1-37) gives rise to the following formulas for determining the dimensionless momentum thickness (for $k = 1.4$);

at $0 < \bar{\Gamma} < 0.7$

$$\bar{\delta}^{**} = \frac{1}{f_1 \text{Re}_L^{0.2}} \left[\bar{\delta}_0^{0.25} \text{Re}_L^{0.25} f_3 + \int_{x_0}^{\bar{x}} f_2 dx \right]^{0.8} \quad (1-38)$$

where

$$\left. \begin{aligned} f_1 &= \lambda_1^{3.31} (6 - \lambda_1^2)^{1.45}; \\ f_2 &= 0.0026 \lambda_1^{3.92} (6 - \lambda_1^2)^{2.81}; \\ f_3 &= \lambda_0^{4.17} (6 - \lambda_0^2)^{1.81}; \end{aligned} \right\} \quad (1-38a)$$

at $0.7 < \bar{\Gamma} < 1$

$$\bar{\delta}^{**} = \frac{1}{\varphi_1 \text{Re}_L^{0.2}} \left[\bar{\delta}_0^{0.25} \text{Re}_L^{0.25} \varphi_3 + \int_{x_0}^{\bar{x}} \varphi_2 dx \right]^{0.8} \quad (1-39)$$

where

$$\left. \begin{aligned} \varphi_1 &= \lambda_1^{2.6} (6 - \lambda_1^2)^{1.3} e^{0.31 \lambda_1^2}; \\ \varphi_2 &= 0.0078 \lambda_1^3 (6 - \lambda_1^2)^{2.62} e^{0.31 \lambda_1^2}; \\ \varphi_3 &= \lambda_0^{3.25} (6 - \lambda_0^2)^{1.62} e^{0.31 \lambda_0^2}. \end{aligned} \right\} \quad (1-39a)$$

In formulas (1-38) and (1-39) critical speed a_* is accepted as a characteristic velocity, and coefficients are calculated for air.

The indicated formulas can be used not only at subsonic but, as calculations show, at low supersonic velocities ($M_1 < 1.5$) for ranges of the flow where shock waves are absent.

§ 1-6. Condition and Criteria of the Boundary Layer Separation

With external flow of potential flow about an arbitrary body, on its surface it is always possible to indicate two points in which the velocity is equal to zero. The first is located on the leading and the second on the trailing edge of the streamlined body. Consequently, on the surface of the body the velocity $c_1(\bar{x})$ is first increased and then decreased to a zero value. Thus, in the intake region there always exists the zone in which the fluid is moved against the increasing pressure. The presence of the boundary layer gives rise to the fact that in this zone, under specific conditions, the kinetic flow energy near the streamlined wall is not sufficient for the flow against the increasing pressure and the feed stagnation point is displaced towards the flow. A similar pattern can take place with the flow in the diffuser channel. In this case, beginning from a certain point S (Fig. 1-13), the lines of flow will move away from the surface, and in the range formed the recurrent fluid flow appears. The zone of separation is the source of formation of stable vortices periodically carried by the main flow.

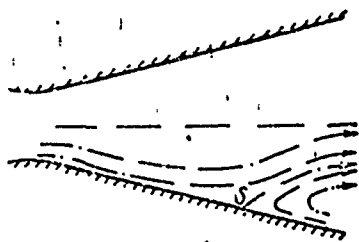


Fig. 1-13. Diagram of detached flow in a flat diffuser.

The separation of the boundary layer from the surface of the streamlined body leads to a sharp increase in drag and is accompanied by increased energy flow losses. Therefore, it is necessary to strive for the displacement of point S towards the exit section of the channel or the trailing edge of the streamlined body.

The position of the separation point is determined by the positive pressure gradient dp/dx and velocity profile in the boundary layer before the separation point. Any increase in dp/dx when an invariable velocity profile gives rise to the displacement in the separation point against the flow. On the other hand, the more complete the velocity profile will be, i.e., the greater the energy possessed by particles of fluid directly at the wall at the assigned pressure gradient dp/dx , the later the separation will begin. Hence there follows the well-known conclusion about the fact that at significant positive pressure gradients it is advantageous to have turbulent flow conditions in the boundary layer, since due to the greater kinetic energy of the particles near the wall separation occurs considerably later than with laminar conditions. Classical experiments with a transversely streamlined cylinder [69] confirm this conclusion.

For the calculation of losses in diffuser channels, just as for the determination of the drag of bodies with external flow, it is necessary to know the position of the separation point determined from condition

$$\left(\frac{dc}{dy}\right)_{y=0} = 0. \quad (1-40)$$

As was already mentioned, the velocity distribution in the boundary layer depends upon the velocity of external flow c_1 , coordinate y , viscosity of fluid ν , pressure gradient or velocity derivative c'_1 and a certain linear dimension, for which it is possible to use the length of the body L , thickness of the layer δ^{**} or any other thickness. Then

$$c = f(c_1; c'_1; \delta^{**}; y; \nu). \quad (1-41)$$

Having turned in expression (1-41) from dimensional magnitudes to dimensionless, and using magnitudes c_1 and δ^{**} , we obtain:

$$\frac{c}{c_1} = f\left(\frac{c'_1 \delta^{**}}{c_1}; \frac{c_1 \delta^{**}}{\nu}; \frac{y}{\delta^{**}}\right). \quad (1-42)$$

Let us expand (1-42) near the surface in series according to the argument y/δ^{**} :

$$\begin{aligned} \frac{c}{c_1} &= \psi_0\left(\frac{c'_1 \delta^{**}}{c_1}; \frac{c_1 \delta^{**}}{\nu}\right) + \\ &+ \psi_1\left(\frac{c'_1 \delta^{**}}{c_1}; \frac{c_1 \delta^{**}}{\nu}\right) \frac{y}{\delta^{**}} + \dots \end{aligned} \quad (1-43)$$

When $c'_1 = 0$ expression (1-43) should coincide with the expression for the appropriate velocity profile on a flat wall. In this case the expansion coefficients with laminar flow do not depend upon the number $Re^{**} = c_1 \delta^{**} / \nu$ [68]. For the turbulent boundary layer the indicated condition for sufficiently large Reynolds numbers also takes place [111].

Therefore, the expansion coefficients ψ_0, ψ_1 etc. should be the function of the product of parameters $(c'_1 \delta^{**} / c_1)^{n_1}$ and $(c_1 \delta^{**} / \nu)^{n_2}$, i.e.,

$$\psi_n = \psi_n \left[\left(\frac{c'_1 \delta^{**}}{c_1} \right)^{n_1} \left(\frac{c_1 \delta^{**}}{\nu} \right)^{n_2} \right]. \quad (1-44)$$

Thus, according to condition (1-40) and formula (1-43), the position of the separation point is determined from the expression

$$\psi_1 = 0. \quad (1-45)$$

Let us expand (1-45) in series and, taking into account that the argument of the expansion $\left[\left(\frac{c'_1 \delta^{**}}{c_1} \right)^{n_1} \text{Re}^{**n_2} \right]$ is small, let us be limited to two terms of the expansion. Then

$$b_0 + b_1 \left[\left(\frac{c'_1 \delta^{**}}{c_1} \right)^{n_1} \text{Re}^{**n_2} \right] = 0.$$

Hence, at the separation point

$$\left(\frac{c'_1 \delta^{**}}{c_1} \right)^{n_1} \text{Re}^{**n_2} = \text{const.} \quad (1-45a)$$

When $n_1 = n_2 = 1$ the obtained expression gives the value of the constant - the shape parameter of L. G. Loytsyanskiy at the separation point f_s . The value of the constant for this case can be shown with sufficient accuracy ($f_s = -0.089$) [68]. When $n_1 = 1$ and $n_2 = 0.25$, the conditions (1-45) gives the parameter of Buri Γ_s at the separation point. At this point the magnitude Γ_s according to experimental data, changes over very wide limits.

Thus, according to experimental data of N. M Markov $|\Gamma_s| = 0.028-0.035$ [71]. According to Nikuradze, G. Shlikhting and Bay Shi-y [4, 111] $|\Gamma_s| = 0.05-0.12$. N. I. Konstantinov's experiments [61] gave $|\Gamma_s| = 0.035-0.09$; P. A. Romanenko and others [90] obtained in their experiment $|\Gamma_s| = 0.05-0.07$.

Instead of the Buri parameter L. G. Loytsyanskiy uses a parameter close to it $f_{Sm} = 153,2 \frac{c'_1 \delta^{**}}{c_1} \text{Re}^{**1/6}$, equal at the separation point to $f_{Sm} = 2-3$, which corresponds to value $|\Gamma_s| = 0.026-0.038$. Such a spread of the numerical values of the Buri parameter at the separation point indicates that the magnitude Γ_s is indefinite, and it is difficult to use this parameter as a criterion of separation.

Furthermore, on the basis of test data in works on the boundary layer, the conclusion is frequently drawn that the one-parameter method of calculation in regions with large positive pressure gradients proves to be invalid, since near the separation point old velocity derivatives, which characterize the prehistory of the flow, acquire vital importance [4, 70]. However, when the velocity distribution at the boundary layer edge can be presented by an analytical dependence, calculations of the thickness δ^{**} according to the one-parameter method give an entirely acceptable agreement with the experimental data almost up to the separation point [11, 23, 25].

It is possible that the effect of the old velocity derivatives near the separation zone is exaggerated, and the probable reason for the spread of values Γ_s can be the low accuracy of measurements in this region and the principal nature of the change in the momentum thickness along the surface at large positive pressure gradients.

Actually the experimental data given in Fig. 1-6 indicate that at $\Gamma < -0.025$ the momentum thickness very weakly depends upon the pressure gradient. In other words, from this moment the magnitude of parameter Γ is determined basically only by values of the velocity and its derivative, and the determination of these magnitudes near the separation point, on the basis of drainage measurements, is insufficiently precise because here the basic condition of the boundary layer $\frac{\partial c_1}{\partial x} \ll \frac{\partial c_1}{\partial y}$ is not fulfilled, and the longitudinal velocity gradient becomes commensurable with the transverse, i.e., $\frac{\partial c}{\partial x} \approx \frac{\partial c}{\partial y}$.

Thus, from the structure of the Buri parameter it follows that its utilization as a criterion of the separation of the turbulent boundary layer is difficult because of the purely physical reasons.

From the aforesaid it follows that for the criterion of separation, it is advantageous to select the parameter dependent directly on the shape of the velocity profile in the boundary layer. The parameter proposed by Grushvits can be used as such a magnitude [4, 111] and equals:

$$\eta = 1 - \left(\frac{c}{c_1} \right)_{y=\delta^{**}}^2 \quad (1-46)$$

Here $\left(\frac{c}{c_1} \right)_{y=\delta^{**}}$ - relative velocity in the boundary layer when $y = \delta^{**}$.

For the gradient-free flow of the turbulent boundary layer, the magnitude $\eta = 0.5$. In diffuser regions the deformation of the velocity profile leads to an increase in η , and at separation point $\eta_s = 0.8$. However, for the determination of the coordinate of this point, it is necessary to construct the law of the change in parameter η along the streamlined surface. For this purpose it is possible to use the empirical relation of Grushvits [4]:

$$\frac{dG}{dx} + 0,00394 \frac{G}{\delta^{**}} = 0,00461 \frac{\rho_1 c_1^2}{2\delta^{**}} \quad (1-47)$$

where

$$G = \frac{\rho_1 c_1^2}{2} \eta.$$

The differential equation (1-47) is solved by the method of successive approximations. Used as the first approximation are values δ^{**} found from the equation of Kármán (1-2).

For a rapid estimate of the possibility of nonseparable flow, it is possible to use the relative momentum thickness $\bar{\delta}^{**} = \delta^{**}/\delta_0^{**}$, where δ_0^{**} - the momentum thickness on a flat plate:

$$\delta_0^{**} = \frac{0,036x}{Re_L^{0,2}}.$$

Considering at the separation point that $\delta_s^{**} = 3$, we obtain the condition for determining the coordinate of the separation point. Figure 1-9 gives the curve of the change in parameter η along the wall of a flat diffuser with the linear law of the velocity change. Here the dependences $\Gamma(\bar{x})$ and $\delta^{***}(\bar{x})$ are given. The value of parameter $\eta_3 = 0.8$ corresponds to the magnitudes Γ_s and $\bar{\delta}_s^{**}$, equal to -0.036 and 3.1 , respectively. Values are obtained very close to these numbers with other laws of the velocity change. In connection with this, in the construction of calculation equations, which determine the change in integral thicknesses along the streamlined surface, the magnitude of the parameter Γ_s at the separation point was accepted equal to -0.036 . Naturally, the indicated value Γ_s , because of reasons noted above, is arbitrary. However, for the majority of the problems the flow at $\Gamma_s > -0.036$, apparently, is nonseparable, and for its calculation the use of the derived dependences (1-32) and (1-33) is admissible.

Without discussing in detail the other criteria of separation, let us say that as such a criterion Tetervin and Dengoff [4] propose using magnitude H relative to which is composed the experimental equation analogous to the equation of Grushvits. However, as the test data show (see Fig. 1-7), this magnitude at the separation point changes from 1.8 to 3.0 [4, 25], which makes it just as indefinite as the parameter Γ_s .

Using the dimensional theory as a basis, G. M. Bam-Zelikovich [5] proposes using at the point of separation the following parameter:

$$\frac{c'_1 \delta^{**}}{c_1} = \eta_0 = 0,005.$$

It is not difficult to see that this parameter results from the parameter of Buri when $m = 0$, and consequently the indicated value 0.005 cannot be recognized as being sufficiently reliable. Furthermore, the magnitude of $\phi_0 = 0.005$ is the first term of the

expansion in series of a certain function about the separation point, and the degree of convergence of this series has not been investigated by the author.

Quite convincing data on the determination of the separation point are given in the work of Stratford [98]. Here, as a criterion of separation, it is proposed to use the following magnitude, which is valid at $Re > 10^6$:

$$(2\bar{p})^{\frac{n-2}{4}} \left(\frac{d\bar{p}}{d\bar{x}} \bar{x} \right)^{0,5} = 1,05\beta (10^{-6} Re_s)^{1/10},$$

where

$$\bar{p} = \frac{p_t - p_0}{\frac{\rho_1 c_{11}^2}{2}}; \quad n = \lg Re_s \approx 7; \quad \beta = 0,66.$$

The given set is obtained as a result of the examination of the form of the velocity profiles near the separation point and, apparently, can serve for the comparatively precise estimate of the possible boundary of separation. In any case the data on the estimate of separation given in work [98] are quite convincing.

In conclusion let us give a table of various criteria at the separation point and tentative ranges from measurements.

Table 1-1

Parameter	Value of Separation Point
$ \dot{r}_s $	0,025 — 0,12
η_s	0,8
H_s	1,8 — 2,6
$k_s = \delta^{**} / \delta^{* *}$	2,8 — 3,0
$\bar{p}^{1,25} \left(\bar{x} \frac{d\bar{p}}{d\bar{x}} \right)^{0,5} (10^{-6} Re_s)^{-\frac{1}{10}}$	0,4

§ 1-7. Effect of the Initial Turbulence on the Boundary Layer Characteristics

The method of calculation of the boundary layer examined above is valid for the certain small turbulence level of external flow. In turbomachines, as a rule, the turbulence level of the main flow proves to be quite large (5-15%). Under these conditions one should expect the noticeable effect of increased turbulence on characteristics of the boundary layer.

The investigation of the effect of the external turbulence until recently was reduced basically to an estimate of the effect of the turbulence on the position of the zone of transition from laminar to turbulent flow conditions. In this case it was considered that with an increase in the degree of turbulence of the external flow, there occurs a reduction in the critical Reynolds number, i.e., the extent of the laminar section is sharply reduced, and characteristics of the turbulent layer are not changed. However, V. A. Vrublevskaya's experiments [13, 14] and the qualitative analysis of equation (1-1) visually show that with an increase in the initial turbulence a noticeable change in the momentum thickness occurs. Thus, Fig. 1-14 gives curves of the change in magnitude $\bar{\delta}^{**}$ on a flat plate at different values of the initial turbulence. A comparison of the curves shows that with an increase in turbulence from 1.5 to 5% the momentum thickness increases almost 2 times. Analogous results were obtained with tests of turbine cascades [14].

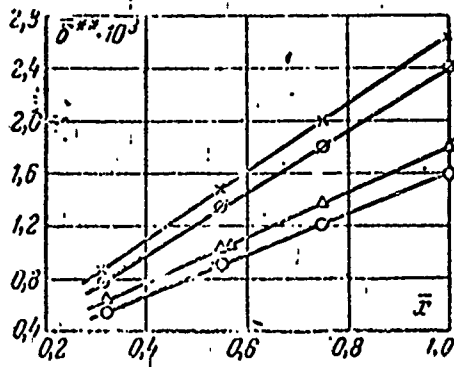


Fig. 1-14. Effect of the turbulence level on the momentum thickness on a flat plate. $\times - \epsilon_0 = 5\%$; $\circ - \epsilon_0 = 4\%$; $\Delta - \epsilon_0 = 2\%$; $O - \epsilon_0 = 1.5\%$.

Therefore, if the degree of turbulence of the flow exceeds 1-2%, it is necessary to introduce a correction into the appropriate calculations of integral thicknesses. Such a correction, according to data [14], is introduced comparatively easily, and for the calculation it is possible to recommend the formula

$$\delta^{**}_0 = \psi(\varepsilon_1 \Gamma) \delta^{**}_{\varepsilon=0} \quad (1-48)$$

Here $\delta^{**}_{\varepsilon=0}$ - the value of the momentum thickness calculated from the relation (1-32), not allowing for the initial turbulence, and function $\psi(\varepsilon_1 \Gamma)$ according to V. A. Vrubl'vskaya's experiments is equal to:

$$\psi(\varepsilon_1 \Gamma) = \left(\frac{0,0131 + 0,14e^{-1,5\Delta\varepsilon} \Gamma}{0,0131 + 0,14\Gamma} \right) e^{0\Delta\varepsilon}, \quad (1-49)$$

where $\Delta\varepsilon = \varepsilon - 0.005$, and Γ is the parameter of Buri found from relations (1-32).

Thus, the calculation of the effect of the initial turbulence level on characteristics of the turbulent layer is not particularly difficult: it is necessary to introduce the correction which considers the increase in integral thicknesses.

§ 1-8. Boundary Layer Calculation on the Basis of the Semiempirical Theories of Turbulence

The engineering method of calculation of the turbulent boundary layer examined above permits finding quite simply its integral thicknesses δ^* , δ^{**} and δ^{***} but does not give a concept about the form of the velocity profile. Furthermore, the possibilities of the method are limited to the fact that with the integration of the equation of Kármán the purely experimental dependence for the resistance coefficient is used, and the accuracy of the calculation is determined actually by the accuracy of the utilized experimental dependence.

The portion of empiricism in the considered question can be substantially decreased if we use the connection between the stress of friction τ and the velocity profile allowed by the theory of turbulence. According to Prandtl this connection is expressed by the relation

$$\tau = \rho l^2 \left(\frac{\partial c}{\partial y} \right)^2, \quad (1-50)$$

where l - mixing length.

If the dependence of τ and l upon the transverse coordinate y is known, then the differential equation (1-50) determines the velocity profile in the following form [105]:

$$\sqrt{\frac{c}{\tau}} = \text{const} + \int \frac{\partial}{l} \sqrt{\frac{\tau}{\tau_w}} d\left(\frac{y}{\delta}\right). \quad (1-51)$$

Expression $\sqrt{\frac{\tau}{\rho}}$ has a dimensionality of velocity and is frequently called "dynamic" velocity (c_*). By changing in an appropriate manner the dependences $\tau/\tau_w = f(y)$ and $l = \phi(y)$, it is possible to obtain a broad class of the profiles whose conformity to the experiment will be determined by how successful the approximating functions are selected.

Thus, when $\tau/\tau_w = 1$ and $l = \kappa y$, where κ - experimental constant,

$$\frac{c}{c_*} = \frac{1}{\kappa} \ln y + B_1 = A_1 \ln \frac{y c_*}{\nu} + B_1. \quad (1-52)$$

Formula (1-52) determines the universal logarithmic velocity profile on the plate and in the pipe and surprisingly concurs with the test data almost in the entire zone of flow, with the exception of the small zone near the wall and exterior of the boundary layer.

In general K. K. Fedyaevskiy (1937) used the empirical formula of Prandtl for the mixing length

$$\frac{l}{\delta} = 0,14 - 0,03 \left(1 - \frac{y}{\delta}\right)^2 - 0,03 \left(1 - \frac{y}{\delta}\right)^4 \quad (1-53)$$

and the polynomial approximation for the stress of friction in the form:

$$\frac{\tau}{\tau_w} = 1 + A \frac{y}{\delta} - (1 + A) \left(\frac{y}{\delta}\right)^2, \quad (1-54)$$

which results from the following boundary conditions:

when $y = 0$

$$\tau = \tau_w; \quad \frac{\partial \tau}{\partial y} = \frac{\partial p}{\partial x}; \quad \frac{\partial^2 \tau}{\partial y^2} = 0;$$

when $y = \delta$

$$\tau = 0; \quad \frac{\partial \tau}{\partial y} = 0.$$

The parameter

$$A = \frac{\delta}{\tau_w} \cdot \frac{\partial p}{\partial x}.$$

Substitution of the accepted dependences into (1-51) determines the velocity profile in the turbulent part of the boundary layer at small negative and any positive gradients.

Taking into account that near the wall the magnitude of eddy viscosity is small as compared with the viscous friction, the lower limit of integration in expression (1-51) is established by the thickness of the so-called viscous sublayer $\eta_n = y_n/\delta$. Moreover, in the subsequent work [105] K. K. Fedyaevskiy showed that the interval of the change in the argument $\eta_n < \eta < 1$ is advantageously divided into two ranges: from η_n to η_0 , where the

dependence $l = 0.4y$ is valid, and exterior part, where the "mixing length" is determined by formula (1-53). Then the velocity profile can be represented in the form:

$$\psi = \frac{c_1 - c}{c_0} = \int_{\eta_0}^1 \varphi(A, \eta) d\eta + \int_{\eta_1}^{\eta_0} \varphi_1(A, \eta) d\eta,$$

where

$$\varphi(A, \eta) = \frac{\sqrt{1 + A\eta - (1 + A)\eta^2}}{0.14 - 0.08(1 - \eta)^2 - 0.05(1 - \eta)^3},$$

and

$$\varphi_1(\eta, A) = \frac{\sqrt{1 + A\eta - (1 + A)\eta^2}}{0.4\eta}.$$



It is easy to calculate the second integral. As a result

$$\begin{aligned} \psi = \frac{c_1 - c}{c_0} = & \int_{\eta_0}^1 \frac{\sqrt{1 + A\eta - (1 + A)\eta^2}}{0.14 - 0.08(1 - \eta)^2 - 0.05(1 - \eta)^3} d\eta + \\ & + 2.5 \left[\sqrt{F} - \ln(2 + A\eta + 2\sqrt{F}) - \right. \\ & \left. - \frac{A}{2\sqrt{A+1}} \arcsin \frac{A - 2(A+1)\eta}{A+2} \right]_{\eta_1}^{\eta_0} - 2.5 \ln \frac{\eta_1}{\eta_0}; \end{aligned} \quad (1-55)$$

$$F = 1 + A\eta - (1 + A)\eta^2.$$

The boundary of the laminar sublayer for the gradient flow, according to work [105], is determined by the following expression:

$$\eta_1 = \sqrt[3]{\frac{200\rho v^3}{d\rho/dx \delta^3}}.$$

The dependence (1-55) is extremely complex for practical calculations, and this explains the fact that its successful use became possible only with the use of electronic computers.

Just as earlier, with the integration of equation (1-2) with the use of experimental dependences, the entire possible range of the nonseparable flow is divided into two regions. For small positive gradients ($0 < |\Gamma| < 2d$), where d is the coefficient dependent on the number Re^{**} , the normal velocity profile (1-55) gives rise to a quadrature of the type (1-27):

$$\frac{\delta^{**}}{L} = \frac{[d(1+m)]^{\frac{1}{1+m}}}{Re_L^{\frac{m}{1+m}} \bar{c}_1^{\frac{3+5m}{1+m}}} \left[\text{const} + \int_{\frac{x}{x_0}}^{\bar{x}} \bar{c}_1^{3+4m} d\bar{x} \right]^{\frac{1}{1+m}} \quad (1-56)$$

The specific value of constants m and d is determined by the range of numbers Re^{**} .

When $\lg Re^{**} = 2.2-4.0$ $d = 0.0103$; $m = 0.222$ and

$$\frac{\delta^{**}}{L} = \frac{1}{Re_L^{0.152} \bar{c}_1^{3.37}} \left[\bar{\delta}_0^{0.122} Re_L^{0.222} \bar{c}_0^{4.11} + 0.0126 \int_{\frac{x}{x_0}}^{\bar{x}} \bar{c}_1^{3.89} d\bar{x} \right]^{0.02} \quad (1-57a)$$

When $\lg Re^{**} = 3.0-5.5$ $d = 0.073$; $m = 0.179$ and

$$\frac{\delta^{**}}{L} = \frac{1}{Re_L^{0.152} \bar{c}_1^{3.31}} \left[\bar{\delta}_0^{0.110} Re_L^{0.179} \bar{c}_0^{2.89} + 0.0386 \int_{\frac{x}{x_0}}^{\bar{x}} \bar{c}_1^{3.72} d\bar{x} \right]^{0.05} \quad (1-57b)$$

When $\lg Re^{**} = 4-6.5$ $d = 0.00521$; $m = 0.148$ and

$$\frac{\delta^{**}}{L} = \frac{1}{Re_L^{0.129} \bar{c}_1^{3.25}} \left[\bar{\delta}_0^{0.115} Re_L^{0.148} \bar{c}_0^{3.74} + 0.0377 \int_{\frac{x}{x_0}}^{\bar{x}} \bar{c}_1^{3.59} d\bar{x} \right]^{0.072} \quad (1-57c)$$

Reproduced from
best available copy.

For the large pressure gradients ($|\Gamma| > 1.5d$), the solution proves to be close to the relation of Ross and Robertson [87]:

$$\frac{\delta^{**}}{\delta^{**}_0} = \left(\frac{c_0}{c_1} \right)^{4.75 - \frac{2}{1+m}} \quad (1-58)$$

If instead of dependence (1-50) we use the relation of Kármán for the stress of friction in the turbulent boundary layer

$$\tau = \alpha^2 \rho \frac{\partial c / \partial y}{(\alpha^2 c' / \partial y^2)^2}, \quad (1-59)$$

then, as A. P. Mel'nikov showed [42], when using the polynomial (1-54) it will be possible to arrive at the following expression for the momentum thickness:

$$\frac{\delta^{**}}{L} = \frac{1}{\text{Re}_L^{0.163} c_1^{0.66}} \left[\delta_0^{**1.2} c_0^{1.4} \text{Re}_L^{0.2} + 0.015 \int_{x_0}^x c_1^{1.2} d\bar{x} \right]^{0.83} \quad (1-60)$$

Reproduced from
best available copy.

The idea of the calculation proposed by K. K. Fedyaevskiy was so fruitful that in the last decade it is used most frequently in works on the boundary layer. Despite the diversity of the procedures, the basis for contemporary calculated methods consists of dependences of the type (1-50) or (1-59), which connect the stress of friction with the profile of the averaged velocities. In this case, just as in work [105], it usually proves to be advisable to use a two-layered or three-layered model of the turbulent boundary layer. In the first case the boundary layer across is divided into a viscous sublayer, where Newton's dependence for the stress of friction $\tau = \mu \frac{\partial c}{\partial y}$ is the basic, and the external turbulent region. In the second case between the viscous sublayer and exterior layer a transition region is located.

An important moment in the development of calculated methods was the research of Clauser, who introduced the concept about equilibrium flows and showed that in the exterior region it is possible to use not Prandtl's relation (1-50), but Boussinesq's formula

$$\tau = \mu_e \frac{\partial c}{\partial y} \quad (1-61)$$

with the coefficient of virtual viscosity μ_e . Under this assumption solutions of D. B. Spolding [94a], Libbey Baronti, Napolitano [67], D. L. Mellor and D. M. Gibson [79], Stratford [98] and others are constructed. Unfortunately, all these methods require numerical integration and do not give such simple expressions for integral thicknesses as the approximation relations (1-27), (1-57) and (1-60) examined above. Since for our purposes the accuracy of these relations is entirely sufficient, the authors considered it possible in this work not to discuss the details of stricter methods of the calculation than the modified method of Buri used in the book. For greater clarity, Table 1-2 gives a comparison of design equations obtained by various authors.

It should be noted that, despite the different approach to the problem in question, the final expressions differ little. The distinction in the coefficients gives rise to noticeable deviations in the computable magnitude in methods of A. P. Mel'nikov, G. M. Bam-Zelikovich and Trukkenbrodt. In the remaining cases the final results prove to be quite close. For a comparison Table 1-3 gives values of the relative momentum thickness with the linear law of the drop in velocity in a flat channel ($\bar{c}_1 = 1 - 0.5\bar{x}$) obtained by calculation in various formulas.

Table 1-2

Author	Formula
Fedyayeskiy, K. K. Kolesnikov, A. V. Smolyaninova, A. N.	$\frac{\delta^{**}}{L} = \frac{1}{\text{Re}_L^{0.152} c_1^{3.37}} \left[\bar{\delta}_0^{**1.22} \text{Re}_L^{0.22} \bar{c}_0^{1.11} + \right. \\ \left. + 0.0126 \int_{\frac{x}{x_0}}^{\bar{x}} \bar{c}_1^{3.09} d\bar{x} \right]^{0.82}$
Mel'nikov, A. P.	$\frac{\delta^{**}}{L} = \frac{1}{\text{Re}_L^{0.166} c_1^{3.65}} \left[\bar{\delta}_0^{**1.3} \text{Re}_L^{0.2} \bar{c}_0^{1.4} + \right. \\ \left. + 0.015 \int_{\frac{x}{x_0}}^{\bar{x}} \bar{c}_1^{1.2} d\bar{x} \right]^{0.83}$
Deych, M. Ye Zaryankin, A. Ye. formula (1-32)	$\frac{\delta^{**}}{L} = \frac{1}{\text{Re}_L^{0.2} c_1^{3.34}} \left[\bar{\delta}_0^{**1.25} \text{Re}_L^{0.25} \bar{c}_0^{1.17} + \right. \\ \left. + 0.0157 \int_{\frac{x}{x_0}}^{\bar{x}} \bar{c}_1^{3.92} d\bar{x} \right]^{0.8}$
Loytsyanskiy, L. G.	$\frac{\delta^{**}}{L} = \frac{1}{\text{Re}_L^{0.153} c_1^{3.4}} \left[\bar{\delta}_0^{**1.16} \text{Re}_L^{0.167} \bar{c}_0^{3.96} + \right. \\ \left. + 0.03765 \int_{\frac{x}{x_0}}^{\bar{x}} \bar{c}_1^{3.8} d\bar{x} \right]^{0.856}$
Maskell	$\frac{\delta^{**}}{L} = \frac{1}{\text{Re}_L^{0.177} c_1^{3.63}} \left[\bar{\delta}_0^{**1.22} \text{Re}_L^{0.22} \bar{c}_0^{1.415} + \right. \\ \left. + 0.0117 \int_{\frac{x}{x_0}}^{\bar{x}} \bar{c}_1^{1.2} d\bar{x} \right]^{0.824}$

Table 1-2 (Continued)

Trukkenbrodt	$\frac{\delta^{**}}{L} = \frac{1}{Re_L^{0.143} \bar{c}_1^3} \left[\bar{\delta}_0^{**+1.167} Re_L^{0.167} \bar{c}_0^{3.5} + 0.6076 \int_{\frac{x}{x_0}}^{\bar{x}} \bar{c}_1^{3.33} d\bar{x} \right]^{0.855}$
Spence	$\frac{\delta^{**}}{L} = \frac{1}{Re_L^{0.167} \bar{c}_1^{3.5}} \left[\bar{\delta}_0^{**+1.2} Re_L^{0.2} \bar{c}_0^{4.2} + 0.0105 \int_{\frac{x}{x_0}}^{\bar{x}} \bar{c}_1^4 d\bar{x} \right]^{0.332}$

Table 1-3

Author	δ^{**}	
	at $Re_L = 10^5$	at $Re_L = 10^6$
Fedyayevskiy, K. K. Kolesnikov, A. V. Smolyaninova, A. N.		
formula (1-57a).....	0.0193	0.0127
formula (1-57b).....	0.0145	0.0102
formula (1-57c).....	0.0142	0.0101
Mel'nikov, A. P.....	0.0262	0.0178
Deych, M. Ye		
Zaryankin, A. Ye		
formula (1-32).....	0.016	0.0110
Loytsyanskiy, L. G.....	0.015	0.0108
Maskell.....	0.018	0.0122
Trukkenbrodt.....	0.0115	0.0082
Spence.....	0.0193	0.013
Bam-Zelikovich, G. M.....	-	0.0248

CHAPTER TWO

METHODS OF CALCULATION AND AERODYNAMIC CHARACTERISTICS OF DIFFUSERS

§ 2-1. Types of Diffusers

Diffuser elements utilized for the conversion of the kinetic energy of the flow into potential energy are completely diverse. Because of this, we will discuss only the basic types of the diffusers which are most frequently encountered in practice.

a) Flat diffusers are the channels, flow passage cross-sectional areas of which are changed in the course of flow in one plane, and the longitudinal linear dimension B (Fig. 2-1) of which considerably exceeds the transverse dimension H_1 in the exit section. The most widespread diffusers of this type are the flat rectilinear and curvilinear diffusers schematically depicted in Fig. 2-1a and b. Since at $H_1/B \ll 1$ the effect of the side walls as a first approximation can be disregarded, the flow in such elements is examined usually only in the meridian plane.

The cross section of the flat rectilinear diffuser is determined by the assignment of the following magnitudes: the height at inlet h , height at the outlet H_1 and the angle of slope of the generatrices α . Together with these magnitudes the length of the diffuser L is frequently introduced into the examination. Any combination of three of these parameters completely determines the shape of the channel in cross section.

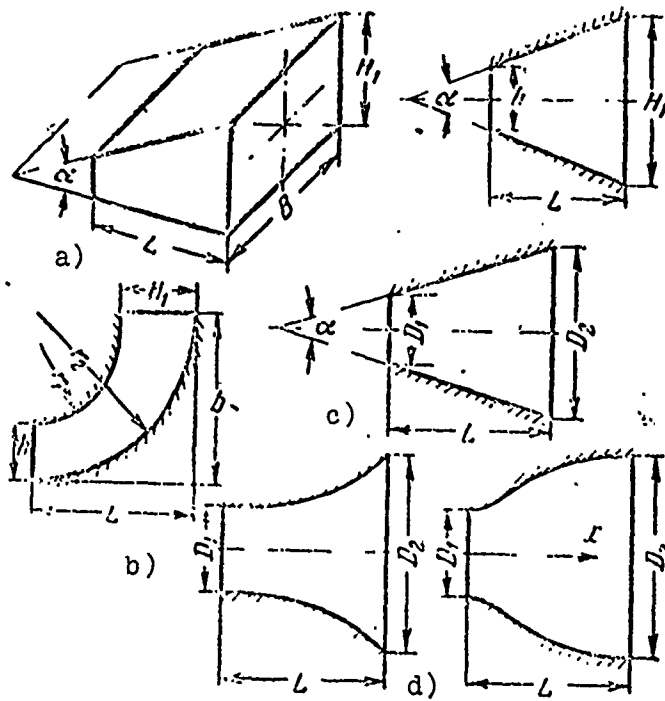


Fig. 2-1. Diagram of flat and conical diffusers. a) flat rectilinear diffuser; b) flat curvilinear diffuser; c) conical diffuser; d) axisymmetric diffuser with curvilinear generatrices.

The number of geometric parameters can apparently, be reduced if we turn to the dimensionless values. Thus, having selected as the basic parameter the height h , we obtain three values: $n = H_1/h$, α and L/h , where n - the expansion ratio of the diffuser, equal to the ratio of the area at the outlet F_2 to the inlet area F_1 . In this case, since the transverse dimensions of the channel are invariable, the area ratio can be replaced by the ratio of appropriate linear dimensions.

The similarity of flat rectilinear diffusers is provided by the equality of any two dimensionless geometric parameters: n and α , n and L/h , α and L/h . The first two parameters are used most frequently.

By examining the flat curvilinear diffuser (Fig. 2-1b), it should be noted that here the minimum number of the geometric parameters which determine the flowing part in meridian section noticeably increases. Thus, for the diffuser depicted in Fig. 2-1b, it is necessary to assign its length L , dimensions b , radii r_1 and r_2 and heights h and H_1 .

Having maintained here as the determining dimension h , we obtain the following dimensionless values:

$$n = \frac{H_1}{h}; \quad \bar{r}_1 = \frac{r_1}{h}; \quad \bar{r}_2 = \frac{r_2}{h}; \quad \bar{L} = \frac{L}{h}; \quad \bar{b} = \frac{b}{h}.$$

Considering, however, that the flow in the curvilinear channel substantially depends upon radius r_1 [109], in certain cases it makes sense to take for the determining dimension not h , but radius r_1 . But both in the first and second cases, when evaluating the similarity of curvilinear diffusers, it is necessary to provide the equality of at least three dimensionless values: n , r_2/r_1 and b/L . The first of these parameters characterizes the expansion ratio of diffusers, the second determines the shape of the channel, and the third indicates its relative curvature.

b) Conical diffusers refer to the most widespread and very simple diffuser elements formed by the surface of a truncated cone (Fig. 2-1c). The meridian section of these diffusers completely coincides with the cross section of the flat rectilinear diffusers and, consequently, is determined by the same geometric parameters. However, instead of heights h and H_1 , here it is advantageous to examine diameters at the inlet D_1 and outlet D_2 . Then for conical diffusers we will have the following systems of dimensionless parameters:

$$\alpha; L/D; n = \frac{D_2^2}{D_1^2}.$$

For the characteristic of the geometric shape of the diffusers in question, just as for the flat ones, it is sufficient to use any two values.

c) The curvilinear axisymmetric diffusers given in Fig. 2-1d are determined by the diameters of the inlet D_1 and outlet D_2 , the length L and the law of the change in area along the x axis $F_x = f(\bar{x})$. Here, for the similarity of the diffusers, it is necessary to provide the equality of the three values: the expansion ratio n , relative length L/D_1 and dimensionless flowing area

$$\bar{F}_x = \frac{D_2^2}{D_1^2} = f\left(\frac{x}{L}\right).$$

d) Annular diffusers with rectilinear generatrices are the necessary elements of the majority of exhaust pipes of gas-turbine installations and are the channels formed by the two coaxial conical surfaces. The meridian section of such a diffuser and its basic dimensions are given in Fig. 2-2a. It is not difficult to see that in this case the geometric parameters which determine the shape of the flowing part are

$$\bar{D}_2 = \frac{D_2}{D_1}; \bar{d}_2 = \frac{d_2}{D_1}; \alpha_1; \alpha_2; \frac{L}{D_1},$$

where d_2 and d_1 - the greatest and least diameters of the internal conical surface, and α_2 - angle at its vertex.

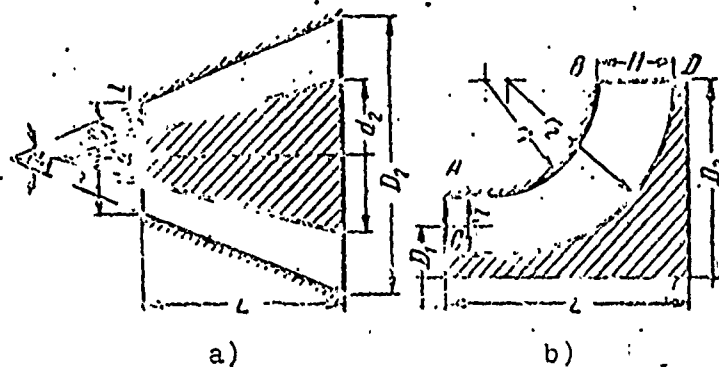


Fig. 2-2. Annular diffuser with rectilinear generatrices a) and a curvilinear annular diffuser b).

For the geometric similarity of two conical annular diffusers, it is necessary to provide the equality of any four of the five indicated values, since the fifth value is not independent.

e) Annular diffusers with curvilinear generatrices (axiradial diffusers), the flowing part and geometrical dimensions of which are given in Fig. 2-2b, are formed by two curvilinear coaxial surface rotations: AB and CD. The shape of the cross sections of these diffusers coincides with the shape of cross sections of flat curvilinear diffusers.

In the simplest case, when the generatrices AB and CD are outlined by radii r_1 and r_2 , and the dimensionless geometric parameters will be

$$n; \frac{r_2}{r_1}; \frac{L}{r_1}; \frac{D_2}{D_1}; \frac{l}{D_1}.$$

The first three parameters given here characterize the shape of the meridian section value D_2/D_1 determines the "radiality" of the diffuser, and $\theta = l/D_1$ characterizes the dimensions of ring at the inlet.

f) Vaned diffusers are the most widespread in centrifugal compressors and some types of axial turbines. As experiments showed [30], the use of vaned diffusers in turbines in a number of cases can give a substantial economic effect.

For the characteristic of vaned diffusers it is advantageous to use the following dimensionless values (Fig. 2-3): relative pitch t_1/b (t/b - for axial cascades) or t_2/b (where b - chord of the airfoil section) relative height l/b ; the expansion ratio of the diffuser as a whole $n = F_2/F_1$; fanning D/l or D_1/b and the angle of deflection of the flow in vane channels.

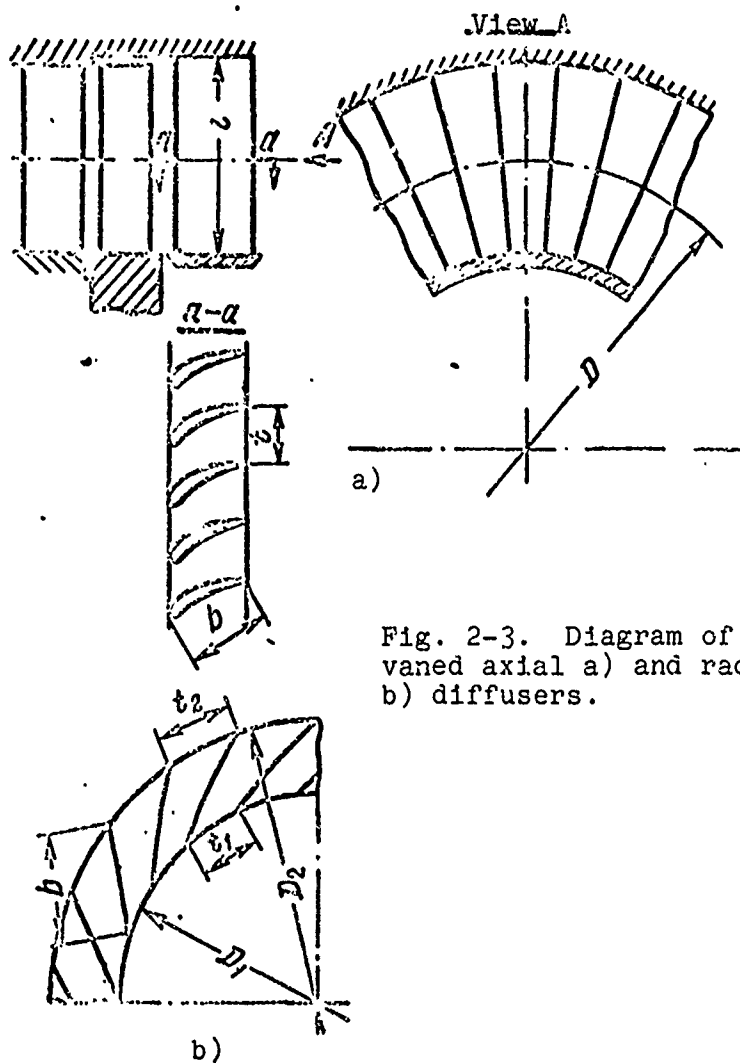


Fig. 2-3. Diagram of vaned axial a) and radial b) diffusers.

It is natural that for the similarity of vaned diffusers, besides the equality of the dimensionless geometric parameters, it is necessary to provide complete geometric similarity of the profiles which form the diffuser channel.

The types of diffusers examined here are the basic elements of the majority of exhaust pipes of turbomachines used for the removal of the working medium in the assigned direction with maximum use of the outlet speed. It is natural that both these requirements should be connected with the arrangement of the entire

The state of the flow after diffuser (point 2) is determined by pressure p_2 , by temperature t_2 and the kinetic energy equivalent to the difference in enthalpy $h_{B.C}$. The parameters of total stagnation p_{01} , t_{01} and p_{02} , t_{02} before the diffuser and after correspond to points O_1 and O_2 .

With isentropic stagnation of the flow, its final state for the assigned diffuser will be expressed by the point which corresponds to maximally possible pressure p_{2T} . However, the energy losses give rise to the fact that the process of stagnation occurs with an increase in entropy along a certain line 1-2, and the pressure in the outlet section p_2 proves to be lower than the pressure p_{2T} .

As a result the energy losses inside the diffuser can be estimated by value Δh , and entering here are both the frictional losses Δh_{TP} , and losses connected with the separation of flow from the walls, Δh_{OTP} (in the case of detached flow).

The coefficient of losses of energy can be obtained either as the ratio of Δh to the kinetic energy at inlet H_0 , or, as is done during cascade tests of turbomachines, as the ratio to the available energy h_0 . Thus, for an estimate of the energy losses, we will obtain two coefficients:

$$\zeta = \frac{\Delta h}{H_0}; \quad (2-1)$$

$$\sigma' = \frac{\Delta h}{h_0}. \quad (2-2)$$

However, these coefficients are insufficient for determining the state of flow at point 2, since in the diffuser element there occurs not only power losses but also the conversion of the kinetic energy of flow into potential energy. The degree of the perfection of this process can be estimated by the coefficient of the recovery of energy, which is the ratio of the increase in potential energy $h_{1.2}$ to kinetic energy at the inlet H_0 :

$$\xi = \frac{h_{1,2}}{H_0} \quad (2-3)$$

For an incompressible fluid the coefficient ξ is frequently called the coefficient of the recovery of pressure and is determined directly according to pressures p_1 , p_2 and p_{01} :

$$\xi = \frac{p_2 - p_1}{p_{01} - p_1}$$

The introduced characteristics are connected by the simple dependence:

$$\zeta = \zeta' (1 - \xi) \quad (2-4)$$

In other words, of the three introduced coefficients only two are independent. Let us use coefficients ζ and ξ as these independent values. Let us note that sometimes the coefficient of the losses in energy is called the resistance coefficient of the diffuser.

When the kinetic energy at the outlet from the diffuser is not used in subsequent elements of the apparatus, an important energy index is the total loss factor ζ_{Π} . To determine this value, let us turn again to Fig. 2-4b. Let us examine the initial (point O_1) and final (point 2) states of the gas.

It is evident that with respect to the outlet pressure p_2 the flow has available energy equivalent to a drop in h_0 , and all this energy is completely expended for the provision of the assigned flow through the diffuser in question with a definite velocity c_2 .

Let us express the value h_0 in portions of H_0 . As a result we will obtain the total loss factor:

$$\zeta_{\Pi} = \frac{h_2}{H_0} \quad (2-5)$$

From the physical point of view the indicated coefficient includes the coefficient of internal losses ζ and the coefficient of outlet losses $\zeta_{B.C}$, being their sum:

$$\zeta_{\Sigma} = \zeta + \zeta_{B.C}$$

Understanding as the coefficient $\zeta_{B.C}$ the ratio $h_{B.C}/H_0$, let us write the energy balance of the diffuser in the following form:

$$H_0 = h_{1,2} + h_{B.C} + \Delta h;$$

$$1 = \frac{h_{1,2}}{H_0} + \frac{h_{B.C}}{H_0} + \frac{\Delta h}{H_0} = \xi + \zeta_{B.C} + \zeta.$$

Hence it follows that for the characteristic of the state of flow in the outlet section of the diffuser, instead of values ζ and ξ , a combination of coefficients ζ and ζ_{Π} or ζ_{Π} and $\zeta_{B.C}$ can be used.

The introduced total loss factor, just as the coefficient of the recovery of energy ξ , quite fully characterizes the energy possibilities of the diffuser and recently increasingly more frequently is used both for calculations and for a comparison of the quality of various diffuser systems and branch connections of turbomachines. Furthermore, it is easy to show that with its help the relative pressure differential $\Delta p/p_{01}$ necessary for passage through the diffuser of an assigned flow is comparatively simply found.

Actually, the enthalpy drop h_0 is equivalent to the square of a certain arbitrary velocity c_0 . If at the outlet section of the diffuser the pressure of total stagnation in the center of the channel is equal to the pressure p_{01} , i.e., flow with a potential nucleus takes place, and velocity c_0 corresponds with the maximum outlet velocity $c_{2\text{макс}}$. Otherwise $c_0 > c_{2\text{макс}}$.

Pressures p_{01} and p_2 and velocity c_0 are connected by the relation

$$\frac{p_2}{p_{01}} = \left(1 - \frac{k-1}{k+1} \lambda_0^2\right)^{\frac{k}{k-1}},$$

where $\lambda_0 = c_0/a_*$ - the dimensionless velocity expressed in the portions of the critical speed a_* .

Hence

$$\frac{\Delta p}{p_{01}} = 1 - \left(1 - \frac{k-1}{k+1} \lambda_0^2\right)^{\frac{k}{k-1}} \approx \frac{k}{k+1} \lambda_0^2.$$

Since

$$\zeta_M = \frac{h_0}{H_0} = \frac{c_0^2}{c_1^2} = \frac{\lambda_0^2}{\lambda_1^2},$$

then

$$\lambda_0^2 = \zeta_M \lambda_1^2.$$

Consequently,

$$\frac{\Delta p}{p_{01}} = \frac{k}{k+1} \lambda_1^2 \zeta_M. \quad (2-7)$$

By using the continuity equation, from formula (2-7) it is possible to introduce the gas flow G . Then

$$\frac{\Delta p}{p_{01}} = \frac{k}{k+1} \zeta_M \frac{G^2}{\rho_1^2 F_1^2 a_0^2}. \quad (2-7a)$$

Here ρ_1 and F_1 - density and area in the narrow cross section of the diffuser.

Used frequently for the diffuser characteristic is its eff η_D , equal to the ratio of the actual increase in potential energy to the maximally possible with isentropic compression, i.e.,

$$\eta_D = \frac{h_{1,2}}{h_{1,2M}}$$

In turn $h_{1,2M} = h_{1,2} + \Delta h$.

Having divided the numerator and denominator of the expression in question by H_0 , we obtain the connection of the eff of the diffuser with the coefficients introduced earlier:

$$\eta_{\mu} = \frac{\xi}{\xi + \zeta} = \frac{\xi}{1 - \zeta_{B.O.}} = \frac{1 - \zeta_n}{1 - \zeta_{B.O.}} \quad (2-8)$$

For the incompressible fluid, the eff of the diffuser is determined by pressures p_1 , p_2 and p_{2T} :

$$\eta_{\mu} = \frac{p_2 - p_1}{p_{2T} - p_1} \quad (2-8a)$$



If during the calculation of the losses we do not consider flow velocity component, then the coefficient of losses with the outlet velocity will be uniquely determined by the expansion ratio of the diffuser n and will be equal to [54]:

$$\zeta_{B.O.} = \left(\frac{\rho_1}{\rho_2} \right)^2 \frac{1}{n^2} \quad (2-9)$$

where ρ_1/ρ_2 is the ratio of average densities in the inlet and outlet cross sections of the diffuser.

Then when $\rho = \text{const}$ the connection between η_{μ} and ζ_n is established by the following relation:

$$\eta_{\mu} = (1 - \zeta_n) \frac{n^2}{n^2 - 1} \quad (2-10)$$

From the other utilized coefficients, let us distinguish the loss factor of total pressure σ_0 and the coefficient of the pressure increase (compression) σ .

The first value is the ratio of the mean pressure of total stagnation after the diffuser p_{02} to the pressure of total stagnation before it p_{01} , and the second gives the ratio of static pressures p_2 and p_1 , i.e.,

$$\sigma_0 = \frac{p_{02}}{p_{01}}; \quad \sigma = \frac{p_2}{p_1}$$

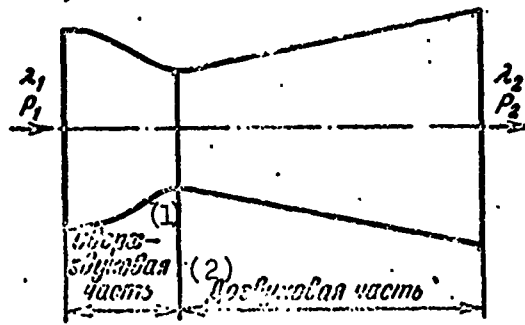
Having expressed these values in terms of the dimensionless velocity at the inlet λ_1 and coefficients ζ and ζ_{Π} , we obtain:

$$\sigma_0 = \frac{p_1}{p_{01}} \cdot \frac{p_{02}}{p_1} = \left[\frac{1 - \frac{k-1}{k+1} \lambda_1^2}{1 - \frac{k-1}{k+1} \lambda_1^2 (1 - \zeta)} \right]^{\frac{k}{k-1}}; \quad (2-11)$$

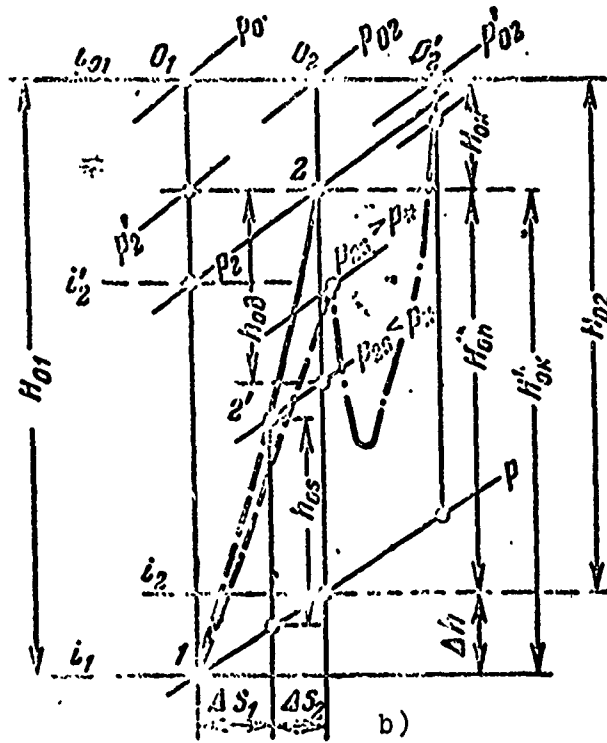
$$\sigma = \frac{p_2}{p_{01}} \cdot \frac{p_{01}}{p_1} = \left[\frac{1 - \frac{k-1}{k+1} \lambda_1^2 \zeta_{\Pi}}{1 - \frac{k-1}{k+1} \lambda_1^2} \right]^{\frac{k}{k-1}}. \quad (2-12)$$

With the transition to supersonic diffusers, the process of the flow is substantially complicated, and here some additional characteristics are introduced. For the development of their physical sense, let us again turn to the thermal diagram (Fig. 2-5).

Point 1 corresponds to the state of flow at the inlet into the diffuser. Line 1-2 conditionally depicts the process of compression of the gas in the system of discontinuities in the supersonic part of the diffuser. The appropriate increase in entropy Δs_1 characterizes wave losses and losses of friction at the inlet part. Behind the discontinuities pressure p_{2s} is established. If $p_{2s}/p_{02} < \epsilon_*$, then after the discontinuities the flow is still supersonic and in the narrowing part of the diffuser the gas compression is continued. At $p_{2s}/p_{02} > \epsilon_*$ the flow behind the discontinuities is subsonic. This means that in the narrowing part up to the minimum cross section the flow will be accelerated, and its pressure will drop. If in the minimum cross section the rate of flow reaches the critical value, then in the expanded part $\lambda > 1$. In this case the stagnation of flow will occur in the system of discontinuities after the narrow cross section. The increase in entropy Δs_2 is conditioned by losses in the subsonic part of the diffuser.



a)



b)

Fig. 2-5. The process of compression in a supersonic diffuser. a) diagram; b) process in an is-diagram.
KEY: (1) Supersonic section; (2) Subsonic section.

Let us note that the total change in potential energy in the supersonic diffuser H_{0n} can be considered as the sum of changes in potential energy in the system of discontinuities h_{0s} and subsonic part h_{0D} .

For an estimate of energy losses in the supersonic diffuser, let us introduce the energy eff into the examination. This value is defined as the ratio of available energy behind the diffuser to the kinetic energy at the inlet (Fig. 2-5b).

$$\eta_{д.э} = \frac{H_{02}}{H_{01}} = \left[1 - \left(\frac{k+1}{k-1} \cdot \frac{1}{\lambda^2} - 1 \right) \frac{1}{\sigma_0} \right]^{\frac{k-1}{k}} - 1. \quad (2-13)$$

The magnitude H_{02} is the sum of the kinetic energy of flow behind the diffuser $H_{0н}$ and changes in potential energy $H_{0п}$. The energy eff $\eta_{д.э}$ can be expressed also in terms of losses in kinetic energy Δh :

$$\eta_{д.э} = \frac{H_{01} - \Delta h}{H_{01}} = 1 - \zeta, \quad (2-14)$$

where, as before, ζ - the coefficient of losses of energy in the diffuser.

Let us note that $\eta_{д.э}$ can be presented in the following form:

$$\eta_{д.э} = \frac{\frac{(p_1/p_{02})^{\frac{k-1}{k}} - 1}{(p_1/p_{01})^{\frac{k-1}{k}} - 1}}$$

The eff of diffuser introduced above $\eta_{д}$, after elementary conversions, can be expressed in terms of dimensionless mean flow velocities λ_1 and λ_2 and the pressure ratio p_1/p_2 in the following manner:

$$\eta_{д} = \frac{1}{2} \cdot \frac{k+1}{k-1} \cdot \frac{1 - \frac{k-1}{k+1} \lambda_2^2}{\lambda_1^2 - \lambda_2^2} \left[1 - \left(\frac{p_1}{p_2} \right)^{\frac{k-1}{k}} \right]. \quad (2-15)$$

If the velocity after the diffuser is low ($\lambda_2 \approx 0$), then the formula (2-15) is simplified:

$$\eta_{\lambda} = \frac{1}{2} \cdot \frac{k+1}{k-1} \cdot \frac{1}{\lambda_1^2} \left[1 - \left(\frac{p_1}{p_2} \right)^{\frac{k-1}{k}} \right] =$$

$$= \left(\frac{1}{2} \cdot \frac{k+1}{k-1} \cdot \frac{1}{M_1^2} \right) \left[1 - \left(\frac{1}{\sigma} \right)^{\frac{k-1}{k}} \right].$$

One should emphasize the distinction in concepts $\eta_{\lambda, \text{э}}$ and η_{λ} . The energy eff depends only upon power losses in the diffuser and does not depend upon the compression ratio σ . Magnitude η_{λ} depends upon the diffuser losses and upon compression ratio. It is easy to see that $\eta_{\lambda, \text{э}} > \eta_{\lambda}$. The connection between these characteristics is illustrated by the formula

$$\eta_{\lambda, \text{э}} = 1 - (1 - \eta_{\lambda}) \frac{H'_{0\lambda}}{i_{01}} = 1 - \xi \left(\frac{1}{\eta_{\lambda}} - 1 \right). \quad (2-16)$$

For the computation of the increase in entropy Δs , let us use the following expression:

$$\frac{\Delta s}{C_p} = \ln \frac{T_0}{T_1} - \frac{k-1}{k} \ln \frac{p_{02}}{p_1} = (1 - \eta'_{\lambda}) \ln \frac{T_0}{T_1},$$

where Δs - the increase in entropy in the diffuser; C_p - the heat capacity of the gas at constant pressure; η'_{λ} - the arbitrary eff of the diffuser:

$$\eta'_{\lambda} = \frac{k-1}{k} \cdot \frac{\ln p_{02}/p_1}{\ln T_0/T_1} = \frac{k-1}{k} \cdot \frac{\ln p_{02}/p_1}{\ln \left(1 + \frac{k-1}{2} M_1^2 \right)} =$$

$$= 1 + \frac{k-1}{k} \cdot \frac{\ln p_{01}/p_{02}}{\ln \left(1 + \frac{k-1}{2} M_1^2 \right)}.$$

The dependence between $\eta_{\lambda, \text{э}}$ and η'_{λ} is defined by the relation

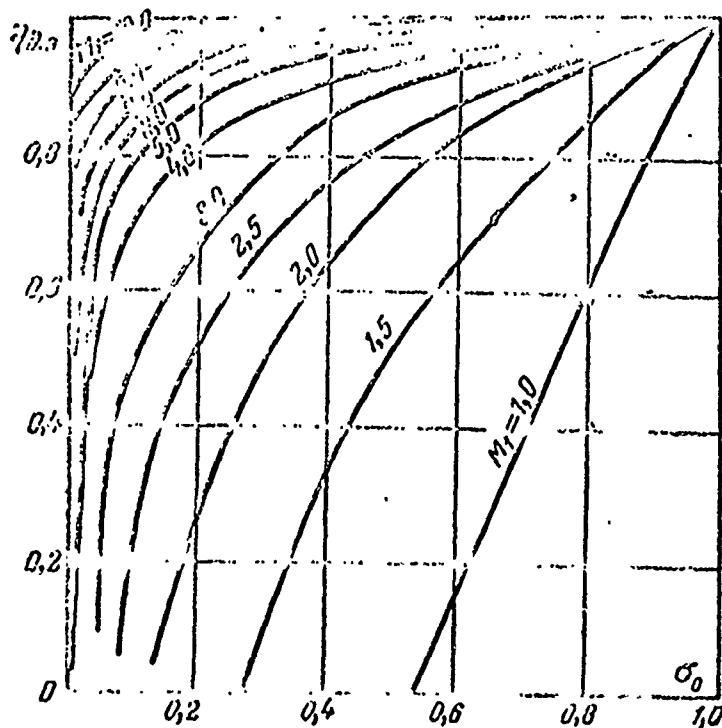
$$\eta_{\lambda, \text{э}} = \frac{1 - (p_1/p_{02})^{\frac{k-1}{k}}}{1 - (p_1/p_{02})^{\frac{k-1}{k\eta'_{\lambda}}} - 1}.$$

The connection between η_D and η'_D is expressed by the formula

$$\eta'_D = \frac{(p_{02}/p_1)^{\frac{k-1}{k}} - 1}{(p_{02}/p_1)^{\frac{k-1}{k\eta'_D}} - 1}$$

Reproduced from
best available copy.

At the fixed values M_1 number at the inlet into the diffuser, the eff $\eta_{D,\text{э}}$, η_D and η'_D are changed in one direction. Therefore, the comparison of various diffusers with an identical velocity at the inlet can be conducted by any eff. However, the substantiated comparison of the diffusers operating at various M_1 numbers can be accomplished only with the correct determination of eff. In this connection let us note that the coefficient of losses of stagnation pressure σ_0 is not the single-valued characteristic of the effectiveness of diffusers. In the comparison of diffusers, this magnitude should be augmented by the compression ratio σ and M_1 number. Only at equal M_1 and p_2/p_1 does the coefficient σ_0 appear as the single-valued diffuser characteristic. The dependence



pressure is shown in Fig. 2-6.

Fig. 2-6. Dependence of the energy eff upon the Mach number and ratio of stagnation pressures σ_0 .

Thus, from an examination of the various coefficients their close interconnections follows. For clarity this connection is given in Table 2-1, where all the coefficients are expressed in terms of the coefficient of losses and the coefficient of pressure recovery.

Table 2-1.

Символы (1)	Формулы связи (2)
ζ	-----
ξ	-----
ζ'	$\zeta' = \zeta(1 - \xi) - 1$
ζ_n	$\zeta_n = 1 - \xi$
η_n	$\eta_n = \frac{\xi}{\xi + \zeta}$
$\eta_{n,0}$	$\eta_{n,0} = 1 - \zeta = 1 - \xi \left(\frac{1}{\eta_n} - 1 \right)$
σ_1	$\sigma_1 = \frac{k-1}{k+1} \lambda_1^2$
σ_0	$\sigma_0 = \left[\frac{1 - \sigma_1}{1 - \sigma_1(1 - \xi)} \right]^{\frac{k}{k-1}}$
σ	$\sigma = \left[\frac{1 - \sigma_1 \zeta_n}{1 - \sigma_1} \right]^{\frac{k}{k-1}}$

KEY: (1) Symbol; (2) Connecting formula.

§ 2-3. Procedure of the Experimental Determination of Aerodynamic Characteristics of Diffusers

The experimental investigation of diffusers is connected with the great expenditure of time, since the nature of the flow in them is determined by the significant number of geometric and mode

parameters. Because of this, those coefficients which can be obtained with minimum difficulties are determined by experimental means. The indicated condition, to the greatest degree, is satisfied by the eff of the diffuser η_D and, the total loss factor ζ_H connected with it by relation (2-8). For their experimental determination, it is necessary to know the pressure p_{01} and temperature T_{01} of total stagnation before the diffuser, static pressures at the inlet into the diffuser p_1 and at the outlet section p_2 . Then we will obtain:

$$\zeta_H = \frac{\lambda_0^2}{\lambda_1^2} \frac{1 - \left(\frac{p_2}{p_{01}}\right)^{\frac{k-1}{k}}}{1 - \left(\frac{p_1}{p_{01}}\right)^{\frac{k-1}{k}}} \quad (2-17)$$

Static pressure in the outlet section of the diffuser p_2 is determined by the environment. At the outlet into the atmosphere $p_2 = B$, where B - barometric pressure.

The pressure p_{01} is found so simply and with high accuracy. The estimate of the mean static pressure p_1 in the inlet section of the diffuser proves to be more complex. Its direct measurement with the help of drainage selections is applicable only for flat and axisymmetric diffusers. When symmetry does not exist, it is necessary to conduct the traverse of the entire inlet velocity field, which is connected with great experimental difficulties, or determine the mean value p_1 on the basis of indirect measurements. The latter way is used most frequently and consists in the fact that, besides pressure p_{01} and temperature T_{01} , the mass flow weight rate G of the working medium through the diffuser is measured, and for the assigned initial parameters the critical flow through the diffuser in question G_{kp} is calculated.

As a result it is possible to find easily the given flow q_1 . Since $G_{kp} = Ap_{01}F_1/\sqrt{T_{01}}$, the formula for the estimate of q_1 assumes the form:

$$q_1 = \frac{G}{G_{\text{кр}}} \cdot \frac{1}{A} \cdot \frac{G \sqrt{T_{01}}}{F_1 p_{01}} \quad (2-18)$$

Here A is the constant dependent on the properties of the working medium, and F_1 is the intake area of the diffuser. For air the coefficient $A = 0.396$, if the flow rate is measured in kg/s, the area - in m^2 , and pressure - in kg/m^2 .

Further, by using the single-valued connection between the pressure p_1 and the given flow q_1 , with the help of tables of gas-dynamic functions all parameters and velocity λ_1 in the inlet section of the diffuser are found.

In certain cases, when the power of the feed source allows achieving the critical flow through the diffuser, the magnitude of the given expenditure q_1 is determined on the basis of direct measurements, since now

$$G_{\text{кр}} = \frac{p_{01}}{p_{01 \text{ макс}}} G_{\text{макс}}$$

$$q_1 = \frac{p_{01 \text{ макс}}}{p_{01}} \cdot \frac{G}{G_{\text{макс}}}$$

Here $G_{\text{макс}}$ - maximum critical flow through the diffuser obtained at the initial pressure $p_{01 \text{ макс}}$.

The given method of the integral estimate of the total loss factor and eff of the diffuser require the minimum expenditure of experimental time, and its accuracy is determined actually by the accuracy of the determination of the flow. If the magnitude of critical flow can be successfully determined directly from the experiment, then the accuracy of the estimate q_1 proves to be even higher. The comparison of coefficients ζ_{Π} and $\eta_{\text{д}}$, obtained on the basis of direct pressure measurements p_1 and calculated by the integral method, shows almost complete convergence of results [44].

Thus, it can be considered that the experimental estimate of the total loss factor is quite reliable. In this connection it is expedient to conduct a comparison of experimental data with data obtained by theoretical methods of the calculation of the diffusers directly according to the total loss factor ζ_{Π} or according to the eff of the diffuser η_{Π} . If a comparison is conducted according to the magnitude of internal losses ζ , then it is necessary to indicate clearly by what manner these losses are obtained.

Most simply the coefficient of internal losses can be found from relation

$$\zeta = \zeta_{\Pi} - \zeta_{\text{B.C.}}, \quad (2-19)$$

where

$$\zeta_{\text{B.C.}} = \frac{c_{2cp}^2}{c_1^2} = \left(\frac{\rho_1}{\rho_2} \right)^2 \frac{1}{n^2}. \quad (2-20)$$

The estimate of the outlet losses of the kinetic energy from relation (2-20) is valid only at a uniform velocity profile in the exit section of the diffuser.

In general for the computation of coefficient $\zeta_{\text{B.C.}}$, it is necessary to use a more complex expression obtained as a result of the averaging of local losses in flow [54].

$$\zeta_{\text{B.C.}}^r = \left(\frac{\rho_1}{\rho_2} \right)^2 \frac{1}{n^2} \int_0^1 \left(\frac{c_2}{c_{2cp}} \right)^3 d \left(\frac{F}{F_2} \right).$$

Having designated by N_2 the magnitude of the integral, we obtain:

$$\zeta_{\text{B.C.}} = \left(\frac{\rho_1}{\rho_2} \right)^2 \frac{N_2}{n^2}. \quad (2-21)$$

Coefficient N_2 depends upon the velocity profile in the outlet section of the diffuser and always, besides a uniform profile, exceeds one.

Consequently, the internal losses calculated on the basis of formulas (2-19) and (2-20) include any (sometimes significant) portion of the outlet losses, and these formulas cannot be used for a comparison with the theoretical methods of calculation which consider the flow velocity component.

At the same time it is necessary to note that the most widespread today semiempirical and purely empirical methods of the calculation of diffusers [34, 39] are based basically on relation (2-19). If for the calculation of total losses such a conditional estimate of internal losses is entirely permissible, then in the determination of the state of flow in the outlet section the accepted conditionality can lead to an appreciable error.

From the aforesaid it follows that the magnitude of total losses and eff of the diffusers do not make it possible to obtain the actual value of the internal losses, for the determination of which a detailed investigation on the outlet velocity field is necessary with the measurement of losses at each point. In this case usually the local coefficient of losses ζ'_1 is determined with respect not to kinetic energy H_0 at the inlet cross section but to the available enthalpy drop h_0 .

For the transition from coefficient ζ' to the coefficient ζ , calculated with respect to H_0 , it is sufficient to make use the relation (2-4), since

$$\zeta = \frac{\Delta h}{h_0} \cdot \frac{h_0}{H_0} = \zeta' \zeta_{H_0}$$

The determination of local values of the coefficient of losses, taking into account mass flow, gives:

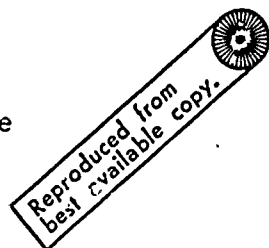
$$\begin{aligned} \zeta &= \frac{\zeta_{H_0}}{m} \int_{F_1} \zeta'_1 dm = \frac{\zeta_{H_0}}{\beta_{2cp} c_{2cp} F_2} \int_{F_1} \zeta'_1 \rho_2 c_{21} dF = \\ &= \zeta_{H_0} \int_0^1 \zeta'_1 \left(\frac{\rho_2}{\beta_{2cp}} \cdot \frac{c_{21}}{c_{2cp}} \right) d \left(\frac{F}{F_2} \right). \end{aligned} \quad (2-22)$$

The connection between the coefficient of local losses ζ'_1 and the velocity in the exit section c_{21} results from the determination of value ζ'_1 . Actually,

$$\begin{aligned} \zeta'_1 &= \frac{h_{21}}{h_0} = \frac{h_{21}}{h_0} = 1 - \frac{c_{21}^2}{c_0^2} \\ &= 1 - \frac{c_{21}^2}{c_{2cp}^2} \cdot \frac{c_{2cp}^2}{c_0^2}. \end{aligned}$$

Hence

$$\frac{c_{21}}{c_{2cp}} = \frac{c_0}{c_{2cp}} \sqrt{1 - \zeta'_1}. \quad (2-23)$$



Here c_0 - the conditional velocity equivalent to the available enthalpy drop h_0 .

Having substituted the obtained relation into formula (2-22), and disregarding the density change in the outlet section, we obtain

$$\zeta = \frac{c_0}{c_{2cp}} \zeta_{11} \int_0^1 \zeta'_1 \sqrt{1 - \zeta'_1} d\left(\frac{F}{F_2}\right).$$

The ratio of velocities c_0/c_{2cp} is easily connected to the total loss factor and the expansion ratio of the diffuser, since

$$\frac{c_0}{c_{2cp}} = \frac{c_0}{c_1} \cdot \frac{c_1}{c_{2cp}} = \sqrt{\zeta_{11}} \frac{\rho_{2cp} F_2}{\rho_1 F_1} = n \sqrt{\zeta_{11}} \frac{\rho_{2cp}}{\rho_1}.$$

As a result the relation for determining internal losses, according to data of probe tests, takes the following form:

$$\zeta = \frac{\rho_{2cp}}{\rho_1} n \sqrt{\zeta_{11}^3} \int_0^1 \zeta'_1 \sqrt{1 - \zeta'_1} d\left(\frac{F}{F_2}\right).$$

It will be possible to present the derived formula of averaging in a somewhat different form, if in correlation (2-22)

we replace the local coefficient of losses ζ' by the ratio of the squares of the appropriate velocities from expression (2-23).

Then

$$\zeta = \zeta_{\text{н}} \frac{c_0}{c_{\text{нр}}} \int_0^1 \frac{c_{2t}}{c_0} \left[1 - \frac{c_{2t}^2}{c_0^2} \right] d \left(\frac{F}{F_2} \right).$$

The obtained integral determines the well-known relative area of the power losses, if velocity c_0 is equal to the maximum speed at the outlet section.

The indicated condition is fulfilled automatically with the equality of the pressure of full stagnation in nucleus $p_{02 \text{ макс}}$ to the initial pressure p_{01} . Otherwise the energy loss thickness, calculated with respect to the maximum speed $c_{2 \text{ макс}}$, in exit section will be less than the examined integral.

Let us introduce the following designations:

$$\bar{\Delta}^{***}_2 = \frac{\Delta^{***}_2 \Pi_2}{F_2} = \int_0^1 \frac{c_{2t}}{c_0} \left(1 - \frac{c_{2t}^2}{c_0^2} \right) d \left(\frac{F}{F_2} \right);$$

$$\bar{\delta}^{***}_2 = \frac{\delta^{***}_2 \Pi_2}{F_2} = \int_0^1 \frac{c_{2t}}{c_{2 \text{ макс}}} \left(1 - \frac{c_{2t}^2}{c_{2 \text{ макс}}^2} \right) d \left(\frac{F}{F_2} \right),$$

$$\bar{\Delta}^{***}_2 = \psi \bar{\delta}^{***}_2;$$

Π_2 - the perimeter of the channel in the outlet section; ψ - the coefficient of the conformity between the introduced values; with $p_{01} = p_{02 \text{ макс}}$ $\psi = 1$; if $p_{01} > p_{02 \text{ макс}}$, then $\psi > 1$; for instance, for the turbulent velocity profile and $p_{02 \text{ макс}}/p_{01} = 0.95$ $\psi = 1.2$; for $p_{02 \text{ макс}}/p_{01} = 0.9$ $\psi = 1.57$.

Thus, to estimate the internal diffuser losses according to the known velocity profile in the outlet section, we will obtain the following relation:

$$\zeta = \zeta_{in} \frac{c_0}{c_1} \cdot \frac{c_1}{c_{2cp}} \frac{\bar{\Delta}^{0.5}}{\Delta^{0.5}} = \zeta_{in}^{3/2} \frac{1}{n \bar{\Delta}^{0.5}} \frac{\rho_{2cp}}{\rho_1}$$

Having replaced here $\bar{\Delta}^{0.5}$ by the common thickness of the energy loss, we obtain:

$$\zeta = \zeta_{in}^{3/2} \frac{1}{n \psi \delta^{0.5}} \frac{\rho_{2cp}}{\rho_1} \quad (2-24)$$

Formula (2-24) allows, on the basis of experimental data, dividing the total losses in diffusers into internal losses and losses with an outlet velocity, since it uniquely connects the outlet normal velocity distribution with coefficients ζ_{in} and ζ . Moreover, this formula solves the problem about the theoretical calculation of total losses in diffusers.

From (2-24) it follows that

$$\zeta_{in} = \left(\frac{\rho_1}{\rho_2} \cdot \frac{\zeta}{n \psi \delta^{0.5}} \right)^{2/3} \quad (2-24a)$$

In such a recording formulas (2-24) and (2-24a) are valid without any restrictions imposed on the flow pattern in the diffuser.

From the given analysis it is clear that the experimental estimate of the internal losses, taking into account the velocity flow component, is a sufficiently prolonged and complex operation. Because of this, in experimental practice estimates from mean flow velocities are more widespread with an arbitrary determination of the coefficient of internal losses ζ according to relation

$$\zeta = \zeta_{in} - \left(\frac{\rho_1}{\rho_2} \right)^2 \frac{1}{n^2} \quad (2-25)$$

It is natural that the results of the calculation according to formula (2-25) cannot be compared with results of the calculation obtained by theoretical methods, which consider the form of

the normal velocity distribution in the outlet section. Because of the aforesaid, more convenient for such comparisons is the total loss factor ζ_{Π} , which we will subsequently use. Furthermore, from the experimental values of magnitude ζ_{Π} it is possible to find the relative arbitrary areas of the boundary layer displacement $\bar{\Delta}^*_2$ in the outlet section of the diffuser, since between ζ_{Π} and $\bar{\Delta}^*_2$ there exists a unique dependence which results from formula (2-17).

Actually,

$$\zeta_{\Pi} = \frac{\lambda_0^2}{\lambda_1^2} = \frac{c_0^2}{c_1^2}.$$

Let us find the ratio of velocities c_0/c_1 from the equation of continuity written for the minimum and outlet sections of the diffuser.

With a uniform velocity field in the inlet section, we will obtain:

$$\rho_1 c_1 F_1 = \rho_2 c_{2cp} F_2.$$

Further from the average speed in the outlet section c_{2cp} let us turn to the arbitrary velocity c_0 and arbitrary effective output area $F_{2\phi}$, considering the velocity distribution c_0 over this entire area uniform. Then

$$\rho_1 c_1 F_1 = \rho_2 c_0 F_{2\phi}. \quad (2-26)$$

If we introduce into examination the arbitrary area of displacement, equal to

$$\bar{\Delta}^*_2 = \int_0^1 \left(1 - \frac{c_{2t}}{c_0}\right) \frac{dF}{F_2}, \quad (2-27)$$

then

$$F_{2\phi} = F_2 - \bar{\Delta}^*_2. \quad (2-28)$$

In the case when in the exit section of the diffuser there is at least one point where the pressure of full stagnation $p_{02 \text{ макс}} = p_{01}$, $c_0 = c_{2 \text{ макс}}$, formula (2-27) determines the common area of displacement δ^*_2 (if the density ratio is considered to be equal to unity).

From expressions (2-28) and (2-26) we will obtain the following relation, which connects coefficient ζ_{Π} with the area of displacement $\bar{\Delta}^*_2$:

$$\zeta_{\Pi} = \frac{c_0^2}{c_1^2} = \left(\frac{\rho_1}{\rho_2} \right)^2 \frac{1}{n^2 (1 - \bar{\Delta}^*_2)^2}. \quad (2.29)$$

Formula (2-29) is valid for any diffuser channel and reduces the calculation of the total loss factor to the problem of the determination of the arbitrary relative area of displacement $\bar{\Delta}^*$. When $p_{02 \text{ макс}} = p_{01}$, $\bar{\Delta}^*_2 = \bar{\delta}^*_2$ and the problem is reduced to the calculation of the integral area of displacement in the outlet section $\bar{\delta}^*_2$ on the basis of the common relations of the boundary layer, and equation (2-29) assumes the form:

$$\zeta_{\Pi} = \left(\frac{\rho_1}{\rho_2} \right)^2 \frac{1}{n^2 (1 - \bar{\delta}^*_2)^2}. \quad (2-29a)$$

Expression (2-29a), obtained by A. S. Ginevskiy [18, 95], is valid for nonseparable flow with the existence of the potential nucleus in the outlet section of the channel. If such a nucleus is absent, then

$$\zeta_{\Pi} = \left(\frac{\rho_1}{\rho_2} \right)^2 \frac{\psi_1}{n^2 (1 - \bar{\delta}^*_2)^2}, \quad (2-29b)$$

where $\psi_1 \geq 1$ - the coefficient of correction dependent on the degree of the loss of pressure of full stagnation in the range of maximum delivery speed.

The given formulas (2-29) and (2-29a) make it possible, on the basis of simple tests, to obtain vast test data on integral thicknesses of the boundary layer and explain the possibility

of the use of a theory for the boundary layer calculation in diffuser channels at various positive pressure gradients.

Let us show further that the use of the integral method does not only make it possible to obtain coefficients ζ_{Π} and η_{Π} , but it also allows finding the loss of pressure of full stagnation σ_0 . For this purpose, by using relation (2-18) and keeping in mind that along the diffuser the mass flow does not change, let us record the equality

$$G = AF_1 \frac{p_{01} q_1}{\sqrt{T_{01}}} = AF_2 \frac{p_{02} q_2}{\sqrt{T_{02}}},$$

where p_{02} and q_2 - values averaged over the flow, and A - the coefficient dependent on properties of the working medium.

Hence, since for the insulated system $T_{01} = T_{02}$,

$$p_{01} q_1 = \frac{p_{02} q_2 F_2}{F_1}.$$

Let us introduce the average static pressures p_1 and p_2 into the last equality in the following manner:

$$\frac{p_{01} q_1}{p_1} = \frac{p_2}{p_1} \cdot \frac{F_2}{F_1} \cdot \frac{p_{02} q_2}{p_2}. \quad (2-30)$$

Magnitude p_0/p is uniquely determined by the dimensionless velocity λ [25]:

$$\frac{p_0}{p} = \left(\frac{k+1}{2} \right)^{\frac{1}{k-1}} \lambda \left(1 - \frac{k-1}{k+1} \lambda^2 \right)^{-1}. \quad (2-31)$$

Then from formula (2-30) we will obtain the equation for determining the average flow velocity at the known values of pressures p_1 and p_2 :

$$\lambda_1 \left[1 - \frac{k-1}{k+1} \lambda_1^2 \right]^{-1} = \frac{p_2}{p_1} \lambda_2 \left[1 - \frac{k-1}{k+1} \lambda_2^2 \right]^{-1}. \quad (2-32)$$

For the facilitation of the calculations, Fig. 2-7 gives the dependence of the complex $\lambda \left[1 - \frac{k-1}{k+1} \lambda^2 \right]^{-1}$ on velocity λ .

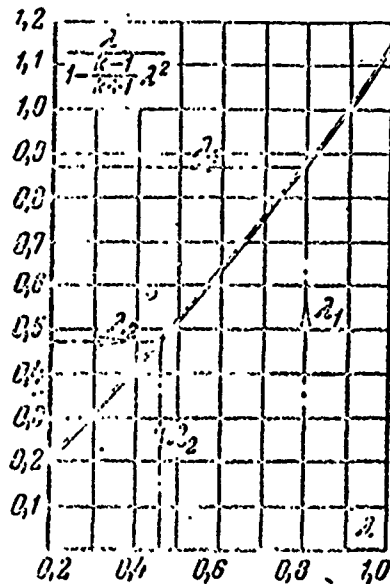


Fig. 2-7. Determination of the mean flow rate in the outlet section of the diffuser.

As a result, having calculated from equation (2-32) the velocity λ_2 , according to tables of gas-dynamic functions it is easy to find the pressure ratio p_2/p_{02} and, consequently, coefficient σ_0 :

$$\sigma_0 = \frac{p_{02}}{p_{01}} = \frac{p_2}{p_{01}} \left(1 - \frac{k-1}{k+1} \lambda_2^2 \right)^{-\frac{k}{k+1}}. \quad (2-33)$$

The examined methods of determining the basic coefficients which characterize the operation of diffusers and the systematic considerations must be considered with the setting of the experiment. Specifically, the system of measurements should provide a reliable determination of the flow of the working medium, initial parameters and pressure in the outlet section of the investigated diffusers.

Besides the indicated basic values, it is extremely advisable to provide the possibility of direct measurements of static

pressure in the inlet section of the diffuser and provide the traverse of the outlet velocity field.

The diagram of the steam experimental circuit of Moscow Power Engineering Institute [MEI] (МЭИ) given in Fig. 2-8 satisfies all the requirements indicated above most fully. Steam to the installation will be fed through the valve [PZ] (ПЗ) with by-pass valve [PB] (ПБ) and small tank 1. Receiver 2 and straight section 3 serve for the damping of the flow. For the purpose of measuring the pressure and temperature along the damping section, measuring ports are provided. The diffusers to be investigated are fastened to flange 4 between the damping section 3 and operating section 5. In the outlet section of the diffuser there is a measuring adapter connected with a traversing probe 7.

After the operating section the steam enters into the exhaust section, where there is the throttle valve 6, with the help of which it is possible over a wide range to change the counter-pressure p_2 .

The exhaust steam enters into the condenser whence the condensate being formed is evacuated by the pump [EKN] (ЭКН) into the measuring tank. The small area of cross section of the measuring tank allows with high accuracy the measuring of not only large but also low flow rates of the steam. From the measuring tank the condensate is dumped into drain tank. The draining of the damping and operating sections is accomplished periodically, and drainage is dumped into a small calibration tank 8 and further into the condenser. The small tank has both vacuum and atmospheric drains. To control the drain there are valves 9 and 10, and a checking of the level is accomplished with the help of gauge glass 11.

The examined diagram allows conducting an independent change in the λ_1 and Re_1 numbers in the following ranges: $\lambda_1 = 0.1-1$; $Re = 3 \cdot 10^4 - 5 \cdot 10^5$.

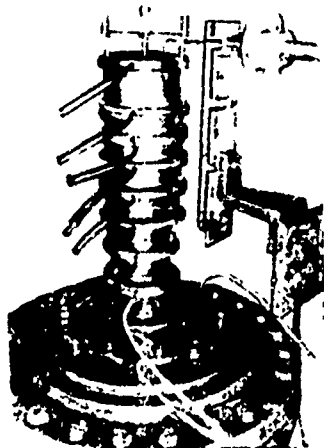


Fig. 2-9. Experimental installation for investigating conical diffusers.

possible changes in regime parameters proves to be considerably narrower than that during steam tests.

§ 2-4. Diffuser Losses and Their Calculation

The flow pattern in diffuser elements is quite complex, which substantially impedes their analytical calculation. As a result until now the most reliable proves to be not the calculated but experimental means of the determining the losses.

However, for an analysis of experimental data and the construction of approximation calculated circuits, it is advantageous to discuss in more detail the mechanism of the formation of diffuser losses. By examining the latter as devices for the effective conversion of the kinetic energy of flow into potential energy, it should be noted that the perfection of this conversion depends both upon the internal losses directly on the diffuser element and on the magnitude of the kinetic energy of flow leaving this element. In general the internal losses in any channel are determined by frictional losses and losses connected with the formation of separation zones. With nonseparable flow a unique source of the losses is internal friction. For flow with the potential nucleus these losses are usually determined according to the integral boundary layer characteristics in the

final cross sections. Using this method, it is possible to obtain comparatively simple calculation formulas for diffusers. Before turning directly to the derivation of such formulas, let us explain the probability of nonseparable flow in diffusers.

Theoretical investigations in the indicated direction, generally speaking, are inconsistent. Thus, according to calculations of N. A. Slezkin [93], S. M. Tarǵ [99] and O. N. Obchinnikov [82] even with laminar flow conditions in the boundary layer the existence of nonseparable flow with expansion ratios $n < 2$ is possible. At the same time an analysis conducted by G. M. Bam-Zelikovich [4] for the turbulent layer showed that at a small intake section before the diffuser separation should occur directly in the throat, if the angle of opening $\alpha > 6^\circ$. Certain clarity into this question has been introduced by the work of Kline [142, 143] who generalized a number of test data and showed on this basis that the range of the limiting geometric parameters, which separate the nonseparable flow from the separable, in flat and conical diffusers is quite significant and actually encompasses the basic group of diffusers used in technology.

For confirmation of the aforesaid, plotted in Fig. 2-10 is the limiting curve 1 with the utilization of data [142, 143], which divides the whole range $\alpha(n)$ into two parts: nonseparable diffusers (range I) and separable (range II); numerals at the experimental points correspond to values of the coefficient of the recovery of energy. Here data obtained at MEI are plotted.

The given experimental results establish a close connection between the expansion ratio n and the maximum angle of opening of the diffuser α . With an increase in the expansion ratio for obtaining nonseparable flow it is necessary to substantially decrease the angle, and with an increase from $n = 2$ to $n \approx 4-5$ $\alpha_{\text{г.акс}}$ drops from 24° to 9° . Such a connection between the limiting parameters is conditioned by the opposite effect of the boundary layer on the flow in the potential nucleus of the flow.

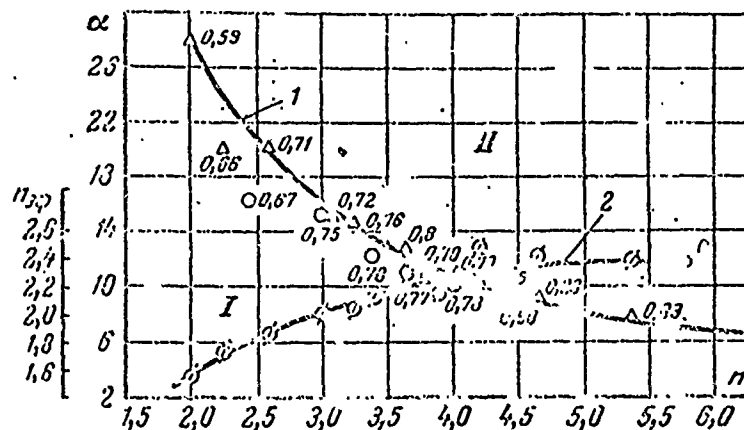


Fig. 2.10. Line of limiting parameters of nonseparable flat and conical diffusers. 1 - dependence $\alpha = f(n)$; O - MEI experiments; Δ - data of Kline; 2 - dependence $n_{\phi} = f(n)$.

This effect can be taken into account if we introduce into the examination not the geometric but the effective expansion ratio of the diffuser determined by relation

$$n_{\phi} = n \left(1 - \frac{\Delta_2^*}{F_2} \right), \quad (2-34)$$

where, as before Δ_2^* - the area equivalent to the arbitrary displacement thickness in the outlet section, and F_2 - the geometric area of the outlet from the diffuser.

By analyzing data in Fig. 2-10 now, it is possible to note that at the large angles of opening and small expansion ratio the length of the diffuser proves to be small. As a result the geometric expansion ratio almost coincides with the effective.

An increase in the geometric expansion ratio n with a simultaneous decrease in α gives rise to more significant deviation of n_{ϕ} from n .

Since the drop in velocity in the nucleus of the flow is determined by the effective value of the expansion ratio, along curve 1 (Fig. 2-10), which corresponds to the limiting drop in

velocity, which ensures the nonseparable flow, $n_{\alpha\phi}$ should be changed within comparatively small limits. Actually, by calculating for the diffusers in question from relation (2-29) the displacement thickness in the outlet section, we obtain along the entire curve value $n_{\alpha\phi} \approx 1.8-2.5$ (curve 2).

In other words, the nonseparable flow in the diffuser proves to be possible only when in the nucleus of the flow the ratio of velocities $c_0/c_1 < 2.5$.

By estimating as a whole the given results, it is necessary to note that the nonseparable flow is possible both at wide angles of opening α and at large geometric expansion ratios, if, of course, with this the correlation established by curve 1 in Fig. 2-10 is not disturbed.

Consequently, the question of the theoretical estimate of frictional losses in diffuser elements represents an entirely specific interest. Considering the aforesaid, let us examine this problem in more detail. Let us assume that as a result of the boundary layer calculation, known to us are all the integral thicknesses in the outlet section of the diffuser, and at the inlet to it the boundary layer is absent. Then according to the physical sense of value δ^{***} losses of energy in the outlet section is expressed by relation

$$\Delta h = \frac{1}{2} \rho_2 c_{2\text{max}}^3 \delta_2^{***} \quad (2-35)$$

Here ρ_2 and $c_{2\text{max}}$ - density and velocity in the nucleus of the flow at the outlet from the diffuser, and δ_2^{***} - the area of the loss of momentum in this cross section.

The magnitude of kinetic energy H_0 at the inlet section of the diffuser at the uniform inlet velocity field and mass flow m is expressed in the following manner:

$$H_0 = \frac{1}{2} m c_1^2 = \frac{1}{2} \rho_1 c_1^3 F_1.$$

Then according to the definition the coefficient of internal losses will be equal to:

$$\zeta = \frac{\Delta h}{H_0} = \frac{\rho_2}{\rho_1} \cdot \frac{c_{2\text{макс}}^3}{c_1^3} \bar{\delta}_2^{***} \frac{F_2}{F_1}.$$

For the connection between maximum velocity $c_{2\text{макс}}$ in the outlet section and velocity c_1 , let us use the equation of continuity and let us introduce into the examination the effective area $F'_{2\text{эф}}$, i.e., the area necessary for the admission of the assigned flow at maximum velocity $c_{2\text{макс}}$ and density in the center ρ_2 :

$$\rho_1 c_1 F_1 = \rho_2 c_{2\text{эф}} F'_{2\text{эф}} = \rho_2 c_{2\text{макс}} F'_{2\text{эф}}.$$

Hence

$$\frac{c_{2\text{макс}}}{c_1} = \frac{\rho_1}{\rho_2} \cdot \frac{F_1}{F'_{2\text{эф}}}$$

and the formula for estimating the coefficient of internal losses ζ takes the form:

$$\zeta = \left(\frac{\rho_1}{\rho_2} \right)^2 \frac{\bar{\delta}_2^{***} n}{n_{\text{эф}}^3}. \quad (2-36)$$

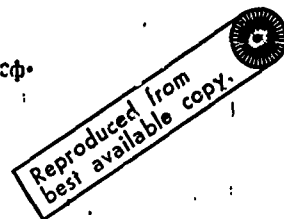
Taking into account that $n'_{\text{эф}} = n(1 - \bar{\delta}^*)$, let us present (2-36) in the following form:

$$\zeta = \left(\frac{\rho_1}{\rho_2} \right)^2 \frac{\bar{\delta}_2^{***}}{n^2 (1 - \bar{\delta}_2^*)^3}. \quad (2-36a)$$

Here $\bar{\delta}_2^{***} = \delta^{***}_2 / F_2$ - the relative area of the energy loss, and $\bar{\delta}_2^* = \delta^*_2 / F_2$ - the relative area of the displacement thickness.

We arrive immediately at expression (2-36a) as a result of the common solution of equation (2-24) and (2-29) when $\bar{\delta}_2^* = \bar{\Delta}_2^*$ and $\bar{\delta}_2^{***} = \bar{\Delta}_2^{***}$.

Formula (2-36a) was derived by A. S. Ginevskiy [18] and is generalized by him for flow with heat exchange and flow with the initial boundary layer.



In the latter case when $\rho_1 = \rho_2$ relation (2-36a) assumes the form:

$$\zeta = \frac{\bar{\delta}^{2**}_2}{r^2 (1 - \bar{\delta}^{2*}_2)^2} \frac{\bar{\delta}^{2**}_1}{(1 - \bar{\delta}^{2*}_1)^2} \quad (2-36b)$$

where the subscript "1" refers to values at the inlet section.

The obtained relations solve the problem of estimating the coefficient of losses in diffusers on the condition that velocity $c_{2\text{макс}}$, determined from the equation of continuity, coincides with the velocity c_0 , equivalent to the enthalpy drop h_0 (see Fig. 2-4).

The indicated condition is reduced to the equality of pressures of full stagnation in the inlet section p_{01} and maximum pressure of full stagnation in the outlet section of the diffuser p_{02} . Otherwise at $p_{02\text{макс}} < p_{01}$ the calculations according to formula (2-36a) substantially understate the magnitude of the coefficient of internal losses.

Let us note that the drop in pressure of full stagnation in the nucleus of the flow is not unique and, perhaps, even not the decisive cause for the divergence of calculated and experimental values. More serious is the absence of reliable test data suitable for a comparison. Even for the simplest conical diffusers in the majority there are given experimental values of coefficients of internal losses obtained not allowing for the flow velocity component, which greatly overstates the magnitude ζ and does not allow the comparing of these data with results of the calculation according to the theoretical methods based upon integral thicknesses of the boundary layer. For an example, let us say, that in a detailed investigation of conical diffusers the following results were obtained by us. The diffuser with a flare angle $\alpha = 7^\circ$ and expansion ratio $n = 3$ and $\lambda_1 = 0.8$ had a total loss factor of $\zeta_{\text{п}} = 16\%$. Its internal losses were with averaging, not allowing for the velocity flow component, $\zeta = 9.5\%$, and

taking it into account, 5.8%. Correspondingly, losses with the outlet velocity were in the first case 6.5, in the second, 10.2%. Above we already indicated that having reached the solution to the problem of the advisability of the utilization of a certain method of calculation, it is necessary to proceed from the comparable total loss factors.

Leaving aside the systematic side of the question, for an agreement of calculated and experimental data when $p_{02\text{макс}} < p_{01}$ it is possible to introduce an additional coefficient ψ_2 dependent on the degree of the loss in pressure of full stagnation in the nucleus of the flow or use the arbitrary boundary layer characteristics Δ^* and Δ^{***} calculated with respect to the arbitrary velocity c_0 . In this case instead of (2-36a) we will obtain:

$$\zeta = \left(\frac{p_1}{p_2} \right)^2 \frac{\bar{\delta}^{00*}_2 \psi_2}{n^3 (1 - \bar{\delta}^{00}_2)^3} = \left(\frac{p_1}{p_2} \right)^2 \frac{\bar{\Delta}^{***}_2}{n^2 (1 - \bar{\Delta}^{00}_2)^3} \quad (2-37)$$

Formula (2-37) generalizes the expression (2-36a) for the general case of nonseparable flow of the flow in channels.

Inequality $p_{02\text{макс}} < p_{01}$ takes place at the joining of the boundary layer. More disputable is the question of the existence of the indicated inequality in the case when the normal velocity distribution at the outlet from the diffuser in the cross section has a clearly expressed section of constant velocity (nucleus of the flow). The accepted division of the examined region of flow into the zone of the boundary layer and potential nucleus with formal approach automatically gives rise to the constancy of the pressure of full stagnation in the nucleus of the flow.

One should, however, keep in mind the asymptotic nature of the normal velocity distribution in the profile of the boundary layer and the conditionality of the determination of its outer edge.

If for problems of the external flow of bodies when the region of the boundary layer is incommensurably small as compared with the external flow, the noted conditionality is entirely permissible, then in conformity with the internal problems, where the boundary layer occupies a greater part of the flow, it is hardly possible to speak about the existence of the potential nucleus in the complete sense of the word. The presence in the central region of a diffuser channel even of a very small eddying of the flow can be the cause of the drop in pressure of full stagnation.

The expressed considerations are confirmed by numerous experiments by the determination of losses in different kinds of channels and diffusers. Thus, during tests of turbine cascades the losses are concentrated not only in the zone of the edge trace, but they exist outside it where the field of average speeds is uniform [25, 26, 27]. The level of losses here is determined basically by the turbulence level of the incoming flow. The same picture is observed in diffuser channels. For example, in Fig. 2-11a relative loss in pressure of full stagnation in the center of the conical diffuser at various expansion ratios and velocities at the inlet λ_1 is plotted. The normal velocity distributions in the outlet section corresponding to these curves, given in Fig. 2-11b, show that the joining of the boundary layer occurs at $n > 3.5$, and the pressure loss p_{01} is noted already at $n > 2.5$. Subsequently, this reduction becomes sufficiently large and increases with an increase in the dimensionless velocity λ_1 .

The noted fact of the drop in pressure of full stagnation in the nucleus of the flow in unjoined boundary layers substantially complicates the theoretical methods of the calculation, even if all boundary layer characteristics in the outlet section of the channel are known. In many cases the ratio $\Delta p_0/p_{01}$ is small, and, for example, Reno and Johnston in work [89] consider it possible for practical calculations to disregard the magnitude $\Delta p_0 = p_{01} - p_{02}$.

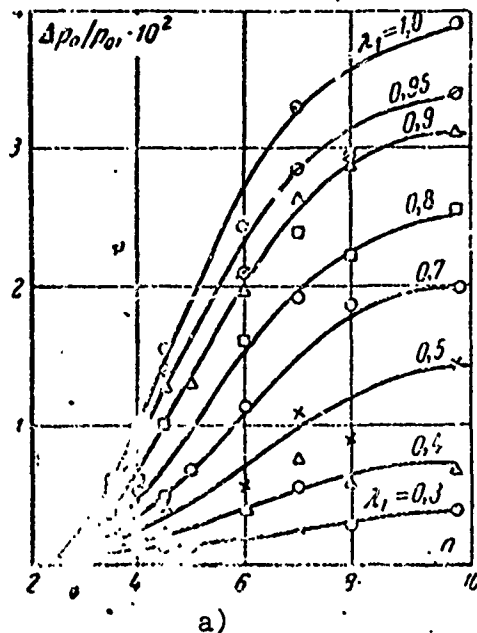
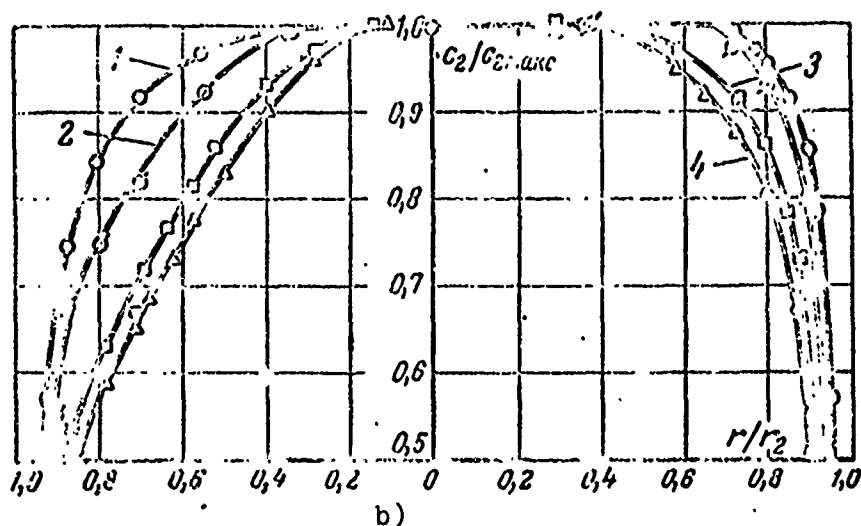


Fig. 2-11. Relative drops in pressure of full stagnation in conical diffusers a) and the normal velocity distributions in the cross section of some channels b). 1 - $\alpha = 7^\circ$; $n = 2$; $\lambda = 0.5$; 2 - $\alpha = 7^\circ$; $n = 2.0$; $\lambda = 0.8$; 3 - $\alpha = 7^\circ$; $n = 3.0$; $\lambda = 0.5$; 4 - $\alpha = 7^\circ$; $n = 3$; $\lambda = 0.8$.



Nevertheless, until now in practice of engineering calculations for estimating the coefficients of losses in diffusers either test data or semiempirical methods have been used. To a considerable degree their distribution is explained by the simplicity of design equations and by the apparent universality, while the use of the formulas of the type (2-36a) requires sufficiently complex calculations for the determination of the integral boundary layer thicknesses, and the region of the use of the obtained results is limited by cases of nonseparable flow.

Because of this let us examine the most widespread method of the calculation of losses based upon the separation of internal losses into losses of friction and expansion. In this method in the calculation of frictional losses, accepted as the initial is the well-known hydraulic formula [34, 54].

$$\Delta h_{fp} = \xi_1 \frac{\rho c^2}{2} \cdot \frac{L}{D}, \quad (2-38)$$

which determines the magnitude of losses on the section of tube with length L and diameter D with stabilized flow. Such a flow takes place at a considerable distance from the inlet section where the joining of the boundary layer occurred, and the typical turbulent normal velocity distribution was established. As a whole it is possible to consider that formula (2-38) gives good agreement with the experimental data in the removal of the examined section at 20-30 gauges from inlet section.

Coefficient ξ_1 , which enters into expression (2-38), depends upon the Re_D number and at $Re_D < 10^6$ is most frequently used in the following form:

$$\xi_1 = 0,316 Re_D^{-1/4}.$$

Let us use formula (2-38) for the calculation of the conical diffuser. For this purpose let us divide it into an infinite number of cylindrical sections with length dx, and let us record formula (2-38) for an infinitesimal section:

$$d(\Delta h) = \xi_1 \frac{\rho c^2}{2} \cdot \frac{dx}{D}. \quad (2-38a)$$

Here ρ , c and D - current values of density, velocity and diameter along the x axis.

Having integrated expression (2-38a) over the entire length, we obtain the complete magnitude of frictional losses in the diffuser. Preliminarily, however, let us establish the connection of diameter D with coordinate x.

From the geometric relations

$$\bar{x} = \frac{D - D_1}{2 \sin \frac{\alpha}{2}}$$

and

$$dx = \frac{dD}{2 \sin \frac{\alpha}{2}} \quad (2-39)$$

For an incompressible fluid ($\rho = \text{const}$) the connection between the velocity and diameter is established from the equation of continuity:

$$c = c_1 \frac{D_1^2}{D^2} \quad (2-39a)$$

Having substituted (2-39) and (2-39a) into (2-38a), as a result of integration from D_1 to D_2 we will obtain:

$$\Delta h_{\text{TP}} = \frac{\rho c_1^2}{2} \frac{D_1^4}{2 \sin \frac{\alpha}{2}} \int_{D_1}^{D_2} \xi_1 \frac{dD}{D^5} \quad (2-40)$$

At large values of the Re_D number coefficient ξ_1 weakly depends upon the diameter and can be carried out from under the integral. Then

$$\Delta h_{\text{TP}} = \frac{\rho c_1^2}{2} \cdot \frac{\xi_1}{2 \sin \alpha/2} \left(1 - \frac{1}{n^2}\right)$$

and for the coefficient of losses ζ_{TP} let us arrive at the following expression:

$$\zeta_{\text{TP}} = \frac{\xi_1}{8 \sin \frac{\alpha}{2}} \left(1 - \frac{1}{n^2}\right) \quad (2-41)$$

The calculation of losses for the diffuser, the geometric parameters of which are given in Table 2-2, gives the following results.

The computed values prove to be quite different from the test data. However, in this case their agreement should not take place.

Table 2-2.

n ($\alpha=3^\circ$)	1,5	2,0	2,5	3,0	3,5	4,0
$\zeta_{\text{расч.}} \%$	1,41	1,50	1,68	1,78	1,92	2,42
$\zeta_{\text{общит.}} \%$	3,2	5,8	7,5	9	10,2	11,5

*Here values of the losses obtained not allowing for the flow velocity component are given.

In fact, with the derivation of formula (2-41) the coefficient of friction is taken as constant not dependent on the expansion ratio of the diffuser, and for its computation expression (2-38a) [34, 54], obtained for the basic section of the circular pipe, is used where there occurs the established normal velocity distribution in the cross section, and the joining of the boundary layer, which is developed on walls of the tube, occurred.

As was already indicated above, the cross section where Blasius's formula is used is located at a distance of 20-30 gauges from the entry into the tube.

At the same time, in analyzing the flow in the diffuser, one should note that on its greater part at $n < 3.5$ and angle $\alpha > 7^\circ$ the joining of the boundary layer does not occur (Fig. 2-11). In other words, when in front of the diffuser a long inlet section does not exist, the flow in it is similar to the flow in the initial section of the tube.

Furthermore, it is necessary to show that the normal velocity distribution in the initial section of the tube is substantially distinguished from the normal velocity distribution in its basic section for which the formula (2-38a) is obtained. Therefore, the utilization of this formula for the calculation of frictional losses to a certain extent is equivalent to the determination of losses in the initial section of the tube according to the relations

valid for the basic section. It is natural, therefore, that frictional losses calculated from formula (2-41) prove to be substantially smaller than the experimental values. This difference can be decreased if into expression for the coefficient ξ_1 we introduce as the determining dimension not the hydraulic diameter but the boundary layer thickness. In this case, however, ξ_1 becomes the velocity distribution function along the axis of the diffuser, i.e., the function of the expansion ratio of the diffuser n , and expression (2-40) even for $\alpha = \text{const}$ is integrated in a considerably more complex manner.

In connection with this in the calculation of losses according to the indicated procedure, it is necessary to introduce into the examination even with nonseparable flow the so-called "losses" of the expansion Δh_p whose ratio to the kinetic energy at the inlet into the diffuser determines the second component of the coefficient of internal losses - the linear coefficient of thermal expansion ζ_p . All additional losses not being considered by formula (2-41) are included here.

By estimating the physical essence of losses of expansion, A. S. Ginevskiy [17] connects them with the deformation of the velocity field in the cross section of the diffuser; I. A. Bindler [7] attempts to explain their increasing turbulence in the course of the flow; N. D. Gryaznov refers these losses only to vortex formation, and in work [35] explanations of losses of expansion actually are not given.

All the expressed points of view give a partial concept about the losses of expansion, but it hardly is worth searching for an explanation of the physical essence of losses being determined by the difference between the experimental values of internal losses ζ and losses calculated from formula (2-41), since the latter, as already mentioned, cannot correctly estimate the order of the frictional losses.

As a result it has been accepted to define all the losses unaccounted for in portions of losses with sudden expansion, considering that

$$\zeta_p = \varphi_p \left(1 - \frac{1}{n}\right)^2. \quad (2-42)$$

The proportionality factor, which obtained the name of the coefficient of the "softening of impact," is considered usually the function only of angle α . According to data [34, 54] its value is weakly changed with a change in the expansion ratio n and barely depends upon the regime parameters.

Considering the small absolute value of frictional losses calculated from formula (2-41), in a number of cases it is advantageous not at all to separate them, estimating internal diffuser losses according to relation [54]:

$$\zeta = \varphi_d \left(1 - \frac{1}{n}\right)^2. \quad (2-42a)$$

The coefficient φ_d entering here is determined on the basis of test data and includes both losses to expansion and losses of friction. Its values, depending on angle α for flat and conical diffusers, are given in Fig. 2-12.

It is necessary to note that formula (2-42a) is sufficiently general and convenient for utilization, since it allows calculating the value of the losses both in separation and nonseparable diffusers. Essentially we are dealing here with the semiempirical method of the estimation of losses. Because of this the range of use of formula (2-42a) is limited, generally speaking, by those diffusers for which the experimental dependence $\varphi_d(\alpha)$ is obtained. However, the simplicity of the method and absence of reliable theoretical solutions led to its widespread use for various classes of diffusers. This method has been developed most fully in works

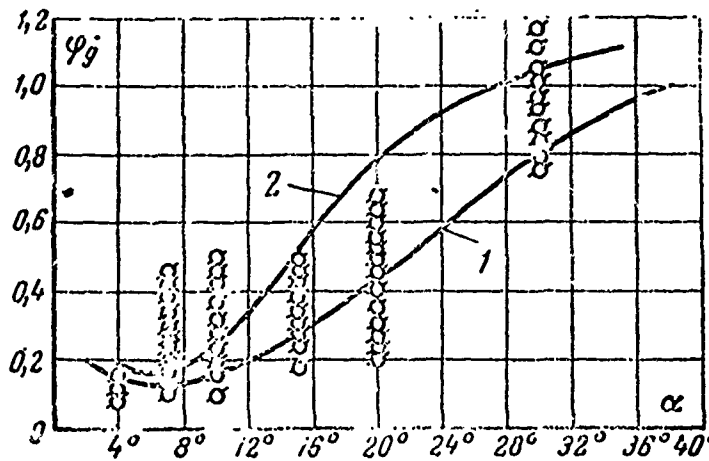


Fig. 2-12. Dependence of coefficient ϕ_g upon angle α . 1 - conical diffusers [54]; 2 - diffuser of square cross section [54]; ϕ - experimental data of L. G. Golovina [21].

[34, 114], where in general it is proposed to estimate losses according to the following relations:

$$\zeta_{rp} = \frac{\xi_1}{4} \int_1^n \frac{df}{f^3 \sin \frac{\alpha}{2}}; \quad (2-43)$$

$$\zeta_p = 2 \int_1^n \varphi(\alpha) \left(1 - \frac{1}{f}\right) \frac{df}{f^2}. \quad (2-44)$$

Here α - the local angle of the diffuser; $\varphi(\alpha)$ - the local coefficient of softening of the impact; $f = F/F_1$ - ratio of flowing area to area at inlet into the diffuser.

When $\alpha = \text{const}$ these formulas convert into the common expressions (2-41) and (2-42) examined above.

For the solution to the problem of the legitimacy of the expansion of the range of use of the initial semiempirical method of calculation, it is advisable to conduct an analysis of the history of internal diffuser losses.

In general losses in the diffusers are determined by regime and geometric parameters. Therefore, for conical and flat diffusers

$$\zeta = \zeta(M, Re, \alpha, n). \quad (2-45)$$

Having expanded expression (2-45) in series with respect to parameter $1/n$ and having been limited to a square term, we obtain:

$$\zeta = \varphi_0 \left(1 + \frac{\varphi_1}{\varphi_0} \cdot \frac{1}{n} + \frac{\varphi_2}{\varphi_0} \cdot \frac{1}{n^2} \right). \quad (2-46)$$

For very small expansion ratios the diffuser losses coincide in practice with losses in the tube equal in length to the diffuser and with diameter D_1 , equal to the inlet diameter of the diffuser. Therefore, at n , striving for unity, losses ζ asymptotically approach losses in the tube, i.e., do not depend upon n . The second asymptote for expression (2-46) takes place in the case of $n \rightarrow \infty$.

Therefore,

$$\left(\frac{\partial \zeta}{\partial n} \right)_{n=1} = 0; \quad (2-47)$$

$$\left(\frac{\partial \zeta}{\partial n} \right)_{n \rightarrow \infty} = 0. \quad (2-47a)$$

Condition (2-47a) is fulfilled automatically, and from relation (2-47) it follows that

$$\varphi_1/\varphi_0 = -2 \frac{\varphi_2}{\varphi_0}.$$

As a result dependence (2-46) is converted:

$$\zeta = \varphi_0 \left[\left(1 - \frac{\varphi_2}{\varphi_0} \cdot \frac{1}{n} \right)^2 + \frac{\varphi_2}{\varphi_0} \cdot \frac{1}{n^2} \left(1 - \frac{\varphi_2}{\varphi_0} \right) \right]. \quad (2-48)$$

With respect to coefficients ϕ_1 let us note that they should be functions M , Re and angle α . At the same time, considering the uniformity of values ϕ_0 and ϕ_1 , it is possible to expect the comparatively weak dependences of their ratio ϕ_2/ϕ_0 upon the indicated parameters. Further, for the convergence of series (2-46) the fulfillment of the condition $\phi_2/\phi_0 < 1$ is necessary. In this case, by using experimental data as a basis, it is admissible, apparently, to consider the ratio ϕ_2/ϕ_0 closer in magnitude to one than to zero. Then, disregarding the second term in the parentheses as compared with the first term in expression (2-48), we obtain:

$$\zeta \approx \varphi_0 \left(1 - \frac{A}{n}\right)^2 \quad (2.49)$$

$(A \equiv \varphi_2/\varphi_0).$

By comparing formulas (2-49) and (2-42a), we see that in structure they prove to be similar and express essentially the same losses. However, the presence in expression (2-49) of coefficient A , generally speaking dependent on the geometric and regime parameters, gives the basis to assume that between values ϕ_0 and ϕ_n a certain distinction should exist.

If in formula (2-49) ϕ_0 is a function of only M and Re numbers and angle α , then coefficient ϕ_n must, evidently depend upon the expansion ratio, whereupon this dependence will be determined by the value of coefficient A , since from a comparison of expressions (2-42a) and (2-49) it follows that

$$\varphi_n = \varphi_0 \left(\frac{1 - \frac{A}{n}}{1 - \frac{1}{n}} \right)^2.$$

Since the ratio $\phi_2/\phi_0 = A < 1$, with an increase in the expansion ratio ϕ_n should somewhat decrease.

The data given by I. Ye. Idel'chik [54] with respect to coefficient ϕ_p indicate that its value depends upon n and in a certain angular region decreases with an increase in the latter. The weak dependence of ϕ_n upon n indicates the fact that the value A is actually close to one.

The analysis conducted here does not pretend to be strict and is oriented basically on the qualitative investigation of formula (2-42a).

Returning now to the question of the possibility of the distribution of the basic dependence (2-42a) on the calculation of more complex diffusers, it should be noted that in this case it is not possible to consider function ϕ_d to be dependent only on the local divergence angle α .

In fact, by turning to circular and curvilinear diffusers and conducting a similar analysis, it is easy to note that in this case the coefficient of the softening of the impact depends not upon one angle α , but also on a number of other parameters which determine the geometry of the diffuser, the effect of which is studied insufficiently. True, the degree of the effect of these additional parameters can be noticeably decreased by means of the successful selection of the so-called "equivalent" angle, but in this case there is always place for the known arbitrariness in its selection.

Furthermore, in the examined works [34, 54] essentially absent are the experimental data which characterize the dependence of coefficient ϕ_d upon the regime parameters, which does not allow with sufficient basis considering this dependence to be self-similar with respect to the numbers M and Re .

Moreover, the test work conducted at MEI by L. G. Golovina [21], with an independent variation in Mach and Reynolds numbers showed that the indicated parameters decisively affect the value of coefficient ϕ_d . Experiments were conducted with conical diffusers with an expansion ratio $n = 3$ and 4 and angles $\alpha = 4, 7, 10, 15, 20$ and 30° . The velocity λ_1 at the inlet was changed from 0.3 to 0.98 , and number Re - from 5×10^4 to $8 \cdot 10^5$.

The results of the experimental determination of coefficient ϕ_D at moderate velocities ($\lambda_1 < 0.6$), given in Fig. 2-12, indicate that even in the subsonic range the change in number Re_1 within limits of $(5-8) \times 10^5$ give rise to the change in coefficient ϕ_D 2-3 times. With an increase in the initial speed (at $\lambda_1 > 0.7$) the effect of the Reynolds number on value ϕ_D proves to be even more significant. Furthermore, it should be noted that the dependence $\phi_D(\alpha)$ does not consider the conditions of the entry and initial turbulence level, and these factors under specific conditions can decisively change the diffuser performances.

The given considerations to a considerable degree lower the value of the procedure in question and do not give basis for its formal distribution beyond the limits of those conditions under which experimental dependence $\phi_D(\alpha)$ is determined. In this connection it is advantageous to turn to the calculation method of frictional losses for the purpose of its possible refinement.

As was already mentioned, the main disadvantage of formula (2-38a) is that losses in an elementary cylindrical section with open boundary layers were estimated according to the correlation valid for the section with the closed boundary layers. Therefore, by preserving the whole methodology of the derivation of constant given above, let us compute the losses in the elementary cylindrical section dx , on the basis of the theory of the boundary layer. In such a section the density and velocity can be considered to be constants, and the frictional losses will be equivalent to the change in the area of the energy loss. Therefore, in this case

$$d(\Delta h) = \frac{1}{2} \rho c^3 d\delta^{***}. \quad (2-50)$$

If we recognize that for the elementary section of the cylindrical tube losses can be expressed in terms of the area δ^{***} according to formula (2-50), then a further derivation will be nothing different from that examined above; it is presented in the works [34, 54].

Let us pass in relation (2-50) to the dimensionless quantities. Using as scale factors density ρ_2 , maximum speed $c_{2\text{макс}}$ and integral area δ^{***}_2 in the outlet section of the diffuser, we will have:

$$d(\Delta h) = \frac{1}{2} \rho_2 c_{2\text{макс}}^3 \delta^{***}_2 \frac{\rho}{\rho_2} \cdot \frac{c^3}{c_{2\text{макс}}^3} d\left(\frac{\delta^{***}}{\delta^{***}_2}\right). \quad (2-50a)$$

The integral of expression (2-50a) gives the absolute value of frictional losses:

$$\Delta h = \frac{1}{2} \rho_2 c_{2\text{макс}}^3 \delta^{***}_2 \int_0^1 \frac{\rho}{\rho_2} \cdot \frac{c^3}{c_{2\text{макс}}^3} d\left(\frac{\delta^{***}}{\delta^{***}_2}\right). \quad (2-51)$$

Hence, for the coefficient of losses we will obtain the following formula:

$$\zeta = \left(\frac{\rho_1}{\rho_2}\right)^2 \frac{\bar{\delta}^{***}_2}{n^2 (1 - \bar{\delta}^*_2)^3} \int_0^1 \frac{\rho}{\rho_2} \cdot \frac{c^3}{c_{2\text{макс}}^3} d\left(\frac{\delta^{***}}{\delta^{***}_2}\right). \quad (2-52)$$

Relation (2-52) according to the sense of the conducted derivation, should be identical to expression (2-37), which is possible under the condition

$$\psi_2 = \int_0^1 \frac{\rho}{\rho_2} \cdot \frac{c^3}{c_{2\text{макс}}^3} d\left(\frac{\Delta^{***}}{\Delta^{***}_2}\right). \quad (2-53)$$

If the considerations given above are conducted on the basis of the arbitrary area of the energy loss Δ^{***} and the arbitrary area of displacement Δ^* , or if we earlier specify that flow with the potential nucleus is examined, then relation (2-52) will be identical with A. S. Ginevskiy's formula and the right side of formula (2-34). This identity gives rise to the condition $\psi = 1$, i.e.,

$$1 = \int_0^1 \frac{\rho}{\rho_2} \cdot \frac{c^3}{c_{2\text{макс}}^3} d\left(\frac{\Delta^{***}}{\Delta^{***}_2}\right). \quad (2-54)$$

In other words, with a correctly calculated boundary layer equation (2-54) should become identical. Hence the reverse sufficiently tempting prospect follows: to use equation (2-54) for the boundary layer calculation. It is understandable that the integral areas Δ^*_2 and Δ^{***}_2 , found from relation (2-54), should coincide for plane and axisymmetric diffusers with analogous values found from equation (1-38).

The comparison given below (see Chapter Three) for conic diffusers confirms well the aforesaid and gives a basis for wide utilization in the calculations of equation (2-54). The found integral areas agree well with results obtained by direct measurements of the boundary layer in the outlet sections of the diffusers and allow with satisfactory accuracy the designing of nonseparable conical and annular diffusers without the attraction of coefficients of correction and additional losses of the type of losses to expansion. The degree of accuracy of such calculations can be judged according to data given in Chapter Three (see Fig. 3-31), Chapter Five (see Fig. 5-11), and tables placed in the appendix.

§ 2-5. The Influence of Conditions of the Inlet on the Gas Flow in Diffuser Elements

The question of the influence of the uniformity of the velocity field at the inlet into the diffuser on the gas flow has been studied comparatively weakly. However, in a number of cases it proves to be possible to indicate the nature of this influence and for some problems to obtain even quantitative estimates.

From a fundamental point of view the greatest interest is a comparison of three possible cases: uniform, convex and concave in the center section of the velocity profiles. These three characteristic input velocity profiles, studied by O. I. Ovchinnikov, are given in Fig. 2-13 [82]. From a practical point of view the greatest interest is in the convex profile of type 2,

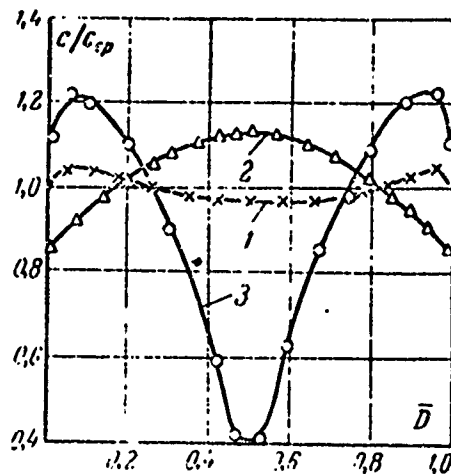


Fig. 2-13. Velocity profiles at the inlet into the diffuser [82]. 1 - uniform; 2 - convex; 3 - concave.

since this form of inlet nonuniformity takes place when before the inlet into the diffuser element the diffuser or gradient-free section are located.

It is not difficult to show that the indicated nonuniformity should lead as compared with the uniform field of velocities, to a substantial increase in losses in diffuser elements and causes an earlier boundary layer separation.

Actually the presence before the inlet into the diffuser of considerable rectilinear sections gives rise to a braking of the flow, and before the diffuser there is already located a more or less developed boundary layer whose growth in the subsequent diffuser section occurs more intensely than at zero thickness of the layer at the inlet (i.e., at a uniform velocity field). As a result an increase in losses to friction takes place, and the possibility of nonseparable flow is sharply decreased.

The aforesaid is confirmed well by curves given in Fig. 2-14 [54]. Here as a characteristic of nonuniformity has been accepted the deviation of maximum velocity on the axis from the average flow rate $k = c_{\text{max}}/c_{\text{cp}}$, and depending on this parameter and flare angle of the conical diffuser α curves of correction factor $K = \zeta_{\text{нep}}/\zeta_{\text{равн}}$, which characterizes the degree of increase in

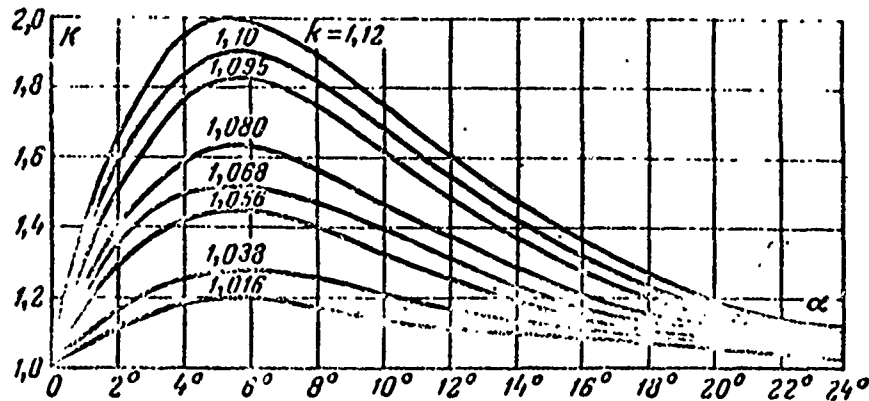


Fig. 2-14. Correction coefficient K , which considers the nonuniformity of the velocity field at the inlet into the diffuser according to I. Ye. Idel'chik [54].

internal losses ζ with the nonuniform velocity field at the inlet with convex profile as compared with the uniform profile.

From the curves it is distinctly evident that in the field of narrow angles there takes place a steep increase in factor K , which reaches a peak value at $\alpha = 5-6^\circ$. A further increase in the angle gives rise to a reduction in value K , and at $\alpha \approx 25^\circ$ the influence of the inlet velocity profile on the diffuser characteristics proves to be insignificant.

The indicated nature of the change in the correction coefficient for the convex velocity profile at the inlet is regular. At small angles α and the uniform inlet velocity field on the entire length of the diffuser, nonseparable flow takes place. The braking of the flow in the boundary layer of the inlet section leads (depending on the length of this section) first to an increase in the boundary layer loss of the diffuser and then to the emergence of the flow separation. The peak value of factor K corresponds to the case of transition from nonseparable flow to flow with separation. In this angular region α almost a crisis increase in losses takes place with an increase in the nonuniformity in question.

With the emergence of separation the influence of the inlet nonuniformity noticeably decreases, since in this case the initial level of losses proves to be high, and a certain displacement of the separation point of flow with an increase in factor k has a slighter effect the relative increase in losses.

Finally, at wide angles ($\alpha = 15-20^\circ$), when separation occurs near the inlet section, the nonuniformity of the inlet velocity profile can affect basically only the intensity of eddy currents. Since for such angles losses are great (30-40%), the relative influence of nonuniformity becomes small.

For an illustration of the aforesaid, Fig. 2-15 gives curves of the change in losses depending on M_1 number for two conical diffusers with angles $\alpha = 6$ and 20° and a radial diffuser tested at the uniform velocity field (curves 1, 2, 3) and the input nonuniformity characterized by a convex profile with factor $k = 1.16$ (curves 4, 5, 6).

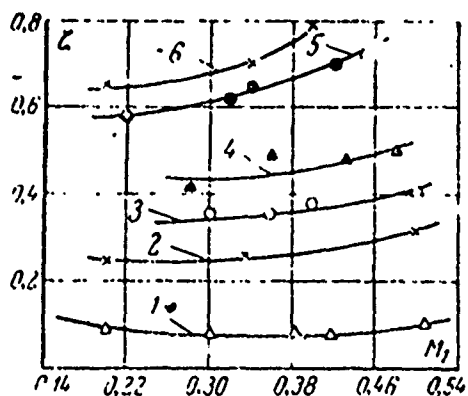


Fig. 2-15. Change in the coefficient of losses ζ depending on M_1 number with a uniform and parabolic inlet profile. 1 and 4 - conical diffuser, $\alpha = 6^\circ$, $n = 2.34$; 3 and 5 - conical diffuser, $\alpha = 20^\circ$, $n = 2.34$; 2 and 6 radial diffuser.

If for a diffuser with angle $\alpha = 6^\circ$ the transition to a nonuniform velocity field led almost to a triple increase in losses, then for a diffuser with angle $\alpha = 20^\circ$ this increase was a total of 60%. It is necessary to show that the absolute increase in losses in both cases compared was noticeable. For $\alpha = 6^\circ$ this increase was $\Delta\zeta = 50\%$, and for $\alpha = 20^\circ$ $\Delta\zeta = 15-25\%$. An

analogous influence can be noted for the radial diffuser where the transition to the nonuniform velocity field increased losses by 40-50%.

Since parabolic nonuniformity examined here is defined basically as the length of the inlet section located in front of the diffuser, in some problems it is advantageous to characterize it by integral boundary layer thicknesses at the inlet into the diffuser, since connected with this are the probability of the emergence of separation in it and, as a consequence, a drop in efficiency.

For representation about the degree of the influence of the inlet boundary layer on the operation of the diffuser, let us examine the experimental dependence given in Fig. 2-16. These data obtained in the work [118] for the diffuser with a flare angle $\alpha = 8^\circ$ and expansion ratio $n = 4$, show that an increase in the relative momentum thickness $2\delta^{**}_1/D_1$ at the inlet from 0.2 to 3% causes a decrease in the eff by 20%. Such a pronounced reduction in efficiency is caused not only by an increase in internal losses but is also connected with an increase in the outlet losses, which depend upon the velocity profile in the outlet section, and the shape of the latter is found to be closely connected to the state of boundary layer at the inlet into the diffuser. These losses increase especially sharply with the emergence of separation, which, apparently, took place here at a large boundary layer thickness at the inlet.

Theoretically the question of the influence of the inlet profile on the efficiency of the diffusers was examined in [95]. The authors used three values as factors which characterize the velocity profile: the coefficient of irregularity of velocity $k_1 = 1/1 - \bar{\delta}^*$, the coefficient of irregularity of the momentum

$$k_2 = \frac{1 - \bar{\delta}^* - \bar{\delta}^{**}}{(1 - \bar{\delta}^*)^2}$$

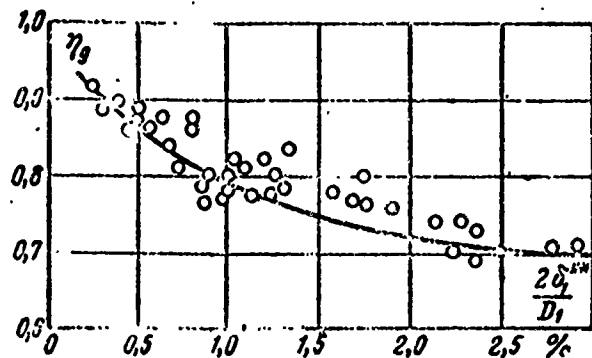


Fig. 2-16. Change in the eff of a conical diffuser depending on the inlet boundary layer thickness [118].

and the coefficient of irregularity of kinetic energy

$$k_3 = \frac{1 - \bar{\delta}^* - \bar{\delta}^{***}}{(1 - \bar{\delta}^*)^2}$$

however, basically the influence of only one coefficient k_1 equivalent to coefficient k in Fig. 2-14 was analyzed. With an increase in this value a reduction in eff was also noted. True, in the analysis of internal losses the authors come to the conclusion that for nonseparable diffusers the nonuniformity characterized by value k_1 causes a reduction in coefficient ζ . Such a result contradicts the curve given above (see Fig. 2-16), obtained by I. Ye. Idel'chik [54], where the growth in nonuniformity at any flare angles of the diffusers gave rise to an intense increase in losses. This contradiction is explained, apparently, by the insufficiently accurate estimate of the energy loss thickness in the final cross section of the diffuser with nonuniform inlet velocity profile.

As a whole the given data give a clear representation of the influence of the inlet nonuniformity on the efficiency of the diffusers.

By examining the influence of the profile concave in center section, it is natural to assume that with such a nonuniformity

the possibility of the emergence of the separation of flow in the diffusers should be reduced.

The velocity profiles in the outlet section of the diffuser (Fig. 2-17), taken at various velocity profiles at the inlet, show that at the uniform velocity field at the inlet in the outlet section a parabolic profile takes place, and with a convex profile there appears the boundary layer separation, as a result of which symmetry of the outlet velocity diagram is disturbed, and the peak value of velocity induced by the decrease in effective area sharply increases.

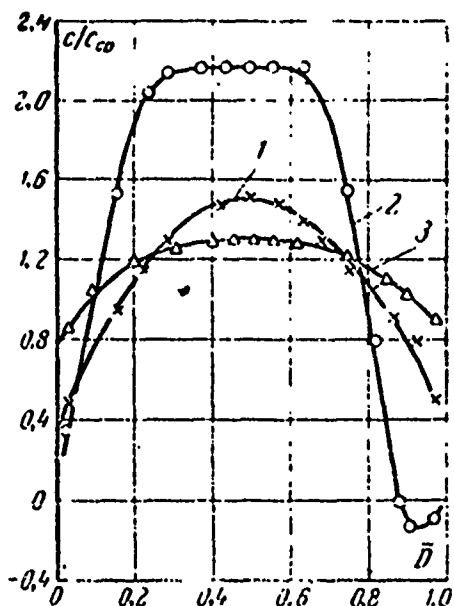


Fig. 2-17. Velocity profiles at the outlet from the diffuser at uniform (1), convex (2) and concave (3) profiles at the inlet.

By estimating the influence of concave inlet profile, one should indicate that, by decreasing the possibility of separation, this profile at large input nonuniformity gives rise to a substantial increase in frictional losses. The last fact is explained by the large transverse gradient of velocities along the length of the diffuser, which gives rise to an increase in turbulent stresses in the flow.

The very characteristic curves of the change in losses, depending on the degree of irregularity, are given in Fig. 2-18. Here, for the characteristic of nonuniformity, coefficient k_3 , defined from the relation [82]

$$k_3 = \frac{1}{F_1} \int_{F_1} \left(\frac{c}{c_{cp}} - 1 \right) dF$$

is accepted.

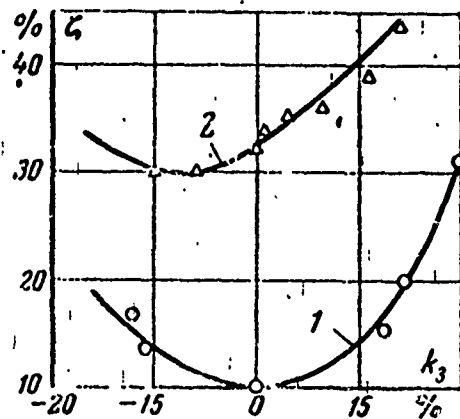


Fig. 2-18. Dependence of the coefficient of losses in conical diffusers upon the nonuniformity of the inlet velocity profile. 1 - $\alpha = 6^\circ$, $n = 3.33$; 2 - $\alpha = 20^\circ$, $n = 3.33$.

From the formula it is evident that for convex profiles $k_3 > 0$, and for concave profiles $k_3 < 0$.

The dependences were diverse for the nonseparable diffuser ($\alpha = 6^\circ$) and for the diffuser having separation even with the uniform velocity field at the inlet ($\alpha = 20^\circ$). If in the first case both the positive and negative nonuniformities gave rise to an increase in losses, then in the second case the transition to negative nonuniformity gave rise to a certain reduction in losses.

The purely qualitative analysis conducted above of the influence of the inlet nonuniformity on the operation of the diffusers to a considerable degree can be supported by the theoretical solutions of S. M. Targ [99] and O. N. Ovchinnikov [82]. These solutions refer to laminar flows, but their importance is not restricted to this case, since they allow

explaining the features of the influence of the degree of irregularity of the inlet field, flare angle and Re_1 number on the operation of the diffusers.

Without discussing in detail all the results, let us examine only the question of the position of the separation point depending on the velocity diagram at the inlet to the diffuser. Figure 2-19, borrowed from [82], gives curves which characterize the position of the separation point in the plane diffuser at various inlet velocity profiles and values of the complex $Re_1\alpha$ for laminar flow. Distinctly visible on the graph are substantial displacements of the separation point along the flow for concave and against the flow for convex velocity profiles. Confirming from the qualitative side the considerations given above, these results can in certain cases be used for quantitative calculations.

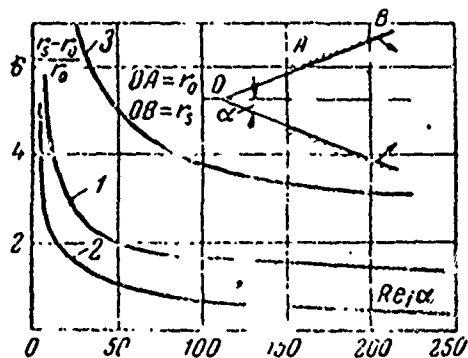


Fig. 2-19. Displacement of the separation point of laminar flow in a plane diffuser at various velocity profiles at the inlet (see designations in Fig. 2-13) [82].

The influence of the inlet nonuniformity on the operation of more complex diffusers (circular axial, axial radial, diagonal and i.e.,) has been studied extremely weakly. However, the available data allow assuming that in this case the inlet nonuniformity seriously deteriorates the operation of the diffusers, whereupon the degree of deterioration also depends upon the form of this nonuniformity.

An interesting investigation in the examined direction was conducted by Johnston [137] for a series of circular axial

diffusers with a constant expansion ratio $n = 3.19$. Tests were conducted at the Reynolds number $Re = 2.5 \cdot 10^5$ on the model whose diagram and basic designations are given in Fig. 2-20a. For a change in the inlet velocity profile in front of the internal cone 1 there was installed an interchangeable shaped fairing 3, with the help of which it was possible to obtain various inlet nonuniformity.

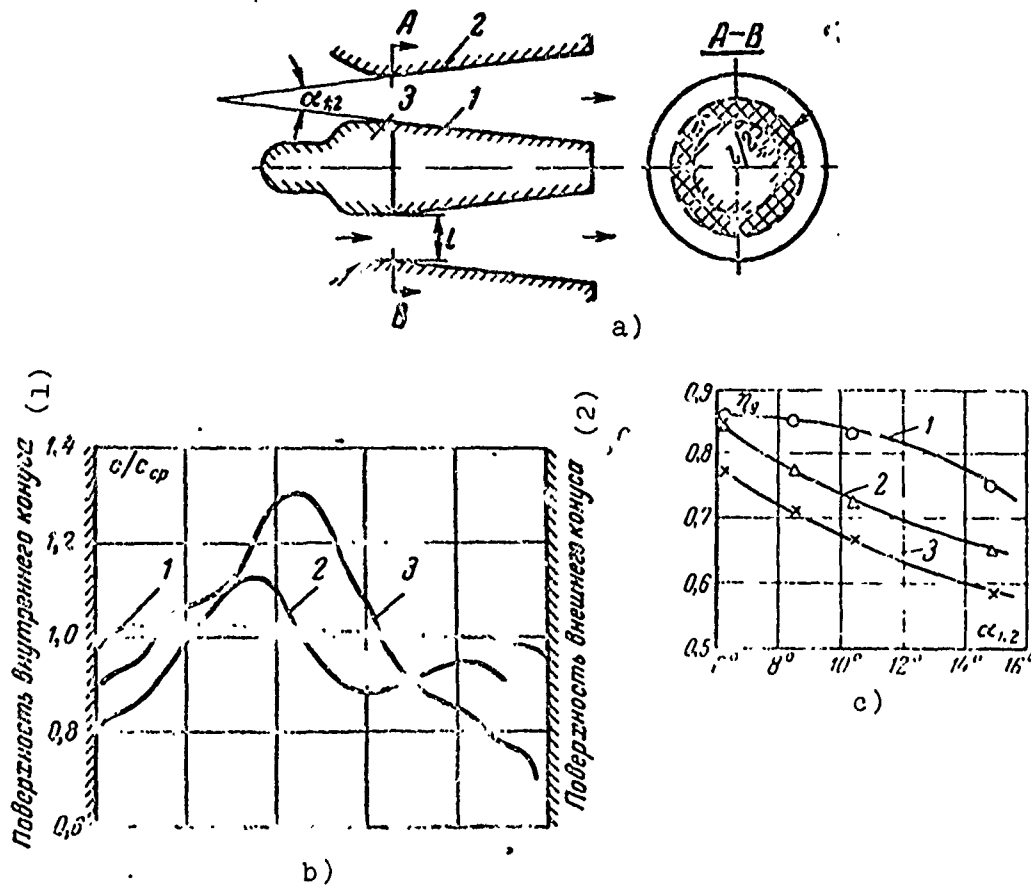


Fig. 2-20. Diagram of an experimental model of the circular axial diffuser a), velocity profiles before the inlet into the diffuser b), and the change in eff of the diffuser depending on the inlet nonuniformity and angle $\alpha_{1,2}$ c). a: 1 - internal cone; 2 - external cone; 3 - shaped fairing; b, c: 1 - profile at the inlet 1; 2 - profile at the inlet 2; 3 - profile at the input 3.
KEY: (1) Surface of internal cone; (2) Surface of external cone.

The shape of the velocity profile before the inlet into diffuser was determined from results of probe measurements. Three such profiles are given in Fig. 2-20b, and their influence on the eff of the diffuser is distinctly evident from curves in Fig. 2-20c, where experimental data obtained during a test of four diffusers which were distinguished only by the magnitude of the total angle $\alpha_{1.2}$ are plotted (Fig. 2-20a). Just as in the case of conical diffusers, the transition from the uniform profile to profiles with a maximum speed in the center led to a noticeable reduction in efficiency, whereupon this reduction was maximum at $\alpha_{1.2}$ of the order of 8-12° and consisted of 17-19%.

The decrease in eff in annular diffusers was close to a drop in eff in conical diffusers at the three percent relative momentum thickness $\bar{\delta}^{**}$ at the inlet (see Fig. 2-16), and the maximum of the increase in losses as compared with the conical diffuser was somewhat displaced to the side of larger angles.

Since annular diffusers are rather frequently installed in branch pipes of turbomachines, where, apart from the significant inlet nonuniformity, there exists in most cases the asymmetry of the velocity profile, the clarification of the question as such asymmetry affects the characteristics of the diffuser is of great interest.

Figure 2-21a gives three velocity profiles investigated in work [137], which are distinguished by the fact that the maximum speed was reached at the external cone (curve 4) in the middle part of the inlet diffuser (curve 5) and at the internal cone (curve 6). Changes in the eff of the annular diffuser corresponding to these profiles, depending on angle $\alpha_{1.2}$, can be seen in Fig. 2-21b.

It was found that the stablest diffuser characteristics are obtained for the case when the maximum of the velocity is shifted to the surface of the external cone. In this case the dependence

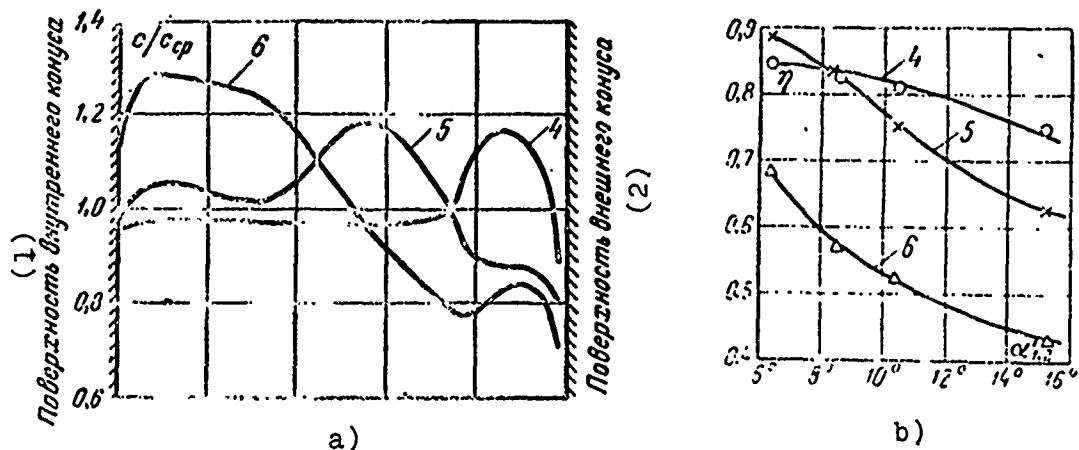


Fig. 2-21. Velocity profiles at the inlet into the circular axial diffuser a) and the change in the eff of the diffuser depending on the inlet nonuniformity and angle $\alpha_{1.2}$ b). a, b: 4 - profile at inlet 4; 5 - profile at inlet 5, (see Fig. 2-21a); 6 - profile at inlet 6.
KEY: (1) Surface of internal cone; (2) Surface of external cone.

of the eff η on angle $\alpha_{1.2}$ practically coincides with the analogous dependence for the uniform velocity profile (curve 1 in Fig. 2-20c). If the maximum velocity is found on the side of internal cone (profile 6 in Fig. 2-21a), then the efficiency of the diffuser for all angles drops by 20-30% (Fig. 2-21b). Such a behavior of the curves is explained by the fact that for profile 6 the probability of the separation of flow from the surface of the external cone sharply increases, whereas for profile 4 the flow in the diffuser, apparently, is nonseparable. Furthermore, on the total diffuser characteristic separation from the surface of internal cone is affected more weakly than from the external cone, where the basic portion of the mass flow passes.

According to the data given in Fig. 2-22 [137] combined curves for all six investigated profiles depending on coefficient k_1 , which characterizes the certain average nonuniformity flow are constructed. Its value is the ratio of velocity c_1 , averaged over area F_1 , which adjoins the internal cone (see Fig. 2-20a), to the average flow rate c_{cp} . From a comparison of the curves it is

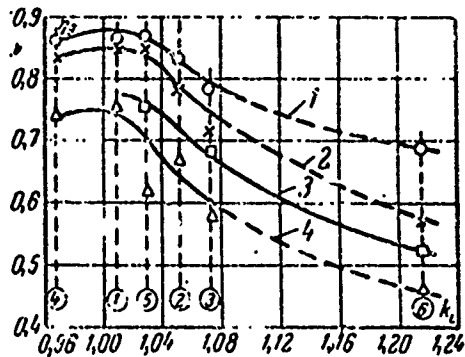


Fig. 2.22. Influence of the average inlet nonuniformity on the eff of circular axial diffusers. 1 - $\alpha_{1.2} = 6.5^\circ$; 2 - $\alpha_{1.2} = 8.5^\circ$; 3 - $\alpha_{1.2} = 10.5^\circ$; 4 - $\alpha_{1.2} = 15^\circ$ (1, 2, 3, 4, 5, 6) numbers in circles - designations of the velocity profiles in Figs. 2-20b and 2-21a.

evident that for all angles the nonuniformity at the inlet gives rise to a reduction in the eff, whereupon the greatest reduction occurs for profile 6 with a maximum velocity of the internal cone.

With the change in nonuniformity estimated by coefficient k_1 , within the limits of $\pm 4\%$ the eff of the diffusers with angles $\alpha_{1.2} < 15^\circ$ is practically not changed. Only when $\alpha_{1.2} = 15^\circ$ and $k_1 \approx 3\%$ does there take place almost a crisis drop in the eff by 14%, which is connected, apparently, with the emergence of the separation.

The given data are not exhausting and do not solve the examined question in question as a whole. However, they give representation about the order of the reduction in efficiency of the diffusers which operate at the nonuniform velocity field at the inlet.

§ 2-6. Selection of Optimum Expansion Ratios of Diffusers

When selecting the rational expansion ratio of diffusers used in turbomachines, it is necessary to consider both the efficiency and permissible overall dimensions of the machine. The latter requirement rather often restricts the expansion ratio of the diffusers, which can lead to a substantial reduction in the coefficient of energy restitution of energy. In connection with this it is necessary, apart from the definition of the optimum expansion ratio n from the minimal condition of losses, to estimate

how greatly the efficiency of diffuser changes with the reduction in value n , having established thereby the definite limitation from the lower side.

It should be noted that the problem in question has a sense only for the diffusers, after which the outlet velocity, and the dependence of the internal losses upon the expansion ratio will be monotonic.

Let us conduct an estimate of the optimum value n from the condition of the minimum of the total loss factor ζ_n . In general the value of ζ_n is added from values of the coefficient of losses to friction up to the separation point of flow ζ_{TP} , coefficient ζ_{OTP} , which characterizes losses in the separation zone, and the coefficient of outlet losses $\zeta_{B.C}$.

The existence of the optimum expansion ratio results from that fact that the components of total losses depend differently upon value n .

Actually, with an increase in value n the internal losses grow, and losses with the outlet velocity drop. At the optimum value n the sum of the outlet and internal losses is minimum.

The specific estimate of the optimum expansion ratio is connected, however, with serious difficulties, since today there are no theoretical bases for the dependence between the components of total losses and value n . Moreover, if formula (2-29a) is used as a basis, then for the incompressible fluid the statement of the determination of the optimum expansion ratio generally meaning, since the total loss factor is connected with the effective expansion ratio by dependence

$$\zeta_n = \frac{1}{n^2 (1 - \delta^*_{\Sigma})^2} = \frac{1}{n_{\Sigma\phi}^2}, \quad (2-29a)$$

which does not give the optimum value of the expansion ratio.

The indicated contradiction is the consequence of the fact that formula (2-29a) was obtained under the assumption of the constancy of the pressure of total stagnation in the flow nucleus and can be used only with the small relative lengths of the diffuser ($L/D_1 \ll 1$) and the small expansion ratios n , when the boundary layer thickness is small as compared with the flow nucleus. Because of this, for the solution to the indicated question it is necessary to proceed from the general formula (2-29b) which is easily converted to the form:

$$\zeta_{II} = \left(\frac{\rho_1}{\rho_2} \right)^2 \left(\frac{c_0}{c_{2maxc}} \right)^2 \frac{1}{n_{\text{эф}}^2}. \quad (2-29c)$$

Here each factor, to a certain degree, depends upon the geometric parameters of the diffuser, especially, upon value n . If the density ratio ρ_1/ρ_2 when $n > 2$ is not changed in practice, then the value of the second factor is determined by the dimensionless length L/D , expansion ratio n and value of turbulence of the incoming flow.

As a result the following function of parameter n will undergo investigation:

$$\zeta_{II} = \frac{f(n)}{n^2}.$$

From the condition of $\partial \zeta_{II} / \partial n = 0$ we will obtain:

$$nf'(n) - 2f(n) = 0. \quad (2-55)$$

Equation (2-55) with the known function $f(n)$ determines the optimum expansion ratio of the diffuser. It should be noted that by using experimental data, it is possible for various diffusers to obtain specific expressions for function $f(n)$ and even extrapolate the obtained data on the definite group of diffusers. However, in the solution to the question of the optimum expansion ratio n , it makes no great sense to construct analytical solutions, since for nonseparable conical diffusers, on the basis of the structure of equation (2-29b), this value will be knowingly more

$n > 2-3$ and the optimum should be very sloping, and with the emergence of separation it is very difficult to select the successful approximating function.

From an analysis of equation (2-55) it follows that the less the loss in pressure in the flow nucleus with an increase in n , i.e., the less $f(n)$ depends upon this parameter, the further the optimum is mixed according to the expansion ratio, and, on the contrary, the worse the diffuser, the more the absolute value of coefficient ζ_n for it, and the less the value of n_{opt} .

For an example, Fig. 2-23 gives dependences of the total loss factor upon the expansion ratio for the conical and three radial diffusers. If for nonseparable flow in conical and radial diffusers the minimum of losses proves to be completely sloping (Fig. 2-23, curve 1, 2), then with the emergence of separation deviation from the optimum expansion ratio gives rise to the steep increase in losses (curve 3), and the point of minimum losses is displaced to the origin of coordinates. The given experimental data show that for the case in question with the emergence of separation (curve 3) the optimum expansion ratio consists of a value of the order of 1.7-2.0.

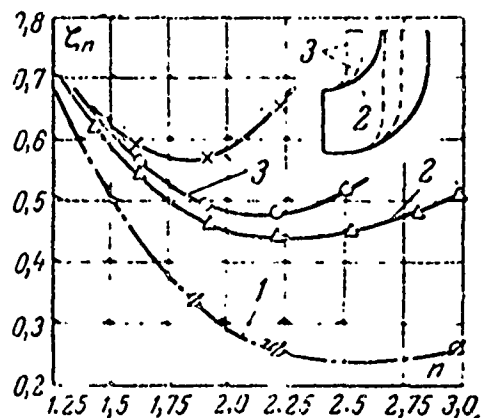


Fig. 2-23. Change in losses depending on the expansion ratio n . 1 - conic diffuser ($\alpha = 15^\circ$); 2 and 3 - radial diffusers.

Numerical values for the optimum expansion ratio and the nature of the change in losses with a change in n allow judging indirectly the flow pattern in the diffuser. In this case one should again emphasize that the dependence of losses upon the expansion ratio in the zone of the optimum value n with nonseparable flow is completely insignificant, and at limited overall dimensions the considerable deviation from n_{opt} to the smaller side is admissible. However, for any diffuser intended for the conversion of kinetic energy of flow in potential energy, the minimum expansion ratio should not be less than 2, since otherwise there occurs a steep increase in losses with the outlet velocity, and correspondingly the coefficient of energy restitution is lowered.

Thus, to obtain the acceptable value of quantity ζ_n , the practical range of the expansion ratio, taking into account the overall dimensions, proves to be comparatively narrow ($2 < n \leq 3$).

CHAPTER THREE

RECTILINEAR PLANE AND AXISYMMETRIC DIFFUSERS

§ 3.1. Flow Pattern in Plane and Axisymmetric Diffusers

By examining the pattern of nonseparable flow in axisymmetric diffusers, it is possible to note its similarity with the pattern of plane flow. As is shown in [68, 70, 93], by means of the appropriate conversion of variables, it is possible to reduce a number of the axisymmetric problems to the two-dimensional case, having substantially simplified thereby the procedure of their solution.

However, with the emergence in the channel of separation the noted analogy is disturbed, and between the characteristics of the plane and axisymmetric diffusers the noticeable distinction is developed. For example, Fig. 2-12 gives coefficients ϕ_A [the coefficient of "softening of the shock" in formula [2-42a)] according to I. Ye. Idel'chik for the conical diffuser (curve 1) and a diffuser with a square cross section (curve 2) depending on angle α .

When $\alpha = 2-8^\circ$, i.e., for nonseparable flow the divergence between the curves comprises a total of 2-4%; when $\alpha > 12^\circ$ the coefficient of internal losses of the square diffuser is almost

2 times more than the conical diffuser. The noted distinction is explained, on the one hand, by the large perimeter of the square diffuser, and on the other, by the different flow pattern in the separation zones of the plane and conical diffusers.

In plane flow, after the separation point, it is possible to observe the stable eddy formations whose intensity is determined by the state of the boundary layer in front of diffuser and weakly changes with time.

In the axisymmetrical channel the separation of flow has a local character, and the intensity of the formed vortices rapidly falls, as a result of which their rate of motion increases and approaches the rate of the main flow.

The characteristic pattern of lines of flow in a plane diffuser at two flare angles ($\alpha = 24$ and 38°) is shown in the photographs (Fig. 3-1). Here the entire flow is moved in the head of the channel, flowing around the eddy regions as certain oval cylinders. This analogy is especially noticeable in the comparison of Fig. 3-1 and Fig. 3-2, where the moment of the origin of the vortex in the flow around the cylinder of plane-parallel flow.

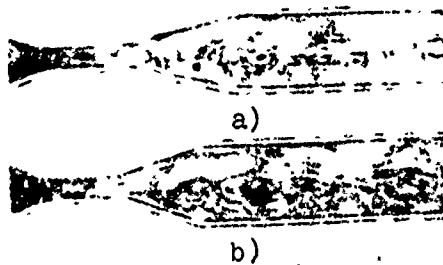


Fig. 3-1. Flow spectrum in a plane diffuser [54].
a) $\alpha = 24^\circ$; b) $\alpha = 38^\circ$.

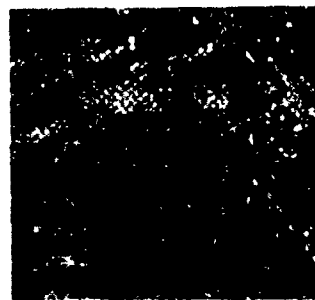


Fig. 3-2. Spectrum of transverse flow of a cylinder.

By examining the flow spectrum at various instants, it is possible to establish that the vortex lines are carried by the flow downstream. The rate of this motion depends upon the vorticity or, if we examine them as some circulatory flows, on the magnitude of the circulation of velocity Γ . The latter can be found from the boundary layer thickness and the velocity at its outer edge at the moment of separation.

In fact, directly before separation the boundary layer velocity profile on its greater part can be approximated by a straight line (Fig. 3-3) [5], i.e., directly at the separation point there takes place the linear normal velocity profile, characteristic for the core of the circulation flow. Then, having used the separation point S as the center of the formed vortex, it is possible to estimate the magnitude of circulation by expression $\Gamma = c_S \delta_S$ and examine further the motion of this vortex in the flow of the source by power Q.

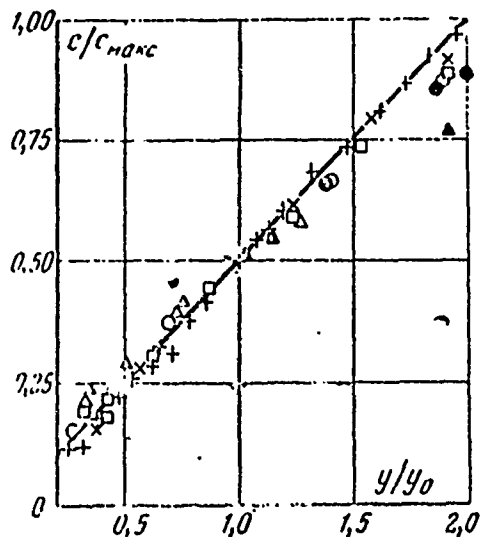


Fig. 3-3. Velocity profiles at the separation point of a turbulent boundary layer [5]. +, O, ●, Δ, ▲ - external flow; □, × - diffusers; y_0 - distance along the normal from the wall to point where $c = 1/2 c_{max}$.

Obviously, the more the magnitude of circulation Γ , the slower at the assigned power Q will be the motion of the vortex along the flow, and, consequently, the more the diffuser losses,

since the vortex zones sharply reduce the effective area and not only give rise to an increase in internal losses, but also cause an increase in outlet losses.

It should be noted that in a plane channel the vortex zones prove to be stable, since in this case the vortices rest by ends on the side walls, and, consequently, the Helmholtz theorem about the conservation of the vortex flow is fulfilled. However, the dissipation of energy gives rise to the fact that the circulation Γ does not remain constant and in the course of time decreases. As a result the rate of motion of the vortices increases, and they decay into smaller formations, and at certain distance it is possible to note only the brightly expressed turbulent nature of the flow.

The qualitative pattern of the flow in separation zones is confirmed well by experimental data, and it shows that for the improvement in the operation of separation diffusers it is necessary, in the first place, to decrease the intensity of the appearing vortices. For this purpose in the separation zones frequently installed grids, which lower the dimensions of discrete vortices and ensure the uniform flow distribution over whole outlet section. For large flare angles finned diffusers [76, 77], which replace the macroseparations by microseparations, appear effective. For this reason the axisymmetric diffusers are more effective than the plane, since separation in such diffusers most frequently has a local character, and the intensity of the formed vortices rapidly falls, whereupon the vortices are considerably less stable (in axisymmetrical channel the fulfillment of the Helmholtz theorem is possible only under the condition of the closing of the vortex into a ring, which in a conical diffuser is unlikely). As a result the velocity of the vortices increases and approaches the velocity of the main flow, and the effectiveness of the axisymmetric diffusers during flow with

separation proves to be substantially higher than that of the plane diffusers.

§ 3-2. Influence of Mode Parameters on Characteristics of Conical Diffusers

Plane and axisymmetric diffusers comprise the most investigated group of the diffuser elements. In spite of this, comprehensive test data for their direct utilization in the definition of the effectiveness of even the most widespread conical diffusers do not exist today. Semi-empirical methods of calculation, based upon formulas of the type (2-42a), also cannot be considered reliable because the utilized experimental dependence of coefficient ϕ_d upon angle α (see Fig. 2-12) was obtained by Gibson in 1910 at an almost constant Reynolds numbers ($Re_1 \approx 2 \cdot 10^5$), constant inlet conditions and low velocities [54].

If for an estimate of the influence of the inlet conditions in literature there are definite data [52, 54, 82, 95, 118, 137], then the influence of mode parameters is investigated very weakly, although with their change the variance of experimental values of coefficient ϕ_d becomes inadmissibly large (Fig. 2-12).

Actually when $Re_1 < 10^5$ and $M_1 > 0.5$ the problem of estimating the characteristics of diffusers becomes indefinite because of the pronounced increase in the role of these criteria, whereupon their influence is not unique and depends upon the geometrical characteristics of the diffusers.

The indicated question was examined in [66, 67]. However, the experimental data obtained in the simultaneous change in numbers M and Re substantially impede the analysis of the influence of each parameter individually.

It was noted above that the independent change in Mach and

Reynolds numbers can be achieved on installations which allow changing over a wide range the counterpressure. Results of such tests conducted at Moscow Power Engineering Institute [MEI] (МЭИ) on a steam test stand with a series of conical diffusers, which were distinguished in flare angles and expansion ratio, are given below.

Since the estimation of the role of the Re_1 number is most complex, we will discuss its influence in more detail.

Theoretically the nature of the change in losses depending on Re_1 can be presented in the following manner (Fig. 3-4). First, at very small Re_1 numbers, when there is no basis for speaking about the boundary layer, an increase in the Reynolds number should give rise to a drop in losses because of the localization of the viscosity near the restricting walls.

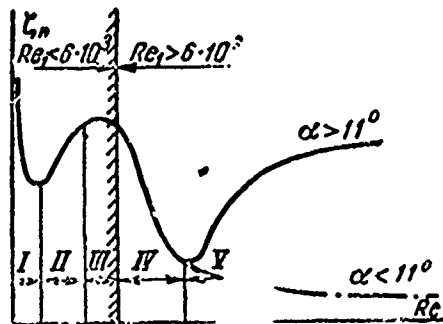


Fig. 3-4. Theoretical dependence of the total loss factor upon the Reynolds number.

Then, depending on angle α , with an increase in Re_1 number there occurs separation of flow from wall and its displacement against the flow (zone II in Fig. 3-4). The emergence of separation and its subsequent displacement against flow are explained by the fact that with an increase in Re_1 number the effective expansion ratio intensely increases, as a result of which the positive pressure gradients increase, and the kinetic energy of the particles found near the wall is already insufficient for overcoming these gradients.

According to theoretical calculations [82, 93, 99], both in plane and conical diffusers the separation point of the laminar boundary layer is asymptotically displaced toward the section with the ratio of areas $F_x/F_1 = 1.65-1.7$.

With the approximation of the separation point toward section F_x , the intensity of the growth of losses is decreased and approaches the stabilization associated with the fact that the position of separation zones with change in Re_1 number is changed insignificantly. The extension of the zone of "stabilization" depends upon the stability of the laminar flow in the boundary layer. Then, on the reaching of the critical state, when the point of the loss in stability (point of "transition") proves to be near the separation point, there occurs a sharp reduction in losses induced by the displacement of the zone of separation to the outlet section as a result of the transition to turbulent flow. This zone, called in [66] the crisis zone, is finished when $Re_1 = (0.8-1.5) \cdot 10^5$. The smaller numbers Re_1 refer to diffusers with larger flare angles α . In other words, at the large values of angle α the crisis zone occupies a smaller extent with respect to the Re_1 number. The further character of dependence $\zeta_n = f(Re_1)$ is wholly determined by the flare angle of the diffuser.

At narrow angles ($\alpha < 11^\circ$) the losses remain practically constant or fall with a change in thickness of the layer and increase in the effective expansion ratio. At large angles ($\alpha > 11^\circ$) with an increase in Re_1 number there again approaches separation of turbulent layer, and the coefficient of losses tends toward a certain constant value (zone V). In the majority of the known works the influence of Re_1 number precisely in this zone is usually investigated, and the zone of smaller values Re_1 remains outside the field of view, although for a number of problems of turbine construction associated with the last stages of steam

turbines, the region $Re_1 < 5 \cdot 10^5$ represents concrete practical interest.

The described hypothetical pattern of flow, based on the analogy of the transverse flow of real flow about a cylinder, can be accepted as the basis if it is possible to prove theoretically or experimentally that in the stabilization zone III the detached flow of the laminar layer actually takes place, and in zone IV the localization of separation or its disappearance occur. Since such a transition is feasible only as a result of the replacement of the form of flow, the given scheme in this case could be considered as proven.

If in zone IV, which still comparatively easily yields to experimental investigation, the flow is nonseparable, then the analysis conducted above should be acknowledged as invalid, and the sharp drop in total losses with an increase in Re_1 number is due to the reduction in losses with outlet velocity.

Thus, for a correct theoretical solution it is necessary to investigate the possible flow conditions both in zone II and zone III. For this purpose let us explain under which conditions in section F_x of the conical diffuser is the separation of the laminar boundary layer possible, since only under these conditions is the pattern examined above possible.

For the laminar boundary layer the momentum thickness is calculated according to formula [68]

$$\frac{\delta^{**}}{L} = \sqrt{\frac{0,44}{\bar{c}^{3,75} Re_L} \int_0^1 \bar{c}^{4,75} d\bar{x}}. \quad (3-1)$$

In the case of incompressible fluid the velocity distribution in the conical diffuser, not allowing for the reverse effect of

the layer, can be represented by a comparatively simple dependence

$$\frac{c}{c_1} = \bar{c} = \frac{1}{[1 + \bar{x}(\sqrt{n}-1)]^2}, \quad (3-2)$$

where c_1 - velocity in the throat of the diffuser, and n - the total expansion ratio.

Having integrated (3-1), taking into account (3-2), we obtain:

$$\bar{\delta}^{**} = \frac{0.242}{\sqrt{Re_L}} \sqrt{\frac{[1 + \bar{x}(\sqrt{n}-1)]^{10.5}}{\sqrt{n}-1} \left[1 - \frac{1}{[1 + \bar{x}(\sqrt{n}-1)]^{7.5}} \right]}. \quad (3-3)$$

Hence it is easy to establish the connection between the Reynolds number, calculated according to thickness δ^{**} , and the number $Re_L = c_1 L / \nu$:

$$Re^{**} = 0.242 \sqrt{Re_L} \times \sqrt{\frac{[1 + \bar{x}(\sqrt{n}-1)]^{10.5}}{\sqrt{n}-1} \left[1 - \frac{1}{[1 + \bar{x}(\sqrt{n}-1)]^{7.5}} \right]}. \quad (3-4)$$

Having used as the separation point the section where the area ratio $F_x/F_1 = 1.7$, i.e.,

$$\bar{x}_{\text{отр}} = \frac{0.305}{\sqrt{n}-1}, \quad (3-5)$$

let us find the value Re^{**} in this section at various expansion ratios and Re_L values.

Substitution into equation (3-4) of $\bar{x}_{\text{отр}}$ gives rise to the very simple dependence:

$$Re^{**} = \frac{0.91}{\sqrt{n}-1} \sqrt{Re_L}. \quad (3-6)$$

Results of calculations according to formula (3-6), presented in Fig. 3-5, show that the intensity of the growth in value Re^{**}

substantially depends upon the expansion ratio of the diffuser n , since with an increase in this parameter the separation point is displaced to the inlet section.

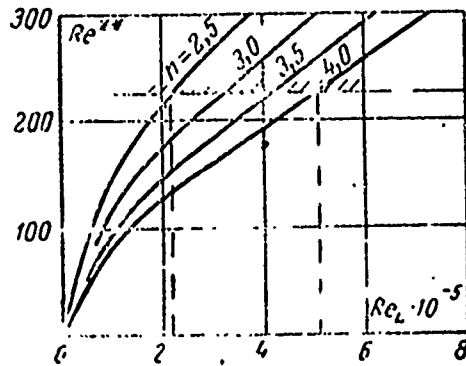


Fig: 3-5. Determination of critical Reynolds numbers at which the transition to the turbulent flow conditions in the boundary layer occurs.

From the given data it is evident that near the separation the Re^{**} number can attain large values. Therefore, the probability of the existence of the laminar boundary layer is sharply decreased, and for the estimation of the possible zone of laminar flow it is necessary to compare the obtained values with the critical value of the Reynolds number. Having used in this question point of view of A. P. Mel'nikov [72], according to which minimum $Re^{**}_{кр}$ near the separation consists of a value equal to 225, and by intersecting on curves of Fig. 3-5 the indicated value, let us find the critical Re_L numbers. According to the calculation the range of critical Re_L numbers consists of $(2-6) \cdot 10^5$.

Thus, the pattern described above of the change in losses proves to be real, and when $Re_L = Re_{L, кр}$ in the diffusers one should expect the "critical region of Reynolds number," i.e., a sharp drop in losses induced by the transition of laminar flow to turbulent.

It is advantageous to note that the experimental data given in [66] confirm well theoretical solutions: for all the diffusers tested the reduction in losses was begun at

$$Re_1 = Re_L \frac{D}{L} \approx 10^6,$$

which approximately corresponded to the critical values.

Analogous results were obtained at MEI during diffuser tests with independent simulation according to the Mach and Reynolds numbers. Thus, Fig. 3-6 shows the dependence of the coefficient of losses upon the Re_1 number for conical diffusers with various flare angles. For every curve in question the M_1 number was maintained constant, i.e., in this case the experimental data reflected only the influence of the Re_1 number.

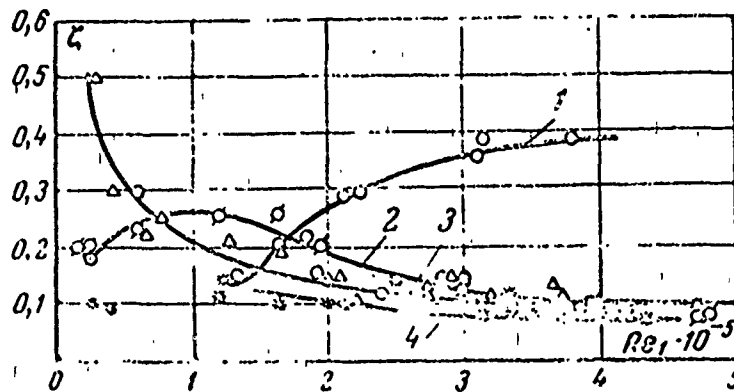


Fig. 3-6. Change in the coefficient of losses depending on the Re_1 number ($n = 4$; $M_1 \approx 0.5$).
 1 - $\alpha = 20^\circ$; 2 - $\alpha = 15^\circ$; 3 - $\alpha = 10^\circ$; 4 - $\alpha = 4^\circ$.

In complete conformity with the pattern described above of the flow of gas in a diffuser with angle $\alpha = 20^\circ$, an increase in Re_1 number caused a growth in losses whose magnitude asymptotically tends to a certain constant value. At the same time in diffusers with angles $\alpha = 15^\circ$ and 10° the losses were intensely lowered and approached constant values when $Re_1 > 5 \cdot 10^5$. Losses plotted on Fig. 3-6 for a diffuser with a flare angle of $\alpha = 4^\circ$ and $n = 3.5$ in practice proved to be not dependent on the Reynolds number. This fact is connected with the fact that at small angles α the

flow in the diffuser in the entire range of Re_1 numbers is non-separable irrespective of the flow conditions in the boundary layer. In this case (small angles) the reverse effect of the boundary layer is very substantial, and the effective expansion ratio does not exceed that value which corresponds to the section of separation. The experimental values of the limiting effective expansion ratio are given in Fig. 3-7 as a function of the λ_1 number.

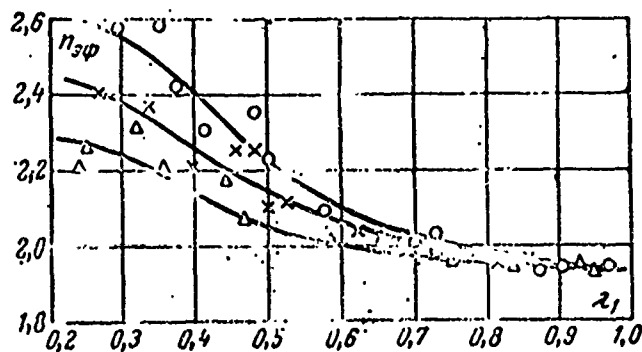


Fig. 3-7. Dependence of the limiting effective expansion ratio $n_{3\phi}$ upon the dimensionless velocity λ_1 at the inlet $Re_1 = (0.8-4.7) \cdot 10^5$; $n = 3-4$; $k = (1.3-1.4)$. \circ - $\alpha = 10^\circ$; \times - $\alpha = 15^\circ$; Δ - $\alpha = 20^\circ$.

With an increase in angle α , at its certain value a critical increase in losses associated with the emergence of separation occurs. The critical angle α_{kp} at which there appears separation depends upon the Re_1 number. If when $Re_1 = 10^5$ $\alpha_{kp} = 8^\circ$, then when $Re_1 = 5 \cdot 10^5$ $15^\circ < \alpha_{kp} < 20^\circ$.

Thus, with the increase in Re_1 number for a large group of diffusers transition is observed from the detached flow to the nonseparable, induced by the replacement of flow conditions in the boundary layer. A clear representation about such a transition can be composed in curves of the changes in pressure (or velocity) along the axis of the diffuser. (*Below it will be shown that α_{kp}

is determined not only by the Reynolds number but also by conditions of the organization of the inlet into the diffuser.)

Figure 3-8 gives a relative drop in velocity in diffusers with angles $\alpha = 15^\circ$ and 10° at various values of the Re_1 number, calculated according to the measured static pressure and constant pressure of full stagnation p_{01} in the flow core.

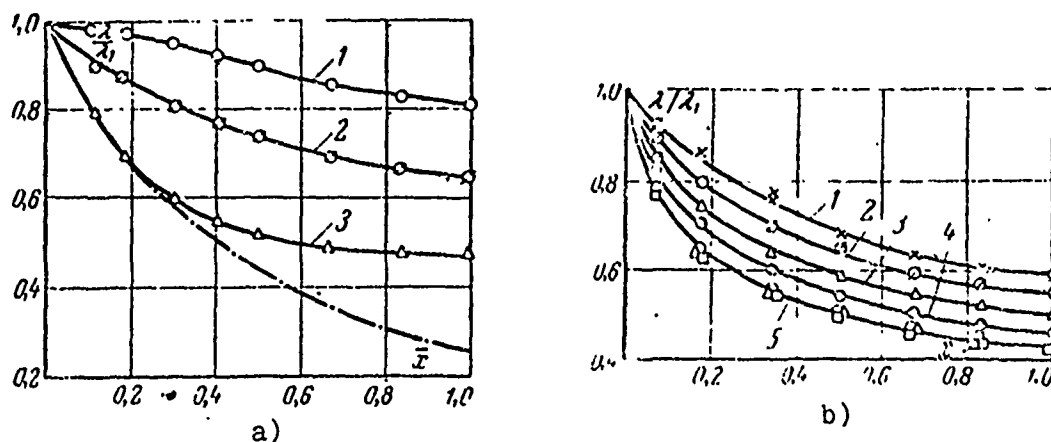


Fig. 3-8. Change in relative velocity λ/λ_1 along the axis of the diffuser ($\lambda_1 \approx 0.8$). a) $\alpha = 15^\circ$; $n = 4$; 1 - $Re_1 = 0.9 \cdot 10^5$; 2 - $Re_1 = 1.2 \cdot 10^5$; 3 - $Re_1 = 4.2 \cdot 10^5$; --- - theoretical dependence $\rho = \text{const}$; b) $\alpha = 10^\circ$; $n = 4$; 1 - $Re_1 = 0.45 \cdot 10^5$; 2 - $Re_1 = 0.66 \cdot 10^5$; 3 - $Re_1 = 1.25 \cdot 10^5$; 4 - $Re_1 = 2.1 \cdot 10^5$; 5 - $Re_1 = 2.8-3.4 \cdot 10^5$.

If when $Re_1 = 0.9 \cdot 10^5$ the velocity in the diffuser is decreased by a total of 18% as compared with the velocity in the inlet section (Fig. 3-8a), which indicates the separation of flow near this section, then with an increase in Re_1 to $1.2 \cdot 10^5$ the decrease in velocity is 35%, and when $Re_1 = 4 \cdot 10^5$ it reaches 55%. For a diffuser with a smaller flare angle the described pattern (Fig. 3-8b) is expressed less brightly, but the maximum drop in velocity comprises a magnitude of the order of 55%, although it is attained at lower Re_1 numbers.

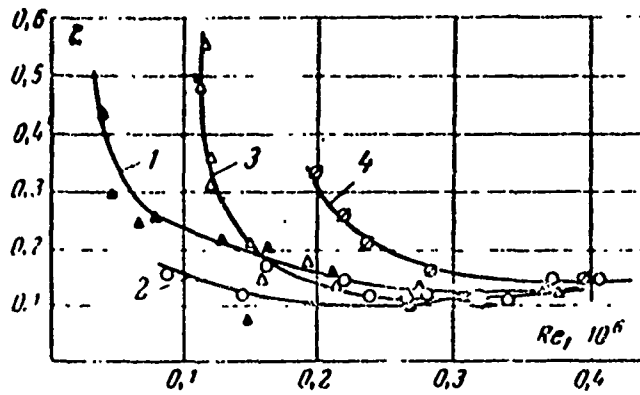
The given value of the maximum drop in velocity is sufficiently characteristic and almost for all nonseparable diffusers when $n > 2.5$ comprises 50-60%, although according to the geometric expansion ratio the maximum outlet velocity should be noticeably less. Such a divergence is the consequence of the loss in pressure of full stagnation in the flow core noted above. By calculating the velocities in the center of the channel not according to pressure p_{01} at the inlet into the diffuser but according to the actual pressure p_{01} in each section, we obtain a sharp reduction in maximum velocities along the diffuser.

The certain fictitious drop in velocity given in Fig. 3-8 gives a clear representation about the local values of the total loss factor. Actually, current velocities λ_1 in this case are calculated with respect to pressures p_1/p_{01} , and velocity λ_1 is determined by ratio p_1/p_{01} . Then by definition of value ζ_n the square of the ratio to velocities λ_1/λ_1 give the local value of the total loss factor and allows determining the local value of the coefficient of recovery of energy. Actually,

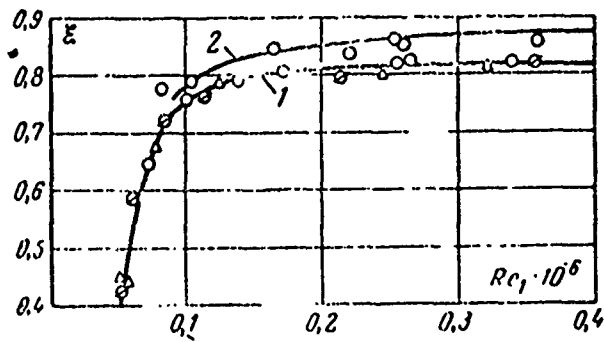
$$\zeta_{nt} = \left(\frac{\lambda_t}{\lambda_1}\right)^2; \xi_t = 1 - \left(\frac{\lambda_t}{\lambda_1}\right)^2.$$

The examined diffuser characteristics are obtained at a constant $M_1(\lambda_1)$ number. However, from curves given in Fig. 3-8, it follows that with a velocity gain the losses can noticeably change, whereupon the magnitude of the change depends upon the Re_1 number.

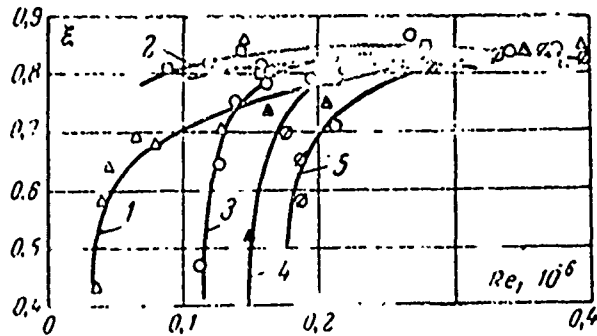
The brightest representation about the interaction of numbers Re_1 and M_1 on the diffuser characteristics is given by curves given in Fig. 3-9. From these curves it is evident that when separation does not exist, in the zone of the large numbers Re_1 ($Re_1 > 4 \cdot 10^5$) the compressibility effect proves to be insignificant. In fact, with an increase in $M_1(\lambda_1)$ number at the inlet into the diffuser there occurs, on the one hand, an increase in inlet pressure gradients, and on the other - the displacement thickness somewhat increases.



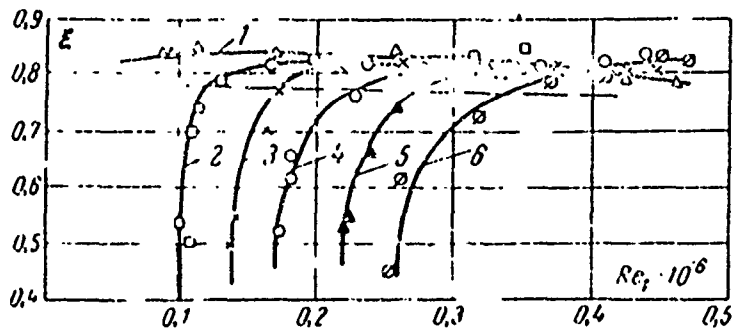
a)



b)



c)



d)

Figure continued on following page.

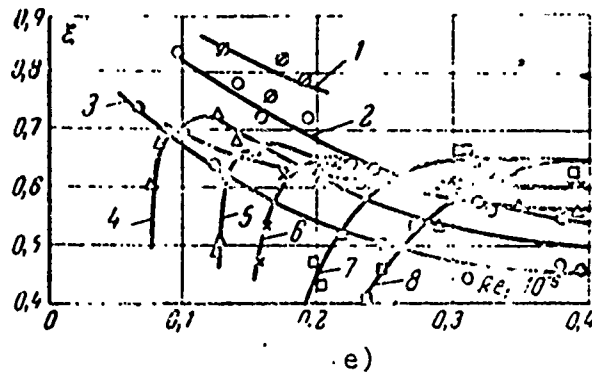


Fig. 3-9. Influence of Reynolds numbers on characteristics of conical diffusers ($n = 4$) when $\lambda_1 = \text{const.}$ a) $\zeta = f(\text{Re}_1)$ $\alpha = 10^\circ$: 1 - $\lambda_1 = 0.126-0.363$; 2 - $\lambda_1 = 0.57-0.7$; 3 - $\lambda_1 = 0.8-0.89$; 4 - $\lambda_1 = 0.98-1.0$; b) $\xi = f(\text{Re}_1)$ $\alpha = 7^\circ$: 1 - $\lambda_1 = 0.4-0.8$; 2 - $\lambda_1 = 0.9$; c) $\xi = f(\text{Re}_1)$ $\alpha = 10^\circ$: 1 - $\lambda_1 = 0.125-0.36$; 2 - $\lambda_1 = 0.57-0.7$; 3 - $\lambda_1 = 0.8-0.89$; 4 - $\lambda_1 = 0.9-0.98$; 5 - $\lambda_1 = 1.0$; d) $\xi = f(\text{Re}_1)$ $\alpha = 15^\circ$: 1 - $\lambda_1 = 0.2-0.33$; 2 - $\lambda_1 = 0.67-0.73$; 3 - $\lambda_1 = 0.77-0.8$; 4 - $\lambda_1 = 0.88-0.92$; 5 - $\lambda_1 = 0.94-0.96$; 6 - $\lambda_1 = 0.98-1.0$; e) $\xi = f(\text{Re}_1)$ $\alpha = 20^\circ$: 1 - $\lambda_1 \approx 0.3$; 2 - $\lambda_1 \approx 0.41$; 3 - $\lambda_1 \approx 0.5$; 4 - $\lambda_1 = 0.6$; 5 - $\lambda_1 = 0.7$; 6 - $\lambda_1 = 0.8$; 7 - $\lambda_1 = 0.95$; 8 - $\lambda_1 = 0.98-1.0$.

The first factor, if it does not cause the separation of flow directly in the inlet section, lowers the intensity of the growth of the displacement thickness along the axis. The second, on the contrary, increases the displacement thickness. As a result of the interaction of two opposite tendencies the effective expansion ration, as experiments show, is lowered somewhat. Furthermore, with a velocity increase the density ratio ρ_1/ρ_2 , which completely compensates the decrease in n_{eff} and leads finally to a drop in coefficient ζ_n and to a growth in the coefficient of recovery of energy, noticeably falls (Fig. 3-10).

The curves given visually show that the compressibility of flow is most greatly developed at small Reynolds numbers, when an increase in inlet dimensionless velocity λ_1 gives rise to a critical drop in the diffuser characteristics. This growth in

losses is caused by the separation of flow in the inlet section under the influence of increase inlet positive pressure gradients.

The dimensionless velocities λ_1 which cause the critical drop in coefficient ξ are determined not only by the Re_1 number but also by the magnitude of angle α .

If for $Re_1 = 10^5$ at angle $\alpha = 10^\circ$ $\lambda_{1 \text{ кр}} \approx 0.65$ (Fig. 3-10b), then $\alpha = 15^\circ$ $\lambda_{1 \text{ кр}} \approx 0.55$ (Fig. 3-10c). With an increase in Re_1 number $\lambda_{1 \text{ кр}}$ also continuously increases, and when $Re_1 > 5 \cdot 10^5$ comprises a value close to one ($\lambda_{1 \text{ кр}} = 0.95-0.98$). The pattern noted is confirmed even in the examination of internal losses (Fig. 3-10a).

The smaller value of $\lambda_{1 \text{ кр}}$ for diffusers with larger flare angles is explained by the fact that at large angles of α , when for an incompressible fluid the inlet pressure gradient is significant, its increase is small enough in order that the separation of flow would begin. The degree of this increase substantially depends upon the λ_1 number.

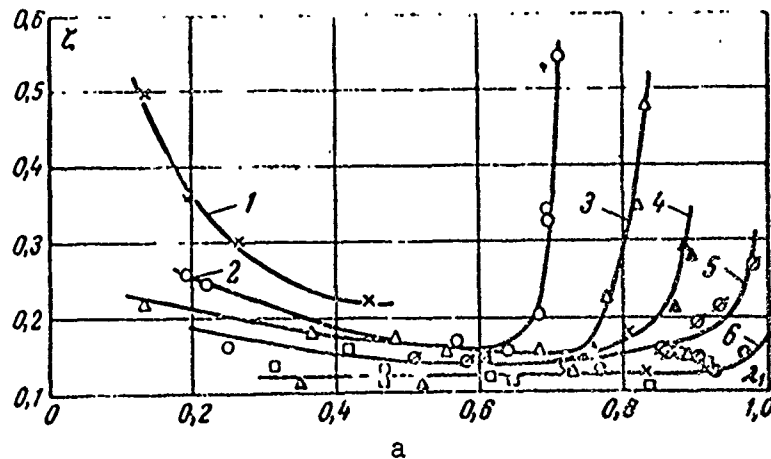
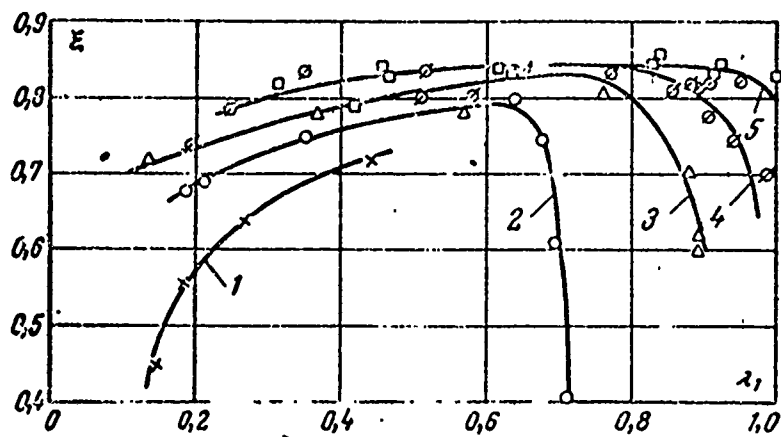
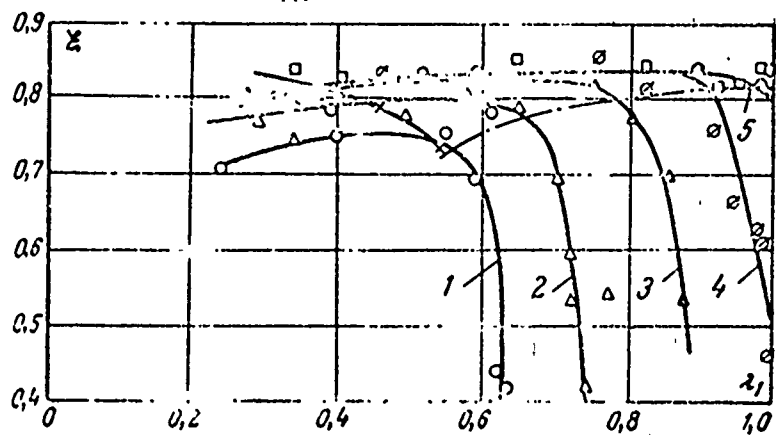


Figure continued on following page.



b)



c)

Fig. 3-10. Influence of λ_1 numbers on characteristics of the conical diffusers when $Re_1 = \text{const}$ ($n = 4$; $k = 1.3$).

a) $\zeta = f(\lambda_1)$ $\alpha = 10^\circ$: 1 - $Re_1 = (0.3-0.65) \cdot 10^5$; 2 - $Re_1 = (0.8-1) \cdot 10^5$; 3 - $Re_1 = (1.1-1.4) \cdot 10^5$; 4 - $Re_1 = (1.5-1.6) \cdot 10^5$; 5 - $Re_1 = (1.7-2.3) \cdot 10^5$; 6 - $Re_1 = (2.6-4.3) \cdot 10^6$; b) $\xi = f(\lambda_1)$ $\alpha = 10^\circ$: 1 - $Re_1 = (0.3-0.65) \cdot 10^5$; 2 - $Re_1 = (0.8-1) \cdot 10^5$; 3 - $Re_1 = (1.1-1.6) \cdot 10^5$; 4 - $Re_1 = (1.7-2.3) \cdot 10^5$; 5 - $Re_1 = (2.6-4.3) \cdot 10^5$; c) $\xi = f(\lambda_1)$ $\alpha = 15^\circ$: 1 - $Re_1 = (1-1.2) \cdot 10^5$; 2 - $Re_1 = (1.25-1.3) \cdot 10^5$; 3 - $Re_1 = (1.6-1.74) \cdot 10^5$; 4 - $Re_1 = (2.3-2.6) \cdot 10^5$; 5 - $Re_1 = (2.8-4.8) \cdot 10^5$.

An increase in the inlet pressure gradient with an increase in the inlet velocity proves to be so considerable that the emergence of separation with an approach to transonic conditions is, in most cases, unavoidable.

At small Re_1 numbers and large α angles when in the incompressible fluid separation appears in the intermediate sections (see Fig. 3-9e), an increase in λ_1 number gives rise to a noticeable growth in losses until the separation approaches the inlet section. From this moment the diffuser characteristics coincide with characteristics of the purely separation diffuser, and the dependence of losses upon λ_1 disappears in practice.

The analysis conducted indicates that the influence of regime parameters $M_1(\lambda_1)$ and Re_1 on diffuser characteristics proves to be complex and depends upon the geometric parameters of the diffuser. At the same time the obtained data allow predicting the general tendency in the changes in coefficients ζ_n and ξ with the change in M_1 and Re_1 numbers.

§ 3-3. Influence of Geometric Parameters on the Aerodynamic Characteristics of Axisymmetric and Plane Diffusers

The geometric parameters of conical and plane diffusers are the dimensionless length \bar{L} , expansion ratio n and flare angle α . Their influence on the aerodynamic characteristics of the diffuser is sufficiently complex and is found in close connection with the regime parameters.

Thus, for example, by changing the angle α with a constant expansion ratio in the zone of small Re_1 ($Re_1 \sim 10^5$) numbers from 4° to 20° , it is possible to arrive at the conclusion about the monotonic increase in the total loss factor from 18 to 28% (Figs. 3-9 and 3-10). The same change in angle α when $Re_1 = 2 \cdot 10^5$ gives a completely different picture: up to $\alpha = 15^\circ$ ζ_n

increases by a total of 4%, and then with transition to $\alpha = 20^\circ$ it is critically increased by 20%. At high speeds ($\lambda_1 \approx 0.8-0.9$) this crisis for a diffuser with angle $\alpha > 15^\circ$ takes place at all Re_1 numbers.

The absence of uniqueness in the examined problem substantially impedes the analysis. However, the physical side of the phenomena which occur in the diffusers with a change in their geometric parameters is sufficiently clear.

For an analysis let us use the numerous experimental data obtained in various works [21, 42, 56, 88, 89, 139, 140, 142, 143, 145, 146, 147, 148]. For the purpose of the greater clarity these data are put by the authors into tables and are placed in the Appendix (see Table A-1), where data on the total loss factors for 300 conical and plane diffusers are gathered, which ensures the definite reliability of the analysis conducted.

Since the basic geometric parameter which characterizes the possibilities of the diffuser is its expansion ratio n , let us begin the examination of the question from this value.

Let us note that the change in the expansion ratio n can be produced either at a constant angle α , when the relative length L/D_1 is changed, or at a constant length, when angle α is changed. Both in the first and second cases the coefficient ζ_n sharply falls with an increase in the expansion ratio, and then it reaches a minimum value and grows further. The intensity of this growth is determined either by angle α or length \bar{L} .

The experimental values of coefficient ζ_n given in Fig. 3-11 visually confirm the aforesaid. The dependence $\zeta_n = f(n)$ when $\alpha = \text{const}$ (Fig. 3-11a) have a very sloping minimum outlined quite clearly only for angles $\alpha = 28-30^\circ$. In the remaining cases coefficient ζ_n with an increase in the expansion ratio

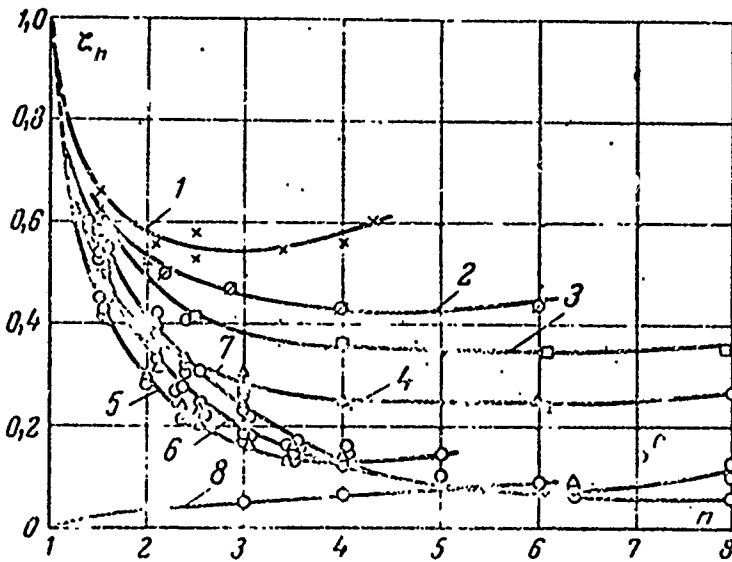
is noticeably decreased in the zone of small values n ($n < 3$), and then when $n > 4$ either it is not changed or is changed insignificantly. The intensity of the reduction in losses with an increase in value n and their absolute level are determined by angle α .

First an increase in the angle from $3^{\circ}30'$ up to $10-12^{\circ}$ gives rise to a comparatively sharp reduction in losses when $n < 4$, and then for $\alpha > 15^{\circ}$ the intensity of the change in coefficient ζ_n falls, and its absolute value continuously increases with an increase in angle α .

The pattern noted is entirely regular. At narrow angles an increase in the expansion ratio gives rise to the continuous reduction in losses with the outlet velocity, and the internal losses determined by friction increase comparatively slowly. The nature of their changes can be judged by curve 8 on Fig. 3-11a, where values of coefficient ζ , obtained as a result of traversing of the outlet velocity field. It is evident that a basic increase in losses occurs at small expansion ratios, and for $n > 4$ these losses increase weakly and cannot substantially influence the nature of the change in the total loss factor.

With the transition to large angles the absolute value of internal losses is decreased due to the reduction of the surface of the diffuser (the reduction in its length), which also causes a reduction in the total losses. However, the noted reduction in losses takes place only up to definite α angles, which ensure the nonseparable flow on the entire length of the channel. Already when $\alpha = 15^{\circ}$ (curve 4) such a flow is possible only for the small expansion ratios ($n < 2.5$), and then the separation of flow from walls approaches, and losses with outlet velocity remain practically constant and do not depend on n . If the separation point of the flow remains fixed, then frictional losses prove to be constant. In the separation zone a vortex flow pattern is

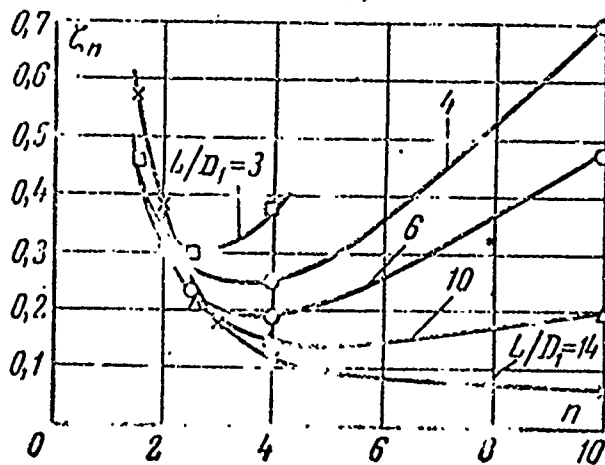
established, and significant dissipation of energy occurs. However, this process cannot have a decisive influence on the total loss factor ζ_n , since the vortex flow is supported because of the energy of the free stream. Consequently, in this case the separation section determines basically the effectiveness of the diffuser, and processes which occur after it are connected with the dissipation of the outlet energy. The expressed consideration is visually confirmed by curves 2, 3 and 4. Here the growth of the expansion ratio from 4 to 8 did not at all lead to a noticeable change in coefficient ζ_n .



a)

Fig. 3-11. Dependence of coefficients ζ_n and ζ upon the expansion ratio n .

a) $\alpha_1 = \text{const}$: 1 - $\alpha = 28-30^\circ$; 2 - $\alpha = 22^\circ$; 3 - $\alpha = 18^\circ$; 4 - $\alpha = 15^\circ$; 5 - $\alpha = 10-12^\circ$; 6 - $\alpha = 6$ to 8° ; 7 - $\alpha = 3.5-4^\circ$; 8 - $\zeta = f(n)$ $\alpha = 7^\circ$;
 b) $L/D_1 = \text{const}$.



b)

At large angles ($\alpha > 30^\circ$) the intensity of the vortex motion proves to be so significant and separation section is so closely located to the inlet section of the diffuser that on curves $\zeta_n = f(n)$ the expressed minimum of losses (curve 1) appears.

If the expansion ratio of the diffuser is changed at constant length only because of an increase in angle α , then the minimum value ζ_n for $\bar{L} = \text{const}$ is determined by such an angle α at which in the diffuser the developed separation of flow from the walls of the channel appears. The nature of the change in curves $\zeta_n = f(n)$ in the case in question is well evident from Fig. 3-11b. At large expansion ratios n ($n > 4$) the growth in this parameter causes an increase in coefficient ζ_n , whereupon smaller values of relative length \bar{L} correspond to the higher level of losses.

The obtained result is the consequence of the fact that the assigned value of parameter n for the longer diffuser is ensured by a smaller angle of expansion α . Thereby the possibility of the flow separation is lowered, and the uniformity of the velocity profile in the outlet section of the diffuser is improved. Thus, for $L/D_1 = 14$ the monotonic reduction in losses with an increase in n is noted.

The pattern is changed in the region of small expansion ratios, where longer diffusers have greater losses than do short ones. In this case the flow in the diffusers is nonseparable, or the separation bears a local character, which increases the role of internal losses. These losses, just as losses in the tube, grow with an increase in the relative length L/D_1 . True, the coefficient ζ changes little and is close to the appropriate values for tubes having the same relative length as that of the diffuser. In [95] even the reduction in the magnitude of coefficients ζ as compared with that for tubes is noted. As a result the approach of all curves occurs and for $n < 2$ the influence of length \bar{L} on coefficient ζ_n decreases.

The examined influence of the expansion ratio of the diffuser on the coefficient of total and internal losses is to a considerable degree unique and is not changed with a change in regime parameters. Only absolute values of coefficients ζ_n and ζ and the position of the minimum on curves $\zeta(n)$, but not the nature of dependence $\zeta_n = f(n)$ can depend on the change in the regime parameters.

For an example Fig. 3-12 gives the dependence of the coefficient of the reduction in energy upon the λ_1 number at various Re_1 numbers for two values of parameter n . At large Re_1 numbers the transition from $n = 3$ to $n = 4$ did not cause changes in the nature of the curves, and for $Re_1 < 10^5$ the maximum distinction in coefficient ξ is about 3%. Let us note simultaneously that the critical reduction in value ξ occurs for both expansion ratios n at the same value of the dimensionless velocity λ_1 . An analogous pattern is noted for diffusers with angles of 4, 10 and 20°.

It is considerably more complex to analyze the influence of angle α . In the majority of works on diffusers, precisely this parameter is considered the basic one which determines the flow pattern in the channel [5, 34, 54, 102, 106, 107]. The value of angle α at invariable remaining parameters, in the first place, is connected with transition from nonseparable to detached flow in the diffusers.

The experimental data given in Fig. 3-13 show that at large Re_1 numbers the change in angle α up to a certain critical value α_{kp} barely changes the coefficient of the recovery of energy, and when $\alpha > \alpha_{kp}$ there occurs its sharp reduction induced by the separation of flow at the throat of the diffuser.

The value of the critical angle depends upon the expansion ratio, the Re_1 number and the dimensionless inlet velocity λ_1 .

For low speeds and large Re_1 numbers the value $\alpha_{кр}$ is determined by the curve given in Fig. 2-10, and it shows that with an increase in the expansion ratio there occurs a reduction in the critical value of angle $\alpha_{кр}$. This dependence follows from curves on Fig. 3-14a. When $n = 2.4$ an increase in coefficient ζ_{Π} occurs, beginning from 15° , and when $n = 4$, $\alpha_{кр} = 10^\circ$.

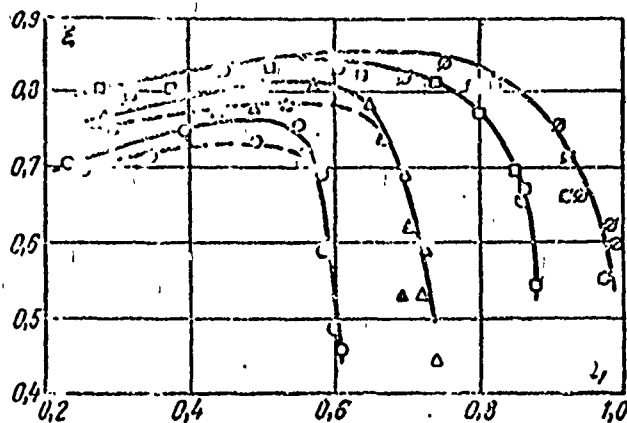


Fig. 3-12. Dependence of coefficient ξ upon λ_1 ($\alpha = 15^\circ$).
 $\bullet, \blacktriangle, \blacksquare$ - $n = 3$; $\circ, \triangle, \square$ - $n = 4$; \circ, \bullet - $Re_1 = 10^5$; Δ, \blacktriangle - $Re_1 = 1.2 \times 10^5$; \square, \blacksquare - $Re_1 = 1.65 \times 10^5$; \bullet - $Re_1 = 2.4 \cdot 10^5$.

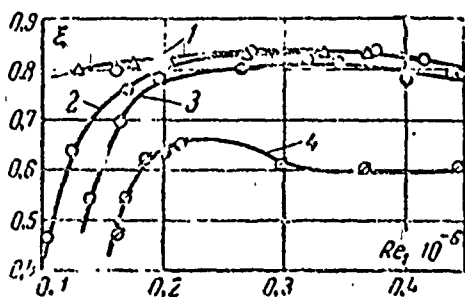


Fig. 3-13. Dependence of coefficient ξ upon Re_1 and angle α ($n = 4$; $\lambda_1 \approx 0.8$).
 1 - $\alpha = 7^\circ$; 2 - $\alpha = 10^\circ$; 3 - $\alpha = 15^\circ$; 4 - $\alpha = 20^\circ$.

With an increase in velocity the range of limiting angles will be narrowed, and with a decrease in Re_1 number in the zone of its small values ($Re_1 < 10^5$) it is possible to obtain non-separable flow when $n = 4$ and angle $\alpha = 20^\circ$. The aforesaid is confirmed by data of an experiment given in Figs. 3-9e and 3-10b.

When $\lambda_1 \approx 0.4$ and $Re = 10^5$ the losses depend upon angle α weakly and even when $\alpha = 20^\circ$ consists of a magnitude of the order

of 27% (Fig. 3-9e). With an increase in velocity ($\lambda_1 = 0.85$) and $Re_1 < 2 \cdot 10^5$ number there occurs a sharp decrease in the coefficient of recovery of energy in the diffuser not only when $\alpha = 20^\circ$ but also when $\alpha \approx 10^\circ$ (Fig. 3-10b).

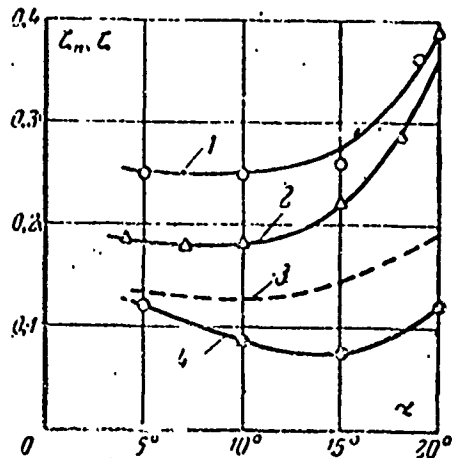
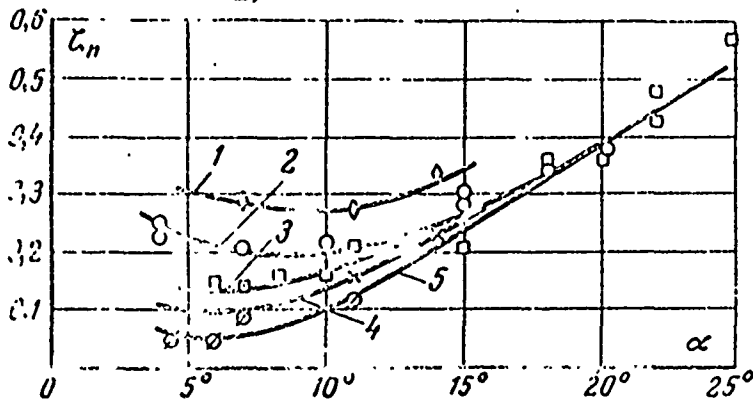


Fig. 3-14. Dependence of coefficients ζ_n and ζ upon angle α .

a): $\left. \begin{array}{l} 1-n=2,4; \\ 2-n=4,0; \end{array} \right\} \zeta_n = f(\alpha);$
 $\left. \begin{array}{l} 3-\zeta = f(\alpha); \\ 4-\zeta = f(\alpha); \end{array} \right\} n=2,4;$

b): 1 - $n = 2$; 2 - $n = 3$; 3 - $n = 4$; 4 - $n = 6$; 5 - $n = 10$ [$\lambda_1 = 0.4$; $Re_1 = (2-3) \cdot 10^5$].



b)

If the upper values of the critical angle depend upon a number of factors and are changed over wide limits, then the lower values are determined more accurately. In accordance with the experimental data, it is possible, apparently, to confirm that when $\alpha < 8^\circ$ the flow in diffusers has basically a nonseparable character.

The angular region from 8 to 15° is transient, but the region of nonseparable conditions and permissible expansion ratios is

still sufficiently wide. At angles from 15° to 20° the zone of nonseparable flows is extremely narrow, and when $\alpha > 20^\circ$ the flow has a clearly expressed separation character, whereupon separation is begun near the inlet section. This is indicated by the curve given in Fig. 3-14b.

If when $\alpha < 20^\circ$ total losses are noticeably changed with a change in the expansion ratio, then for $\alpha > 20^\circ$ all curves converge, and the dependence of value ζ_n on n in practice disappears.

By examining the nature of the change in total losses in the zone of nonseparable flow, it is possible to note their weak dependence upon angle α . At the same time internal losses noticeably fall with an increase in α and reach a minimum value near the limiting angle. The change in internal losses, depending on this value for diffusers with a constant expansion ratio ($n = 2.4$), is given in Fig. 3-14a (curve 4). The experimental points are obtained as a result of the traversing of entire outlet section of the diffuser and subsequent averaging taking into account the flow velocity component. Here, for a comparison, the dependence of internal losses (curve 3) upon angle α , obtained without allowing for the flow velocity component is plotted.

If at narrow angles ($\alpha < 5^\circ$) the method of averaging plays a comparatively small role, then when $\alpha = 10^\circ$ the divergence of the compared curves comprises 4%, and when $\alpha = 15^\circ$ the losses differ almost 2 times, and then with the emergence of separation this distinction is barely changed.

The given comparison indicates the fact that with an increase in the flare angle of the diffuser there occurs a noticeable deformation in the outlet velocity field, which leads to an increase in the ratio $c_{2\text{max}}/c_{2\text{cp}}$. Having calculated for the given case

the coefficient of energy N_2 in the outlet section, we obtain its continuous increase ($N_2 = 1.09$; $\alpha = 5^\circ$, $N_2 = 1.58$; $\alpha = 15^\circ$).

In other words, with an increase in angle α up to the limiting value, internal losses decrease, and losses with the outlet velocity increase. The decrease in coefficient ζ with an increase in angle α at a constant expansion ratio is explained by the decrease in length of the diffuser and, consequently, by the decrease in the rubbing surface. At the same time the deformation of the outlet velocity profile gives rise to the increase in the coefficient of losses with the outlet speed $\zeta_{B.C.}$. The intensity of the growth in coefficient $\zeta_{B.C.}$ when $\alpha > 7-8^\circ$ exceeds the intensity of the decrease in the coefficient of internal losses, and as a result of the optimum with respect to total losses appears shifted to the side of smaller α as compared with the optimum angle in internal losses.

In analyzing the influence of angle α , one should keep in mind that with its increase the effective expansion ratio increases. As a result the deformation of the velocity profile in the outlet section and as consequence the noted increase in the coefficient of energy N_2 occur. If with this the outlet losses are estimated according to the mean flow rate by relation

$$\zeta_{B.C.} = \left(\frac{\rho_1}{\rho_2} \right)^2 \frac{1}{\eta^2},$$

then the portion of losses unaccounted for here with outlet velocity enters into the internal losses and lowers the intensity of their change with an increase in angle α (Fig. 3-14). At narrow angles ($\alpha < 6-8^\circ$), when the flow is still distant from the pre-separation state, this portion of outlet losses is insignificant and cannot change the nature of the dependence of the coefficient of losses ζ_{Π} upon angle α . With an approach to the pre-separation state coefficient N_2 and the total losses begin to grow with an increase in angle α .

By estimating the internal losses according to the difference between total losses and losses with the outlet velocity, calculated according to the formula $\zeta_{B.C.} = 1/n^2$, we obtain that the optimum value of the angle is 6-10°. During probe diffuser tests, when averaging is conducted without allowing for the flow component, the portion of losses indicated above with the outlet velocity is also automatically included into the internal losses.

When estimating the total losses in principle it is no different than when averaging is conducted: taking into account the flow velocity component or without it, since they represent the sum of internal and outlet losses, and the method of averaging leads only to the redistribution of components of total losses.

The aforesaid is confirmed by the experimental data in Fig. 3-15, where given are test data of a series of conical diffusers with a constant expansion ratio $n = 2.33$ for four values of the M_1 number. Here it is possible to distinguish three zones. With an increase in the angle up to 6° a reduction in losses occurs. Then when $6^\circ < \alpha < 15^\circ$ the losses comparatively weakly increase (in practice according to the linear law). This zone is characterized by the high-frequency pulsations induced by the appearance of small nonstationary separation zones. However, the developed separation zones are not detected, and the losses increase a total of 3-5%. The extent of the second zone depends upon the Mach number at the outlet into the diffuser and Re_1 number and is continuously reduced with an increase in M_1 .

When $\alpha > 15-20^\circ$ the losses intensely increase, and the flow acquires a pulsing character with clearly expressed vortex regions carried downstream, whereupon the ripple frequency decreases with an increase in the angle.

Thus, minimum losses correspond to the comparatively narrow angular region (6-10°). For the purpose of decreasing the axial

dimensions of the diffusers, it is admissible for low velocities and high Re_1 numbers to use angles of the order of 15° (without a noticeable deterioration of aerodynamic characteristics). By explaining such a pronounced influence of angle α on the flow pattern in the diffusers, authors of some works [34, 54] make attempt to connect value α with the Buri [Translator's note: name not verified] parameter Γ and thus explain not only the deformation of the velocity profile in the outlet section but also the emergence of separation when $\alpha > \alpha_{np}$.

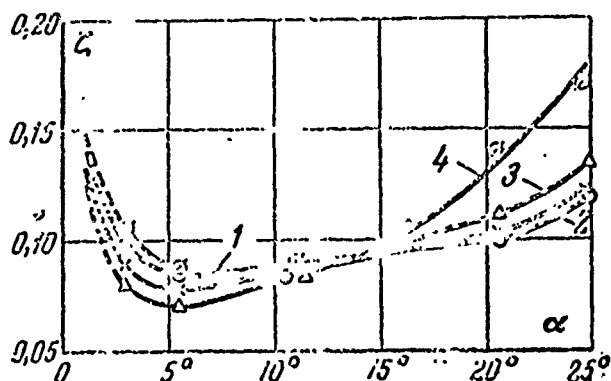


Fig. 3-15. Dependence of ζ upon angle α at various initial velocities.

1 - $M_1 = 0.25$; 2 - $M_1 = 0.4$;
3 - $M_1 = 0.51$; 4 - $M_1 = 0.7$.

The reasoning is based on fact that with an increase in angle α there occurs a growth in parameter Γ in connection with the growth of both the velocity gradient dc/dx and the boundary layer thickness. As a result value Γ rapidly reaches the separation value Γ_s , and a further increase in the angle gives rise to the displacement of the separation point against the flow. However, it is not complicated to show that the Buri parameter Γ does not depend upon angle α , and, consequently, the considerations given above prove to be invalid.

In fact, let us rewrite (1-26) in the following form:

$$\Gamma = \frac{dc}{dx} \cdot \frac{\delta^{**1,25}}{c^{0,75} v^{0,25}} = \frac{d\bar{c}}{d\bar{x}} \cdot \frac{\bar{\delta}^{**1,25}}{\bar{c}^{0,75}} \left(\frac{Lc_1}{v} \right)^{0,25},$$

where accepted as the velocity scale is the velocity at the inlet into the diffuser, and the length scale - the length of the generatrix L .

The dimensionless momentum thickness $\bar{\delta}^{**}$, the velocity \bar{c} and the velocity gradient are determined only by the dimensionless coordinate \bar{x} and for assigned expansion ratio do not depend upon angle α . For the laminar boundary layer this conclusion was made by Pol'gauzen [111].

Thus, in the explanation of separation in diffusers with an increase in angle α , one should proceed from different premises. Specifically, let us note that with an increase in angle α at an invariable relative length there occurs a reduction in the reverse effect of the boundary layer, and the effective expansion ratio approaches the geometric, i.e., an increase in the actual expansion ratio occurs. Furthermore, an increase in the angle causes a significant local disturbance at the inlet into the diffuser. This disturbance lowers the boundary layer stability and gives rise to its separation when $\alpha > \alpha_{np}$.

The influence of conditions of entry (evenness of transition) is illustrated by velocity profiles in the outlet section of the seven-degree diffuser given in Fig. 3-16. If at angular fracture ($r_1 = 0$) in the transition point to the diffuser part in the outlet section was fixed detached flow, then the rounding of angle ($r = 2$ mm) gave rise to the liquidation of the separation. The last fact gives the basis to connect the emergence of separation with the degree of the inlet disturbance induced by the angular fracture.

If the flow plane contains singular points of the pole type, then in their environs the common boundary layer theory is inapplicable, and in this region a special analysis of the flow is required. The aforesaid results from the sense of Prandtl equations, since near the angular points $\partial p / \partial y \neq 0$.

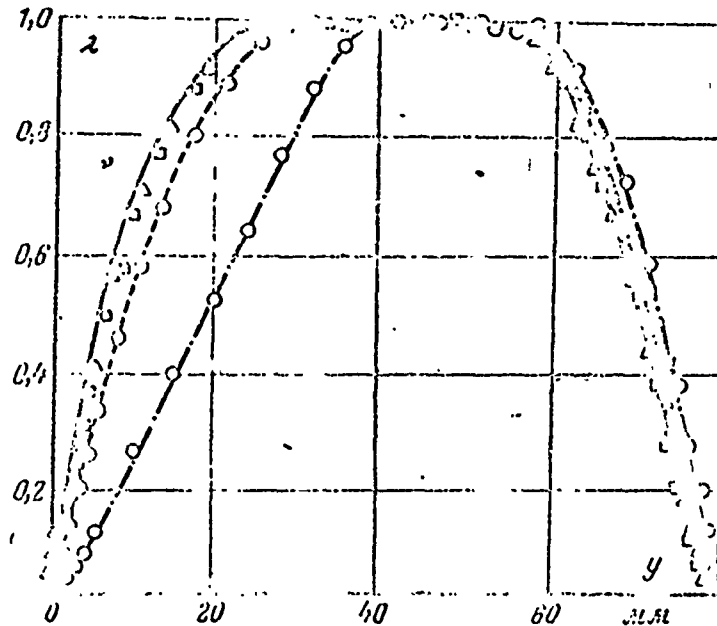


Fig. 3-16. Velocity profiles at the inlet section of the conical diffuser under various conditions of the inlet ($\alpha = 7^\circ$; $n = 4$; $\lambda_1 = 0.82$). $\circ - r_1 = 0$; $\bullet - r_1 = 1$ mm; $\square - r_1 = 2$ mm; $\Delta - r_1 = 4$ mm.

In the remaining space, excluding the zone of separation, where also $\partial p / \partial y \neq 0$ [65], it is possible to use as a basis methods and derivation of the boundary layer theory used for the internal problem. However, unlike the external problem, here the reverse effect of the boundary layer on the distribution of pressures along the limiting walls is considerably greater and can lead to a substantial deviations of results from values calculated for the ideal fluid.

For a solution to the problem of the flow pattern in diffusers, apart from a general analysis based upon the known distribution of pressures and velocities, it is necessary to examine the fluid flow with finite viscosity near angular points and explain the validity of the assumption made above about the role of angular fractures. For this purpose let us examine results of an investigation of the plane channel depicted in Fig. 3-17a and which is a unidirectional diffuser with flare angles α equal respectively to 5, 10, 20 and 30°.

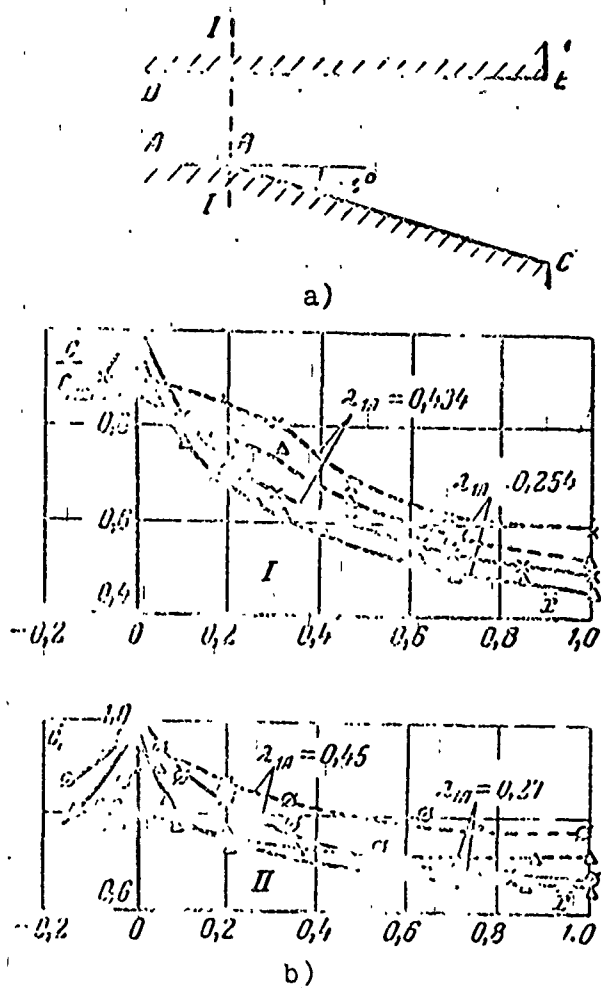


Fig. 3-17. Diagram of the channel investigated a) and the change in relative velocities in this channel b). I - $\alpha = 10^\circ$; II - $\alpha = 20^\circ$; — - along wall ABC; - - - - along wall DE.

For an experimental estimate of the velocities both the lower and upper walls of the channel had a series of drain holes, and in fracture zone they were located at a distance of 1-2 mm from each other. Furthermore, directly in section I-I (Fig. 3-17a) with the help of a stanton tube the boundary layer velocity profile, which allowed obtaining a representation about the disturbance introduced by the fracture was measured.

Figure 3-17b gives values of the relative velocity along the wall ABC at various values of the dimensionless velocity at initial point A (λ_{1A}) for two values of angle α equal to 10° and 20° . For the convenience of comparison the current velocity everywhere refers to the velocity at point B. All velocities here

are calculated according to static pressure on wall p_1 and the initial pressure p_0 .

From the curves it is evident that influence of the fracture has quite a great effect and is extended for a considerable distance upstream. With an approach to the angular point the velocity on the small section increases by almost 30%, and then just as sharply its decrease in the diffuser part occurs. Simultaneously it is possible to note that on the opposite wall DE the velocity increases by a total of 2-5%.

The indicated results from the qualitative side agree well with theoretical solutions for the flow of ideal fluid about a convex angle [64]. However, the absolute velocity increase remains limited although very noticeable.

By estimating the practical velocity increase near the pole, V. V. Golubev [20] considers that the pressure force at this point cannot be less than the friction forces. Hence, by knowing the order of minimum pressure, it is possible to determine the order of maximum velocity. Such an approach is more physically substantiated and allows conducting certain quantitative estimations.

For a comparison of the theory with experimental data, it is hardly possible to use the curves given above, since near the angular point not only a longitudinal but also a substantial transverse pressure gradient should take place even within limits of the boundary layer. This is confirmed completely by the measurements of static pressure across the channel with the help of a stanton tube of static pressure [52].

From the given results it follows that the disturbances introduced into flow by the fracture increase with an increase in the M_1 number and depend upon the angle of fracture α . A clear

representation about the influence of the indicated parameters near the point in question can be obtained from Fig. 3-18. Plotted here along the axis of the ordinates is the mean flow rate in section I-I (see Fig. 3-17a) and along the axis of the abscissas - the local velocity in the section of fracture on both walls of the channel. In the indicated coordinates the degree of deviation of the experimental points from the bisectrix gives the difference between the local and average velocities at various angles in the whole subsonic (in average speeds) range.

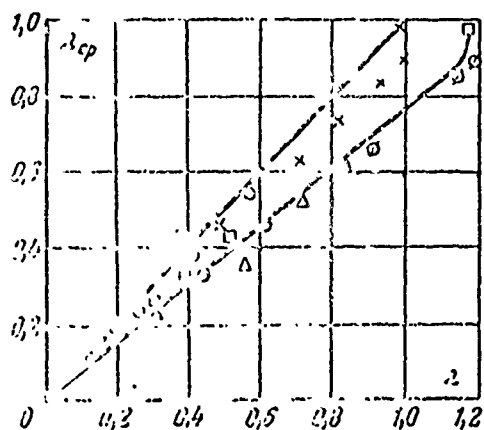


Fig. 3-18. Dependence between the average (λ_{cp}) and local (λ) relative velocities at the inlet into the diffuser. \square - $\alpha = 5^\circ$; \emptyset - $\alpha = 10^\circ$; Δ - $\alpha = 20^\circ$ - wall ABC; \times - $\alpha = 10^\circ$; o - $\alpha = 20^\circ$ - wall DE.

It is evident that on wall DE the local velocities coincide in practice with the mean value and are somewhat increased with the approach to the speed of sound. On wall ABC at point B the difference in question proves to be substantial and almost in the whole subsonic range is equal to 30-35%. With this the absolute divergence between the velocity at point B and its mean value continuously increases. For $\lambda_{cp} = 0.75$ $\lambda_B = 1$. A further increase in the average velocity gives rise to the appearance near the fracture of the zone of local supersonic velocities. The transverse extent of the region of increased velocities is small. However, its influence on the further development of flow in the part of the channel being expanded frequently proves to be decisive, since it gives rise to the sharp increase in the local positive pressure gradients.

Bearing in mind what has been said, let us examine the dependence of maximum velocity at point B upon α . This dependence, given in Fig. 3-19, proves to be discontinuous. First, with an increase in angle α the local acceleration of the flow increases continuously. Then when $\alpha > 10^\circ$ the intensity of this growth is slowed down, and when $\alpha = 20-25^\circ$ function $\lambda_B/\lambda_{cp} = f(\alpha)$ undergoes discontinuity, and the local velocity approaches the mean value. With an increase in velocity the point of discontinuity is displaced to the side of smaller angles, and the disturbance introduced by the fracture increases.

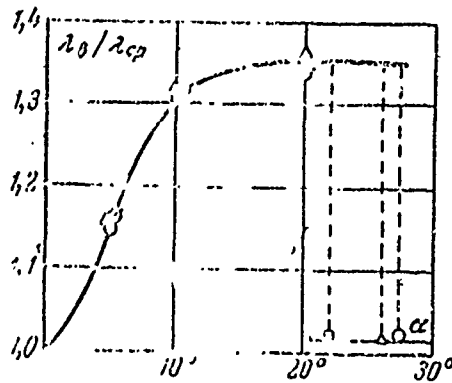


Fig. 3-19. Dependence of maximum velocity at the fracture point on angle α and average velocity λ_{cp} .
 $\circ - \lambda_{cp} = 0.2$; $\Delta - \lambda_{cp} = 0.44$;
 $\square - \lambda_{cp} = 0.65$.

Thus, if angle α is comparatively small, then the disturbance induced by them does not have a substantial influence on the subsequent flow, and the position of the separation point can be determined on the basis of the theory of the boundary layer. However, with an increase in the angle the zone of the disturbed flow includes more significant regions and substantially increases the local positive pressure gradient directly at the inlet into the diffuser (see Fig. 3-17b), which gives rise to a reduction in the stability of the velocity profile, and in flow local zones of nonstationary separations appear.

The theoretical calculation of the indicated flow is extremely complex, and thus far it has been necessary to be

oriented on experimental data which, incidentally, due to the nonstationary character of the flow are also rather inconsistent.

It is natural that the emergence of nonstationary separation in the angular region in question ($\alpha = 10-25^\circ$) depends upon the total expansion ratio of the diffuser n . The larger the angle, the less the limiting value n , which ensures the nonseparable flow. Let us note simultaneously that an analogous conclusion can be made with respect to the compressibility effect (the more velocity at the assigned angle α , the less the limiting value of the expansion ratio should be). The reason for such a limitation is clear from the previous presentation.

By examining finally diffusers with angles greater than 20° , it is possible to note the emergence of the separation directly at the inlet section. From this moment the flow in the diffuser acquires a stream character, and the influence of angular point B upstream is little. In Fig. 3-19 the transition to the indicated flow conditions corresponds to the point of discontinuity.

With the emergence of the stream separation the flow in the diffuser becomes identical with the flow at sudden expansion, and for the evaluation of the power losses ζ it is possible to use the widely known formula (2-42a). In connection with this it is interesting to indicate that the values obtained here of angles which correspond to the transition to stream separation in a rectangular diffuser coincide for low velocities with the data given in work [54], where the value $\phi_{\Delta} = \phi(\alpha)$ becomes equal to one for angle $\alpha = 26^\circ$.

Thus, the presence in the flow of angular points can decisively influence the flow pattern in the subsequent diffuser regions, since the introduced disturbances will noticeably redistribute the velocities in the cross section of the channel. The indicated disturbances are somewhat decreased if in front of the fracture

there is an inlet section. Then the inlet boundary layer gives rise to the smooth change in longitudinal velocities, "smoothing" the influence of the fracture. It is necessary, true, to keep in mind that, by decreasing the disturbance induced by the fracture, the inlet boundary layer deteriorates the aerodynamic characteristics of the diffusers and also promotes early separation. However, in this case the possible point of separation is located in the expanded part of the channel, and its position can be predicted as a result of theoretical calculations.

In the examination of flow at the inlet section of the diffuser the author of work [5] made a theoretical conclusion about the inevitability of separation if the length of the section in front of the diffuser exceeds two inlet gauges and angle $\alpha > 6^\circ$.

The experimental data given above obtained at the inlet section equal to three gauges, and subsequent experiments with a longer inlet, and also data examined in the works [21, 88, 89, 140] indicate the nonseparating state of the flow at angles which considerably exceed 6° . This fact is especially brought out in work [88]. In our experiments even when angle $\alpha = 20^\circ$ the flow in the inlet region of the diffuser had a nonseparable character, and only in the subsequent sections did nonstationary separation appear. This is indicated by experimental values of the coefficient of the recovery of pressure given on Figs. 3-9 and 3-10.

The study of the flow pattern near angular points can give valuable data for the explanation of the critical increase in diffuser losses in transonic conditions, when with an increase in velocity there occurs a sharp increase in the inlet disturbance and, as a consequence, the separation of flow near the inlet section.

In connection with that stated we will discuss the question of the rational law of the decrease in velocity along the axis of the diffuser, which ensures minimum losses and the greatest zone of nonseparable flow. For this purpose let us examine the following laws of the change in the dimensionless velocities:

$$\frac{c}{c_1} = 1 - \bar{x} \frac{n-1}{n}; \quad (3-7a)$$

$$\frac{c}{c_1} = \frac{1}{1 + \bar{x}(n-1)}; \quad (3-7b)$$

$$\frac{c}{c_1} = 1 - \sqrt{\bar{x}} \frac{n-1}{n}. \quad (3-7c)$$

Curves which correspond to these dependences when $n = 2$ are given in Fig. 3-20. It is not difficult to see that the formula (3-7b) corresponds to the theoretical decrease in the velocity in a plane diffuser when $\rho = \text{const}$.

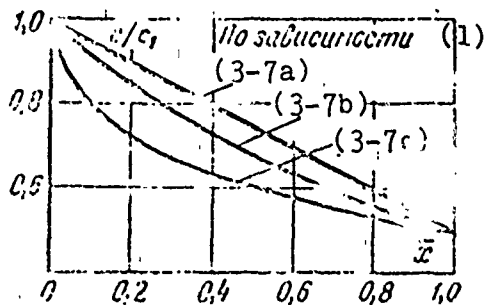


Fig. 3-20. Different laws of the velocity change in the diffuser.
KEY: (1) According to relation.

Having calculated from formulas (3-7a), (3-7b) and (3-7c) the value of parameter Γ , we obtain for the case of formula (3-7a):

$$\Gamma = 3,24 \cdot 10^{-3} \left[1 - \frac{1}{\left(1 - \bar{x} \frac{n-1}{n} \right)^{4,62}} \right]; \quad (3-8a)$$

when using of formula (3-7b)

$$\Gamma = 5,5 \cdot 10^{-3} \{ [1 + \bar{x}(n-1)]^{2,62} - 1 \} \quad (3-8b)$$

and formula (3-7c)

$$\Gamma = 5,5 \cdot 10^{-3} \frac{n}{(n-1)} \cdot \frac{1}{\sqrt{\bar{x}}} \times \left[\frac{1}{\left(1 - \sqrt{\bar{x}} \frac{n-1}{n}\right)^{4,32}} - 4,72 \frac{n-1}{n} \sqrt{\bar{x}} \right], \quad (3.8c)$$

The curves plotted according to these formulas of the change in parameter Γ along the diffuser for $n = 2$ (Fig. 3-21) show that the intensity of its growth substantially depends upon the law of the velocity change. With the linear law (3-7a) the separation value Γ_s is reached in the section $\bar{x} = 0.85$. However, on the initial section value Γ proves to be minimum, i.e., from the point of view of disturbances at the inlet, it is advantageous to have as far as possible a smooth transition to the diffuser section. With a sharp decrease in velocity at the inlet [law (3-7a)] parameter Γ attains in this region the maximum value, although in finite sections its values are less than those with a linear dependence for velocity.

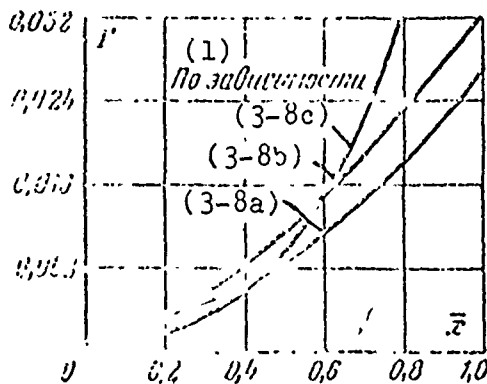


Fig. 3-21. Change in parameter Γ along the diffuser at various laws of the velocity change.

KEY: (1) According to relation.

Thus, for the provision of nonseparable flow in finite sections, it is advantageous to have in the region of the minimum section a sharper decrease in the velocity. The examination of laminar flow in the diffuser leads to this result.

At the same time for short diffusers, when angle $\alpha > 11^\circ$ and the effective expansion ratio approaches the geometric, it is advantageous to provide a smooth transition from the cylindrical

section to the expanded channel. In this case the so-called isograde diffusers, having at $L/D_1 < 2$ somewhat smaller losses than the plane diffusers are most frequently used.

However, at angles $\alpha < 10-11^\circ$ and $L/D_1 > 2$ it is most advantageous to use common conical or plane diffusers, and at low speeds it is admissible to change to diffusers with increased expansion near the inlet section. The shape of such a diffuser is shown in Fig. 3-22a.

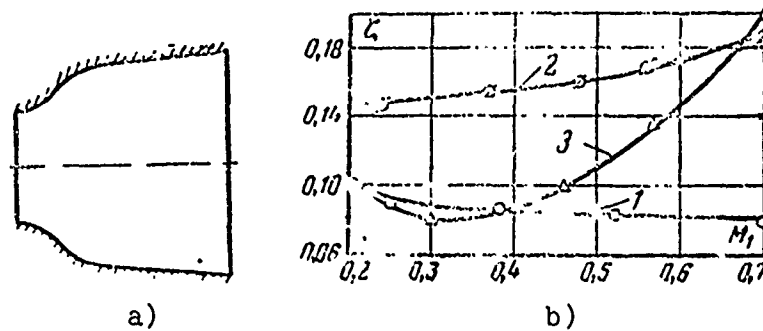


Fig. 3-22. Diagram of a profiled diffuser a) and the dependence of coefficient ζ upon M_1 for various diffusers b) ($n = 2.33$). 1 - conical diffuser; 2 - isograde diffuser; 3 - profiled diffuser.

The considerations stated are confirmed well by curves of losses in Fig. 3-22b. Let us note that when $n = 2.33$ and the relative length $L/D_1 = 2$, only in the conical diffuser does non-separable flow take place in a wide range of M_1 numbers. In an isograde diffuser (curve 2) separation occurs during all conditions and in a diffuser with the inverse curvature of the wall (curve 3) at $M_1 > 0.45$, when the local inlet velocity gradient noticeably increases.

The analysis conducted of the influence of the flare angle on the flow pattern in diffuser channels shows that α essentially characterizes the degree of the inlet disturbances. The magnitude of the latter increases intensely both with an increase in the angle and with an increase in the inlet velocity. Here the local pressure gradients considerably exceed values of $\partial p / \partial x$ calculated

according to the mean flow rate.

For a reduction in the negative effect of angular fractures, the small rounding of the diffuser inlet section frequently proves to be sufficient. Thus, in Fig. 3-16 examined above when $r_1 = 0$, when the transition from a cylindrical to a conical section was accomplished without rounding, in the exit section of the diffuser the flow had a separation character, and when $r_1 = 1$ mm separation was eliminated, despite the high inlet velocities. A further change in radius r_1 no longer gave rise to any noticeable deformation of outlet profile.

The dependence of the coefficient of recovery of energy upon number λ_1 (Fig. 3-23) also shows that the smooth coupling of the diffuser with the inlet section even with a small radius ($r_1 > 2$ mm) substantially decreases the losses.

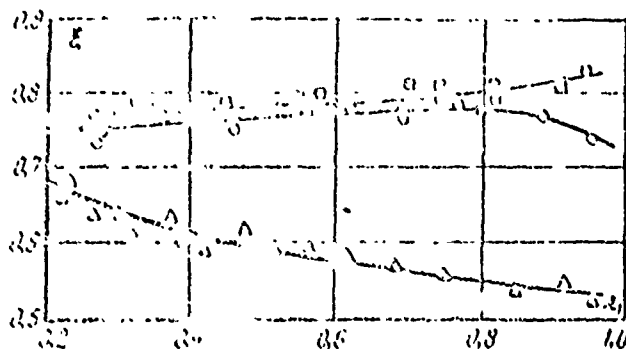


Fig. 3-23. Effect of the inlet into the diffuser on the coefficient of pressure recovery.

□, ○, △ - $r_1 = 2.0$ mm;
 ■, ●, ▲ - $r_1 = 4$ mm; □, ■ - $\alpha = 7^\circ$; ○, ● - $\alpha = 10^\circ$;
 △, ▲ - $\alpha = 20^\circ$.

The influence of the last of the determining geometric parameters of conical diffusers (value L/D_1) on the total loss factor ζ_n essentially was already examined above. In explicit form the relations

$$\zeta_n = f(L/D_1) \text{ for } n = \text{const}$$

are given in Fig. 3-24a and for $\alpha = \text{const}$ in Fig. 3-24b. In both the first and second cases (except $\alpha > 22^\circ$) with an increase in the length, the total losses continuously decrease. The decrease

in coefficient ζ_n in Fig. 3-24a is connected with the fact that an increase in parameter L/D_1 occurs with a simultaneous decrease in angle α , and in Fig. 3-24b the latter is explained by the growth in the expansion ratio. Both the decrease in angle α and the growth in value n lower losses with the outlet velocity, and the certain increase in internal losses with an increase in the length of the diffuser cannot substantially influence the character of the dependence $\zeta_n = f(L/D_1)$.

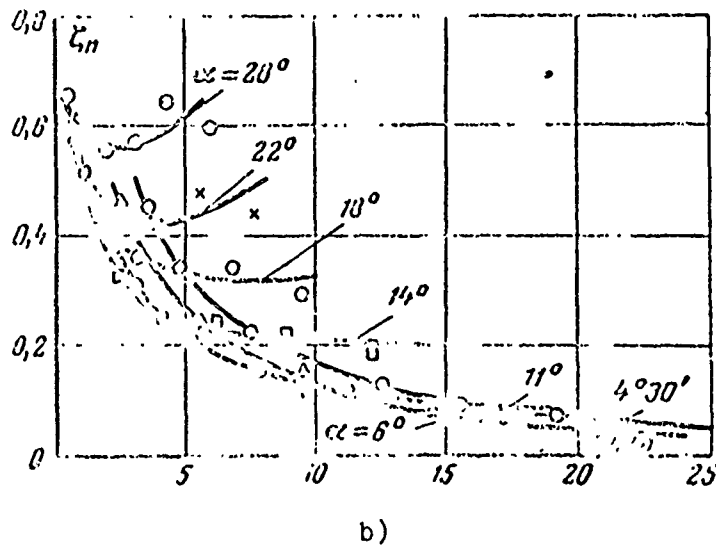
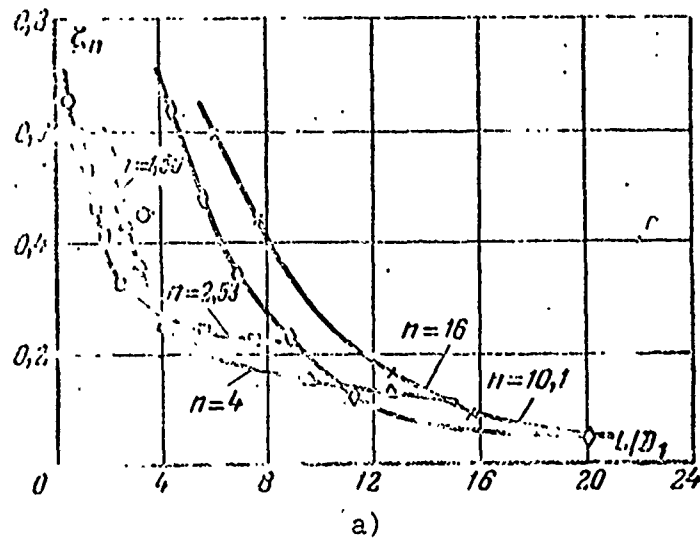


Fig. 3-24. Dependence of the total loss factor upon value L/D_1 . a) $n = \text{const}$; b) $\alpha = \text{const}$.

The examined experimental data refer to the axisymmetric diffusers. However, they are completely used for an analysis of the flow in plane channels. True, this analysis is somewhat complicated for diffusers whose width B is commensurable with the height H (see Fig. 2-1a), since in this case the magnitude of losses is significantly affected by the correlation of longitudinal and transverse dimensions of the inlet and outlet sections.

§ 3-4. Calculation of Losses in Conical and Plane Diffusers According to Boundary layer Characteristics

The calculation of the effectiveness of diffusers is reduced finally to the estimation of coefficients of total (ξ) and internal (ξ_{in}) losses. At known boundary layer characteristics in the outlet section of the diffuser channel, the values of these coefficients are defined by relations

$$\xi_{\text{in}} = \left(\frac{p_1}{p_2} \right)^2 \frac{1}{n^2 (1 - \bar{\Delta}^{*2})^2}; \quad (2-29)$$

$$\xi = \left(\frac{p_1}{p_2} \right)^2 \frac{\bar{\Delta}^{***2}}{n^2 (1 - \bar{\Delta}^{*2})^2}, \quad (2-37)$$

where $\bar{\Delta}^*_2$ and $\bar{\Delta}^{***}_2$ - the relative areas of displacement and energy losses connected with the velocity profile c_{2l} in the outlet section and with the arbitrary velocity c_0 which corresponds to the pressure ratio p_2/p_{01} :

$$\bar{\Delta}^{*2} = \int_0^1 \left(1 - \frac{c_{2l}}{c_0} \right) d \left(\frac{F}{F_2} \right);$$

$$\bar{\Delta}^{***2} = \int_0^1 \frac{c_{2l}}{c_0} \left(1 - \frac{c_{2l}^2}{c_0^2} \right) d \left(\frac{F}{F_2} \right).$$

If in the center of the flow the potential core (the zone where $p_{01} = p_{02\text{max}}$) is preserved, then $c_0 = c_{2\text{max}}$ and the

introduced values $\bar{\Delta}^*_2$ and $\bar{\Delta}^{***}_2$ are identical with the relative area of displacement $\bar{\delta}^*_2$ and the area of the energy loss $\bar{\delta}^{***}_2$ determined from formulas (1-3) and (1-5).

If $p_{01} > p_{02\text{макс}}$, then $\bar{\Delta}^*_2 > \bar{\delta}^*_2$ and $\bar{\Delta}^{***}_2 > \bar{\delta}^{***}_2$. Above it was noted that condition $p_{01} = p_{02\text{макс}}$ for nonseparable flow is disturbed not only with the joining of the boundary layer but also somewhat earlier under the adverse conditions of the entry into the diffuser and increased flow turbulences. Considerable distinctions between pressures p_{01} and $p_{02\text{макс}}$ and respectively between velocities c_0 and $c_{2\text{макс}}$ in the case of nonseparable flow take place at comparatively large expansion ratios ($n > 3$), when values of the coefficients ζ_n are small and the absolute error of the calculations is found within limits of the accuracy of the experiment ($\Delta\zeta_n \approx 3-5\%$).

For an example Fig. 3-25 gives the correlations between velocities $c_0(\lambda_0)$, $c_{2\text{макс}}(\lambda_{2\text{макс}})$ and $c_{2\text{ср}}(\lambda_{2\text{ср}})$ in a seven-degree diffuser with various expansion ratios n . With an increase in this parameter average speed (curve 1) is decreased most sharply. The intensity of the decrease in the maximum speed ($\lambda_{2\text{макс}}$), determined according to the maximum pressure of full stagnation of the inlet section and static pressure p_2 , is noticeably less (curve 2), and the arbitrary velocity λ_0 coinciding with the rate $\lambda_{2\text{макс}}$ up to $n = 2.0$ is reduced only by 66% of the initial velocity λ_1 , but then when $n > 4$ it is almost not changed (curve 3).

Thus, in practice for important expansion ratios ($n < 4$) it is possible not to take into consideration the drop in pressure of the full stagnation, and to use the common definition of integral areas of the boundary layer.

From the aforesaid it is clear that the accuracy of determining coefficients ζ_n and ζ depends upon the accuracy of the computation of values $\Delta^*(\delta^*_2)$ and $\Delta^{***}_2(\delta^{***}_2)$. For a calculation

of the arbitrary thicknesses let us use formula (1-32) and convert it taking into account the axial symmetry of the problem, to the form [69]

$$\frac{\delta^{*2}}{L} = \frac{0,033}{Re_1^{0,2} c_2^{0,34} D_2} \left[\int_0^1 \bar{D}^{1,25} \bar{c}^{0,67} d\bar{x} \right]^{0,8} \quad (3-9)$$

(here $\bar{D} = D_1/D_2$).

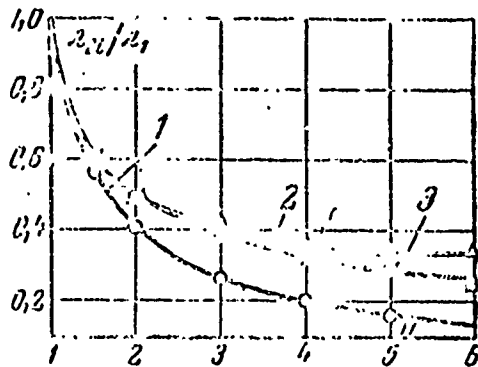


Fig. 3-25. Dependence of relative velocities in the inlet section upon the expansion ratio n .

1 — λ_{203}/λ_1
 2 — λ_{1110}/λ_1
 3 — λ/λ_1

The dimensionless velocity $\bar{c} = c/c_1$ entering here is determined by the law of the change in area along the channel. However, as was already mentioned above, in plane and conical diffusers the nature of its change along the x axis is considerably different from the theoretical dependence.

If in the initial section the agreement of experimental and calculation data still takes place, then with an approach to the outlet section due to the growth in the boundary layer the decrease in velocity is sharply reduced (see Fig. 3-8b).

Consideration of the reverse effect of the boundary layer can be realized if we introduce the local area of displacement δ^*_1 into the examination. Then from the continuity equation the law of the velocity change in the diffuser channel will be expressed by the following relation:

Reproduced from
best available copy.

$$\frac{c}{c_{10}} = \frac{\rho_1 \bar{v}_1 (1 - \delta^{*2}_1)}{\rho_2 \bar{v}_2 (1 - \delta^{*2}_2)} \quad (3-10)$$

With a comparatively thin boundary layer

$$\bar{\delta}^{*2}_2 = \frac{\delta^{*2}_2}{D_2} \quad (3-11)$$

If the boundary layer occupies almost the entire channel, then the correlation between the relative area of displacement $\bar{\delta}^{*2}_2$ and the thickness δ^{*2}_2 proves to be more complex:

$$\delta^{*2}_2 = \frac{D_2}{2} (1 - \sqrt{1 - \bar{\delta}^{*2}_2}) \quad (3-11a)$$

The combined use of equations (3-9), (3-10) and (3-11a) gives rise to the following integral equation, which determines the area of displacement $\bar{\delta}^{*2}_2$:

$$\bar{\delta}^{*2}_2 = 1 - \left\{ 1 - B \frac{(1 - \bar{\delta}^{*2}_2)^{1.4}}{2\sqrt{n}} \left[\int_0^1 \frac{dx}{D^{0.8} (1 - \delta^{*2}_1)^{1.02}} \right]^{0.8} \right\}^2 \quad (3-12)$$

Here

$$B = \frac{0.144H}{Re_1^{0.2}} \left(\frac{L}{D_1} \right)^{0.8}; \quad H = \frac{\delta^*}{\delta^{*2}}$$

Quantity H depends basically upon the expansion ratio n and relative length L/D₁.

As a first approximation let us assume

$$H = \frac{\delta^*}{\delta^{*2}} = 1.4 \left[1 + \frac{\sqrt{n} - 1}{(L/D_1)^{0.12}} \right] \quad (3-13)$$

Qualitatively the relation (3-13) expresses that fact that with an increase in the expansion ratio at constant length \bar{L} the velocity profile in the outlet section approaches the separation form for which coefficient H = 2-2.8 [71, 111] when n = 1 H = 1.4, which corresponds to its value for the gradient-free flow.

The degree of approximation (3-13) can be judged from Fig. 3-26, where experimental values of parameter H, obtained by L. G. Golovina and V. V. Ett as a result of the traversing of the outlet velocity field of the diffuser with $\alpha = 7^\circ$ are given.

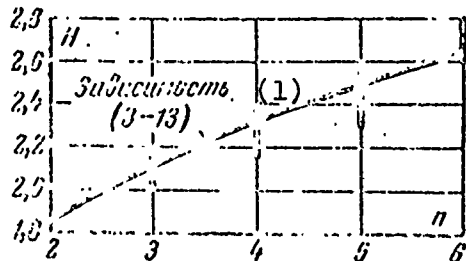


Fig. 3-26. Change in parameter H depending on the expansion ratio n. ████████ - zone of experimental values H for $M_1 = 0.5-0.8$ (experiments of MEI).

KEY: (1) Relation.

Using the obvious relation

$$\bar{D}_1 = \frac{D_1}{D_2} = \frac{1 + \bar{x}(\sqrt{n} - 1)}{\sqrt{n}} \quad (3-13a)$$

let us present (3-12) in the form

$$\bar{\delta}_2^* = 1 - \left\{ 1 - B \frac{(1 - \bar{\delta}_2^*)^{2.02}}{2} n^{2.02} \times \left[\int_0^1 \frac{dx}{[1 + \bar{x}(\sqrt{n} - 1)]^{2.02} (1 - \bar{\delta}_1^*)^{2.02}} \right]^{0.8} \right\}^2$$

and express the current area of displacement $\bar{\delta}_1^*$ in the following manner:

$$\bar{\delta}_1^* = \bar{\delta}_2^* f(\bar{x}). \quad (3-14)$$

The unknown function $f(\bar{x})$, which determines the law of the change in value $\bar{\delta}_1^*$ along the \bar{x} axis, continuously increases from zero to one and can be approximated by the power function of the form:

$$f(\bar{x}) = \bar{x}^m.$$

Then

$$\bar{\delta}_2^* = 1 - \left\{ 1 - B \frac{(1 - \bar{\delta}_2^*)^{3.34} n^{2.34}}{2} \times \right. \\ \left. \times \left[\int_0^1 \frac{d\bar{x}}{[1 + \bar{x}(\sqrt{n} - 1)]^{0.6} (1 - \bar{x}^m \bar{\delta}_2^*)^{0.92}} \right]^{0.9} \right\} \quad (3-15)$$

or

$$\bar{\delta}_2^* \cong B (1 - \bar{\delta}_2^*)^{3.34} n^{2.34} \times \\ \times \left[\int_0^1 \frac{d\bar{x}}{[1 + \bar{x}(\sqrt{n} - 1)]^{0.6} (1 - \bar{x}^m \bar{\delta}_2^*)^{0.92}} \right]^{0.9} \quad (3-15a)$$

In equation (3-15) at fixed values of quantities m and n , a unique unknown is the area of displacement $\bar{\delta}_2^*$ at the outlet of the diffuser.

Concrete calculations show that the change in the exponent m in rather wide limits (from 0.5 to 1.0) changes the final result little. On this basis it would be possible to use the simplest linear approximation. However, experimental values $f(\bar{x})$ (Fig. 3-27) show that good agreement with experiment takes place when $m = 0.8$.

The structure of the expression obtained for $\bar{\delta}_2^*$ is complex, and its solution in each case requires significant computational work, which lowers the practical value of the examined method. In this connection L. M. Dyskiny conducted computations of the area of displacement $\bar{\delta}_2^*$ for a whole series of conical diffusers on a digital computer. Results of the calculations are given in the Appendix (see Fig. A-1) in the form of a nomogram. Using the expansion ratio n as a parameter, it is possible to construct value $\bar{\delta}_2^*$ depending on coefficient

$$B = \frac{0.20}{\text{Re}_1^{0.2}} \left(\frac{L}{D_1} \right)^{0.8} \left[1 + \frac{\sqrt{n} - 1}{(L/D_1)^{0.2}} \right] \quad (3-16)$$

Thus, the entire calculation is reduced to the definition of coefficient B and finding on the nomogram of the area of

$$\Delta^{***}_1 = \frac{0,036H^*}{Re_1^{0,2}} \left(\frac{L}{D_1}\right)^{0,3} \frac{D_1}{(c_1/\bar{c}_1)^{1,2}} \bar{x}^{0,8}.$$

Hence

$$d\Delta^{***}_1 = \frac{0,0283H^*}{Re_1^{0,2}} \left(\frac{L}{D_1}\right) \frac{D_1 d\bar{x}}{\bar{c}_1^{0,2} \bar{x}^{0,2}}. \quad (3-17)$$

Here $H^* = \Delta^{***}/\Delta^{**}$ (for gradient-free flow $H^* = 1.8$). Having substituted (3-17) into expression (2-54), and having replaced the ratio of velocities \bar{c}_1 according to formula (3-10) and the ratio of diameters according to relation (3-13a), we obtain:

$$\Delta^{***}_2 = \frac{0,0288}{Re_1^{0,2}} H^* D_1 \left(\frac{L}{D_1}\right)^{0,3} (1 - \bar{\Delta}^*_2)^3 n^{0,2} \times \\ \times \int_0^1 \left(\frac{\rho_2}{\rho_1}\right)^{1,8} \frac{n^{2,3} d\bar{x}}{[1 - (V\bar{n} - 1)\bar{x}]^{4,0} (1 - \bar{\Delta}^*_2)^3 \bar{x}^{0,2}}.$$

Let us use for the relative area $\bar{\Delta}^*_1$ the relation of the (3-14) type with the same function $f(\bar{x})$ as earlier, and let us pass from the energy thickness to the relative area of displacement $\bar{\Delta}^*_2$, keeping in mind that

$$\Delta^{***}_2 = \frac{H^*}{H} \Delta^*_2 = \frac{H^*}{H} \cdot \frac{D_2}{2} (1 - \sqrt{1 - \bar{\Delta}^*_2}).$$

As a result the integral equation which determines the area of displacement takes the form

$$\bar{\Delta}^*_2 = 1 - \left[1 - B_1 \frac{(1 - \bar{\Delta}^*_2)^3}{2} n^2 \times \right. \\ \left. \times \int_0^1 \left(\frac{\rho_2}{\rho_1}\right)^{1,8} \frac{\bar{x}^{-0,2} d\bar{x}}{[1 - (V\bar{n} - 1)\bar{x}]^{4,0} (1 - \bar{x}^{0,8} \bar{\Delta}^*_2)^{2,8}} \right]^2, \quad (3-18)$$

where the parameter

$$B_1 = \frac{0,115}{Re_1^{0,2}} \left(\frac{L}{D_1}\right)^{0,8} H. \quad (3-19)$$

As yet let us eliminate the density ratio ρ_2/ρ_1 appearing in formula (3-18) from the examination, since the density is changed basically only on the initial section of the diffuser, and then it remains almost constant (Fig. 3-28).

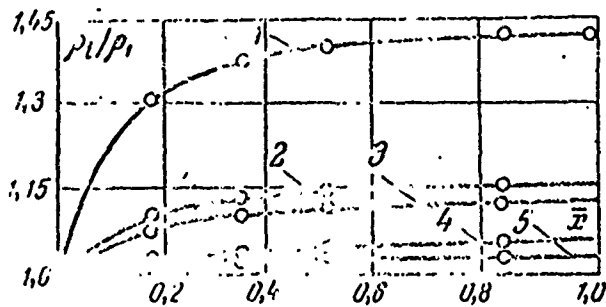


Fig. 3-28. Density change along a conical diffuser ($n = 4$; $\alpha = 10^\circ$; $Re_1 = 2 \cdot 10^5$): 1 - $\lambda_1 = 0.98$; 2 - $\lambda_1 = 0.63$; 3 - $\lambda_1 = 0.57$; 4 - $\lambda_1 = 0.4$; 5 - $\lambda_1 = 0.3$.

For value H let us use the approximation (3-13) introduced above. Then we will obtain

$$B_1 = \frac{0.161}{Re_1^{0.2}} \left(\frac{L}{D_1} \right)^{0.8} \left[1 - \frac{V\bar{n} - 1}{(L/D_1)^{0.2}} \right]. \quad (3-19a)$$

As a whole equation (3-18) is simpler than equation (3-15), and in its derivation we did not use in explicit form the condition of the potentiality of flow in the flow core. The physical basis for formula (3-18) is the replacement of the real flow on an infinitely small section of the diffuser $d\bar{x}$ by a certain fictitious flow in a circular tube of the same length $d\bar{x}$ at the same distance \bar{x} from the inlet, and having in the center of flow the same velocity c_1 as that of the section of the diffuser in question [see formula (2-54)].

The numerical comparison of calculations according to formulas (3-15) and (3-18) shows that both methods give sufficiently close results. In Appendix the nomogram (see Fig. A-2) based upon equation (3-18) with parameter B_1 being defined from formula (3-18a) is given.

Representation about the accuracy of definition of relative areas of displacement in the inlet section of the diffuser is given on Fig. 3-29, where both methods of the calculation are compared with experimental values obtained as a result of the traversing of the outlet velocity field in seven-degree diffusers which differ in the expansion ratio n . The agreement of calculation and experimental values $\bar{\delta}^*_2$ should be recognized as being entirely satisfactory. At the same time it is necessary to note that the arbitrary area of displacement \bar{A}^*_2 when $n > 4$ is noticeably distinguished from value \bar{S}^*_2 . This difference is caused by the drop in pressure of full stagnation in the flow (see Fig. 3-25). Hence the limitation of the examined method of the calculation of total loss factors ζ_n by moderate expansion ratios $n < 3.5-4$ follows.

In all the given relations except the geometric, only one regime parameter - the Reynolds number appears. The absence here of the Mach number is explained by the fact that directly on the integral thicknesses δ^*_2 , δ^{**}_2 and δ^{***}_2 in the outlet section this parameter has little effect. Basically the Mach number changes the flow pattern in the intake of the diffuser, where its growth gives rise to an increase in the inlet positive pressure gradients. However, this disturbance, if it does not cause boundary-layer separation, is smoothed in the subsequent flow, and the whole compressibility effect is reduced finally to a density change along the diffuser, which gives rise to an increase in value $\bar{\delta}^*_2$. The degree of this increase is traced on Fig. 1-11, where with the change in inlet velocity from $\lambda_1 = 0.3$ to $\lambda_1 = 1.1$ the maximum growth in value $\bar{\delta}^*_2$ was 20%. In principle this growth should be kept in mind, and it can be taken into account if we do not reject the density ratio in formula (3-18), and, by using the mean value theorem, include the ratio $\left(\frac{\rho_2}{\rho_1}\right)^{1.8}$ into parameter B_1 .

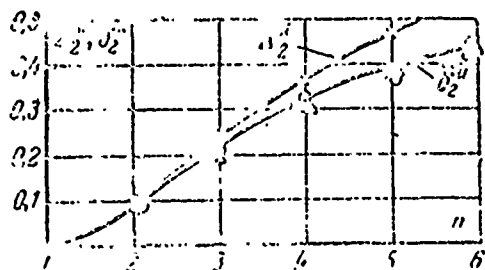


Fig. 3-29. Comparison of results of calculations according to formulas (3-15) and (3-18) with test data. Δ - calculation by formula (3-15); \emptyset - calculation by formula (3-18); \odot - experimental values δ_2^* ; \times - experimental values $\bar{\Delta}_2^*$.

As a result it is possible to use the same nomogram of the Appendix but define the coefficient B_1 by relation

$$B_1 = \frac{0,161}{Re_1^{0,2}} \left(\frac{L}{D} \right)^{0,8} \left[1 - \frac{\sqrt{n}-1}{(L/D_1)^{0,2}} \right] \left(\frac{\rho_2}{\rho_1} \right)_{\bar{x}}^{1,8}. \quad (3-20)$$

The ratio of densities in the certain section \bar{x} is expressed in the following manner:

$$\left(\frac{\rho_2}{\rho_1} \right)_{\bar{x}} = 1 + a \left(1 - \frac{\rho_2}{\rho_1} \right), \quad (3-21)$$

where coefficient $a < 1$, and ratio ρ_2/ρ_1 is connected with velocities λ_0 and λ_1 by relation [25]:

$$\frac{\rho_2}{\rho_1} = \frac{\left(1 - \frac{k-1}{k+1} \lambda_0^2 \right)^{\frac{1}{k-1}}}{\left(1 - \frac{k-1}{k+1} \lambda_1^2 \right)^{\frac{1}{k-1}}}. \quad (3-21a)$$

It was noted above that the relative velocity λ_0 is distinguished by not more than 2.5 times from velocity λ_1 (see Fig. 3-25). Then, assuming $\lambda_0^2 = \lambda_1^2/5$, we obtain:

$$\frac{\rho_2}{\rho_1} = \frac{1 - \frac{\lambda_1^2}{5(k+1)}}{\left(1 - \frac{k-1}{k+1} \lambda_1^2 \right)^{\frac{1}{k-1}}}. \quad (3-22)$$

As a whole formula (3-22) gives an approximate representation of the order of the density ratio and can be used not only in the computation of parameter B_1 but also in the relations which define the complete (2-29) and internal (2-34) diffuser losses.

The nature of the density change along the diffuser at various velocities λ_1 is sufficiently clear from the curves given in Fig. 3-28, which allow using coefficient a in formula (3-21) of the order of 0.4.

Taking into account the aforesaid, we will obtain

$$B_1 = \frac{0,161}{Re_1^{0,2}} \left(\frac{L}{D_1} \right)^{0,8} \left[1 - \frac{V\bar{n}-1}{(L/D_1)^{0,2}} \right] \times \left\{ 1 + 0,4 \left[1 - \frac{1 - \frac{\lambda_1^2}{5(k+1)}}{\left(1 - \frac{k-1}{k+1} \lambda_1^2 \right)^{\frac{1}{k-1}}} \right] \right\}^{1,8} \quad (3-23)$$

The examined procedure is easily generalized on arbitrary diffusers with a rectilinear axis. In this case instead of the formula (3-18), we will obtain the following general expression:

$$\bar{\Delta}^2 = B_1 n^{0,2} (1 - \bar{\Delta}^2)^2 \frac{b_1}{b_2} \int_0^1 \left(\frac{\rho_2}{\rho_1} \right)^{1,8} \times \left(\frac{F_2}{F_1} \right)^{2,6} \frac{\Pi_1}{\Pi_2} \frac{d\bar{x}}{Re^{0,2} [1 - \bar{\Delta}^2 f(\bar{x})]^{2,8}} \quad (3-24)$$

Here

$$B_1 = \frac{0,0238H}{Re_{01}^{0,2}} \left(\frac{L}{b_1} \right)^{0,8} \frac{b_2 \Pi_2}{F_2};$$

L - the length of the channel on the center line; b_1 and b_2 are the characteristic dimensions of the inlet and outlet section
 Π_1 and Π_2 - current perimeter and perimeter of the channel in the outlet section.

Results of the calculation according to formula (3-24) depend upon the concrete channel, and because of this they cannot be obtained earlier. However, having isolated the definite group of one-type diffusers, it is not difficult to obtain simple calculated nomograms for them.

For plane diffusers equation (3-24) is considerably simplified. In this case, having used as characteristic dimensions h and H_1 (see Fig. 2-1a), we obtain

$$\bar{\Delta}^*_{22} = B_1 (1 - \bar{\Delta}^*_{22})^3 n^2 \int_0^1 \frac{d\bar{x}}{[1 + \bar{x}(n-1)]^{2.3} (1 - \bar{x}^{0.9} \bar{\Delta}^*_{22}) \bar{x}^{0.2}}, \quad (3-25)$$

$$B_1 = \frac{0.0576H}{\text{Re}_h^{0.2}} \left(\frac{L}{h}\right)^{1.9} \left(\frac{\rho_2}{\rho_1}\right)^{1.8}. \quad (3-26)$$

By examining the pyramidal diffuser depicted on Fig. 3-30, it is easy to see that in this case the calculation is considerably complicated. Actually, here the ratios of areas and perimeters entering into formula (3-24) are expressed in the following manner:

$$\frac{F_1}{F_2} = \frac{h \left[1 + \bar{x} \left(\frac{H_1}{h} - 1 \right) \right] + b \left[1 + \bar{x} (B/b - 1) \right]}{H_1 (1 + B/H_1)};$$

$$\frac{P_1}{P_2} = \frac{n}{\left[1 + \bar{x} \left(\frac{H_1}{h} - 1 \right) \right] \left[1 + \bar{x} (B/b - 1) \right]}.$$

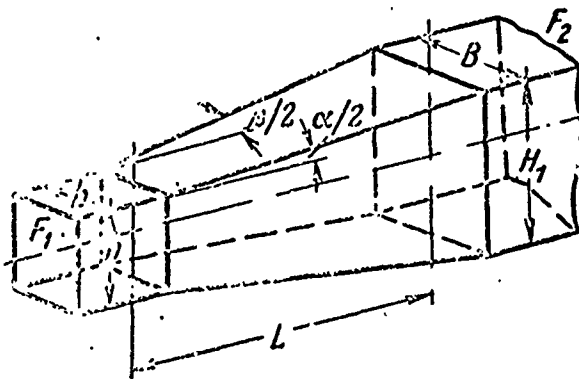


Fig. 3-30. Diagram of a pyramidal diffuser.

As a result the calculation of area $\bar{\Delta}^*_{22}$ must be conducted not with one parameter n but with three additional values:

$$\frac{H_1}{h}, \quad \frac{B}{b}, \quad \text{and} \quad \frac{B}{H}.$$

This fact impedes the construction of the universal nomograms

of the type examined above, and it gives rise to the necessity for the determining $\bar{\Delta}_2^*$ by the method of successive approximations according to equation (3-24).

§ 3-5. Comparison of Calculated and Experimental Data

The examined calculation procedure of diffusers according to formulas (3-15) and (3-18) when using nomograms of the stagnation differs little in laboriousness from the calculation method according to the coefficient of "softening" of the impact ϕ_d . However, the question of laboriousness is not decisive but rather the accuracy of the final result.

By using experimental data given in Table A-1 of the Appendix, let us compare them with the theoretical values found both on the basis of the boundary layer characteristics and on the basis of formula (2-42a).

For a comparison let us use the data on the conical diffusers with angles $\alpha < 11^\circ$, and let us limit the maximum expansion ratio $n \leq 6$. In other words, let us distinguish the group of nonseparable diffusers, since only for them is it possible to conduct the calculation of losses on the basis of nomograms.

Furthermore, for the correctness of the use of the curve in Fig. 2-12, which links the coefficient ϕ_d with angle α , let us use the test data obtained at low velocities at the inlet ($\lambda_1 < 0.4$) and similar Reynolds numbers ($Re_1 = (2-3) \cdot 10^5$). Data selection according to such a principle of 35 diffusers are placed in the first part of Table A-1, and for them the calculated values of coefficients ξ_n are determined.

Results on the comparison conducted are clearly visible from Fig. 3-31.

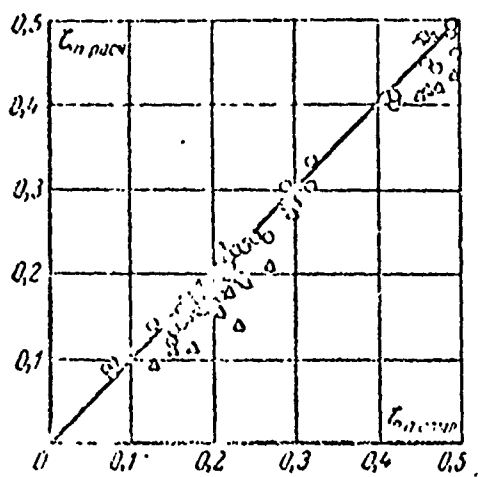


Fig. 3-31. Comparison of the calculated and experimental values of coefficient ζ_{π} . O - calculation by nomograms of the Appendix; Δ - calculation by formula (2-42a).

Deviation of the applied points from the bisector of the quadrant gives the absolute value of the divergence between the calculations and experiment. The comparison conducted illustrates visually the advantage of the examined method of calculation for nonseparable flow. In this case the absolute deviation in the points from the bisector does not exceed 3%, and the maximum relative error is 15%. At the same time the use of the coefficient of softening of the impact ϕ_{Δ} increases the relative error to 25%, and the general divergence of the points is noticeably worse than that in the case of calculation according to boundary layer characteristics.

Furthermore, it should be kept in mind that we actually eliminated from the examination the mode parameters - Mach and Reynolds numbers. Otherwise the error of calculation according to coefficient ϕ_{Δ} could exceed the absolute value of the definable value ζ_{π} , since the relation $\phi_{\Delta} = f(\alpha)$ is far from being universal. Considering the wide distribution of the relation and its use for the performance calculation of all possible diffusers, Fig. 3-32 gives values of ϕ_{Δ} depending on angle α obtained on the basis of the experimental data gathered in the Appendix. It is evident that at the same angle the value of coefficient ϕ_{Δ} can change

several times in the zone of narrow angles and by 30-50% when $\alpha > 15^\circ$. Hence it follows that the relation in question (2-42a) can be used for an estimate of the order of losses with the emergence of separation, but it does not solve the problems in the zone of small angles ($\alpha < 11^\circ$) when the flow is not separated. Here the advantage of theoretical methods is evident.

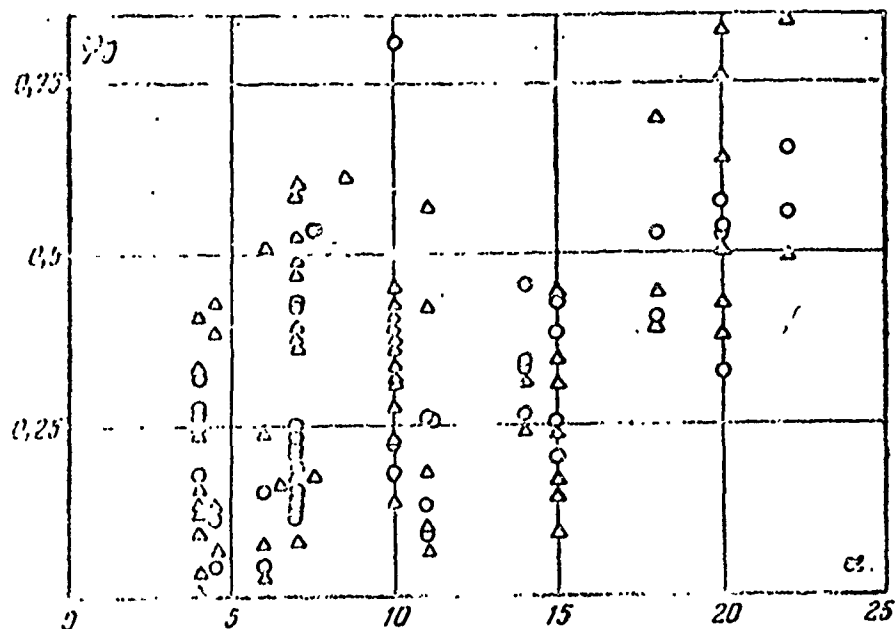


Fig. 3-32. The experimental values of coefficient ϕ_D depending on angle α .

Considering the significant quantity of experimental material attracted for analysis, the estimate of losses in conical diffusers can be conducted directly according to the experimental dependences depicted on Figs. 3-11, 3-14 and 3-24. In this case not only the direct but also the inverse problem is easily solved: according to the prescribed value of coefficient ζ_n select the adequate geometric parameters of the conical diffuser. For instance, setting $\zeta_n = 0.4$, from Fig. 3-11a we find that this condition satisfies a number of diffusers with angles $\alpha = 4-18^\circ$ and value $n = 1.6-2.8$.

If according to design considerations a short diffuser is required, then the most suitable parameters will be $\alpha = 15^\circ$ and $n = 2.0$. If it is required to provide stable flow in variable modes, then it is advantageous to decrease angle α and use $\alpha = 7^\circ$ and $n = 1.9$.

§ 3-6. Detached Flows in Flat and Conical Diffusers

The visual study on the flow pattern in diffusers, conducted in works [88, 142, 143], showed that the separation of flow from walls of the channel occurs at a definite correlation between the flare angle of the diffuser and the expansion ratio (see Fig. 2-10).

A small increase in limiting values of α_{np} and n_{np} causes at first nonstationary separation. The small eddy regions appearing in this case are easily carried away by the flow without causing a substantial drop in the efficiency of the diffuser. Subsequently, however, with an increase in the angle α or the expansion ratio, there appear more powerful eddy formations, which sharply change the flow pattern in the outlet section of the diffuser. These changes are most noticeable in flat diffusers. If during non-separable flow the flow lines of ordered motion fill the whole outlet section of the diffuser, then with the separation of flow the zero line of current will move away from the wall of the diffuser, and in the region between this line and the wall the vortex fluid flow is established. In the zone of separation there can be formed either the stationary vortex, which rests on the side walls of the channel, or the system of vortices¹ of smaller intensity being transported together with the flow. The diagram of such a flow is given on Fig. 3-33. The zero line of current ABC at point B moves away from the wall and separates the

¹Here and further we will understand by the word "vortex" purely circulation flow.

zone of vortex currents from the main stream.

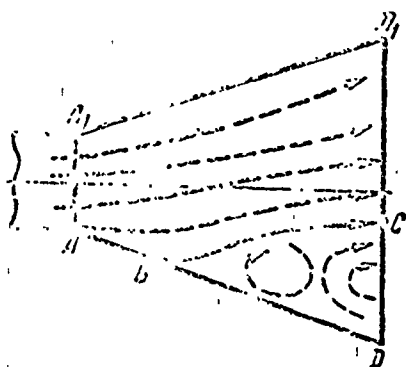


Fig. 3-33. Diagram of detached flow in a plane diffuser.

Thus, with the emergence of separation, the section of the channel which passes the assigned fluid flow rate is sharply reduced, and in the zone lying over the line of separation the flow which is close to being gradient-free is established. It is natural that in connection with the decrease in effective output area $F_{2\phi}$ an increase in the total loss factor occurs, and, correspondingly, the coefficient of the recovery of energy is lowered.

The theoretical determination of area $F_{2\phi}$ with the emergence of separation is associated today with insurmountable difficulties. Because of this, for the calculation of losses in separation diffusers, it is necessary to use either the purely experimental data or semi-empirical relations of the type of formula (2-42a). As was already mentioned above, the accuracy of the estimate of coefficients ζ_n and ζ in such case proves to be low. With emergence in the zone of the separation of a stationary vortex approximately the same accuracy can be obtained by means of the following rough estimation of the effective expansion ratio.

Let us assume that in the vortex zone CD (Fig. 3-33) the flow-rate velocity component is equal to zero, and in zone CD_1 the velocity profile is close to being uniform. Then

$$n_{0\phi} = n(1 - CD/F_1 n)$$

and for determining the total loss factor when a stationary vortex exists, in the plane diffuser we will obtain:

$$\zeta_{11} = \frac{1}{n^2 (1 - CD/F_1 n)^2} \quad (3-27)$$

The value of coefficient ζ_{11} , calculated on the basis of formula (3-27), should be somewhat lower than the experimental value, since it is obtained as a result of the estimate of the effective expansion ratio according to the value of average velocity in zone CD_1 and not velocity c_0 , which corresponds to the available enthalpy drop in the diffuser. This inaccuracy can be compensated by the line shift of section BC to the side of the main flow. It is clear that such a means of the calculation of losses, to a considerable degree, is arbitrary. However, it can be recommended for the comparative performance estimate of various diffusers if we use the same procedure of the determination of the zone line of current ABC.

Before accepting any method of drawing the line ABC, let us explain in which cases the existence in a plane diffuser of a stationary vortex is possible. For this purpose let us maximally simplify the problem and let us examine the flow of inviscid fluid in the plane of the complex variable z from the source by power Q placed at point 0 and the vortex with intensity Γ located at point z_0 (Fig. 3-34a). Let us assume that the region of flow is limited by sector BOB_1 with angle $\alpha = \pi/m$. Then the fluid flow rate in this region will be equal to $Q/2m$, and the coordinate of the center of the vortex in polar coordinates will be defined by relation

$$z_0 = r_0 \exp(i\alpha_0). \quad (3-28)$$

Let us map the indicated region on a strip of width π . As is known [64], such a mapping is accomplished with the help of function

$$\omega = \eta \ln z. \quad (3-29)$$

The mutual uniqueness of the mapping (3-29) provided automatically if

$$0 < \arg z < \alpha. \quad (3-30)$$

With this point z_B goes over to point ω_B , and point 0 - to infinity, and values of the power of the source and vortex strength with conformal mapping remain without changes.

Therefore, from the initial case we turn to the problem about the flow of a vortex with intensity Γ , located inside a strip with width π , and plane-parallel flow with a velocity at infinity equal to

$$c_\infty = u_\infty = \frac{Q}{2\pi m}. \quad (3-31)$$

In such a formulation the problem is close to that examined in [62]. The analytical extension of the chosen region on the whole plane is attained, representing its infinite number once relative to each wall. We will obtain the double vortex chain, which consists of equidistant vortices with opposite intensities Γ and $-\Gamma$ [62]. Let the coordinates of the first vortex system be ω_{k1} and ω_{-k1} , and of the second ω_{k2} and ω_{-k2} (Fig. 3-34b). These values are easily expressed in terms of coordinates of vortex ω_B in the assigned strip:

$$\left. \begin{aligned} \omega_{k1} &= \omega_B + 2\pi ki; \\ \omega_{-k1} &= \omega_B - 2\pi ki; \\ \omega_{k2} &= -\omega_B + 2\pi ki; \\ \omega_{-k2} &= -\omega_B - 2\pi ki. \end{aligned} \right\} \quad (3-32)$$

Taking into account the aforesaid, the complex potential from the first vortex system will be equal to

$$W_1 = \frac{-\Gamma}{2i} \ln \left\{ \frac{\omega - \omega_B}{2i} \Pi \left[1 - \left(\frac{\omega - \omega_B}{2\pi ki} \right)^2 \right] \right\} = \frac{-\Gamma}{2i} \ln \sin \frac{\omega - \omega_B}{2i}. \quad (3-33)$$

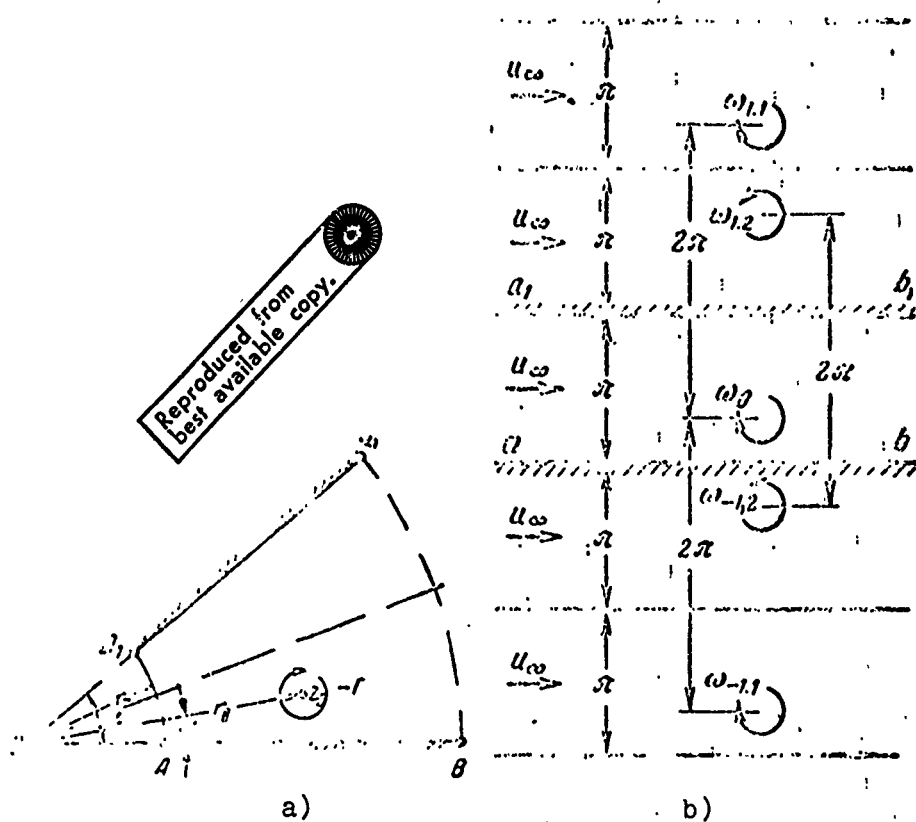


Fig. 3-34. Design diagram of flow in a diffuser a) and the region of flow in the plane of the complex variable b).

Analogously, for the second vortex system we will obtain

$$W_2 = \frac{\Gamma}{2\pi i} \ln \sin \frac{\omega - \bar{\omega}_2}{2i}. \quad (3-34)$$

Finally, let us present the complex potential of plane-parallel flow in the form of

$$W_3 = u_\infty \omega \frac{Q}{2\pi m} \omega. \quad (3-35)$$

Thus, for the complex flow induced by the double vortex chain and the plane-parallel flow, the complex potential will be equal to

$$W = \frac{\Gamma}{2\pi i} \ln \frac{\sin \frac{\omega - \bar{\omega}_2}{2i}}{\sin \frac{\omega - \omega_2}{2i}} + \frac{Q}{2\pi m} \omega. \quad (3-36)$$

It is easy to note that the pressure and velocity on both sides of the lines dividing the plane into strips with width π are equal. Therefore, each such line can be used as the restricting wall, and expression (3-36) gives the complex potential for flow in the infinite channel with the vortex being located at point z_0 .

Having substituted into (3-36) the value ω from formula (3-29), we obtain the value of the complex potential in plane z for flow in the diffuser with the vortex at point z_0 :

$$W = \frac{\Gamma}{2\pi i} \ln \frac{\operatorname{sh} \left(\frac{m}{2i} \ln z/z_0 \right)}{\operatorname{sh} \left(\frac{m}{2i} \ln z/z_0 \right)} + \frac{Q}{2\pi} \ln z. \quad (3-37)$$

Let us turn to polar coordinates according to relation (3-28), then

$$W = \frac{\Gamma}{2\pi i} \ln \frac{\operatorname{sh} \frac{m}{2i} \left[\ln r/r_0 + i(\alpha + \alpha_0) \right]}{\operatorname{sh} \frac{m}{2i} \left[\ln r/r_0 + i(\alpha - \alpha_0) \right]} + \frac{Q}{2\pi} (\ln r + i\alpha). \quad (3-38)$$

For a definition of the stream function, it is sufficient in expression (3-38) to separate the imaginary part. For this purpose let us present (3-38) in the form of

$$W = \frac{\Gamma}{2\pi i} \ln \frac{\operatorname{sh} \left[\frac{m}{2} \ln r/r_0 + \frac{im}{2} (\alpha + \alpha_0) \right]}{\operatorname{sh} \left[\frac{m}{2} \ln r/r_0 + \frac{im}{2} (\alpha - \alpha_0) \right]} + \frac{Q}{2\pi} (\ln r + i\alpha).$$

Hence

$$\psi = -\frac{\Gamma}{2\pi} \ln \left| \frac{\operatorname{sh} \left[\frac{m}{2} \ln r/r_0 + \frac{im}{2} (\alpha + \alpha_0) \right]}{\operatorname{sh} \left[\frac{m}{2} \ln r/r_0 + \frac{im}{2} (\alpha - \alpha_0) \right]} \right| + \frac{Q\alpha}{2\pi}.$$

or

Reproduced from
best available copy.

$$\psi = \frac{\Gamma}{2\pi} \ln \frac{\left(\frac{r}{r_1}\right)^m + \left(\frac{r}{r_2}\right)^{-m} + 4\sin^2 \frac{m}{2} (\alpha + \alpha_0) - 2}{\left(\frac{r}{r_1}\right)^m + \left(\frac{r}{r_2}\right)^{-m} + 4\sin^2 \frac{m}{2} (\alpha - \alpha_0) - 2} + \frac{Q\alpha}{2\pi} \quad (3-39)$$

To obtain the concrete line of flow in expression (3-39) let us assume:

$$\psi = \psi_0 = \frac{Q\alpha_0}{2\pi m} = \text{const.} \quad (3-40)$$

As a result we will obtain:

Reproduced from
best available copy.

$$\frac{\left(\frac{r}{r_1}\right)^m + \left(\frac{r}{r_2}\right)^{-m}}{\left| 1 - \exp 2 \frac{Q}{\Gamma} (\alpha - \alpha_0) \right|} \times$$

$$\frac{\left\{ 4 \sin^2 \frac{m}{2} (\alpha - \alpha_0) - 2 \right\} - 4 \sin^2 \frac{m}{2} (\alpha + \alpha_0) + 2}{\dots}$$

The right side of the equation is a function of angle α and three parameters: Q/Γ , α_0 and α_0 , i.e.,

$$\psi \left(\alpha; \frac{Q}{\Gamma}; \alpha_0; \alpha_0 \right) = \frac{\exp \left[2 \frac{Q}{\Gamma} (\alpha - \alpha_0) \right] \left\{ 4 \sin^2 \frac{m}{2} (\alpha - \alpha_0) - 4 \sin^2 \frac{m}{2} (\alpha + \alpha_0) \right\} + 2}{1 - \exp \left[2 \frac{Q}{\Gamma} (\alpha - \alpha_0) \right]} \quad (3-41)$$

As a result for determining the zero line of flow, we will obtain equation

$$\left(\frac{r}{r_1}\right)^{2m} - \psi(\alpha) \left(\frac{r}{r_2}\right)^{2m} + 1 = 0,$$

the solution of which will give:

$$\left(\frac{r}{r_1}\right)^{2m} = \left[\frac{\psi(\alpha)}{2} \pm \sqrt{\frac{\psi^2(\alpha)}{4} - 1} \right] \quad (3-42)$$

If the center of the vortex is located on ray $\arg z = \alpha_0$, then, as calculations show, it is possible to consider that the whole

"vortex atmosphere"¹ is located in the angle α_0 the definable equality

$$0 < \arg z < 2,1\alpha_0. \quad (3-43)$$

Since points of the "vortex atmosphere" belong to the zero line of flow, we assume that the tangent to the contour of the "vortex atmosphere" has a length of the order of r_B , i.e., $r/r_B = 1$. Then from (2-42) it follows that

$$\psi(\alpha) = 2. \quad (3-44)$$

For the fulfillment of this equality in equation (3-41), it is necessary to place:

$$\alpha_0 = 0;$$

$$\alpha = 2,1\alpha_0.$$

As a result the condition (3-44) takes the form:

$$\exp 2,1 \frac{Q}{\Gamma} \alpha_0 = \frac{\sin (1,55m\alpha_0)}{\sin (3,55m\alpha_0)}. \quad (3-45)$$

Its solution for the given value Q/Γ makes it possible to determine the ray along which the displacement of the center of vortex occurs. The graphical solution of this equation for different values of Q/Γ shows that with a decrease in the vortex strength Γ and an increase in the flow rate Q the ray $\arg z = \alpha_B$ approaches the real axis, i.e., near a "vortex atmosphere" the dimensions are sharply decreased. This direction is influenced by the decrease in flare angle of the diffuser characterized by parameter m .

The obtained relations allow determining the velocity, from which the center of the vortex will be carried away by the flow downstream. For this it is sufficient to differentiate expression (3-36) with respect to variable ω and to assume $\omega = \omega_B$. Then the value of the complex velocity will be equal to

¹Here and further we will understand by "vortex atmosphere" as the closed line which limits both adjacent vortices.

$$u_{\alpha} - iv_{\alpha} = \left[-\frac{\Gamma}{4\pi} \operatorname{ctg} \frac{\omega_1 - \bar{\omega}_1}{2i} + \frac{Q}{2\pi m} \right] \frac{d\omega}{dz}. \quad (3-46)$$

Since the difference $\frac{\omega_1 - \bar{\omega}_1}{2i}$ is a real number, from (3-46) we will obtain

Reproduced from
best available copy.

$$u_{\alpha} = \frac{Q}{2\pi m} - \frac{\Gamma}{4\pi} \operatorname{ctg} \frac{\omega_1 - \bar{\omega}_1}{2i}; \quad v_{\alpha} = 0. \quad (3-46a)$$

In the particular case $Q = 0$ the solution of (3-46a) coincides with the result obtained by N. Ye. Kochinyy, A. I. Kibel' and N. V. Roze [62].

Replacing ω_1 according to equation (3-29) and having passed over to polar coordinates, we find the velocity of motion of the center of the vortex in the diffuser:

$$u_r = \frac{Q}{2\pi r} - \frac{\Gamma m}{4\pi r} \operatorname{ctg} m\alpha_1. \quad (3-47)$$

Hence it is apparent that the velocity of motion of the vortex substantially depends upon the value of the circulation Γ and flow rate Q with the certain relation between these values $u_r = 0$. This case correspond to the fixed stationary vortex inside the diffuser, and from (3-47) the simple condition of its existence follows:

$$\frac{Q}{\Gamma} = \frac{m}{2} \operatorname{ctg} m\alpha_1. \quad (3-48)$$

With the fulfillment of equality (3-48) we will obtain from (3-45) the value of the argument α_1 , which corresponds to the ray on which the center of the stationary vortex should be located. For this case equation (3-45) assumes the form

$$\exp \left[1,05 \frac{m\alpha_1}{\operatorname{tg} m\alpha_1} \right] = \frac{\sin 1,55m\alpha_1}{\sin 0,55m\alpha_1}. \quad (3-49)$$

Hence for angle α_1 we will obtain

$$\alpha_1 = \frac{0,475}{m}. \quad (3-50)$$

Consequently, the center of the stationary vortex should be located on ray (3-50), and the ratio of the source power to the vortex strength Γ is determined by equality

$$\frac{Q}{\Gamma} = 0,975m. \quad (3-51)$$

If $Q/\Gamma > 0.975m$, then the vortex will be carried away downstream. When $Q/\Gamma < 0.975m$ the vortex will be moved against the flow. The velocity of motion of the vortex can be found from expression (3-47).

Taking into account (3-50) and (3-52), equation (3-41) is considerably simplified and depends only upon parameter α_0 :

$$\psi(\alpha, \alpha_0) = 4 \frac{\exp[1,95m(\alpha - \alpha_0) \sin^2[0,5m\alpha - 0,237]]}{1 - \exp[1,95m(\alpha - \alpha_0)]} \frac{\sin^2[0,5m\alpha + 0,237]}{1 - \exp[1,95m(\alpha - \alpha_0)]} + 2. \quad (3-52)$$

Let us give as an example the calculation of lines of flow in a plane diffuser when $m = 8$. The accepted value of m corresponds to a diffuser with a flare angle $\alpha = 22^\circ 31'$. For the construction of the pattern of flow in diffuser from the results of a calculation, it is necessary to determine the value of the radius r_B from the center of the vortex. Having assumed that the branch point of the zero line of flow is the separation point of flow from the wall, we obtain for the diffuser in question:

$$r_B = 1,11r_{027}.$$

The greatest difficulties usually appear in the definition of the coordinate of the separation point. As was already mentioned above, not one of the known criteria of separation based upon results of the boundary layer calculation gives sufficient accuracy in determining the indicated coordinate. In this direction some help can be given by purely statistical data. Thus, in [167] vast statistical material about the emergence of separation in compressor cascades is given. It was found that in almost all

cases the separation of flow from the walls began with the reduction in maximum speed in the channel of approximately 2 times, which for incompressible fluid corresponds to the effective expansion ratio $n_{\phi S} = 2$. It is interesting to note that this value in the zone of turbulent flow was found not dependent on the Reynolds number. Analogous results were obtained even at MEI during tests of conical diffusers.

Figure 3-7 gives the limiting values of the effective expansion ratios determined according to the velocity c_0 , which corresponds to the available enthalpy drop in the diffuser, depending on the input dimensionless velocity λ_1 at various Re_1 numbers for the large series of conical diffusers.

The obtained test data indicate that the value $n_{\phi S}$ is considerably affected by the compressibility of gas. With a velocity increase from $\lambda_1 = 0.3$ to $\lambda_1 = 1$, $n_{\phi S}$ is decreased from 2.4 to 2.0.

The influence of the flare angle of the diffuser α is noted only at low velocities. Here, as one would expect, with an increase in the angle from 10° to 20° , $n_{\phi S}$ drops from 2.5 to 2.3. When $\lambda_1 > 0.7$, for all diffusers tested both on air and steam, $n_{\phi S} = 2$.

The decrease in the influence of the flare angle on the limiting effective expansion ratio of the diffuser with the increase in inlet velocity is connected with the feature of the flow of flow near the sharply changing curvature in the inlet of the diffuser. In the examination of this question it was indicated that near the angular point there occurs a sharp increase in the pressure gradients dependent both on the flare angle and the flow rate. If at low velocities the angle is of decisive importance, then, with an increase in velocity the noted local increase is basically determined by velocity λ_1 .

The use of the value of the limiting effective expansion ratio, along with the known criteria of separation, allows approaching the solution to the problem of the separation point of the boundary layer.

Since in this case flow not in conical but in plane diffuser is examined, let us use on the basis of [167] $n_{\text{эфс}} = F_{\text{отр}}/F_1 = 2.0$, where $F_{\text{отр}}$ - the area of pressure of the diffuser at the separation point B.

Since in a plane diffuser

$$F_1 = 2r_H \sin \alpha / 2m;$$

$$F_{\text{отр}} = 2r_{\text{отр}} \sin \alpha / 2m,$$

then $r_{\text{отр}} = 2r_H$, where r_H - the radius of the inlet section of the diffuser (see Fig. 3-34a). Hence

$$r_{\text{отр}} = 2,2r_H. \quad (3-53)$$

The pattern of flow of an ideal fluid in a plane diffuser when in it there is a stationary vortex located at the point with coordinates α_B and r_B , determined by equalities (3-50) and (3-53), is represented in Fig. 3-35. From the spectrum of lines of flow it is clearly evident that the presence in the diffuser of a stationary vortex is equivalent to the appearance inside the channel of a certain solid contour outlined by the line BNM, which coincides with the "vortex atmosphere" of the vortex.

By comparing the given pattern of the flow of the ideal fluid with the real spectra of flow when separation exists, (see, Fig. 3-1a), it is possible to note the qualitative concurrence of the lines of the flow of ideal and real flows.

Thus, appearance in the flow of a stationary vortex gives rise to the noticeable decrease in the cross section of the channel. With a uniform velocity vector its effective cross section in the zone of location of the vortex is defined by segment NN_1 .

the cross section of separation. With an increase in the expansion ratio at a constant flare angle, the effective area in outlet section will be decreased as compared with area NN_1 , which can lead to an increase in total losses.

The aforesaid is confirmed well by the experimental data given in Fig. 3-11a. Here minimum losses for angle $\alpha = 22^\circ$ are about 0.41 when $n = 4$, which coincides in practice with the computed value of quantity ζ_n . Further, ζ_n somewhat increases with an increase in the expansion ratio n .

The derived formulas for the calculation of losses in plane separation diffusers are completely approximate, and they should be examined only as one of the possible ways of solving this complex problem. At the same time the obtained results are interesting from a physical side, since they allow explaining the reason for the reduction in channel losses examined above, where by various measures it is possible to divide the basic vortex into a number of vortices of less strength. Actually, according to formula (3-48) for existence in the channel of stationary vortex, it is necessary that between the vortex strength and flow rate there would be a completely definite correlation. With the disturbance of this ratio, especially with the decrease in the magnitude of circulation, the vortex begins to be carried away with the flow downstream.

The indicated motion of the vortices is one of the conditions of the reduction in channel losses which operate with the boundary layer separation, since in this case the "fixed obstacle" in the form of "a vortex atmosphere" is replaced smaller in dimensions and by the "solid" contours moved together with the flow, and therefore the "shadow regions" disappear, and on whole outlet section of the channel the mean flow rate is established.

However, the appearance in the flow of the moving vortex regions gives rise to the appearance of rather powerful pulsations. The latter is explained by the fact that the passage of the vortex through the channel is equivalent to the motion in the channel of a certain solid contour, and with the exit of the vortex from the channel its resistance sharply falls due to an increase in the effective flow area. The formation of the following vortex again gives rise to the contraction of the cross section. As a result pulsating flow is established with the frequency dependent on the velocity of motion of the vortices.

Low-frequency pulsations take place at low velocities of motion of the vortex, i.e., at a considerable magnitude of circulation Γ . On the other hand, high-frequency pulsations appear at the powerful fragmentation of the basic vortex. It is understandable that in the latter case channel losses fall more intensely, since with a reduction in the vortex strength the velocity of the vortex approaches the velocity of the main flow, and the whole cross section is filled with the flowing fluid. In this respect the experiments having the purpose of decreasing the resistance of the diffusers with the help of the grids placed inside the channel are characteristic [54]. The presence of such additional resistances in diffusers allows in a number of cases lowering their total resistance; in this case the basic vortex is divided into number of small vortices, and over the whole cross section the mean flow rate is established. If the grid resistance is less than the resistance induced by the "shading" of the channel by a stationary vortex, then the total losses of diffuser decrease. Analogously, the reduction in losses in finned diffusers can be explained [46], where the transverse grooves cause microseparations of the flow with the formation of vortices of small strength, which are easily carried away by the flow, without disturbing the total picture of the flow.

The obtained results from a qualitative side are valid even

for axisymmetric diffusers. However, quantitative estimates in this case prove to be different: in an axisymmetric diffuser in most cases local separations appear, and the formation of closed vortex rings is observed extremely rarely.

§ 3-7. Procedure for Calculating Losses with the Sudden Flow Expansion

The sudden flow expansion, i.e., flow with a sharp change in the flow area, is frequently encountered in various technical problems.¹ The solution to this problem includes the procedure of calculating losses in conical diffusers at flare angles $\alpha > 30^\circ$, when it is recommended to turn to sudden expansion [34].

In most cases for the estimate of losses with sudden expansion, the authors [34, 54] in one form or another use the formula of Borda-Carnot

$$\zeta = \left(1 - \frac{1}{n}\right)^2. \quad (3-55)$$

where $n = F'_2/F_1$ - ratio of appropriate areas.

A simple analysis shows that the mechanical use of formula (3-55) for a number of problems can lead to the perceptible errors. In connection with this let us indicate the prerequisites and limitations which were placed as a basis for the solution of formula (3-55). Let us examine the flow in the cylindrical channel by radius r_0 (Fig. 3-36) and radius r_2' connected in the cross section I-I with a tube. During such a transfer in flow it is possible to distinguish the two characteristic zones - the zone of the free jet *adec* and the equalizing zone *dekl*.

¹In turbine construction problems about sudden expansion include the calculation of losses in the presence of a cover at the inlet into operating grid and nozzle apparatus, the calculation of losses beyond the control valves, and in a revolving diffuser with partial losses the calculation of boundary losses and so on.

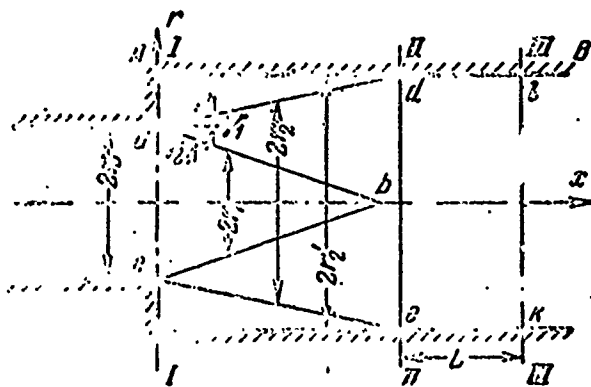


Fig. 3-36. Diagram of flow with sudden expansion.

Reproduced from
best available copy.

In the section in question one usually assumes that the pressure changes only along the axis of the channel and does not depend upon the transverse coordinate r . At the same time the velocities change both across and along the x axis. In this case in the open jet there exist the potential core abc , within the limits of which the longitudinal velocity c_1 depends only upon coordinate x , and the zone where the velocities in a transverse direction are changed from the value in potential core c_1 up to zero on the jet boundary. In a known sense this zone can be called the zone of boundary layer, bearing in mind, of course, the conditionality of such a definition.

From the diagram of the flow presentation in Fig. 3-36, it follows that along the x axis the sharp contraction of the potential core and the expansion of the jet occur.

For the computation of losses between cross sections I-I and III-III, in these cross sections the equations of energy and momentum are recorded, the common solution of which gives rise to the following relation [54]:

$$\zeta = \frac{2M_2 - N_2}{n'^2} + N_1 - \frac{2M_1}{n'} \quad (3.56)$$

The coefficients of the momentum M_1 and M_2 and also coefficients of kinetic energy N_1 and N_2 are determined by the

velocity profiles in the cross sections in question and are calculated according to formulas

$$M_1 = \frac{1}{F_1} \int_{F_1} \left(\frac{c}{c_{0p}} \right)^2 dF; \quad M_2 = \frac{1}{F_2} \int_{F_2} \left(\frac{c}{c_{0p}} \right)^2 dF;$$

$$N_1 = \frac{1}{F_1} \int_{F_1} \left(\frac{c}{c_{0p}} \right)^3 dF.$$

Since it is assumed that in cross section III-III the flow was equalized and has a turbulent velocity profile, for which $N_2 \approx M_2 \approx 1$, for the calculations a simpler relation is recommended:

$$\zeta = \frac{1}{n'^2} + N_1 - \frac{2M_1}{n'}. \quad (3-57)$$

If we assume that in cross section I-I the uniform velocity field takes place, then $N_1 = M_1 = 1$, and formula (3-57) turns into widely used relation (3-55).

However, calculations according to formula (3-56) give the basis to assume that strongly it minimizes losses with the non-uniform output field and the small expansion ratio. Actually, let us determine losses in cross section III-III (Fig. 3-36), where the velocity profile took the typical form characteristic for developed turbulent flow, with the uniform field before the sudden expansion and $n' = 1.2$.

For the exponential velocity profile, beginning with index $m = 1/7$, the coefficients are equal, respectively, to $M_2 = 1.015$ and $N_2 = 1.043$, i.e., actually very close to one. But in this case the result proves to be completely different if we assume $M_2 = N_2 = 1$.

Having calculated the losses for $M_2 = N_2 = 1$, we find: $\zeta = 0.0143$. If we use the actual values M_2 and N_2 , then we will obtain $\zeta = -0.0137$.

The noted feature of relation (3-56) is connected partially with the fact that with its derivation in the momentum equation, written for cross sections I-I and III-III, the momentum of frictional forces in section L is not considered. In connection with this formula (3-56) gives substantially fewer losses, but at small expansion ratios n the losses generally become negative. The particular form of formula (3-55) is unacceptable both in the zone of the free jet and outside the equalizing section, since in the first zone coefficients M_2 and N_2 are different from one, and in the second zone frictional forces on the restricting walls are not considered.

Since the length of the equalizing zone II-III is of the order of $(10-20)r'_2$, the error at large n can show. In fact, if we introduce into the momentum equation the momentum of frictional forces and assume the velocity field in cross section I-I to be uniform, then in cross section III-III for determining losses connected with the sudden expansion, we obtain the following expression:

$$\zeta = \left(1 - \frac{1}{n'}\right)^2 + \frac{16L}{D'_2} \cdot \frac{C_{fcp}}{n'^2} \quad (3-58)$$

Here $C_{fcp} = \frac{0,022}{Re_{D_2}^{0,25}}$ - the resistance coefficient on the

equalizing section L.

Having estimated the value of the additional term in formula (3-58) when $L/D_2 = 10$ and number $Re_{D_2} = 10^5$, we obtain that for the expansion ratio $n = 2$ the correction is 9%, or with respect to the first term, 36%. Thus, in the computation of losses in pipelines with a sudden change in the flow area it is more correct to use formula (3-58) and not (3-55). In this connection it is necessary to show that for rectangular cores with expansion of the area in only one plane, the formula of the

type (3-56), apparently, cannot generally be used, because in this case the momentum of frictional forces on the side walls proves to be of the same order as the momentum of forces of pressure, and calculation of these become difficult.

Furthermore, the sudden expansion of the cross section in one plane substantially changes the whole pattern of flow. In this case with the transition to the wide cross section the boundary sections of the jet lose stability and are displaced into vortex lines, forming along channel stable vortex regions which induce additional velocities in the main jet. The pattern of flow proves to be complex, and the equalizing zone is stretched far along the flow.

The examined cases of the use of formula (3-55) refer to the long channels where section L is great and the velocity profile assumes the form characteristic for turbulent flow. For short channels, where the outlet section at best is located in cross section II-II, the equalizing of the velocity field does not occur, and for the estimate of losses it is necessary to know the form of the normal velocity profile in the free section of the jet. For this purpose we approximate the velocity profile by the following polynomial:

$$c = a_0 + a_1 r + a_2 r^2 + a_3 r^3. \quad (3-59)$$

We compute coefficient a_0 , a_1 , a_2 and a_3 from the following obvious boundary conditions:

when $r = r_2$

$$1) c = 0; \quad 2) \frac{\partial c}{\partial r} = 0;$$

when $r = r_1$

$$3) c = c_{\text{max}}; \quad 4) \frac{\partial c}{\partial r} = 0. \quad (3-60)$$

Then we will obtain

$$\frac{c}{c_{\text{max}}} = 3 \left(\frac{r_2 - r}{r_2 - r_1} \right)^2 - 2 \left(\frac{r_2 - r}{r_2 - r_1} \right)^3. \quad (3-61)$$

Here r_1 - the radius of the potential core; r - flowing radius in the given cross section (Fig. 3-36).

The velocity profile, plotted from expression (3-61), is represented in Fig. 3-37 by the solid curve. Plotted here are test data taken at different distances from the inlet section I-I in various pressure differentials. The calculated velocity profile adequately coincides with experiment 1 results on the boundary of the core of the jet and somewhat deviates from experimental points in the exterior, which is explained by the suction of flow in the space between the open jet and wall AB. As a result the second condition in relations (3-60) is fulfilled approximately. However, as a whole it is possible to consider that equation (3-61) correctly describes the velocity profile with sudden expansion and can be used for determining the area of displacement $\bar{\delta}^*$ and the area of energy loss $\bar{\delta}^{***}$ in the longitudinal cross section of the open jet. The appropriate calculations give rise to the following relations:

$$\bar{\delta}^* = \frac{1}{F_2} \int_0^{F_2} \left(1 - \frac{c}{c_{\text{max}}} \right) dF = 0,7 (1 - b^2) - b (1 - b); \quad (3-62)$$

$$\bar{\delta}^{***} = \frac{1}{F_2} \int_0^{F_2} \frac{c}{c_{\text{max}}} \left(1 - \frac{c^2}{c_{\text{max}}^2} \right) dF = 0,2 (1 - b^2) - 0,35 (1 - b) b, \quad (3-63)$$

where $b = r_1/r_2$ - the parameter dependent on the jet cross-sectional area.

Analogous expressions can be obtained if as the velocity profile we use [111].

$$\frac{c}{c_{\text{max}}} = \left[1 - \left(\frac{1-b}{1+b} \right)^{3/2} \right]^2. \quad (3-64)$$

The divergence in the integral areas $\bar{\delta}^*$ and $\bar{\delta}^{***}$, calculated on the basis of profiles (3-61) and (3-64), is small and when $b = 0$ is 4%.

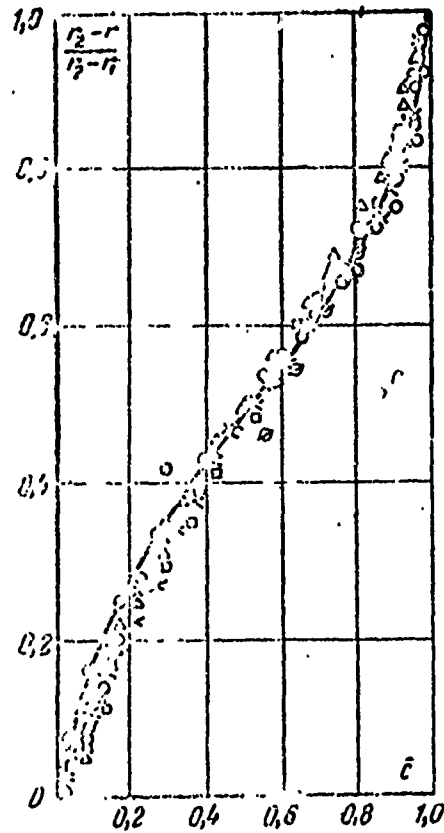


Fig. 3-37. Velocity profile in a jet with sudden expansion.

Values of the relative areas of displacement and energy losses, depending on parameter b , are given in Fig. 3-38. With a decrease in b from one to zero $\bar{\delta}^*$ monotonically increases, and $\bar{\delta}^{***}$ reaches a peak value when $b = 0.38$. Since along the jet the ratio r_1/r_2 falls, the curves given in Fig. 3-38 define the laws of the change in the area of displacement and area of the energy loss in zone $adec$ (see Fig. 3-36).

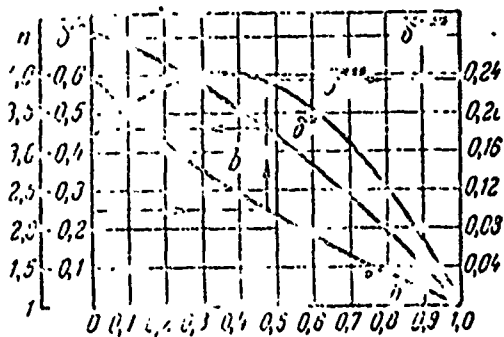


Fig. 3-38. The change in integral areas $\bar{\delta}^*$ and $\bar{\delta}^{***}$ along the jet with sudden expansion.

If we assume the jet boundary to be rectilinear, then it will be easy to connect value b to the expansion ratio:

$$b = \left[\frac{1}{\sqrt{n}} \left(\frac{\tan \gamma_1}{\tan \gamma_2} + 1 \right) - 1 \right] \frac{\tan \gamma_2}{\tan \gamma_1},$$

where $n = \left(\frac{r_3}{r_0} \right)^2 = \left(1 + \frac{x}{r_0} \tan \gamma_1 \right)^2$; γ_1 and γ_2 - the external and internal angles of lines limiting the zone of the viscosity effect on the section of the open jet.

In cross section II-II $n' = n$; having designated the ratio $\tan \gamma_1 / \tan \gamma_2$ by d , we obtain:

$$b = \left(\frac{d+1}{\sqrt{n}} - 1 \right) \frac{1}{d}. \quad (3-65)$$

With the change in the expansion ratio the correlation between angles γ_1 and γ_2 does not remain constant, i.e., value d is also a function of the expansion ratio. At first the value d grows with an increase in n and reaches a peak value equal to 2-2.2 when $n = 2$, and then it falls and when $n \approx 4$ approaches one. According to experiments conducted by B. B. Ett, this dependence can be approximated by the following relation:

$$d = \frac{1}{2} n (5 - n) - 1. \quad (3-66)$$

The noted change in parameter d is connected with the fact that at first the growth in the expansion ratio gives rise to a sharp increase in the rarefaction directly in the region of the change in flow area. As a result the external jet boundary is deflected to the large angle γ_1 , and the internal angle γ_2 is decreased somewhat. For large values of n ($n > 2$) the rarefaction drops, and the free jet boundary is noticeably lengthened, and angles γ_1 and γ_2 become approximately equal.

The specific values of the angles in question are given below. It should be noted that relations (3-62), (3-63), (3-65)

and (3-66) allow completely solving the problem of the estimate of internal and total losses with sudden expansion near the cross section II-II (see Fig. 3-36), when the jet completely fills the channel examined. For this purpose it is sufficient to use formulas (2-29) and (2-36)

$$\zeta = \frac{\bar{\delta}^{***}}{n^2(1-\bar{\delta}^*)^2}; \text{ and } \zeta_{\text{ex}} = \frac{1}{n^2(1-\bar{\delta}^*)^2},$$

having substituted in them for the prescribed value n the area of displacement $\bar{\delta}^*$ and the area of the energy loss $\bar{\delta}^{***}$ defined by formulas (3-62), (3-63), (3-65) and (3-66).

For the facilitation of the indicated calculations, plotted in Fig. 3-38 is dependence $b = f(n)$, which allows immediately finding the desired characteristics for the assigned expansion ratio. The order of the use of a nomogram in Fig. 3-38 is shown by dot-and-dash line and is not required in additional explanations.

Figure 3-39 gives the calculation and experimental values of the coefficient of recovery of energy ξ for various expansion ratios n . The use of formula (3-55) for determining this value gives rise to the dependence depicted by curve 1. At first an increase in the expansion ratio causes an intense increase in the coefficient ξ , and for $n = 2$ it reaches its peak value $\xi = 0.5$. A further increase in parameter n does not give a positive effect, and the conversion of the kinetic energy of flow into potential occurs with increased losses (when $n = 4$ $\xi = 0.385$).

Figure 3-39 gives experimental values of the coefficient of recovery of energy obtained in the channel with the sudden expansion of the area and relative length L/D_0 , which ensures maximum ξ with sudden expansion (curve 2). If when $n = 2$ the experimental and computed values ξ coincide, then subsequently the empirical curve is noticeably distinguished from the calculated one, and

when $n = 4$ the error is almost 22%.

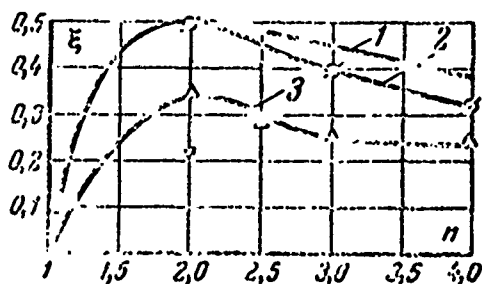


Fig. 3-39. The dependence of the coefficient of recovery of energy ξ upon the expansion ratio with sudden expansion. 1 - calculation by means of formula (3-55); 2 - experimental dependence; 3 - calculation formula (2-29) with the use of nomograms in Fig. 3-38; Δ - experimental values with the joining of the jet with the wall.

The obtained results confirm well the considerations expressed above about the necessity for the introduction of a correction into formula (3-55), which considers the momentum of frictional forces on the side of the restricting walls on the equalizing section.

When $n \leq 2$ the length of the free section of the jet is small, and the zone of nonuniformity of the velocity profile is also insignificant. In these conditions the additional losses, not being considered by formula (3-55), are small and practically do not affect the final result. When $n > 2$ the zone of equalizing is stretched, and, furthermore, losses in jet itself increase. As a result the additional term in formula (3-58) begins to play a noticeable role, and it is already necessary to consider it.

For the case when the length of the equalizing zone is equal to zero, i.e., when the jet wholly fills the outlet section, the calculated dependence $\xi = f(n)$, obtained by means of the nomogram in Fig. 3-38 and formula (2-29), is represented by curve 3. Here also the greatest value of the coefficient of recovery of energy is reached when $n = 2$, but its absolute value is substantially less and comprises only 0.34. A further increase in the expansion ratio gives rise to a drop in coefficient ξ . Experimental values of ξ confirm not only qualitatively but also quantitatively the

calculated dependence $\xi = f(n)$ well.

If in outlet section the diameter of the jet is less than the diameter of the channel, i.e., the flow does not fill the entire outlet section, in the space between the jet and wall there appears an intense return flow, which increases the losses and sharply lowers the coefficient of recovery of energy. From the aforesaid it follows that for the complete realization of sudden expansion, considerable length of the channel, determined by the total expansion ratio n and value of the external angle γ_1 is necessary.

For an example Fig. 3-40 gives curves of the change in coefficient ξ at various relative lengths of the wide part of the channel for three values of the expansion ratio n (vertical lines denote cross sections where the jet completely fills the outlet section of the channel). The nature of the given curves was different. When $n = 2$ the effectiveness of sudden expansion with an increase in L/D_0 grows very rapidly and reaches its greatest value when $L/D_0 = 6-7$, whereupon it is possible to note a certain drop (by 2-2.5%) in the coefficient ξ .

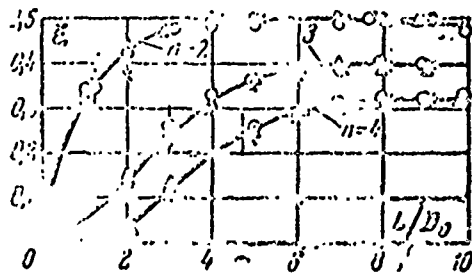


Fig. 3-40. Change in the coefficient of recovery of energy ξ with sudden expansion depending on the length of the wide part of the channel for various expansion ratios.

With an increase in the expansion ratio to $n = 3$, the intensity of the growth in ξ noticeably falls, and its greatest value ($\xi = 0.4$) corresponds to $L/D = 8-10$. The even more clearly expressed regularity is characteristic for $n = 4$, where generally at first ($L/D_0 < 2$) the coefficient of the recovery of energy ξ is close to zero. Only with an increase in the relative length

of the wide part of the channel ($L/D_0 > 2$) is there noted an increase in the coefficient ξ , the maximum value of which (0.33) is reached when $L/D_0 > 10$.

The noticeable decrease in total losses and the appropriate growth in value ξ after the filling with the flow of the entire channel located after the sudden expansion are explained by the sudden decrease in losses with the outlet velocity induced by the equalizing of the velocity field. The latter occurs at considerable length and is accompanied by additional internal losses.

The data given in Fig. 3-40 do not only allow observing the change in the diffuser effect with an increase in length, but also make it possible to estimate angle γ_1 for the given expansion. This value was equal to $9^\circ 30'$ for $n = 2$, 7° for $n = 3$ and $5^\circ 30'$ for $n = 4$, i.e., with a decrease in the diffuser effect (with a decrease in rarefaction in the region of sudden expansion), there occurs a decrease in angle γ_1 and its approximation to the value characteristic for the free jet.

The examined theoretical and experimental data show that the maximally attainable coefficient of recovery of pressure with sudden expansion is 0.50 for $n = 2$ and can be obtained only with long length of the channel.

For a determination of the minimum length of the wide part of the channel, which ensures the filling with the flow of its outlet section, it is possible to use the simple geometric relation

$$r_{\text{min}} = \frac{x}{r_0} = \frac{\sqrt{n-1}}{\text{tg } \gamma_1} \quad (3-67)$$

In this case the calculation of internal and total losses can be conducted on the basis of formulas (2-29) and (2-36) with

the use of the nomogram in Fig. 3-38.

As was already mentioned above, at wide flare angles of conical diffusers ($\alpha > 40^\circ$) and small axial dimensions, it is sometimes recommended to turn over to the diagram with the sudden expansion of flow [34]. In light of the given data, such a conclusion is insufficiently substantiated, because to obtain an acceptable diffuser effect in a scheme with sudden expansion it is necessary to have considerable axial dimensions ($L/D_0 > 5-6$), and at such a length it is always possible to use a non-detached diffuser having higher aerodynamic characteristics.

In conclusion let us point to the original method of the implementation of the sudden expansion proposed in work [160]. The form of channel for two-dimensional flow in this case is depicted on Fig. 3-41.

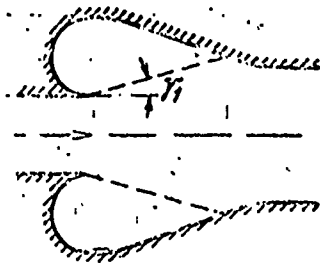


Fig. 3-41. Diameter of vortex diffuser.

Here directly after the sudden expansion "pockets" are created which facilitate the formation at the inlet of two stationary vortices which play the role of unique vortex "pumps." According to work [160] such a system has small total losses and allows obtaining the coefficient of recovery of energy at a level of 80%.

§ 3-8. Change in the Flow Parameters Along the Axis of the Conical Diffuser

The problem of the calculation of flow parameters along the axis of plane and axisymmetric channels for an ideal fluid

is solved within the framework of the one-dimensional theory comparatively simply [25].

When friction exists, the initial differential momentum equation is written by taking into account the unit impulse of frictional forces $L_{\tau p}$ and take the following form [25, 34]:

$$c dc - \frac{dp}{\rho} - dL_{\tau p} = 0. \quad (3-68)$$

Here c , p and ρ - velocity, pressure and flow density in the given cross section.

With the known law of the change in the frictional forces, equation (3-68) by means of equations of continuity and energy is solved in quadratures.

As a result for conical diffusers the following connection can be established between the flowing area F and dimensionless velocity λ [34]:

$$\frac{F_1}{F} = \frac{\lambda \left(1 - \frac{k-1}{k+1} \lambda^2\right)^\beta}{\lambda_1 \left(1 - \frac{k-1}{k+1} \lambda_1^2\right)^\beta} \times \left(1 + \sqrt{\frac{k-1}{k+1}} \lambda\right)^{\alpha \lambda_1} \times \frac{1}{\left(1 + \sqrt{\frac{k-1}{k+1}} \lambda_1\right)^{\alpha \lambda_1}}, \quad (3-69)$$

where

$$\beta = \frac{1}{k-1} (\gamma_1 + 1); \quad \alpha = \frac{k \gamma_1}{\sqrt{k^2 - 1}}; \quad F_1 \text{ and } \lambda_1$$

are the area and velocity in the inlet section, and ϕ_A - the coefficient of the "softening of shock" in formula (2-42a), which defines the losses ζ in the diffuser.

Relation (3-69) represents the common equation of continuity, in which the density ratio ρ_1/ρ_1 is connected with the velocity

and losses, namely:

$$\frac{\rho_2}{\rho_1} = \frac{\left(1 - \frac{k-1}{2} \lambda_1^2\right)^2 \left(1 + \sqrt{\frac{k-1}{k+1}} \lambda_1\right)^{\alpha \lambda_1}}{\left(1 - \frac{k-1}{2} \lambda_1^2\right)^2 \left(1 - \sqrt{\frac{k-1}{k+1}} \lambda_1\right)^{\alpha \lambda_1}}$$

With $\lambda \rightarrow 0$ $\rho_2/\rho_1 \rightarrow 1$, and formula (3-69) expresses the distribution of average velocities in the incompressible fluid:

$$\frac{c_2}{c_1} = \frac{F_1}{F_2}$$

If in the assigned cross section of the diffuser the mean dimensionless velocity is found, then the remaining values are easily located by means of gas-dynamic functions.

Unfortunately, for the calculation of mean velocities according to formula (3-69) it is necessary to know the coefficient of "softening" of the shock ϕ_d . This value, as was shown above, depends upon a number of factors and changes within inadmissibly wide limits (see Fig. 3-32). True, the structure of the formula (3-69) is such that at low velocities the error in the accepted value of coefficient ϕ_d weakly affects final results. However, for high velocities, when the density ratio changes greatly, the error can become perceptible. In connection with this let us examine the solution to the stated problem within the framework of the theory of the boundary layer, being restricted to the case of nonseparable flow.

The viscosity effect gives rise to the intense braking of the fluid near walls of the channel and to the "displacement" of it in the external part of the flow. From a physical point of view the viscosity effect causes a change in the effective flow area. Its magnitude is easily found after the appropriate boundary layer calculation and determination of the area of displacement. Then, having replaced the actual channel by a certain

arbitrary channel, the cross section of which at the known value of quantity δ^*_1 is calculated according to formula

$$F_{\text{ср}} = F_t - \delta^*_t,$$

it is possible to conduct the calculation of velocities with respect to relations of the ideal fluid.

With the practical use of the indicated method the greatest difficulties with calculations are usually connected with the definition of integral area δ^*_1 . For plane and conical diffusers the change in this value along walls can be calculated earlier, and then the construction of the equivalent channel will be reduced to purely a mechanical operation.

Above the distribution of the area of displacement δ^*_1 along the diffuser was approximated by the exponential function of the form

$$\delta^*_t = \delta^*_2 \bar{x}^m,$$

with the exponent $m = 0.8$, where the value δ^*_2 can be found from the nomogram of the Appendix (see Fig. A-1).

As a result the flowing effective area $F_{1 \text{ эф}}$ in any cross section \bar{x} will be determined by relation

$$F_{1 \text{ эф}} = F_t \left(1 - \frac{F_t}{F_t} \delta^*_2 \bar{x}^{0.8} \right).$$

For the calculation of the flow parameters along the axis of the thus obtained equivalent channel, it is most rational to use tables of gas-dynamic functions. With their use the calculation is constructed in the following manner:

1. According to the known flow rate, area at the inlet F_1 and parameters of full stagnation, we determine the given flow rate of the inlet section:

$$q(\lambda_1) = 0,326 \frac{GT_0}{F_1 p_{01}}$$

and from tables we find the dimensionless velocity λ_1 .

2. Using the following obvious relation

$$q_2(\lambda) = q(\lambda_1) \frac{F_1}{F_{1cp}}$$

with the help of tables with respect to q_1 we determine the moving values of velocity λ_1 , relative pressure p_1/p_{01} , relative density ρ_1/ρ_{01} and relative temperature T_1/T_0 .

On the sense of conclusion all the found values refer to the potential flow core, but hence it is easy to turn to their mean values. For this purpose let us write the continuity equation in the arbitrary cross section \bar{x}_1 :

$$F_1 \rho_1 \lambda_1 = F_{1cp} \rho_{1cp} \lambda_{1cp}$$

Hence

Reproduced from
best available copy.

$$\frac{F_{1cp}}{F_1} \frac{\rho_{1cp}}{\rho_1} \lambda_{1cp} = \frac{\rho_1}{\rho_{1cp}} \frac{\left(1 - \frac{k-1}{k+1} \lambda_{1cp}^2\right)}{\left(1 - \frac{k-1}{k+1} \lambda_1^2\right)} \frac{F_1 \lambda_1}{F_{1cp} \lambda_{1cp}} \quad (3-70)$$

Since the mean static pressure in the axisymmetric and plane duct is equal to the pressure p_1 in its center, formula (3-70) allows finding the mean dimensionless velocity λ_{1cp} and further from the tables all the averaged parameters in assigned cross section of the diffuser.

The mean pressure of full stagnation p_{01cp} is defined by expression (2-33):

$$(p_{01})_{cp} = p_1 \left(1 - \frac{k-1}{k+1} \lambda_{1cp}^2\right)^{\frac{k}{k-1}}$$

The examined method of the calculation of parameters along

the axis of the diffuser allows finding both the mean flow parameters and parameters in the center of the channel.

Let us note that the experimental velocity distribution, found with the help of drainage measurements of pressure and pressure of full stagnation p_{01} , corresponds not to the mean but maximum velocity in the given cross section, and in the comparison of calculated values with the experimental data this fact should be kept in mind. For example, Fig. 3-42 gives calculated and experimental curves of the change in relative velocity along the axis of the diffuser. As a whole the agreement of the calculation with experiment should be recognized as being satisfactory.

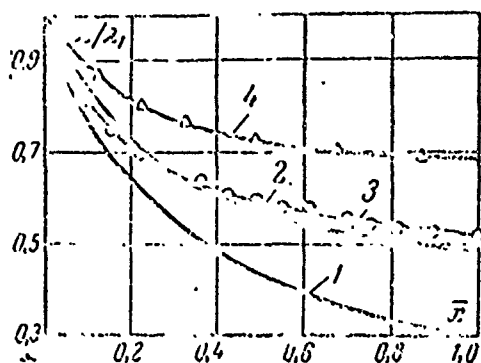


Fig. 3-42. Change in relative velocities along the axis of the diffuser. 1 - calculated curve of mean velocity; 2 - empirical curve ($\alpha = 10^\circ$; $n = 3$) of maximum velocity; 3 - calculation taking into account the boundary layer; 4 - empirical curve for a detached diffuser ($\alpha = 20^\circ$; $n = 3$).

§ 3-9. Example of the Calculation of a Diffuser with a Rectilinear Axis

As an example let us examine the calculation of a conical diffuser for the following conditions:

1. Mass flow weight rate $G = 5 \text{ kg/s}$.
2. Dimensionless velocity at the inlet into the diffuser $\lambda_1 = 0.5$.
3. Pressure of full stagnation $p_0 = 1.2 \text{ bar}$.

4. Stagnation temperature $T_0 = 450^\circ\text{K}$.

Since in the calculation it is convenient to use tables of gas-dynamic functions, let us introduce additionally the following designations:

q - reduced flow rate;

$\bar{\rho}$ - relative density;

T - relative temperature;

R - gas constant equal for air to $287 \text{ J/deg}\cdot\text{kg}$ and for vapor, $470 \text{ J/deg}\cdot\text{kg}$;

ρ_* - critical density.

The area of the inlet section of the diffuser is determined from the formula

$$F_1 = \frac{G}{\rho_1 c} = \frac{G \sqrt{T_0}}{0.385 \rho_0 q_1}$$

By knowing $\lambda = 0.5$, we find in the tables $q_1 = 0.71$, and, consequently,

$$F_1 = \frac{5 \sqrt{455}}{0.385 \cdot 1.2 \cdot 10^{-3} \cdot 0.71} = 0.0315 \text{ m}^2.$$

Reproduced from
best available copy.

It is advantageous to conduct further calculation of the diffuser in tabular form (see Table 3-1).

Table 3-1. Calculation of the conical diffuser.

Name	Designation	Unit of measurement	Calculation equation	Numerical value
Diameter at input	D_1	m	$D_1 = \sqrt{\frac{L_1^2}{\pi}}$	0,285
Relative temperature at inlet	$\frac{t_1}{t_0}$	—	Determined from table on λ_1	0,934
Temperature at inlet	T_1	°K	$T_1 = T_0 \bar{T}_1$	437
Critical velocity	a_x	m/s	$a_x = 13,3 \sqrt{T_0}$	386
Velocity at inlet into diffuser	c_1	m/s	$c_1 = a_x \lambda_1$	193
Relative density at inlet into diffuser	$\bar{\rho}$	—	Determined from gas-dynamic tables	0,9
Density at inlet into diffuser	ρ_1	$\frac{\text{kgf} \cdot \text{s}^2}{\text{m}^4}$	$\rho_1 = \bar{\rho} \frac{p_0}{R T_0}$	0,01
Coefficient of dynamic coefficient of viscosity	μ	$\frac{\text{kgf} \cdot \text{s}^2}{\text{m}^2}$	Found according to temperature from tables	$3,15 \cdot 10^{-6}$
Coefficient of kinematic viscosity	ν_1	$\frac{\text{cm}^2}{\text{sec}}$	$\nu_1 = \mu_1 / \rho_1$	$3,45 \cdot 10^{-8}$
Reynolds number calculated by conditions at inlet	Re_1	—	$Re_1 = \frac{D_1 c_1}{\nu_1}$	$1,1 \cdot 10^6$
Flare angle of diffuser	α	deg	Assumed depending on velocity at inlet	7
Expansion ratio of diffuser	n	—	Assumed from the condition of nonseparable flow	3

Table 3-1. (Cont'd.).

Name	Designation	Unit of measurement	Calculation equation	Numerical value
Relative length	L/D_1	—	$\frac{L}{D_1} = \frac{\sqrt{n}-1}{2 \sin \alpha/2}$	6
Length of diffuser	L	m	$L = D_1 \frac{L}{D_1}$	1,2
Parameter	H	—	$H = 1,4 \left(1 + \frac{\sqrt{n}-1}{L^{0,2}} \right)$	2,2
Value	B	—	$B = \frac{0,115}{Re^{0,2}} L^{0,2} H$	0,036
Relative area of displacement in outlet section	$\bar{\Delta}_2$	—	Determined from the nomogram of Appendix. (see Fig. A-2)	0,178
Total losses in diffuser	ζ_n	%	$\zeta_n = \frac{1}{n^2 (1 - \bar{\Delta}_2)^2}$	16,7
Internal losses	ζ	%	$\zeta = \frac{H^* / H \bar{\Delta}_2}{n^2 (1 - \bar{\Delta}_2)^2}$	3,8
Losses with outlet velocity	$\zeta_{a,c}$	%	$\zeta_{a,c} = \zeta_n - \zeta$	12,9
Pressure at inlet into diffuser	p_1	bar	$p_1 = p_0 z_1$	1,035
Pressure at outlet from diffuser	p_2	bar	$p_2 = (1 - \zeta_n) \frac{\rho_1 c_1}{2} - p_1$	1,170

CHAPTER FOUR

TRANSONIC AND SUPERSONIC DIFFUSERS

The characteristics of conical diffusers examined in the previous chapter show that an increase in the mach number at the inlet does not cause qualitative changes in the coefficients of internal and total losses. However, with approach to the speed of sound the picture is changed: almost in all cases it is possible to note a critical increase in losses. This fact gives rise to the necessity of dividing the transonic diffusers into a separate group, the examination of which is the subject of the first part of this chapter.

§ 4-1. Effect of the Reynolds Number and Compressibility (Mach Number) on the Diffuser Performances at High Subsonic Speeds. Transonic Diffusers

Physically the effect of compressibility velocities is seen in the increase in the longitudinal pressure gradients, which is explained by the density change of gas at significant numbers $M_1 < 1$. Actually, in accordance with conclusions of the one-dimensional theory, the longitudinal gradients of pressure and velocity in the elastic fluid are defined by formulas [25]:

$$\frac{dp}{dx} = \frac{\rho c^2}{F} \cdot \frac{1 - \frac{k-1}{k+1} \lambda^2}{1 - \lambda^2} \cdot \frac{dF}{dx} \quad (4-1)$$

$$= \frac{2k}{k+1} \cdot \frac{\rho}{F} \cdot \frac{\lambda^2}{1 - \lambda^2} \cdot \frac{dF}{dx}$$

$$\frac{d\lambda}{dx} = \frac{\lambda}{F} \cdot \frac{1 - \frac{k-1}{k+1} \lambda^2}{\lambda^2 - 1} \cdot \frac{dF}{dx}, \quad (4-1a)$$

Hence it follows that when $dF/dx > 0$ and $\lambda < 1$ $dp/dx > 0$ and $d\lambda/dx < 0$, where with an increase in λ the gradients of pressure and velocity increase. Consequently, the effect of compressibility is most perceptible in the diffuser inlet where the λ (M) numbers reach a maximum value. The final result of this effect is the critical drop in the diffuser performances with the approach to high subsonic and transonic velocities, and the beginning of crisis depends upon the magnitude of the aperture angle α [97] and the state of flow in the inlet section [150].

The greater the angle α or the boundary layer thickness at the inlet, then at smaller values of the dimensionless velocity λ_1 the critical reduction in the efficiency of diffusers, induced by the separation of flow directly in the inlet section is begun (see Fig. 3-9 and 3-10). A most clearly indicated pattern is traced if the coupling of the expanded part of the diffuser with the inlet section is accomplished by a small radius or generally with an angular break. In this case an increase in inlet gradients of pressure and velocity with an approach to the speed of sound becomes most noticeable. For example Fig. 4-1a gives the distribution of the relative static pressure along the outline of the inlet section of two conical diffusers, which are distinguished by angle α , for the dimensionless velocities of λ_1 equal to 0.4 and 0.85. All pressures are

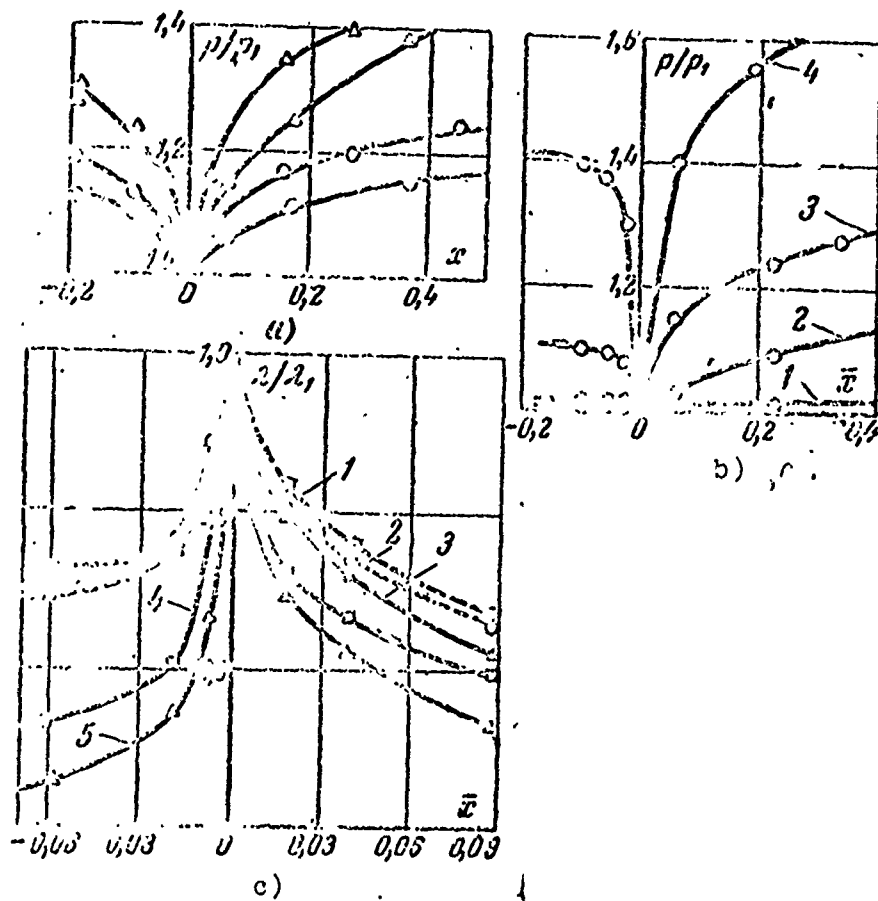


Fig. 4-1. Changes in static pressure and velocity on the inlet circuit of plane and conical diffusers. a) conical diaphragm; $p/p_1 = f(\bar{x})$;

○	$-\alpha = 7^\circ$;	} $\lambda_1 = 0.4$;
○	$-\alpha = 15^\circ$;	
△	$-\alpha = 7^\circ$;	} $\lambda_1 = 0.85$;
△	$-\alpha = 15^\circ$;	

b) plane diffuser; $p/p_1 = f(\bar{x})$: 1 - $\lambda_1 = 0.24$; 2 - $\lambda_1 = 0.57$; 3 - $\lambda_1 = 0.77$; 4 - $\lambda_1 = 1$; c) plane diffuser; $\lambda/\lambda_1 = f(\bar{x})$: 1 - $\lambda_1 = 0.4$; 2 - $\lambda_1 = 0.62$; 3 - $\lambda_1 = 0.7$; 4 - $\lambda_1 = 0.8$; 5 - $\lambda_1 = 0.94$.

expressed in fractions of the static pressure in the throat, and the longitudinal coordinate x is referred to the length of the expanded part of the diffuser L and is counted off from its inlet section.

The existence in the flow of the angular point, which is the specific point of the pole type leads, as was already mentioned above (see Chapter 3), to the local acceleration of flow on the side of the inlet and to its intense braking in the expanded part of the channel. Figure 4-1a visually shows an increase in the pressure gradients with an increase in the velocity and angle α . The same pattern is observed in the case of a plane diffuser (Fig. 4-1b), where for transonic velocity (curve 4) both negative (on the inlet side) and positive (in the expanded part) pressure gradients reach a peak value. The velocities corresponding to these gradients are shown in Fig. 4-1c. In the inlet plane section when $\lambda_1 = 0.94$ near the angular point the velocity increases almost to 30% (curve 5), whereas when $\lambda_1 = 0.4$ this increase is 14-15%.

Apart from the increase in the longitudinal pressure gradients, in the inlet region of the diffuser substantial transverse gradients of pressure [52] appear. In the inlet section the static pressure increases stably from the wall to the center of the flow. With an increase in the initial velocity and the approach to the angular point the transverse nonuniformity of the velocity and pressure fields increases, reaching about 32% when $\lambda_1 = 0.93$.

Thus, the disturbances induced by transition to the expanded part of the channel cover sufficiently vast regions and cause substantial nonuniformity of flow both in the longitudinal and transverse directions. The local pressure gradients in the wall region prove to be considerably increased as compared with

the gradients calculated according to mean flow rate λ_{1cp} . The noted features of flow give rise to substantial changes in the flow pattern in the inlet section, which is well noticeable in the examination of the boundary layer velocity profiles given in Fig. 4-2 and taken before the inlet section ($\bar{x} = -0.05$), in the inlet section ($\bar{x} = 0.1$). With their construction the transverse change in static pressure was considered. With an increase in the relative velocity λ_1 to 0.7, as one would expect, there occurs the filling of the velocity profiles, since the local convergence in the inlet part of the channel noticeably increases (see Fig. 4-1). However, when $\lambda_1 > 0.7-0.75$ the deformation behavior of the velocity profiles proves to be somewhat unexpected.

Despite an even further sharp increase in the convergence of the flow with an increase in λ_1 , the filling of the velocity profiles is sharply decreased (profile 4). Such a phenomenon is all the more strange as in experiments the velocity gain λ_1 was accompanied also by an increase in Re_1 number. Actually this means that in the range of high subsonic and transonic velocities an increase in λ_1 gives rise to a drop in the momentum of particles of fluid of the wall before the inlet section of the diffuser.

The given experimental data allow inferring about the presence of substantial changes in the flow pattern in the range of the inlet section of the diffuser at high subsonic and transonic velocities λ_1 . The mechanism for these changes can be represented in the following manner.

At low velocities, ($\lambda_1 = 0.34-0.37$, Fig. 4-2a) in the channel the typical turbulent velocity profile (profile 1) takes place. With an increase in λ_1 in the zone of the angular

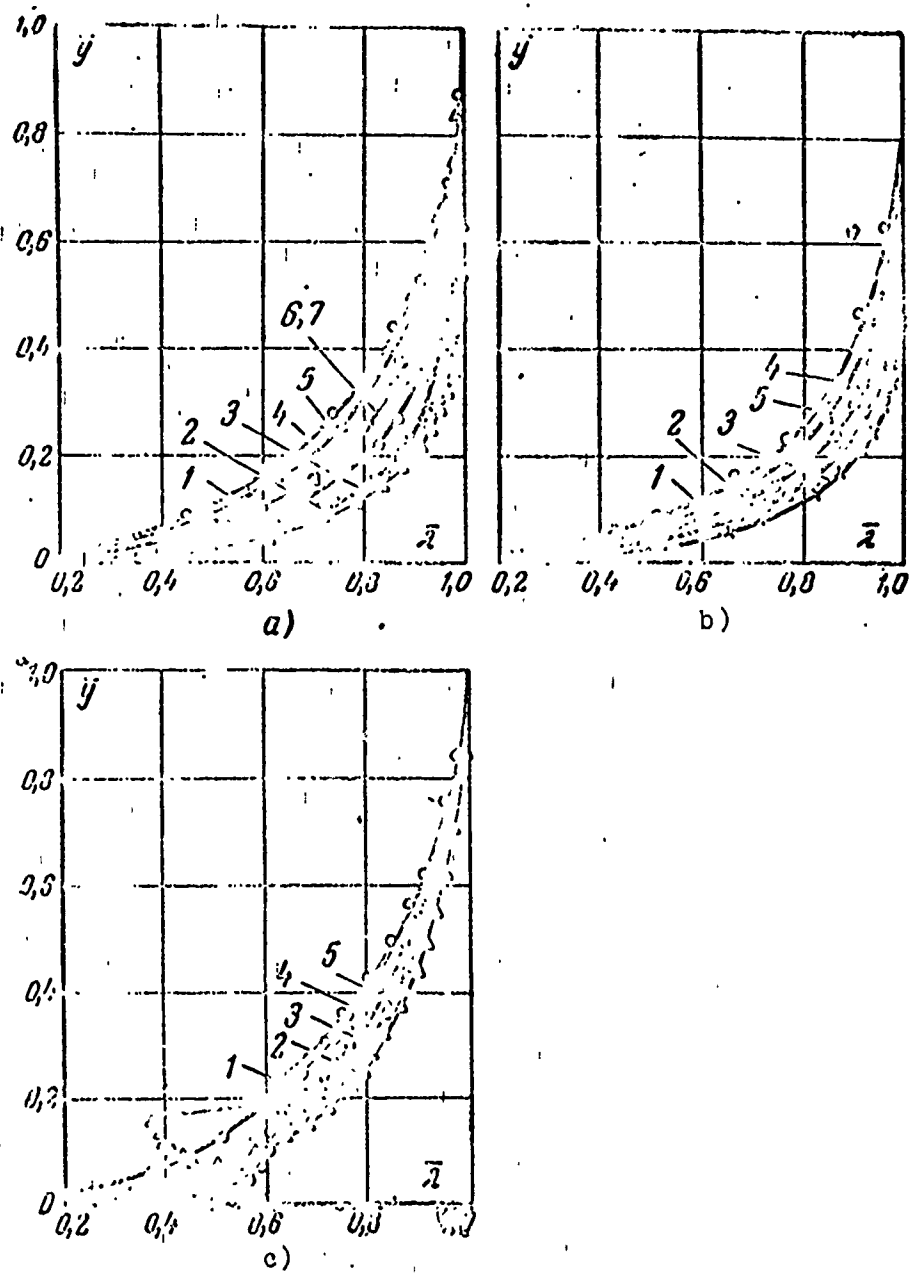


Fig. 4-2. Boundary layer velocity profiles in the inlet section of the plane diffuser ($\alpha = 10^\circ$).

$a - \bar{x} = 0.65$; $1 - \lambda_1 = 0.2$; $Re_1 = 0.21 \cdot 10^3$;
 $2 - \lambda_1 = 0.57$; $Re_1 = 0.23 \cdot 10^3$; $3 - \lambda_1 = 0.65$;
 $Re_1 = 0.25 \cdot 10^3$; $4 - \lambda_1 = 0.73$; $Re_1 = 0.4 \cdot 10^3$;
 $5 - \lambda_1 = 0.87$; $Re_1 = 0.43 \cdot 10^3$; $6 - \lambda_1 = 0.91$;
 $Re_1 = 0.44 \cdot 10^3$; $7 - \lambda_1 = 0.95$; $Re_1 = 0.45 \cdot 10^3$;
 $b - \bar{x} = 0$; $a - \bar{x} = 0.1$; $1 - \lambda_1 = 0.37$; $2 - \lambda_1 =$
 0.62 ; $3 - \lambda_1 = 0.7$; $4 - \lambda_1 = 0.95$; $5 - \lambda_1 = 0.93$.

break there occurs the sudden acceleration of flow noted above, the result of which is the deformation of the normal velocity profile characteristic for common convergent flow (profiles 2 and 3). However, with an increase in the local convergence there occurs a reduction in turbulent fluctuations in the flow [110], and, consequently, the transverse transfer of the momentum is decreased. As a result with a certain magnitude of the negative pressure gradient, being determined in this case by the value λ_1 , in the shaping of the velocity profile near the wall an ever greater importance is begun to be played by the viscous friction, and the "turbulent" friction will move away to the second plan, and when $\lambda_1 = 0.78-0.85$ (profiles 4, 5 and 6) the completeness of the profiles is substantially decreased. The velocity profile acquires a form characteristic for laminar flow.

The indicated changes in the flow pattern are an important feature of the transonic gas flows, which has a decisive importance for determining the behavior of subsequent flow in a diffuser.

Actually at high subsonic and transonic velocities λ_1 , on one hand, negative pressure gradients in the diffuser range increase (see Fig. 4-1), and on the other - there occurs a noted replotting of the velocity profile in the section before the inlet into the diffuser, as a result of which kinetic energy of particles of flow in the region near the wall is decreased (Fig. 4-2a). Both factors create conditions for the separation of flow directly after the inlet section of the diffuser. Thus, with the approach to transonic speeds there increases the possibility of the emergence of the separation of flow as a result of specific changes in the structure of the boundary layer.

Considering the varied viscosity effect on the gas flow pattern in diffusers [157, 165], the experimental investigation

of the compressibility effect on the effectiveness of diffusers must be conducted at the constant values of the Reynolds number over a wide range of its change.

Figure 3-10b and c gives experimental values of the coefficients of recovery of energy ξ , depending on the initial relative velocity λ_1 . Every curve corresponds to the narrow range of the changes in the Re_1 number. As one would expect, in the zone of the high subsonic and transonic speeds a sharp drop in the coefficient of recovery of pressure is observed, and a critical lowering of the efficiency of the diffusers depends both upon λ_1 and upon the Re_1 number. The greater Re_1 , then up to higher values of the relative velocity λ_1 nonseparable flow exists. This experimental fact agrees well with the structural changes in the boundary layer examined above with the approach to the inlet section of the diffuser.

Actually, with an increase in the Reynolds number the intensity of the transverse turbulent transition increases, and, consequently, large negative pressure gradients are necessary (high velocities of $\lambda_1 = 1$) for the degeneration of turbulence and adverse from the point of view of the separation of the deformation of the velocity profile. With an increase in Re_1 number the degree of degeneracy of turbulence at the inlet into the diffuser is decreased, and the zone of nonseparable flows according to velocity λ_1 is expanded.

The found connection of the critical drop in the diffuser performances from the combination of Re_1 and λ_1 numbers is very important and can be completely revealed only experimentally with an independent change in these criteria. If the change in Re_1 number is reached by the appropriate velocity change, then it is possible to arrive at the erroneous conclusion about the independence of the aerodynamic characteristics of diffusers from the compressibility of the fluid. Actually such a conclusion is made in work [66], whose author up to the velocity

$\lambda_1 = 0.96$ did not detect any compressibility effect on the coefficient of losses of the diffusers, since the increase in the Reynolds number simultaneously with an increase in the dimensionless velocity λ_1 ensured the mutual compensation of their effects and moved aside the critical drop in the characteristics into the zone of almost transonic speeds.

From the given experimental data obtained with independent simulation according to λ_1 and Re_1 numbers, it follows that compressibility can most decisively influence the energy performances of the diffuser with the approach to transonic speeds, whereupon the critical value of velocity λ_1 depends upon the Reynolds number and flare angle of the diffuser. The connection between these values, obtained on the basis of the examined experiments, is given in Fig. 4-3. This dependence allows determining the flow pattern in the inlet section of the diffuser for the assigned regime parameters.

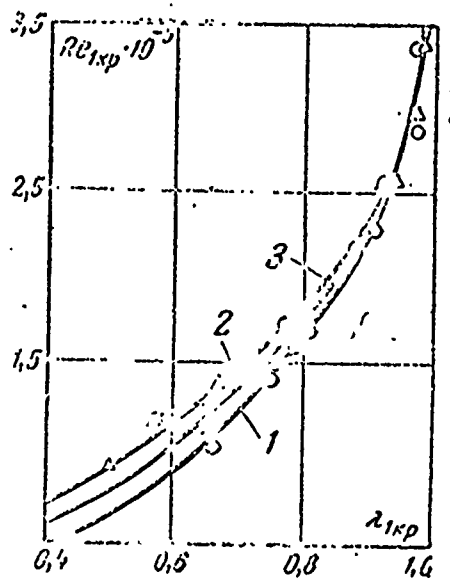


Fig. 4-3. Connection between the critical values of the Reynolds number and relative velocity at the inlet into the diffuser. 1 - $\alpha = 10^\circ$; 2 - $\alpha = 15^\circ$; 3 - $\alpha = 20^\circ$.

Thus, if the point which corresponds to the given initial parameters lies above the curve $Re_{1KP} = f(\lambda_{1KP})$, the flow will be nonseparable, and if it lies below it, the separation of flow occurs directly in the inlet section. For instance, if the velocity λ_1 in the diffuser with the flare angle $\alpha = 10^\circ$ is equivalent to 0.8, then for the provision of nonseparable flow the Re_1 number should be not less than $1.6 \cdot 10^5$. At smaller values of it, as experiments show, the separation of the flow will occur.

The dependence $Re_{1KP} = f(\lambda_{1KP})$ is determined also by the aperture angle of the diffuser α . The greater the angle α , the more the critical value of the Re_1 number for the given velocity. Physically such a dependence is entirely regular. The large angle α corresponds to the increased pressure gradients in the range of the inlet section of the diffuser, and consequently, the separation of flow appears at a lower velocity λ_1 . Let us note that the effect of angle α is developed only at moderate values of the velocity λ_1 . With its increase compressibility acquires primary importance, and the effect of angle α will move away to the second plan. When $\lambda_1 \rightarrow 1$ (transonic flows) the value of Re_{1KP} for all angles α approaches very large values, and the possibility of nonseparable flow is sharply lowered.

There is specific interest in results of the study of the mode which corresponds to low supersonic velocity at the inlet into the diffuser. In this case separation occurs before the shock wave at the inlet expanded part of the diffuser.

The modes in question ($\lambda_1 = 1.0-1.15$) are characterized by the constant (critical) values of velocity and pressure in the minimum (inlet) cross section of the diffuser. In accordance with this the stratification of curves of relative velocities (pressures), depending on mode, is noted after the inlet section

and is determined basically by the position of the shocks (or the system of shocks) in the expanded part of the diffuser. Prior to the shock the flow in the inlet part is convergent. An increase in pressure occurs in the shock and the expanded part after it during separation and nonseparation flows. In this connection it should be noted that if the section of laminarization of the boundary layer is stretched up to the shock, then the latter always causes separation. When the region of transition of the laminar layer into the turbulent is located before the shock, the separation is shifted along the flow.

The minimum intensity of the shocks which cause separation was determined experimentally. Figure 4-4 gives the appropriate relation of I. S. Grodzovskiy and L. Ya. Lazarev for laminar and turbulent boundary layers. For the laminar boundary layer the appropriate pressure ratio on the shock is 1.50-1.58 and for the turbulent boundary layer, 1.8-2.1. In proportion to the development of the process of the degeneration of turbulence, the intensity of the shock which causes separation is decreased, and with completely completed reversed transfer the broken and solid lines merge.

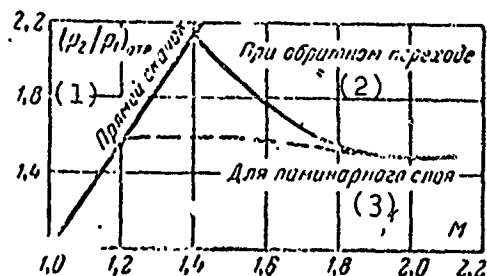


Fig. 4-4. Intensity of the shock causing separation of the boundary layer. (Experiments of I. S. Grodzovskiy and L. Ya. Lazarev, MEI)

KEY: 1 - normal shock; 2' - with inverse transition; 3 - for laminar flow.

The location place of the shock in the modes in question is established by the method known from the theory of variable modes of the Laval nozzle [25]. The use of this method is all the more justified in that the modes of operation of the diffuser when $\lambda_1 \geq 1.0$ completely correspond to modes of the operation of the Laval nozzle with an increased ratio of pressures,

when in the expanded part shocks are formed. One should keep in mind that the form of the shock to a great degree depends upon the flare angle of the diffuser. Thus, for instance, in a diffuser with $\alpha = 15^\circ$ experiments record the system of two oblique shocks, and in a diffuser with $\alpha = 7^\circ$ - one curvilinear shock. The position of the shock in the diffuser also substantially depends upon the flare angle.

The discharge characteristics of diffusers at transonic speeds show that the relative gas flow through the diffuser increases with an increase in λ_1 up to 1.0. A further increase in λ_1 does not give rise to a change in the flow rate.

For the characteristic of transonic diffusers it is advantageous to compare values of theoretical and actual pressure ratios.

The appropriate graphs are given in Fig. 4-5. Curve 1 corresponds to the calculated theoretical pressure ratio p_{2T}/p_1 (without allowing for diffuser losses). Curve 2 is obtained experimentally and represents the relation of the product of the pressure ratio and coefficient of recovery of the stagnation pressure:

$$\frac{p_2}{p_1} \cdot \frac{p_{01}}{p_{02}} = \frac{p_{2T}}{p_1}$$

The agreement of the calculated 1 and experimental 2 curves proves to be satisfactory. The divergence between curves 2 and 3-8 reflects the effect of the Reynolds number and dimensionless velocity λ_1 on the pressure ratio in the diffuser. With a decrease in the Reynolds number an intense reduction in the pressure ratio is noted. In accordance with data of Fig. 4-3 critical values of λ_{1kp} decrease with a decrease in the Reynolds number.

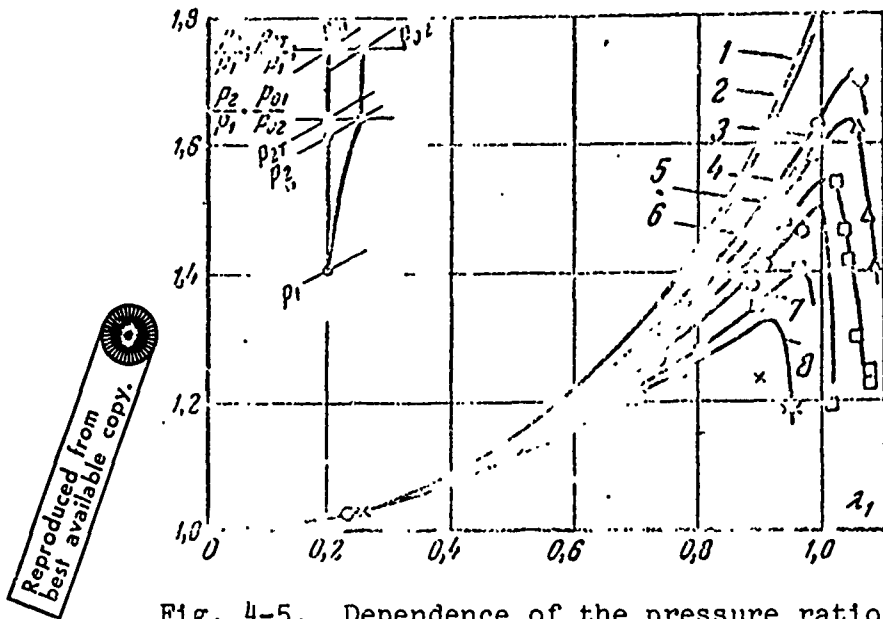


Fig. 4-5. Dependence of the pressure ratio in conical diffuser upon the Reynolds number and dimensionless velocity λ_1 ($\alpha = 15^\circ$; $n = 4$; tests with superheated steam). 1 - theoretical curve

$\frac{p_2}{p_1} / \frac{p_01}{p_02}$; 2 - $\frac{p_2}{p_1} \cdot \frac{p_01}{p_02}$; 3 - p_2/p_1 ; 8 - $Re_1 = (0.5 \div 0.9) \cdot 10^5$; 7 - $Re_1 = (1.0 \div 1.2) \cdot 10^5$;
 6 - $Re_1 = (1.5 \div 1.8) \cdot 10^5$; 5 - $Re_1 = (2.02 \div 2.5) \cdot 10^5$; 4 - $Re_1 = (2.8 \div 3.3) \cdot 10^5$;
 3 - $Re_1 = (4.4 \div 4.8) \cdot 10^5$.

The graphs in Fig. 4-5 reflect the compressibility effect on the pressure ratio - the most important diffuser performance. Here it is clearly evident when $\lambda_1 < 0.5$ the compressibility effect is imperceptible in practice. At large Reynolds numbers ($Re_1 > 4 \cdot 10^5$) the diffuser with the flare angle $\alpha = 15^\circ$ and $n = 4$ has a maximum compression ratio when $\lambda_1 \approx 1-1.05$.

In connection with that expounded above, one should note the influence of the initial turbulence level on the diffuser performances. The increase in the degrees of turbulence at small and moderate Re_1 values gives rise to a noticeable improvement in the diffuser performances, since the transition region

with the mixed boundary layer is shifted against the flow, which in a number of cases eliminates separation. However, with a very high initial turbulence the thickness of the boundary layer sharply increases, and the effective value of the expansion ratio is decreased. An increase in the turbulence level causes an increase in frictional losses. For these reasons at small Re_1 and λ_1 numbers the energy losses in the diffuser with an increase in ϵ_0 are at first lowered but then increased. An example of such a dependence is shown in Fig. 4-6. With a decrease in Re_1 when $\lambda_1 \approx 0.4$, the minimum of losses in the range $\epsilon_0 = 2-3\%$ is developed more clearly.

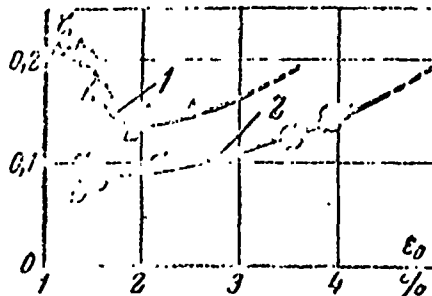


Fig. 4-6. Effect of initial degree of turbulence on losses in conical diffusers at various Reynolds numbers ($\lambda_1 = 0.40$; $n = 3$; $\alpha = 10^\circ$). 1 - $Re_1 = 2.2 \cdot 10^4$; 2 - $Re_1 = 10^6$.

Experiments show that the effect of the initial turbulence on the diffuser performances at high subsonic speeds is maintained qualitatively the same as that for the incompressible fluid. The data given in Fig. 4-6 can be used for the introduction of appropriate corrections at significant λ_1 numbers.

Thus, the transition to high subsonic speeds does not give rise to noticeable changes in losses and recovery ratio in diffusers. If the flow conditions are self-similar according to Re_1 number, then an increase in λ_1 number from 0.3 to 0.6-0.7 does not cause a substantial change in the diffuser performances. The latter means that the intensification of the flow of process in diffusers according to λ_1 number up to the indicated limits is rational.

In conclusion it is necessary to emphasize that at small Re_1 numbers a favorable effect on the diffuser performances is rendered by the blowing of the boundary layer. The use of suction gives rise to a noticeable increase in the effective expansion ratio and a decrease in frictional losses.

§ 4-2. Reverse Transition of the Turbulent Boundary Layer into Laminar

Let us examine in more detail the phenomenon of reverse transition in the boundary layer and the laminarization of the velocity profile at transonic speeds.

In the laboratory of [MEI] (MЭИ) Moscow Power Engineering Institute) the transition of the turbulent layer into a laminar layer was investigated on four different models 1) axisymmetric "two-throat" channel; 2) plane "two-throat" channel; 3) nozzle curvilinear channel; 4) plane diffuser. Some results of this study are stated below.

In axisymmetric and plane straight channels there is the possibility of obtaining the characteristic flow conditions, the basic features of which are the following: in the second "throat" of the channel there occurs the secondary transition of flow through the speed of sound, whereupon the flow before the second "throat" is created greatly turbulent by the shock wave which appears after the first throat of the channel. The pressure distribution along the wall of the channel (Fig. 4-7a) clearly shows that behind the diffuser section in the middle part of the channel the flow is characterized by very large positive velocity gradients $\left(\frac{\partial c_{\max}}{\partial x} \approx 2 \cdot 10^4 \frac{1}{s}\right)$.

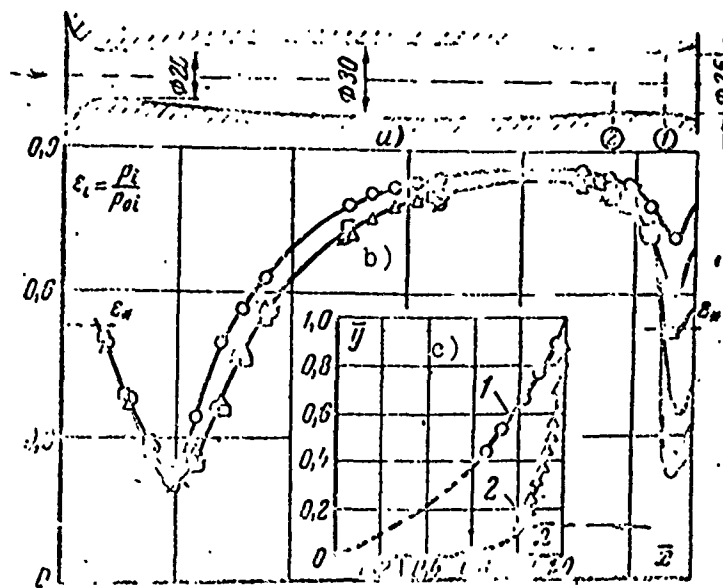


Fig. 4-7. Diagram of a "two-throat" channel (a), pressure distribution along its length; (b) and boundary layer velocity profile $\epsilon_a = 0.210$ (c). b) $\circ \epsilon_a = p_2/p_{01} = 0.700$; $\bullet \epsilon_a = 0.514$; $\Delta \epsilon_a = 0.350$; $\square \epsilon_a = 0.309$; $\nabla \epsilon_a = 0.262$; $\emptyset \epsilon_a = 0.209$; c) 1 - section 1; 2 - section 23 mm to the left of section 1 (section 2).

The presence of such velocity gradients should facilitate and, probably, basically determine the transition of the turbulent boundary layer into the laminar one. This transition was confirmed by measurements of the velocity distribution in the boundary layer before and after the second throat. If before the second throat of the channel the velocity profile is clearly turbulent (Fig. 4-7c), then after the second throat profile has another form - laminar.

In a plane two-throat channel measurements of pressure fluctuations were conducted at a distance of ~ 0.8 mm from

the wall, i.e., almost in the boundary layer, in three characteristic sections: in the first throat, in the section of maximum width and in the second throat. Fluctuations were measured by an extensometric probe and recorded on the film of a loop oscillograph. It is evident that in such a channel there should also take place the characteristic conditions of reverse transition which were observed in the axisymmetric channel. Figure 4-8 shows oscillograms of the measurement of fluctuations of the total pressure in the mode $\epsilon_a = 0.25$. One can see well that in the first minimum cross section of the channel there are practically no fluctuations. In the maximum section of the channel fluctuations of large amplitude and sufficiently low frequency (~ 20 Hz) take place. This order is characteristic for large-scale turbulent fluctuations. It should be noted that in this mode the amplitude of fluctuations comprised about 10% of the total pressure. In the second minimum section the fluctuations were sharply attenuated and were absent in practice. The measurements of fluctuations described above show that in the second throat of the channel the boundary layer became laminar, although before the second throat the flow had a clearly turbulent behavior.

The curvilinear channel was investigated along the straight and convex walls in oblique shear (Fig. 4-9). By examining the distribution of relative pressures $\epsilon_1 = p_1/p_{01}$ along the contour of the channel, it is possible to note that up to the emergence of the shock wave on the convex wall the positive velocity gradient was of the order of $(6-8) \cdot 10^3$ 1/s, whereupon in this section the rates of flow were changed from $M = 0.4-0.5$ to $M = 1.85-2.0$ in the mode $\epsilon_a = 0.23$. It is interesting that the extension of the section in which the large positive velocity gradients took place considerably increased with an increase in the M_2 number at the outlet from the channel. This is clearly

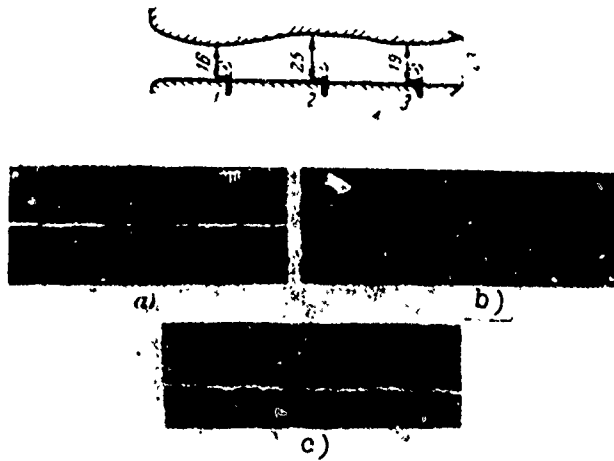


Fig. 4-8. Fluctuations of the total pressure (measurements in the plane "two-throat" channel; $\epsilon_a = 0.25$).
 a) section 1; b) section 2; c) section 3.

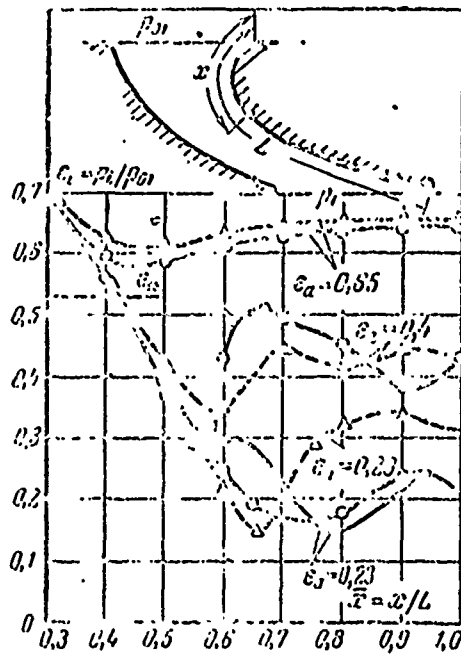


Fig. 4-9. Pressure distribution along walls of the curvilinear nozzle channel at different pressure ratios. \circ - convex wall; Δ - straight wall.

Reproduced from
 best available copy.

evident in Fig. 4-10 where plotted along the axis of the ordinates is the relative extension of the section $\Delta x/L$ (L - length of the wall) with the velocity gradient, and along the axis of the

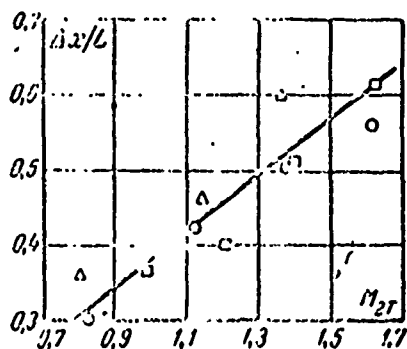


Fig. 4-10. Extension of the section of the channel with maximum velocity gradients. Δ - convex wall; \circ - straight wall; \square - concave wall.

abscissae - the Mach number at the outlet from the channel determined from pressures before and after the channel. As can be seen from Fig. 4-10, the extension of the section with maximum gradients depends little upon the surface shape of the channel. It should be noted that, as was expected, the maximum gradients of velocity (pressure) were attained in the narrow sections of the channel, i.e., in the region where the number $M \rightarrow 1$.

The channel tested was established in a wind channel, the turbulence level of the flow in which was approximately 1%. For the agitation of the boundary layer before the throat of the channel on the convex surface ($\bar{x} = 0.15$) a turbulent wire with a diameter $d = 0.8$ mm was installed. As measurements of the boundary layer the velocity profile showed in mode $\epsilon_a = 0.286$, in sections $\bar{x} = 0.483$ and $\bar{x} = 0.512$ on the convex wall the boundary layer was turbulent (Fig. 4-11). With the advancement along wall from the narrow section ($\bar{x} = 0.483$) to the outlet section, there occurred the laminarization of the boundary layer velocity profile, i.e., the filling of the profile was decreased, and under a sufficiently prolonged effect of the negative pressure gradient the velocity profile became laminar. The laminar boundary layer further interacted with the shock wave which appeared on the convex wall as a result of the overexpansion of the flow and was separated by this shock (the characteristic separation

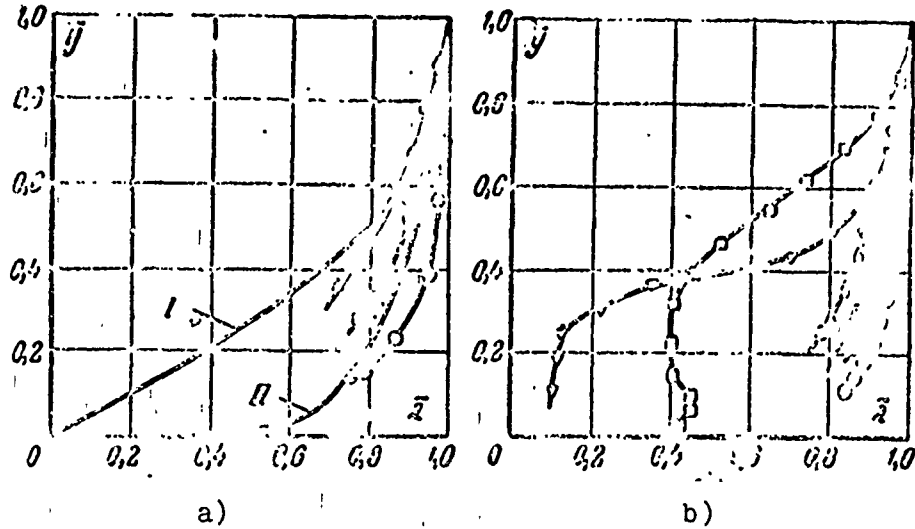


Fig. 4-11. Boundary layer velocity profiles on walls of a curvilinear channel. a) straight wall ($\epsilon_a = 0.250$):
 \circ - $\bar{x} = 0.485$; \otimes - $\bar{x} = 0.616$; Δ - $\bar{x} = 0.673$; I - laminar profile; II - turbulent profile; b) convex wall ($\epsilon_a = 0.253$): \circ - $\bar{x} = 0.473$; Δ - $\bar{x} = 0.512$; \odot - $\bar{x} = 0.559$; \square - $\bar{x} = 0.623$; \diamond - $\bar{x} = 0.673$; ∇ - $\bar{x} = 0.969$.

velocity diagrams in the boundary layer are presented in Fig. 4-11b). It should be noted that at a relatively small length of the effect of the negative pressure gradients, i.e., at smaller Mach numbers, the total laminarization of the velocity profile was not observed, and the turbulence degenerated partially. The analogous change in the velocity profile occurred even on straight wall of the channel.

In the investigation of the transition of the laminar boundary layer into the turbulent, usually the position of the transition is determined from the nature of the change in the boundary layer thickness δ^{**} . Let us note that the same boundary layer characteristics can be used for determining the point of the transition of the turbulent mode into the laminar mode.

There is specific interest represented in data given in Fig. 4-12, where the change in the dimensionless boundary layer thickness $\delta \sqrt{\frac{c_{x, \max}}{\nu x}}$ depending on the $Re_x = c_{x, \max} x / \nu$ number, calculated on the coordinate along the rectilinear wall of the channel is represented. According to Blasius's solution, the dimensionless boundary layer thickness with laminar flow along the plate has a constant value equal to ~ 5 . But as soon as the Re_x number becomes more than the critical, the dimensionless thickness of the layer begins to increase sharply. It is logical to assume that in the case of the transition of the turbulent boundary layer into a laminar one, a reverse pattern will be observed, i.e., with the degeneration of turbulence the dimensionless boundary layer thickness will be decreased along the back edge up to the achievement of a certain constant value. The achievement of a constant value means that the boundary layer became laminar. Such an assumption is confirmed well by an experiment. For flow without a vortex generator (Fig. 4-12b) the thickness without a vortex generator (Fig. 4-12b) the thickness $\delta \sqrt{\frac{c_{x, \max}}{\nu x}}$ remained constant up to $Re_x = (1.8-2.0) \cdot 10^5$, and then it sharply increased, which indicates the transition to the turbulent mode induced by the shock wave. For the case with a vortex generator (Fig. 4-12a) the dimensionless boundary layer thickness was first rather rapidly decreased to the value equal to ~ 10 , and then it remained constant (the turbulent layer turned into the laminar), and when $Re_x = 2.15 \cdot 10^5$ it sharply increased (the laminar layer again turned into the turbulent in the shock wave).

Completely analogous results were obtained during the study of the boundary layer on the convex wall of the channel. These results show some features of reverse transition. It is evident that transition zone in the case of reverse transition should have a large extension, since a significant section of the flow

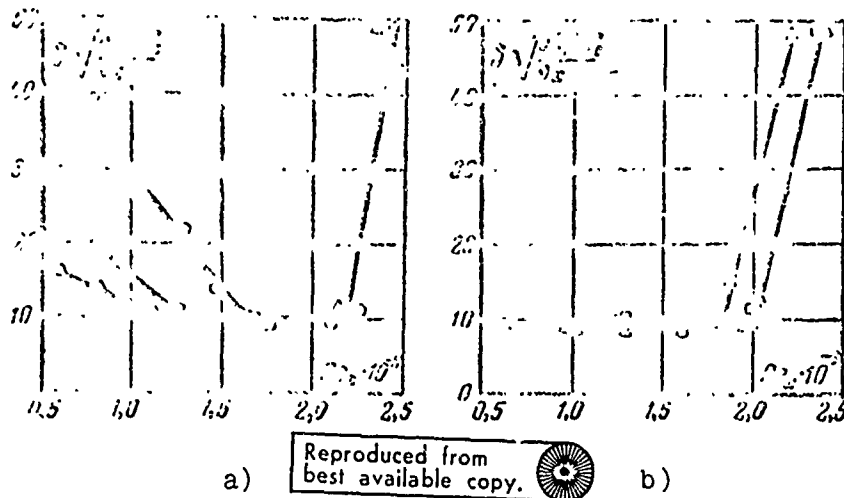


Fig. 4-12. Change in the dimensionless boundary layer thickness along walls of the curvilinear channel. a) with a vortex generator: \circ - straight wall ($\epsilon_a = 0.230$); \square - convex wall ($\epsilon_a = 0.284$); Δ - convex wall ($\epsilon_a = 0.325$); b) without a vortex generator: Δ - straight wall ($\epsilon_a = 0.230$); \blacktriangle - straight wall ($\epsilon_a = 0.318$); \square - convex wall ($\epsilon_a = 0.330$).

for the degeneration of turbulence is necessary. It is natural that the length of this section will depend upon the magnitude of the velocity change. Furthermore, as is known, the instantaneous transition of laminar conditions into turbulent (for instance, at the height of the protuberances of the roughness more than limiting) is possible, and in the case of reverse transition in principle this is impossible - the zone of transition should have an extension.

Usually when estimating the flow stability, the basic stability criterion is the Reynolds number. Figure 4-13 gives the change in the $Re^{**} = C_{x\max} \delta^{**} / \nu$ number and $Re^{**}_{кр}$, calculated according to the empirical correlation of A. P. Mel'nikov, for straight and convex walls in the oblique shear of the channel with the vortex generator when $\epsilon_a = 0.23$ and $\epsilon_a = 0.286$,

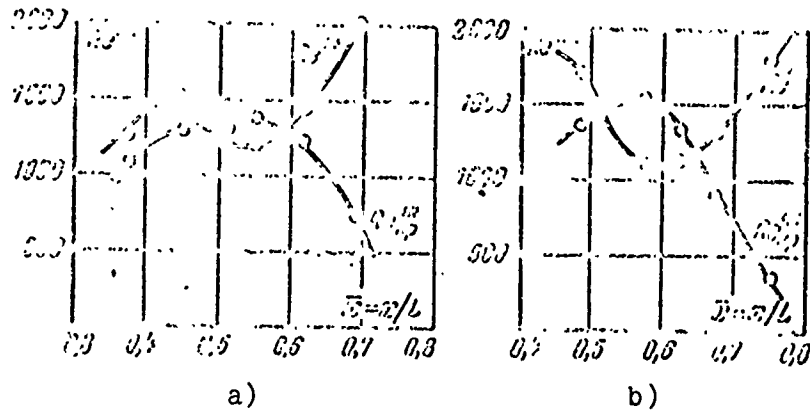


Fig. 4-13. Change in numbers Re^{**} and $Re^{**}_{кр}$ along walls of a curvilinear channel. a) convex back edge; b) straight wall.

respectively. In Fig. 4-13 for the convex wall it is clearly evident that after the vortex generator the $Re^{**}_{кр}$ number is less than Re^{**} , i.e., the boundary layer is turbulent. During motion along the wall $Re^{**}_{кр}$ increases, and Re^{**} is decreased and in the section with coordinate $\bar{x} = 0.490$ the two curves intersect. When $\bar{x} > 0.490$ the number $Re^{**} < Re^{**}_{кр}$, i.e., the layer became laminar - "reverse" transition occurred. When $\bar{x} > 0.590$ the Re^{**} number again proves to be more than $Re^{**}_{кр}$ and on the wall turbulent flow conditions in the boundary layer is established.

One should note the satisfactory coincidence of the point of the transition of the turbulent flow conditions into laminar determined by two methods: as points of the intersection of curves $Re^{**}(\bar{x})$ and $Re^{**}_{кр}(x)$ in Fig. 4-13 and as the beginnings of the plane section on the curve of the dependence of the dimensionless boundary layer thickness upon Re_x (Fig. 4-12). Their coordinates are respectively equal to 0.490 and 0.509.

Thus, the experimental investigation of the boundary layer on various models confirmed the emergence of the transition of

the turbulent boundary layer into laminar, or of the "reverse" transition, at large longitudinal negative pressure gradients.

The maximum negative pressure gradients correspond to the transonic gas flows. Consequently, during the transition through the speed of sound the possibility of the degeneration of the turbulence proves to be maximum. The "reverse" transition is an important feature of transonic flows of viscous gas, which is the reason for the separation of flow with the emergence of the shock wave directly after the section of the reverse transition where the boundary layer is laminar.

Experimental investigations showed that the transition of the turbulent boundary layer occurs gradually in the significant transition section. According to preliminary data, this section has an extension of the order of $(15-25)\delta$ (δ - the physical boundary layer thickness in the beginning of the transition zone). However, the extension of the zone of transition should depend upon the magnitude of the velocity gradient and is in need of refinements. Important also is a definition of conditions necessary for the reverse transition, i.e., a definition of the correlation between the magnitude of the velocity gradient (or intensity of cooling of the wall) and the extension of the zone of transition.

It is necessary to emphasize especially that in many instances in the sharply convergent gas flows only partial degeneration of the turbulence in the boundary layer and core of the flow will occur. The partial degeneration of turbulence gives rise to the characteristic deformation of the velocity profile near the wall, which is expressed in the reduction in local velocities. The effect of the positive pressure gradients on the flow with a partially degenerating turbulence also gives rise to its separation.

The phenomenon of partial or complete laminarization of the flow at transonic speeds is revealed when the boundary layer thickness at the inlet into the diffuser reaches large values.

In convergent flow the reverse transfer in the boundary layer, connected with the partial or complete degeneration of turbulence, gives rise to a reduction in losses to friction.

The investigation of the boundary layer in diffusers whose results are given in Fig. 4-1 and 4-2 shows that with alternating pressure gradients at the feed and inlet sections of the diffuser the phenomenon of partial or complete degeneration of turbulence is observed. The flow of features in these sections at transonic speeds, which are expressed in an increase in the pressure gradients in convergent and diffuser regions, should give rise to the critical increase in losses in connection with the unavoidable separation in inlet sections of diffusers. In this aspect becoming quite clear are results of the experiment, which showed the dependence of $\lambda_{\text{кр}}$ upon the Reynolds number, since the possibility of partial or complete extinguishing of the turbulence is determined by the value Re_1 .

The basic regularities of the "reverse" transition stated above are confirmed well by data of other researchers. We will discuss some of these works briefly.

Interesting research on the flow pattern under the effect of high accelerations was carried out at the end of the 1950's by Senno [168] and A. A. Sergeyenko and V. K. Gretsov [94]. In [168] the boundary layer on the back edge of the profile of the turbine nozzle grid was studied. The boundary layer in the throat section was always laminar even when prior to the throat turbulent flow conditions were recorded. The flow pattern up to the throat

almost did not affect the structure of the boundary layer near the throat. After the minimum section the flow again became turbulent, which confirmed the measurements of fluctuations and the appearance of noise in a stethoscope. An analysis of the flow of structure was realized on the basis of the theory of a three-dimensional laminar boundary layer, whereupon the convergence of the calculation and experiment was satisfactory. Values of the Reynolds number in the throat section were $Re^{**} < 600$, which confirms the stability of such a flow.

In [94] test data of an axisymmetric convergent-divergent nozzle are given. Velocity profiles in the superimposed section and at the outlet from the nozzle were measured. Measurements were conducted in two modes: under pressures in the receiver of 0.3 and 1.0 bar. For both modes the velocity gradients on the axis were equal, respectively: to $dc_{max}/dx = 2730$ l/s (in the throat) and 2720 l/s (at the outlet from the nozzle). The velocity profiles at the outlet from the nozzle in the first mode had the distribution characteristic for laminar conditions, although in the superimposed section layer it was always turbulent. In the second mode no peculiarities were noted.

A detailed study of the degeneration of turbulence was conducted by a group of colleagues under the guidance of A. A. Gukhman. Part of the works (they were carried out in the 1950's and beginning of the 1960's) was based on the use of a design apparatus of a one-dimensional model. Used as the working sections were the convergent-divergent nozzles of small conicity with an aperture angle less than 1° . On the basis of careful measurements of the distribution of static pressure and (in experiments with heat exchange) local thermal flows along the nozzle, the coefficients of friction and thermal conductivity along the length of channel were determined. These experimental

values were the basis for the analysis of structural changes in the flow. Such a method, naturally, could not lead to reliable conclusions, since it is based on considerably important assumptions whose validity must be proved. In this connection a direct study of the flow pattern is more interesting [24a]. The same channels of small conicity served as the working sections. An experimental installation allowed over a wide range a changing of the Reynolds numbers irrespective of the Mach number. Velocity profiles before the nozzle inlet and at the outlet from it at various distances from the entrance. The studies showed the following:

1. Under the effect of the negative pressure gradients the turbulence in the flow begins to degenerate, which under specific conditions gave rise to the reconstruction of the velocity profile. Simultaneously, under the action of high accelerations the boundary layer thickness was considerably decreased.

2. The stability of changes in the structure of the boundary layer considerably depended upon the Reynolds and Mach number. Only at small Re_1 was the flow stabler and preserved the laminated form of the profile at a distance of the order of 2 gauges behind the throat. At large Re_1 numbers even in the cross sections close to entrance, laminated profiles were not detected.

3. The effect of laminarization was characterized by the presence of two regions in the boundary layer: the wall region with a velocity distribution close to the laminar, and the external region with a velocity profile close to turbulent. The magnitude of the wall region exceeded the thickness of the viscous sublayer by one order. In accordance with the nature of the velocity distribution, the frictional resistance of the laminated flow was, according to the calculation, considerably (2-2.5 times) less than the resistance of the turbulent boundary

layer for conditions under which the reverse transition was observed.

4. The depth of the changes which occurred under the action of the large negative pressure gradients depended upon the conditions of flow (magnitude of the acceleration of flow, the Re_1 and M_1 numbers). With this the values of negative gradients and the time of their effect appeared as interdependent causes of the same phenomenon. The depth of the laminarization depended upon the combination of these factors.

5. The effect of degeneration was developed to the greatest degree at a certain distance from the place of the effect of high accelerations. In certain cases, apparently, the secondary transition managed to occur earlier than laminarization was developed.

It is natural that both the results obtained by the authors and data of the other researchers described above do not exhaust the entire complexity and uniqueness of the problem of reverse transition. Additional studies are necessary with the use of the low-inertia probes, which allow measuring the spectrum of the fluctuations of parameters, the correlation between fluctuations, etc. Such measurements help understand better the nature of the reverse transition.

In conclusion it is necessary to emphasize that for the first time the phenomenon of reverse transition in convergent gas currents discovered in the works of A. A. Gukhman and M. Ye. Deych, is found in complete conformity with conclusions of the stability theory.

§ 4-3. The Flow of Gas in Supersonic Diffusers

Supersonic diffusers have an extensive application as a component element of aircraft and other flight vehicles and engines and also experimental installations. Examined below are only tube diffusers used in wind tunnels, ejectors, MHD generators and so on. There is certain interest in such diffusers for special turbine stages having supersonic velocities at the outlet from the operating cascade. Therefore, even a brief examination of features of the physical process in supersonic diffusers is entirely justified.

From the basic equation of one-dimensional flow [25], it follows that supersonic diffusion can be accomplished in a tube of varying section, the inlet part of which is made constricted and the outlet - expanded. In the first part the velocity is decreased and reaches a critical value in the minimum section. Then in the expanded part the process of the compression of subsonic flow is continued.

Supersonic diffusers can be divided into two basic types:

- 1) without a central body;
- 2) with a central body.

Within limits of every type, diffusers can be divided in diffusers with multishock, isentropic and combined compression. The distinction in the indicated types is easily understood from the examination of diagrams in Fig. 4-14.

Diffusers without a central body are accomplished according to the diagrams given in Fig. 4-14a and b. As an "ideal" diffuser

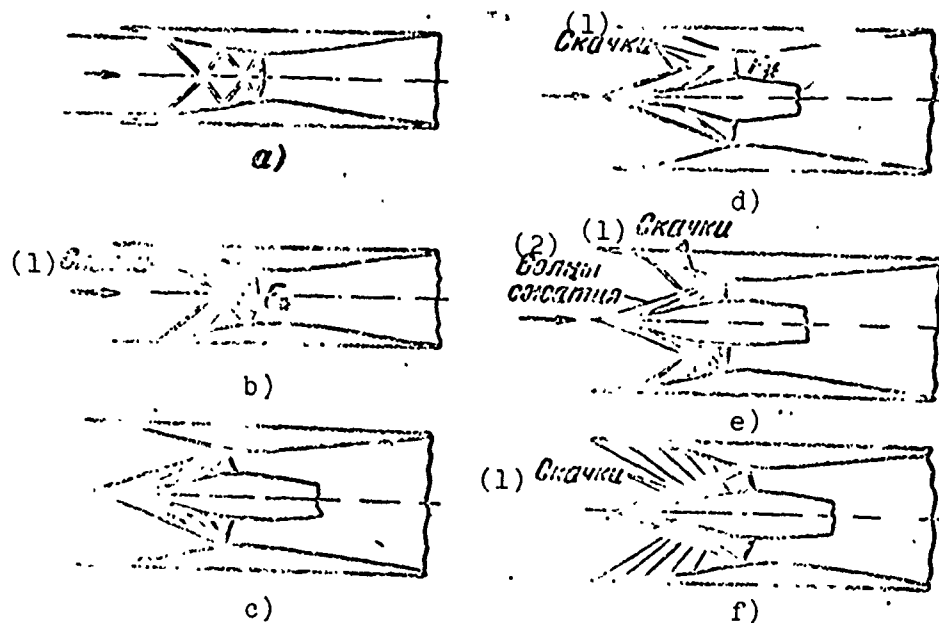


Fig. 4-14. Schematic diagram of supersonic tube diffusers.
KEY: (1) Shocks; (2) Compression wave.

with isentropic compression it is possible to use a convergent-divergent nozzle with profiled walls, assuming the flow in it is reversed. Because of the evenness of the profiled walls, at every point of which the flow accomplishes a turn at a small angle, in the diffuser inlet a system of weak compression waves (characteristics) should arise. In passing through this system, the flow is braked isentropically. The system of weak compression waves in this case coincides completely with the system of the weak rarefaction waves (characteristics) in the expanded part of the nozzle. In the entrance the flow acquires a critical velocity ($\lambda = 1$). In the expanded part of the diffuser the velocities are subsonic, which are decreased in the flow direction. In actuality, however, it is not possible to accomplish such a diffuser, since the flow in it proves to be unstable: slight disturbances at the inlet give rise to finite disturbances at the outlet. This is explained by the fact that

with a small decrease in M_1 number at the inlet in the minimum section critical speed is not established, as a result of which before tapered part the departing wave appears.

The field of flow which enters from the Laval nozzle, as a rule, is nonuniform and saturated irregularly. Furthermore, as a result of the emergence of losses in the inlet part and the formation of the boundary layer, the nature of the change in flow areas will not correspond to those calculated. As a result in the inlet part the system of shocks appears. Therefore, one should consider more advisable the step braking of supersonic flow at the inlet in the specially organized system of oblique disturbances. The system of shocks can be organized by two different means. One of them consists in the fact that the walls of the inlet section are made with breaks (Fig. 4-14b). When the flow flows, about the angular turns with supersonic velocity oblique shock waves, which interfere near the axis of the channel with walls of the inlet part, appear. Depending on the number of angular turns and conditions of the organization of the flow in the outlet points of shocks on the wall, the intensity of the shock braking can be different.

Best results can be obtained with the help of a profiled needle, which ensures either isentropic (Fig. 4-14c) or shock (Fig. 4-14d) compression of the flow. Circular supersonic diffusers with an inner body (regulating needle) having an axial movement prove to be more economic with variable modes of operation. The use of combined designs of diffusers which ensure the isentropic or shock and also mixed compression on the wall and during the flow of the inner body is possible (Fig. 4-14e and f).

One should emphasize that for the reduction in wave losses at the inlet a system of reflected shocks is also used.

Thus, a characteristic feature of any supersonic diffuser is the section of compression located after the inlet section.

Comparative merits and shortcomings in various designs of the inlet part of supersonic diffusers can be established basically experimentally. With this the best design should correspond to the following requirements:

1. Losses of kinetic energy (losses of stagnation pressure at the given value of the M_1 number) should be minimum.
2. The velocity field behind the diffuser should be uniform.
3. The diffuser should have satisfactory characteristics over a wide range of modes.

The possibility of satisfying the indicated requirements is connected not only with the finishing of the inlet part of the supersonic diffuser. As a more detailed analysis of physical processes which occur in diffuser shows, the most important is the section near the throat (minimum) area. Taking into account the processes which occur near the throat, one should estimate the perfection of a certain design. Actually, as experiments show, the maximum positive longitudinal pressure gradients on the surface of the inner body and on the contour of the diffuser are developed near the throat section. As was indicated in § 4-1, this feature is characteristic for transonic speeds, whereupon the direction of the pressure change along the flow (convergent or diffuser) is not important. Consequently, irrespective of the intensity of compression in the inlet section, in the entrance of the diffuser a region with maximum longitudinal pressure gradients is located. It is evident that in this section with maximum diffusivity the boundary layer separation or its most intense swelling are most probable.

Experiments confirm the emergence of separations near the throat area where the longitudinal pressure gradients reach maximum values. Hence it follows that the shaping of wall and central body of supersonic diffusers in the zone of throat area acquires an exceptional importance. The basic problem is reduced to the reduction in longitudinal pressure gradients in this section and the organization of the blowing of the boundary layer in the sections located before separation.

Keeping in mind the noted features of transonic diffuser flows, it is possible to assume that in the correct organization of flow at the inlet the maximum power losses appear in the zone of the minimum section and in the initial section of the expanded subsonic part.

Of significant interest is the comparison of diffusers with shock and isentropic compression. It is known that the number of shocks necessary for effective compression depends upon the effective range of M_1 numbers. This conclusion is confirmed by the dependences in Fig. 4-15 plotted for an ideal gas. Here curves 1-4 refer to optimum multiple-shock diffusers. As it appears, the compression in a three-shock system when $M_1 \leq 1.8$ does not give noticeable advantage as compared with a two-shock system. In the range $M_1 = 2.0-2.5$ the three-shock system gives a gain in the recovery of the stagnation pressure from 5 to 10%. At large M_1 numbers the use of four or five jumps is advantageous; however, in these cases combined compression should be used.

The attainable values of the coefficient of recovery of the stagnation pressure during isentropic compression with the focusing of the Mach waves at one point are shown in Fig. 4-15 by curves a and b. Less recovery (curve a) refers to the case when the requirement of the equality of pressures from two sides



Fig. 4-15. Theoretical values of the coefficient of recovery of stagnation pressure σ_0 in various systems of shock waves during external and internal compression in a supersonic diffuser (numbers near the curves correspond to the number of shocks).

of the discontinuity surface after the focusing point is fulfilled.

Curves a' and b' in Fig. 4-15 are plotted under the assumption of the combined isentropic compression for diffusers with fixed geometry. These data show that isentropic diffusers have a noticeable advantage. It should be considered that this advantage will be greater if we take into account the interaction of shocks with the boundary layer, as a result of which there occurs intense swelling and in certain cases separation of the layer. The effect of friction and separation on the recovery of the total pressure, not taken into account in the curve plotting in Fig. 4-15, is especially great at the small Reynolds numbers and large M_1 numbers.

It should be noted that in diffusers with variable geometry (adjustable diffusers) the magnitude of the recovery of stagnation pressure can be substantially higher.

§ 4-4. Characteristics of Transonic and Supersonic Diffusers.

At high velocities of the flow of gas in the diffuser (subsonic and supersonic), its characteristics are determined

by taking the compressibilities into account. For supersonic diffusers we will use (see § 2-2) the following characteristics introduced above: the eff of the diffuser η_D (energy eff η_{λ^3} and arbitrary eff η'_D), the coefficient of the recovery of stagnation pressure σ_0 and the pressure ratio σ .

The sections of the supersonic diffuser are designed from the equation of continuity, which (for the tapered part) can be recorded in the form:

$$\rho_1 \lambda_1 F_1 = \rho'_* \lambda'_* F_{*D},$$

where ρ'_* and λ'_* - density and velocity in the minimum section of the diffuser F_{*D} ; F_1 - inlet section of the diffuser.

After transformation we will obtain

$$\frac{F_1}{F_{*D}} = \frac{\frac{\rho'_*}{\rho'_{0*}} \lambda'_* \rho'_{0*}}{\frac{\rho_1}{\rho_{01}} \lambda_1 \rho_{01}} = \left(\frac{1 - \frac{k-1}{k+1} \lambda'^2_{0*}}{1 - \frac{k-1}{k+1} \lambda_1^2} \right)^{\frac{1}{k-1}} \frac{\lambda'_*}{\lambda_1} \cdot \frac{\rho'_{0*}}{\rho_{01}} = \frac{q'_{*}}{q_1} \cdot \frac{\rho_{0*}}{\rho_{01}} = \frac{q'_{*}}{q_1} \sigma_{01},$$

where q_1 , q'_{*} - the reduced gas flows in the inlet and minimum sections.

If in the minimum section the critical velocity $\eta'_* = 1$ ($q'_{*} = 1$), then

$$\frac{F_1}{F_{*n}} = \frac{\sigma_{01}}{q_1} \quad (4-2)$$

The coefficient of recovery of the stagnation pressure in the inlet section of the diffuser is defined from formula [25]

$$\sigma_{01} = \left[\frac{1 - m\lambda_1^2}{1 - m\lambda_1^2(1 - \zeta_{n1})} \right]^{\frac{k}{k-1}}, \quad (4-3)$$

where $m = \frac{k-1}{k+1}$; ζ_{n1} — the coefficient of losses in the tapered part of the diffuser.

Substitution of σ_{01} into formula (4-2) gives

$$\frac{F_1}{F_{*n}} = \left(\frac{2}{k+1} \right)^{\frac{1}{k-1}} \frac{1 - m\lambda_1^2}{\lambda_1 [1 - m\lambda_1^2(1 - \zeta_{n1})]^{k/k-1}} \quad (4-2a)$$

The formula shows that with an increase in losses in the tapered part the ratio of the sections F_1/F_{*n} is decreased. Hence it also follows that for the fixed value F_1/F_{*n} the change in parameters at the inlet leads to the change in losses in the tapered part.

By comparing the two modes of the flow under equal initial conditions with the various losses, from expression (4-2a) it is possible to obtain the dependence which shows that the minimum section of the diffuser should increase in proportion to the stagnation pressure change in section F_{*n} :

$$\frac{F_{0n}}{F_{*n}} = \frac{\rho'_{0n}}{\rho_{0n}}$$

or

$$\frac{F_1}{F'_{*R}} = \frac{F_1}{F_{*R}} \cdot \frac{p'_{0*}}{p_{0*}}$$

Here values of the parameters without the prime refer to one mode, and with a prime - to another mode.

For the calculation of the inlet part of the supersonic diffuser, it is necessary to know the magnitude of the coefficient of losses ξ_{q1} and, consequently, the structure and shock position in this section. The system of shocks at the inlet is selected from the condition of the minimum wave losses. In the selected and calculated system of shocks it is not difficult to determine the recovery of the total pressure and the coefficient of wave losses in the system of shocks [25].

Then according to the pressure distribution on surfaces of the inner body and inlet part the calculation of the boundary layer in the supersonic section is produced, and frictional losses are determined. The section of the minimum sections and expanded outlet part is further profiled. The outlet part of the diffuser is designed from the selected rational distribution pressure or on the basis of experimental data. Results of the boundary layer calculation allow establishing the energy losses in the subsonic part of the diffuser. At small supersonic velocities ($M_1 \approx 1.3-1.4$) it is possible to consider that in the inlet part there is only one normal shock. Value ξ_{q1} in this case will depend upon the position of the normal shock. If the shock is formed in section F_1 , then the energy losses will be maximum; if the shock is located in the cross section, then the losses will be considerably decreased.

For an illustration Fig. 4-16 gives the appropriate computed values of the eff of the diffuser η_d and η'_d for two limiting cases (1 - with a normal shock in the entrance and 2 - with a normal shock in the inlet section and also experimental points. A comparison shows the satisfactory agreement of the calculated and experimental values.

The outlet section of the diffuser is defined from the equation of continuity. The coefficient of losses in the expanded part of the diffuser can be used as a first approximation according to tests of subsonic diffusers. The outlet velocity from the diffuser is assigned.

The complete coefficient of losses in the diffuser is found by using formula (when $\lambda'_* = 1$)

$$\zeta_d = 1 - \eta_d = \zeta_{d1} + \frac{\zeta_{d2}}{\lambda_1^2}.$$

The pressure of stagnation after the diffuser is defined from relation (4-3):

$$p_{02} = p_{01} \left[\frac{1 - m\lambda_1^2}{1 - m\lambda_1^2(1 - \zeta_d)} \right]^{\frac{k}{k-1}}. \quad (4-3a)$$

One should again emphasize the necessity for the careful shaping of the walls in the zone of the throat (minimum) section, ensuring the very smooth transition to this section by lines of small curvature. It is evident that the shaping of the initial section of the expanded part of the diffuser should also be subordinated to the condition of the smooth change in the section along the flow, since here also the rates of the flow are close to being sonic.

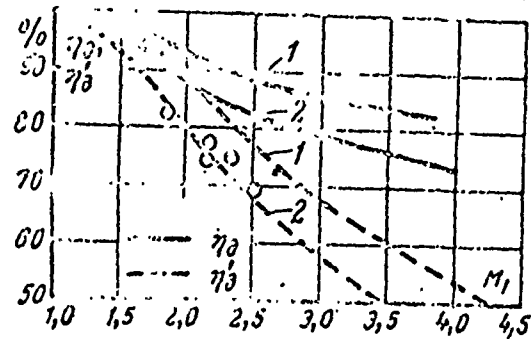


Fig. 4-16. Dependence of eff of diffusers upon the Mach number M_1 at the inlet; $k = 1.4$.

The outlet subsonic section is shaped on the basis of conditions described in Chapter 3. In the simplest case this section can be fulfilled with linear generatrices.

At transonic and small supersonic velocities at the inlet ($M_1 < 1.3$) the usual expanded subsonic diffusers are used. In this case before the expanded part there appears a normal shock wave, in which the flow passes over to subsonic velocities. In the expanded part the compression of subsonic flow is continued. Losses in such a diffuser can be moderate, since when $M_1 < 1.3$ wave losses in normal shocks are small. The calculation of diffusers can be realized by the following scheme. Determined is the pressure ratio which corresponds to the appearance of critical velocity in the inlet section with the help of the semiempirical formula

$$\frac{p_{2np}}{p_{01}} = \sigma_n + (1 - \sigma_n) \sqrt{1 - \frac{1}{n\sigma_0}}, \quad (4-4)$$

where $\sigma_0 = p_{02}/p_{01}$ - the coefficient of recovery of the stagnation pressure; p_{01} , p_{02} - the stagnation pressure before and after the diffuser; $\sigma_{cr} = \left(\frac{2}{k+1}\right)^{\frac{k}{k-1}}$ - critical pressure ratio; n - expansion ratio of the diffuser; p_{2kp} desired discharge pressure, which corresponds to such a limiting mode.

If the assigned ratio p_2/p_{01} is less than that value calculated from formula (4-4), then the diffuser operates with the shock wave in the expanded part. In this case on the basis of the theory of variable modes of supersonic nozzles [25] the position of shock and its intensity are found and the possibility of nonseparable flow is checked (see Fig. 4-4). With nonseparable flow the energy losses in shocks and the losses of friction after the shock are determined. Losses in the convergent section prior to the shock can be disregarded.

In solving the problem of the emergence of separation, one should consider the possibility of a reverse and direct transition in the boundary layer. Depending on the flow conditions in the boundary layer, the flow can cause separation. With laminar conditions separation is observed, as a rule, in all cases.

§ 4-5. Variable Modes and Some Results of the Experimental Study of Supersonic Diffusers

Let us examine some features of the operation of supersonic diffusers without an inner body under partial load conditions. The mode in the diffuser can be changed as a result of the change in the flow conditions at the inlet (M_1 , p_1 , p_{01}) and, consequently, the gas flow and discharge pressure p_2 .

Let us allow first that the flow conditions at the inlet and the gas flow through the diffuser remain constant, and let us observe the effect of the changing counterpressure p_a . Let us assume that in the initial section the velocity is equal to the critical, and the pressure of the medium is considerably lower than calculated ($p_a < p_{2m}$). In this case the expanded part of the diffuser works as a convergent-divergent nozzle. On the shear of the outlet part, depending on p_a rarefaction waves or oblique shocks appear. With an increase in p_a in the outlet section there is a bridge-like shock; a further increase in p_a leads to the displacement of the shock inside the expanded part toward the minimum section. With limiting counterpressure $p_a = p_{2m}$ the shock is located in the entrance of the diffuser (narrow section) and the flow in the expanded part is completely subsonic. Such a mode with a shock in the entrance corresponds to the maximum compression ratio in the diffuser.

The appropriate graphs of the pressure distribution along the diffuser without the inner body are given in Fig. 4-17a. The curve OAC corresponds to the limiting mode of operation of the diffuser with critical pressure in the minimum section. Curves OAB, OADE and others correspond to reduced pressures after the diffuser $p_a < p_{2m}$, and curve O_1A_1L - to the increased pressure $p_a > p_{2m}$. With this the pressure in the throat section proves to be higher than the critical pressure.

Let us examine now the effect of changes in the flow conditions at the inlet into diffuser. Let us assume that the pressure after the diffuser is maintained constant ($p_a < p_{2m}$). The dimensionless velocity at the inlet λ'_1 increases. At subsonic velocities at the inlet ($\lambda'_1 < 1$) in the tapered part, the flow is accelerated and maximum velocity is reached in the narrow section F_{*d} . As λ'_1 increases the gas flow and velocity in the narrow section λ'_* increase.

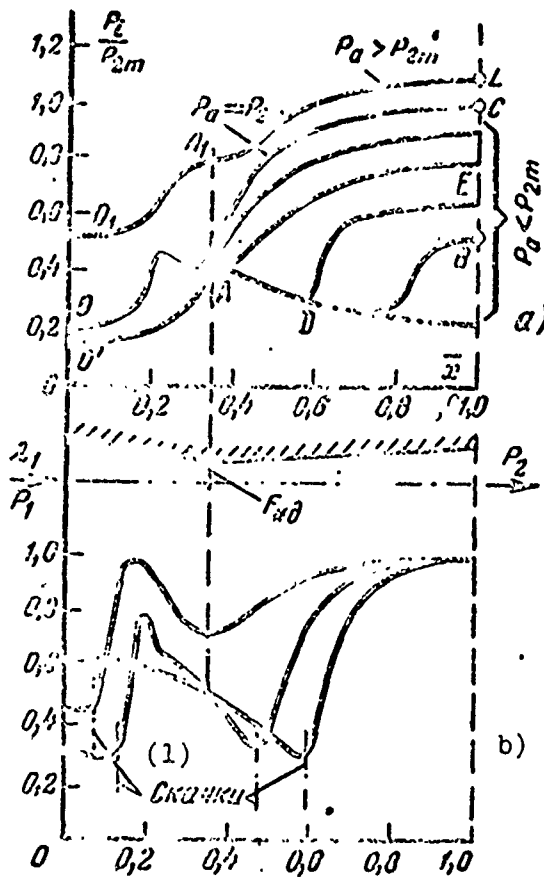


Fig. 4-17. Pressure distribution in a supersonic diffuser at various modes. a) $p_a = \text{var}$; b) $p_a = \text{const}$; $\lambda'_1 = \text{var}$; $p_1 = \text{var}$.

KEY: (1) Shocks.

At a certain value $\lambda'_{1\text{кр}} < 1$ the velocity in the section F_{*d} is equal to the critical ($\lambda'_* = 1$). A further increase in flow rate at invariable static pressure before the diffuser becomes impossible. In accordance with this, the velocity gain $\lambda'_1 > \lambda'_{1\text{кр}}$ will entail a pressure increase in the inlet section of the diffuser and in all other sections of the tapered part; as a result when $\lambda'_1 > 1$ a shock appears before the diffuser. With an increase in λ'_1 the shock approaches the diffuser and at a certain value λ'_1 is located in the inlet section F_1 . If the

shock at the inlet is normal, then in the tapered part of the diffuser the flow is subsonic and is accelerated towards the minimum section. In order that the normal shock (or system of shocks) penetrates into the tapered part of the diffuser, a further velocity gain λ'_1 is necessary.

Since with the motion of the shock toward the entrance the power losses are decreased, then in the minimum section the critical speed can again arise. In certain cases when $p_a < p_{2m}$ with transition into the expanded part, the flow continues to be accelerated and becomes supersonic. Then in the expanded part of the diffuser shocks appear. In such modes the diffuser losses sharply increase¹. The examined modes are illustrated by graphs of the pressure distribution in Fig. 4-17b. With the simultaneous appearance of shocks in the tapered and expanded parts of the diffuser, curves of the pressure distribution acquire a characteristic loop form.

Experimental results allow concluding that the form and correlations of the flow area of the diffuser have a very great effect on its effectiveness. The most considerable effect is in the change in angles of the tapered and expanded parts and also the length of the entrance. The research of P. Simons and others [161] allows evaluating of the effect of these angles for the simplest design of a diffuser without an inner body. Figure 4-18 gives a pressure distribution along the circuit of a supersonic wind tunnel for three angles of the expanded part of the diffuser, which shows that the greatest recovery of pressure in the expanded part corresponds to $\alpha \approx 6^\circ$.

The effect of the angle of the tapered part should be examined in connection with the selection of the geometric

¹The case in question is shown by dot-and-dash line on the diagram of Fig. 2-5b.

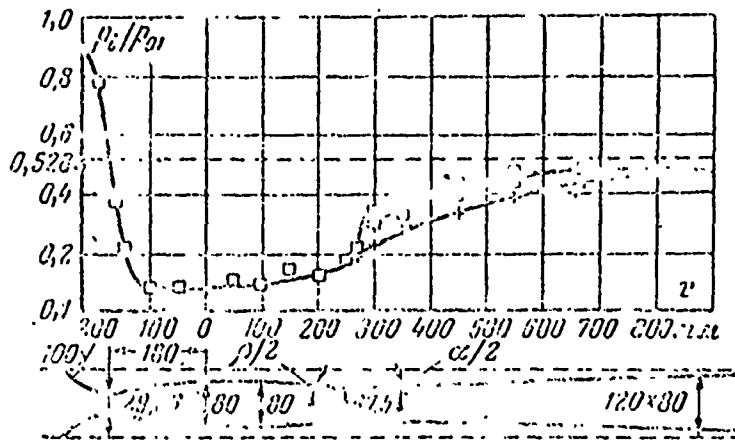


Fig. 4-18. Pressure distribution along the circuit of a supersonic wind tunnel at various flare angles of the subsonic part of the diffuser ($M_1 = 2.57$).

x - $\alpha = 3.32^\circ$; o - $\alpha = 5.35^\circ$; \square - $\alpha = 7.32^\circ$.

parameter F_1/F_{*d} (or F_{*d}/F_{*c} , where F_{*c} - the area of the minimum section of the nozzle installed before the diffuser). Figure 4-19a gives dependences of these geometric parameters upon the M_1 number before the diffuser. Let us note that the curve for the diffuser with a smaller angle β of the convergent section, i.e., with its greater length, lies below the curve obtained for the short convergent section.

Figure 4-19b gives values of the limiting angle of the tapered part, which corresponds to the minimally permissible value F_{*d}/F_{*c} . It should be noted that for the transonic diffuser ($M_1 \approx 1^\circ$), the value $\beta_{\text{lim}} \approx -1^\circ$, i.e., the inlet section must be made with a small expansion, which compensates for the building up of the boundary layer. For the short inlet section the limiting angles β (curve 1) should be greater than that for the long inlet section (curve 2).

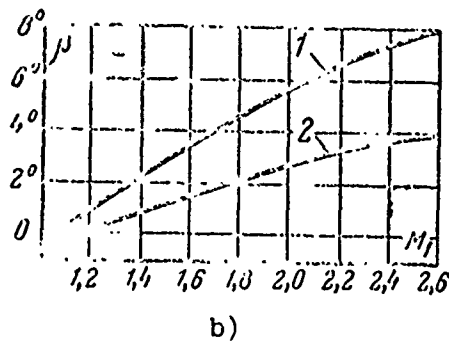
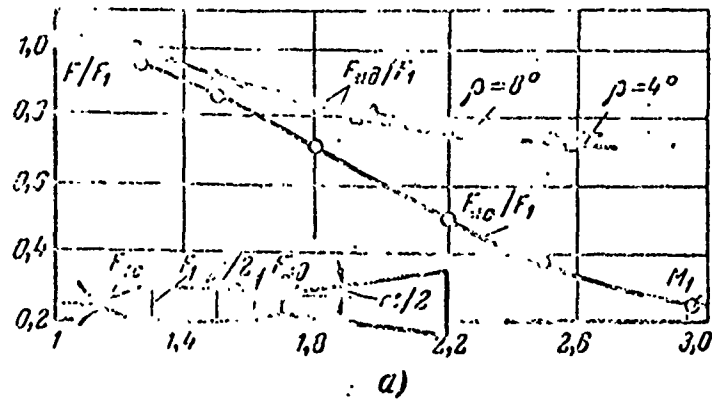


Fig. 4-19. The change in relative minimum areas of the diffuser, depending on M_1 number (a), and limiting angles β of the tapered part of the supersonic diffuser (b).

Results of a comparison of two types of diffusers without an inner body made with the tapered and expanded ($\beta = -1^\circ$) inlet section are of interest. At low supersonic velocities both diffusers are equivalent (Fig. 4-20). With an increase in M_1 the advantage of the diffuser with the tapered inlet section becomes obvious, and when $M_1 = 2.9$ the recovery of stagnation pressure in this diffuser is 25% more.

An examination of the operating conditions of the supersonic diffuser during partial load conditions (see Fig. 4-19) shows

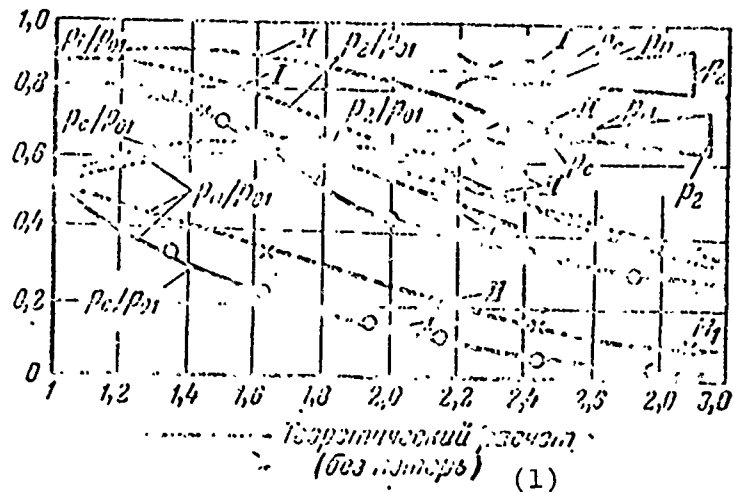


Fig. 4-20. The pressure of recovery in super-sonic diffusers without the tapered section I (with small expansion) and with a tapered inlet part II according to experimental data (P. Simons's experiments [161] and by calculation. KEY: (1) theoretical calculation (without losses).

that the ratio of the sections F_{*d}/F_1 should be changed with a change in flow conditions at the inlet or outlet. During the launching phase the ratio F_{*d}/F_1 should be maximum. With starting any disturbance of the mode can be partially compensated by the appropriate change in ratio F_{*d}/F_1 .

Let us analyze in more detail the variable modes of the diffuser with minimum section changing during the operation. If the minimum section is gradually decreased from $F_{*d} = F_1$ up to that value for which the velocity $M_* = 1$, then the gas flow through the diffuser will be maintained constant ($G = \rho_1 c_1 F_1$). However, if the area of the entrance will be decreased further, then the flow-rate through the diffuser will be lowered. With this near the narrow section a shock wave will arise since the narrowed entrance is an additional resistance. Because of the increase in entropy in the shock, the pressure in minimum cross section will fall, and the velocity and temperature will be

maintained constant. As a result of the decrease in density ρ_* , the flow rate is decreased to an even greater degree, and the shock will be shifted against the flow. At this the intensity of jump will increase. The motion of the shock against the flow will be continued until it falls outside the limits of the inlet section F_1 ; depending on the form of the feed section, the position of the shock relative to F_1 can be different. If in the inlet section after the shock the possibility of the bypass of part of gas beyond the limits of the diffuser will be provided for, then with a further decrease in F_{*D} the shock will move against the flow toward the Laval nozzle, ensuring the necessary reduction in flow rate through the diffuser; the intensity of the shock will be maintained practically constant (Fig. 4-21a).

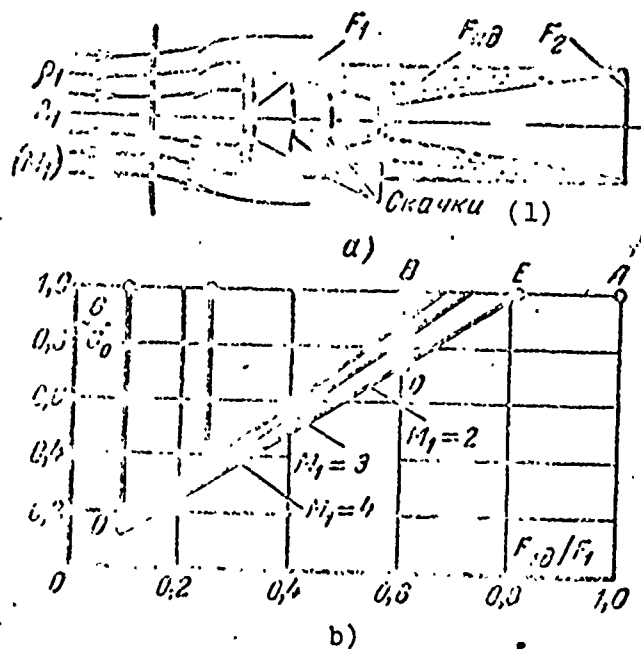


Fig. 4-21. Diagram of a diffuser with a variable minimum section a) and its discharge characteristics b) during various modes.

KEY: (1) Shocks.

By examining now the reverse process - the increase in F_{*d} , it can be concluded that if F_{*d} reaches the value during which appeared the shock for the first time, then the shock will not disappear, since the reduced density in entrance will cause the partial displacement of the gas mass beyond the limits of the diffuser. Consequently, F_{*d} must be increased to such limits in order to compensate for the decrease in density in the entrance. A subsequent increase in F_{*d} leads to a displacement of the shock inside the diffuser and provides a constant maximum flow rate through the diffuser.

That which has been expounded shows that in a diffuser with a variable section of entrance hysteresis effects will be observed. Graphs in Fig. 4-21b illustrate this. In the diagram of dependence of G/G_0 upon F_{*d}/F_1 (G - flow rate through the diffuser; $G_0 = \rho_1 c_1 F_1$), it is possible to indicate point A, which corresponds to $F_{*d} = F_1$ ($G = G_0$). With a decrease in F_{*d} the flow rate is maintained constant up to point B, which corresponds to $M_* = 1$ in the entrance; before the diffuser there appears a shock, and the flow rate falls down to the value at point D. A further decrease in F_{*d} gives rise to the change in flow rate along line DO.

With an increase in F_{*d} the shock before the diffuser is maintained up to that value of F_{*d} which corresponds to point E. The diffuser returns to the origin A along the line ODEA. As a result the hysteresis loop EBDE is formed, and in order to establish the state of flow in the diffuser at arbitrary F_{*d} , it is necessary to know what the direction of change in F_{*d} was.

It is necessary to emphasize that the modes with shock waves before the diffuser are characterized by a sudden increase in resistance. The dimension of the hysteresis loop depends upon the M_1 number, with an increase in which segment BD moves to the left (Fig. 4-21b). It should be noted that the region between the curves characterizes the unstable modes of operation of the diffuser, during which the shock can appear and disappear.

As was indicated, used in practice variable supersonic diffusers with step braking at the inlet (with an inner body). When the internal cone has the possibility of axial movements, it is possible not only to improve the conditions of starting and operation of a supersonic diffuser but also to provide the higher eff during calculated and partial load conditions.

Thus, the features of the operation of supersonic diffusers during variable modes distinctly show that the multimode diffusers should be made variable. In tube diffusers two methods of the control of the mode are used: a) a control needle and; b) flexible walls in the region of the minimum section. Furthermore, the control of mode can be accomplished by means of the bypass of the excess in the flow rate through openings in walls of the subsonic part of diffusers and the bypass of the excess of gas through the drilled walls of the inlet supersonic section of the diffuser.

The indicated methods of control are based on the use of diffusers with variable geometry. It should be noted that the use of any means of the control of flow through the diffuser does not take away the question of the advisability of the use of blowing of the boundary layer in sections of surfaces where the emergence of separation or the sudden swelling of layer are possible.

Experiments showed [127] that with detached flows near the throat it is advantageous to make the section of constant cross section in the zone of critical speed, which facilitates the stabilization of separation. Experiments confirmed also that the decrease in the aperture angle of the subsonic (expanded) part of the diffuser in the initial section and its increase in the outlet section give a positive result if the aperture angles do not exceed the permissible limits. This result confirms the advisability of such a profiling in the region of transonic velocities, which ensures the lowering in the longitudinal pressure gradients.

A large series of experiments with uncontrolled supersonic diffusers is described in [128]¹. The effect of the compression ratio and form of the inlet part and the effect of the form of the inner body on the coefficient of recovery of the stagnation pressure σ_0 . Experiments were conducted for single-shock and multishock inner bodies whereupon the shocks were focused on the inlet edge of the conical casing. For every stage of compression on the inner body the intensity of the shocks was selected less than limiting in order to eliminate the boundary layer separation ($p_2/p_1 < 1.8$). The latter angular turn was selected so that the M number on the leading edge of the conical casing would be 0.1 more than the M_1 number at which detachment of the shock occurs. The total aperture angles of the subsonic diffuser was 6, 9 and 21°. One of the models was made with the bleed of the layer on the surface of the inner body directly after the shock reflected from the conical casing.

The shape of the diffuser and experimental results are presented in Fig. 4-22. In the study of the effect of internal compression the magnitude of this compression was changed by

¹In [128] results are given of the study of the supersonic diffuser of a jet engine with the so-called "combined compression." Cited here are some data which are of interest in designing of tube diffusers.

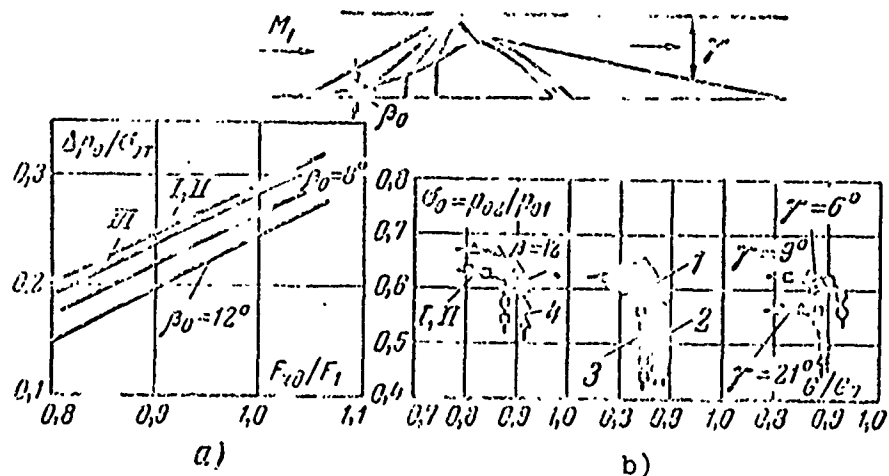


Fig. 4-22. Results of the experimental investigation of a plane supersonic diffuser with combined compression [128]. a) Roman numerals correspond to the number of shocks; b) 1 - optimum bleed; 2 - maximum bleed; 3 - without bleed; 4 - minimum bleed.

appropriate empirical curves in Fig. 4-22a represent the relative stagnation pressure change Δp_0 in the portions of the theoretical value of the coefficient of recovery σ_{0T} . Experiments showed that the effect of the use of the internal compression changes weakly depending on the system of shocks at the inlet, and the angle of the undercut of the conical casing and increases with an increase in F_{*a}/F_1 .

The effect of the bleed of the boundary layer was investigated for the three-cascade system at the inlet (Fig. 4-22b). Experiments showed that with an increase in the quantity of the air being drawn off by more than 1-3%, the coefficient σ_0 is decreased. With the correct selection of the dimensions of the slot and its position, the bleed allows increasing the effectiveness of the diffuser, giving an increase in σ_0 of 2-3%.

The effect of the subsonic section of the diffuser can be evaluated also according to curves in Fig. 4-22b. As it appears,

with the transition to the large aperture angle (21°), a sharp drop in the coefficient of recovery is noted. The aperture angles of $6-9^\circ$, apparently, are close to the optimum, which coincides with the experimental data in Fig. 4-18.

The experiments in question allow revealing the rational method of organizing compression on the inner body. Peak values of σ_0 at the given M_1 are given by the four-cascade system and isentropic wedge.

As the discharge characteristics show, the actual flow rate for the majority of the models was lower than that calculated. This is explained by the fact that the angle of the first oblique shock of the system was more than that calculated and also by the fact that throat section was insufficient. In this connection the specific features of the location of the discharge characteristics of supersonic diffusers should be noted (Fig. 4-22b). At first, with an increase in relative flow rate G/G_0 the coefficient of recovery is weakly changed. With the achievement of critical velocity in the throat section the actual flow rate is not changed, and the coefficient of recovery falls (vertical section of the diffuser performance). The presence of this section is explained by the additional losses in the system of shocks being changed over with a change in the parameters of the undisturbed flow and by an increase in losses in the throat section of the diffuser.

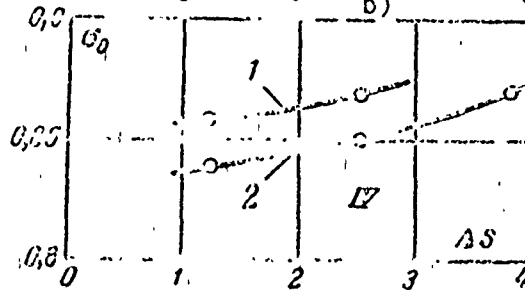
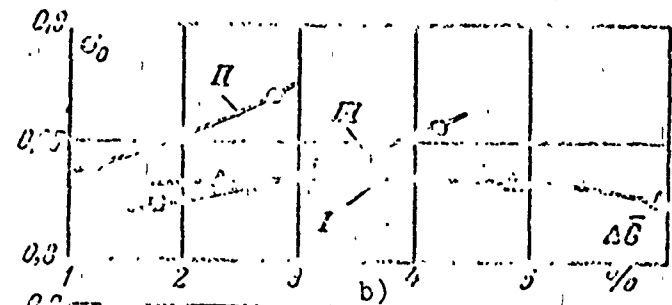
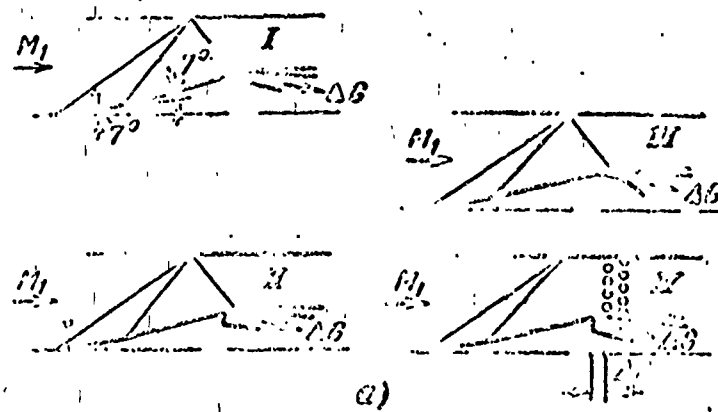
In diffusers with a control wedge (cone) the change in velocity M_1 gives rise to the disturbance of the calculated system of shocks. Modes $M_1 < M_{1p}$ cause an especially sharp increase in the wave losses, since in this case reflected shocks are formed. A study of two types of diffusers at variable velocities at the inlet showed that the coefficients of losses

when $M_1 < M_{1p}$ increase more intensely than for diffusers with an inner body. Minimum losses correspond to conditions close to the rated.

As was already mentioned, attempts to improve the characteristics of supersonic diffusers should be oriented for the improvement of the flow near the throat section. Most advisable is the organization of the bleed of the boundary layer and the use of vortex generators located on the inner body. The available experimental data show that in the correct organization of the bleed (i.e., with the correct selection of the shape, dimensions and place of the location of the slot) the bleed gives positive results and increases the coefficient of recovery of the total pressure [126].

Various methods of organization of bleed before the throat section of the diffuser at a constant $M_1 = 2.2$ number were investigated in [152]. Experiments showed (Fig. 4-23) that the bleed through slot of the scoop type (variant I) does not give rise to a noticeable improvement in the diffuser performances, and the coefficient of recovery of the stagnation pressure proves to be minimum weakly dependent on the quantity of the air being drawn off $\overline{\Delta G}$. The mean value of the coefficient of recovery for variant I is equal $\sigma_0 = 0.835$ (computed value $\sigma_0 = 0.939$). Considerably better results were achieved when using a stepped type of slot (variant II). In this case with the flow rate of the air being drawn off $\overline{\Delta G} = 2.8\%$ the coefficient of recovery $\sigma_0 = 0.87$ is obtained, whereupon an increase in $\Delta G > 2.8\%$ should give rise to a further increase in σ_0 . The rounded slot (variant III) gives intermediate values of σ_0 , whereupon a noticeable reduction in the energy losses, as compared with variant I, is reached only at large flow rate of the air being drawn off.

A comparison of the three variants clearly confirms the advantages of the variant with the stepped slot. A shortcoming



Reproduced from
best available copy.

Fig. 4-23. The effect of various methods of the organization of the bleed a) on diffuser performances (b and c). c) 1 - with a bleed on the side wall; 2 - without a bleed on the side wall.

of the scoop type of slot is that its drag proves to be considerable, and a detached curvilinear shock appears before it. Furthermore, the slot is made protruding into the flow, which gives rise to a relatively great change in the area of the section in the zone of transonic speeds, which is most sensitive to the

geometric effect. It is evident that the rounded slot in practice possesses the same shortcomings.

The given results explain the comparatively small effect of the bleed illustrated by graphs in Fig. 4-22. Also used here was a rounded slot for the bleed.

The organization of the bleed from the side walls (variant IV) led to an increase in the coefficient of recovery of the total pressure of approximately 1.5% (Fig. 4-23c). In this case, according to an approximate estimate through openings in the side walls up to 8% of the air through the diffuser was drawn off. It should be noted that scheme of the bleed through a group of openings is unsuccessful, since the resistance of such a system proves to be considerable. Substantially the best results can be obtained by means of making on the side walls of vertical slots or increasing the dimension of the stepped slot (variant II) near the side walls.

In summing up, let us note that the effectiveness of the bleed of the boundary layer before the throat section of the diffuser depends upon the geometric parameters of the inlet (supersonic) and outlet (subsonic) sections of the diffuser. The changes in angles of inclination of surfaces of the wedge and aperture angle of the subsonic section give rise to the change in σ_0 at the assigned values M_1 and $\overline{\Delta G}$. Qualitatively the effect of these factors is reflected in Fig. 4-22. The experiments in question showed that this effect is conditioned by the change in the Mach number before the closing shock in the bleed zone. Experiments confirmed also the noticeable effect of the Reynolds number or σ_0 . With an increase in the Re_1 numbers losses in the diffuser were decreased.

Experiments confirmed also the advisability of the use of vortex generators, which expand the zone of the stable operation

of diffusers. However, positive results were achieved only at definite positions of the vortex generators and with the correspondingly correct selection of their construction [127].

It is evident that the methods in question should supplement the methods for increasing the effectiveness of supersonic diffusers based upon the rational profiling of throat section and supersonic and subsonic sections adjoining it.

There is considerable interest in results of the study of supersonic diffusers with drilled walls of the supersonic section [125, 150]. In [125] results of the study of a diffuser with a drilled similar part are presented (Fig. 4-24a). The change in the coefficient of recovery of the stagnation pressure σ_0 , depending on the variable relative inlet area, is shown in Fig. 4-24c. The peak value of the coefficient of recovery $\sigma_{0max} = 0.81$ was obtained at ratios of the area of the inlet section to the area of the throat $F_1/F_{*d} = 1.33$ and the area of the drilled surface to the throat area $\Delta F_{nep}/F_{*d} = 4.28$. A further increase in F_1/F_{*d} gives rise to a change in σ_0 according to the law close to the hyperbolic. With $F_1/F_{*d} \leq 0.6$ in the diffuser there appears an unstable motion (surge), which is characterized by the fluctuation of the parameters. The actual distribution of ratio $\Delta F_{nep}/F_{*d}$ along the diffuser is shown in Fig. 4-26b, depending on the local value of the M number in the tapered section of the diffuser.

Returning to Fig. 4-24a, let us note the physical features of the gas flow in a diffuser with drilled walls. When drilling is not included (diagram I) before the diffuser there appears a bow shock, whereupon the peripheral part of the incoming flow within limits of the inlet section will pass into the zone of

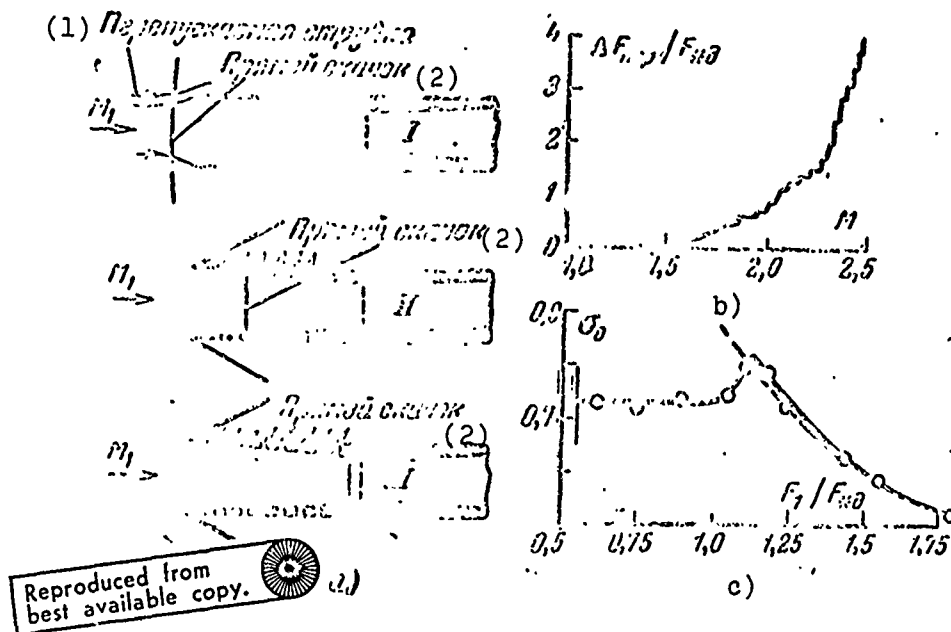


Fig. 4-24. Characteristics of a supersonic diffuser with a drilled inlet section [125]. a) diagrams of flow in the diffuser; b) relative area of the drilling depending on the M number; c) coefficients of recovery of the stagnation pressure depending on the relative inlet area. KEY: (1) Stream being passed; (2) Normal shock.

reduced static pressure at the external surface. After the shock the flow is subsonic and convergent.

With a partially included drilling (diagram II) the normal shock moves inside the diffuser. Part of the drilling will pass supersonic flow, and the pressure in direction toward the shock grows. From the inlet edges in the external flow an oblique shock is propagated. After a normal shock the pressure increased, which is decreased along the flow. With an increase in the outlet section F_2/F_{*d} the normal shock moves toward the throat section; in this case the area of the drilling increases and the quantity of the jettisonable air increases. Diagram III corresponds to the mode of operation of the diffuser which is close to that calculated. This mode corresponds to the maximum recovery of coefficient σ_0 (Fig. 4-24c).

The examined experiments showed that with the help of drilling it is possible to obtain high recovery of coefficients σ_0 ; however, in this case the part of gas is lost. There is special interest, therefore, in a drilled supersonic diffuser with a variable drilling. After the starting of the diffuser the openings can be closed, which allows maintaining the total gas flow rate in design conditions. The calculation of the drilled diffuser can be produced if the discharge coefficients through the openings for supersonic and subsonic flows are known.

CHAPTER FIVE

ANNUAL DIFFUSERS WITH LINEAR GENERATRICES

§ 5-1. The Effect of Geometric and Mode Parameters on the Characteristics of Annular Diffusers with a Rectilinear Axis

Circular axisymmetric diffusers with a rectilinear axis are rather often used as elements of exhaust ducts of turbomachines. Their designs and basic designations are given in Fig. 2-2. Such diffuser systems formed by two conical surfaces are characterized by the assignment of the following geometrical dimensions (see Chapter 2): inlet diameters D_1 and d_1 , outlet diameters D_2 and d_2 , and length l .

These dimensions are not unique ones which determine the geometric form of annular diffusers. For this purpose these parameters (Chapter 2) can be used: D_1 , d_1 , α_1 , α_2 , L , where α_1 and α_2 - angles of inclination of generatrices of conical surfaces, or D_{1cp} , l , α_1 , α_2 , n . Here: D_{1cp} - the mean diameter of the inlet section; l - height at the inlet and n - expansion ratio of the diffuser.

Consequently, in the examination of annular diffusers it is necessary to deal with the following geometrical dimensions: D_1 , d_1 , D_{1cp} , D_2 , d_2 , α_1 , α_2 , L , l , and n . Five values from this set completely determine the geometry of the diffuser.

True, the selection of the characteristic dimensions cannot be arbitrary. They should include two parameters connected with internal and external cones and one general parameter for the entire diffuser. For example: d_1, d_2, l_1, α_1 , and L or $D_{1cp}, l, \alpha_1, \alpha_2$, and n . The latter combination is, in our opinion, the most successful one. Having passed to the dimensionless parameters and selected as the determining dimension D_{1cp} , we obtain a set of four characteristics: $l/D_{1cp}, \alpha_1, \alpha_2$ and n , with the help of which it is possible to express all the remaining values in terms of relations:

$$\begin{aligned}
 \bar{D}_1 &= 1 + \frac{l}{D_{cp}}; \\
 \bar{d}_1 &= 1 - \frac{l}{D_{cp}}; \\
 \bar{L} &= \frac{\sqrt{l/D_{cp}} (l/D_{cp} - n)}{\operatorname{tg} \frac{\alpha_1}{2} - \operatorname{tg} \frac{\alpha_2}{2}}; \\
 \bar{D}_2 &= 1 + \frac{l}{D_{cp}} + \frac{2 \operatorname{tg} \frac{\alpha_1}{2} \sqrt{\frac{l}{D_{cp}} \left(\frac{l}{D_{cp}} - n \right)}}{\operatorname{tg} \frac{\alpha_1}{2} - \operatorname{tg} \frac{\alpha_2}{2}}; \\
 \bar{d}_2 &= 1 - \frac{l}{D_{cp}} + \frac{2 \operatorname{tg} \frac{\alpha_2}{2} \sqrt{\frac{l}{D_{cp}} \left(\frac{l}{D_{cp}} - n \right)}}{\operatorname{tg} \frac{\alpha_1}{2} - \operatorname{tg} \frac{\alpha_2}{2}}.
 \end{aligned} \tag{5-1}$$

Here and further $D_{cp} = D_{1cp} = D$.

Thus, in examining the influence of geometric parameters, we will discuss the clarification of the role of dimensionless inlet diameter D/l , angles α_1 and α_2 and the expansion ratio of the diffuser n . For the solution of the stated problem by experimental means, changing each parameter 4 times, it is necessary to test 1820 variants. Being limited to three changes, the number of these variants can be reduced to 220.

The given numbers give a graphic representation about the necessary minimum volume of experimental work. In the study of conical diffusers being determined by two dimensionless quantities (for instance, \bar{L} and n), complete test data with fixed mode parameters can be obtained as a result of tests of a total of 28 variants.

Today the bibliography on the experimental investigation of annular diffusers is comparatively small [1, 10, 22, 41, 51, 131, 137], but the number of variants investigated in the zone of low Mach numbers and numbers $Re_1 \approx 10^5 - 10^6$ approaches the numeral 220.

For the clarity of the performed analysis, given in Table A-2 of the appendix are test data of 174 annular diffusers conducted by various authors in different organizations. On the basis of this statistical material, let us conduct an analysis of the effect of the indicated geometric parameters.

a) Effect of the dimensionless inlet diameter. In examining annular diffusers from the point of view of their use in the system of exhaust of turbomachines, it should be noted that the value D/l characterizes, on one hand, the stage of the turbomachine, and on the other - determines dimensions of the inlet section of the diffuser connected with the given stage. In other words, the value D/l is the assigned design parameter determined by dimensions of the stage of the turbomachine. The limits of its changes is sufficiently wide, but the greatest interest is in the range of 2.5-3.0 to 10. As a whole the effect of D/l on internal losses proves to be sufficiently complex, but it is possible to expect that with an increase in this parameter the losses will increase. Actually the absolute value of losses in the diffuser during non-seperable flow is proportional to the streamlined surface, and the available energy at the given velocity is determined by the inlet section area (mass flow). As a result the coefficient of losses in a rough approximation proves to be proportional to the relative length L/D and to the parameter D/l , i.e.,

$$\zeta \sim \frac{D}{l} \cdot \frac{L}{D}.$$

The change in value D/l at a constant expansion ratio can be accomplished either at a constant relative length or at constant angles α_1 and α_2 . In the first case conditions $n = \text{const}$ and $\bar{L} = \text{const}$ give rise to the necessity for the changing of angles α_1 and α_2 . In the second case when $n = \text{const}$ and at constant angles the length \bar{L} is changed. In accordance with this one should expect a different dependence of losses upon D/l for the indicated extreme variants.

The experimental investigation of diffusers as a whole confirms the aforesaid. Thus, Fig. 5-1 gives the dependence of total losses upon value D/l , obtained as a result of a test of 20 annular diffusers the geometrical characteristics of which are placed in Tables 5-1 and 5-2.

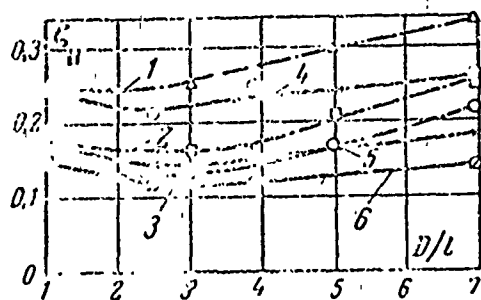


Fig. 5-1. Dependence of ζ_n on D/l for annular diffusers.

$1-n \sim 2$ } $d_1 = d_2$ } $d_2 > d_1$.
 $2-n \sim 3$ } $d_1 = d_2$ } $d_2 > d_1$.
 $3-n \sim 4$ } $d_1 = d_2$ } $d_2 > d_1$.
 $4-n = 2$ } $d_2 > d_1$.
 $5-n = 3$ } $d_2 > d_1$.
 $6-n = 4$ } $d_2 > d_1$.

(Experiments of Moscow Power Engineering Institute [MEI] (МЭИ)).

Table 5-1. Conical annular diffusers with a cylindrical [U] inner body ($d_1 = d_2$).

Designations	D_1, mm	D_{cp}, mm	l, mm	D/l	d_1, mm	\bar{d}_r	d_2, mm
1/1 U 1/2 U 1/3 U	49	35	14	2,5	21	0,43	21
2/1 U 2/2 U 2/3 U 2/4 U	49	39	10	3,9	29	0,43	29
3/1 U 3/2 U 3/3 U 3/4 U	49	43	6	7,17	37	0,43	37

Table 5-1 Continued.

Designations	\bar{d}_2	D_2, mm	\bar{D}_2	L, mm	n	L/D_1
1/1 II	0,3	67,1	1,37	143,2	2,67	3,62
1/2 II		80,9	1,53	254,2	3,01	5,92
1/3 II		89,4	1,62	332,2	3,63	7,10
2/1 II	0,43	63,3	1,29	117,1	2,63	2,4
2/2 II		74,8	1,53	212	3,01	4,34
2/3 II		80,0	1,63	254,2	3,56	5,7
2/4 II		84,9	1,73	294,4	4,03	6,60
3/1 II	0,43	56,6	1,15	62,3	1,773	1,27
3/2 II		63,3	1,29	117,1	2,55	2,40
3/3 II		67,1	1,37	148,2	3,01	3,02
3/4 II		74,8	1,53	212	4,09	4,33

Table 5-2. Conical annular diffusers with a conical [H] inner body ($d_2 > d_1$).

Designation	D_1, mm	D, mm	l, mm	D/l	d_1, mm	\bar{d}_1	d_2, mm
1/1 K	49	36,75	12,25	3	21,5	0,5	31,7
1/2 K							42,5
1/3 K							49,0
2/1 K	49	40,25	8,15	5	32,7	0,67	43,2
2/2 K							56,7
							65,4
3/1 K	49	42,25	6,15	7	33,3	0,75	52
3/2 K							63,8
3/3 K							73,6

Designation	\bar{d}_2	D_2, mm	\bar{D}_2	L, mm	n	L/D_1
1/1 K	0,71	69,3	1,415	163,3	2	3,4
1/2 K	0,87	84,9	1,73	201,4	3	6,0
1/3 K	1,00	93	2,0	201,9	4	3,2
2/1 K	0,94	69,3	1,415	163,3	2	3,4
2/2 K	1,16	84,9	1,73	201,4	3	6,0
	1,335	93	2,0	201,9	4	3,2
3/1 K	1,06	69,3	1,415	163,3	2	3,4
3/2 K	1,29	84,9	1,73	201,4	3	6,0
3/3 K	1,50	93	2,0	201,9	4	3,2

If for diffusers with a cylindrical inner generatrix (curves 4, 5 and 6) losses in the region of small and moderate values D/l increases insignificantly, then when $\bar{L} = \text{const}$ (curves 1, 2 and 3), it is possible to note an almost linear dependence of the total loss factor on the dimensionless inlet diameter.

The studies conducted in work [105] for diffusers with large values D/l ($D/l > 7$) confirm the fact of an increase in losses with an increase in D/l , and this increase becomes sufficiently intense with a cylindrical inner generatrix.

b) Effect of angles α_1 and α_2 . By examining the effect of the angles, one should keep in mind that their change with a constant expansion ratio n leads to a noticeable change in the relative length, and when $\bar{L} = \text{const}$ the expansion ratio changes. Hence, at first sight, it is sufficiently simple to predict the dependence of the total loss factor upon the indicated angles. Actually, with an increase, for example, of angle α_1 when $n = \text{const}$, it is possible to expect a reduction in losses due to the decrease in length of the diffuser, and when $\bar{L} = \text{const}$ total losses must drop due to an increase in the expansion ratio. In a certain range of the change in angles, such a pattern is observed in actuality. For an example Fig. 5-2 gives the dependence of losses in annular diffusers upon angle α_1 (Fig. 5-2b) with a cylindrical internal generatrix and upon angle α_2 (Fig. 5-2a) with a cylindrical external generatrix¹ and at a constant value of the expansion ratio. In both cases the growth at angles of up to 10° gave rise to a certain decrease in losses, and then the coefficient ζ_n sharply increased, whereupon not only qualitative but quantitatively the effect of the angles examined was almost identical.

¹The minus at coordinate α_2 indicates that the top of the internal cone is located behind the exit section of the diffuser.

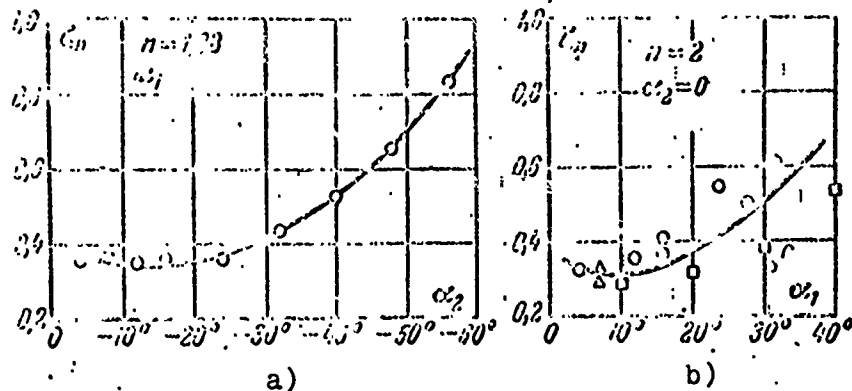


Fig. 5-2. Dependence of the total loss factor ζ_n upon angles α_2 (a) and α_1 (b).

O — $Re_1 = (1.5-2.3) \cdot 10^5$; $M_1 = 0.25-0.71$ [2]; \square — $Re_1 = (1.9-6.3) \cdot 10^5$; $M_1 = 0.1-0.4$; Δ — the experiments of MEI.

Reproduced from
best available copy.

Sometimes instead of angles α_1 and α_2 , which characterize the geometry of the annular diffuser, the plane angle $\theta = \alpha_1 - \alpha_2/2$ (here angle α_2 is taken with its sign) is used. In this case the number of independent geometric parameters is reduced, and the experimental data can be presented as a function of one angle θ . Such a dependence when $n = \text{const}$ (Fig. 5-3) has a minimum when $\theta = 4-5^\circ$, whereupon again an intense increase in losses occurs.

If we examine the effect of angle θ on the total loss factor at a constant relative length $\bar{L} = \text{const}$ (Fig. 5-4), then it is possible to note that here first a reduction in losses takes place. True, in this case the minimum of losses is reached at large values of angle θ , and the intensity of their increase when $\theta > 10^\circ$ is small.

The disturbance of the expected pattern at large angles of taper is connected with the feature of the flow near the angular points. A detailed study of this question examined above (see Chapter 3) showed that near an obtuse angle a sharp increase in the local pressure gradients occurs. Up to a definite limit the noted local disturbance of flow does not change the qualitative pattern

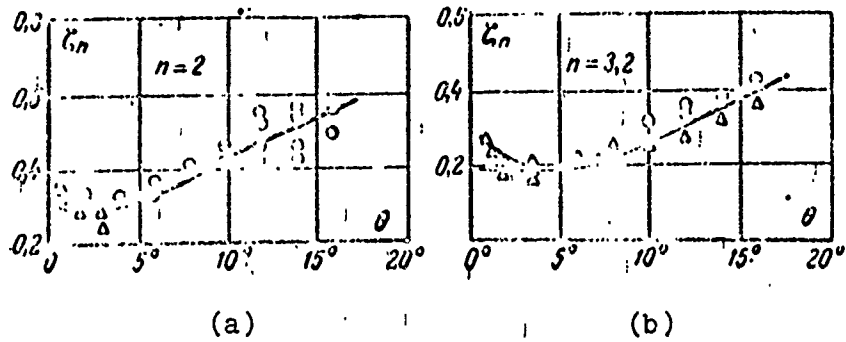


Fig. 5.3. Dependence of the coefficient ζ_n upon the plane angle θ when $n = \text{const}$.

O - experiments of Gurevich [22]; ● - experiments of Dovzhik and Morozov [41]; Δ - experiments of MEI; ▲ - experiments of Johnson [137]

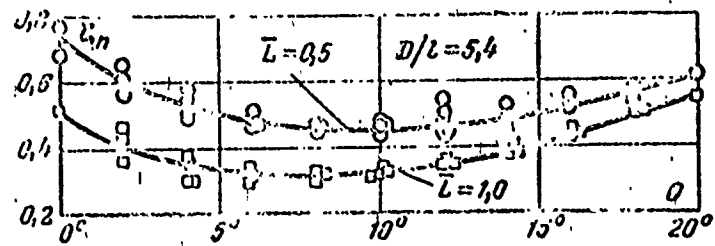


Fig. 5-4. Effect of plane angle θ on coefficient ζ_n when $\bar{L} = \text{const}$.

of flow, and losses with the increase in the angle decrease. However, at large angles ($\alpha/2 > 5^\circ$) the local positive pressure gradients increase so substantially that they give rise to the separation of flow, the result of which is an increase in losses when $\alpha > 10^\circ$. If a change in the coefficient of losses with a constant expansion ratio is examined, then the effect of the separation of flow is sufficiently great since it gives rise to a sharp reduction in the effective output area and, consequently, to an increase in the total energy balance of a portion of the output losses.

At a constant relative length of the diffuser the effect of the separation of flow, induced by the increase in angles, is compensated by the simultaneous growth in the geometric expansion

ratio. As a result the minimum of losses with respect to angle θ on curve in Fig. 5-4 proves to be more slanting.

The given test data give the basis for some practical recommendations for the choice of angles α_1 and α_2 . Thus, keeping in mind the local disturbances introduced by the angular break, it is inexpedient to increase angle α_1 above 10° and to select less than angle α_2 10° . (Let us recall that the minus sign at angle α_2 indicates the location of the vertex of internal conical surface after the outlet section of the diffuser.) Thus, the maximum magnitude of the plane angle θ proves to be limited to 10° . It should be noted that the design of the diffuser in question, with respect to design considerations, is rarely used in turbomachines. More widespread is the design with a positive angle α_2 at the location of the vertex of the internal conical surface before the inlet section. In such a circuit the internal angular break is the zero point and forms the closed separation zone whose extension increases with an increase in angle α_2 .

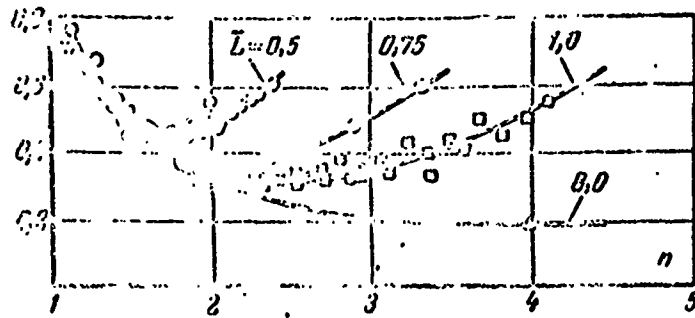
If in this case limitations with respect to angle α_1 indicated above are adhered to, then the value of the plane angle θ will be very small and at the assigned expansion ratio will sharply increase the linear overall dimensions of the diffuser, and at limited length \bar{L} the expansion ratio n will approach unity. In this case it is frequently necessary to increase angle α_1 to $20-25^\circ$ at angle α_2 equal to $10-15^\circ$, which corresponds to a plane angle θ of the order of 5° . Such an increase in angles in the scheme of diffuser in question at a limited plane angle θ proves to be permissible, since the closed separation zone near the internal surface smooths the local positive pressure gradient in the zone of angle α_1 and the total effect is defined basically by the magnitude of the plane angle θ . The experimental data plotted in Fig. 5-4 confirm this fact sufficiently well. At the same time it is necessary to note that to obtain a high effectiveness of annular diffusers, it is necessary to pay serious attention to the provision for normal inlet conditions. For this purpose the transition from the

cylindrical inlet section to conical surfaces forming the diffuser is advantageously carried out without angular breaks with a smooth coupling of cylindrical and conical surfaces.

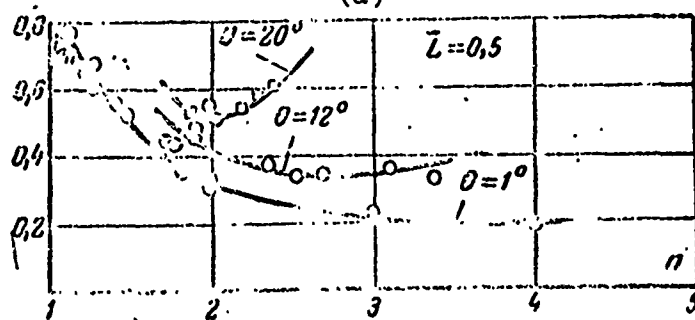
c) Effect of the expansion ratio of the diffuser. The expansion ratio of the diffuser is the basic geometric parameter which determines the effectiveness of the process of the conversion of kinetic flow energy into potential pressure energy. The effect of this parameter at constant relative inlet diameter, just as for the previous parameters, can be examined while maintaining constant one of two dimensions: the relative length \bar{L} or plane angle θ . Then in the first case the expansion ratio will be changed because of angle θ and in the second - because of length \bar{L} .

The dependence of total losses upon the expansion ratio in both cases in question is given in Fig. 5-5 and proves to be, as one would expect, not monotonic. With an increase in the expansion ratio the coefficient of losses ζ_n first falls to a certain minimum value and then begins to increase intensely. At a constant length of the diffuser the position of the minimum on the examined dependences is determined by the value of the relative length \bar{L} . The less the relative length of the diffuser, then at smaller expansion ratios this minimum is reached. Thus, for instance, when $\bar{L} = 0.5$, $n_{opt} = 1.8$; when $\bar{L} = 0.75$, $n_{opt} = 2.1$; when $\bar{L} = 1.00$, $n_{opt} = 2.5$, and when $\bar{L} = 8$ in the investigated range of the expansion ratios the minimum of the losses is not detected at all.

This type of dependence is regular and results from the effect of angles α_1 and α_2 examined above. Actually, at a constant length the small expansion ratios correspond to small values of plane angles θ . Under these conditions the disturbances introduced by angular breaks in the inlet section of the diffuser still do not substantially change the flow pattern inside the channel, and the coefficient of losses with the outlet velocity is intensely decreased with an increase in n , causing such an intense decrease in value ζ_n .



(a)



(b)

Fig. 5.5. Dependence of ζ_n upon the expansion ratio n when $\bar{L} = \text{const}$ (a) and $\theta = \text{const}$ (b) ($D/L = 5.4$).

However, with an increase in the expansion ratio the negative effect of angles α_1 and α_2 increases, and the intensity of the reduction in losses with the outlet velocity ζ_{BC} falls, and at certain value n the minimum level of losses is reached. Naturally, the greater the length \bar{L} , the larger the expansion ratio can be achieved at equal critical values of angle θ . In accordance with this, the displacement of the optimum expansion ratios noted in Fig. 5.5a occurs to the side of larger values with an increase in length \bar{L} , and there is an appropriate reduction in the minimum value of coefficient of total losses.

With an increase in the expansion ratio above optimum value, inside the diffuser channel the separation of flow occurs, and the separation is shifted toward the entrance with an increase in the expansion ratio n (with the increase in θ).

At a very long length (in the case in question when $\bar{L} = 8.0$) the range of the change in the plane angle θ for the achievement of

large expansion ratios becomes small ($\theta < 5^\circ$), the flow inside the channel is maintained nonseparable, and at a small level of internal losses the optimum according to the expansion ratio becomes more slanting, being displaced into the zone of practically unused expansion ratios.

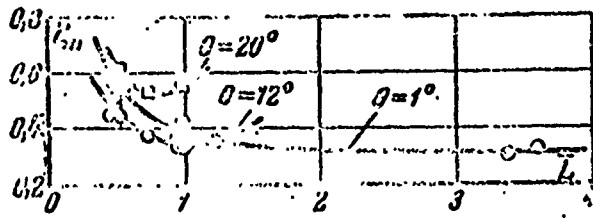
The pattern analogous to that examined is observed in the case when the expansion ratio changes because of the length \bar{L} at a constant angle θ . Here (Fig. 5-5b) when $\theta = 1^\circ$ with an increase in the expansion ratio at first an intense drop in the coefficient of total losses ζ_n occurs, and then when $n > 3$ its magnitude is not changed in practice. In other words, in this case the growth in internal losses with an increase in n (with an increase in length \bar{L}) is completely compensated by the reduction in losses with the outlet velocity.

If angle θ proves to be large, then with a comparatively small increase in length \bar{L} an intense increase in the expansion ratio occurs. Under such conditions a local increase in the positive pressure gradients in the inlet section, together with an increase in the average diffusivity in the channel, gives rise to the separation of flow in the region of small values n . In accordance with this, on curves ζ_n there appears a clearly marked minimum, determined by angle θ and value n .

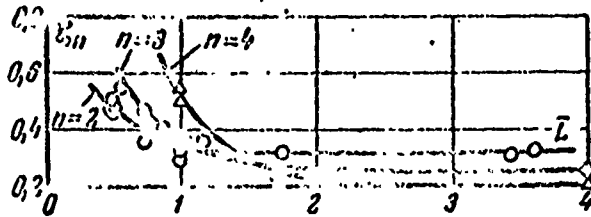
d) Effect of relative length \bar{L} . The relative length does not enter into the number of basic geometric parameters selected above for the characteristic of annular diffusers, and, consequently, its effect can be estimated on the basis of the given experimental data. Actually to the role of this parameter was already indicated during the analysis of the dependence of losses both upon D/l and the expansion ratio n .

Considering, however, that the relative length is rather often assigned according to purely design considerations let us construct the dependence of total losses upon \bar{L} at constant plane angles θ

(Fig. 5-6a) and expansion ratios n (Fig. 5-6b).



(a)



(b)

Fig. 5-6. Dependence of ζ_n upon dimensionless length \bar{L} when $\theta = \text{const}$ (a) and $n = \text{const}$ (b) ($D/l =$

The first dependence is obtained by means of the replotting of Fig. 5.5a, and the second results from Fig. 5-5b.

When $\theta = \text{const}$ with an increase in \bar{L} a change in the expansion ratio occurs. It is natural that when separation does not exist, ($\theta = 1^\circ$) the increase in length \bar{L} leads here to the drop in losses due to the reduction in delivery speed. When the emergence of separation ($\theta > 10^\circ$) on the curves in question the points of the minimum of losses, which correspond to critical values of the length \bar{L}_{kp} (critical expansion ratios) are well visible. The larger the angle θ , the smaller the value \bar{L}_{kp} and higher the level of losses at minimum point.

By examining the change in losses depending on length \bar{L} at a constant expansion ratio n , we obtain their monotonic reduction with an increase in \bar{L} (Fig. 5-6b), induced by a simultaneous decrease in losses when $\bar{L} > 1$ noticeably drops and depends upon the expansion ratio n . The larger n is then to a greater extent the effect of the relative length \bar{L} is apparent. However, in all cases beginning with $\bar{L} > 2$, the effect of this parameter becomes unimportant. Hence there follows the important practical conclusion about the

possibility of the building of highly economical annular diffusers with a constructively acceptable length \bar{L} .

e) Effect of mode parameters. The majority of the experimental data gathered in the appendix refers to incompressible fluids and encompasses a narrow range according to the Reynolds number. Actually there is no systematic data on the effect of Mach and Reynolds numbers on the efficiency of annular diffusers. The position is complicated still by the fact that the effect of these parameters cannot be examined separately without the connection with the geometrical dimensions, which can considerably affect the flow pattern inside the diffuser.

However, the present experimental data show that from the qualitative side the role of the mode parameters proves to be the same as that for the conical diffusers examined earlier (see Chapter 3). For an example, Fig. 5-7 gives results of experimental research on diffusers placed in Tables 5-1 and 5-2 at numbers $\lambda_1 = 0.3-1.0$. Here in all cases at subsonic velocities the flow remained nonseparable, and the reduction of losses was recorded everywhere with an increase in the dimensionless velocity λ_1 . The magnitude of this reduction, just as earlier [see formula (2-29)], is determined basically by the density change between the inlet and outlet sections of the diffuser and can be taken into account with the help of the following expression:

$$\zeta_n^c = \zeta_n^H \left(\frac{\rho_1}{\rho_2} \right)^m, \quad (5-2)$$

where ζ_n^c - total losses in the flow of compressible fluid;
 ζ_n^H - total losses in the flow of incompressible fluid;
 ρ_1 and ρ_2 - densities at inlet and outlet of the diffuser;

$$m = 1-2.$$

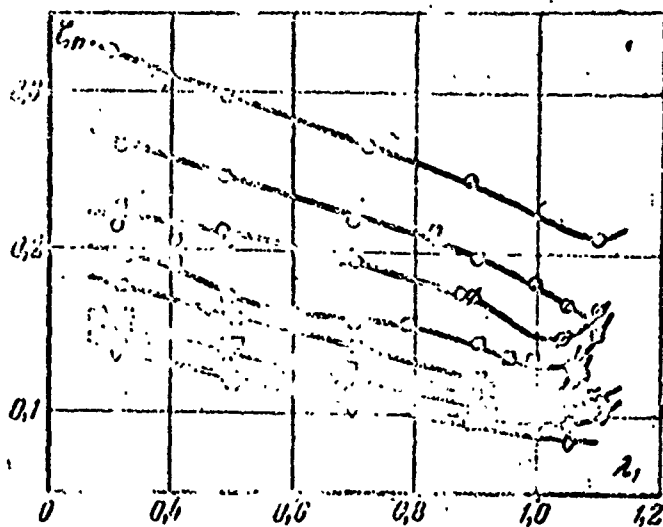
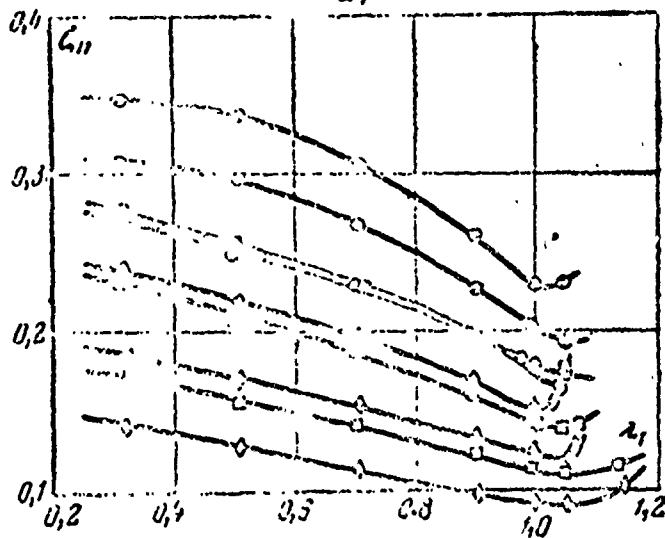


Fig. 5.7. Effect of compressibility on coefficient ζ_n .

a) diffusers according to Table 5-1: \bigcirc -1/1U;
 \odot -2/1U; \ominus -3/1U; \square -1/2U;
 \boxtimes -2/2U; \otimes -3/2U; \circ -1/3U;
 \ast -2/3U; α -3/3U; ∇ -2/1U;
 \diamond -3/1U;

a)



b) diffusers according to Table 5-2: \bigcirc -1/1K;
 \odot -2/1K; \ominus -3/1K; \square -1/2K;
 \boxtimes -2/2K; \otimes -3/2K; \circ -1/3K; ∇ -2/3K;
 \diamond -3/3K;

Designations:
 U = cylindrical
 K = conical

b)

The validity of formula (5-2) results from the theoretical solutions (see Chapters 2 and 3) and for nonseparable flows is confirmed experimentally. In the case in question good agreement with the experimental data is observed when $m = 1.6$.

Let us note that the curves in Fig. 5-7 were obtained during the investigation of diffusers in air in an open circuit, i.e., here simultaneously with a change in the Mach number a change in the Reynolds number occurred. However, the change in the latter in

the zone of high velocities was small, and at the relative velocity $\lambda_1 > 0.8$ simulation only according to the number M_1 (λ_1) was accomplished in practice.

For nondetached annular diffusers the velocity increase in the inlet section at a constant counter pressure gave rise to a disproportionate increase in the Reynolds number, since simultaneously with an increase in velocity in the inlet section the density was intensely lowered, and at transonic velocities the magnitude of the specific mass flow rate incoming into the Re_1 number is changed insignificantly.

The connection in question, constructed on the basis of direct measurements in the inlet section of the diffusers, is given in Fig. 5-8. If in the zone of low velocities the dependence $Re_1 = f(\lambda_1)$ is almost linear, then in the transonic zone the change in velocity of 40% gives rise to an increase in the Re_1 number of a total of 10-15%.

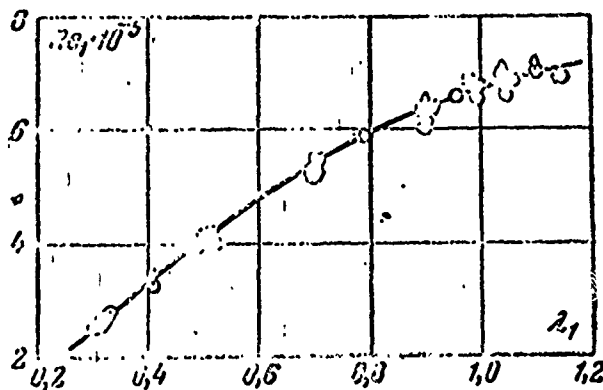


Fig. 5.8. Dependence of the Re_1 number upon velocity λ_1 at the inlet into the diffuser.

○—1/3K; ◇—1/2K; ○—1/3K; } (see
 ◇—3/2K; ○—3/3K; ○—3/2K. } Table
 5-2).

The noted fact is important during the study of transonic flows because it allows distinguishing the effect of the Mach number almost in pure form of open experimental contours.

§ 5-2. Calculation of Annular Diffusers in an Equivalent Angle

The analytical calculation of diffusers, especially annular, is based basically on semiempirical relations. For practical purposes the method of calculation in equivalent angles is most frequently used. The essence of the method is that the arbitrary diffuser channel is placed into conformity to a certain conical diffuser, and for this equivalent diffuser on the basis of experimental data the magnitude of the coefficient of losses is calculated or estimated.

The use of such a method of calculation is very tempting because it allows reducing the problems to a simpler one. As a result the accuracy of the final result depends upon the accuracy of determining losses in the conical diffuser. The calculation of energy characteristics of the latter (see Chapter 2) is based on the elementary relation

$$\zeta = \phi_D \left(1 - \frac{1}{n}\right)^2, \quad (5-3)$$

where ζ - the coefficient of internal losses, and ϕ_D - the experimental coefficient whose magnitude according to [54] is determined only by the flare angle of the diffuser α . The limits of changes ϕ_D , as was noted above, are quite wide and vary from 0.1 to 1.1. For any diffuser it is possible to match the experimental data with the formula (5-3) by means of the appropriate selection of the equivalent angle α_9 . The magnitude of this angle must, apparently, depend upon a number of parameters which define both the geometry of the channel and the flow conditions in it.

Actually, for annular diffusers the coefficient of internal losses on the basis of experimental data given above should be expressed by the following relation:

$$\zeta = f(n; D/l; \alpha_1; \alpha_2; M_1; Re). \quad (5-4)$$

By comparing formulas (5-3) and (5-4), we arrive at the conclusion that the coefficient ϕ_D should be determined by taking into account all the given parameters, i.e., it is possible to record

$$\varphi_{ik} = \varphi(\alpha_3),$$

and

$$\alpha_3 = f_1(n; D/l; \alpha_1; \alpha_2; M_1; Re). \quad (5-5)$$

In such a form the problem still remains sufficiently complex, since the magnitude of the equivalent angle α_3 is determined by six variables, the connection between which is unknown. In striving to reduce the number of variables, the effect of the mode parameters is usually disregarded and angle α_3 only according to geometric parameters is estimated. For low velocities ($M_1 < 0.3$) and large Re_1 numbers ($Re_1 > 10^6$), such a simplification is admissible, and the connection between the remaining variables depends upon how the equivalent diffuser is determined.

Most frequently as the equivalent diffuser the conical diffuser is assumed as having the same length L , the expansion ratio n and the inlet area F_1 as does the diffuser channel in question. In this case the equivalent angle α_3 is determined by the relation

$$\alpha_3 = 2 \arcsin \sqrt{\frac{F_1}{\pi L^2} (\sqrt{n} - 1)}. \quad (5-6)$$

For annular diffusers $F_1 = \pi D l$ and

$$\alpha_3 = 2 \arcsin \frac{1}{L} \sqrt{\frac{l}{D}} (\sqrt{n} - 1). \quad (5-7)$$

Formula (5-7) links the equivalent angle with the geometric parameters of the annular diffuser and allows defining according to Fig. 2-12 the value of the coefficient ϕ_D .

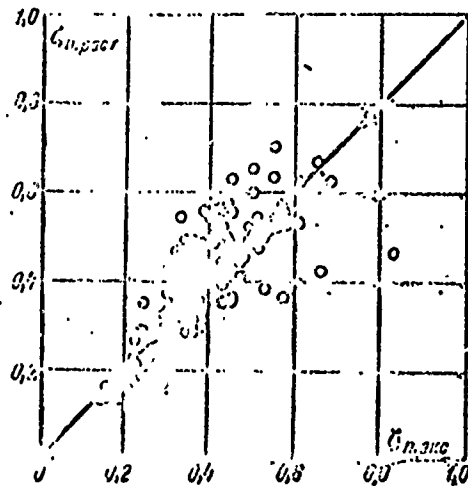


Fig. 5-9. Comparison calculated [see formula (5-3)] and the experimental values of coefficient ζ_n .

In analyzing the change in angle α_3 , it is possible to note that with an increase in length \bar{L} the magnitude of the equivalent angle is decreased, and an increase in the expansion ratio gives rise to an increase in α_3 . Since the higher values of angle α_3 correspond to higher coefficients ϕ_A and, consequently, larger values of coefficients of losses, formula (5-7) qualitatively agrees with the test data. However, in a quantitative respect such an agreement does not always prove to be sufficient. For an example in Table A-2 of the appendix values of equivalent angles are calculated, calculation data are given on all the gathered diffusers, and Fig. 5-9 gives their comparison with experimental data on 155 diffusers.

On the average the experimental points are grouped around the bisector of the right angle; however, their spread proves to be inadmissibly large, whereupon this spread ($\pm 20\%$) takes place not only in the zone of large absolute values of losses, where the flow bears a separation character, but it remains important even for nondetached diffusers. Thus, at the same calculated losses equal to 0.25, the experimentally determined losses are changed from 0.15 to 0.30. Such an error, naturally, is great even for a rough approximation. The limited possibilities of the calculation of diffusers in equivalent angles are indicated in [10].

Nevertheless, in striving to use an apparent simplicity of the method, and by attempting as far as possible to take into account fully the law of the change in the geometric characteristics of diffusers, the authors of work [34, 114] introduce the concept of the local equivalent angle, defining it by relation

$$\alpha_3 = 2 \operatorname{arctg} \left(\frac{1}{\Pi} \cdot \frac{dF}{dx} \right), \quad (5-8)$$

where Π - wetted perimeter, and F - area in the given section at distance x from the inlet.

For annular diffusers the use of formula (5-8) gives

$$\alpha_3 = 2 \operatorname{arctg} \left[\operatorname{tg} \theta \left(1 + \frac{1}{1 + \frac{y_0}{x - x_0} \operatorname{ctg} \alpha_1} \right) \right]. \quad (5-9)$$

Here

$$\theta = \frac{\alpha_1 - \alpha_2}{2}; \quad \alpha = \frac{\alpha_1 + \alpha_2}{2},$$

x_0, y_0 - coordinates of the intersection of the generatrices of the diffuser (Fig. 5-10).

In such a definition it is possible to indicate only two types of annular diffusers with a constant equivalent angle:

1. Diffuser with a cylindrical axial surface, when $\alpha_1 = -\alpha_2$.
2. Diffuser for which $y_0 = 0$.

In the first case $\alpha_3 = 2\alpha$, and in the second $\alpha_3 = 2 \operatorname{arc} \operatorname{tg} 2 \operatorname{tg} \theta$.

In all the other cases the calculation on the basis of formula (5-3), taking into account relation (5-9), requires numerical or graphical integration, which increases computational difficulties and impeded the theoretical analysis.

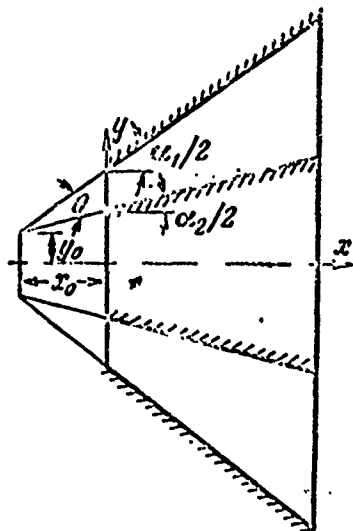


Fig. 5-10. Determination of a local equivalent angle.

Furthermore, the accuracy of calculations with the introduction of local angles proves also to be low, and in certain cases in principle it is impossible to expect correct results.

For example, it is possible to indicate the calculation of equiangular diffusers. In this particular case the magnitude of the equivalent angle will depend only upon the correlation of angles α_1 and α_2 . All the remaining geometric parameters will not enter into the examination. Hence in the comparison of two equal angular diffusers having identical angles α_1 and α_2 , but different relative lengths \bar{L} or different relative diameters D/l , we obtain equal calculated coefficients of losses. At the same time the experimental data indicate the distinction in losses with the change in length \bar{L} or diameter \bar{D} .

Using the method of equivalent angles, it is possible, apparently, for a definite group of diffusers, by the appropriate selection of angle α_3 , to attain the agreement of experimental and experimental data. However, with entire simplicity the method possesses a fundamental shortcoming, which consists in the fact that the consideration of the effect of geometric factors during any selection of the equivalent angle has to a considerable degree a formal character and does not consider the features of flow in

the diffuser channel.

For the indicated reason the method of calculation of the diffuser on the basis of the boundary layer theory is more promising although less widespread.

§ 5.3. Calculation of Losses in Annular Diffusers on the Basis of Characteristics of the Boundary Layer

The fundamental relations for determining the total and internal losses were derived in Chapter 2.

Design equations (2-29) and (2-34) show that the problem in question is reduced finally to definition of the area of the energy losses $\bar{\Delta}^{***}_2$ and the area of displacement $\bar{\Delta}^*_2$ in the exit section of the diffuser. The basis for the definition of the indicated values can be equation (3-9) or (2-54).

Since an almost complete agreement of results of the calculation in formulas (3-9) and (2-54) with comparatively small expansion ratios ($n < 3$) was shown above, the selection of the basic design equations is determined only by the simplicity of the calculation. In this sense relation (2-54) is more convenient. However, the use of formulas based upon the integral equation of Kármán (1-1), is more usual, and when using electronic computers computational difficulties no longer have a decisive importance. Because of this the calculated nomograms given in the appendix are obtained as a result of the use of equation (3-9). This relation converted for annular diffusers with a rectilinear axis, has a sufficiently complex structure:

$$\bar{\delta}_2^* \approx \bar{\Delta}_2^* = B \frac{(D_2^2 - d_2^2)^{0.24} (1 - \bar{\Delta}_2^*)^{0.24}}{D_2^2 (D_2 - d_2) (1 - \bar{d}_1^2)^{0.2}} \times$$

$$\times \left[\int_0^1 \frac{[1 + \bar{x} (D_2 - 1)]^{1.25} d\bar{x}}{\left\{ [1 + \bar{x} (D_2 - 1)]^2 - \bar{d}_1^2 \left[1 + \bar{x} \left(\frac{d_2}{d_1} - 1 \right) \right]^2 \right\}^{0.2}} \times \dots \right]$$

$$\left[\dots \times (1 - \bar{x}^{0.5} \bar{\Delta}_2^*)^{0.2} \right]^{0.8} \quad (5-10)$$

Here all the geometrical dimensions are referred to diameter D_1 (see Fig. 2-2), and parameters B and H are equal, respectively:

$$B = \frac{0.144}{\text{Re}_1^{0.2}} \left(\frac{L}{D} \right)^{0.8} H; \quad (5-11)$$

$$H = 1.4 \left[1 - \frac{\sqrt{n} - 1}{(L/l)^{0.2}} \right]. \quad (5-12)$$

These relations, obtained when using equations (2-54), take the form

$$\bar{\Delta}_2^* = B_1 n^{0.2} (1 - \bar{\Delta}_2^*)^2 \frac{(1 + d_1) (D_2 - d_2)^{0.8}}{(D_2 + d_2)} \times$$

$$\times \int_0^1 \frac{\{ [1 + \bar{x} (D_2 - 1)]^2 - [d_1 + \bar{x} (d_2 - d_1)]^2 \}^{-1} d\bar{x}}{[(1 - d_1) + \bar{x} (D_2 - 1 + d_1 - d_2)] (1 - \bar{x}^{0.5} \bar{\Delta}_2^*)^{0.8}}, \quad (5-13)$$

where

$$B_1 = \frac{0.0376H}{\text{Re}_1^{0.2}} \left(\frac{L}{D} \right)^{0.8} \frac{D_{20p}}{l_s}. \quad (5-14)$$

The comparison of formulas (5-10) and (5-13) gives rise to conclusion that as compared with conical diffusers the number of parameters which determine the area of displacement was sharply increased. At the same time for a specific diffuser these relations are considerably simplified, and value $\bar{\Delta}_2^* \approx \bar{\delta}_2^*$ can be found with the method of successive approximations.

To reduce the volume of computational work, in the appendix (see Fig. A-3) nomograms are given for the calculation of the area of displacement $\bar{\Delta}^*_2$ (δ^*_2) in annular diffusers with linear generatrices at different values of the geometric parameters. The given nomograms encompass essentially all the annular diffusers the most used in turbomachines and reduce the entire calculation to simple arithmetical operations. Actually for the assigned diffuser it is sufficient to determine the relative dimensions \bar{D}_2 , \bar{d}_1 , and \bar{d}_2 and calculate, according to formulas (5-11) and (5-12), parameter B in order from the appropriate curve of the appendix to find $\bar{\Delta}^*_2$ (δ^*_2) and, consequently, the total loss factor ζ_n . Such calculations for nondetached diffusers in (Table A-2 of the appendix) showed satisfactory accuracy. The appropriate comparison which was shown in Fig. 5-11 confirms that the absolute error does not exceed 5-8%, and the relative error lies within limits of 15%.

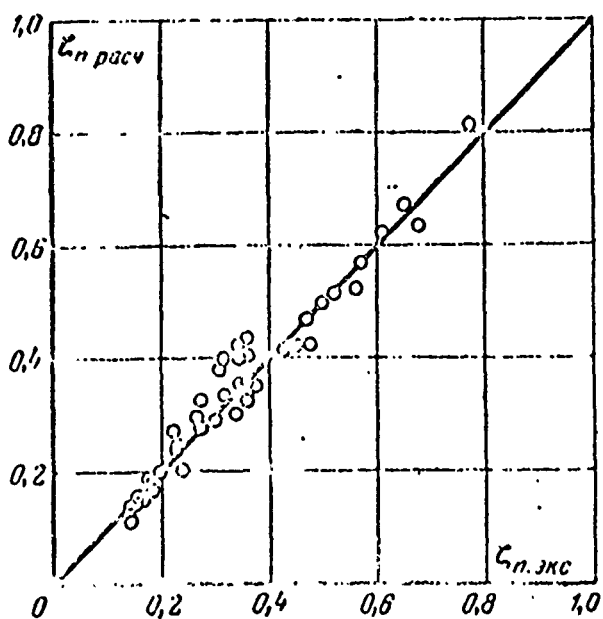


Fig. 5-11. Comparison calculated [see formula (5-10)] and experimental values of coefficient ζ_n .

§ 5-4. Calculation of Annular Diffusers in Experimental Nomograms

The examined analytical method of the calculation of annular diffusers allows estimating their energy characteristics with definite accuracy. In certain cases the accuracy of such estimates can be raised, and the labor input of the calculations is decreased by means of the direct use of experimental data. With the appropriate selection of variables these experimental data can be assumed as the basis for the construction of simple calculated nomograms. For annular diffusers such a nomogram is given in Fig. 5-12. Given in its upper part is the experimental dependence of the total loss factor upon the equivalent angle α_3 at a constant relative length \bar{L} , constructed on the basis experimental data of various authors [1, 22, 41, 103] for $D/l = 5.4$.

Attention is given to the fact that all 85 experimental points in the selected coordinate system obey the definite regularity noted above in the examination of the effect of geometric parameters. Thus, at a constant length \bar{L} the increase in angle α_3 leads first to a drop in losses, and then they reach a minimum value and further comparatively slowly increase.

With an increase in length when $\alpha_3 < 20^\circ$ the coefficient of losses is lowered, and the optimum magnitude of angle¹ α_3 develops a tendency toward a decrease.

The noted regularity is explained by the fact that at constant length \bar{L} and invariable diameter \bar{D} the increase in the equivalent angle is accompanied by an increase in the expansion ratio.

¹By optimum angle α_3 we understand as the angle at which the minimum of losses is attained.

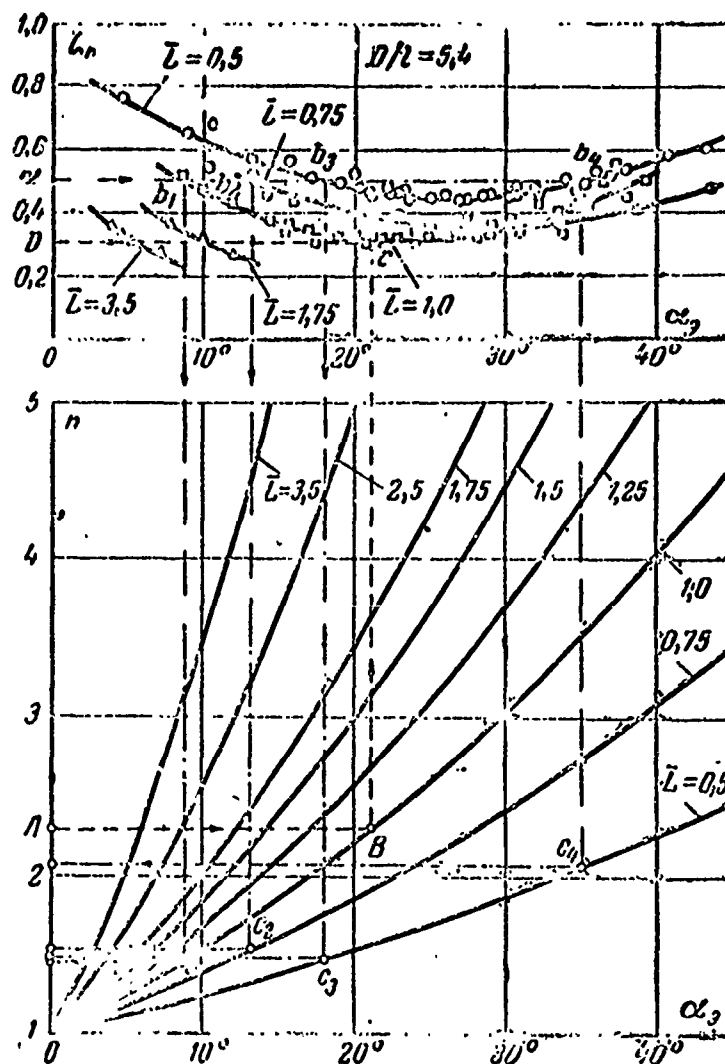


Fig. 5-12. Experimental nomogram for the calculation of annular diffusers with a rectilinear axis ($D/l = 5.4$).

At narrow angles α_3 an increase in the expansion ratio n is accompanied by an intense drop in losses with the outlet velocity and small increase in internal losses. However, with the transition to large angles α_3 ($\alpha_3 > 20^\circ$) the nature of the flow in the diffuser is changed. Here the intensity of the increase in internal losses, induced by the appearance of separation zones, exceeds the positive effect of the increasing expansion ratio, and the total losses increase. With an increase in length this process is begun at

smaller equivalent angles, since in this case the magnitude of internal losses increases, and the large expansion ratios are reached at comparatively narrow angles α_3 . In accordance with what has been said, the right branches of the curves in question are built up more steeply with an increase in length.

For the practical use of a nomogram, given in its lower part is the relation between basic geometric parameters of the diffusers. Taking into account this addition, it proves to be possible with maximum simplicity to estimate losses in the annular diffuser of assigned geometry or, having been assigned the level of losses, to find the geometric parameters of the diffuser. In the first case the problem has a unique solution, and in the second diverse variants are possible.

For instance, it is required to find the total loss factor for the diffuser with the relative length $\bar{L} = 1$ and expansion ratio $n = 2.3$. Using the lower part of the nomogram, on the axis of the ordinates we find point A, which corresponds to $n = 2.3$. Moving from it in parallel to the axis of abscissae up to the intersection with the curve $\bar{L} = 1$, we find the magnitude of the equivalent angle ($\alpha_3 = 21^\circ 15'$), and in the upper part of the nomogram we obtain the total loss factor, $\zeta_n = 0.30$ (point D).

Somewhat more complex proves to be the solution to the problem of the planning of a new diffuser according to the tolerance level of losses. Let us assume that it is required to determine the geometric parameters of the diffuser, the level of losses in which should not exceed $\zeta_n < 0.5$. In this case, by using the upper part of the nomogram, let us move from point a, which corresponds to the assigned losses, in parallel to the axis of the abscissae up to the intersection with the experimental curves at points b_1, b_2, b_3 and b_4 , obtaining four solutions equivalent in losses. The practical selection of the diffuser is determined further, on the strength of additional conditions.

For turbomachines the requirement of dimensionality is important. Then in the case in question one should discuss the third variant, which determines a diffuser with the following parameters: $n = 1.5$; $\bar{L} = 0.5$; $\alpha_3 = 18^\circ$.

The obtained results, naturally, should be corrected to the assigned relative diameter of the inlet, which can be made with the help of curves in Fig. 5-1.

§ 5-5. Effect of Structural Elements and Shape of the Channel on the Efficiency of Annular Diffusers

The examined characteristics of annular diffusers were obtained with a uniform inlet velocity field and free annular channel not blocked by the structural elements, the most important of which are fins.

If the influence of the inlet nonuniformity in annular diffusers to a certain extent has been examined in [137] and has been touched upon in Chapter 2, then the data which allow estimating the effect of fins are extremely small.

In this connection the investigations conducted at MEI with a series of annular diffusers, the meridian sections of which are given in Fig. 5-13 and geometric parameters are reduced in Table 5-3 are of definite interest.

It is evident that with identical shape of the blading diffusers Nos. 1 and 4 differed in practice only by the ratio D/l . Diffusers Nos. 2 and 3 had a cylindrical internal bushing, identical inlet and outlet dimensions, but different configuration of the channel in meridian of plane. If diffuser No. 2 had a conical external generatrix, then the external generatrix of diffuser No. 3 was made curvilinear, as a result of which a sharp increase is noted in the area of the sections at the inlet section.

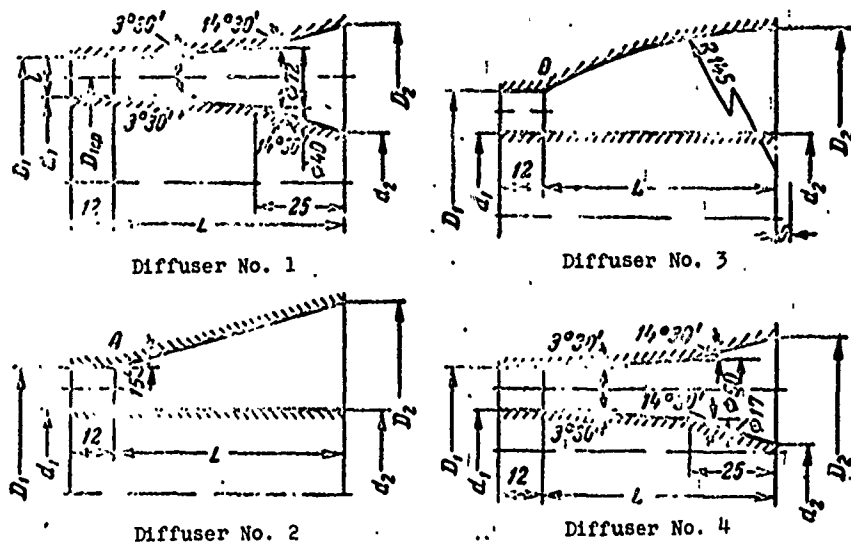


Fig. 5-13. Meridian sections of annular diffusers tested at MEI.

Table 5-3.

Number of Diffusers	D_1, mm	D_2, mm	l, mm	D/l	d_1, mm	\bar{d}_1	d_2, mm
1	67	56	11	5,1	45	0,67	27
2	67	56	11	5,1	45	0,67	45
3	67	56	11	5,1	45	0,67	45
4	45	33,5	11,5	2,9	22	0,49	4

Table 5-3 Continued

Number of Diffusers	\bar{d}_2	D_2, mm	\bar{D}_2	L, mm	\bar{L}	n
1	0,4	35	1,27	65	0,97	2,64
2	0,67	162	1,52	65	0,97	3,5
3	0,67	102	1,52	65	0,97	3,5
4	0,09	63	1,40	65	1,44	2,57

Furthermore, all the diffusers were divided by longitudinal fins into six insulated sectors and were tested both with inlet fairings and without them.

In this case the improvement in conditions of the inlet by means of the installation of fairings did not affect in practice the total loss factor (Fig. 5-14). This result is the consequence of the fact that in the insulated sectors the flow pattern is determined not by conditions of feed but by those disturbances which are introduced by the fins. The installation of the latter not only blocks the inlet section, but it leads also to the emergence of stable separation zones in the channel. Indirectly the separation flow pattern is indicated by the level of the coefficient of losses ζ_n and the absence of its dependence upon the Reynolds number. This conclusion is confirmed by direct measurements of the velocity field in the outlet sections.

As a whole, as one would expect, the best in efficiency proved to be diffusers No. 1 and No. 4 (Fig. 5-14a and d) ($\zeta_n = 0.50-0.55$).

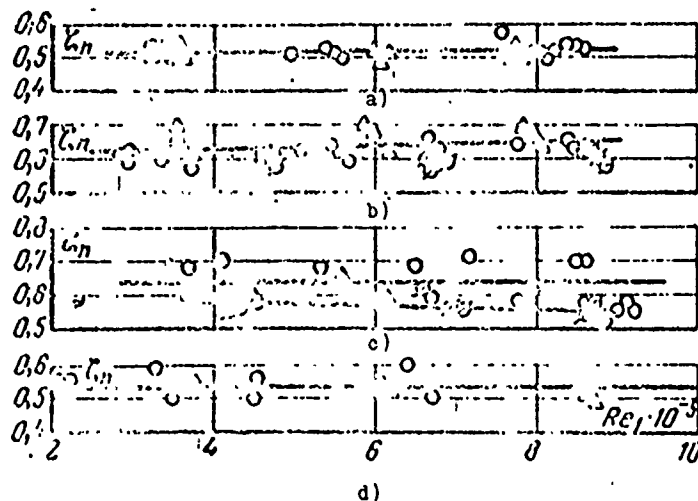


Fig. 5-14. Dependence of coefficient ζ_n upon Reynolds number. a) diffuser No. 1; b) diffuser No. 2; c) diffuser No. 3; d) diffuser No. 4; \circ - experiments without fairing; \blacktriangle - experiments with fairing; \emptyset - experiments with smooth inlet.

The transition to large equivalent angles and, respectively, with equal length \bar{L} to the large expansion ratios n did not give

Table 5-4.

Name	Notation	Unit of Measurement	Design Equations	Result of the calculation
External diameter at the inlet	D_1	m		0,293
Internal diameter at the inlet	d_1	m		0,502
External diameter at the outlet	D_2	m		0,352
Internal diameter at the outlet	d_2	m		0,216
Length	L	m		0,111
Expansion ratio	n		$n = \frac{D_2^2 - d_2^2}{D_1^2 - d_1^2}$	1,29
Mean diameter at the inlet	D	m	$D = \frac{1}{2} (D_1 + d_1)$	0,247
Height of throat	l	m	$l = \frac{1}{2} (D_1 - d_1)$	0,0455
Relative diameter of the stage	D/l			5,43
Relative internal diameter at the input	\bar{d}_1		$\bar{d}_1 = d_1/D_1$	0,69
Relative internal diameter at the outlet	\bar{D}_2	—	$\bar{D}_2 = \frac{D_2}{D_1}$	1,2
Relative internal diameter at the outlet	\bar{d}_2	—	$\bar{d}_2 = \frac{d_2}{D_1}$	0,85
Relative length	\bar{L}	—	$\bar{L} = \frac{L}{D_1}$	0,38
Equivalent flare angle	α_0	deg	$\alpha_0 = \arctg \left[\frac{\sqrt{1 - \bar{d}_1^2}}{2\bar{L}} (\sqrt{n} - 1) \right]$	15°20'
Gas velocity at inlet	c_1	m/s	Calculated from parameters at the inlet	178
Gas density at the outlet	ρ_1	$\frac{kg \cdot s^2}{m^4}$	The same	0,0705
Gas density at the outlet	ρ_2	$\frac{kg \cdot s^2}{m^4}$	Calculated from parameters at the outlet	0,0713
Viscosity of gas at the inlet	ν_1	m^2/s	Estimated according to parameters at the inlet	$6,65 \cdot 10^{-6}$
Reynolds number	Re_1		$Re_1 = \frac{c_1 D_1}{\nu_1}$	$8,63 \cdot 10^6$
Shape parameter of the boundary layer	H		$H = 1,4 \left[1 + \frac{\sqrt{n} - 1}{(L/l)^{0,2}} \right]$	1,565

Table 5-4 Continued

Name	Notation	Unit of Measurement	Design Equations	Result of the calculation
Complex parameter	B		$B = \frac{0.144R}{Re_{D_1}^{0.2}} \left(\frac{L}{D} \right)^{0.8}$	0.0077
Arbitrary relative area of displacement	$\bar{\Delta}^*$		Calculated from (5-10) or graphs in the appendix	0.025
Coefficient of internal losses	ζ		$\zeta = \left(\frac{\rho_1}{\rho_2} \right)^2 \frac{1}{n^2} \left[\frac{1}{(1-\bar{\Delta}^*)^2} - 1 \right]$	0.0266
Total loss factor	ζ_{II}		$\zeta_{II} = \left(\frac{\rho_1}{\rho_2} \right)^2 \frac{1}{n^2(1-\bar{\Delta}^*)^2}$	0.53
Coefficient of the "completeness" of the shock	φ_A	—	Found on Fig. 2-12 (54)	0.4
Coefficient of internal losses	ζ		$\zeta = \varphi_A \left(1 - \frac{1}{n} \right)^2$	0.112
Total loss factor	ζ_{II}		$\zeta_{II} = \zeta + \left(\frac{\rho_1}{\rho_2} \right)^2 \frac{1}{n^2}$	0.63
Total loss factor	ζ_{II}		On the nomogram of Fig. 5-12	0.52

positive result. The total loss factor for diffusers Nos. 2 and 3 was raised to 0.60-0.70. This increase is connected in the first place with the appearance in the channel of sharp angular breaks (see points A and B in Fig. 5-13). The smooth coupling of the generatrices at points A and B by radius $r_1 = 10$ mm reduced the losses by 5-7% for diffuser No. 2 and 10-15% for diffuser No. 3. The obtained results again confirm the conclusion made in Chapter 3 about the role of angular points and indicate the necessity for smooth couplings in the diffuser inlet.

§ 5-6. Example of the Calculation of an Annular Diffuser¹

Given below is the calculation of an annular diffuser made by three methods: according to boundary layer characteristics, the equivalent angle of expansion, and experimental data.

¹Calculations were carried out by engineer L. M. Dyskin.

Results of the calculation give good agreement of the total loss factors calculated in the boundary layer characteristics with the experimental data. The difference between the indicated coefficients comprises here a total of 1%, which indicates the sufficiently great accuracy of the theoretical method of the calculation of losses in diffusers based upon boundary layer characteristics.

The distinction between the total loss factors calculated in the equivalent angle of expansion α_3 and the experimental data comprises 11% in the given example.

The geometric mode parameters and results of the calculation of the diffuser are given in a Table. A diagram of the diffuser is shown in Fig. 2-2.

CHAPTER SIX

CURVILINEAR DIFFUSERS. FLOW PATTERN IN CURVILINEAR CHANNELS

§ 6-1. Secondary Flows in Curvilinear Channels

As is known [15, 17, 19], with flow in curvilinear channels secondary flows appear. Let us examine the mechanism of secondary flows for a channel of the parallel section in which the flow accomplishes a turn of 90° (Fig. 6-1a). Let us assume first that the velocities of motion in the channel are low as compared with the speed of sound, so that the compressibility effect can be disregarded. In connection with the fact that particles of gas move along curved paths, the pressures on the external (concave) and internal (convex) walls of the channel prove to be different and change differently in the direction of the motion. Since particles of the flow core under the action of centrifugal forces are forced back toward the external wall, then the pressure along AB increases as compared with the pressure of the influx p and is decreased along A_1B_1 . After a turn the pressure on the concave wall is lowered, and on the internal wall it is increased; at a significant distance after the turn the pressures are equalized.

Thus, in sections of the curvilinear channel a nonuniform distribution of velocities and pressures is established; here transverse pressure gradients appear. The particles of fluid which

move in the boundary layer along flat walls are under the effect of a pressure differential and, by possessing low speed in the direction of the basic motion overflow to the internal wall, undergoing greater deflection than particles far from the walls. According to the condition of continuity in the flow core, compensating flows directed toward the external wall should appear. As a result in the channel secondary vortex motion, which is superimposed on the main flow, is formed. Lines of flow of the secondary flow are closed in the cross section of the channel (Fig. 6-1b).

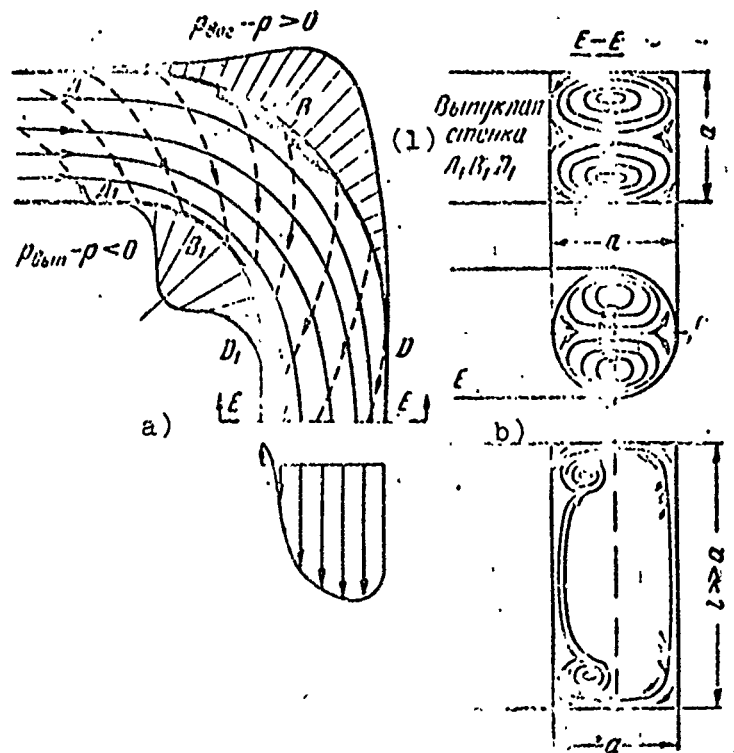


Fig. 6-1. Diagram of flow in curvilinear channels with a different shape of the profile.
KEY: (1) Convex wall.

The secondary flow consists of two flows which near the flat walls are directed toward the convex surface of the channel and, in center - toward the concave surface. Consequently, the secondary flow has a symmetrical-helical behavior. The lines of flow of the secondary flow on the flat walls are shown by a dashed line in Fig. 6-1a.

Along the section of the concave wall AB and section of the convex wall B_1D_1 the flow is divergent, and depending on the shape of the curvilinear channel separations can appear here. Separation on the concave wall AB can be localized by the subsequent convergent flow in section BD. Separation in section B_1D_1 has a more significant extension along the flow.

The structure of the secondary flow in the curvilinear channel and the additional energy losses being caused by it considerably depend upon the geometric shape of the channel and flow regime (Re and M numbers). Experiments show that the structure of secondary flows is changed with a change in the shape of the section of the channel (Fig. 6-1b). The greatest distinctions from the diagram examined above are revealed in channels with a rectangular shape of the section ($l \gg a$ and $l \ll a$). In the case $l \gg a$ the secondary flow of gas over the concave and convex walls is difficult, since the particles should accomplish the long path and overcome frictional resistance. Such an overflowing proves to be possible only in the boundary layer along the flat walls; it is begun on the concave surface (near the flat walls) and is continued on the flat walls in the direction toward the convex surface, where the boundary layer, which participates in the peripheral motion, merges with the boundary layer of the main flow and swells intensely. At the same time, as was already indicated, because of the motion in the boundary layer from the concave surface to the convex in the flow core of flat walls the compensating flows directed toward the concave wall are formed. These flows together with the boundary layer, which moves along the flat walls in the opposite direction,

form the closed eddy regions which encompass not the whole section of the flow but only its part near the convex surface and flat walls. In the rectangular channel in question the secondary flow degenerates into a pair of vortices, which are rotated in the opposite directions.

In channels with $z \ll a$ the secondary flow is difficult by the friction on flat walls, the effect of which is seen in the flow core, which gives rise to the extinguishing of the compensating flows from the convex to concave surface. As a result in such channels the secondary motion degenerates into small vortices, which are concentrated near the corners of channel.

The important features of the flow pattern are reached in annular curvilinear channels. Actually by comparing the distribution of losses in the exit section of annular curvilinear channels at ratios $d_1/d_2 = 0, 0.19, 0.31, \text{ and } 0.6$ (Fig. 6-2), it is possible to note the qualitative change in the structure in the transition from the cylindrical curvilinear channel ($d_1/d_2 = 0$) to the annular. In the first case the zone of sharply increased losses is located in the lower part of the flow near the convex wall and reflects the effect of the separation, which is formed in the diffuser region. In annular channels there are several zones of increased losses symmetrically located along the circumference. The number of these zones does not depend within certain limits on the relation of the internal and external diameters of the channel, but the level of losses in them is basically defined by d_1/d_2 . With an increase in parameter d_1/d_2 losses at all points of the section substantially increase, especially intensely in the nucleus of regions of increased losses. This result is confirmed also by measurements of total channel losses with various d_1/d_2 (Fig. 6-3a). Thus, in the transition from $d_1/d_2 = 0$ to $d_1/d_2 = 0.6$ the coefficient of losses increases almost twice. Curves in Fig. 6-3a show that with an increase in M_2 number in all channels the losses are reduced.

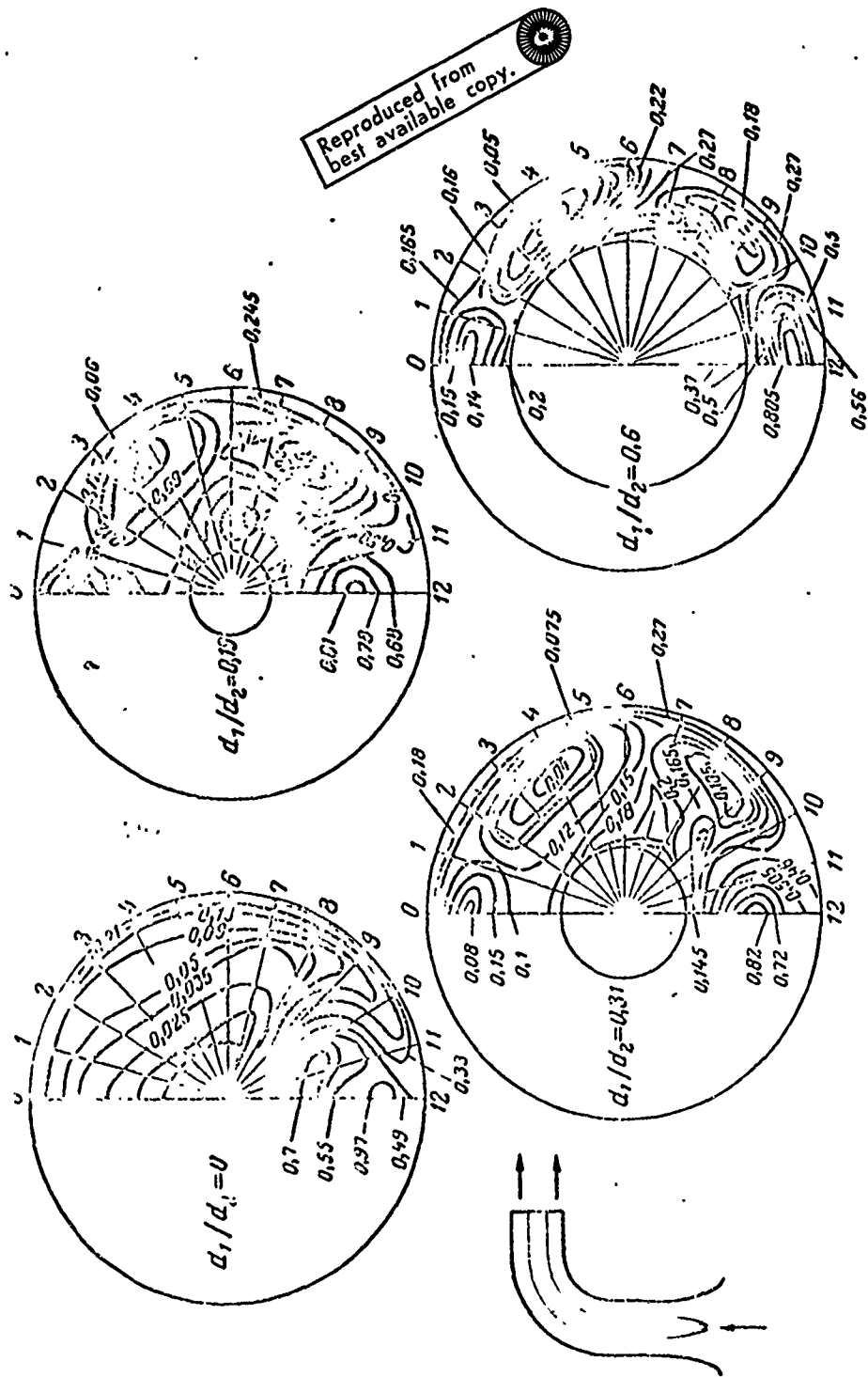
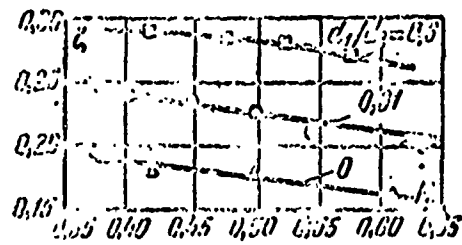


Fig. 6-2. Distribution of losses in the outlet section of an annular curvilinear channel at different values of parameter d_1/d_2 .

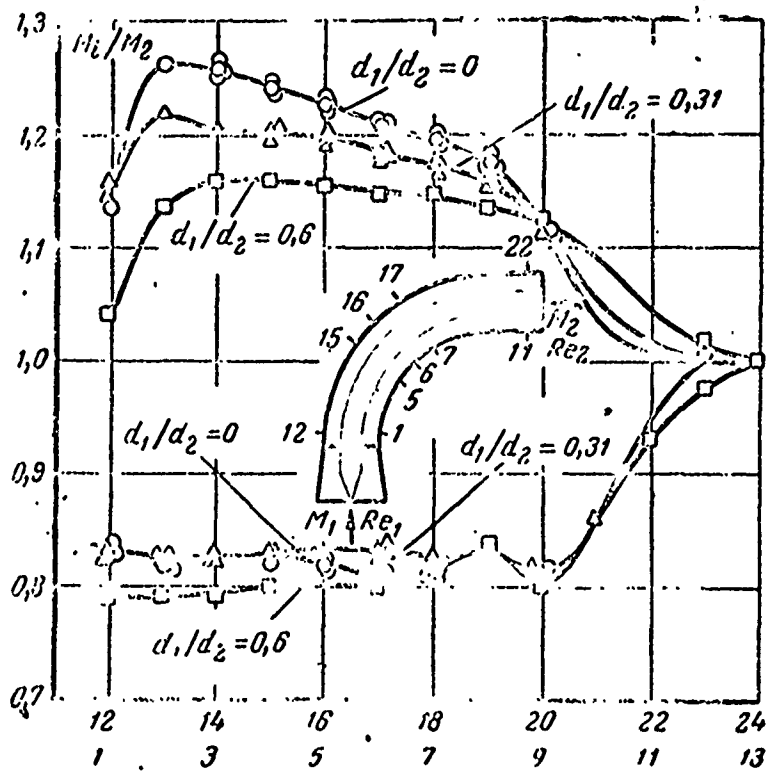
The physical flow pattern in the annular curvilinear channel is illustrated by graphs of the distribution of relative velocities over contours of the channel (Fig. 6-3b). Here it is clearly evident that the differences in the velocities between the concave and convex walls of the channel and also the values of velocities at various points of the contour are substantially changed depending on d_1/d_2 . With an increase in d_1/d_2 the indicated difference in the velocities is lowered; the relative velocities at all points of the contour with the exception of the outlet section are decreased somewhat.

The given experimental data show that in the curvilinear annular channel the secondary flows have a different structure. The systems of two vortices disintegrate; in such a channel, depending on the ratio d_1/d_2 , six vortex regions, evenly arranged over the circumference are formed. In the secondary flows a boundary layer participates both on the external and internal contours. Under the effect of the transverse pressure gradient there occurs a runoff of the layer at several points of the internal surface and its entrainment into the zones of compensating flows. An increase in losses in the annular curvilinear channels is explained also by an increase in the rubbing surface in the boundary layer on the internal contour. One should consider that the motion of the layer occurs on the helixes of flow, which increases the actual rubbing surface.

It is necessary to keep in mind that because of the intense accumulation of the layer on the convex surface of the external contour and internal surface of the insert, the separation, detectable after the turn, proves to be considerably more developed than that in the case of a common curvilinear channel.



a)



(1) Номера точек замера
b)

Fig. 6-3. Characteristics of the curvilinear annular channel of constant section. (Experiments of Moscow Power Engineering Institute [MEI] (МЭИ))
a) total channel losses depending on M_2 for various d_1/d_2 ; b) velocity distribution over the contour of the channel.
KEY: (1) Numbers of measuring points.

§ 6-2. Effect of the Basic Geometric and Mode Parameters on the Effectiveness of Plane Curvilinear Diffusers

Let us examine the basic characteristics of plane curvilinear diffusers according to data of experimental investigations. The formation of the secondary flow in curvilinear diffusers (channels) is due to part of the kinetic flow energy being expended. The energy losses, conditioned by the curvature of the channel, can be considered as a sum of: a) additional frictional losses as a result of the secondary motion; b) vortex losses in the zones of separation; c) losses induced by vortex compensating flows. The greatest part of the losses comprise the vortex losses as a result of separation.

Figure 6-4 gives data of H. Nippert which characterize the effect of certain geometric characteristics of the channel on the coefficient of losses. Here the coefficient ζ is defined as the difference in total energies at the inlet and outlet referred to the velocity head at the inlet into the channel. As can be seen from Fig. 6-4, ζ considerably depends upon the internal r_1 and external r_2 of radii of curvature, basically upon the expansion ratio of the channel defined by the ratio $n = a_2/a_1$ (if $n < 1$, then the channel is convergent; if $n > 1$, then the channel is divergent). At the assigned n the change in r_1 or r_2 gives rise to a change in the ratio $\bar{a}_m = a_m/a_1$ and, consequently, the area of the section along the axis of the flow. The points of the minimum of curves ζ correspond to different $\bar{r}_2 = r_2/a_1$ depending on $\bar{r}_1 = r_1/a_1$. The optimum values of \bar{r}_1 are somewhat less than \bar{r}_2 . At the given \bar{r}_1 an increase in $\bar{r}_2 > \bar{r}_{2opt}$ gives rise to an especially sharp increase in losses. In this case the curvilinear channel acquires a converging-diverging shape; the rate of flow on the turn and losses increase.

The curves in Fig. 6-4 also reflect the effect of the basic parameter n . In the diffuser channels ($n > 1$) the losses are substantially higher than those in channels of constant section

($n = 1$) and convergent channels ($n < 1$). In the whole range of values \bar{r}_1 and \bar{r}_2 the envelope $\zeta(\bar{r}_2, \bar{r}_1)$ lies higher for the diffuser channel ($n = 1.30$). An intermediate position is occupied by the channel of constant section ($n = 1$).

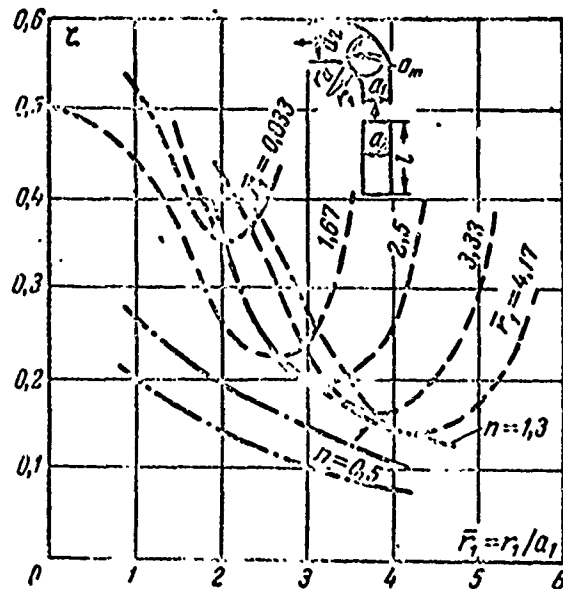


Fig. 6-4. Effect of the radii of curvature of concave and convex walls of a plane curvilinear channel with the angle of turn of 90° on the coefficient of losses of energy for various expansion ratios n .

A similar effect of the geometric parameter n is revealed for a channel with an angle of turn of 180° . The minimum of the losses in this case corresponds to values $n < 1$, and the optimum compression in the outlet part of the channel is decreased with a transition to converging channels ($n > 1$).

Let us examine some results of research on curvilinear diffuser channels which were made in MEI by V. I. Nikitin. Graphs of the pressure distribution along the generatrix of the channel (Fig. 6-5), plotted for various M_1 and Re_1 numbers, show that at the inlet into the channel (points 27-21) on the concave surface

the diffuser section with large pressure gradients is formed. The diffuser region on convex wall of the outlet (points 9-11). An important aspect is the fact that after the diffuser section on the concave surface there follows the region of convergent flow (points 20-12), in which there occurs the localization of separation if it appears in the preceding diffuser section. On convex wall the separation which appears in the diffuser region near the outlet section is not localized.

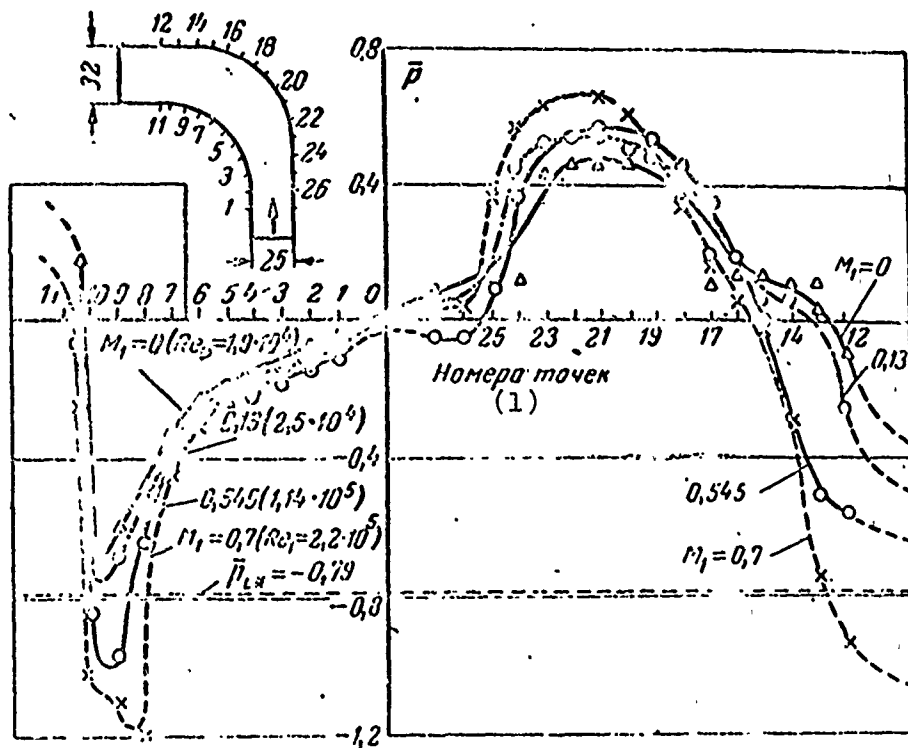


Fig. 6-5. Pressure distribution over concave and convex walls of a plane curvilinear diffuser at various M_1 and Re_1 numbers.

KEY: (1) Numbers of points.

With an increase in M_1 number the pressure gradients both in the diffuser and, in particular, in the convergent sections of the channel noticeably increase. The general nonuniformity of the pressure distribution in the channel increases. It should be noted

that at number $M_1 = 0.7$ at points 8-10 on the convex wall supersonic velocities are reached, since the pressure ratios at these points prove to be lower than the critical value $\bar{p}_{1*} = 0.79$ at this value of M_1 (Fig. 6-5). Let us note also that the divergence of curves \bar{p} for numbers $M_1 \approx 0$ and $M_1 = 0.13$ is explained by the Reynolds number effect.

The distribution of the coefficients of losses over the channel width in the outlet section confirms that near the convex wall a separation appears (Fig. 6-6a). Here the energy losses sharply increase, which is characteristic for the developed regions of separation. Let us note that with an increase in the height of the channel \bar{z} losses near the convex wall increase, and near the concave wall they decrease. Consequently, the secondary overflowing of boundary layers from the plane wall to the convex gives rise to a decrease in the extension of the separation zone and a certain reduction in the energy losses. The indirect confirmation of this assumption can be the graphs in Fig. 6-6b, where presented is the distribution of losses over the channel width for various distances from the plane wall. In the zone of secondary boundary layer flows near the plane walls ($\bar{z} = z/l = 0.014$ and $\bar{z} = 0.083$), values of the coefficients of losses near the convex wall were lower than those in sections far from the plane walls ($\bar{z} = 0.18$ and $\bar{z} = 0.5$).

Of interest is the distribution of losses over the height of the channel (Fig. 6-6c), which shows that the altitude effect in the diffuser curvilinear channels, the motion in which occurs with separation, proves to be complex. Separation on the convex wall does not reach the flat walls because the secondary flows are convergent. The secondary flows restrict the development of the separation zone along the convex wall and push back this zone to the middle sections where the losses increase due to this.

Curves in Fig. 6-6 allow drawing the conclusion about the sharply nonuniform distribution of the flow conditions along the

section, which, naturally, is explained not only by the effect of the secondary flows, but also, mainly, by the effect of separation. The lines of constant coefficients of losses for channels with $\bar{z} = 0.625$ and $\bar{z} = 1.125$ (Fig. 6-7) show that at a smaller height \bar{z} there occurs not only the joining of the secondary flows but also the deformation of the vortex region on the internal wall because of the secondary flows. The reduction of this region at very low levels facilitates the reduction in losses because of the decrease in fundamental component - eddy losses in the separation zone.

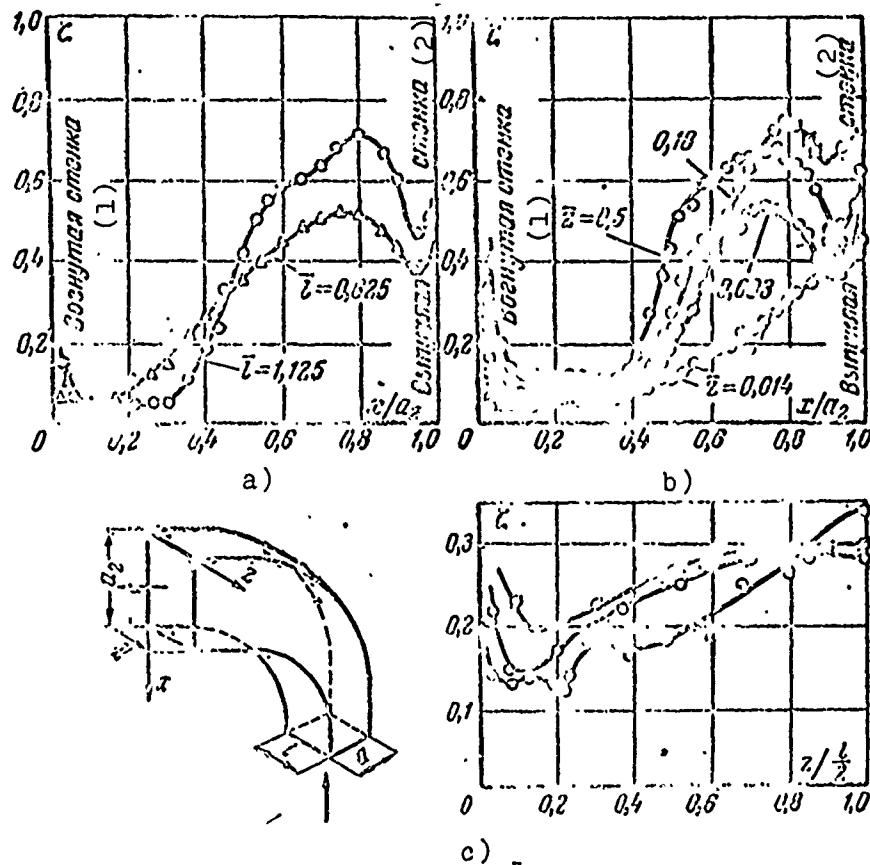


Fig. 6-6. Distribution of the coefficients of losses over the width (a and b) and the height (c) of a plane curvilinear diffuser with an angle of turn of 90° . (experiments of MEI).
 KEY: (1) Concave wall; (2) Convex wall.

The secondary flows, which limit the separation zone on the convex wall, simultaneously push this zone aside into the flow core (region I in Fig. 6-7); the dimensions and extent of region II (maximum losses) change with a change in height of the channel. The forcing back of the detached flow into the flow core is also characterized by the displacement of vortex zones III toward the axis of the outlet section and by the increase in their dimensions.

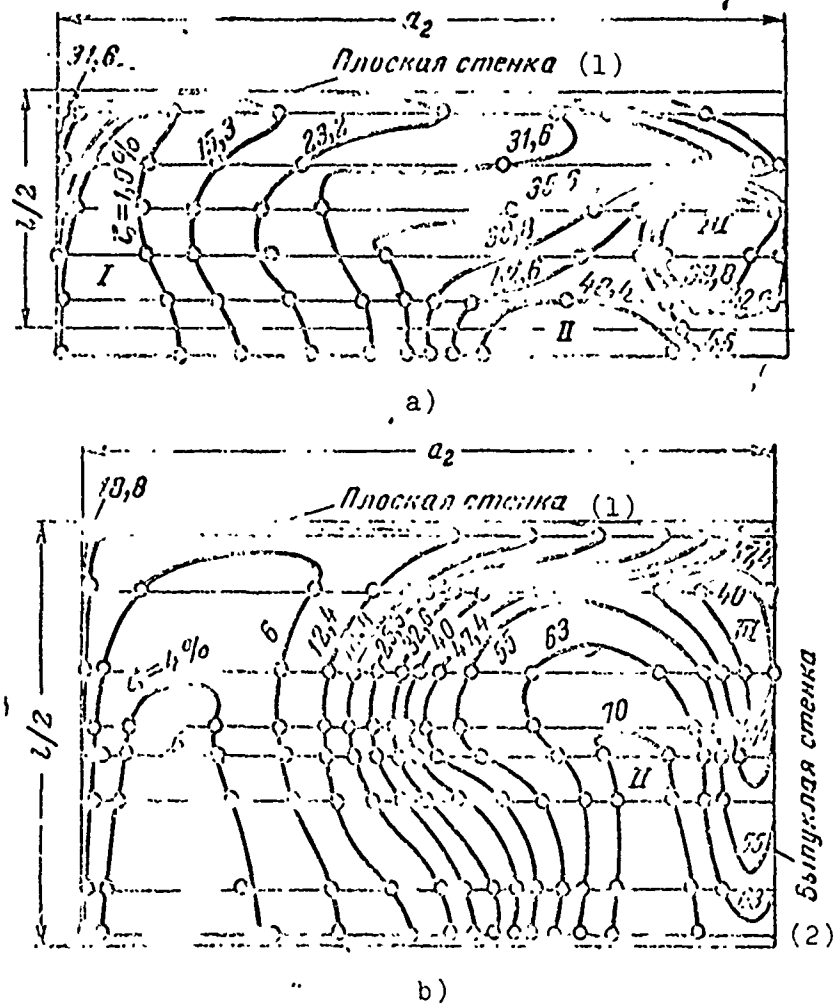


Fig. 6-7. Distribution of coefficients of losses of energy in the outlet section of plane curvilinear diffusers of different height ($M_1 = 0.76-0.8$; $Re_1 = 2.1 \cdot 10^5$. Experiments of MEI). a) $\bar{z} = z/a_2 = 0.625$; b) $\bar{z} = 1.125$. KEY: (1) Flat wall; (2) Convex wall.

The joining of secondary flows under conditions of separation occurs also on the convex wall, and the vortex zones III preserve their structure here. The penetration of secondary flows into the region of separation gives rise to a certain reduction in losses near the convex wall. This result is explained by the fact that the secondary flow possesses the greater kinetic energy than the flow in the separation zone. However, the pushing back of zone II exerts a negative effect on the core of the region I (near the concave channel wall). Zone I is narrowed, and losses in it increase. The boundary of the vortex zone II is concave, and flat walls form the fictitious channel with a decreased section along the flow. In this case in zone II the stationary vortex or the system of periodically formed vortices of smaller intensity are formed. In the latter case the flow will be periodically non-stationary (pulsating).

The effect of the basic geometric parameter (relative height) and mode parameters (M_1 and Re_1 numbers) on losses in the diffuser channel with the angle of turn of 90° can be seen in Fig. 6-8. Primarily it should be noted that the dependence ζ upon the height is not linear (Fig. 6-8a). An especially intense increase in losses with a decrease in height is noted when $l/\bar{l} \leq 1.0$. If the number $M_1 > M_{1*}$ (M_{1*} - critical M_1 number for the curvilinear channel), then the dependence ζ (l/\bar{l}) is changed: with a decrease in height losses in the beginning are lowered and then are somewhat increased. In the channel with $\bar{l} = 1.875$ when $M_1 > M_{1*}$ the shock wave, which closes the local supersonic region on the convex wall, gives rise to separation, whereupon the separation region is extended to the entire height of the channel. It is natural that in this case the losses sharply increase as compared with subcritical modes.

Figure 6-9 gives values of the optimum radius of curvature and ratios of the characteristic sections of the channel, which ensure the minimum intensity of secondary flows in the curvilinear

diffuser channel with the angle of turn of flow of 90° . From the graphs it follows that in the diffuser and weakly convergent channels it is advantageous to make the middle section of the channel a_m increased ($\bar{a}_m = a_m/a_1 > 1$) and then to ensure the convergent flow by the corresponding compression. In this case the pressure differential is decreased between the concave and convex surfaces in the sections, where the curvature of the channel is maximum, and, consequently, the intensity of the secondary flows is lowered. Furthermore, the compression of the output part of the channel reduces the region of separation on the convex wall AB (see Fig. 6-1a) and in certain cases prevents separation. Experiments of H. Nippert showed that depending on the angle of turn and the radii of curvature of the concave and convex walls, the optimum correlations of values a_m and a_1 are changed. This result is confirmed also by experiments of MEI.

The indicated correlations depend also on the geometric diffusivity of the channel, i.e., on n . Experiments show that with an increase in the radii of curvature of the back edge and the concave surface, losses from the secondary flows are decreased. At the same time (Fig. 6-9a) with an increase in the radius of curvature of the convex wall \bar{r}_1 , the optimum value \bar{a}_m at the given angle of turn and expansion ratio n increases. The dependence of \bar{a}_m upon n , which corresponds to minimal losses in the curvilinear channel with the angle of turn of 90° , is shown in Fig. 6-9b. One should also note the effect of the relative height of the channel \bar{l} on the optimum value of parameter \bar{a}_m . The relation $\bar{a}_m = f(\bar{l})$ should have a maximum the position of which will be determined by the geometric degree of diffusivity of the channel n . The most important geometric parameter of the curvilinear channel is the angle of turn of the flow. At MEI the plane curvilinear channels with angles of turn of 150° , 180° and 250° were investigated. H. Nippert determined the optimum dimensions of channels with an angle of turn of 180° . With a change in the angle of turn the intensity of the secondary flows and the position and number of

vortex zones and regions of separations should be changed. In channels with angles of turn of 150-180° the region of separation in the initial section of the convex wall can be substantially developed in the subsequent curvilinear flow if we do not use special methods of shaping.

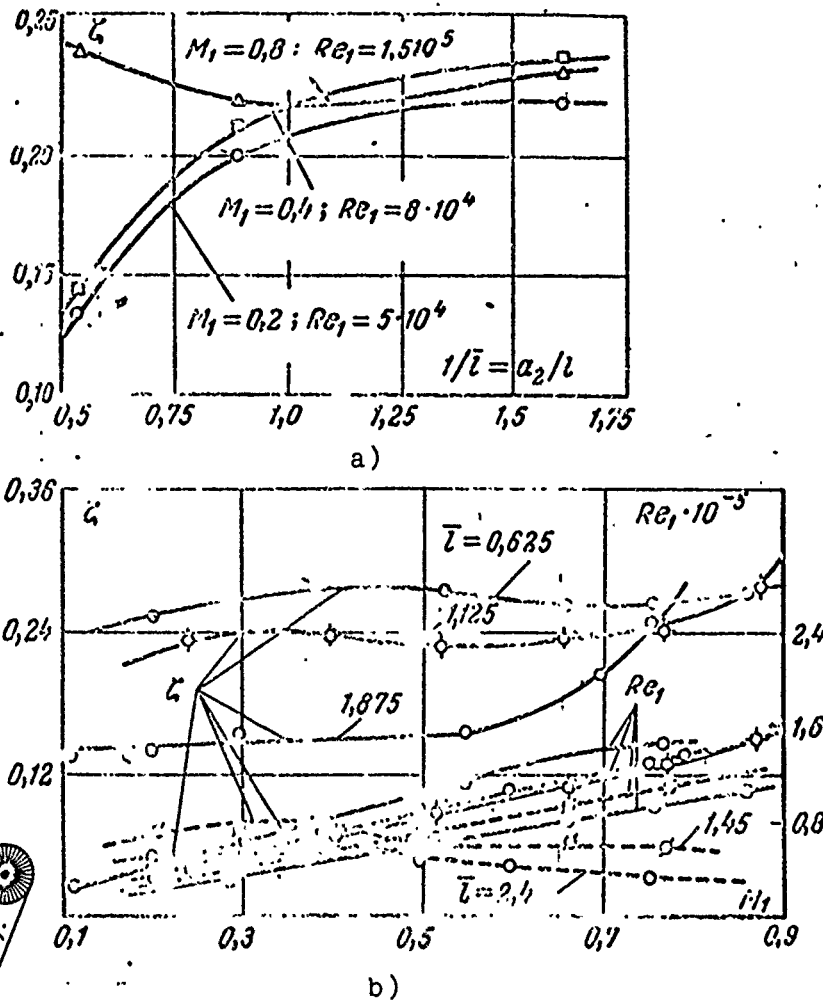


Fig. 6-8. Effect of relative height a) and number M_1 b) on losses in a plane curvilinear diffuser channel with the angle of turn of 90°.

Reproduced from
best available copy.

Reproduced from
best available copy.

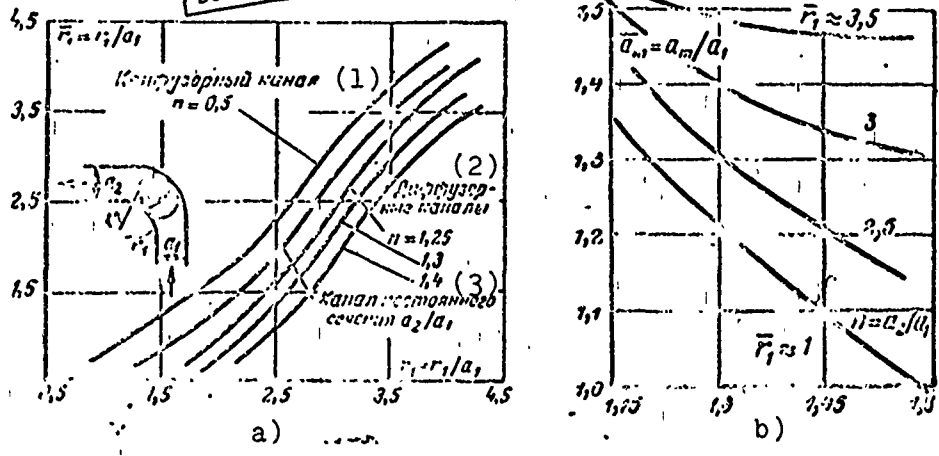


Fig. 6-9. Optimum geometric parameters of plane curvilinear diffusers. a) relative radii of curvature of the walls; b) degree of the diffusivity of the inlet section for the angle of turn of 90° .
KEY: (1) Convergent channel; (2) Divergent channels; (3) Channel of the stood section.

The appropriate experimental data are given in Fig. 6-10 and 6-11. It should be noted that with an increase in n the convergence of the outlet section \bar{a}_m should be decreased for channels with such angles of turn. However, the diffusivity of the inlet section, determined by the ratio $\bar{a}_m = a_2/a_1$, increases with an increase in n (Fig. 6-10b). With sufficiently large expansion ratios of the channel n , the construction of the channel with $\bar{a}_m > 1$ and $\bar{a}'_m > 1$ can cause some difficulties, since these parameters will not be in the optimum zone. Some deviations from the recommended parameters (Fig. 6-10a) do not cause a noticeable change in characteristics of the curvilinear diffuser channel. Consequently, in channels with large angles of turn it proves to be advisable to decrease the velocity before the turn (introduce the local diffusivity $\bar{a}_m > 1$) and after the turn to increase the velocity by the introduction of the local convergence ($\bar{a}'_m > 1$).

The appropriate results were obtained at MEI for channels with angles of turn of $150-250^\circ$. As can be seen from Fig. 6-10b, for

channels angled turn of 150° and 180° the optimum diffusivity of the inlet section is approximately equal. For the plane channel with the angle of turn of 250° , it was necessary to introduce successively two diffuser and two compression sections (Fig. 6-11). In this case the energy losses were minimum but quite high. At angles of turn $0 > 180^\circ$ the length of the section of constant cross section after the first turn is of importance.

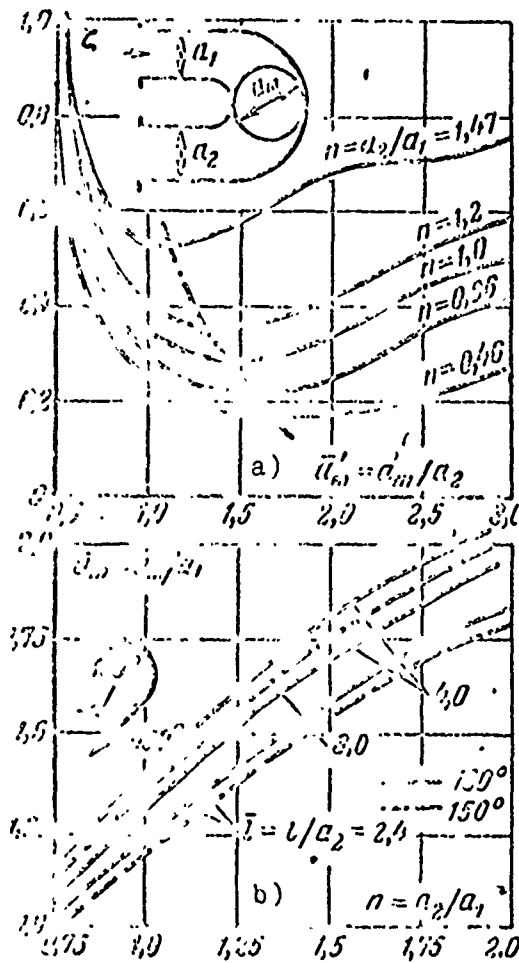
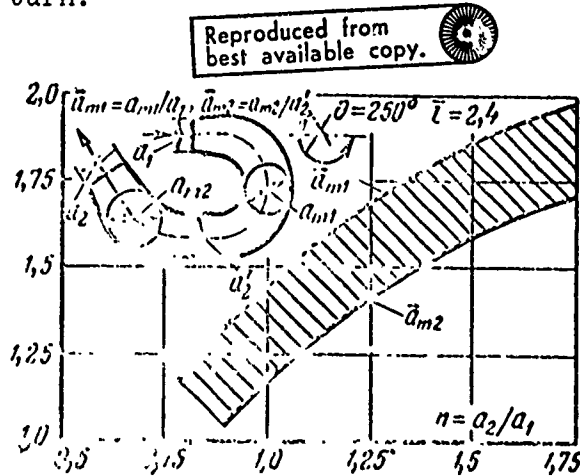


Fig. 6-10. Effect of the expansion ratio n and compression ratio of the outlet section \bar{a}'_m of the curvilinear diffuser with the angle of turn of 180° on the energy losses a) and the dependence of the optimum expansion ratio of the inlet section \bar{a}'_m upon the expansion ratio of the channel n for channels with angles of turn of 150° and 180° b).

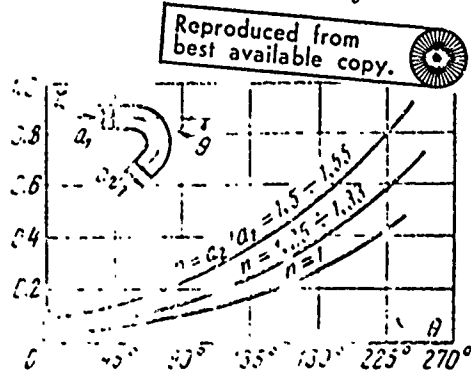
Reproduced from
best available copy.

Generalized graphs of energy losses in curvilinear diffuser channels are shown in Fig. 6-12. It is easy to see that the effect of the angle of turn of the channel sharply increases with an increase in the expansion ratio. Moreover, with the correct

organization of the flow in the curvilinear diffuser channel it is possible to provide moderate energy losses even at large angles of turn.



Plotted on the axis of the ordinates in Fig. 6-12 are coefficients of losses in straight diffusers with the appropriate expansion ratios and small flare angles. A comparison with these values allow estimating the additional losses in curvilinear diffusers conditioned by secondary flows and separations.



Important results were obtained in the study of the effect of the expansion ratio of curvilinear diffusers with constant angles of turn of the flow. An increase in n should give rise to an increase in the energy losses and the formation of separation. The existence of the dependence of the limiting expansion ratio of the curvilinear diffuser upon the angle of turn of flow was

established (Fig. 6-13). When $n > n_{np}$ the recovery of pressure in the curvilinear diffuser was sharply lowered, and the diffuser practically stopped operating. It is natural that in the curvilinear diffusers the maximally attainable expansion ratio n_{np} was substantially lower than that in the rectilinear diffusers.

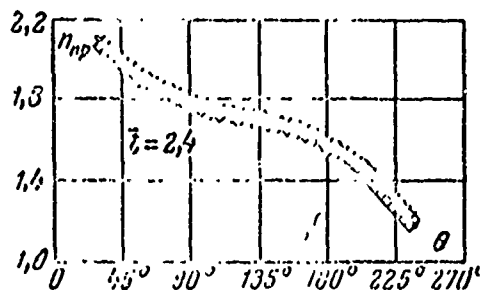


Fig. 6-13. Limiting expansion ratios of a plane curvilinear diffuser depending on the angle of turn θ .

A noticeable improvement in the structure of the flow and a reduction in the loss in the curvilinear plane diffuser can be attained by the use of blowing of the boundary layer before the zone of separation on the convex wall near the outlet section. Furthermore, in those cases when blowing cannot be accomplished it is advisable to install moving blades with nonuniform pitch. The number of the installed blades should be a minimum (1-2).

The recently conducted experiments showed that the use of a short separating rib on the concave wall of the channel (over the entire length) and blind grooves on flat walls near the convex surface allows noticeably reducing the losses and increasing the limiting expansion ratio.

It is rational to use the indicated methods, having provided the optimum geometric parameters of the diffusers, especially, the radii of curvature of the concave and convex walls of the channel and the degree of diffusivity of the inlet section \bar{a}_m .

The effect of the two most important mode parameters (Re_1 and M_1 numbers) on losses in curvilinear channels with various

angles of turn has still been studied insufficiently. With an increase in Re_1 losses in the channel are decreased. The turbulence of the layer near the separation gives rise to a line shift of separation along the flow, which also causes a sharp reduction in the losses.

The compressibility effect at subcritical velocities is indicated in the fact that the intensity of the secondary flows is lowered. An analysis of curves of pressure distribution (See Fig. 6-5) shows that with an increase in Mach number the transverse pressure gradients in the channel are decreased, since the pressure ratios increase more intensively on the convex wall than on the concave wall.

§ 6-3. Effect of Basic Geometric and Mode Parameters on the Operation of Annular Curvilinear Diffusers

The experimental investigation of the effect of geometric parameters on the operation of annular curvilinear diffusers is associated with great difficulties. They result from the fact that for the characteristic of even a plane curvilinear diffuser the assignment of five dimensionless quantities is necessary, and with the transition to the axiradial variant (see Fig. 2-2b) their number increases to six. Then, having changed each of six parameters 4 times, let us arrive at the conclusion that to obtain the total test data on annular curvilinear diffusers, it is necessary to test an unreally large quantity of variants determined by the number of combinations of 24 elements with 6 each, i.e.,

$$C_{24}^6 = \frac{24!}{6!18!} = 134\,594 \text{ variants.}$$

As a result in the study of axiradial diffusers, they are restricted to the geometric parameters whose effect should be decisive.

The present experimental data on the indicated group of diffusers, generally speaking, are limited and show in the majority the effect of only one-two parameters. Furthermore, results of some studies prove to be inconsistent.

The most complete research on axiradial diffusers was conducted by N. M. Kondak [60]. The shapes of vaneless annular turns examined by him were unsuccessful and led the author to the conclusion about inexpediency of the use of vaneless axiradial diffusers. These results, however, contradict the previous studies [7, 15, 70] and were not confirmed in the subsequent work [8, 41, 103].

Thus, I. A. Bindler obtained in the axiradial diffuser with the expansion ratio $n = 2$ the total coefficient of losses $\zeta_n \approx 0.61$.

In experiments of R. N. Bogomolov and L. A. Dorfman [8] the minimum total loss factor ζ_n was 43%. At this level there were losses in experiments of M. P. Umanskiy [103] and S. A. Dovzhik and P. I. Morozov [41].

Thus, in the correct selection of the relations between geometric parameters in annular curvilinear channels, it is possible to transform into the gravitation energy of pressure more than 50% of the kinetic flow energy at the inlet. For the solution to this problem, however, it is necessary to examine the effect of the most important geometric parameters.

Let us examine the following dimensionless parameters of the diffusers: the dimensionless diameter at the inlet $\theta = D/l$, "radiality" D_2/D_1 , "intensity" of turn L/l , dimensionless radius $\bar{r}_2 = r_2/r_1$, and the expansion ratio n .

Each of the given parameters has a definite physical sense. Thus, θ characterizes the inlet conditions and the structure and

intensity of the secondary flows, r_2/r_1 determines the shape of the channel in the meridian section of the diffuser, L/l shows how "sharply" the turn occurs and so on.

All the experiments were conducted in air at constant values of mode parameters M_1 and κe_1 equal, respectively, to 0.3 and $5 \cdot 10^5$.

The dimensionless geometric parameters of the investigated diffusers, optimum expansion ratios and minimum values of losses are given in Table 6-1.

Table 6-1

No.	Группа диффуза- ров	D/l	D_2/D_1	r_2/r_1	L/l	n_{opt}	$\zeta_{n, min}$	
1	I	6	2	0	2,5	2,3	0,60	$r_2/r_1 = \text{var}$
2		6	2	0,4	2,5	2,3	0,59	
3		6	2	0,7	2,5	2,3	0,51	
4		6	2	1,0	2,5	2,3	0,52	
5		6	2	1,1	2,5	2,3	0,53	
6		6	2	1,4	2,5	2,3	0,64	
7	II	6	2	1,0	1,0	1,7	0,66	$L/l = \text{var}$
8		6	2	1,0	1,5	2,2	0,57	
9		6	2	1,0	2,5	2,3	0,53	
10		6	2	1,0	3,4	2,6	0,48	
11		6	2	0,9	4,5	2,7	0,46	
12	III	6	2,67	0,85	4,2	2,7	0,38	$D_2/D_1 = \text{var}$
13		6	2,34	0,95	3,4	2,7	0,40	
14		6	2,00	0,87	3,54	2,6	0,46	
15	IV	6	2,00	1,0	1,5	2,2	0,57	$D_2/D_1 = \text{var}$
16		6	1,88	1,0	1,5	2,0	0,64	
17		6	1,75	1,0	1,5	1,8	0,72	
18		6	1,58	1,0	1,5	1,7	0,75	
19	V	10	1,6	0,8	3,16	2,84	0,615	$\theta = \text{var}$
20		8	1,75	0,85	3,16	2,40	0,620	
21		6	1,80	0,95	3,2	2,30	0,60	
22		4,5	1,78	0,8	3,0	2,5	0,60	

KEY: (1) Group of diffusers.

Five series of diffusers were tested. In the first series the effect of the shape of the flowing part characterized by the ratio of radii r_2/r_1 was investigated; in the second series the relative length L/l was changed; in the third and fourth series "radiality" was changed, and in the fifth series the role of the inlet diameter was investigated.

a) *Effect of radii r_1 , r_2 and the expansion ratio n .* Since losses in the annular curvilinear diffusers depend basically upon the velocity distribution about the contours AB and CD and the latter are determined by shape of the meridian section, let us explain first the effect of radii r_1 and r_2 and the expansion ratio n . For this purpose let us examine results of the experimental research on diffusers at various shapes of the meridian sections. These sections, given in Fig. 6-14, are outlined by the invariable radius r_1 and continuously decreasing radius r_2 , as a result of which the effect of the vertical section of contour CD is similar to the effect of the turning shield of the annular curvilinear diffuser.

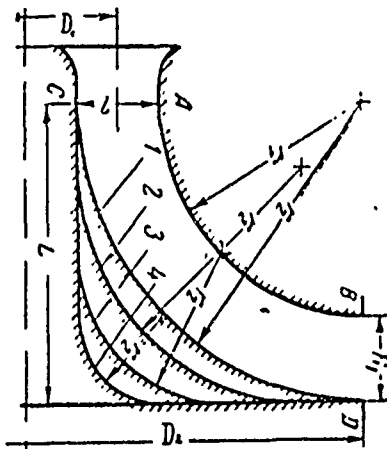


Fig. 6-14. Shapes of meridian sections of radial diffusers and basic designations.
 1 - $\bar{r}_2 = 1.2$; 2 -
 $\bar{r}_2 = 1.1$; 3 - $\bar{r}_2 = 0.7$;
 4 - $\bar{r}_2 = 0.4$.

Tests of the indicated diffusers, whose results are presented in Fig. 6-15, indicate that between radii r_1 and r_2 there exists a certain optimum relation, the deviation of which with small expansion ratios gives rise to a noticeable increase in losses.

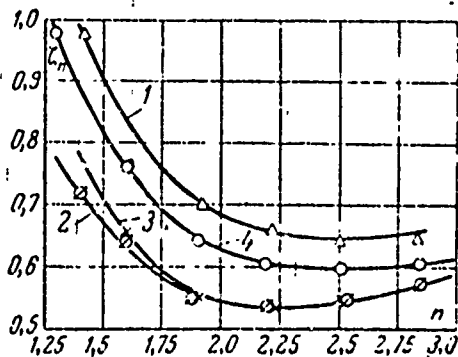


Fig. 6-15. Dependence of losses in axiradial diffusers upon the expansion ratio n in various ratios of radii r_2/r_1 . 1 - $\bar{r}_2 = 1.2$; 2 - $\bar{r}_2 = 1.1$; 3 - $\bar{r}_2 = 0.7$; 4 - $\bar{r}_2 = 0.4$.

For the greater clarity Fig. 6-16 depicts the relation $\zeta_n = f(\bar{r}_2)$ obtained in the zone of optimum values of n ($n_{\text{опт}} = 2.2-2.3$).

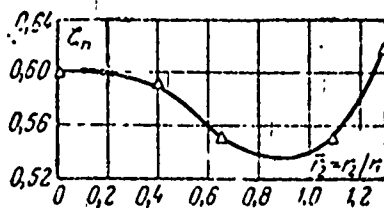


Fig. 6-16. Variation in losses depending on \bar{r}_2 in the zone of optimum expansion ratios.

From the given curve it follows that with an increase in \bar{r}_2 first a certain reduction in losses occurs. When $\bar{r}_2 = 0.7-1.1$ the losses reach a minimum value, and then for $\bar{r}_2 > 1.1$ they rather sharply increase. Such a nature of the change in losses is connected with the shape of the channel in the meridian section of the diffuser or, more accurately, with the nature of the change in velocities along the convex AB and concave CD (see Fig. 6-14) contours which form the channel.

It is obvious that when $\bar{r}_2 < 1$ the basic braking of the flow occurs in the inlet, and a further turn is accomplished with reduced velocities. If we depict for this case the change in areas along the center line, then the corresponding dependence will be

close to curves F for the most effective nondetached conical diffusers. With an increase in the radius \bar{r}_2 the braking of the flow is transferred to the zone of turn and then into strictly the radial part. As a result the distribution of velocities on the convex contour noticeably deteriorates, and there appears an open separation zone on the convex wall, which decreases the effective expansion ratio of the diffuser. In this case the losses increase.

On the other hand, the value of the radius \bar{r}_2 is limited on the lower side, since at small values of \bar{r}_2 there occurs an abrupt braking of the flow by the concave contour, which causes the appearance of a closed separation zone of the concave wall. However, the effect on the total losses of internal separation is considerably less, since it does not cause a substantial change in effective outlet area, i.e., an area with a positive value of the flow velocity component. This circumstance explains the fact that even when $\bar{r}_2 = 0$ the losses are increased in comparison with the minimum value a total of 9%.

Thus, with the optimum relation between radii r_1 and r_2 the shape of the channel in the meridian section of the diffuser should ensure nondetached flow of contours AB and CD or the minimum extent of the separation zones. From this viewpoint the fulfillment of inlet with maximum diffusivity is also justified: in this case the maximum positive pressure gradient acts on the comparatively thin boundary layer, and the probability of nondetached flow increases. If the zone of braking of the flow is far from the inlet section, then the effect of the positive pressure gradient on the thicker boundary layer in most cases gives rise to a separation on the convex contour.

One should emphasize that the discussed test data of axial-radial diffusers confirm the data on the advisable shape of the curvilinear diffusers given in § 6-1.

The curves given in Fig. 6-15 visually confirm the aforesaid about the role of the radius \bar{r}_2 . Actually when $\bar{r}_2 = \bar{r}_{2\text{max}}$ in the whole range of values of the expansion ratio the losses have a peak value. Then when $\bar{r}_2 = 1.1$ and 0.7 these losses become minimal and practically equal, and with a further decrease \bar{r}_2 they again increase. Furthermore, it is clearly evident that the losses substantially depend upon the expansion ratio. Thus, if when $n = 1.5$ the maximum change in losses, depending on \bar{r}_2 , is 20%, and then for $n = 2.8$ it is decreased to 5-7%.

The noted distinction in quantitative results is connected with the fact that in the experiments the expansion ratio was changed by means of the displacement of the contour CD along the longitudinal axis. As a result with small expansion ratios, any deformation of the contour CD substantially changed the velocity distribution on the contour AB. With an increase in n , when the contour CD was remote, its effect on the flow pattern along the contour AB was decreased.

Thus, the estimate of the effect of the radius r_2 must be conducted taking into account the expansion ratio n . If for large values of n the use of arbitrary values of the radius r_2 is admissible, then with decrease in n it is necessary to approach the observance of the optimum relations between radii r_1 and r_2 .

By comparing the relations $\zeta_n = f(n)$ for the conical and annular diffusers, it is possible to note the substantial reduction in the zone of optimum expansion ratios, which in the case in question changes from 2.2 to 2.5. A decrease in n_{opt} is connected with the fact that nondetached flow in the annular radial diffuser is possible only with small expansion ratios.

Visual observations and the shape of the velocity profiles in the outlet section showed that with an increase in n in the outlet part of the contour AB there appears the separation of the

flow, which is continuously displaced inside the channel. As a result there occurs a decrease in effective area at the outlet from the diffuser and an increase in internal losses, and their magnitude rather rapidly becomes of the same order as that of the outlet losses. A further increase in the expansion ratio is given in Fig. 6-17.

b) *Effect of the relative length (the "intensity" of the turn).* The following very important geometric parameter of the axiradial diffuser is the dimensionless length L/l .

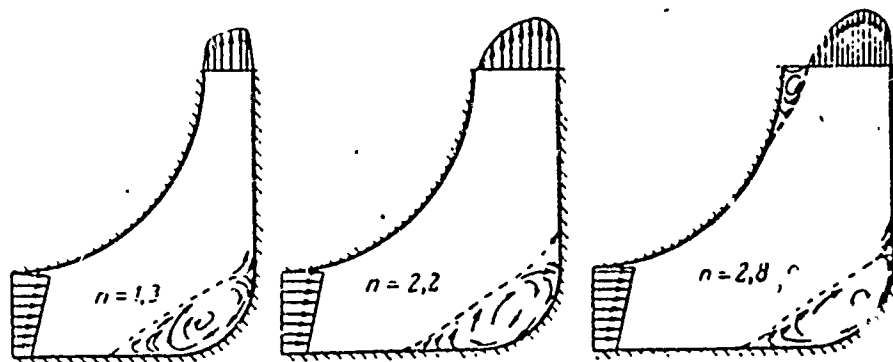


Fig. 6-17. Diagram of the redistribution of separation zones in an annular diffuser with an increase in the expansion ratio n .

The data given in Fig. 6-18 indicate that with an increase in the nondimensional distance \bar{L} there occurs a continuous decrease in the total loss factor, and the optimum expansion ratio increases (Table 6-1). Geometrically with an increase in \bar{L} the axiradial diffusers approximate the axial annular diffusers. It is natural that with this the portion of the losses connected with the turn of the flow should be continuously decreased. On the contrary, with an increase in the "intensity" of the turn, i.e., with a decrease in the axial length of the diffuser, one should expect an increase in losses. Simultaneously, to provide for such a turn more active effect on the flow of the concave contour CD is necessary, which requires its approach with the convex contour AB

and gives rise to a decrease in the optimum expansion ratio. At the same time the curve given in Fig. 6-18 shows that the intensity of the reduction in losses, with an increase in value \bar{L} , decreases. If an increase in dimension \bar{L} from 1.0 to 3.0 gives rise to a decrease in losses by 18%, then with a change in \bar{L} from 3 to 4.5 the losses decrease a total of 2%.

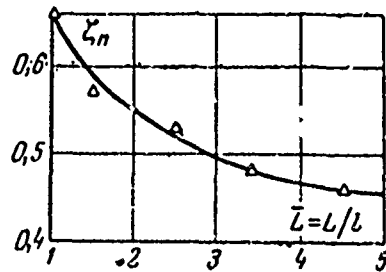


Fig. 6-18. Dependence of the total loss factor ζ_n upon parameter \bar{L} .

Thus, for a reduction in the losses it is necessary to strive for a decrease in the "intensity" of the turn. However, to increase dimension \bar{L} more than 2.5-3.0 is hardly advisable: the economic effect in this case is comparatively small, and the overall axial dimensions of the diffuser substantially increase. The expressed considerations apropos of the selection of the dimension \bar{L} completely refers to the dimensionless radius of the convex contour.

Let us note that the curves in question are obtained with the optimum relation between radii r_1 and r_2 .

With a decrease in \bar{L} from 3.5 to 2.0 the minimum magnitude of the losses increases by 12%, and the optimum expansion ratio is decreased from 2.2 to 1.8. If we examine the effect of \bar{L} with a constant expansion ratio n , equal to 2.2, then the indicated decrease in axial dimension increases the losses by 22%. Such a sharp increase in losses with an increase in the "curvature" of the radial diffuser is caused by the substantial deterioration of flow along the contour AB, where even with a small expansion ratio

n separation appears.

c) *The effect the "radiality" of diffusers D_2/D_1 .* The effect of "radiality" was investigated in the third and fourth series of the diffusers.

The distinction between the indicated series was that in the first case the ratio of the diameters was changed because of radii r_1 and r_2 and in the second case - because of the radial cutting of the same diffuser.

From a qualitative side the dependence of losses from the dimensionless ratio D_2/D_1 in both cases was equal (Fig. 6-19): with an increase in "radiality" the energy losses were decreased. In this case it is possible to note that in the third series of experiments the optimum expansion ratios were changed very weakly, whereas in the fourth series simultaneously with a decrease in the ratio of diameters D_2/D_1 a noticeable reduction in the optimum expansion ratio and a sharp increase in losses occurred.

The obtained results reflect the effect of the shape of the diffuser channel. If the "radiality" of the diffuser was changed with variations of radii r_1 and r_2 with close expansion ratios, then this gave rise to the approach of convex and concave contours. As a result the reverse boundary layer effect increased, since the same geometric diffusivity was accomplished on a large length, and the gas flow in the whole channel could be nondetached. From this viewpoint, when evaluating the optimum value of "radiality," it is possible, apparently, to proceed from the same consideration as when evaluating the optimum flare angle of a conical diffuser.

On the one hand, the increase in ratio D_2/D_1 causes an increase in the fairing and, consequently, an increase in frictional losses. On the other hand, the distribution of the assigned diffusivity at the greater length gives rise to a reduction in the

longitudinal positive pressure gradients and increases the probability of nondetached flow. The optimum ratio of diameters D_2/D_1 according to the available data comprises a magnitude of the order of 2.5-3.0.

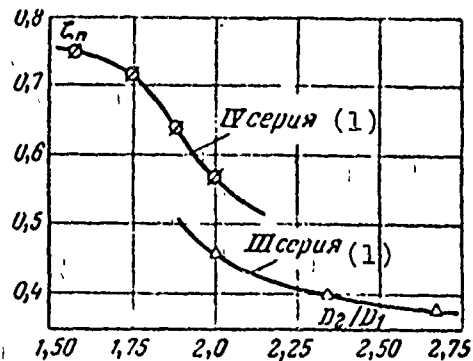


Fig. 6-19. The effect of "radiality" of the annular diffuser D_2/D_1 on the total loss factor ζ_n .

KEY: (1) Series.

If the "radiality" is changed by means of radial trimming, then the shape of diffuser substantially changes, and with large sections it approaches the diagonal shape and further to the axial variant with a large opening angle and shield at the outlet. The motion in such a diffuser occurs usually with the separation of flow and is accompanied by increased losses, and the optimum conditions of flow correspond to the reduced geometric diffusivity. A certain concept about the effect of the "radiality" in such a case can be obtained from curves in Fig. 6-20, where curves of losses in four diffusers differing only by the ratio D_2/D_1 are given. The remaining parameters in this series of experiments are: $\theta = 6$; $\bar{L} = 2.5$ and $\bar{r}_2 = 1$.

From the curves in Fig. 6-20 it follows that with a decrease in D_2/D_1 a very sharp increase in losses takes place. Thus, having kept n invariable and equal to 2 and having decreased D_2/D_1 from 2 to 1.6, we obtain an increase in losses of 22%. For $n = 2.5$ this increase consists of 30%, and in the zone of small expansion ratios ($n = 1.4$) losses with a change in D_2/D_1 were practically not changed.

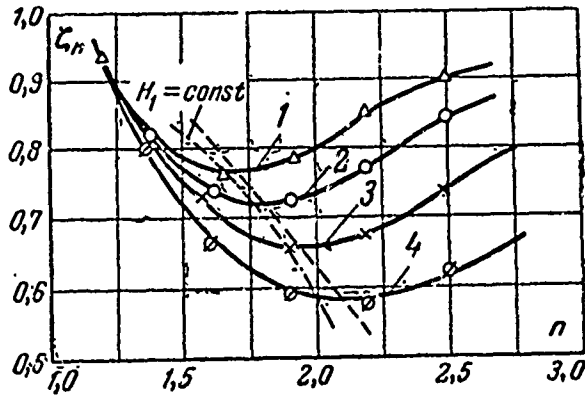


Fig. 6-20. Dependence of the coefficient of total losses upon the expansion ratio n for various values of D_2/D_1 . 1 - $D_2/D_1 = 1.58$; 2 - $D_2/D_1 = 1.75$; 3 - $D_2/D_1 = 1.88$; 4 - $D_2/D_1 = 2.0$.

The noted effect of "radiality" is explained by the fact that with a decrease in ratio D_2/D_1 , to preserve the invariable expansion ratio it is necessary to increase the width of the outlet section by means of the axial displacement of the external contour CD (see Fig. 6-14). As a result the conditions of flow on the contour AB noticeably deteriorate, which leads in this region to the separation of flow whose zone is continuously expanded with an increase in the outlet dimension.

With a small expansion ratio ($n \approx 1.4$), when the flow in meridian plane is not accompanied by separation, the reduction in the "radiality" has an insignificant effect, since in this case the displacement of the contour CD leads only to an increase in boundary layer losses, without causing its separation. When separation does not exist, and with a constant output dimension H_1 the reduction in the ratio to diameters D_2/D_1 causes an increase in the losses with an outlet velocity within bounds of a decrease in the expansion ratio and gives rise to a certain reduction in internal losses due to the reduction of the streamlined perimeter.

For an illustration of the aforesaid, in Fig. 6-20 a line of the change in losses is plotted with a change in "radiality" but at constant value H_1 . Here the dashed line represents the calculated increase in total losses induced by the reduction in the expansion ratio. A certain divergence between these curves in the zone of small values n is connected with the reduction in internal losses noted above.

A similar curve, plotted for the region of large values of the outlet dimension H_1 , when inside the channel detached flow takes place, gives a more intense increase in losses as compared with the calculation; here the decrease in "radiality" along with an increase in losses in outlet velocity gives rise to an increase in internal losses. The latter is caused by the fact that with a decrease in D_2 the internal local separation in the region of the turn turns into the open zone of the separation, lowering the effective outlet area.

d) *The effect of dimensionless inlet diameter θ .* The next parameter, investigated in experiments of the fifth series, was the dimensionless inlet diameter $\theta = D/l$. In turbomachines this parameter serves as one of the basic stage characteristics. Therefore, in this case a comparatively wide range of the variation of θ from 4.5 to 10 was investigated, which corresponds to a large number of stages of steam and gas turbines.

By estimating the effect of the dimensionless inlet diameter on the operation of the diffuser with invariable remaining dimensions, it is possible to note that if a change in θ is accomplished only because of the diameter at a constant absolute value of the inlet dimension l , then the effect of this parameter proves to be weak. In fact, with an increase in θ the streamlined surface increases, but simultaneously with this there is an increase in the inlet section area of the diffuser, which increases the value of the available kinetic flow energy at a constant differential

pressure on the diffuser. As a result the coefficient of losses, which represents the ratio of internal diffuser losses to the kinetic energy at the inlet, is changed insignificantly. As a whole, according to the data given in Table 6-1, the change in this parameter from 4.5 to 10 causes an increase in losses of approximately 1-1.5%. If θ is changed because of the height l , then in the axiradial diffusers a noticeable increase in losses occurs.

e) *The effect of the smoothness of the contours outlining the meridian channel of the diffuser and fastening ribs on losses in axiradial diffusers.* As was already mentioned, with small radius r_2 on the concave contour closed detached zone is formed (see Fig. 6-1). In this case between the main flow and the zone of separation an intense energy exchange is established, which maintains a vortex flow pattern here.

The magnitude of additional losses connected with the formation of separation on the concave contour of the diffuser substantially depends upon the extension of the detached zone, and therefore, for their decrease it is necessary either to reduce the extension of the vortex zone or reduce the intensity of the energy exchange with the main flow. In this direction good results can be achieved in the replacement of the smooth concave contour in meridian plane by a contour composed of segments of straight lines. Tests of such a diffuser with three different contours (Fig. 6-21) showed that with the transition to a broken generatrix (curve 2, Fig. 6-21) losses in the zone of optimum expansion ratio are lowered by almost 10%.

At small expansion ratios ($n < 2$) the effect of the shape of the broken contour proves to be insignificant. However, when $n > 2.0$ it is advantageous in zone of high velocities to have a smaller angle of break of the generatrix, since at a small angle of break the basic zone of separation is transferred into the region of lower velocities, and with an increase in this angle the

extension of the separation zones at conjugation points proves to be approximately equal (Fig. 6-14, contour CD). The reduction in losses during the replacement of the smooth contour by a broken line is explained by the fact that with such contour the zones of separation are localized at angular points, and their extension is noticeably reduced.

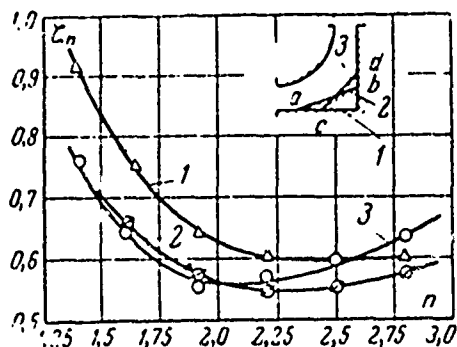


Fig. 6-21. Effect of the shape of the concave contour of axiradial diffusers on total losses in it.

The obtained results are important, since the technology of the manufacture of radial diffusers for exhaust ducts of powerful steam turbines is considerably simplified, since in the transition to a broken contour the execution of a welded construction proves to be possible. From this viewpoint it was advisable to examine the question of the replacement of the smooth convex contour of the diffuser with a broken line. Two variants of the contour are depicted on Fig. 6-22a, and test data at various values of n are given in Fig. 6-22b.

Here, just as one would expect, the disturbance of the smoothness of the contour led to a substantial increase in losses, since unlike the internal contour, where at angular points local separation took place, in this case the angular points were the sources of the developed separation zones, which sharply narrow the effective output area of the diffuser. In this case not only the internal diffuser losses but also the outlet increased.

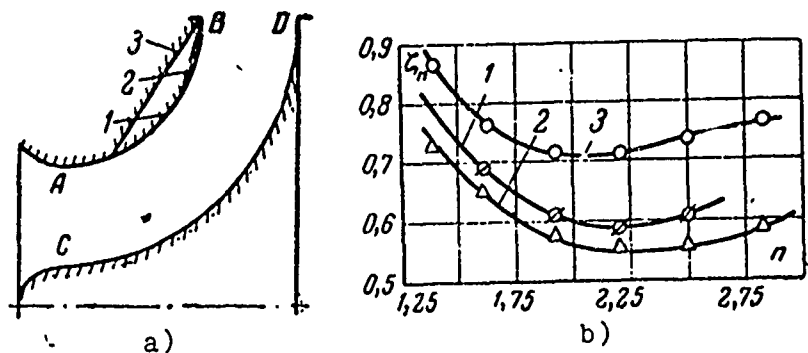


Fig. 6-22. Variants of convex contours a) and the dependence of losses upon the expansion ratio at various contours AB b).

It should be noted, however, that the magnitude of the losses depended upon the position of the angular point on the external contour. If the smoothness of the contour was disturbed only in the outlet part (contour 2, Fig. 6-22a), then the change in losses proved to be unimportant. Moreover, at small radii r_2 this gave rise to a certain reduction in the losses. However, the approach of the angular point to the inlet section caused a sharp increase in losses irrespective of the magnitude of the radius r_2 (contour 3, Fig. 6-22a). From what has been said it follows that in the designing of the radial diffuser it is necessary to pay serious attention to the outlines of the convex contour and then select the most optimum shape of the concave part of the axiradial diffuser.

Since in most cases with the installation of axiradial diffusers after the stage of the turbomachine, according to design consideration, it is necessary to provide rigid coupling of the external and internal contours, let us examine the effect of the internal coupling elements on the magnitude of the diffuser losses. Used most frequently as such elements are longitudinal ribs. As experiments show, the location of these ribs can substantially

change the whole pattern of flow. Thus, with the installation of the continuous longitudinal ribs, which divide the channel of the diffuser into a number of isolated segments, one should expect a noticeable increase in the losses; in this case in each segment there occur complex secondary flows, which cause the separation of the flow at connecting places of the ribs with the contours of the diffuser.

The test data of an axiradial diffuser given in Fig. 6-23 show that with the installation in it of three continuous ribs losses increase by 5-8%.

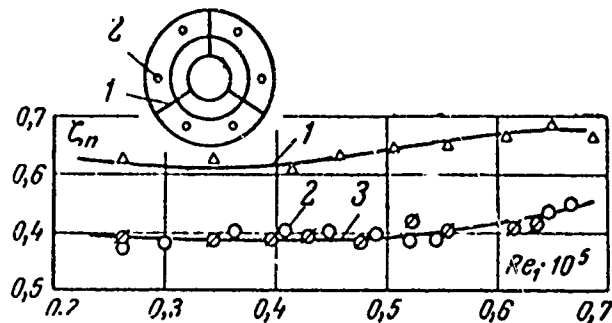


Fig. 6-23. Effect of ribs on the operation of axiradial diffusers. 1 - Flat ribs; 2 - Round rods; 3 - Ribs are absent.

The picture proves to be completely different, if from continuous longitudinal ribs we turn to slotted ribs or ribs installed only in the outlet section, where the transverse pressure gradient is minimal. In this case the effect of the ribs proves to be insignificant. With the installation in the diffuser of six round rods the losses were practically not changed (Fig. 6-23, point 2). Thus, at the inlet into the diffuser it is necessary to install as small a quantity of narrow ribs as possible and place the main power ribs in the outlet section.

We will discuss further the effect of misalignments and eccentricity of the installation of the concave contour of the diffuser relative to its convex part. Such disturbances are always possible with the assembly of a diffuser, and, as the conducted experiments show they can noticeably be reflected on the efficiency of the entire machine.

Thus, Fig. 6-24 gives curves of the change in local coefficients of pressure recovery over the circumference of the axiradial diffuser with the concentric and eccentric location of the concave contour.

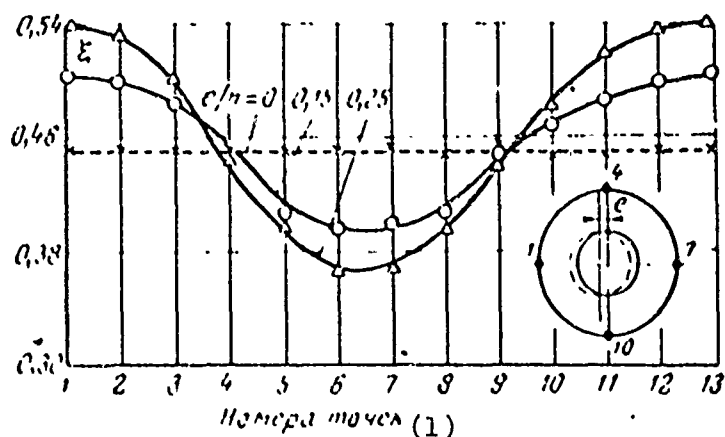


Fig. 6-24. Measurement of the coefficients of pressure recovery over the circumference of an axiradial diffuser with a disturbance in the concentricity of the installation.

KEY: (1) Numbers of points.

Experiments showed that even with a small eccentricity its presence gives rise to a noticeable change in the local coefficients of pressure recovery. If the mean value of these coefficients in comparable cases is approximately equal, then the local nonuniformity was increased almost 2 times, which can have a noticeable effect on the operation of the last stage of a turbomachine. From this viewpoint one should, apparently,

estimate the effect of the eccentricity and misalignments of the exhaust diffuser of the turbomachine.

§ 6-4. Some Problems in the Analytical Determination of Losses in Axiradial Diffusers

The calculation of curvilinear diffusers represents today the greatest difficulties, since their shape is determined by a large number of geometric parameters which affect the structure of the flow. Because of this attempts to use for calculation here a formula of the type (2-42a) cannot give positive results. At the best by such a method the probable order of the coefficient of losses can be found, because, on the one hand the equivalent angle even on a qualitative side cannot take into account the effect the most important geometrical parameters of axiradial diffusers, and on the other hand — the relation $\phi_{\Delta} = \phi_{\Delta}(\alpha_{\Theta})$ (see Fig. 2-12) is far from being universal.

In attempting to solve the indicated problem, W. Albring [114] offered to examine not the equivalent but the local angle determined by formula

$$\alpha_{\Theta} = 2 \operatorname{arctg} \left(\frac{1}{\Pi_1} \cdot \frac{df}{dx} \right).$$

Thus, an attempt is made to introduce into calculation as large geometric parameters of complex diffusers as possible and by subsequent integration of local losses over the whole channel to find the total magnitude of the loss factor ζ . This method of calculation has been developed most fully in [34, 38, 39]. However, as was already mentioned above, the method based on the use of the coefficient of softening of the shock ϕ_{Δ} can give correct result if the experimental dependence $\phi_{\Delta} = f(\alpha)$ is single-valued. Unfortunately, there is no such uniqueness even for the simplest conical diffusers. Fig. 3-32 already gave values of coefficient ϕ_{Δ} for various angles of α , calculated from experimental values of

the coefficient of losses ζ [51, 66, 110, 142, 148]. Even with the same mode parameters the same angle corresponds to a number of coefficients ϕ_d . Thus, for $\alpha = 4.0^\circ$, $0.4 \leq \phi_d \leq 0.8$, for $\alpha = 7^\circ$, $0.1 < \phi_d < 0.6$, for $\alpha = 15^\circ$, $0.1 < \phi_d < 0.4$, etc. Nevertheless, the method expounded in [34, 38, 39] is still the only one for the analytical calculation of losses in curvilinear diffusers.

The use for calculation of boundary layer characteristics in this case also encounters difficulties in the determination of the area of displacement Δ^* and the area of energy losses $\bar{\Delta}^{***}$. However, with some assumptions it is possible to determine the magnitude $\bar{\Delta}^*$ and by using formula (2-29) find the total loss factor ζ_n .

For this purpose let us introduce into the examination not the equivalent angle but the equivalent channel, i.e., the channel with a rectilinear axis whose areas, perimeters and the law of the change in these values along the x axis coincide with analogous values of the assigned curvilinear diffuser. Let us present the law of the velocity change along the axis of such a channel in the form of

$$\frac{c_1}{c_2} = \frac{F_1}{F_2 (1 - \bar{\Delta}_1^*)} \quad (6-1)$$

Let us designate further the length of the external contour of diffuser AB (see Fig. 6-14) by L_1 and the internal CD by L_2 . Then on these contours in the inlet section, when using expression (3-9) and formula (6-1), we will obtain the following values of the displacement thickness:

$$\Delta_{2,1}^* = \frac{0.036H}{\text{Re}_1^{0.2}} u^{3.31} (1 - \bar{\Delta}_2^*)^{1.31} D \left(\frac{L_1}{D} \right)^{0.8} \times \left[\int_0^1 \left(\frac{D_1}{D_2} \right)^{1.23} \left(\frac{F_1}{F_2} \right)^{2.92} \frac{d\bar{x}}{(1 - \bar{\Delta}_1^*)^{3.92}} \right]^{0.8}; \quad (6-2)$$

$$\Delta_{2,2}^* = \frac{0,036H}{\text{Re}_1^{0,2}} n^{3,54} (1 - \bar{\Delta}_2^*)^{2,34} D \left(\frac{L_2}{D} \right)^{0,8} \times$$

$$\times \left[\int_0^1 \left(\frac{D_t}{D_2} \right)^{1,25} \left(\frac{F_t}{F_1} \right)^{3,92} \frac{d\bar{x}}{(1 - \bar{\Delta}_t^*)^{2,92}} \right]^{0,8} \quad (6-3)$$

Hence

$$\bar{\Delta}_2^* = \frac{\bar{\Delta}_{1,2}^* + \bar{\Delta}_{2,2}^*}{2} = B n^{3,34} (1 - \bar{\Delta}_2^*)^{3,34} \times$$

$$\times \left[\int_0^1 \frac{\Phi(\bar{x}) d\bar{x}}{(1 - \bar{\Delta}_t^*)^{2,92}} \right]^{0,8} \quad (6-4)$$

where

$$\Phi(\bar{x}) \equiv \left(\frac{D_t}{D_2} \right)^{1,25} \left(\frac{F_t}{F_1} \right)^{3,92};$$

parameters B and H are determined by formulas

$$B = \frac{0,036H}{\text{Re}_1^{0,2}} \left(\frac{L_2}{D_{1cp}} \right)^{0,8} \frac{D_{1cp}}{h} \left[1 + \left(\frac{L_1}{L_2} \right)^{0,8} \right];$$

$$H = 1,4 \left[1 + \frac{n^{0,8} - 1}{(L/D_{1cp})^{0,2}} \right]; \quad (6-5)$$

h - the channel width in meridian plane at the outlet from the diffuser.

Formula (6-4) is a generalization of the earlier derived expressions (3-12) and (5-10). Actually for annular diffusers with linear generatrices $L_1 = L_2$; $h = D_2 - d_2/2$ and

$$\frac{F_t}{F_1} = \frac{D_i^2 - d_i^2}{D_i^2 - d_i^2} = \frac{1 - d_i^2}{D_i^2 - d_i^2}$$

The substitution of these values into (6-4) gives rise to relation (5-10). Thus it is possible to show the identity of formulas (6-4) and (3-12).

In general function $\Phi(\bar{x})$ is changed arbitrarily, and for the assigned channel the calculation of area is reduced to the solution of the integral relation (6-4). For the purpose the facilitation of calculations, let us approximate the function $\Phi(\bar{x})$ by the following expression:

$$\Phi(\bar{x}) = \frac{1}{[1 + (n-1)\bar{x}^m]^{1,92}} \quad (6-6)$$

By changing the exponent m , it is possible at the assigned expansion ratio n to achieve the close coincidence of the actual function $\Phi(\bar{x})$ and the approximating expression (6-6):

$$\Phi(\bar{x}) = \left(\frac{D_{icp}}{D_2}\right)^{1,25} \left(\frac{F_1}{F_t}\right)^{1,92} \approx \frac{1}{[1 + (n-1)\bar{x}^m]^{1,92}} \quad (6-6a)$$

Then the calculation according to formula (6-4) can be noticeably facilitated if under condition (6-6) earlier we calculate for different values of parameter B of the area of displacement $\bar{\Delta}^*_2$. These calculations, conducted by L. M. Dyskin, are presented in the form of a nomogram in the appendix (see Fig. A-4), constructed for the exponent $m = 1.5$. As specific calculations show, for axiradial diffusers the value m is changed from 1.5 to 2.0.

Let us note that, just as in the case of conical diffusers, the use of the simpler formula (2-54) instead of (3-9) leads almost to the same quantitative results, and with the expansion ratios $n > 2$ it gives the best agreement with the experimental data. However, in considering the definite discussion of formula (2-54) and the degree of approximation of the evaluation of losses

in axiradial diffusers, we are limited here to the use of the more usual relations.

The greatest difficulties in the analytical calculation of axiradial diffusers are connected with the estimate of the flow pattern in them, since all the given conclusions are valid only for nondetached flows taking place with defined relations between the geometrical parameters. These optimum relations, based upon results of the experiment, are examined in the previous paragraph. For the concept about the possibilities of the calculated method, let us conduct an estimate of the losses in the axiradial diffuser with the expansion ratio $n = 2.3$ and $D/l = 2.5$ whose contours are outlined from one center. In this case the calculated distribution of the dimensionless velocities along the center line of the diffuser proves to be very unfavorable.

Actually, if in the conical diffuser the basic drop in velocity occurs in the initial section of the diffuser where the thickness of the boundary layer is small, then here the maximum velocity gradients are displaced to the outlet part of the channel, and there is complete basis for expecting the boundary layer separation.

The comparative performance calculations of the boundary layer in diffusers at various distributions of velocities (see Fig. 3-20 and 3-21) show that with a linear drop in velocity for $n > 2$ practically does not succeed in avoiding the boundary layer separation.

However, with a sharp increase in the displacement thickness Δ^*_1 an intensive reduction in the effective expansion ratio occurs. As a result the actual drop in velocity, as was already repeatedly noted, will be less intense, and with small geometric expansion ratios the flow will be kept nondetached.

Results of the calculation give for the diffuser in question a magnitude of the total loss factor of about 45%. An analogous coefficient for a conical diffuser with the same expansion ratio and same relative length consists of 27%, i.e., according to the recovery ability even with nondetached flow radial diffusers are considerably inferior to conical and axial diffusers, and the magnitude of the total coefficient of losses, equal to 40-45%, is, apparently, minimal.

CHAPTER SEVEN

EXHAUST DUCTS OF TURBOMACHINES

§ 7.1. Fundamental Design of Exhaust Ducts and Their Effect on the Efficiency of Turbomachines

When selecting a design scheme and design of the exhaust ducts of turbomachines, it is necessary to consider the requirements dictated by considerations of the efficiency of reliability of the machine. The created branch connection should:

- 1) ensure the removal of the working medium from the turbomachine in an assigned direction with minimum aerodynamic losses;
- 2) ensure the uniform pressure field after the last stage, i.e., possess equal flow friction in all the directions discharging the working medium to the outlet section;
- 3) have a uniform velocity field at the outlet;
- 4) in all modes ensure the stationary stable flow pattern;
- 5) possess high rigidity;
- 6) have acceptable design overall dimensions.

The execution of requirements of points 2, 3, and 4 will allow successfully solving the complex problems of the increase in the vibration reliability of the blades of the last stage. The creation of a branch connection which satisfies all these requirements is quite complex, and the problem is to find an acceptable compromise solution. In the designing of branch connections the bases are requirements of rigidity, overall dimensionality, and, being determined by thermal and layout schemes, the direction of the removal of the working medium. The tendency to implement the remaining requirements sometimes creates insurmountable difficulties.

The maximally complete execution of the first requirement is the main thing, since, as a rule, at the low total flow friction of the branch connection the subsequent three are automatically executed.

Depending on the flow direction, designs with the axial, diagonal and radial exhaust relative to the rotating axis. The first two designs (Fig. 7-1) are the most simple in a design respect and consist of annular rectilinear (Fig. 7-1a) or curvilinear (Fig. 7-1b) diffusers, which ensure the symmetrical exhaust from the stage of the turbomachine. It is natural that such an organization of flow allows obtaining the highest coefficients of pressure recovery.

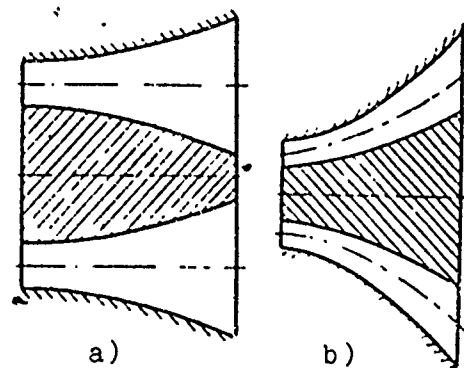


Fig. 7-1. Diagram of an exhaust duct with axial a) and diagonal b) exhaust.

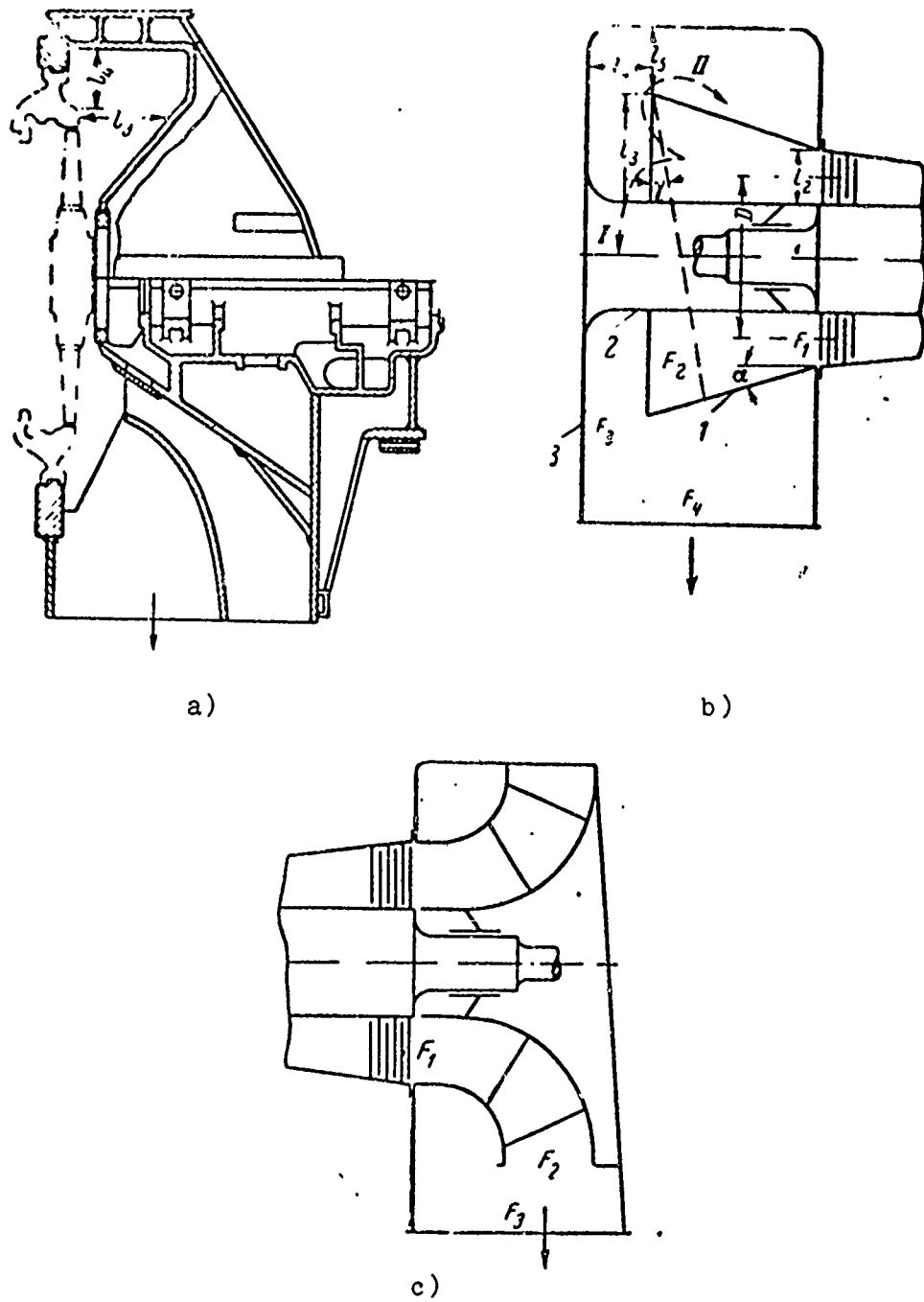


Fig. 7-2. Diagrams of exhaust ducts without a diffuser a), and with axial b) and radial c) diffusers.

The solution to the indicated problem can be achieved with the installation after the stage of the appropriate diffuser. Depending on its type, branch connections with axial (Fig. 7-2b) and radial (Fig. 7-2c) diffusers are distinguished. The first design is most frequently used for gas turbine installations, but here the axial overall dimensions of the branch connection are usually commensurable with the axial overall dimensions of the entire gas-turbine installation. Therefore, for the steam turbines having limited axial overall dimensions and the exhaust at an angle of 90° to the axis of the machine, designs with axial-radial annular diffusers are widely used. Their efficiency as compared with other types of diffusers is somewhat less, but with the correct selection of geometric parameters it is quite possible to convert to a pressure of about 60-65% of input kinetic flow energy [17, 22, 81]. The preservation of these criteria for the entire branch connection as a whole is very tempting. However, during the solution to this problem it is necessary to contend with the problem of the arrangement of flow beyond limits of the diffuser element with limited overall dimensions. It is sometimes considered that since the velocities after the diffuser are low, the flow after it can no longer lead to substantial losses. Such a point of view is erroneous, since when a symmetrical exhaust does not exist and with limited overall dimensions of the branch connection according to design considerations, the flow distribution after the diffuser proves to be extremely nonuniform. As a result there are zones where the flow again undergoes local accelerations, zones of overexpansion where there occurs its kind of sudden expansion, and zones of stable vortex motions, which sharply lower the effective output area of the branch connection.

From the outside the flow in such a branch connection reminds one of the flow in the simplest conical diffuser with high output resistance. How seriously this fact can affect the aerodynamic characteristics of the entire system as a whole can be seen in Fig. 7-3, where given are curves of the coefficients of the

recovery of energy in the conical diffuser, which operates with the output resistance in the form of grids (curves 3, 4) and without it (curves 1, 2). Characteristic are curves of the change in static pressure along the axis of this diffuser (Fig. 7-4). Actually here the whole pressure increase inside the diffuser is expended for the overcoming of the resistance of the grids.

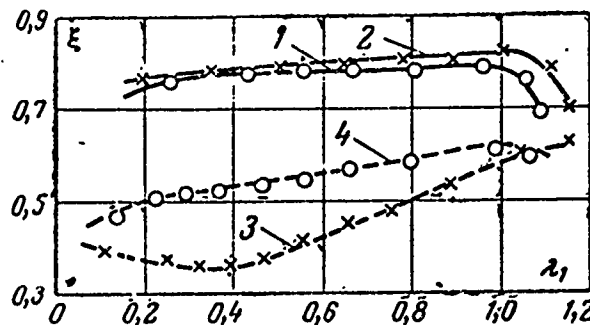


Fig. 7-3. Coefficient of recovery of energy in a conical diffuser with the output resistance and without it. 1 - $n = 3$; $\alpha = 4^\circ$; 2 - $n = 3$; $\alpha = 10^\circ$ (without resistance); 3 - $n = 3$; $\alpha = 4^\circ$, 4 - $n = 3$; $\alpha = 10^\circ$ (with resistance).

With the external similarity of the pattern in question with the flow in the exhaust ducts of the turbine a qualitative difference exists.

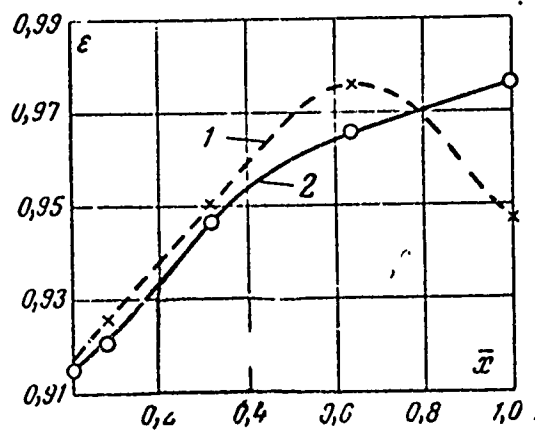


Fig. 7-4. Change in the relative static pressure along a diffuser with resistance (curve 1) and without it (curve 2) ($n = 3$; $\alpha = 4^\circ$).

In the given experiments with conical diffusers the output resistance was assigned and was determined only by geometric parameters of the output grid. In the branch connection the resistance after the diffuser has a purely aerodynamic origin and is the result of the unsuccessful arrangement of the flow.

If when structural resistance exists, after the stage of the turbomachine (for instance, the regenerator in the Gas Turbine Installation [GTU] (ГТУ) the installation of the diffuser is unconditionally justified, then in a steam turbine the total resistance of the branch connection with the diffuser and without it in a number of cases can be of one order. In fact, with the installation of a diffuser the active passage area in the assembly part of the branch connection is considerably reduced, and when the special organization of flow does not exist the increased resistance of the remaining part of the branch connection reduces the pressure increase in the diffuser itself to a zero effect.

Hence it follows that with the working out of the exhaust duct it is necessary to pay serious attention to the arrangement of flow in all its parts. A highly economical diffuser is a necessary but far from being a sufficient means of lowering the resistance of the exhaust ducts.

This conclusion was repeatedly confirmed in a number of the published works [73, 100] and is indisputable.

At the same time it is not possible to exaggerate the role of that part of the branch connection where motion from the diffuser to the outlet section (scroll of the branch connection) occurs. Sometimes for the calculation of this part a different kind of the relation of one-dimensional flow is used, and walls of the branch connection are shaped according to quite complex laws [34, 36]. Such a means can be useful for the calculation of branch connections of small turbomachines and hardly solves problems for energy turbomachines.

However, the axial and diagonal exhausts are used basically for transport and low-power stationary turbomachines. In powerful machines, according to design considerations, in most cases it is necessary to discharge the working medium at right angles to the rotating axis, using for this highly diverse design schemes.

The simplest is the design given in Fig. 7-2a, where the special organization of flow is generally absent. The air drag of the branch connection proves to be high, since in it a significant place is occupied by zones of three-dimensional separation, which are the source of the origin of vortex formations. The latter, in moving together with the flow, will narrow the effective flow passage area, induce additional velocities, and thus create the basic component of aerodynamic losses. By measuring the velocity field in the outlet section of the branch connection, it is possible to note that the area with the positive velocity component $F_{2\phi}$, as a rule, is distinguished little from the area of the outlet of flow from stage F_1 , and it sometimes proves to be even less than the latter, although geometrically area F_2 is 2-3 times more than area F_1 .

Hence naturally appears the tendency to arrange the flow in order to expand the effective output area of the branch connection, having approximated it to the geometric. The simplest solution by this means is the use of various guide vanes and ribs. Such measures usually lower the total losses by 10-20% but do not solve the problems, since they become the source of additional frictional losses, and at the best the pressure after the stage proves to be close to the pressure in the shear of the branch connection. In other words, when using guide vanes and ribs it is possible to create a branch connection the hydraulic losses of which would be covered because of the kinetic energy of flow leaving the last stage of the turbine. Problem is to partially convert this energy into the potential energy of pressure.

$h_{B.C}$ - the drop equivalent to the kinetic flow energy after the last stage, and ζ - the coefficient of the recovery of kinetic energy in the branch connection.

By estimating the relative blade eff of the turbine $\eta_{0.n}$ as the ratio of the used drop to the available, we obtain

$$\eta_{0.n} = \frac{H_t}{H_0} = \frac{H^*_t - h_{B.C}}{H'_0 - \xi h_{B.C}}$$

Hence :

$$\eta_{0.n} = \frac{\eta^*_{0.n} - \zeta_{B.C}}{1 - \xi \zeta_{B.C}} \quad (7-1)$$

In formula (7-1) $\eta^*_{0.n}$ - blade eff of flowing part with the complete use of the outlet velocity; $\zeta_{B.C} = h_{B.C}/H'_0$ - the coefficient of losses with the outlet velocity. The last value refers to the turbine and is calculated in portions of the available drop on the turbine, while the coefficient ξ and, connected with it, the total loss factor $\xi_n = 1 - \xi$ refer to the branch connection and are expressed in this case in the portions of output energy of the turbine $h_{B.C}$. Having replaced ξ by ζ_n , we obtain

$$\eta_{0.n} = \frac{\eta^*_{0.n} - \zeta_{B.C}}{1 - \zeta_{B.C}(1 - \zeta_n)} \quad (7-2)$$

Expression (7-2) allows examining the effect of the exhaust duct on the eff of the turbine at various values of coefficients ζ_n and $\zeta_{B.C}$. On Fig. 7-6 curves are plotted of the change in the eff $\eta_{0.n}$ depending on $\zeta_{B.C}$ for various values of the coefficient ζ_n when $\eta^*_{0.n} = 0.9$.

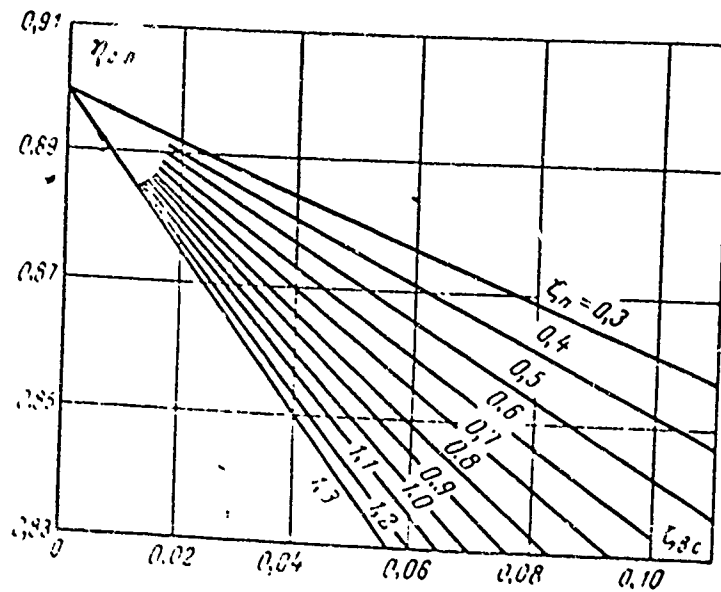


Fig. 7-6. Dependence of the relative blade eff of a turbine upon losses with the outlet velocity and on the total loss factor of the branch connection.

From curves in Fig. 7-6 it follows that with the improvement in the aerodynamic characteristics of the branch connection, a noticeable increase in the eff of the turbine takes place. Thus, for instance, by estimating the losses with the outlet speed from the turbine at 5%, we obtain with the reduction in the total loss factor of the branch connection 3 times an increase in the eff of 3.5%. This gain considerably increases with an increase in the outlet velocity and when $\zeta_{B.C} = 10\%$ comprises about 7%.

For powerful steam turbines the loss with an outlet velocity with respect to the whole available enthalpy drop varies from 1.5 to 3.0%, which allows with the reduction in the coefficient ζ_{11} of 1.3 to 0.7 increasing the eff by 1-1.5%. The absolute increase in the power of turbine installation in this case is proportion to the increase in the eff and comprises

$$\Delta N_i = N_i \frac{\Delta \eta}{\eta_{01}}$$

When $N_1 = 200-1000$ MW, $\Delta N_1 = 2.2-12$ MW.

For a representation about the order of losses with the outlet velocity in contemporary turbine installation Table 7-1 gives for different units data on the power, steam parameters and the absolute value of losses with the outlet velocity h в.с.

Table 7-1.

(1) Тип установки	(2) Мощ. по т.б. Мвт	(3) П.пар. р-н п.д.			h кал/кг	(4) Завод или фирма-изготовитель
		t_0 , °C	p_0 , ат	p_k , ат		
ВКТ-100	100	535	90	0,035	8,2	ХГТЗ
ВК-100-6	100	535	90	0,035	11,4	ЛМЗ
ПВК-150	150	565	130	0,03	9,9	ХГТЗ
ПВК-200	200	535	130	0,035	8,6	ЛМЗ
К-300-240	300	565	240	0,035	6,4	ХГТЗ
К-300-240	300	565	240	0,035	8,2	ЛМЗ
Эйвон № 8 (5)	250	593	247	0,035	22,5	Вестингауз (14)
Эддистоун № 1 (6)	325	650	352	0,035	7,7	.
Брид № 1 (7)	500	566	247	0,052	7,5	ДЖИИ
Таннерс Крик № 4 (8)	600	538	247	0,052	5,0	.
Бул Ран № 1 (9)	900	538	247	0,052	8,0	.
Кейстоун № 1, 2 (10)	900	538	258	0,066	6,5	.
Кардинал № 1, 2 (11)	615	538	247	0,035	7,0	Вестингауз (14)
Уидоус Крик № 7 (12)	500	566	170	0,052	10,5	ДЖИИ
Уил Каунти № 4 (13)	530	538	170	0,035	10,5	.

KEY: (1) Type of installation, (2) Power; (3) Steam Parameters, (4) Factory or manufacturing firm, (5) Avon No. 8, (6) Eddystone No. 1, (7) Breed No. 1; (8) Tanners Creek No. 4, (9) Bull Run No. 1, (10) Keystone No. 1, 2, (11) Cardinal No. 1, 2, (12) Widows Creek No. 7, (13) Will County No. 4, (14) Westinghouse Designations: ЛМЗ = Leningrad Metal Plant; ХГТЗ = Kar'kov gas Turbine Plant; ДЖИИ = unknown; мвт = MW; ат = at; кал/кг = cal/kg.

Thus, the working out of bran ducts can allow considerably increasing the eff of turbine at the prescribed value of outlet losses or noticeably increasing the outlet speed at an invariable level of eff. The last problem can be of interest for gas turbines of maximum power when it is necessary to provide maximum volumetric flow rate through the last stage.

Let us examine now the possibilities of the conversion of kinetic flow energy into potential energy in various diffuser elements. For this purpose Fig. 7-7 gives values of total losses depending on the M_1 number for various diffuser systems. The best prove to be conical diffusers for which ζ_n has a value of the order of 0.25-0.3, whereas for the remaining diffusers $\zeta_n = 0.35-0.6$. The given results indicate the sufficiently high efficiency of the inherent diffuser element.

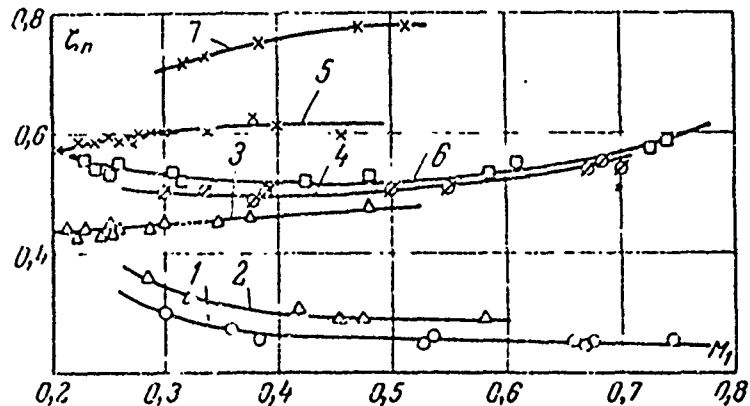


Fig. 7-7. Dependence of total losses in various diffuser systems upon the M_1 number. 1 - conical; 2 - annular; 3 - annular with radial turn; 4 - axiradial; 5 - branch connection with an obliquely cut diffuser; 6 - branch connection with a radial diffuser and guide vane at the outlet; 7 - branch connection with an axiradial diffuser.

However, in the system of the branch connection the operating conditions of the diffuser noticeably deteriorate, and the efficiency of the entire branch connection depends upon the method of the removal of the flow after the diffuser element. Thus, if the annular diffuser with radial turn has losses of the order of 50% (curve 4 in Fig. 7-7), then with its joint operation with the discharge housing of the branch connection the magnitude of losses increases to 70-80%, and with an unfavorable outline of the contours of the housing this magnitude is of the order of 100-130%.

Such a sudden increase in the losses is explained by the fact that the flow, falling into the composite housing, is very unevenly distributed over its exit section. Rather often the effective area of the exhaust $F_{2\text{э}\phi}$ (area with a positive value of the velocity) comprises a total of 50-60% of the geometric area. Furthermore, when the special arrangement of the flow does not exist, on the path from the outlet section of the diffuser to the outlet section of the branch connection are formed zones of intense vortex currents. As a result losses of the housing, which consist of internal losses and losses with outlet velocity, prove to be of the same order, and sometimes exceed losses in the inherent diffuser element. It should be noted that due to the sharp reduction in effective area, in a number of cases in the balance of the losses the basic portion is comprised of outlet losses.

In accordance with the considerations discussed above, for the improvement in branch connections one should pay great attention to the arrangement of flow in the composite housing. In this case, however, it is difficult to indicate how many general rules of the design of branch connections there are, since their shape and dimensions are closely connected with the construction of the entire installation, and their possible changes are extremely limited. As a result the branch connection of each new installation requires a prolonged and laborious working out.

In connection with that expounded at the Department of Steam and Gas Turbines of MEI (Moscow Power Engineering Institute), an attempt was undertaken to develop the branch connections having satisfactory characteristics with the simplest shape of the composite housing.

To a considerable degree the stated purpose was achieved because of the use of diffusers obliquely sheared in the direction of the exhaust. This simple change, which is that the external cone of the annular diffuser will be cut at a certain angle γ to the longitudinal axis of the machine (see Fig. 7-2b), allowed approximating the aerodynamic characteristics of the branch connection to the characteristics of the best diffusers (see § 7-3).

Curve 5 given in Fig. 7-7, obtained for the same branch connection as that of curve 7, but with the shear of the external cone at an angle $\gamma = 15^\circ$, visually indicated the noticeable reduction in losses whose magnitude is of the order of $\zeta_n = 55-60\%$, whereupon these values are preserved for different variants of the composite housings.

The skew shear of the external cone ensures an almost free outlet of flow from the diffuser directly into the outlet section of the branch connection, which expands the effective area of the exhaust. Furthermore, the flow which leaves the branch connection almost over the whole exit section creates an ejecting effect, which ensures the reduction in internal losses in the housing. Both these reasons substantially raise the efficiency of branch connections with obliquely sheared diffusers.

Since the examined way for the improvement in exhaust ducts of GTU requires in practice no changes in design of installation, it is possible not only to use it extensively in the designing of new turbines but also to use it in the modernization of the operating gas turbines.

In certain cases the overall dimensions of the installation do not allow using in the exhaust system annular diffusers with radial turn and it is necessary to replace them with more compact

axiradial diffusers. The efficiency of the latter also proves to be high if we select the optimum geometric relations. However, a large number of free geometric parameters impedes the designing of such a diffuser element.

Furthermore, with a radial diffuser it is considerably more complex to organize a one-way exhaust from the turbine with minimum losses in the exhaust duct, since the flow after the stage is turned at first 90° relative to the axis of the turbine in the radial diffuser and then in upper part makes one additional 90° turn in the transition into the housing. These two successive turns give rise to the formation of stable vortex filaments, which lower the effective area and increase the internal losses in the branch connection. As a result branch connections with axiradial diffusers rarely have losses less than 80-85%, although by means of a different location of the separating ribs inside the composite housing it succeeds in sometimes obtaining satisfactory results.

The investigations conducted at MEI showed that the efficiency of the indicated branch connections can be raised if directly in the outlet section of the radial diffuser a guide vane is installed with compressor profiles, which ensure in the left and right halves of the housing the turn of flow in the direction of the outlet section of the branch connection. The test data of the examined system represented in Fig. 7-7 by curve 6 show that also in this case it proves to be possible to obtain in the branch connection losses at a level of 50%.

Thus, according to economic data both variants of the improved exhaust ducts are approximately equal.

Besides the examined designs, for turbines of maximum power "multilayer" diffusers can be useful. The variant of the branch connection with such a diffuser is given in Fig. 7-8. The basic

feature of such a design is the replacement of the general diffuser by the system of separating annular channels, each of which is made with optimum flare angles and moderate expansion ratios.

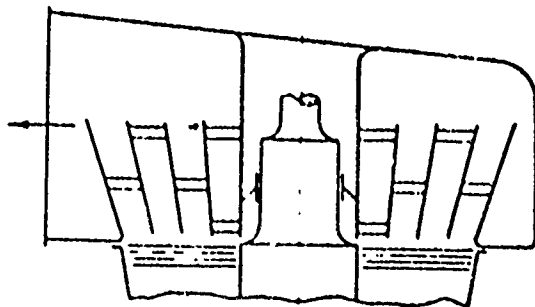


Fig. 7-8. Diagram of a branch connection with a "multilayer" diffuser.

The effectiveness of the system in question substantially depends upon the law of the change in the inlet areas F_{11} over the radius. As was shown above (see Chapter Five), the preservation of value F_{11} constant in each diffuser can lead to a substantial increase in losses with a decrease in l_2/D , since in this case the perimeter of the fairing increases while maintaining the invariable available energy. However, if with a transfer to a smaller dimension l_2/D F_1 is simultaneously increased. Thereby increasing the available kinetic energy at the inlet, it is possible to obtain rather high results at small values of l_2/D . Thus the experimental data given in Fig. 5-1 show that in this case a decrease in l/D from 0.3 to 0.15 gives a rise to an increase in losses by a total of 3-5%.

In the case of the use of "multilayer" diffusers, good results can be achieved if in each channel an approximately equal absolute inlet height l is maintained.

Returning to the question of the effect of outlet ducts on the efficiency of the turbine, let us say that the obtained

results allow raising the eff by 1-2% with a fixed value of outlet energy losses or increasing the outlet velocity with a fixed eff level.

In the latter case it appears possible to increase the gas flow through the stages of maximum dimensions by 30-40%, having raised approximately in the same ratio the power of the entire turbine.

After a brief survey of the possible designs of exhaust ducts, let us turn to the detailed examination of each design separately.

§ 7-2. Exhaust Ducts with Axial Annular Diffusers

Exhaust ducts with axial annular diffusers are most frequently used in gas-turbine installations. The typical such branch connection, given in Fig. 7-2b, consists of an annular diffuser 1, rotary shield 2 and composite housing 3.

For the maximum use of the kinetic flow energy which leaves the last stage of the turbomachine, it is necessary to provide quite definite geometric relations between the indicated elements of the branch connection. With this one should consider assigned the dimensions of the last stage, which is characterized by the dimensionless mean diameter $\theta = D/l_2$ (referred to the height of the rotor blades l_2), and the selection of remaining dimensions should be produced from the condition of minimum losses and permissible overall dimensions of the branch connection.

The solution to the stated problem today is possible only empirically, and this gives rise to the necessity for the individual development of a branch connection with a change in the dimensions of the last stage of the turbine.

Conducted at MEI was a series of tests of exhaust ducts with axial annular diffusers at various distances between shield and the diffuser and different values of θ , which allowed explaining the role of this parameter and establishing the effect of the rotary shield on the magnitude of losses with the fixed simplest construction of the housing 3 [28].

Table 7-2 gives the range of the changes in geometric parameters of the tested branch connections, which encompasses the majority of the real dimensions which are encountered in gas-turbine construction. This range is so close to the natural range of the mode parameters M_1 and Re_1 .

Table 7-2

D/l_2	i_2/l_2	L/l_2	M_1	Re_1	n
4	1-7	4,7-8	0,15-0,6	$(0,5 \div 3) \cdot 10^5$	2,22
6	1-6	6,7	0,15-0,4	$(0,5 \div 2) \cdot 10^5$	2,21
8	1-6	6,7	0,15-0,3	$(0,5 \div 1,5) \cdot 10^5$	2,20
10	1-6	6,7	0,15-0,5	$(0,5 \div 1,0) \cdot 10^5$	2,15

When evaluating the efficiency of one or another system the total loss factor ζ_n , calculated with respect to the kinetic energy at the inlet into the branch connection was used.

Since the efficiency of the branch connection is determined to a considerable degree by the diffuser element, let us begin examination from characteristics of the annular diffusers used.

According to Table 7-2 the diffusers had an approximately equal expansion ratio, equal to ~ 2.2 , and an equal relative length of $\bar{L} = 6.7$, which corresponds to the angle $\alpha_{\text{ЭKB}} = 7-8^\circ$.

The accepted dimensions are close to the optimum but should ensure the coefficient of recovery of pressure at a level of 75-60% (the total losses in this case will be $\zeta_n = 25-40\%$).

However, with the installation of the turning shield losses in the diffusers are changed and depend upon the distance between the outlet section and the shield l_4 . The nature of this dependence can be judged by the curves in Fig. 7-9a, where is presented the change in total losses depending on the relative distance \bar{l}_4 for different values of θ .

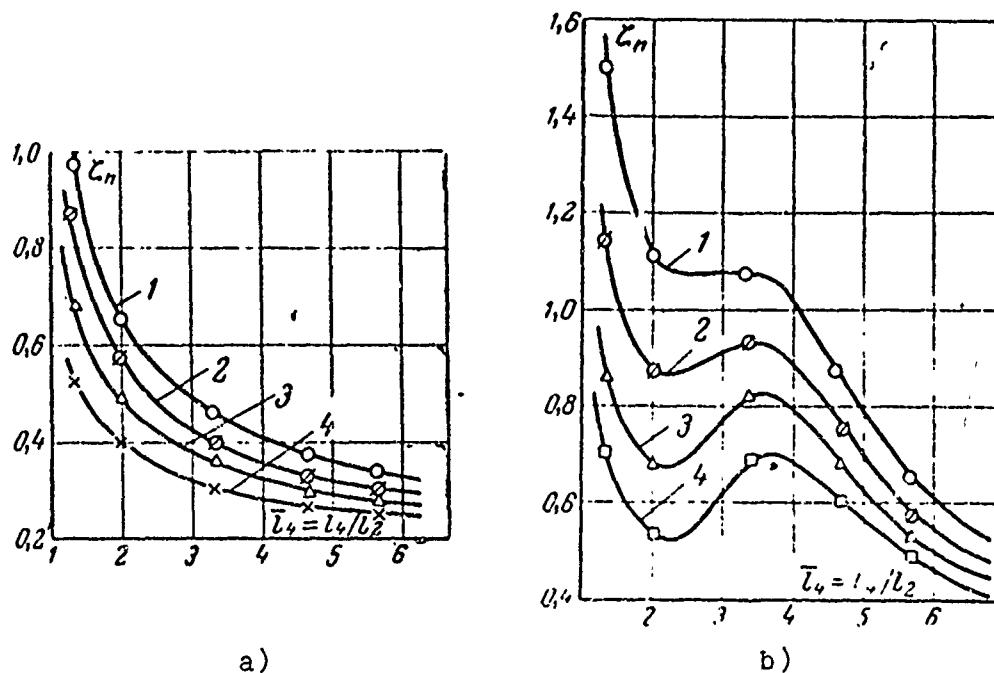


Fig. 7-9. Variation in the total loss factor ζ_n depending on \bar{l}_4 and $e = D/l_2$ for annular diffusers with a shield a) for branch connections b). 1 - $\theta = 10$; 2 - $\theta = 8$; 3 - $\theta = 6$; 4 - $\theta = 4$.

As one would expect, with a decrease in distance \bar{l}_4 irrespective of D/l_2 a continuous increase in the losses occurred, since for nondetached conical and annular diffusers the installation

of the shield should give rise to additional losses connected with the turn of the flow. The magnitude of these additional losses continuously increases with the approach of the shield to the diffuser, and at small values of \bar{l}_4 , when the circular area F_3 becomes commensurable with the area F_2 (see Fig. 7-2b), a sharp increase in not only internal but also outlet losses should take place. As a result at small values of \bar{l}_4 it is possible to note an intense increase in the total losses.

The indicated dependence can be different if we use short annular diffusers with a large expansion ratio, for which, as is known [54], the zone of optimum values \bar{l}_4 exists. However, even in this zone the minimum value of losses in such systems proves to be high. Certain data, which estimates the effect of the relative length \bar{L} , will be given below, and let us now examine the operation of nondetached diffusers together with a housing.

Results of the tests given in Fig. 7-9b indicate that the installation of the housing substantially changes the nature of the dependence of losses upon the nondimensional distance \bar{l}_4 . First with the approach of the shield the losses increase and more intensely than without a housing. Then when $\bar{l}_4 = 3.3$ the coefficient ζ_n reaches a maximum value and a further decrease in \bar{l}_4 leads for small values D/l_2 almost to a critical reduction in the losses (curves 3, 4), and for large D/l_2 the losses are maintained constant (curve 1). For all the tested branch connections the zone of minimum losses corresponds approximately to the identical value \bar{l}_4 equal to 2.2.

When $\bar{l}_4 < 2.2$ losses begin again to intensely increase and the effect of the housing is decreased. The degree of this effect in the whole range of distances \bar{l}_4 can be judged by the curves in Fig. 7-10, where has been given the differences between losses in the branch connection and its diffuser system with a different location of the turning shield.

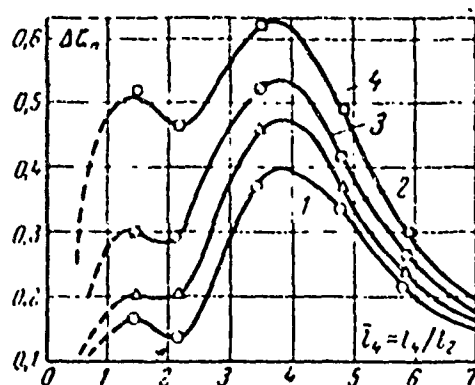


Fig. 7-10. Effect of the presence of a housing on losses in the branch connection.
 1 - $\theta = 4$; 2 - $\theta = 6$; 3 - $\theta = 8$;
 4 - $\theta = 10$.

As a whole the effect of the housing proves to be very important but not monotonic. With the approach of the shield to the diffuser the portion of the losses in the housing increases, reaching at $\bar{\tau}_4 = 3.8$ a peak value equal to 40% for $\theta = 4$ and 62% for $\theta = 10$. Then $\Delta\zeta_n$ falls and comprises at $\bar{\tau}_4 = 1.8-2.0$ for the same values of θ , respectively, 12 and 47%. A further decrease in $\bar{\tau}_4$ gives rise to a certain increase in $\Delta\zeta_n$, and then the effect of the housing again begins to be reduced.

The obtained dependence has an important practical value. Thus, if the distance $\bar{\tau}_4$ in the branch connection is selected in the zone of maximum values $\Delta\zeta_n$ by means of treatment of the composite shell, it is possible to attain a substantial reduction in the losses. However, in most cases such means gives rise to an increase in the overall radial dimensions of the machine. At the same time from the curves it follows that the improvement in the aerodynamic characteristics of the branch connection can be achieved by the simple decrease in axial distance $\bar{\tau}_4$. This means is especially effective for small relative diameters, but when $\theta = 10$ the advisability of the transfer from $\bar{\tau}_4 = 3.0-3.5$ to $\bar{\tau}_4 = 2.0-2.5$ is obvious, since it gives rise to the decrease in the overall axial dimensions without an increase in the total losses.

If in the initial branch connection $\bar{l}_4 = 2$, then at small \bar{l}_4 the treatment of the shell proves to be practically aimless: in this case the basic portion of the losses are in the diffuser system, and the portion of losses in the housing comprises an insignificant magnitude.

The examined effect of the housing is connected with the specific features of the flow in branch connections with a one-way exhaust.

In fact, at large distances \bar{l}_4 the flow from the upper part of the branch connection is able comparatively easily to turn to the side of the outlet section, considerably disturbing the symmetry of the flow. With the approach of the shield to the diffuser the asymmetry of the flow substantially increases, which gives rise to a noticeable increase in the resistance of the branch connection. However, thus far resistance on path I (see Fig. 7-2b) is less than the resistance being exerted by the clearance l_5 on path II, and the main flow from the upper part of the branch connection is superimposed on the flow in its lower half and moves not along possible path II but along the path I, substantially deteriorating the outlet conditions.

With the equality of the resistances in question the losses reach an extreme value. This mode is characterized by the erratic operation of the branch connection, since now the exhaust from upper half can occur both on path I and path II. The transition to such a mode is accompanied by standard noise of variable intensity and is clearly recorded.

A noted fact should be kept in mind, since the unstable mode is accompanied not only by a noise effect but also leads to the fluctuation of pressure at the inlet into the branch connection, which can have very serious consequences from the point of view of the strength of the blades of the last stage of the turbomachine.

A further displacement of the shield to the outlet section of the diffuser ensures the removal of flow from the upper part of the branch connection along path II, the resistance of which proves to be less than the resistance of path I. As a result the effective area of the branch connection at the outlet (area with a positive value of the flow rate component) noticeably increases and the conditions of the removal of flow from the lower part improve, since now on path I a smaller part of the working medium is discharged.

The indicated reasons causes a reduction in the total losses whose magnitude approaches losses in the free diffuser system. This reduction occurs until area F_3 in magnitude is of the same order as that of area F_2 . From this time on, the decrease in dimension \bar{l}_4 gives rise to a sharp increase in losses induced by the reduction in the expansion ratio of the diffuser system of the branch connection. In these modes the effect of the housing is again decreased.

For the clarification of the role of relative diameter $\theta = D/l_2$, let us examine the dependence of losses at a constant distance \bar{l}_4 upon this parameter. The curves given in Fig. 7-11a for the diffuser system and in Fig. 7-11b for the entire branch connection as a whole indicate that the effect of this parameter is noticeable even for the free annular diffuser. Thus, the change in θ from 4 to 10 gives rise to an increase in losses of 5% (curve 1 in Fig. 7-11a). With the installation of the turning shield this increase is 15-33% (curves 2 and 3), and in the branch connection it reaches 55% (curve 1 in Fig. 7-11b) and depends upon the distance \bar{l}_4 , decreasing with its increase. In this case the effect of the housing is simultaneously decreased.

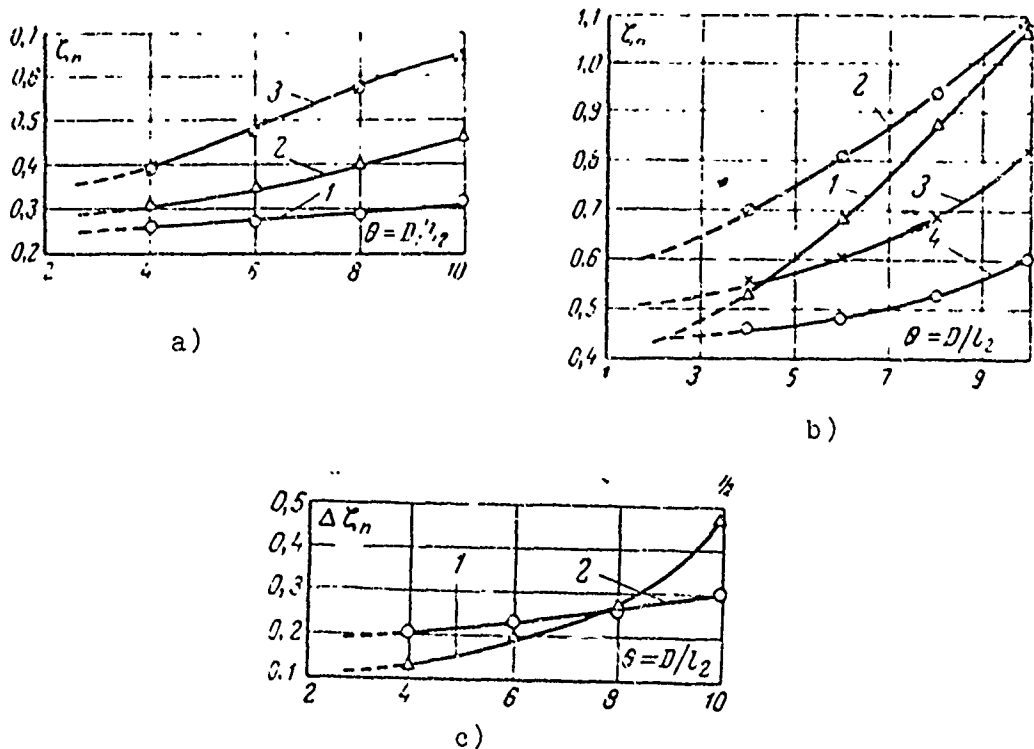


Fig. 7-11. Effect of the dimensionless input diameter $\theta = D/l_2$ on coefficient ζ_n . a) diffusers: 1 - $\bar{\tau}_4 = \infty$; 2 - $\bar{\tau}_4 = 3.3$; 3 - $\bar{\tau}_4 = 2$; b) branch connection; 1 - $\bar{\tau}_4 = 2.2$; 2 - $\bar{\tau}_4 = 3.3$; 3 - $\bar{\tau}_4 = 5.0$; 4 - $\bar{\tau}_4 = 6.0$; c) 1 - $\bar{\tau}_4 = 2.0$; 2 - $\bar{\tau}_4 = 5.7$.

Thus, if in the zone of optimum values $\bar{\tau}_4$ an increase in θ from 4 to 10 gives rise to an increase in losses in the housing of 35% (curve 1 in Fig. 7-11c), then for $\bar{\tau}_4 = 5.7$ this increase is 9-10% (curve 2).

Such a great effect of the parameter θ is connected with the fact that its increase leads as a rule, to an increase in the total surface streamlined by the flow and, therefore, to an increase in frictional losses. In the free diffuser, as was already noted, frictional losses increase by 5% (see curve 1 in Fig. 7-11a and Fig. 5-1).

With the installation of a shield losses for large θ increase even more intensely, since now on the internal generatrix of the diffuser the boundary layer development occurs with an increased positive pressure gradient, and with the approach of the shield the possibility of separation of the layer becomes more probable.

The separation flow pattern is indicated by the obtained level of losses at large θ . It is natural that in this case the conditions of the flow in the composite housing, i.e., its negative effect becomes more noticeable.

The tests conducted clearly showed that the optimum designs of the exhaust ducts are determined by dimensions of that stage behind which they are installed.

At small θ and optimum geometry of the diffuser it proves to be possible to obtain a high coefficient of the recovery of pressure at limited axial and radial overall dimensions of the branch connection; in this case the following ratios between the areas are maintained: $F_1:F_2:F_3:F_4 = 1:2.6:3.5:4.0$.

With an increase in θ the reduction in losses in the branch connection can be achieved basically because of the treatment of the composite housing and increase in the axial overall dimensions or by the method indicated in [100].

By examining the design of the branch connection with an annular diffuser, it is easy to note that dimension \bar{l}_4 can be changed not only by means of the movement of shield 2 but also owing to the use of shorter diffusers, especially when a shield exists, according to [54], sufficiently high coefficients of the recovery of pressure in short diffusers are ensured. For the clarification of this question in the system of the branch connection three diffusers with different relative lengths were tested. The test data are given in Fig. 7-12. Diffuser systems

tested without a housing at almost all distances of the shield were equivalent (curves 4, 5, 6), and their tests together with the shell showed that the short diffusers ($L/l_2 = 4.7$) are noticeably worse than the long ones ($\bar{L} = 8$).

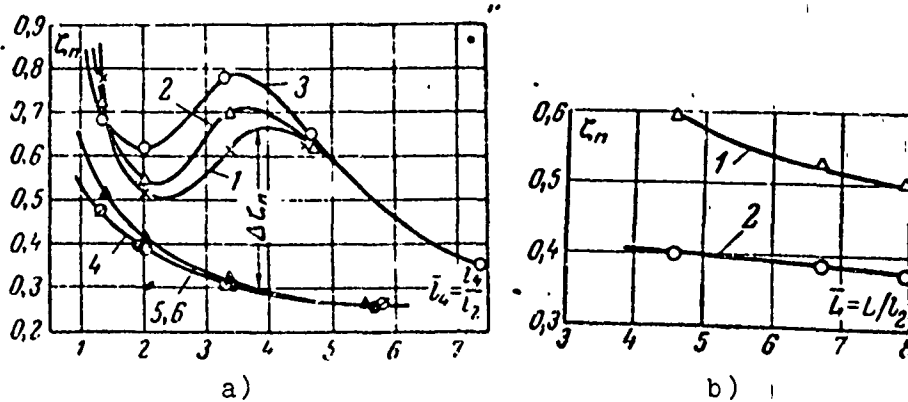


Fig. 7-12. Effect of the relative length of the diffuser L/l_2 on losses in the diffuser and branch connection ($\theta = 4$).

$$\begin{array}{l}
 a: \left. \begin{array}{l} 1 - \bar{L} = 8.0; \\ 2 - \bar{L} = 6.7; \\ 3 - \bar{L} = 4.7 \end{array} \right\} \text{ losses in branch connection;} \\
 \left. \begin{array}{l} 4 - \bar{L} = 8.0; \\ 5 - \bar{L} = 6.7; \\ 6 - \bar{L} = 4.7 \end{array} \right\} \text{ diffuser losses;}
 \end{array}$$

b) $\bar{l}_4 = 2.2$; 1 - losses in the branch connection; 2 - diffuser losses.

Over a wide range of values \bar{l}_4 the change in losses comprises 10-15%. Such a behavior of the curves is connected with the unsymmetric flow pattern noted above in the branch connection with one-way exhaust. The asymmetry of the exhaust noticeably disturbs the flow in the diffuser, and this disturbance is greater the less the length of the diffuser.

It is natural therefore that the installation of the housing causes a more intense increase in losses in a short diffuser (curve 3) than in a long one (curve 1), and only at the very close location of the shield ($\bar{z}_4 < 2$), when the effect of the external asymmetry is small, and the expansion ratio of the diffuser system begins to decrease, do losses in the long diffuser due to an increase in the streamlined surface prove to be great.

Here one should especially emphasize that the tendency to move the shield away from the diffuser by means of a decrease in the length in its generatrix can lead not to a decrease in losses but to their great increase (up to 25% at small θ), if the initial distance \bar{z}_4 is located in the zone of optimum values. Thus, a decrease in dimension \bar{z}_4 because of the length of the diffuser is inexpedient if, of course, this decrease is not dictated by the necessity of a reduction in the axial overall dimensions of the machine. In the latter case an increase in angle α up to 15-18° is admissible while maintaining the invariable expansion ratio of the diffuser.

The conducted analysis of the effect of the basic geometric parameters on the efficiency of the exhaust ducts refers to the fixed number $M_1 = 0.30$ (in practice an incompressible fluid). The effect of this mode parameter on the operation of the diffusers in question and branch connections can be observed on Fig. 7-13; where curves of the change in coefficients ζ_n for branch connections with different D/l_2 depending on M_1 are given.

It is possible to note that in all cases with a speed gain a certain increase in losses occurs. This is connected with the fact that in this case with an increase in M_1 numbers an increase in the positive pressure gradient and an increase in the available separation zones occurs.

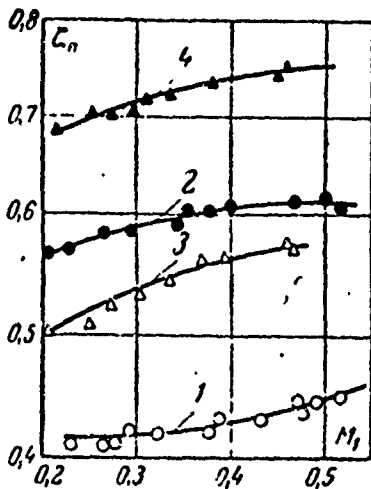


Fig. 7-13. Change in diffuser losses and branch connections depending on M_1 number.

$$\begin{array}{l}
 1-\theta = 4; \\
 3-\theta = 6 \\
 2-\theta = 4 \\
 4-\theta = 6
 \end{array}
 \left. \begin{array}{l}
 \\
 \\
 \\
 \end{array} \right\} \bar{T}_1 = 2 \text{ (diffuser);}$$

$$\left. \begin{array}{l}
 \\
 \\
 \\
 \end{array} \right\} \bar{T}_1 = 2 \text{ (branch connections).}$$

Since in gas-turbine installations the M_1 number does not exceed 0.3-0.5, it is possible to consider that the relations obtained above between the geometrical dimensions of exhaust ducts with annular diffusers can be without great error assumed the basis for their design. It should be noted that in the exhaust systems in question with limited axial and radial overall dimensions, the negative role of the composite housing is very significant and the average level of losses in the branch connection comprises a magnitude of the order of 65-80%. In connection with this the creation of a diffuser system which adequately operates with simplest form of the composite housing is advisable. As was already mentioned above, good results in the solution to such a problem can be obtained as a result of the use of obliquely cut diffusers in the direction of the outlet.

§ 7-3. Exhaust Ducts with Obliquely Cut Diffusers

The text data of exhaust ducts examined in the previous section with annular diffusers showed that the losses in them substantially depend upon the correct correlation between the basic geometrical dimensions. On the basis of the data given

above, such dimensions can be considered as the relative diameter at the inlet $\theta = D/l_2$ and relative distances $\bar{l}_5 = l_5/l_2$ and $\bar{l}_4 = l_4/l_2$ ¹ (see Fig. 7-2b).

For the given value of θ and the fixed value of \bar{l}_5 the decrease in the dimension of \bar{l}_4 causes an intense increase in the losses. However, in a certain zone this increase is slowed down, and for small θ it is possible to indicate the region in which losses with the approach of the shield to the outlet section of the diffuser do not increase, but decrease.

The dependence given in Fig. 7-9b is very characteristic for exhaust ducts with annular diffusers and clearly shows the effect of the housing in various positions of the turning shield.

The negative effect of the housing can be decreased if the axial (\bar{l}_4) or radial (\bar{l}_5) dimension is greatly increased. The first means is usually unacceptable for design considerations, because for satisfactory results it is necessary to have $\bar{l}_4 < 6$, i.e., one should sharply increase the overall axial dimensions of the machine.

A second means is used considerably more frequently [73], whereupon the obtained gain substantially depends upon the magnitude of the relative diameter θ and dimension \bar{l}_4 .

¹Instead of the linear ratios it is more correct to use the area ratios F_4/F_1 and F_3/F_1 . However, since the experimental data are obtained for the branch connection with the housing, in which along the circumference the dimension l_5 remained constant, in the examination of obliquely cut diffusers we will use ratios of linear dimensions.

According to the experimental data obtained at MEI, an increase in the radial dimension gives a maximum reduction in the losses when $\bar{r}_4 = 3-3.5$ and a minimum result when $\bar{r}_4 = 2.2$, and the difference between these values is continuously reduced with an increase in θ .

Test data of the branch connections at different values of \bar{r}_5 are given in Fig. 7-14.

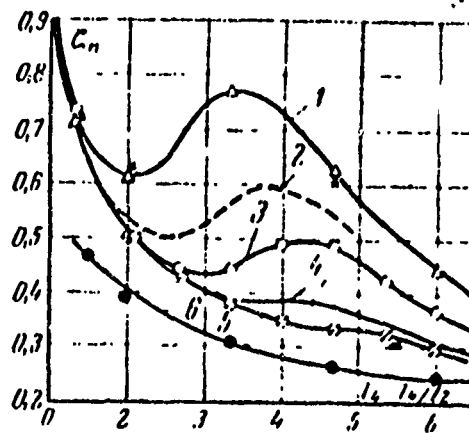


Fig. 7-14. Effect of radial dimension \bar{r}_5 on the efficiency of exhaust ducts. 1 - $\bar{r}_5 = 1.0$; 2 - $\bar{r}_5 = 1.5$; 3 - $\bar{r}_5 = 2.0$; 4 - $\bar{r}_5 = 3.0$; 5 - $\bar{r}_5 = 4.0$; 6 - $\bar{r}_5 = \infty$ ($\theta = 4$).

Thus, for the symmetrical annular diffuser and one-way outlet the reduction in losses to a certain degree is connected with an increase in the overall dimensions of the branch connection and frequently requires a complex shaping of the composite housing. At the same time, by rejecting the symmetrical diffuser, it is possible to obtain a noticeable reduction in the losses, having kept the remaining elements of the branch connection fixed. In this direction the use of obliquely cut annular diffusers in the direction of the exhaust was quite effective [29]. The diagram of the branch connection given in Fig. 7-2b remains essentially without any changes, and the plane of the output

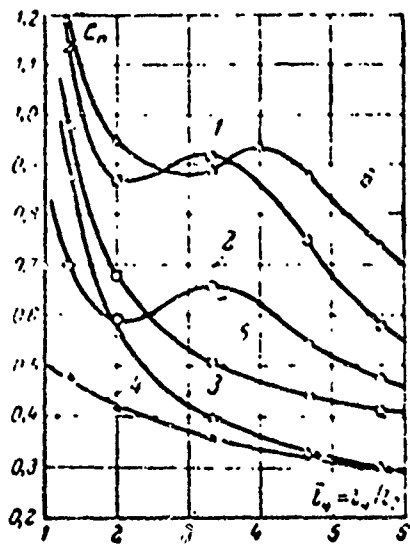
of flow from the diffuser is arranged by means of the shear of external cone at angle γ to the vertical plane.

It is interesting to note that the indicated unsymmetric diffuser during operation with a shield gives with close location of the latter a noticeable reduction in losses. The aforesaid is clearly confirmed by the test data given in Fig. 7-15a. If for the symmetrical diffuser (curve 3) the reduction in the dimension of \bar{l}_4 from 6 to 1.3 caused an increase in losses of 60%, then when a shear exists, the same change increased the losses at a total of 18% (curve 4). Approximately to the same degree losses in obliquely cut diffusers and at other values of θ increase.

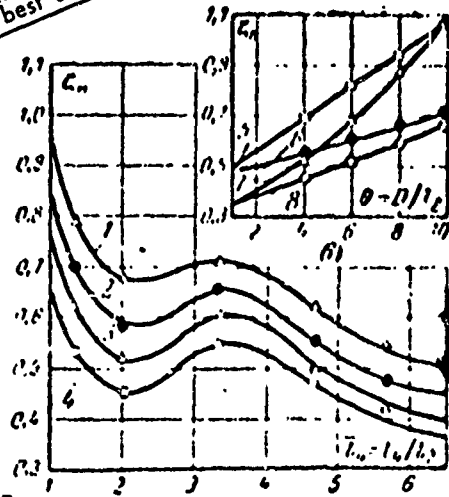
Curve 2 given in Fig. 7-15a shows that with the introduction of an oblique shear losses in the branch connection were decreased in practically the whole range of values \bar{l}_4 . Moreover, when $\bar{l}_4 = 1.3$ the effectiveness of the branch connection with a diffuser having a skew shear was higher than in the branch connection with a symmetrical diffuser by almost 15%. Therefore, there is the real possibility of using the kinetic energy of flow which leaves the last stage of the turbine without an increase in the overall dimensions of exhaust duct.

Representation about the magnitude of losses in the indicated systems can be obtained from Fig. 7-15b and c, where coefficients ζ_{Π} are given for four branch connections with obliquely cut diffusers which differ by parameter θ . As a whole all the curves are arranged almost equidistantly, although the level of losses, just as for the insulated diffusers, proves to be higher with an increase in θ .

Reproduced from
best available copy.



a)



b)

Fig. 7-15. The change in total losses in branch connections and diffusers depending on the relative distance \bar{l}_4 . a)
 1 - branch connection with an annular diffuser ($\theta = 8$; $n = 2.4$);
 2 - branch connection with an annular obliquely cut diffuser ($\theta = 8$); 3 - annular diffuser ($\theta = 8$; $n = 2.4$); 4 - annular obliquely cut diffuser ($\theta = 8$); 5 - shortened diffuser ($\theta = 8$; $n = 1.7$); 6 - branch connection with the shortened diffuser;

b) $\theta = 10$;
 $n = 8$;
 $\theta = 6$;
 $n = 1$ } branch connections with obliquely cut diffusers:

c) $\bar{l}_4 = 3.3$;
 $\bar{l}_4 = 2.2$ } branch connections with annular diffusers without section.

$\bar{l}_4 = 1.3$;
 $\bar{l}_4 = 1.2$ } branch connections with obliquely cut diffusers.

One should emphasize, however, that the introduction of shear noticeably lowers the intensity of the increase in losses in the branch connection with an increase in θ . If for the normal system (see Fig. 7-11b) an increase in θ from 4 to 10 gives rise to an increase in losses from 70 to 108% when $\bar{l}_4 = 3.3$ (curve 2) and from 52 to 105% when $\bar{l}_4 = 2.2$ (curve 1), then in the branch connection with an obliquely cut diffuser (Fig. 7-15c) the same increase in θ causes an increase in losses from 55 to 70% for $\bar{l}_4 = 3.3$ (curve 6) and from 45 to 68% for $\bar{l}_4 = 2.2$ (curve 8).

Thus, the branch connection ensures the use of 30 to 55% of the input kinetic flow energy, and the effect of the shape of the composite housing proves to be insignificant.

The absolute reduction in losses in branch connections with obliquely cut diffusers $\Delta\zeta_{\Pi} = \zeta_{\Pi} - \zeta_{\Pi.c}$, where ζ_{Π} - total losses in the initial variant and $\zeta_{\Pi.c}$ - in the examined variant with shear (Fig. 7-16), proves to be more substantial than in intrinsic diffuser systems.

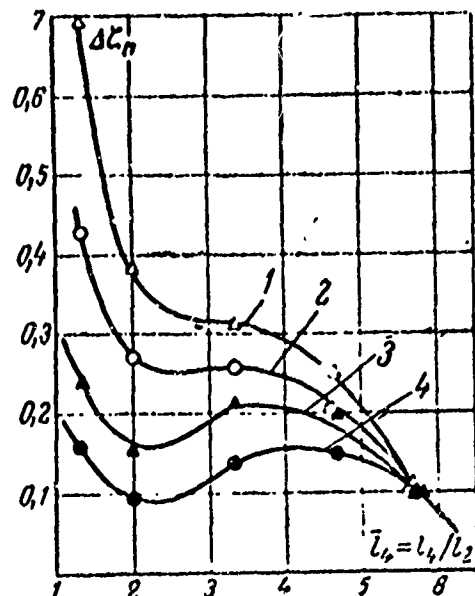


Fig. 7-16. Absolute reduction in losses in branch connections in the transition to obliquely cut diffusers. 1 - $\theta = 10$; 2 - $\theta = 8$; 3 - $\theta = 6$; 4 - $\theta = 4$.

Thus, if the use of an oblique shear in a diffuser with a turning shield at $\theta = 10$ increases its effectiveness by 20% at $\bar{r}_4 = 2$, then in the system of branch connection the losses at $\theta = 10$ and $\bar{r}_4 = 2$ are lowered by 38% (curve 1 in Fig. 7-16). These data indicate the fact that the effectiveness of the branch connection with an obliquely cut diffuser increases not only because of the improvement in operation of the diffuser but also owing to the more rational arrangement of flow in the composite housing.

In the usual scheme the flow coming out of the diffuser at a distant location of the shield turns directly into the direction of the outlet section not only in the lower but also from the upper half of the diffuser, moving along path I (see Fig. 7-2b). With the approach of the shield the resistance for this part of flow continuously increases, and the flow from the upper half of the diffuser begins to flow not only along the path I, but also along path II. It is natural that the larger the dimension \bar{r}_5 , i.e., the further composite housing is arranged, the less resistance the flow in path II undergoes, and, therefore, the less intensely losses with the approach of the shield increase.

The comparison of the total losses ζ_{Π} , obtained in the branch connection with increased dimension \bar{r}_5 (see Fig. 7-14), and curves 1 and 2 in Fig. 7-15a shows that in this case the nature of the change in the losses proves to be approximately the same as that for the branch connection with an oblique shear. In other words, the flow in the composite housing with an obliquely cut diffuser and with increased radial dimension \bar{r}_5 from a qualitative side proves to be identical.

In fact, with the introduction of an oblique shear the flow after the diffuser in the lower part fills the greater part of the passage discharge area of the branch connection, sharply

increasing the area with a positive flow component. As a result, together with the reduction in resistance for the flow coming out of the upper part of the diffuser on path I, resistance on path II is noticeably reduced; since with an increase in the degree of filling of the outlet section the ejecting effect of the flow which leaves branch connection increases.

With the approach of the shield the air drag in path II for flows in the upper part of the diffuser first approaches the resistance on path I, and then it becomes less than the latter. The indicated redistribution of resistance explains, especially, the certain reduction in the losses in Fig. 7-15b at $\bar{L}_4 = 2-3$.

By estimating the role of the oblique shear, it is advantageous to examine the operation of the branch connection with a shortened diffuser, since in this case, while maintaining the external overall dimensions distances \bar{L}_4 and \bar{L}_5 noticeably increase, which on the whole lowers the air drag of the subsequent channel. Test data is given in Fig. 7-15a, where curve 5 refers to the shortened diffuser and curve 6 - to the corresponding branch connection.

As a whole the conducted change did not give positive results, because simultaneously with an increase in distance \bar{L}_4 there occurred the displacement of the extreme value of losses to the side of large values of \bar{L}_4 , which was caused by the decrease in the resistance in the upper part of the branch connection due to an increase in the dimension \bar{L}_5 .

Furthermore, the straight shear of the diffuser decreased its expansion ratio from 2.2 to 1.7. As a result the output losses were increased by 12%, and the total losses were respectively increased (curve 5). In this case, naturally,

a portion of the losses in the composite housing was increased, since at smaller expansion ratio of the diffuser the flow after it occurred with higher rates.

Thus, from a comparison of the shortened diffuser with an oblique shear the obvious advantage of the latter follows.

The results examined above were obtained at the fixed value of the angle of shear $\gamma = 18^\circ$. It is possible to expect that the magnitude of the angle should have an optimum value, since with an increase in γ , on the one hand, the conditions of flow after the diffuser are improved, and, on the other hand, the expansion ratio of the diffuser is lowered, and in the limit from the lower it is possible to shear completely the conical surface.

A study of the effect of angle γ confirms the inferred well. Figure 7-17 gives the relative decrease in losses in the three branch connections with an increase in the angle of shear γ . The tested branch connections in the initial variant were distinguished only by the expansion ratio of the diffuser at constant length. Therefore, in this case the change in the expansion ratio was accomplished by a change in angle α (see Fig. 7-2b). The qualitative nature of the obtained curves was approximately equal for all branch connections. First with an increase in angle γ a reduction in losses occurred; with angle γ of the order of $18-22^\circ$ the losses reached a minimum value, and with a further increase in the angle of shear they increased.

However, the quantitatively effect of angle γ was different for different diffusers. With a large expansion ratio ($n = 2.8$) the diffuser cut at an optimum angle γ led to a decrease in

losses of 10% (curve 1), whereas when $n = 2$ (curve 3) a similar shear improved the efficiency up to 20%. This distinction is explained by the fact that for the large value of n the velocity in the outlet section of the diffuser is small, and the improvement in outlet conditions of flow affects the total losses to a lesser degree than with moderate values of the expansion ratio.

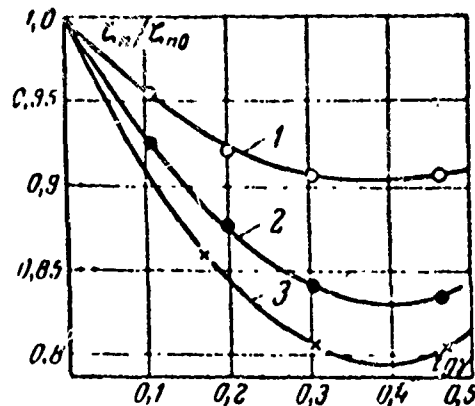


Fig. 7-17. Effect of the angle of the shear of the diffuser γ on the relative reduction in losses. 1 - $n = 2.8$; 2 - $n = 2.4$; 3 - $n = 2$.

Let us note that at the small relative lengths of the external cone ($L/D_1 < 1.0$, where D_1 - diameter at the inlet) the shear of the diffuser at an optimum angle cannot be accomplished, because in the lower part the shear plane emerges beyond the limits of the diffuser. In this case it is necessary to decrease the shear angle γ in such a way that the shear plane intersects the lower generatrix on half of the initial length L .

The indicated limitation enters into force if

$$L/D_1 < 0,8\sqrt{n_1},$$

where n_1 - the expansion ratio of the external cone which forms the annular diffuser.

Otherwise the fulfillment of obliquely cut diffusers with optimum angles of shear equal to 15-20° does not create special difficulties.

The examined results have a practical importance, since they allow obtaining the acceptable values of coefficients of pressure recovery at limited overall dimensions and simple configuration of the branch connection and allow comparatively simply reconstructing the exhaust ducts of the operating installations, the air drag of which exceeds the dynamic head of the flow at the outlet from the last stage. The obtained values of the total loss factor for branch connections with obliquely cut diffusers show that with such reconstruction it is quite realistic to increase the absolute value of the eff of the turbine by 0.5-1%. As a result the increase in the efficiency of entire gas-turbine installation will be 1.5-2%.

Further from the obtained results there ensure quite specific ways for improvement in the branch connections, and these ways considerably depend upon the type of the stage after which the branch connection is installed.

For small values of θ good results can be achieved with the correct selection of the combination of the obliquely cut diffuser and distance \bar{l}_4 , the optimum value of which comprises on the basis of tests of a considerable series of branch connections $\bar{l}_{4opt} = 2.2$. With an increase in θ , as was already mentioned above, losses in branch connections increase even at optimum values of \bar{l}_4 and obliquely cut diffusers (see Fig. 7-15c). Therefore, here one should focus great attention on the design of a composite housing, increasing, especially, the dimension \bar{l}_5 .

Let us note that since for large value θ the mean level of losses is 60-70%, it is advantageous, apparently, in this

case to turn from axial diffusers to axiradial. Losses in the latter have approximately the same order, but the overall axial dimensions are substantially less. Furthermore, by using special circular grids, here it is possible to attain good results, having lowered the losses down to 50% [30].

§ 7-4. Exhaust Ducts with Radial Diffusers

Exhaust ducts with radial diffusers are widely used in steam turbines. However, with an increase in the power and dimensions of the last stage the difficulties connected with the selection of optimum contours of the radial diffuser substantially increase. At the same time a sharp increase in recent years of unitary powerful steam turbines with limited dimensions of the last stage led to a perceptible increase in the outlet losses. In absolute values these losses for machines of types VK-150, PVK-200 and K-300 comprise 6-10 kcal/kg (see Table 7-1). It is natural that the recovery of even a small part of this energy would lead to a noticeable increase in the efficiency of the entire installation.

However, an increase in the power of the turbines is accompanied by considerable changes in the design of exhaust ducts. In the majority taken as the basis is the branch connection of the turbine VK-100 [LMZ] (ЛМЗ) Leningrad Metal Plant (Fig. 7-2a), despite the fact that according to results of aerodynamic tests the coefficient of losses of the indicated branch connection ζ_{Π} , depending on the design features and mode of operation, varies within limits of 1.2-1.6. Thus, in this case for the overcoming of air drag of the branch connection all the kinetic energy of flow which leaves the last stage of the turbine is expended in the best variant. The reason for such high losses consists in the absence of the general diffuser element in which the recovery of pressure could take place. At the same time an analysis of the change in the flow passage cross-sectional area shows that on the path of steam flow there are many local diffuser sections the nondetached flow in which is practically impossible. Furthermore, the geometric area sharply increases at the inlet into the branch connection, and

then is decreased to the outlet section.

The indicated shortcomings were to a considerable extent eliminated in the branch connection of the turbine PVK-200 (LMZ), where by means of a certain increase in the transverse overall dimensions of the branch connection, by the introduction of smooth contours and by means of the creation of the nonsymmetric radial diffuser with the subsequent direction of the flow along the defined channels bounded by curvilinear ribs, it was possible to obtain in the effective range of velocities the coefficient ζ_n , equal to 0.84-0.9 [100].

Similar changes were introduced into the branch connection of the turbine T-50 [STMZ] (CTM3) Stalinsk Metal Plant [47]. A diagram of this branch connection is given in Fig. 7-18. The indicated branch connection was tested in detail in MEI, whereupon the tests were conducted both in air and steam. Since data on steam tests is small, and the results obtained during these tests represent a definite interest, we will discuss them in more detail.

In the air tests the common scheme described in [44] was used. Steam tests were conducted on an installation whose diagram is given in Fig. 7-19.

The tested branch connection 1 was fastened to the steam box 2 of the experimental turbine, from which the rotor was removed. Thus, the whole system of the feed and removal of steam to the branch connection proved to be inside the turbine casing 3, which ensured the sufficient density of the entire system and the most simple method of the removal of steam to the condenser 4.

To maintain the assigned counterpressure to the installation a three-stage ejector 5 was connected, which allowed changing

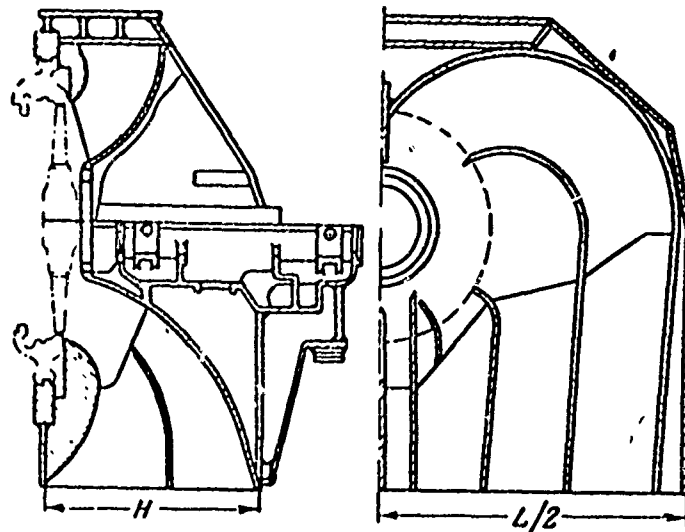


Fig. 7-18. Diagram of an improved branch connection of the turbine T-50 (STMZ).

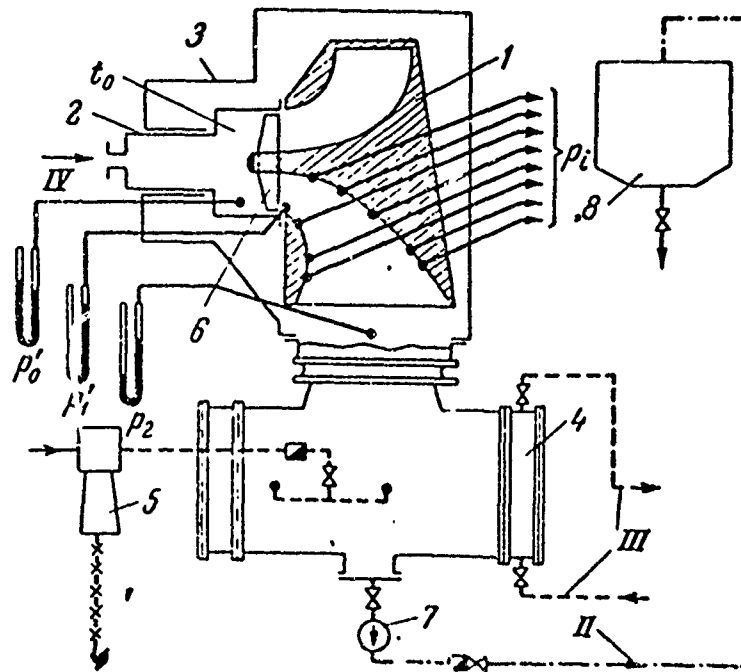


Fig. 7-19. Diagram of a test stand for the conducting of steam tests of branch connections. 1 - steam-water mixture; II - condensate; III - circulation water; IV - steam.

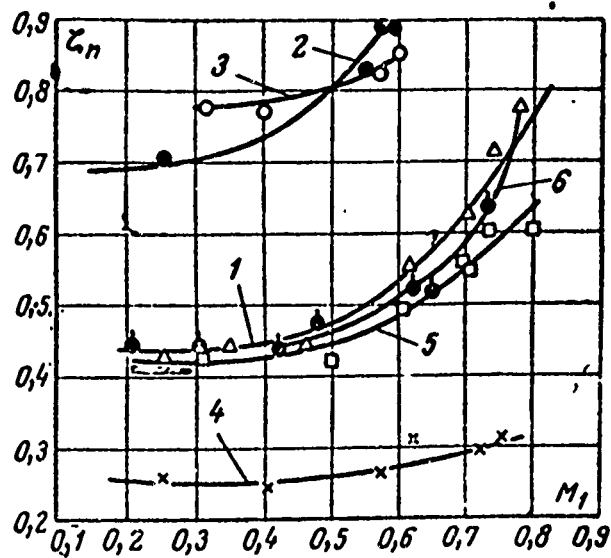
over wide limits the counterpressure p_2 and conducting tests with independent changes in the Mach and Reynolds numbers. Before the entry into the branch connection a grid 6, which simulated the turbine stage was installed.

Pressure measurement was conducted by means of mercury manometers, and the temperature was determined by the thermocouples installed in the steam box of the installation. To determine the flow rate, the condensate by condensate pump 7 was pumped into the gauging tank 8. The pressure in the mouth of the condenser was determined by means of the averaging of pressures measured at 14 points of the cross section of the mouth.

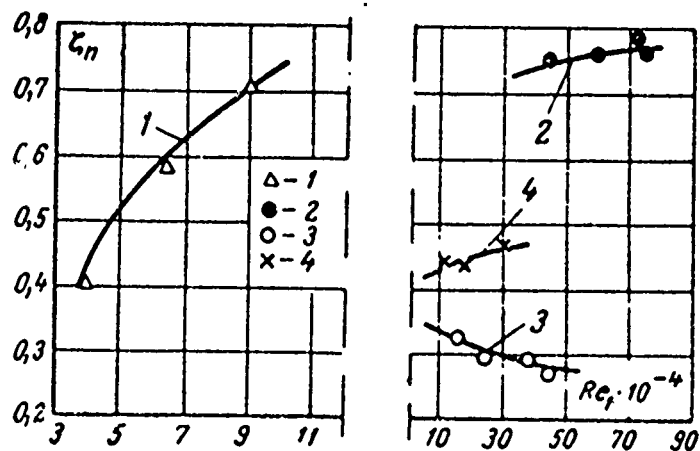
All tests were conducted over a wide range of Mach numbers at the inlet ($M_1 = 0.2-0.9$) and at various values of the Re_1 number. The coefficients of the branch connection ζ_{Π} , obtained as a result of these tests, are given depending on the M_1 and Re_1 numbers in Fig. 7-20. The dependence on the M_1 number is obtained for two values of the Reynolds number (lines 1 and 2). Plotted here is the curve from results of air tests (curve 3). In this case separate simulation according to M_1 and Re_1 numbers was not provided.

It is interesting to note that the air tests showed the same order of losses as the steam tests at the number $Re_1 = 8.2 \times 10^4$, but the nature of the change in losses depending on M_1 number was somewhat different.

Taking into account that in the turbine the Reynolds number, calculated according to the diameter of the last stage and rate at the inlet into the branch connection, is of the order $(2-5) \times 10^5$, when evaluating the quality of the branch connection in question it follows to be oriented on curves 2 and 3 in Fig. 7-20a



a)



b)

Fig. 7-20. Dependence of coefficient ζ_n upon M_1 a) and Re b) for various objects. a; 1 - branch connection of the turbine T-50; $Re_1 = 4 \cdot 10^4$; 2 - branch connection of the turbine T-50, $Re_1 = 8.2 \cdot 10^4$; 3 - branch connection of the turbine T-50 (air tests); $Re_1 = (2-6.5) \cdot 10^5$; 4 - conical diffuser ($\alpha = 8^\circ$; $n = 2.34$); 5 - variant of a branch connection with a vane and smooth radial diffuser; 6 - variant of a branch connection with a vane and welded radial diffuser; b: 1 - branch connection of the turbine T-50; $M_1 = 0.35$ (steam tests); 2 - branch connection of turbine T-50; $M_1 = 0.15-0.37$ (air tests); 3 - conical diffuser ($\alpha = 8^\circ$; $n = 2.34$); 4 - conical diffuser; $M_1 = 0.13-0.43$ ($\alpha = 30^\circ$; $n = 2,34$).

i.e., in the effective range of the velocities (0.5-0.7) M_1 the total losses in the branch connection will comprise a noticeable magnitude ($\zeta_n = 0.8-1.0$).

From the given curves it follows that with an increase in M_1 and Re_1 numbers an increase in the coefficients of losses occurs. As experiments showed, an increase in Re_1 number 2 times when $M_1 = 0.33$ (Fig. 7-20b) gives rise to an increase in losses of 28%, and an increase in M_1 number from 0.35 to 0.72 when $Re_1 = 2 \cdot 10^4$ causes an increase in losses of 27%.

Let us discuss the effect of M_1 and Re_1 numbers in more detail. Figure 7-20b gives the dependence of the coefficient of losses for a number of tested objects upon the Re_1 number. It is interesting that in the region of small values of Re_1 with its increase there occurs not a decrease but an increase in losses (curve 1). A certain increase in losses with an increase in the Re_1 number was noted during air tests of a branch connection (curve 2) in the zone of higher values of the Reynolds number.

For a comparison Fig. 7-20b plots test data of two conical diffusers with an equal area ratio $n = 2.34$ and flare angles $\alpha = 8$ and 30° . In the first diffuser the flow in all the modes occurred without boundary layer separation, and in the second one detached flow took place.

The test data showed that increase in Re_1 number led to a decrease in losses in the nondetached diffuser (curve 3) and to the increase in diffuser losses with angle $\alpha = 30^\circ$ (curve 4).

As was already mentioned above (see Chapter 3), with an increase in the Re_1 number there occurs a certain decrease in the boundary layer thickness and as a consequence a reduction in losses. An increase in losses with an increase in Re_1 number

with the appearance of separation is explained by the displacement of the separation point against the flow, whereupon in the region of large values of the Re_1 number the position of the separation zones is stabilized and the effect of the Re_1 number proves to be weak. That fact that in the branch connection in question (Fig. 7-20b) with an increase in the Re_1 number the losses increase confirms that the flow in its elements occurs with separations.

An increase in the M_1 number has a similar effect. Since with an increase in the Mach number the positive pressure gradients increase, then at large M_1 numbers the previous boundary layer separation and the sharp increase in energy losses occur.

A pressure measurement along the circumference of the internal contour of the branch connection showed that the resistance of all the channels is practically identical, the reverse effect of the branch connection on the operation of the last stage of the turbine is insignificant.

By comparing the improved variant of the branch connection with the previous one, let us note that for the turbine T-50 the transition to a new design means the reduction in losses expressed in power units by 200-300 kW.

Naturally, the obtained results are not limiting. In order to be convinced of this, let us return to Fig. 7-20a, where plotted is the curve of the change in coefficient ζ_n depending on the M_1 number for a conical diffuser with the expansion ratio $n = 2.34$ (curve 4). In comparing these data with data on branch connections, we see that in the range of high velocities the distinction in coefficients ζ_n for the diffuser and branch connection is 40-60%.

The reason for the sharp increase in losses in the branch connection as compared with that in the diffuser with an increase in the M_1 number is the fact that in design considerations the radial diffuser of the branch connection must be made unsymmetric.

If in the upper part of the branch connection the axial opening of the radial diffuser is small, then in the outlet section for the provision of normal flow it is necessary to introduce additional guide ribs. As a whole losses in such an unsymmetric diffuser are intensely changed with a change in M_1 number which is clearly evident in Fig. 7-20a (here in the analysis one should compare curves 2 and 4, since they were obtained at approximately equal Re_1 numbers).

Furthermore, the presence in the branch connections of developed ribs, which separate the flow on the outlet section, substantially increases the rubbing surface and gives rise to additional losses which are not always compensated by that gain, which gives such an arrangement of flow behind the radial diffuser. For the clarification of the role of the ribs in the given branch connection, a determination of the coefficient of losses ζ' in whole exit section was conducted by means of probe tests. In this case the losses were determined not allowing for outlet losses and were referred to the energy of the completely stagnation flow.

Test data are given in Fig. 7-21, where values of the losses averaged over the height H (see Fig. 7-18) are plotted. For a comparison the curve of losses, obtained during tests of a branch connection without ribs is given. A comparison of these curves visually shows that near the ribs a sharp increase in losses occurs.

Thus, on the basis of the conducted analysis, it is possible to confirm that the examined design of the branch connection from

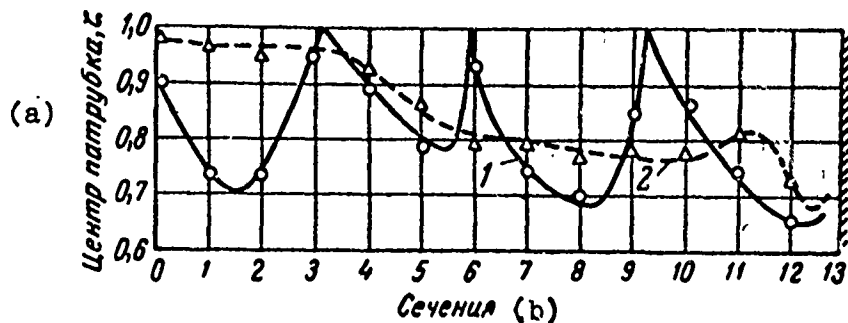


Fig. 7-21. Variation in losses in the outlet section of the branch connection of the turbine T-50. 1 - branch connection with ribs; 2 - branch connection without ribs.
KEY: (a) Center of branch connection; (2) Sections.

an aerodynamic point of view is not optimum, although it is better than the initial variant.

The noted shortcomings were eliminated to a considerable degree in the branch connection designed in MEI (Moscow Power Engineering Institute). Its diagram is given in Fig. 7-22.

The main part of branch connection consists of a symmetrical radial diffuser and the subsequent vane diffuser installed at the outlet from the radial diffuser. The transition to the coupling dimension of the condenser is accomplished by means of a sudden expansion from the outlet area of the vaned diffuser in its lower part to the final dimension. To provide for a more uniform field, in the outlet section of the branch connection an equalizing grid with a cell with a dimension of 10×10 mm is arranged. Such a design ensures the satisfactory operation of the branch connection during various modes of operation over a wide range of velocities.

In this case the basic braking of the flow is accomplished in a symmetrical radial diffuser. The subsequent grid, installed in the range of reduced velocities, ensures further braking and,

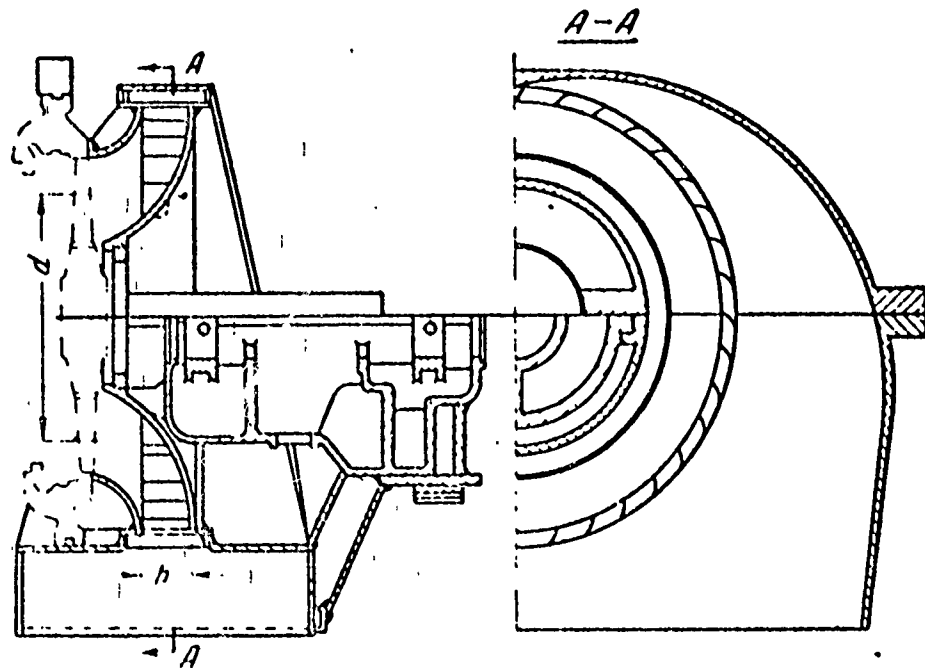


Fig. 7-22. Diagram of a branch connection of MEI with radial and vaned diffusers.

most importantly, guides the flow into the composite chamber of the branch connection. Furthermore, a certain additional pressure of recovery takes place with the sudden expansion of flow at the inlet into the composite chamber. These design changes led to a substantial increase in the aerodynamic characteristics of the branch connection and provided its stabler operation with a change in flow rate at the inlet.

Thus, from curve 5, given in Fig. 7-20a, it follows that over a wide range of velocities the coefficient of losses of the branch connection was changed in the range of 0.45-0.7, i.e., in the given branch connection it was reduced from 30 to 55% of the kinetic energy of flow which entered into the branch connection.

The obtained curve is close to the analogous dependence for the branch connection of the turbine T-50 taken at small Re_1 numbers. However, since in the turbine the order of the number $Re_1 \approx 10^5$, we should produce all comparisons with curve 2.

For a clarification of the possibility of making the examined branch connection welded, tests of a radial diffuser with the external contour composed of two cones were conducted.

The test data showed that with the correct selection of nondimensional distance $\bar{l}_4 = l_4/l_2$, where l_4 - the width of radial diffuser at the outlet, and l_2 - the height of the inlet section, it is possible to obtain approximately the same values of characteristics of the branch connection as with a smooth contour.

A study of the role of the guide vane showed that its installation increases the degree of pressure recovery by 5-7%, whereupon the quality of the manufacture of the vane and shape of the profile weakly affect the total characteristics of the branch connection. The known freedom in the selection of the type of vane is explained by the fact that the main braking occurs in the radial diffuser, and the portion of losses in the vane, referred to the kinetic energy of flow at the inlet into the diffuser, is small.

§ 7-5. Exhaust Branch Connections with Axiradial Elliptical Diffusers

The diagram examined above (see § 7-4) of the exhaust duct with a circular grid installed behind the axiradial diffuser, with good aerodynamic characteristics, possesses a considerable design shortcoming. Actually, for the removal of flow behind the grid with minimum losses, it is necessary to increase noticeably

the transverse dimensions of the branch connection (Fig. 7-22). As a result its outlet section takes the form of an elongated rectangle located across the axis of the machine. If for gas turbine this shortcoming to a certain degree is compensated by a gain in efficiency, then for steam turbines the elongated rectangular exhaust duct complicates the joint of the branch connection with the existing condensers. Hence there results the necessity to create an economic branch connection with limited transverse dimensions and adequate shape of the outlet section.

Here it is possible to propose for use as one of the possible solutions axiradial elliptical diffusers, the minor axis of which is arranged perpendicular to the axis of the machine in a horizontal plane. Then while maintaining the design described in § 7-4, it appears possible to eliminate the shortcomings noted above.

Before turning to the branch connection as a whole, let us examine results of the experimental investigation of such diffusers given in Fig. 7-23.

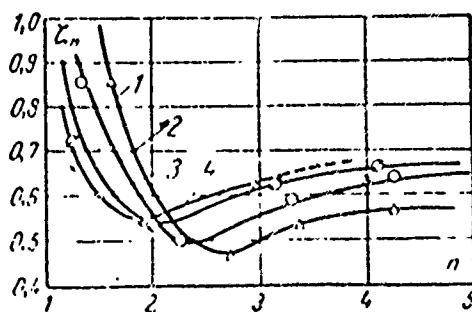


Fig. 7-23. Dependence of losses upon the expansion ratio for elliptical diffusers. 1 - $a/b = 1.0$; 2 - $a/b = 0.89$; 3 - $a/b = 0.834$; 4 - $a/b = 0.722$.

The dependences of the total loss factor upon the expansion ratio at various relations between the major and minor axes of the ellipse from a qualitative side were identical.

However, with a decrease in ratio a/b there occurs a certain increase in losses, and the displacement of the optimum expansion ratio to the side of smaller values is clearly noticeable. Thus, if when $a/b = 1.0$, $n_{\text{опт}} = 2.8$, then when $a/b = 0.8$, $n_{\text{опт}} = 1.9-2.0$.

Of specific interest is the behavior of the curves in question in the zone of small expansion ratios, since because of the limited axial dimensions of steam turbines it is rarely possible in radial diffusers to maintain the optimum value of n .

In deviating from $n_{\text{опт}}$ to the smaller side, with a normal axiradial diffuser ($a/b = 1.0$) we will obtain that when $n = 1.5$ the coefficient of recovery proves to be close to zero ($\zeta_n = 1.0$). At the same time for the elliptic diffuser this magnitude is preserved at a level of 40%. Such a valuable quality can be successfully used in the designing of exhaust ducts of steam turbines. One of its possible variants is given in Fig. 7-24. The aerodynamic scheme of this branch connection consists in the axiradial diffuser 1 (Fig. 7-24a), guide blades 2 (Fig. 7-24b), a separating "plug" rib 3 (Fig. 7-24c), guide and force ribs 4 and a housing 5.

The basic element of the branch connection, which converts the kinetic energy of flow into potential energy of pressure, is the axiradial diffuser, which consists of two halves separated by rib 3. In the upper part its contour is outlined by the circumference, and the lower half is made with a considerable side shear, which allows increasing the free passage area after the diffuser without an increase in the overall radial dimensions of the branch connection.

Entering into the diffuser, the flow is separated by rib 3, installed on horizontal joint, into two almost isolated parts, which subsequently are connected only in the outlet section of the branch connection.

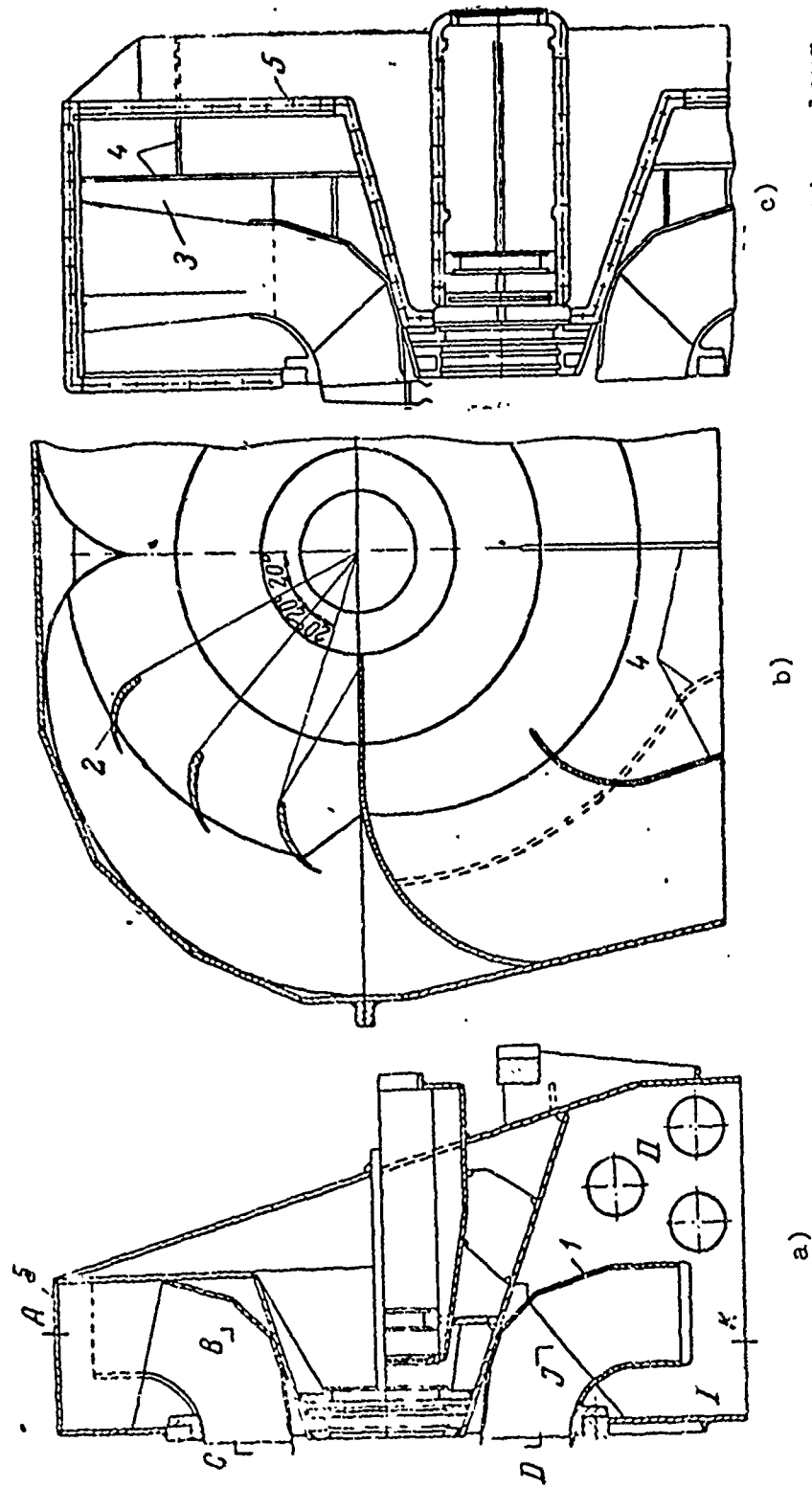


Fig. 7-24. Diagram of the exhaust duct of MEI. a) meridional section; b) section along ABC and DJK; c) view of branch connection from the side of the joint.

Installed in the radial part of the upper half of the diffuser are guide vanes which turn the flow around in the direction toward the outlet section of the branch connection. Simultaneously with this, they are the basic force elements which ensure the rigidity of the upper half of the branch connection. The flow directed thus toward the horizontal joint by the "plug" rib is thrown off into the free chambers I and II of the lower half of the branch connection (Fig. 7-24a).

The removal of the flow from the lower half of the diffuser and its distribution along the outlet section are accomplished by the usual guide ribs, which together with the longitudinal ribs form the rigid stressed frame of the lower half of the branch connection.

The examined organization of the flow of flow behind the diffuser has as a goal the complete use of the structural flow passage cross-sectional areas and the liquidation of vortex regions.

It should be noted that the indicated design allows preserving all the coupling dimensions, and if there is a decrease in "radiality" of the diffuser, then the external overall dimensions of the branch connection with a certain reduction in its efficiency can remain constant.

Results of comparative tests of the initial design (see Fig. 7-2a) and the modernized variant were encouraging. If in the initial variant the total losses at the velocity at the inlet of $M_1 = 0.45$ comprised $\zeta_n = 1.3$, then upon the introduction of the design changes examined above this value was lowered to $\zeta_n = 0.62$. In other words, in the new variant 38% of the kinetic energy of flow which leaves the last stage of the turbine is recovered, and the total gain with respect to the initial variant is 68%.

Here it is interesting to indicate that the half-welded construction of the diffuser, tested without a branch connection, gave losses at a level of 60%, i.e., in the indicated arrangement of the flow behind the diffuser losses in the free part of the branch connection were very small, since in all of its parts the flow was characterized by insignificant velocities.

Simultaneously with a decrease in air drag in the new branch connection, the nonuniformity of pressure behind the stage was lowered and zones of reverse currents in the outlet section disappeared. The last fact can substantially affect the effectiveness of the operation of the condenser, since it ensures a uniform distribution of steam flows along tube banks.

The numbers of losses given above are obtained not allowing for the inlet nonuniformity being created by the runner. Therefore, the absolute values of losses in the real machine can be different. However, the relative improvement should remain of approximately the same order as that with static tests.

§ 7-6. Operation of Exhaust Ducts when the Stage of the Turbomachine Exists

The test data given above were obtained with a uniform axial velocity field at the inlet into the branch connection. It is natural that when the stage of turbomachine exists, the inlet field can be substantially nonuniform. Furthermore, the deviation of the mode of operation of the machine from that calculated leads to the appearance of flow spin. According to experimental data the small flow spin takes place in design conditions.

A certain idea about the flow pattern after the turbine stage can be obtained from experimental data of Central Scientific Research, Planning and Design Boiler and Turbine Institute im. I. I. Polzunov [TsKTI] (ЦКТИ) [23]. Figure 7-25 gives curves of changes in the angle and velocity of the outlet for four turbine stages with $\theta = 5$ which were different only by the type of blading.

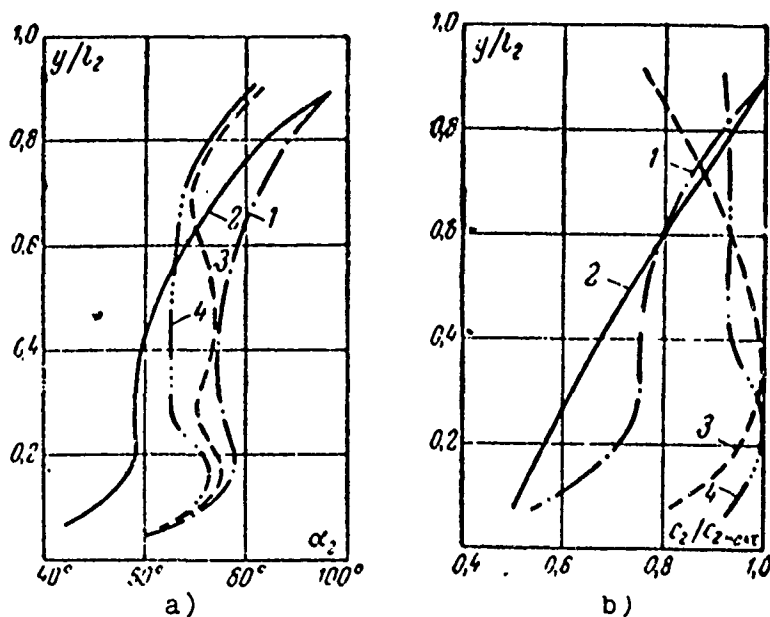


Fig. 7-25. Change in the angle of outlet α_2 a) and velocity at the outlet c_2 b) along the radius of the turbine stage [23].

Stage 1 was designed according to the law of constant circulation:

$$c_u r = \text{const}; c_z = \text{const.}$$

Stage 2 is constructed according to the law

$$c_u r^{f(n)} = \text{const}; \rho c_z = \text{const.}$$

Stage 3 is designed with a constant reaction along the radius, and stage 4 had cylindrical blading. (Numbers of the curves in Fig. 7-25 correspond to the numbers of stages).

In all cases it is possible to note a certain spin of the flow on the greater part of the radius and the nonuniformity of the velocity profile. Consequently, in the final evaluation of the effectiveness of a certain exhaust of system, it is necessary to introduce the corrections which consider both factors.

For the characteristic of the nonuniformity of the inlet profile in [54] the coefficient $k_1 = c_{\text{макс}}/c_{\text{ср}}$, which represents the ratio of the maximum flow rate to the mean flow rate, is used. The coefficient $k_2 = c_{\text{макс}}/c_{\text{мин}}$ is similarly introduced [82]. However, both these coefficients characterize the velocity profile quite unilaterally since they do not consider the sign of heterogeneity. In this sense the coefficient

$$k_3 = \int_F \left(\frac{c}{c_{\text{ср}}} - 1 \right) dF,$$

used in work [82] is more successful.

It is not difficult to see that for the convex velocity profiles $k_3 > 0$, for the concave $k_3 < 0$, and for the uniform $k_3 = 0$.

Thus, by taking as an argument the coefficient of nonuniformity k_3 , it is necessary to construct the functional dependence of losses upon this coefficient.

The theoretical solution to the stated problem for laminar flow conditions in the boundary layer was obtained by O. N. Ovchinnikov. However, for the solution to this problem, in general it is necessary to use experimental data. According to the latter, dependence $\zeta/\zeta_0 = f(k_3)$, where ζ_0 - the coefficient of losses with a uniform velocity profile, can be represented by a certain parabola the vertex of which for nondetached flow is located at point $k_3 = 0$ (curve 1 in Fig. 7-26) and is shifted to the side of negative values k_3 with detached flow (curve 2).

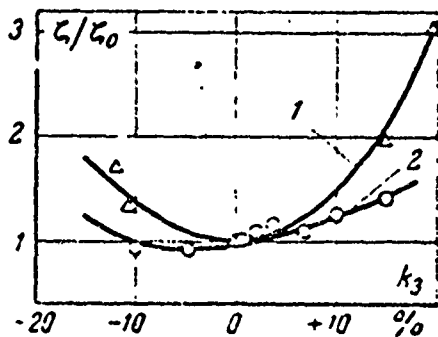


Fig. 7-26. Effect of the non-uniformity of the velocity profile at the inlet to losses in branch connection. 1 - non-separable flow; 2 - separation flow.

For experimental velocity profiles after the last stage given in Fig. 7-25b, the coefficient $k_3 \approx 0-3\%$, and, consequently, the maximum increase in losses because of the nonuniformity of the velocity profile at the inlet into the branch connection will comprise 10-15% of the initial level of losses.

The given numbers should be examined only as a first approximation, because for the final conclusions the experimental data are clearly insufficient.

Besides the radial nonuniformity of the inlet velocity profile, the efficiency of exhaust duct can be substantially affected by the spin of the flow behind the stage, characterized by the circular component c_u of absolute velocity c .

Flow in the diffusers when the indicated component exists was experimentally investigated little [3, 22, 145, 147], but the

obtained results are of great theoretical and practical interest.

It was found that up to a definite limit the appearance of a circular velocity component favorably affects the aerodynamic characteristics of diffusers of all types. The greatest improvement in characteristics is noted for wide-angle conical diffusers [147]. The least sensitivity to the twist of flow was showed by axiradial diffusers [3, 22].

The positive effect of the twist of flow on the efficiency of diffusers is connected with the fact that the development of the flow in the zone of positive pressure gradients occurs in the field of centrifugal forces, which prevent the emergence of the separation of the flow. If in wide-angle conical diffusers this field prevents the emergence of the separation of flow from walls of the channel, then in annular diffusers, simultaneously with the stabilization of the flow on the external surface, the deterioration of conditions of the flow on the internal surface occurs. As a result in annular diffusers, depending on their shape, a small positive effect of the spin is noticeably observed.

For an illustration of the aforesaid, Fig. 7-27 gives the dependence of the coefficient of losses ζ_n upon the angle of twist of the flow β for conical and axiradial annular diffusers.

If for one conical diffuser an increase in angle β up to 30° led to a reduction in losses of more than 25%, then for axiradial diffusers the losses were practically not changed. The results in question were obtained during a test of free diffusers. At the same time being of interest is the effect of the twist of flow not only on diffuser systems but also on the characteristics of exhaust ducts as a whole. Such results were obtained at MEI during research on the exhaust duct in static conditions. The basic geometric parameters of an axiradial diffuser used in the branch connection is given in Table 7-3. Given here for a comparison are data on diffusers [3, 22].

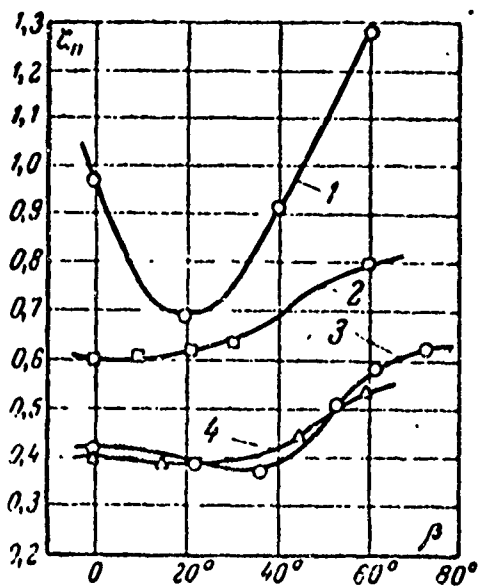


Fig. 7-27. Dependence of coefficient ζ_n upon the angle of twist β . 1 - conical diffuser ($\alpha = 25^\circ$) [147]; 2 - axiradial diffuser [22]; 3 - axiradial diffuser [3]; 4 - experiments of MEI.

Research on the effect of the twist of the flow was conducted at angles β equal to 0, 15, 45, and 60°. The dependence of the coefficient of total losses for the system in question upon angle β , presented in Fig. 7-27 (curve 4), as a whole confirmed the results of work [3, 22]. Here, just as during the test of axiradial diffusers, an increase in the angle β to 30° in practice did not cause a change in the value ζ_n . A further increase in twist led to negative results, and when $\beta = 60^\circ$ the total loss factor was increased by 15%. With this coefficient of the recovery of energy ξ was decreased from 60 to 40-45%.

The reduction in the recovery ability of an axiradial diffuser with a transition to a significant twist of flow is illustrated well by the distribution of the local coefficients of pressure recovery on the external (Fig. 7-28a) and internal (Fig. 7-28b) contours of the diffuser. The coefficient ξ_1 used here constitutes the following value:

$$\xi_1 = \frac{p_1 - p_1}{E_0},$$

where p_1 - static pressure at the point of the contour in question; p_1 - mean static pressure in the inlet section; E_0 - inlet kinetic energy of the flow.

Table 7-3.

Type of diffuser	n	$H/D_{1,P}$	$H/D_{2,P}$	γ/μ	\bar{D}_1	\bar{D}_2	\bar{r}_1	\bar{L}	R, mm	$\frac{r_2}{r_1}$	$P_{1,P}, \text{mm Hg}$
Experiments of Gurevich [22].	2.45	0.184	0.141	0.018	1.18	2.41	0.82	—	53	1.33	146.5
Experiments Amelyushkin-Uman [3].	3.0	0.21	0.12	1.75	1.12	2.0	0.88	0.91	—	—	—
Experiments of MEI.	2.06	0.208	0.171	1.215	1.11	1.69	0.83	0.64	53	1.08	216

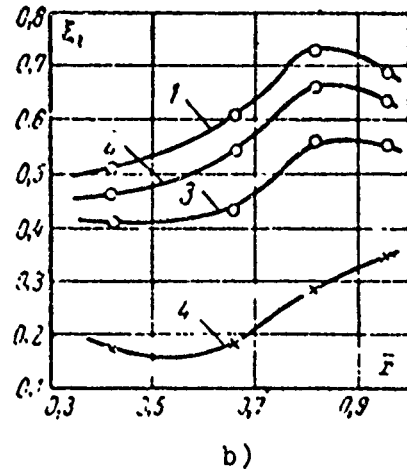
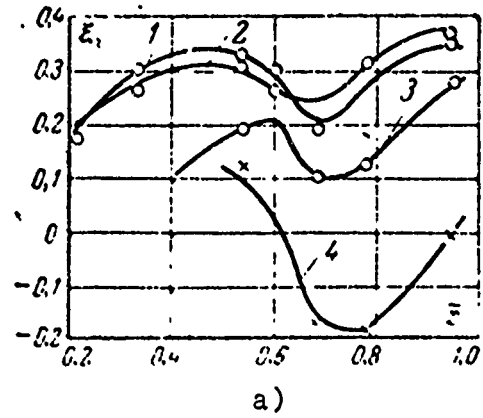


Fig. 7-28. Variation in the local coefficients of pressure recovery along the contours of an axiradial diffuser. a) external contour AB; b) internal contour CD; 1 - $\beta = 0^\circ$; 2 - $\beta = 15^\circ$; 3 - $\beta = 45^\circ$; 4 - $\beta = 60^\circ$.

With the axial entry of flow ($\beta = 0$) on the external contour a pressure increase p_1 in the axial part of the diffuser takes place. Then when $\bar{x} > 0.5$ in the zone of the turn the flow is accelerated, and subsequent braking occurs at the output part of the external contour ($\bar{x} > 0.7$).

On the internal contour the picture is somewhat different. The braking of the flow, beginning from the entry, intensely builds up, attaining a peak value in the zone of the turn ($\bar{x} = 0.7-0.8$), whereupon a certain acceleration of the flow and, correspondingly a decrease in the coefficient of pressure recovery occur.

With a significant deviation in the flow from the axial entry ($\beta = 45, 60^\circ$) the distribution of ξ_1 along the surfaces which limit the channel is qualitatively preserved without a change. However, the numerical values of coefficient ξ_1 fall very noticeably, and at angle $\beta = 60^\circ$ on the external contour there are zones where the local static pressure p_1 proves to be less than the mean pressure in the inlet section of the branch connection. On the internal contour the coefficient ξ_1 maintains at all tested angles β a positive value, but its absolute value at $\beta = 60^\circ$ drops by approximately 30%.

The noted reduction in the effectiveness of the axiradial diffuser with the appearance of a noticeable circular velocity component is caused by the following fact.

With the axial entry and nondetached flow the effectiveness of the conversion of the kinetic energy of flow into potential energy is basically determined by the law of the change in the mean flow rate dependent on the flow passage cross-sectional area of the channel.

The appearance of the circular velocity component complicates the flow pattern, but now it is possible to consider that during

braking dominant role is played by the axial or in this case it is more correct to say the meridian velocity component c_m . Then, by considering the proportionality of pressure to the square of the velocity, we obtain that at narrow angles of β (small values of c_u) the square of the meridian velocity c_m is little distinguished from this value with the axial entry of flow, and the additional centrifugal-force field induced by the twist has as a whole a favorable effect on the development of flow in the diffuser channel.

Since the angle β at the assigned absolute velocity uniquely determines its components c_u and c_m ($c_u = c \sin \beta$), we obtain with an increase in twist the drop in value of c_m and increase in c_u .

If one assumes that along the diffuser channel the intensity of the drop in the meridian velocity component exceeds the intensity of the drop in its circular component, then the reduction in the effectiveness of the diffusers noted in the experiments at angles $\beta > 30^\circ$ becomes entirely regular. This regularity remains valid even for detached diffusers. True, in this case at moderate angles β ($\beta < 30^\circ$) there occurs a sharp reduction in the total losses induced by the displacement of point of separation in the direction toward the outlet section, which gives rise to a well expressed optimum with respect to the angle of the twist of flow (see curve 1, Fig. 7-27).

The quantitative estimate of the possible displacement of the separation point depending on the twist is quite complex and at present is impracticable in practice. However, the qualitative change in the limiting values of parameters of the boundary layer can be predicted.

Actually, having used for certainty as a parameter of the boundary layer the Buri [Translator's Note: name not verified] parameter Γ , let us present the condition of nondetached flow

on the external contour of the diffuser in question in the form of

$$\Gamma = \frac{\delta^{**}}{c} \cdot \frac{dc}{dx} Re^{**m} \leq A_1 + A_2 \frac{\delta^{**}}{r_1} \sin^2 \beta - A_3 \frac{\delta^{**}}{r_1} \cos^2 \beta. \quad (7-1)$$

Here: A_1 , A_2 and A_3 are certain constants whose value should be determined from the experiment; δ^{**} - the momentum thickness.

The expression (7-1) written on the basis of purely qualitative considerations expresses the fact that the limiting value of parameters of separation during the motion of swirling flow in the curvilinear channel cannot be constant and is determined by conditions of the flow. Moreover, the experimental values of Γ , obtained for flat channels at the axial entry of the flow, indicate that in this comparatively simple case the limiting value of the parameter Γ is changed over wide limits. In other words, the coefficient A_1 , which enters into expression (7-1), generally speaking, is not constant, and also depends upon the flow conditions. According to our data, quite good results during the processing of experimental data can be obtained if we present the coefficient A_1 in the form of

$$A_1 = B \frac{p_1}{\rho c_1^2 / 2} = B \bar{p}_1,$$

where B is the experimental constant, and \bar{p}_1 is the local pressure ratio.

The relation (7-1) given above is very debatable and can be recommended for quantitative calculations only after serious test work.

By examining the effect of twist, it is necessary to indicate even the effect of the fastening ribs installed usually in the

exhaust ducts of the diffusers. This question is investigated most comprehensively in [3]. The study was conducted with a different location of eight fastening stiffening ribs.

As one would expect, the location of the ribs directly at the inlet section gave rise to a sharp increase in losses with a deviation of the velocity vector from axial direction (Fig. 7-29, curve 1). With removal of the ribs from the inlet their negative effect decreases and with the location of the ribs near the outlet section a twist of the order of 15-20° practically did not change the magnitudes of the losses. Hence it follows that with the correct position of the stiffening ribs it proves to be possible, by estimating the efficiency of the branch connections, not to consider the twist of the flow in design conditions.

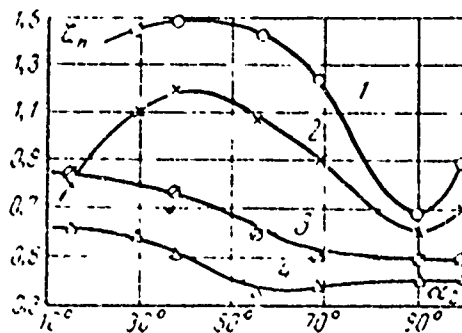


Fig. 7-29. Dependence of losses upon the outlet angle of flow α_2 for a curvilinear diffuser with different length of the ribs [3]. 1 - $\bar{\delta} = 0.3$; 2 - $\bar{\delta} = 1.0$; 3 - $\bar{\delta} = 3.1$; 4 - diffuser without ribs; $\bar{\delta} = \delta/l_2$ - dimensionless distance from the inlet to the ribs.

With a deviation from the design conditions, when the twist of the flow exceeds 30°, a noticeable increase in total losses, which is connected both with the separation of flow under the action of centrifugal forces and with an increase in losses of friction in sections of nondetached flow occurs. It is natural that the quantitative estimates in this case can be conducted only on the basis of experimental data. A certain representation about the intensity of the increase in losses can be given by curves in Fig. 7-29 [3]. These data, besides estimating the role of the twist, allow quantitatively estimating the effect of the ribs.

At $\beta \approx 0^\circ$, i.e., when there is no separation of flow from the ribs induced by twist, it is possible to observe the degree of the reduction in losses with a decrease in the fairing. Thus, with the location of the ribs along the whole curvilinear diffuser, the total losses in it were $\zeta_n \approx 0.68$ (curve 1), and with a reduction in their length by approximately 9 times the losses were decreased by 18% (curve 3, $\zeta_n = 0.50$). The complete removal of the ribs (curve 4) reduced the losses down to 0.40-0.42.

As a whole the reduction in losses by 28% as a result of the removal of the continuous ribs is caused not only by the reduction in the fairing but also by the noticeable change in the flow pattern in the curvilinear diffuser with the replacement of continuous channel with a series of sections.

The given results give an indirect idea about the possible change in characteristics of the exhaust duct during its operation with the rotor wheel. It is understandable that decisive importance in this question belongs to the direct experiment. Unfortunately, such data at present are insufficient for final conclusions. Nevertheless, some experiments are of doubtless interest and allow conducting an estimate at least from a qualitative side. In this sense a sufficiently detailed study of the exhaust duct, which operates together with the stage of the gas turbine, was conducted by R. I. D'yakonov, A. M. Drokonov and R. V. Kus'michev at the Bryansk Institute of Transportation Machinery [BITM] (БИТМ) [39a]. The stage had a comparatively small hub-tip ratio ($D/l_2 = 3.34$ at the span of the blade $l_2 = 125$ mm) and a high value of the coefficient of outlet losses ($\zeta_{B.C} = 0.11$). Results of the test with the exhaust into the atmosphere, given in Fig. 7-30 (curve 3), show that the maximum efficiency level in this case was $\eta_{01} = 83.8\%$. The same stage, tested with an axial diffuser ($n = 1.9$; $r_2/r_1 \sim 1.3$; $D_2/D_1 = 2.25$ and $L/r_1 \sim 1$), had a maximum eff $\eta_{01} = 86.6\%$ (curve 1).

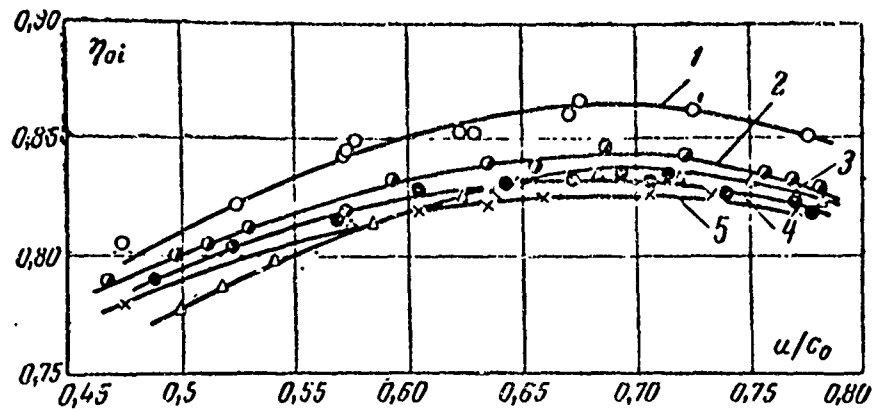


Fig. 7-30. Variation in the eff of the axial stage of the turbine depending on u/c_0 from experiments of BITM. 1 - stage with diffuser; 2 - stage with branch connection ($F_3/F_1 = 3.82$); 3 - stage with exhaust into the atmosphere; 4 - stage with branch connection ($F_3/F_1 = 3.35$); 5 - stage with branch connection ($F_3/F_1 = 2.98$).

The established increase in the eff of 3% when using a diffuser visually shows the effectiveness in its installation behind the last stage.

For our purposes it is advantageous to distinguish the characteristic of the intrinsic diffuser. Such a characteristic is given in Fig. 7-31, where the dependence of total losses in the diffuser ζ_n upon the mean angle of departure of the flow from the stage α_2 . Just as with static tests, the reduction in the α_2 up to 70° , i.e., the twist of the flow within limits of 20° , affected little the magnitude of the total losses. A more perceptible effect was an increase in angle α_2 , with an increase of which up to 102° losses increased from 0.61 to 0.67. It is interesting to note that the coefficient of losses in the given diffuser, according to results of static tests, was about 0.55. Approximately the same value of losses ($\zeta_n = 0.51$) is obtained as a result of theoretical calculations. Thus, in this case the effect of the rotating grid proves to be unessential, and its portion makes up about 5-6% of the losses. Basically this effect

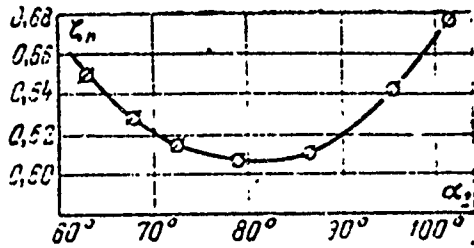


Fig. 7-31. Variation in total losses in an axiradial diffuser, tested together with the operating grid, at various angles of the flow from the rotor wheel α_2 . (Experiments of BITM.)

is explained by the increased turbulence level of the flow which leaves the stage. Under such conditions in the flow it is not possible to isolate the region where the pressure of full stagnation p_{01} would be maintained constant, and everywhere in the outlet section the pressure p_{02} proves to be below p_{01} . Above it was indicated (see Chapter Two) that if $p_{02} < p_{01}$, then the losses should be determined according to the arbitrary relative areas of the boundary layer $\bar{\Delta}^*$ and $\bar{\Delta}^{**}$, which consider the difference in the pressures of full stagnation.

Results of the detailed study on the velocity field in front of the diffuser and behind it, in the optimum ratio u/c_0 , are given in Figs. 7-32 and 7.33 (experiments of BITM).

When the diffuser is not present, the static pressure behind the stage, expressed in the portions of the initial pressure before the stage (Fig. 7-32), was distinguished little from the ambient pressure and was insignificantly changed along the height of the blade (curve 1). The setting of the diffuser led to a noticeable pressure change in the direction from the root to the top of the blade and increased rarefaction behind the stage (curve 2). However, the distribution of the angles and velocities was changed to a lesser degree. The output angles of flow along the height of the blade α_2 were practically not changed (Fig. 7-32b), curves 1 and 2), and on the velocity profile (Fig. 7-32c, curve 1) it is possible to note the local acceleration of flow near the top of the blade. The given dependences confirm the assumption about the absence of the twist of flow in the mode in question and sufficient uniformity of the velocity field in front of the

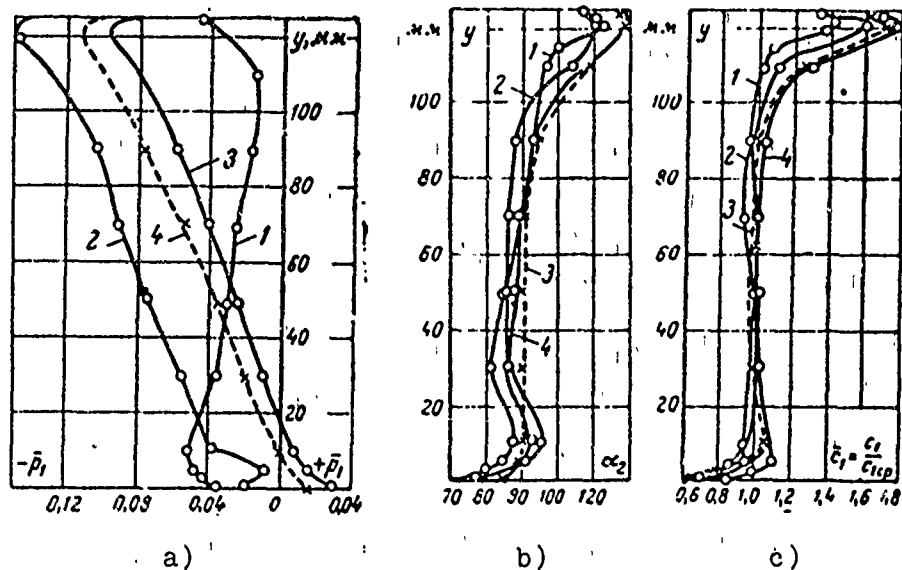
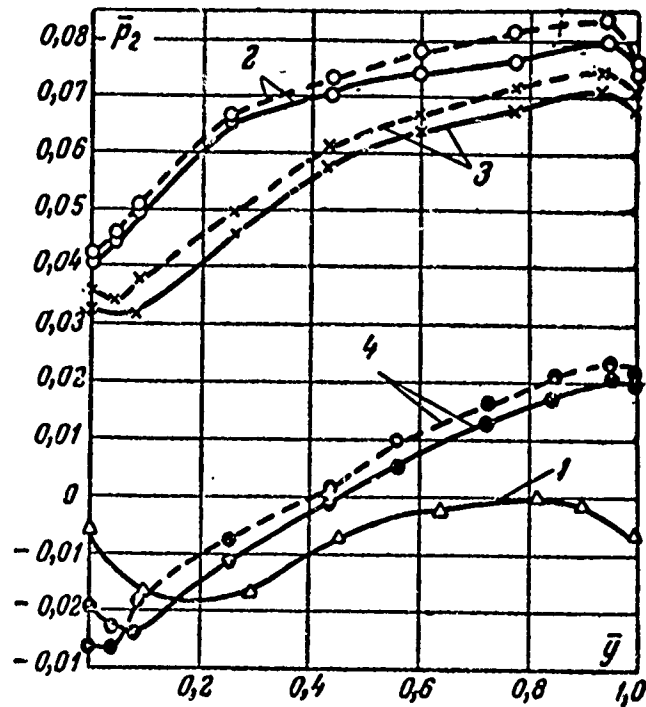


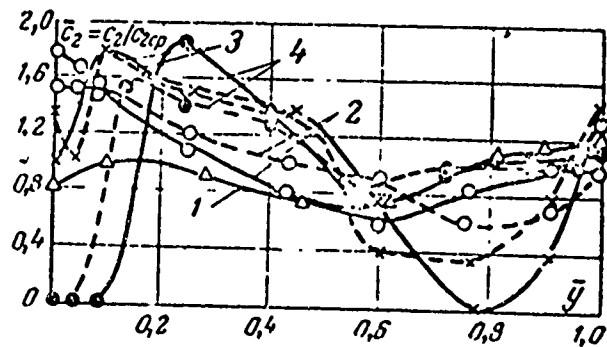
Fig. 7-32. Variation in relative static pressure a), angles α_2 b) and relative velocities c) behind the turbine stage. (Experiments of BITM.) 1 - free exhaust; 2 - stage with diffuser; 3 - stage with branch connection ($F_3/F_1 = 3.35$); 4 - stage with branch connection ($F_3/F_1 = 3.82$).

entry into the diffuser. Hence it is quite evident that the characteristics of the intrinsic diffuser, tested with a stage and without it, differ little. Research on the flow pattern in its outlet section showed the almost uniform velocity distribution over the whole cross section (Fig. 7-33b, curve 1).

With a transition to smaller values of u/c_0 , the operating conditions of the diffuser are changed, and the velocity field in the outlet section is deformed. For example in Fig. 7-34 velocity profiles taken at various ratios of u/c_0 are compared. In the optimum mode ($u/c_0 = 0.675$) the instantaneous values of velocity are distinguished from average velocity by 15-20% and are changed from the external to the internal contour almost according to the sinusoidal law.



a)



b)

Fig. 7-33. Variation in the relative static pressure a) and relative velocities b) in the outlet section of the diffuser along the radius. (Experiments of BITM.) 1 - free outlet; 2 - closed side of branch connection; 3 - middle section; 4 - open side; ($F_3/F_1 = 3.82$ and 2.98).

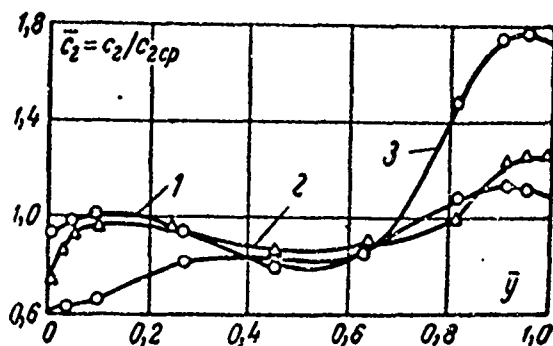


Fig. 7-34. Velocity distribution at the outlet from the diffuser at various values of $u/c_0 = 0.675$; 2 - $u/c_0 = 0.575$; 3 - $u/c_0 = 0.475$.

For $u/c_0 = 0.575$ (curve 2) an increased drop in velocity directly in the external contour, a more uniform distribution in the middle part, and an increase in velocity of 30% from the middle level of the internal contour are characteristic. A further reduction in u/c_0 led to an increase in velocity near the internal outlet. Thus, with nonaxial entry, when there exists a circular velocity component, in the axiradial diffuser the displacement of flow from the external to the internal outlet occurs. As a result the effective expansion ratio of the diffuser is lowered, which gives rise to an increase in energy losses, and the eff of the whole installation is noticeably lowered. If for $u/c_0 = 0.675$ the increase in the eff induced by the diffuser is $\Delta\eta_{01} = 3\%$, then for $u/c_0 = 0.475$ it is lowered to 0.5% (see Fig. 7-30).

As was already mentioned above, the aerodynamic characteristics of the exhaust system is defined not only by the diffuser, but to a considerable degree it depends also upon the correct arrangement of the flow in the housing of the branch connection. When special measures do not exist, for this the effectiveness of diffuser can be reduced to zero.

The aforesaid is convincingly confirmed not only by results of static tests but by the examined experiments of BITM [39a], where the operation of the stage together with the simplest branch connection was investigated. A diagram of the latter is given in Fig. 7-35. Tests were conducted in three positions of the side walls, which ensured the following relation between the intake area F_1 , the area of the outlet from the diffuser F_2 and the area

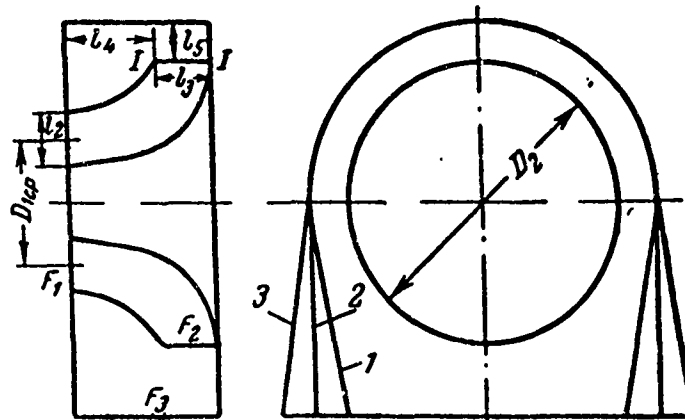


Fig. 7-35. Diagram of the investigated branch connection [39a].

of the outlet from the branch connection F_3 : 1) $F_1:F_2:F_3 = 1:1.9:1.57$; 2) $F_1:F_2:F_3 = 1:1.9:1.76$; 3) $F_1:F_2:F_3 = 1:1.9:2.0$.

The first variant immediately gave a negative result, having caused a reduction of 5% in the eff of the turbine as compared with the free diffuser and 2% as compared with the open exhaust into the atmosphere (curve 5 in Fig. 7-30). The second variant was somewhat better (curve 4), and only in the third case (curve 2) did the branch connection on the whole provide a small diffuser effect, raising the eff by approximately 0.5-0.6%.

Such a sharp negative effect of the housing is explained by the positive relation between the area of the outlet from the diffuser and the area of the outlet from the branch connection. The ratio F_3/F_2 for the branch connection without the arrangement of flow behind the diffuser according to the work [28] should be of the order of 3-3.5. The numbers given above are 1.5-2 times less than these values. The necessity for having a large reserve of output area is dictated by the fact that the flow distribution in the housing is extremely uneven, and with a small ratio F_3/F_2 the effective outlet area, i.e., the area with a positive component of flow rate, proves to be less than the area of the outlet from the diffuser ($F_{3\text{eff}}/F_2 < 1$).

As a result additional local accelerations of flow and an intense vortex formation in the housing of the branch connection appear, and the latter causes increased air drag of the outlet channel.

With installation of the housing conditions at the inlet into diffuser are changed little. Diagrams of the distribution of angles α_2 and velocities c_1 along the height of the blade are practically not changed (see Fig. 7-32b and c), and the distribution of static pressure, in preserving the general regularity in connection with the additional drag of the channel, is noticeably raised (curves 3 and 4).

More important changes are observed in the outlet section of the diffuser. Here the asymmetry of the outlet disturbs the uniformity of flow in various sections. On the closed side of the diffuser (section I-I in Fig. 7-35) the static pressure (see Fig. 7-33a, curve 2) sharply increases, and the velocity near the external contour increases (Fig. 7-33b, curve 2). In the middle section the static pressure is also noticeably higher than the pressure in the outlet section, and the velocity distribution indicates the emergence of small separation zones near the internal contour (curve 3 in Fig. 7-33b).

On the open side of the diffuser, as one would expect, the mean pressure is almost equal to the atmospheric (curve 4) and increases from the external contour, where there is the zone of separation of the flow (curve 4 in Fig. 7-33b), to the internal contour. The examined data indicate that the presence of the axial stage in front of the branch connection does not cause sudden changes in the quantitative characteristics.

The effect of the operating grid in the case of the axial stage, where at the inlet into the branch connection there is increased nonuniformity of velocity field, proves to be

more important. Results of such tests together with the branch connection (see Fig. 7-24) are given in Fig. 7-36.¹ Experiments were conducted with superheated (curve 1) and moist (curves 2 and 3) steam. It was found that the value ζ_{Π} substantially depends upon the mode of operation of the turbine characterized by the ratio u/c_0 . With a small ratio of u/c_0 , not dependent from the initial state of the steam, the coefficient ζ_{Π} was everywhere more than unity, i.e., the kinetic energy at the outlet from the grid proved to be insufficient for the overcoming of the air drag of the branch connection. With an increase in value u/c_0 there occurred an intense decrease in the coefficient ζ_{Π} and for superheated steam, when $u/c_0 = 0.55$ ζ_{Π} , reached the minimum value equal to 0.9.

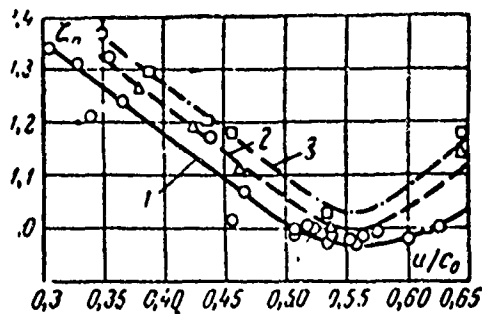


Fig. 7-36. Dependence of the total loss factor upon u/c_0 . 1 - dry steam; 2 - moisture $y = 3\%$; 3 - moisture $y = 6\%$.

It was noted above that for this branch connection, according to static tests $\zeta_{\Pi} = 0.68$, i.e., in this case the noticeable deterioration of the aerodynamic characteristics of the branch connection was noted.

A further increase in parameter u/c_0 again gave rise to the increase in coefficient ζ_{Π} .

The nature of the dependence in question was not changed even with transition to moist steam, but numerical values of ζ_{Π}

¹Experiments were conducted by Engineer Ye. N. Myslitskiy.

prove to be different. With the initial moisture of the steam in front of the turbine equal to 3%, $\zeta_{\text{п.мин}} = 1.0$, and with its increase of 6% $\zeta_{\text{п.мин}} = 1.1$. In other words, with an increase in moisture an increase in the total loss factor occurred, and this fact must be considered if the discussion concerns the exhaust ducts of steam condensation turbines.

Unfortunately, for a quantitative estimate of the effect of moisture, at present there is still very little experimental data.

APPENDICES

Table A-1. Conical diffusers.

N ^o	α	n	l/D_1	λ_1	Re · 10 ⁻³	ζ_n	ζ_p	ζ_{II}	Remarks
1	1°	1,3	4	0,43	0,2	0,65	0,604	0,592	[Л. 120]
2	2°	1,64	8	0,3	0,2	0,5	0,491	0,38	[Л. 142] МЭИ (air)
3	2°	2,43	16	0,42	0,2	0,3	0,318	1,1755	
4	3°30'	2,1	18			0,42	0,408	0,241	МЭИ (steam)
5	4°	1,3	2	0,47	0,2	0,6	0,64	0,595	
6	4°	3	10,5	0,368	0,295	0,228	0,194	0,138	МЭИ (air)
7	5°	3,5	12,45	0,316	0,038	0,176	0,198	0,1124	
8	4°	3,5	12,45	0,478	0,218	0,163	0,168	0,1124	МЭИ (air)
9	4°	3,5	12,45	0,555	0,301	0,178	0,164	0,1124	
10	4°30'	2,4	18			0,41	0,334	0,195	[Л. 143]
11	4°30'	2,4	18			0,32	0,334	0,196	
12	4°30'	2,4	18			0,3	0,334	0,196	[Л. 140]
13	4°30'	2,53	7,47		0,16	0,222	0,207	0,178	
14	4°30'	4,0	12,65		0,16	0,128	0,144	0,0964	[Л. 142] МЭИ
15	4°30'	6,35	19,52		0,16	0,071	0,096	0,0671	
16	5°	1,5	6			0,530	0,530	0,454	[Л. 140]
17	6°	1,59	2,48	0,32	0,16	0,465	0,453	0,41	
18	6°	2,38	5,62			0,268	0,239	0,204	[Л. 142]
19	6°	25,3	5,65		0,16	0,243	0,229	0,189	
20	6°	4	9,5		0,16	0,149	0,131	0,113	МЭИ
21	6°	6,35	14,5		0,16	0,078	0,085	0,0882	
22	6°30'	3,0	18			0,27	0,244	0,158	[Л. 142]
23	7°	1,5	1,84	409	0,323	0,4556	0,482	0,461	
24	7°	2,0	3,375	0,403	0,32	0,287	0,3	0,277	МЭИ
25	7°	2,5	4,75	0,3	0,243	0,22	0,218	0,2	
26	7°	3	6	0,294	0,238	0,186	0,171	0,16	

[MEI] (МЭИ) = Moscow Power Engineering Institutes; Л = Bibliography references.

Table A-1 (Cont'd.).

No	α	"	L/D ₁	λ_1	Re·10 ⁻⁶	ζ_n	ζ_p	ζ_n	Remarks
27	7°	3,5	6,875	0,307	0,248	0,173	0,14	0,138	[Л. 142]
28	7°	4	8,19	0,301	0,244	0,152	0,121	0,1244	[Л. 120]
29	7°	45	8,48	0,305	0,246	0,1475	0,104	0,1159	
30	7°30'	1,8	6			0,41	0,401	0,33	
31	8°	1,3	1	0,42	0,2	0,61	0,615	0,655	
32	8°	2,43	4	0,22	0,2	0,3	0,218	0,211	
33	8°20'	3,45	5,77	0,5		0,16	0,137	0,155	МЭИ
34	9°30'	1,5	3,0			0,53	0,506	0,46	[Л. 142]
35	9°30'	3,87	5,8		0,2	0,2	0,126	0,149	[Л. 148]
36	10°	3	4,19	0,434	0,136	0,17	0,163	0,182	
37	10°	4	5,715	0,314	0,054	0,136	0,126	0,152	МЭИ
38	10°	4	5,715	0,325	0,145	0,133	0,114	0,152	
39	10°30'	2,1	6,0		0,16	0,38	0,31	0,276	[Л. 139]
40	11°	2,38	2,81	0,32		0,275	0,215	0,237	МЭИ
41	11°15'	2,3	2,58	0,15		0,27	0,227	0,245	[Л. 148]
42	12°	1,6	1,25		0,2	0,55	0,419	0,419	
43	14°	1,43	0,8		0,2	0,6	0,508	0,534	
44	4°	3,5	12,45	0,344	0,249	0,222	0,1124	0,1124	
45	4°	3,5	12,45	0,397	0,098	0,101	0,1124	0,1124	
46	4°	3,5	12,45	0,484	0,165	0,135	0,1124	0,1124	
47	4°	3,5	12,45	0,61	0,206	0,164	0,1124	0,1124	
48	4°	3,5	12,45	0,314	0,1937	0,144	0,1124	0,1124	
49	4°	3,5	12,45	0,385	0,1756	0,154	0,1124	0,1124	
50	4°	3,5	12,45	0,44	0,25	0,173	0,1124	0,1124	
51	4°	3,5	12,45	0,556	0,122	0,207	0,1124	0,1124	
52	4°	3,5	12,45	0,556	0,0514	0,169	0,1124	0,1124	

Table A-1 (Cont'd.).

N_r	α	n	L/D_1	λ_1	$Re \cdot 10^{-4}$	ζ_n	ζ_n^p	ζ_n^v	Remarks
53	4°	3,5	12,45	0,62	0,22	0,13	0,1124	0,1124	МЭИ
54	7°	3	6	0,486	0,234	0,33	0,1588	0,1588	
55	7°	3	6	0,591	0,238	0,285	0,1588	0,1588	МЭИ
56	7°	3	6	0,459	0,191	0,326	0,1588	0,1588	
57	7°	3	6	0,48	0,113	0,379	0,1588	0,1588	
58	7°	3	6	0,354	0,052	0,373	0,1588	0,1588	
59	7°	3	6	0,598	0,37	0,305	0,1588	0,1588	
60	7°	3	6	0,582	0,317	0,298	0,1588	0,1588	
61	10°	3	4,187	0,482	0,208	0,234	0,1822	0,1822	
62	10°	3	4,187	0,603	0,14	0,185	0,1822	0,1822	
63	10°	3	0,4187	0,403	0,0514	0,294	0,1822	0,1822	
64	10°	3	0,4187	0,518	0,225	0,236	0,1822	0,1822	
65	10°	4	0,4187	0,363	0,2735	0,187	0,1822	0,1822	
66	10°	4	0,4187	0,4955	0,0666	0,275	0,1822	0,1822	
67	10°	4	0,4187	0,503	0,115	0,249	0,1822	0,1822	
68	10°	4	0,4187	0,505	0,331	0,16	0,1822	0,1822	
69	10°	4	0,4187	0,57	0,206	0,159	0,1822	0,1822	
70	15°	4	3,8	0,5053	0,227	0,1954	0,2145	0,2145	
71	15°	4	3,8	0,36	0,249	0,176	0,2145	0,2145	
72	15°	4	3,8	0,413	0,11	0,144	0,2145	0,2145	
73	15°	4	3,8	0,467	0,095	0,154	0,2145	0,2145	
74	15°	4	3,8	0,552	0,051	0,257	0,2145	0,2145	
75	20°	4	2,84	0,336	0,218	0,31	0,3045	0,3045	
76	20°	4	2,84	0,4755	0,31	0,42	0,3045	0,3045	
77	20°	4	2,84	0,4155	0,251	0,246	0,3045	0,3045	
78	20°	4	2,84	0,589	0,365	0,526	0,3045	0,3045	

Table A-1 (Cont'd.).

λ_s	α	n	L/D_1	λ_1	$Re \cdot 10^{-4}$	ζ_n	ζ_n^p	ζ_n^q	Remarks
79	20°	4	2,84	0,4155	0,2245	0,358		0,3045	МЭИ
80	20°	4	2,84	0,42	0,1855	0,272		0,3045	
81	20°	4	2,84	0,577	0,25	0,486		0,3045	МЭИ (steam)
82	20°	4	2,84	0,586	0,313	0,541		0,3045	
83	30°	4	1,869	0,394	0,092	0,8866		0,5065	
84	30°	4	1,869	0,565	0,124	0,707		0,5065	
85	30°	4	1,869	0,382	0,15	0,575		0,5065	
86	30°	4	1,869	0,402	0,178	0,767		0,5065	
87	30°	4	1,869	0,416	0,169	0,78		0,5065	
88	30°	4	1,869	0,447	0,183	0,588		0,5065	
89	1°	3	10,5	0,493	0,383	0,222		0,1377	
90	4°	3	10,5	0,597	0,444	0,223		0,1377	
91	4°	3,5	12,45	0,372	0,289	0,251		0,1123	
92	4°	3,5	12,15	0,574	0,43	0,2		0,1123	
93	7°	1,5	1,84	0,503	0,386	0,428		0,461	
94	7°	1,5	1,84	0,599	0,445	0,411		0,461	
95	7°	2,0	3,375	0,3	0,243	0,273		0,275	
96	7°	2,5	4,75	0,506	0,388	0,205		0,1996	
97	7°	3	6	0,294	0,238	0,186		0,1599	
98	7°	3	6	0,506	0,388	0,182		0,1599	
99	7°	3	6	0,602	0,446	0,172		0,1599	
100	7°	3	6	0,55	0,415	0,207		0,1599	
101	7°	3,5	6,875	0,398	0,315	0,1625		0,1379	
102	7°	3,5	6,875	0,606	0,449	0,149		0,1379	
103	7°	4	8,19	0,401	0,317	0,146		0,1244	
104	7°	4	8,19	0,599	0,445	0,145		0,1244	

Table A-1 (Cont'd.).

№	α	n	L/D_s	λ_s	$ke \cdot 10^{-6}$	ζ_n	ζ_p	ζ_n	Remarks
105	7°	4	8,19	0,486	0,376	0,161		0,1599	
106	7°	4,5	8,48	0,495	0,381	0,136		0,1159	
107	7°	4,5	8,48	0,6	0,446	0,133		0,1159	
108	7°	5	10,1	0,5	0,243	0,139		0,1104	
109	7°	5	10,1	0,606	0,449	0,123		0,1104	
110	7°	6	11,85	0,418	0,329	0,123		0,1041	
111	7°	6	11,85	0,607	0,5	0,121		0,1041	
112	7°	7	13,45	0,301	0,244	0,13		0,1004	
113	7°	7	13,45	0,602	0,447	0,115		0,1004	
114	7°	8	14,92	0,41	0,324	0,113		0,0999	
115	7°	8	14,92	0,501	0,384	0,105		0,0999	
116	7°	9	16,35	0,407	0,321	0,112		0,0992	
117	7°	9	16,35	0,61	0,452	0,1		0,0992	
118	7°	10,0	17,67	0,304	0,246	0,112		0,0991	
119	7°	10,0	17,67	0,4876	0,374	0,1		0,0991	
120	10°	3	4,187	0,458	0,357	0,272		0,1822	
121	10°	3	4,187	0,404	0,32	0,217		0,1822	
122	10°	3	4,187	0,559	0,42	0,213		0,1822	
123	10°	4	5,715	0,4475	0,35	0,184		0,1525	
124	15°	3	2,78	0,454	0,355	0,249		0,231	
125	15°	3	2,78	0,601	0,446	0,267		0,231	
126	15°	3	2,78	0,332	0,267	0,283		0,231	
127	15°	3	3,8	0,411	0,324	0,205		0,1245	
128	15°	4	3,8	0,4895	0,378	0,217		0,2145	
129	20°	3	2,075	0,312	0,251	0,337		0,3025	
130	20°	3	2,075	0,474	0,367	0,377		0,3025	

Table A-1 (Cont'd.).

N ^o	α	n	L/D ₁	λ_1	Re · 10 ⁻⁶	ζ_H	ζ_H^P	ζ_U^P	Remarks
157	22°	1,59	0,67	0,16	0,618	0,42		0,46	
158	22°	2,53	1,52	0,16	0,466	0,1845		0,462	
159	22°	4,0	2,57	0,16	0,429	0,095		0,331	
160	22°	6,35	3,91	0,16	0,423	0,0535		0,362	
161	22°	10,11	5,61	0,16	0,482			0,4	
162	22°	16	7,72	0,16	0,44			0,43	
163	28°	1,59	0,522	0,16	0,656	0,432		0,502	[Jl. 139, 140]
164	28°	2,53	1,18	0,16	0,58	0,19		0,412	
165	28°	4,0	2,0	0,16	0,559	0,089		0,456	
166	28°	6,35	3,05	0,16	0,57	0,04		0,518	
167	28°	10,11	4,37	0,16	0,643			0,577	
168	28°	16	6,02	0,16	0,596			0,624	
169	4°30'	1,59	3,29	0,16	0,455	0,474		0,404	
170	4°30'	2,53	7,47	0,16	0,235	0,243		0,178	[Jl. 139, 140]
171	4°30'	4,0	12,65	0,16	0,132	0,144		0,0962	
172	11°	1,59	1,35	0,16	0,443	0,439		5,421	
173	11°	2,53	3,07	0,16	0,252	0,206		0,222	
174	11°	4,0	5,19	0,16	0,144	0,11		0,1725	[Jl. 140]
175	7°	1,56	2		0,47	0,461		0,43	
176	7°	2,22	4	0,3	0,258	0,235		0,235	
177	7°	3,015	6			0,22		0,156	
178	7°	3,91	8			0,18		0,126	
179	7°	4,95	10			0,175		0,078	
180	7°	6,1	12			0,17		0,1	
181	6°	3,38	8			0,25		0,137	
182	7°	3,01	6			0,3		0,159	[Jl. 148] (uniform velocity profile at the inlet)

Table A-1 (Cont'd.).

No	α	n	L/D	λ_s	$Re \cdot 10^{-6}$	ζ_n	ζ_n^p	ζ_n^φ	Remarks
183	7°30'	2,55	4,8			0,35		0,1856	[Л. 148] (uniform velocity profile at the inlet)
184	8°30'	2,32	3,5			0,4		0,224	
185	10°	2,08	2,5			0,45		0,273	
186	14°	2,23	2			0,34		0,282	
187	14°	3,94	4			0,25		0,214	
188	14°	6,1	6			0,24		0,216	
189	14°	8,8	8			0,22		0,224	
190	14°	12	10			0,2		0,234	
191	14°	15,6	12			0,14		0,24	
192	14°	7,3	15			0,15		0,093	
193	7°30'	5,95	11			0,25		0,1	
194	11°	3,0	3,8			0,3		0,19	
195	12°	2,4	2,6			0,5		0,24	
196	14°	2,23	2			0,43		0,282	
197	14°	3,94	4			0,4		0,214	
198	14°	6,1	6			0,38		0,216	
199	14°	8,8	8			0,375		0,224	
200	14°	12	10			0,37		0,234	
201	14°	15,6	12			0,4		0,24	
202	14°	2,15	1,9			0,35		0,285	
203	14°30'	1,9	1,5			0,4		0,33	
204	15°	1,7	1,15			0,45		0,39	
205	16°	1,5	0,8			0,5		0,47	
206	9°30'	1,5	3,0			0,58			[Л. 142] (plane diffuser)
207	9°30'	1,5	3,0			0,52			
208	14°	1,8	3,0			0,59			
209	14°	1,8	3,0			0,51			

Table A-1 (Cont'd.).

No	α	n	L/D_1	λ_1	$Re \cdot 10^{-6}$	ζ_n	ζ_n^p	Remarks
210	14°	1.8	3.0					[JL. 142] (plane diffusers)
211	21°	2.1	3.0					
212	21°	2.1	3.0					
213	21°	2.1	3.0					
214	26°	2.4	3.0					
215	26°	2.4	3.0					
216	26°	2.4	3.0					
217	5°	1.5	6.0					
218	5°	1.5	6.0					
219	5°	1.5	6.0					
220	7°30'	1.8	6.0					[JL. 142, 143] (plane diffusers)
221	7°30'	1.8	6.0					
222	10°30'	2.1	6.0					
223	10°30'	2.1	6.0					
224	13°30'	2.4	6.0					
225	16°	2.7	6.0					
226	19°	3.0	6.0					
227	19°	3.0	6.0					
228	3°30'	2.1	18					
229	6°30'	3.0	18					
230	11°	4.5	18					[JL. 139] (extended velocity profile at the inlet)
231	4°30'	1.59	3.29					
232	4°30'	2.53	7.47					
233	4°30'	4	12.65					
234	4°30'	6.35	19.25					
235	4°30'	10.11	27.6					
236	4°30'	16	37					

Table A-1 (Cont'd.).

Nr	α	n	L/D ₁	λ_1	Re·10 ⁻⁴	ζ_n	ζ_n^p	ζ_n^w	Remarks
237	6°	1,59	2,48			0,57		0,410	[Л. 139] (extended velocity profile at the inlet)
238	6°	2,53	5,63			0,348		0,193	
239	6°	4	9,55			0,252		0,118	
240	6°	6,35	14,5			0,22		0,096	
241	6°	10,1	20,8			0,225		0,091	
242	6°	16	28,6			0,222		0,092	
243	11°	1,59	1,35			0,612		0,422	
244	11°	2,53	3,07			0,388		0,224	
245	11°	4,0	5,19			0,287		0,166	
246	11°	6,35	7,9			0,26		0,156	
247	11°	10,1	11,3			0,235		0,160	
248	11°	16	15,57			0,245		0,167	
249	14°	1,59	1,06			0,638		0,431	
250	14°	2,53	2,4			0,447		0,248	
251	14°	4	4,07			0,317		0,203	
252	14°	6,35	6,18			0,285		0,202	
253	14°	10,1	8,87			0,322		0,212	
254	14°	16	12,2			0,311		0,224	
255	18°	1,59	0,821			0,688		0,446	
256	18°	2,53	1,86			0,518		0,288	
257	18°	4	3,15			0,365		0,264	
258	18°	6,35	4,8			0,352		0,281	
259	18°	10,1	6,88			0,383		0,302	
260	18°	16	9,47			0,408		0,321	
261	22°	1,59	0,67			0,755		0,465	
262	22°	2,53	1,516			0,569		0,339	
263	22°	4	2,57			0,491		0,343	

Table A-1 (cont'd.).

No	α	n	L/D_1	λ_1	$Re \cdot 10^{-6}$	ζ_n	ζ_n^p	ζ_n^y	Remarks
264	22°	6,35	3,91			0,444		0,380	[Л. 139] (extended velocity profile at the inlet)
265	22°	10,1	5,61			0,439		0,415	
266	22°	16	7,72			0,512		0,444	
267	23°	1,59	0,522			0,769		0,496	
268	26°	2,53	1,18			0,708		0,419	
269	28°	4	2,0			0,591		0,467	
270	28°	6,35	3,05			0,558		0,536	
271	28°	10,1	4,37			0,593		0,594	
272	28°	16	6,02			0,629		0,638	
273	4°30'	1,59	3,29			0,572		0,405	
274	4°30'	2,53	7,47			0,341		0,191	
275	4°30'	4,0	12,65			0,265		0,099	
276	11°	1,59	1,35			0,6		0,422	
277	11°	2,53	3,07			0,394		0,224	
278	11°	4,0	5,19			0,265		0,166	
279	31,2°	4,48	2	0,27		0,65		0,531	
280	31,2°	4,48	2	0,33				0,531	
281	8°	8,27	13,4	0,26				0,107	
282	8°	8,27	13,4	0,43				0,107	
283	15,8°	8,27	6,7	0,22				0,231	
284	15,8°	8,27	6,7	0,46				0,231	
285	31,2°	8,27	3,85	0,2				0,633	
286	31,2°	8,27	3,85	0,3				0,633	
287	31,5°	8,27	3,85	0,43				0,633	
288	2°	1,3	4	0,25				0,592	
289	2°	1,3	4	0,3				0,592	

[Л. 120]

Table A-1 (Cont'd.).

No.	α	n	L/D_1	λ_1	$Re \cdot 10^{-6}$	ζ_n	ζ_n^p	ζ_n^q	Remarks
290	4°	1, 3	2	0, 21		0, 630		0, 595	
291	4°	1, 3	2	0, 41		0, 62		0, 595	
292	8°	1, 3	1	0, 29		0, 61		0, 655	
293	2°	1, 64	8	0, 23		0, 50		0, 38	
294	2°	1, 64	8	0, 46		0, 47		0, 38	
295	8°	1, 64	2	0, 2		0, 480		0, 495	
296	8°	1, 64	2	0, 38		0, 48		0, 405	
297	8°	1, 64	2	0, 45		0, 47		0, 405	
298	15, 8°	1, 64	1	0, 22		0, 52		0, 446	
299	15, 8°	1, 64	1	0, 38		0, 60		0, 446	
300	2°	2, 43	16	0, 22		0, 30		0, 175	
301	2°	2, 43	16	0, 33		0, 32		0, 175	
302	8°	2, 43	4	0, 3		0, 3		0, 211	
303	8°	2, 43	2	0, 43		0, 32		0, 211	
304	15, 8°	2, 43	2	0, 26		0, 52		0, 266	
305	15, 8°	2, 43	2	0, 38		0, 52		0, 266	
306	31, 2°	2, 43	1	0, 2		0, 65		0, 447	
307	31, 2°	2, 43	1	0, 34		0, 70		0, 447	
308	31, 2°	2, 43	1	0, 4		0, 78		0, 447	
309	4°	4, 48	16	0, 26		0, 160		0, 086	
310	4°	4, 48	16	0, 44		0, 17		0, 086	
311	8°	4, 48	8	0, 23		0, 18		0, 122	
312	8°	4, 48	8	0, 42		0, 21		0, 122	
213	15, 8°	4, 48	4	0, 25		0, 48		0, 218	
314	15, 8°	4, 48	4	0, 45		0, 46		0, 218	
315	31, 2°	4, 48	2	0, 23		0, 73		0, 531	

[Л. 120]

Table A-2 Annular diffusers.

Author	λ	n	$\frac{D_{3:2}P}{l}$	T	\bar{L}	\bar{d}_1	\bar{d}_2	\bar{D}_2	α_1	α_2	α_3	θ	$\zeta_{n,arc}$	[Л. 54] $\zeta_{n,расч}$	$A_{n, \%}$
	1	2,07	2,5	0,286	3,02	0,43	0,43	1,37	7°	0°	7°28'	3°30'	22,5	26,65	15,6
	2	3,04	2,5	0,286	5,2	0,43	0,43	1,63	7°	0°	7°20'	3°30'	15,7	16,52	4,95
	3	3,86	2,5	0,286	6,8	0,43	0,43	1,82	7°	0°	7°20'	3°30'	14,6	13,57	7,6
	4	2,06	3,9	0,204	2,39	0,592	0,592	1,29	7°	0°	8°20'	3°30'	26,7	27,22	1,91
	5	3,04	3,9	0,204	4,33	0,592	0,592	1,53	7°	0°	7°50'	3°30'	17,9	16,5	8,5
	6	3,56	3,9	0,204	5,2	0,592	0,592	1,63	7°	0°	7°50'	3°30'	15,7	14,37	9,25
	7	4,08	3,9	0,204	6,0	0,592	0,592	1,73	7°	0°	7°50'	3°30'	14,3	13,2	8,4
	8	1,778	7,17	0,122	1,27	0,755	0,755	1,16	7°	0°	9°45'	3°30'	34,5	34,8	0,56
	9	2,55	7,17	0,122	2,39	0,755	0,755	1,29	7°	0°	9°20'	3°30'	22,8	20,95	8,6
	10	3,04	7,17	0,122	3,02	0,755	0,755	1,37	7°	0°	9°10'	3°30'	19,6	17,63	11,2
	11	4,09	7,17	0,122	4,33	0,755	0,755	1,53	7°	0°	8°48'	3°30'	16,0	14,55	9,95
	12	2	3	0,25	3,4	0,5	0,708	1,42	7°	3°30'	6°	1°45'	27,7	28,12	1,49
	13	3	3	0,25	6,0	0,5	0,868	1,73	7°	3°30'	6°	1°45'	17,5	16,66	5,05
	14	4	3	0,25	8,2	0,5	1,0	2,0	7°	3°30'	6°	1°45'	14,3	13,27	7,8
	15	2	5	0,166	3,4	0,668	0,942	1,42	7°	4°40'	5°10'	1°10'	30,8	28,25	9,05
	16	3	5	0,166	6,0	0,668	1,16	1,73	7°	4°40'	5°10'	1°10'	23,2	16,88	37,4
	17	4	5	0,166	8,2	0,668	1,33	2,0	7°	4°40'	5°10'	1°10'	18,7	13,55	38
	18	2	7	0,125	3,4	0,75	1,06	1,42	7°	5°14'	4°36'	0°53'	34,7	28,5	21,7
	19	3	7	0,125	6,0	0,75	1,3	1,73	7°	5°14'	4°35'	0°53'	27,7	17,33	59,8
	20	4	7	0,125	8,2	0,75	1,5	2,0	7°	5°14'	4°36'	0°53'	24	14,12	70
	21	2	5,5	0,153	3,6	0,693	0,693	1,23	4°	0°	4°60'	2°	33	32,3	2,16
	22	2	5,5	0,153	1,73	0,693	0,693	1,23	8°	0°	10°	4°	32	34	5,9
	23	2	5,5	0,153	1,17	0,693	0,693	1,23	12°	0°	15°	6°	36	42,2	14,5
	24	2	5,5	0,153	0,88	0,693	0,693	1,23	16°	0°	19°30'	8°	41	48,5	15,6
	25	2	5,5	0,153	0,555	0,693	0,693	1,23	24°	0°	30°	12°	55	70	21,4
	26	1,88	5,5	0,153	7,6	0,693	0,156	1,0	0°	-4°	2°	2°	36	28,74	25,3

МЭИ

[Л. 22]

[MEI] (МЭИ) = Moscow Power Engineering Institute; Л = Bibliography references.

Table A-2 (Cont'd.).

Author	N ^o	n	$\frac{D_{\text{ср}}}{l}$	T	\bar{L}	\bar{d}_1	\bar{d}_2	\bar{D}_2	α_1	α_2	α_3	θ	$\zeta_{\text{п.экс}}$	$[\zeta_{\text{п.экс}}]$	$\Delta \bar{n}, \%$
[Л. 22]	27	1,88	5,5	0,153	1,0	0,693	0,156	1,0	0°	-8°	4°	4°	36	29,4	22,4
	28	1,88	5,5	0,153	2,4	0,693	0,156	1,0	0°	-12°	6°	6°	35	30,5	14,8
	29	1,88	5,5	0,153	1,91	0,693	0,156	1,0	0°	-16°	8°	8°	36	31,05	15,9
	30	1,88	5,5	0,153	1,27	0,693	0,156	1,0	0°	-24°	12°	12°	36	32,48	10,8
	31	1,88	5,5	0,153	0,95	0,693	0,156	1,0	0°	-32°	16°	16°	43,2	34,9	23,8
	32	1,88	5,5	0,153	0,75	0,693	0,156	1,0	0°	-40°	20°	20°	53,2	37,76	41
	33	1,88	5,5	0,153	0,6	0,693	0,156	1,0	0°	-48°	25°	24°	60,2	42,16	57
ИАМИ [Л. 130]	34	1,88	5,5	0,153	0,515	0,693	0,156	1,0	0°	-56°	30°	28°	83,2	46,13	80,5
	35	2,9	6,5	0,133	1,34	0,733	0,733	1,66	16°	0°	13°40'	8°	28	21,35	31,2
	36	2,44	5,14	0,163	0,965	0,674	1,27	1,74	42°	0°	24°	3°30'	57	37,25	53
	37	2,22	5,4	0,156	1	0,688	0,688	1,28	16°	0°	20°	8°	32,5	33,3	2,4
	38	2,58	5,4	0,156	1	0,688	0,688	1,35	20°	0°	24°40'	10°	32,5	37,8	14,0
	39	2,97	5,4	0,156	1	0,688	0,688	1,43	24°	0°	29°10'	12°	35	45,7	24,0
	40	3,37	5,4	0,156	1	0,688	0,688	1,5	28°	0°	33°30'	14°	40	53,8	25,7
[Л. 41]	41	3,82	5,4	0,156	1	0,688	0,688	1,58	32°	0°	38°	16°	45	62,5	28,0
	42	1,57	5,4	0,156	0,5	0,688	0,688	1,14	16°	0°	20°20'	8°	47,5	46,44	2,28
	43	1,59	5,4	0,156	0,5	0,688	0,688	1,18	20°	0°	21°15'	10°	45	46,27	2,74
	44	1,895	5,4	0,156	0,5	0,688	0,688	1,22	24°	0°	30°20'	12°	45	46,4	3,02
	45	2,07	5,4	0,156	0,5	0,688	0,688	1,25	28°	0°	35°10'	14°	49	48,7	0,62
	46	2,26	5,4	0,156	0,5	0,688	0,688	1,29	32°	0°	40°	16°	56	52,3	7,06
	47	2,53	5,4	0,156	1	0,688	0,55	1,28	16°	-8°	24°	12°	34	37,2	8,6
	48	2,82	5,4	0,156	1	0,688	0,55	1,35	20°	-8°	27°30'	14°	38	42,9	11,4
	49	3,24	5,4	0,156	1	0,688	0,55	1,43	24°	-8°	38°10'	16°	43	51,75	16,9
	50	3,68	5,4	0,156	1	0,688	0,55	1,50	28°	-8°	36°30'	18°	50	59,4	15,8
51	4,10	5,4	0,156	1	0,688	0,55	1,58	32°	-8°	37°20'	20°	55	63	12,7	
52	2,33	5,4	0,156	1	0,688	0,62	1,28	16°	-4°	21°30'	10°	32,5	34,1	4,7	

[NAMI] (НАМИ) = Central Scientific Research Institute of Automobiles and Automobile Engines)

Table A-2 (Cont'd.).

Author	N _e	n	$\frac{D_{icp}}{l}$	T	L	\bar{d}_1	\bar{d}_2	\bar{D}_2	α_1	α_2	α_3	θ	$S_{n, \text{max}}$	[Л. 54] n. Paca	$\Delta_{\text{п.}} \%$
	53	2, 7	5, 4	0, 156	1	0, 688	0, 62	1, 35	20°	-4°	36°10'	12°	35	40, 3	13, 1
	54	2, 07	5, 4	0, 156	1	0, 688	0, 62	1, 43	24°	-4°	30°20'	14°	38	48, 4	21, 5
	55	3, 5	5, 4	0, 156	1	0, 688	0, 62	1, 5	28°	-4°	34°50'	16°	44	56, 7	40
	56	3, 97	5, 4	0, 156	1	0, 688	0, 62	1, 58	32°	-4°	39°20'	18°	50	65, 15	23, 2
	57	2, 0	5, 4	0, 156	1	0, 688	0, 76	1, 28	16°	+4°	17°	6°	34	33, 25	23, 25
	58	2, 35	5, 4	0, 16	1	0, 688	0, 76	1, 35	20°	+4°	21°40'	8°	32	36, 4	12, 1
	59	2, 71	5, 4	0, 16	1	0, 688	0, 76	1, 43	24°	+4°	26°10'	10°	32	40, 3	20, 6
	60	3, 11	5, 4	0, 16	1	0, 688	0, 76	1, 43	28°	+4°	30°45'	12°	36	49	26, 5
	61	3, 58	5, 4	0, 16	1	0, 688	0, 76	1, 5	32°	+4°	35°30'	14°	41	57, 85	29, 2
	62	1, 82	5, 4	0, 16	1	0, 688	0, 83	1, 28	16°	8°	14°25'	4°	37, 5	35, 36	6, 05
	63	2, 15	5, 4	0, 16	1	0, 688	0, 83	1, 35	20°	8°	19°	6°	32	32, 7	2, 14
	64	2, 53	5, 4	0, 16	1	0, 688	0, 83	1, 43	24°	8°	24°	8°	30	37, 1	19, 1
	65	2, 96	5, 4	0, 16	1	0, 688	0, 83	1, 5	28°	8°	29°	10°	33	45, 7	27, 6
	66	3, 38	5, 4	0, 16	1	0, 688	0, 83	1, 58	32°	8°	33°40'	12°	33	64, 26	39, 2
	67	1, 54	5, 4	0, 16	1	0, 688	0, 9	1, 25	16°	12°	10°	2°	47	44, 22	7, 3
	68	1, 9	5, 4	0, 16	1	0, 688	0, 9	1, 35	20°	12°	15°30'	4°	35	33, 93	3, 16
	69	2, 27	5, 4	0, 16	1	0, 688	0, 9	1, 43	24°	12°	20°40'	6°	30	33, 6	10, 7
	70	2, 71	5, 4	0, 16	1	0, 688	0, 9	1, 5	28°	12°	26°10'	8°	32	40, 3	20, 6
	71	3, 12	5, 4	0, 16	1	0, 688	0, 9	1, 58	32°	12°	30°30'	10°	34	49, 15	30, 8
	72	1, 66	5, 4	0, 156	1	0, 688	0, 98	1, 35	20°	16°	12°	2°	43	39, 3	9, 9
	73	2, 03	5, 4	0, 156	1	0, 688	0, 98	1, 43	24°	16°	17°25'	4°	30	33, 3	9, 9
	74	2, 42	5, 4	0, 156	1	0, 688	0, 98	1, 5	28°	16°	22°40'	6°	32	35, 4	9, 6
	75	2, 87	5, 4	0, 156	1	0, 688	0, 98	1, 58	32°	16°	28°10'	8°	32	44	27, 3
	76	1, 48	5, 4	0, 156	1	0, 688	1, 12	1, 43	24°	24°	8°50'	0°	52	46, 09	10, 4
	77	1, 91	5, 4	0, 156	1	0, 688	1, 12	1, 5	28°	24°	15°40'	2°	36	33, 86	6, 3
	78	2, 32	5, 4	0, 156	1	0, 688	1, 12	1, 58	32°	24°	21°20'	4°	30	34, 1	12, 0

[Л. 41]

Table A-2 (Cont'd.).

Author	N ^o	n	$\frac{D_{10P}}{l}$	T	Z	\bar{d}_1	\bar{d}_2	\bar{D}_3	α_1	α_2	α_3	θ	$\zeta_{n,exc}$	$\left[\frac{\Delta \sigma}{\sigma} \right]_{n, pacu}$	$\Delta \sigma, \%$
	79	1,72	5,4	0,156	0,5	0,688	0,62	1,14	16°	-8°	25°10'	12°	45	34,91	31,2
	80	1,89	5,4	0,156	0,5	0,688	0,62	1,18	20°	-8°	30°10'	14°	45	36,2	24,3
	81	2,06	5,4	0,156	0,5	0,688	0,62	1,22	24°	-8°	34°50'	16°	47	48,7	3,5
	82	2,2	5,4	0,156	0,5	0,688	0,62	0,15	28°	-8°	38°	18°	54	51,1	5,7
	83	2,4	5,4	0,156	0,5	0,688	0,62	1,29	32°	-8°	43°20'	20°	61	53,1	14,9
	84	1,64	5,4	0,156	0,5	0,688	0,65	1,14	16°	-4°	22°30'	10°	46	45,64	0,79
	85	1,78	5,4	0,156	0,5	0,688	0,65	1,18	20°	-4°	27°	12°	44	45	2,22
	86	1,96	5,4	0,156	0,5	0,688	0,65	1,22	24°	-4°	32°15'	14°	46	47,1	2,34
	87	2,14	5,4	0,156	0,5	0,688	0,65	1,25	28°	-4°	37°	16°	52	50,3	3,38
	88	2,3	5,4	0,156	0,5	0,688	0,65	1,29	32°	-4°	40°10'	18°	58	52,5	10,5
	89	1,47	5,4	0,156	0,5	0,688	0,72	1,14	16°	+4°	17°15'	6°	51	49,56	2,9
	90	1,65	5,4	0,156	0,5	0,688	0,72	1,18	20°	+4°	23°	8°	46	45,17	1,84
	91	1,79	5,4	0,156	0,5	0,688	0,72	1,22	24°	+4°	27°20'	10°	44	45,2	2,66
	92	1,91	5,4	0,156	0,5	0,688	0,72	1,25	28°	+4°	30°40'	12°	48	46,3	4,06
	93	2,11	5,4	0,156	0,5	0,688	0,72	1,29	32°	+4°	36°	14°	53	49,4	7,3
	94	1,23	5,4	0,156	0,5	0,688	0,79	1,14	16°	12°	9°	2°	65	66,5	2,26
	95	1,4	5,4	0,156	0,5	0,688	0,79	1,18	20°	12°	10°30'	4°	54	52,38	3,1
	96	1,58	5,4	0,156	0,5	0,688	0,79	1,22	24°	12°	21°	6°	47	46,2	2,6
	97	1,76	5,4	0,156	0,5	0,688	0,79	1,25	28°	12°	26°10'	8°	46	44,95	2,34
	98	1,95	5,4	0,156	0,5	0,688	0,79	1,29	32°	12°	32°10'	10°	48	47	2,13
	99	1,14	5,4	0,156	0,5	0,688	0,83	1,14	16°	16°	5°46'	10°	77	77,15	0,195
	100	1,28	5,4	0,156	0,5	0,688	0,83	1,18	20°	16°	10°40'	2°	61	61,82	1,33
	101	1,46	5,4	0,156	0,5	0,688	0,83	1,22	24°	16°	17°10'	4°	50	50,3	0,6
	102	1,65	5,4	0,156	0,5	0,688	0,83	1,25	28°	16°	23°15'	6°	47	45,18	4,04
	103	1,84	5,4	0,156	0,5	0,688	0,83	1,29	32°	16°	28°40'	8°	46	45,5	1,1
	104	1,28	5,4	0,156	0,5	0,688	0,9	1,22	24°	24°	10°40'	0°	68	61,82	10

[Л. 41]

Table A-2 (Cont'd.).

Author	N ^o	n	$\frac{D_{icp}}{l}$	T	Z	\bar{d}_1	\bar{d}_2	\bar{D}_3	α_1	β_3	α_3	θ	$\zeta_{n, \text{max}}$	[Л. 54] $\zeta_{n, \text{max}}$	$\Delta \zeta_n, \%$
[Л. 41]	105	1,42	5,4	0,156	0,5	0,688	0,9	1,25	28°	24°	15°40'	2°	66	61,95	7,8
	106	1,62	5,4	0,688	0,5	0,688	0,9	1,29	32°	24°	22°10'	4°	48	45,6	5,5
	107	1,34	5,4	0,156	0,5	0,688	0,76	1,14	16°	8°	13°10'	4°	57	56,86	0,25
	108	1,52	5,4	0,156	0,5	0,688	0,76	1,18	20°	8°	19°	6°	49	47,92	2,25
	109	1,66	5,4	0,156	0,5	0,688	0,76	1,22	24°	8°	23°40'	8°	44	45,41	3,17
	110	1,85	5,4	0,156	0,5	0,688	0,76	1,25	28°	8°	29°	10°	46	45,75	0,55
	111	2,03	5,4	0,256	0,5	0,688	0,76	1,29	32°	8°	34°	12°	51	48,2	5,8
	112	3,19	6,95	0,126	2,48	0,75	0,475	1,275	6°	-6°	12°	6°	22	18,35	19,9
	113	3,19	6,95	0,126	1,93	0,75	0,475	1,275	8°	-8°	15°20'	8°	22	22,61	2,7
	114	3,19	6,95	0,126	1,53	0,75	0,475	1,275	10°	-10°	19°10'	10°	24,5	28,75	14,8
	115	3,19	6,95	0,126	1,28	0,75	0,475	1,275	12°	-12°	22°40'	12°	27	34,9	22,6
	116	3,19	6,95	0,126	1,08	0,75	0,475	1,275	14°	-14°	27°	14°	30,7	43,45	29,4
	117	3,19	6,95	0,126	0,97	0,75	0,475	1,275	16°	-16°	29°50'	16°	35	48,15	27,4
	118	1,353	3,44	0,225	0,735	0,55	0,55	1,12	9°	0°	10°36'	4°30'	57,5	55,65	3,33
	119	1,377	3,44	0,225	0,735	0,55	0,55	1,16	12°	0°	11°12'	6°	51	53,87	5,32
120	1,656	3,44	0,225	0,735	0,55	0,55	1,2	16°	0°	11°20'	8°	40	42,3	5,43	
121	1,844	3,44	0,225	0,735	0,55	0,55	1,26	20°	0°	23°06'	0°	31	41	24,4	
122	2,045	3,44	0,225	0,735	0,55	0,55	1,31	24°	0°	27°24'	12°	30	42,9	30	
123	2,24	3,44	0,225	0,735	0,55	0,55	1,36	28°	0°	31°42'	14°	32	46,7	31,5	
124	2,47	3,44	0,225	0,735	0,55	0,55	1,42	32°	0°	35°48'	16°	41	50,5	18,8	
125	1,384	4	0,2	0,735	0,6	0,6	1,12	9°	0°	11°18'	4°30'	55	53,4	3,0	
126	1,41	4	0,2	0,735	0,6	0,6	1,16	12°	0°	12°12'	6°	49	51,8	5,4	
127	1,715	4	0,2	0,735	0,6	0,6	1,2	16°	0°	20°36'	8°	39	41,8	6,7	
128	1,92	4	0,2	0,735	0,6	0,6	1,26	20°	0°	24°36'	10°	35	40,8	14,2	
129	2,14	4	0,2	0,735	0,6	0,6	1,31	24°	0°	29°36'	12°	35	44,6	21,5	
[Л. 3]															

Table A-2 (Cont'd.).

Author	λ	n	$\frac{D_{1cp}}{l}$	\bar{t}	\bar{L}	\bar{d}_1	\bar{d}_2	α_1	α_2	α_3	θ	$\zeta_{п.экс}$	[Л. 34] $\zeta_{п.расч}$	$\Delta\zeta_{п.}\%$
	130	2,36	4	0,2	0,735	0,6	1,36	28°	0°	0°	14°	37,5	48,5	22,7
	131	2,6	4	0,2	0,735	0,6	1,42	32°	0°	0°	16°	42	53,5	21,5
	132	1,458	5,25	0,16	0,735	0,68	1,12	9°	0°	0°	4°30'	52	49,1	5,9
	133	1,49	5,25	0,16	0,735	0,68	1,16	12°	0°	0°	6°	45	47,5	5,47
	134	1,85	5,25	0,16	0,735	0,68	1,2	16°	0°	0°	8°	39	40,9	4,65
	135	2,095	5,25	0,16	0,735	0,68	1,25	20°	0°	0°	10°	34	43,6	22
	136	2,355	5,25	0,16	0,735	0,68	1,31	24°	0°	0°	12°	37,5	48,1	22
	137	2,62	5,25	0,16	0,735	0,68	1,36	28°	0°	0°	14°	41	53,9	24
	138	2,91	5,25	0,16	0,735	0,68	1,42	32°	0°	0°	16°	48	—	—
	139	1,592	7	0,125	0,735	0,75	1,12	9°	0°	0°	16°	48	—	—
	140	1,6	7	0,125	0,735	0,75	1,16	12°	0°	0°	4°30'	48	41,9	6,9
	141	2,045	7	0,125	0,735	0,75	1,2	16°	0°	0°	6°	42,5	43,8	2,16
	142	2,045	7	0,125	0,735	0,75	1,26	20°	0°	0°	8°	38	43	11,5
	143	2,66	7	0,125	0,735	0,75	1,31	24°	0°	0°	10°	38	48,2	21,2
	144	2,99	7	0,125	0,735	0,75	1,36	28°	0°	0°	12°	45	55,1	18,4
	145	3,34	7	0,125	0,735	0,75	1,42	32°	0°	0°	14°	50	—	—
	146	1,885	9	0,125	0,735	0,75	1,42	32°	0°	0°	16°	60	—	—
	147	1,945	9	0,1	0,735	0,8	1,12	9°	0°	0°	4°30'	47	40,8	15,2
	148	3,11	9	0,1	0,735	0,8	1,16	12°	0°	0°	6°	40	41,3	3,15
	149	4,14	9	0,1	0,735	0,8	1,26	20°	0°	0°	10°	48	—	—
	150	4,69	9	0,1	0,735	0,8	1,36	28°	0°	0°	14°	62,5	—	—
	151	2	3,4	0,225	1,72	0,55	1,42	32°	0°	0°	16°	72	—	—
	152	2	3,4	0,225	0,85	0,55	1,303	10°	0°	0°	5°	29,5	29,5	0
							1,303	20°	0°	0°	10°	31,5	38,75	18,7

[Л. 3]

[Л. 1] {

Table A-2 (Cont'd.).

Author	β	n	$\frac{D_{12}p}{l}$	T	Z	$\bar{\pi}_1$	$ \bar{\pi}_2 $	\bar{D}_2	α_1	α_2	α_3	δ	$\zeta_{n, \text{arc}}$	$ \bar{D}_1 $ % Facs	$A_{\alpha_1}^{\circ}, \%$
	153	2	3.44	0.225	0.57	0.55	0.55	1.303	30°	0°	33°48'	15°	38.5	48	19.8
	154	2	3.44	0.225	0.43	0.55	0.55	1.303	40°	0°	43°48'	20°	54.25	—	—
	155	2	3.44	0.225	0.33	0.55	0.55	1.303	50°	0°	55°24'	25°	71.9	—	—
	156	2	3.44	0.225	0.26	0.55	0.55	1.303	60°	0°	67°16'	30°	83.9	—	—
	157	2	3.44	0.225	0.22	0.55	0.55	1.303	70°	0°	76°16'	35°	90.25	—	—
	158	2	3.44	0.225	0.18	0.55	0.55	1.303	80°	0°	87°36'	40°	92.5	—	—
	159	3, 8	3.44	0.225	4.68	0.55	0.55	1.72	10°	0°	11°	5°	29.2	16, 68	75
	160	3, 8	3.14	0.225	2.0	0.55	0.55	1.72	20°	0°	22°24'	10°	32	35, 63	10, 2
	161	3, 8	3.14	0.225	2.0	0.55	0.55	1.72	20°	0°	22°48'	15°	38.5	55, 73	31
	162	3, 8	3.44	0.225	1.0	0.55	0.55	1.72	40°	0°	43°12'	20°	53.4	—	—
	163	3, 8	3.44	0.225	0.77	0.55	0.55	1.72	50°	0°	54°30'	25°	70.6	—	—
	164	3, 8	3.44	0.225	0.62	0.55	0.55	1.72	60°	0°	65°14'	30°	82.3	—	—
	165	3, 8	3.44	0.225	0.51	0.55	0.55	1.72	70°	0°	75°48'	35°	88.8	—	—
	166	3, 8	3.44	0.225	0.43	0.55	0.55	1.72	80°	0°	85°12'	40°	91	—	—
[11. 1]	167	2	3.44	0.225	2.57	0.55	0.325	1.225	5°	-5°	7°40'	5°	28.75	28, 25	1, 77
	168	2	3.44	0.225	1.28	0.55	0.325	1.225	10°	-10°	15°24'	10°	28.8	32	10
	169	2	3.44	0.225	0.85	0.55	0.325	1.225	15°	-15°	23°	15°	31.5	38, 75	18, 7
	170	2	3.44	0.225	0.64	0.55	0.325	1.225	20°	-20°	30°12'	20°	37	45, 5	18, 7
	171	2	3.44	0.225	0.51	0.55	0.325	1.225	25°	-25°	37°36'	25°	43.75	50, 2	17, 8
	172	2	2.44	0.225	0.42	0.55	0.325	1.225	30°	-30°	44°48'	30°	52	—	—
	173	2	3.44	0.225	0.36	0.55	0.325	1.225	35°	-35°	51°24'	35°	58	—	—
	174	2	3.44	0.225	0.31	0.55	0.325	1.225	50°	-40°	58°20'	40°	62.5	—	—

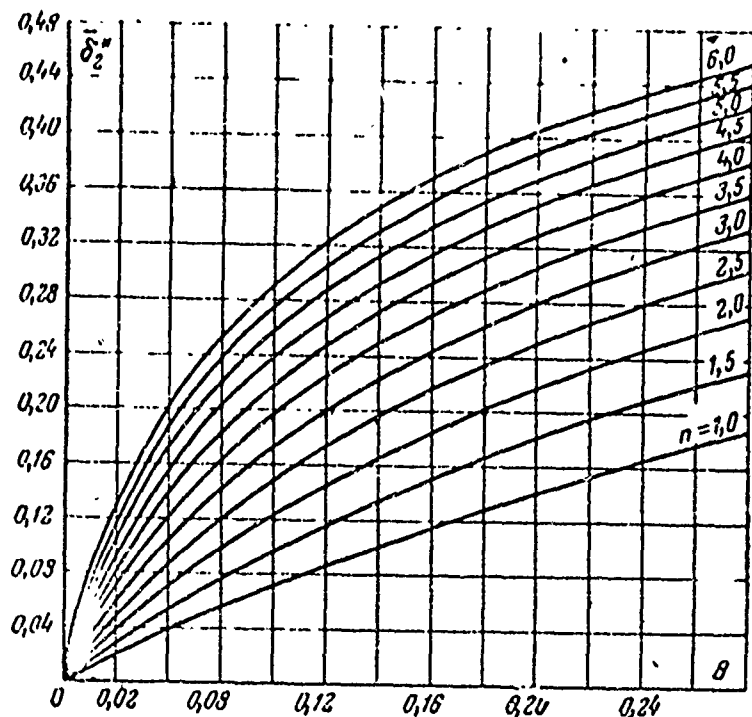


Fig. A-1. Nomogram for calculation of δ_2^* by formula (3-15).

Fig. A-2. Nomogram for calculation of $\bar{\Delta}_2^*$ by formula (3-18).

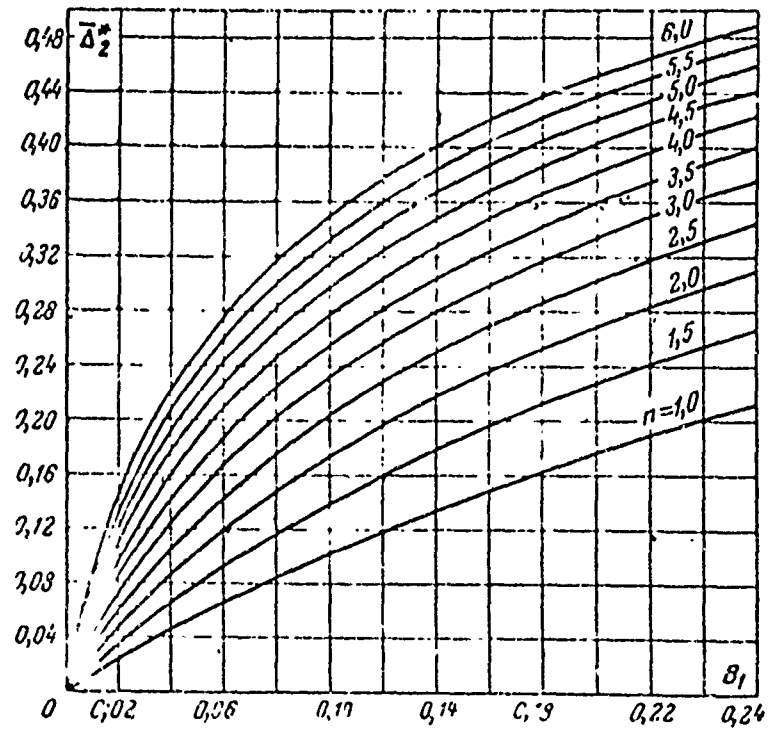
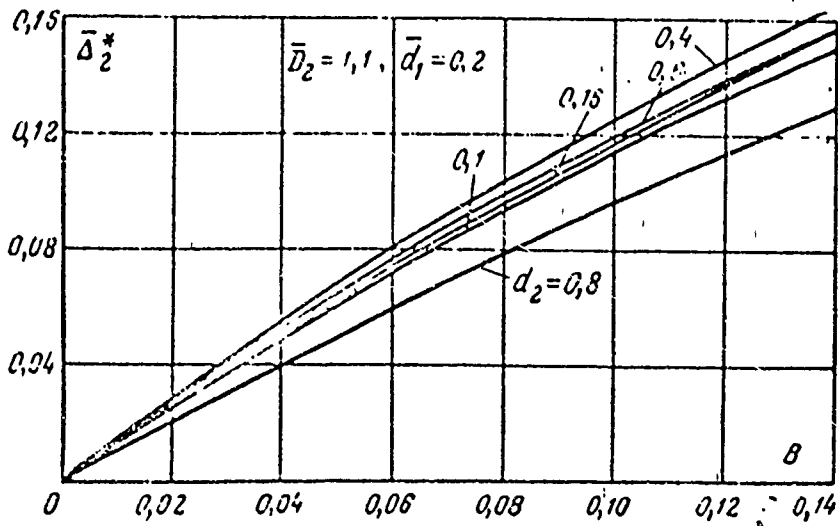
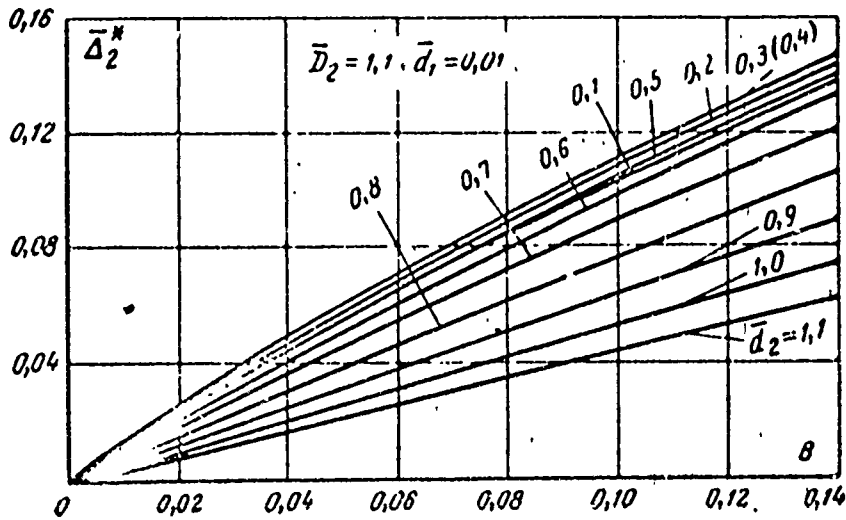
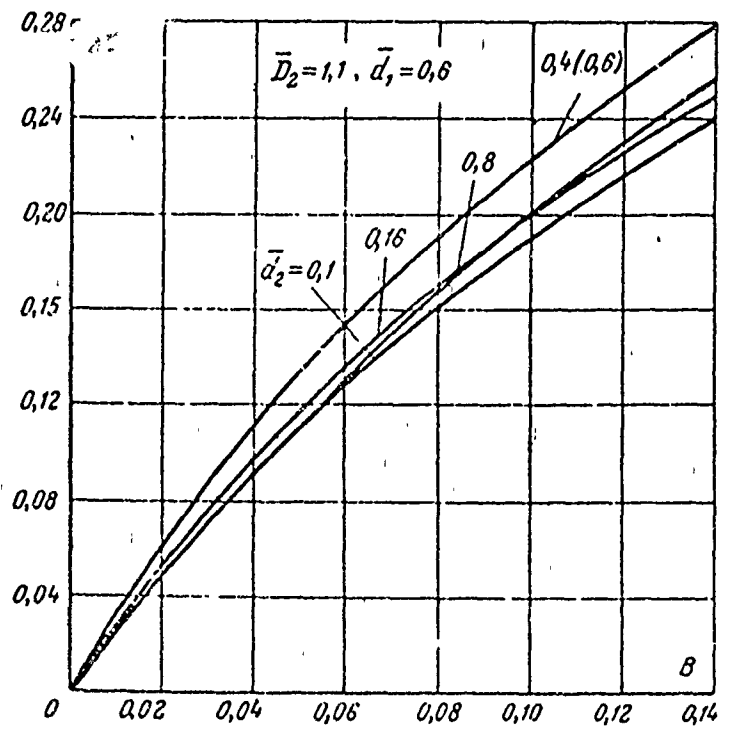
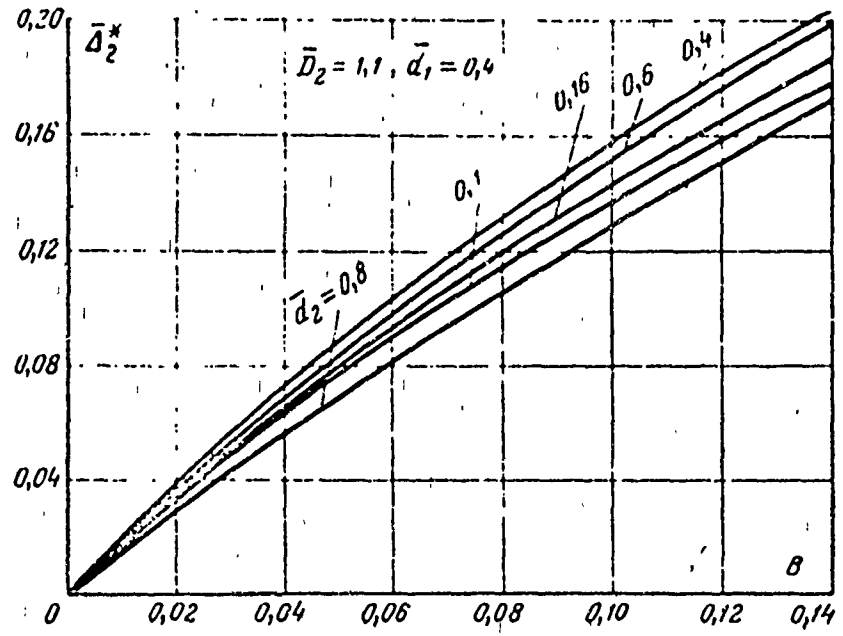
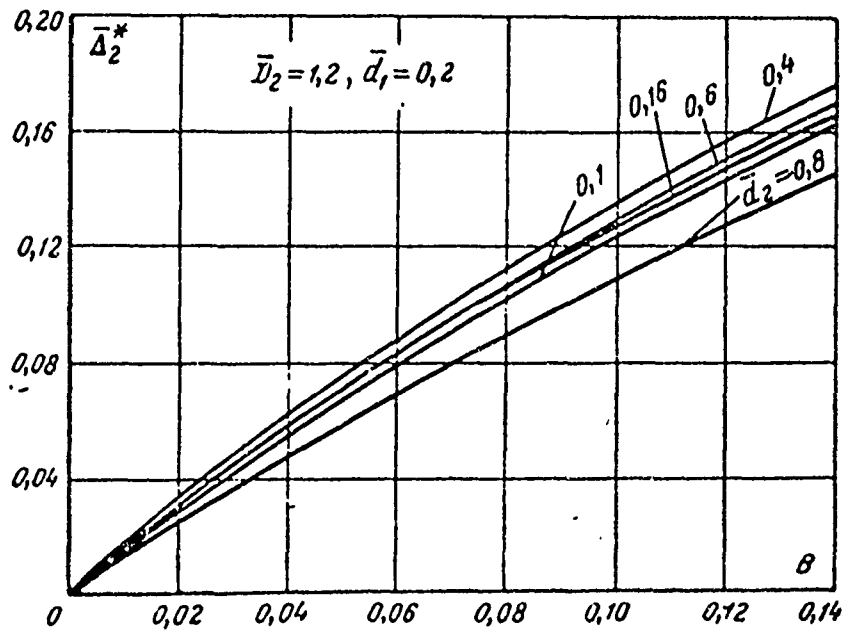
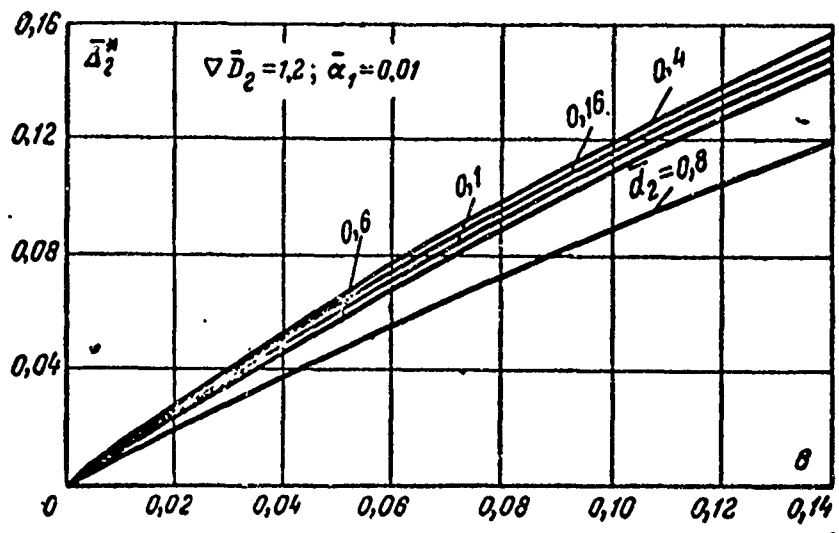
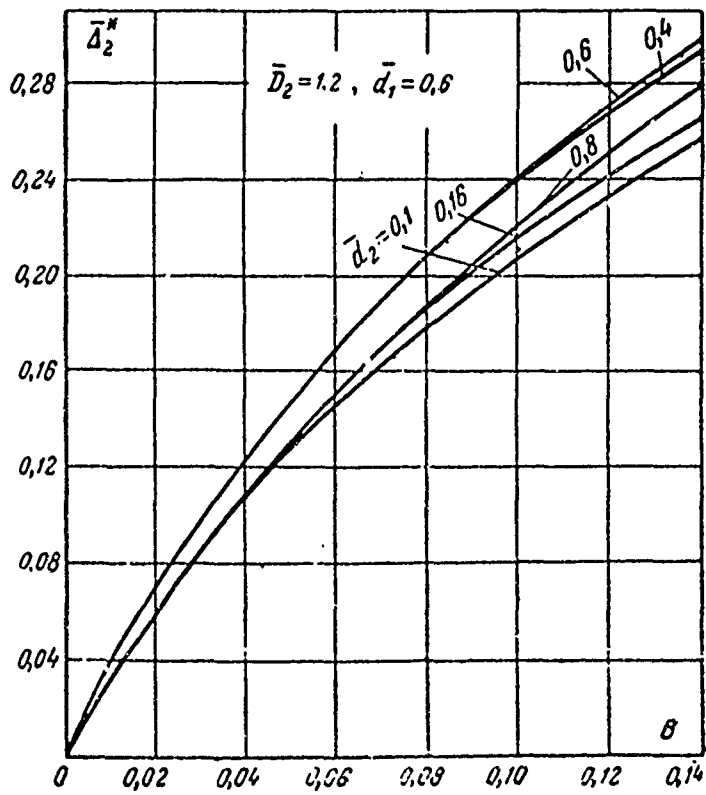
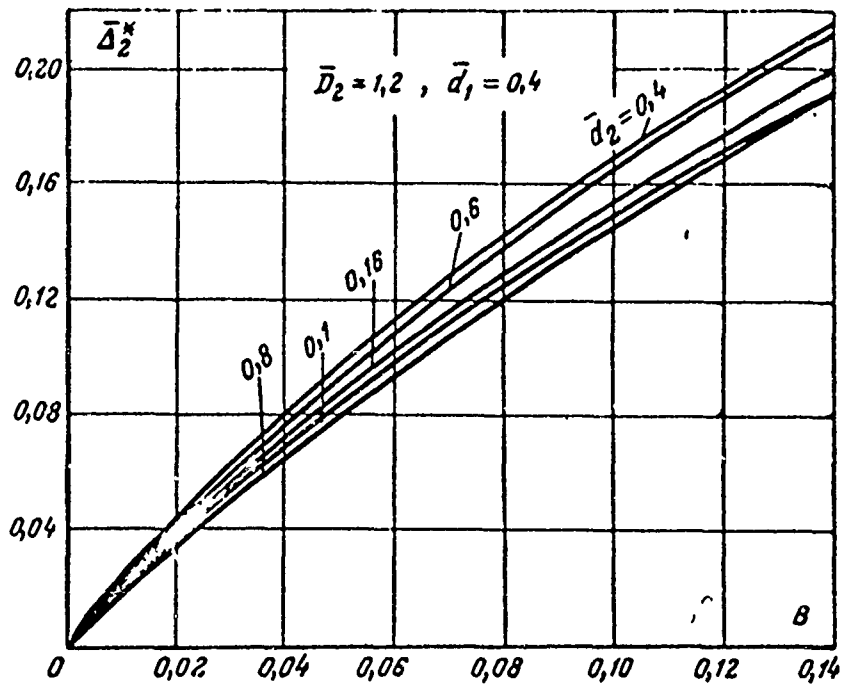


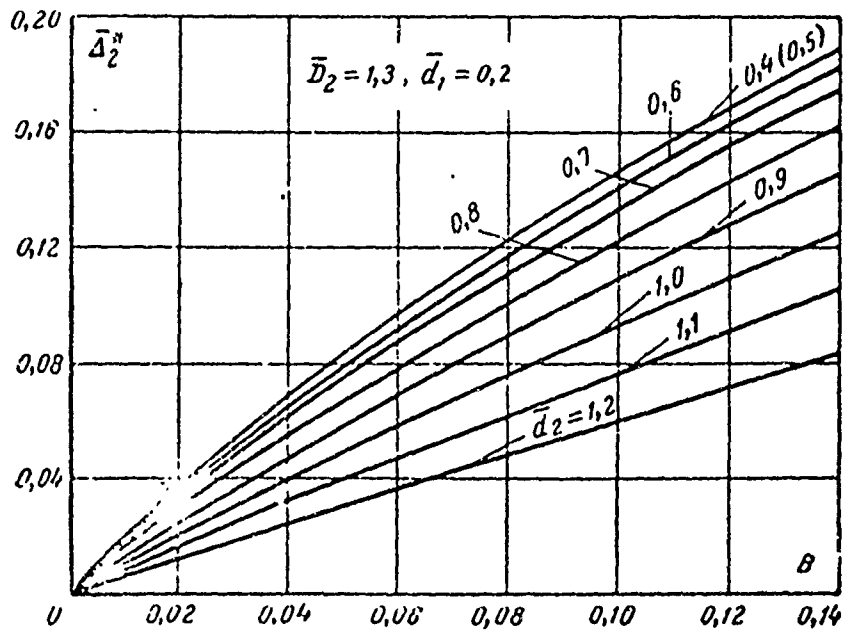
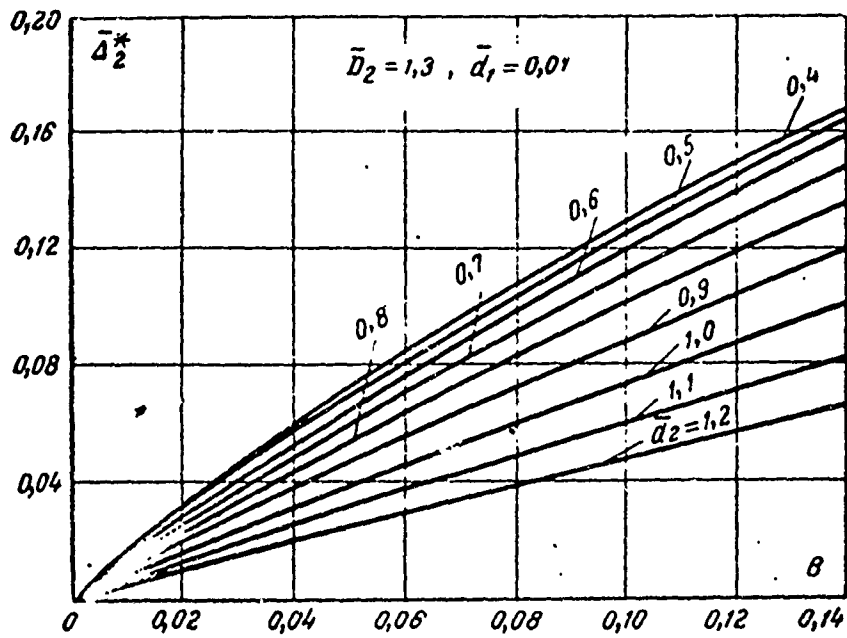
Fig. A-3. Nomograms for calculation of Δ_2^* by formula (5-10).

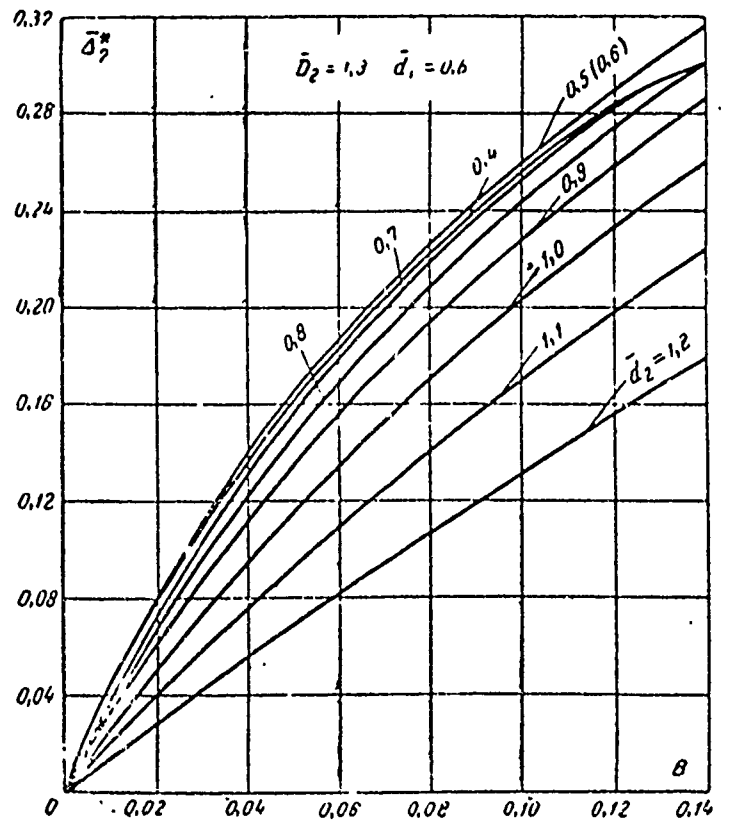
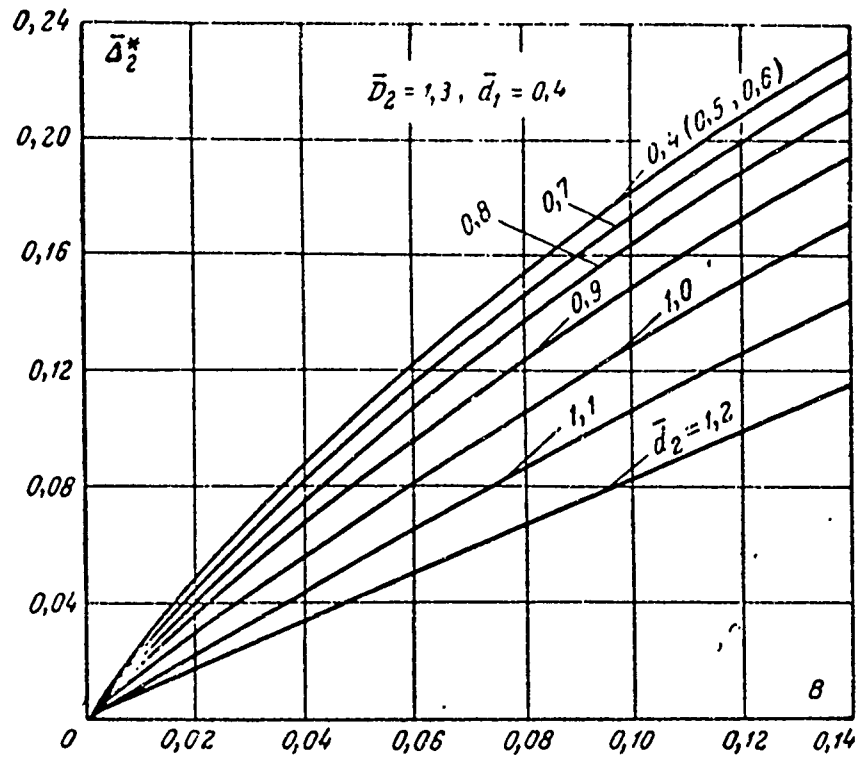


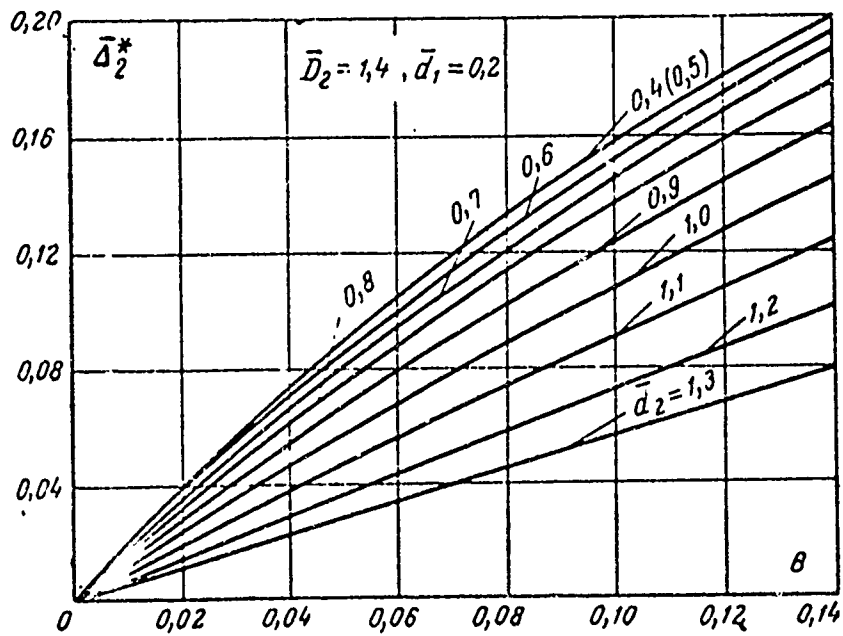
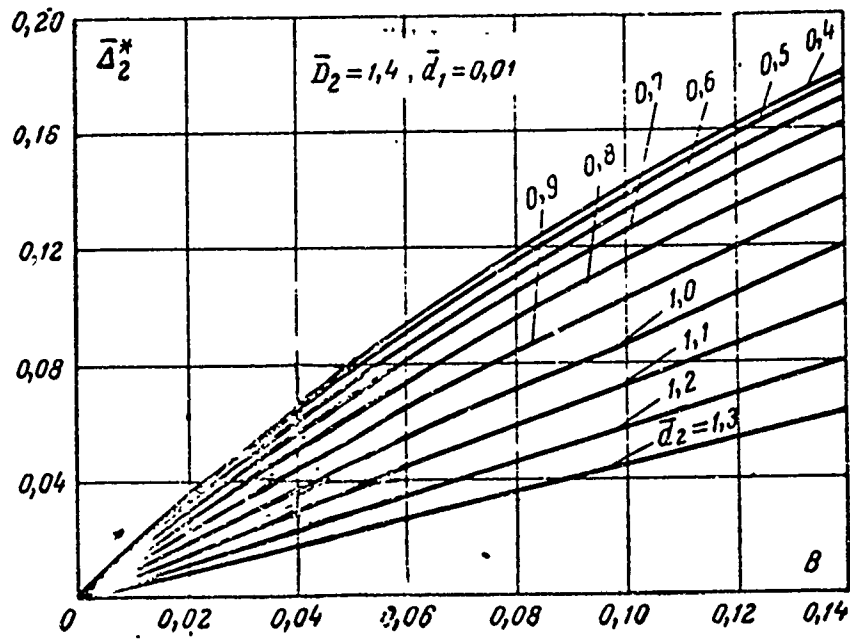


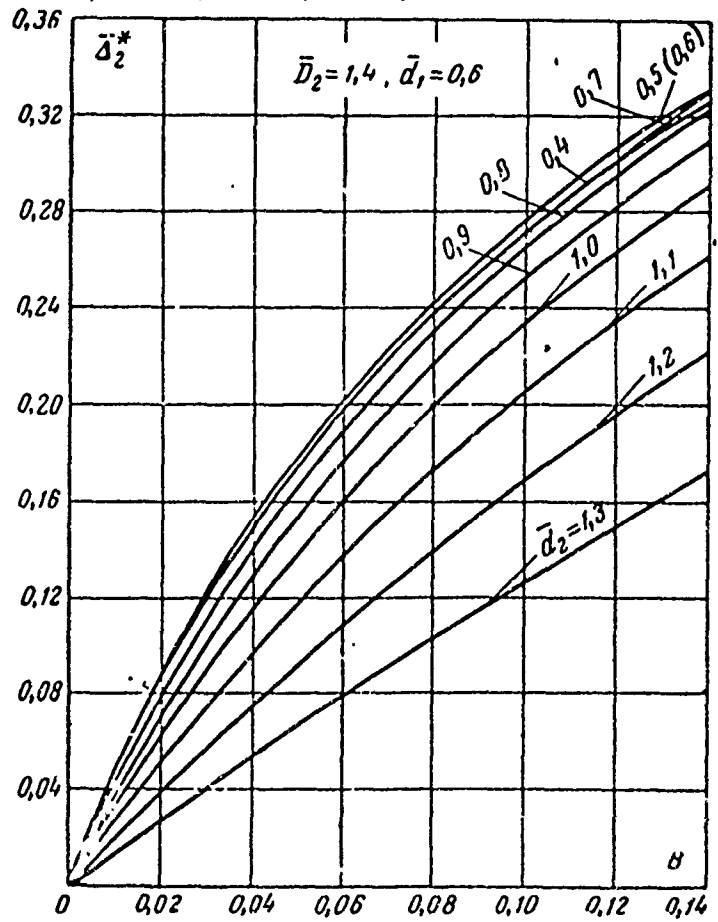
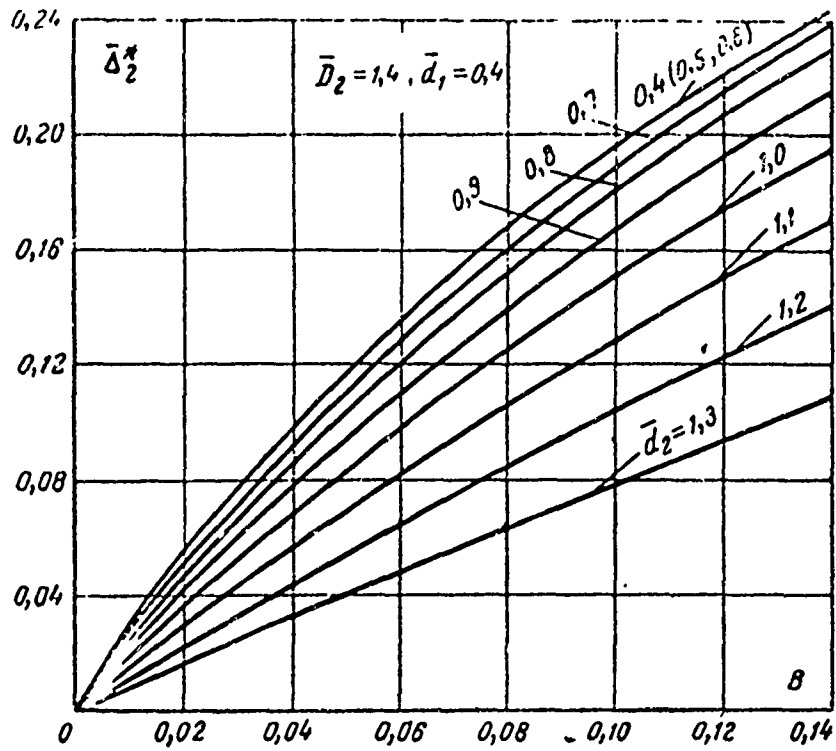


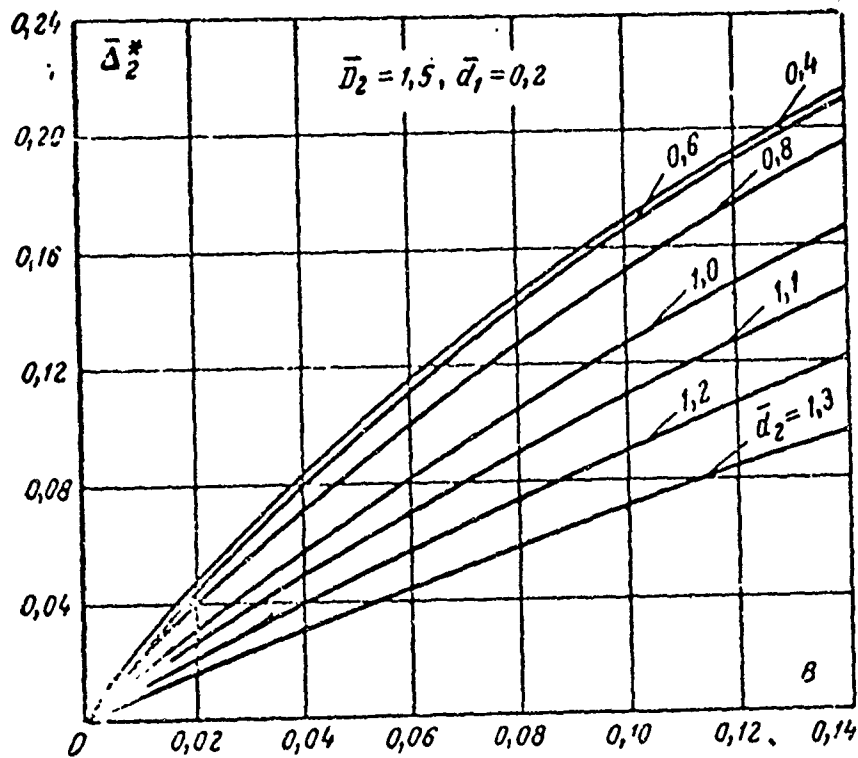
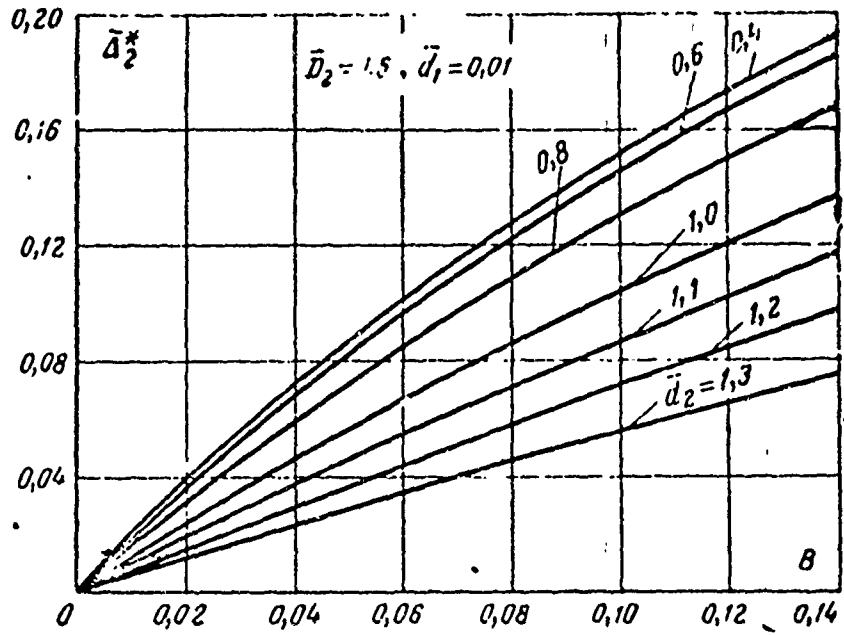


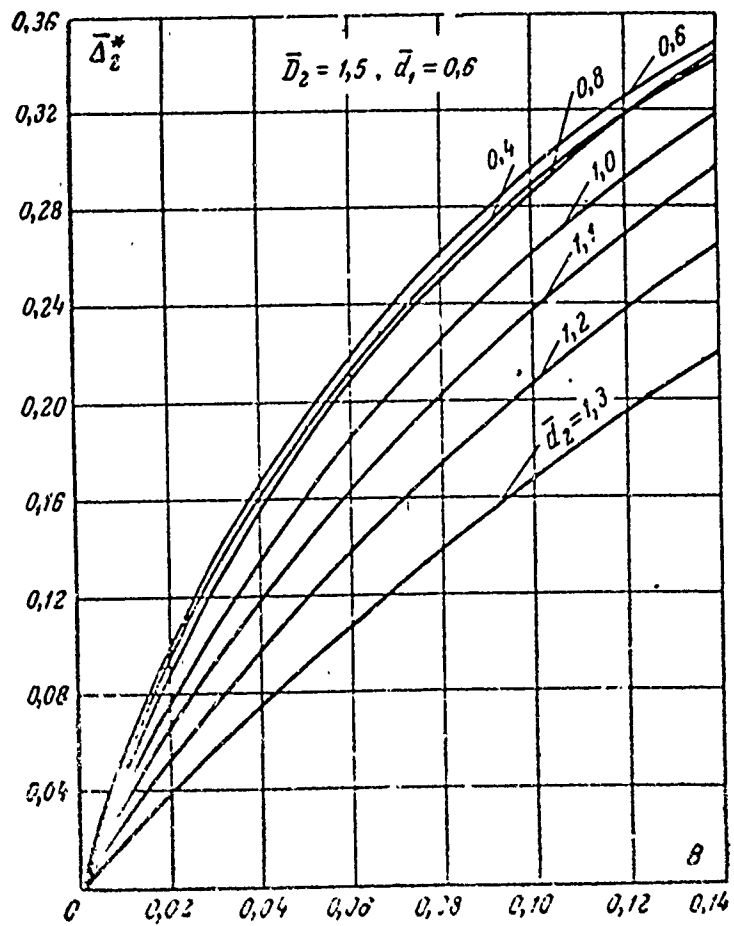
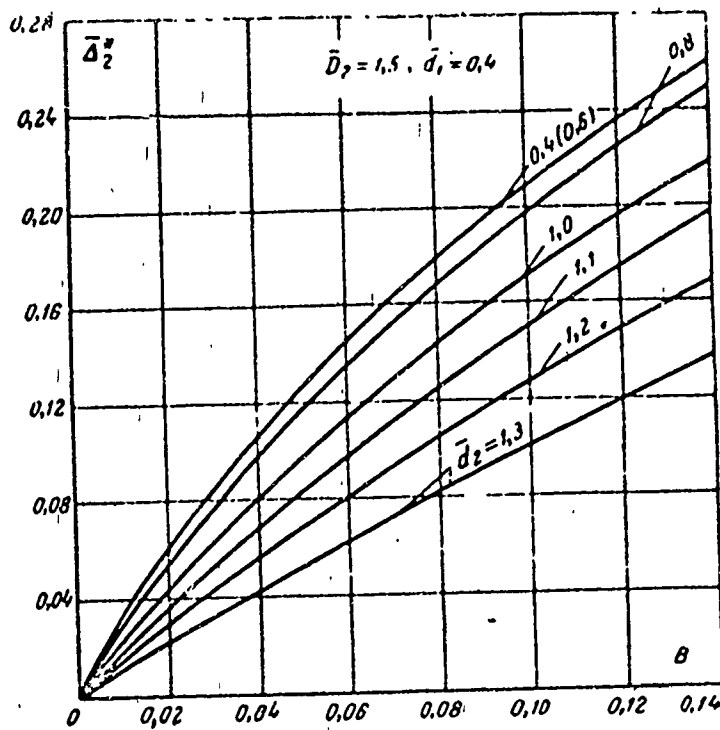


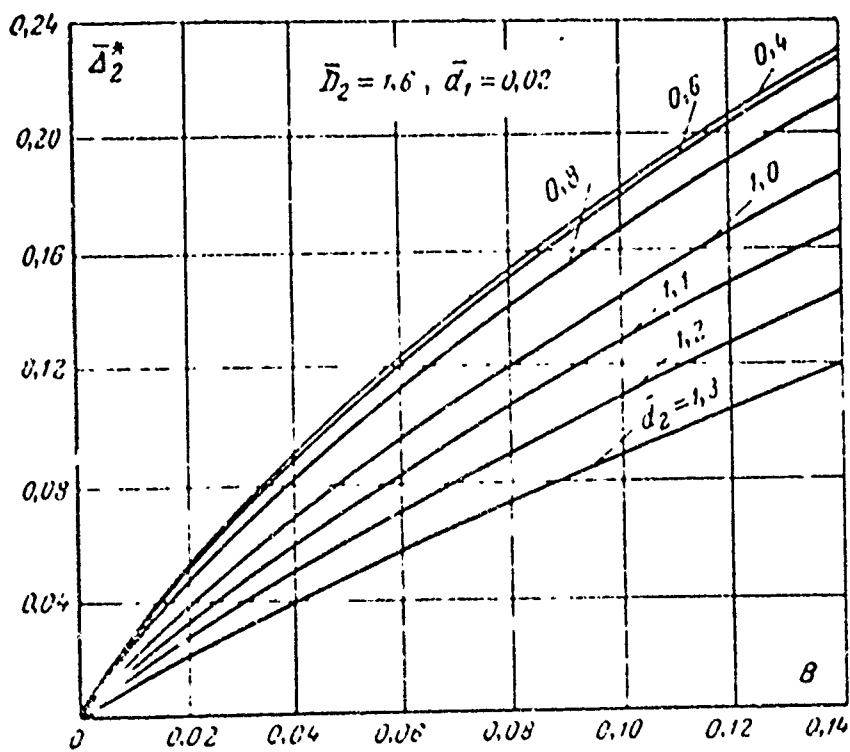
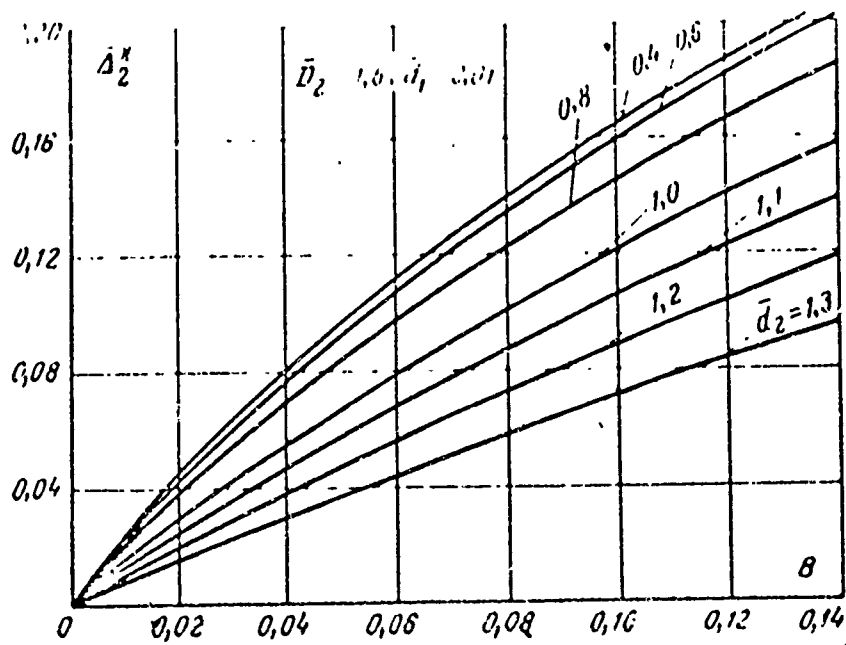


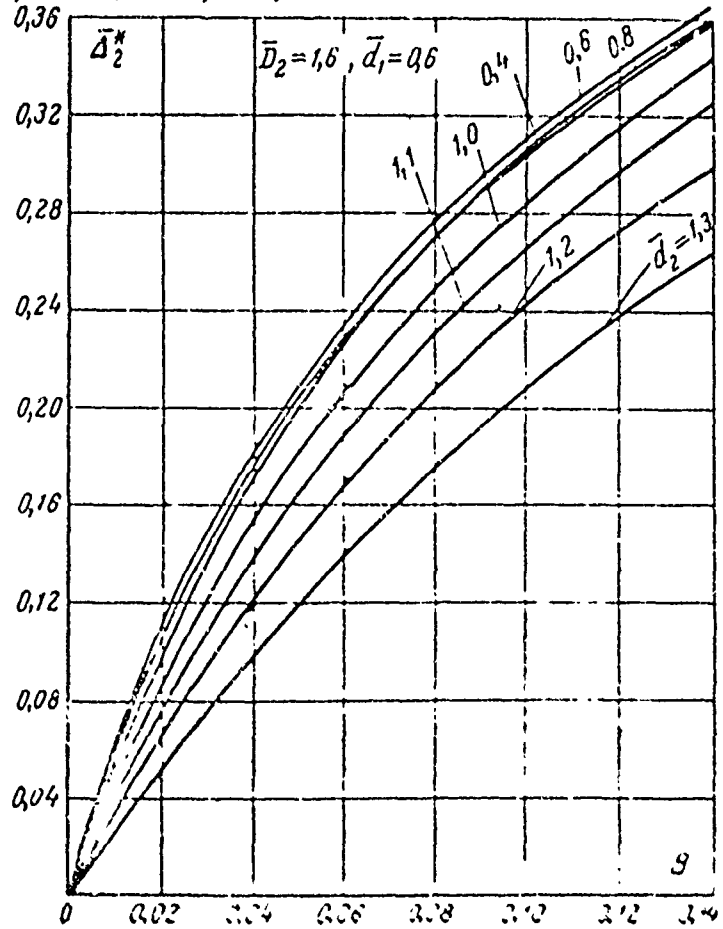
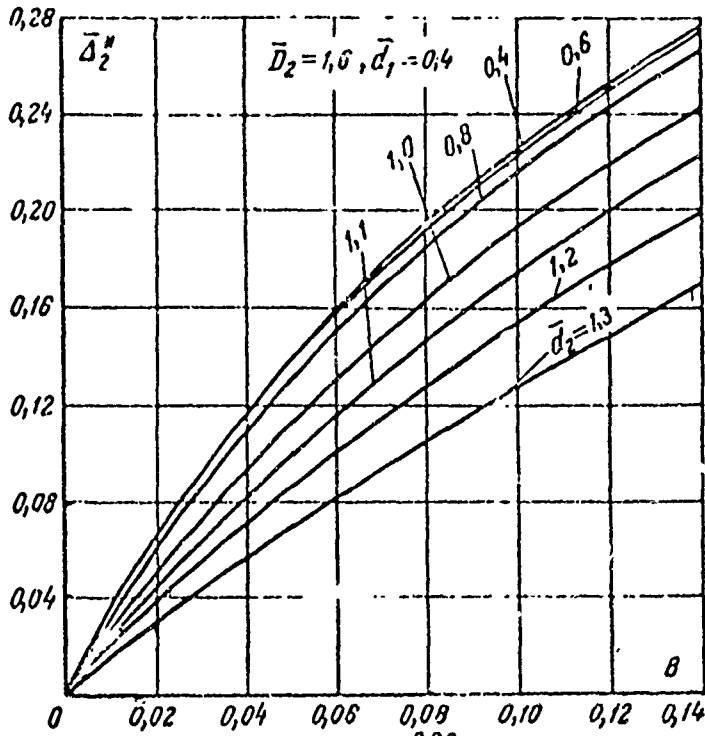


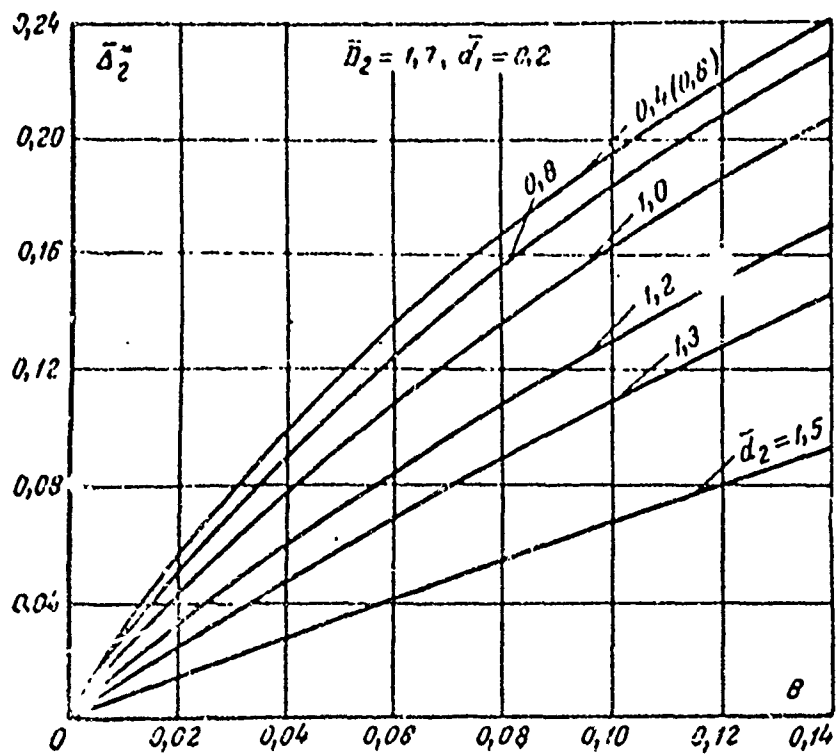
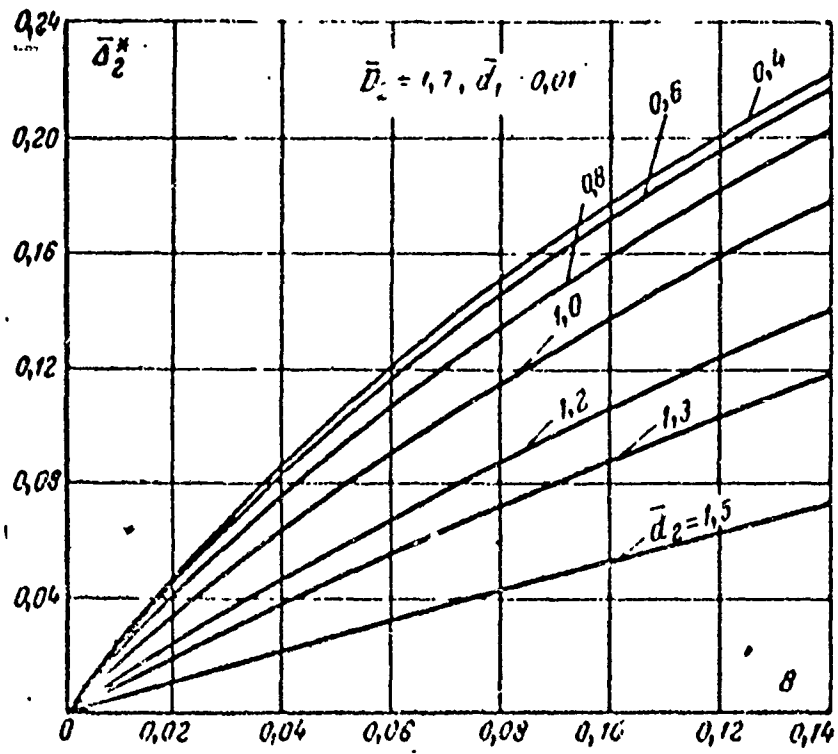


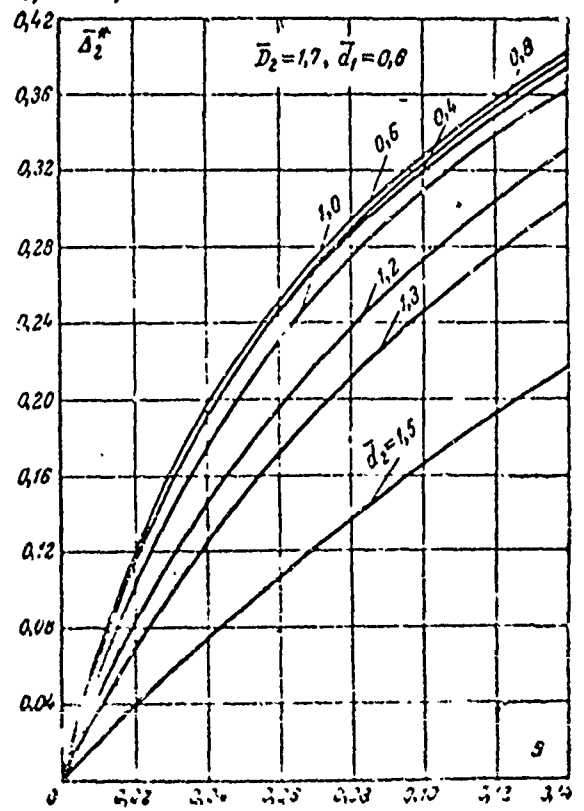
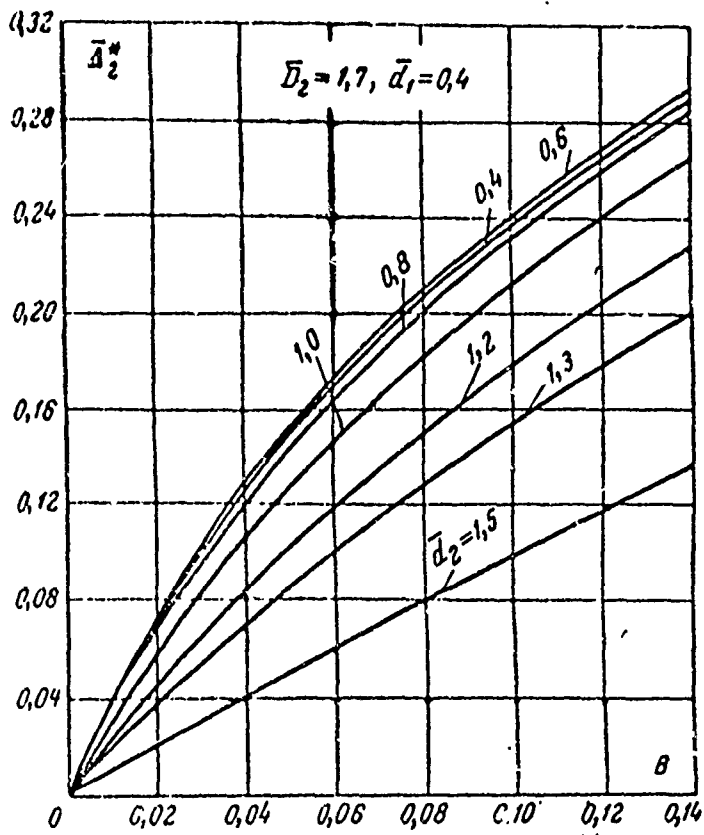


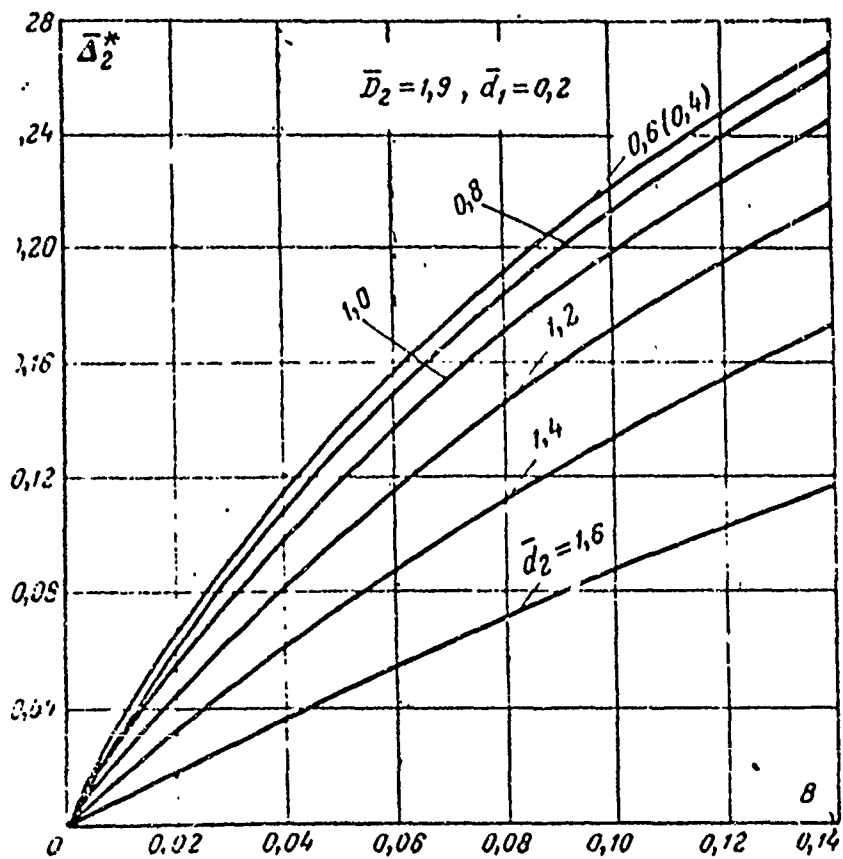
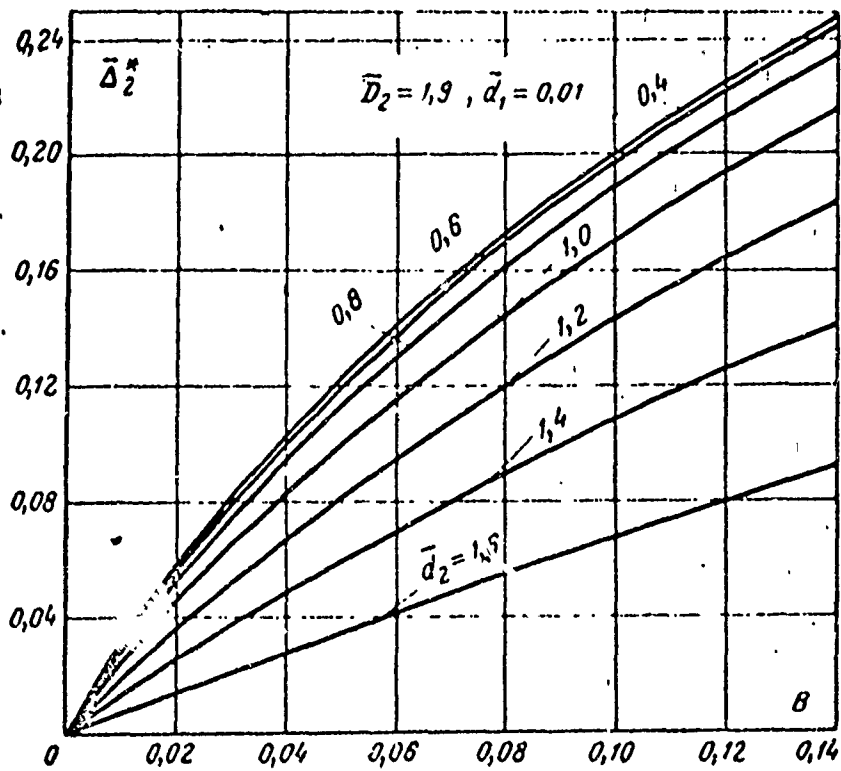




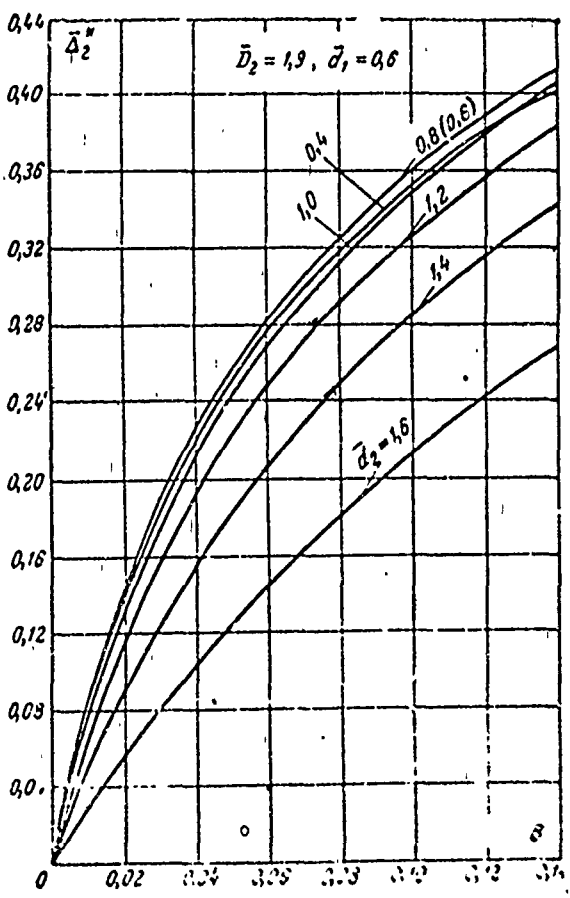
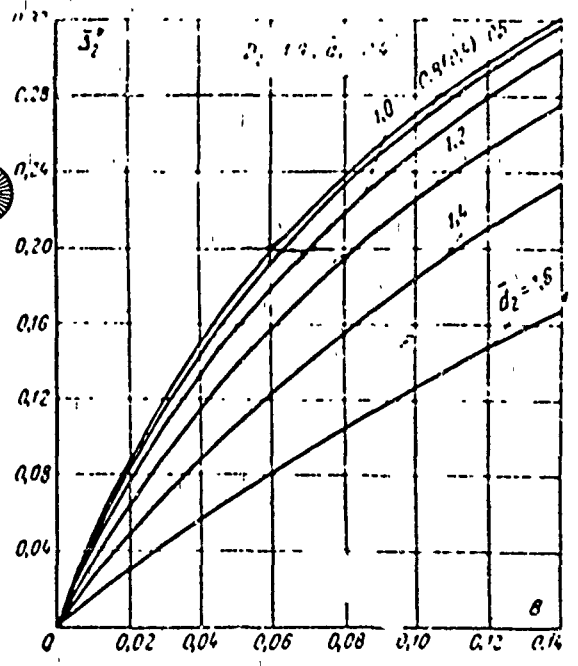


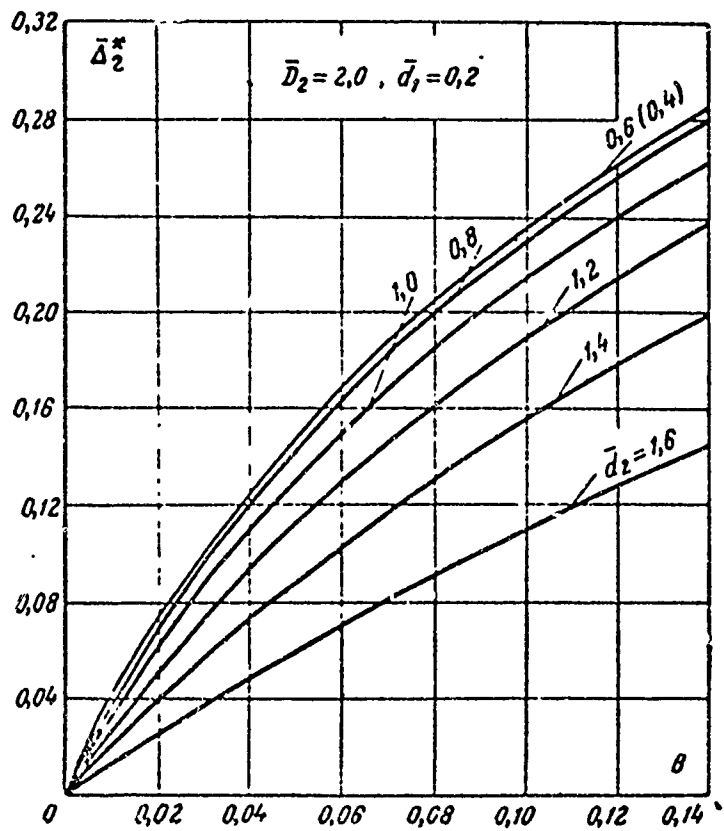
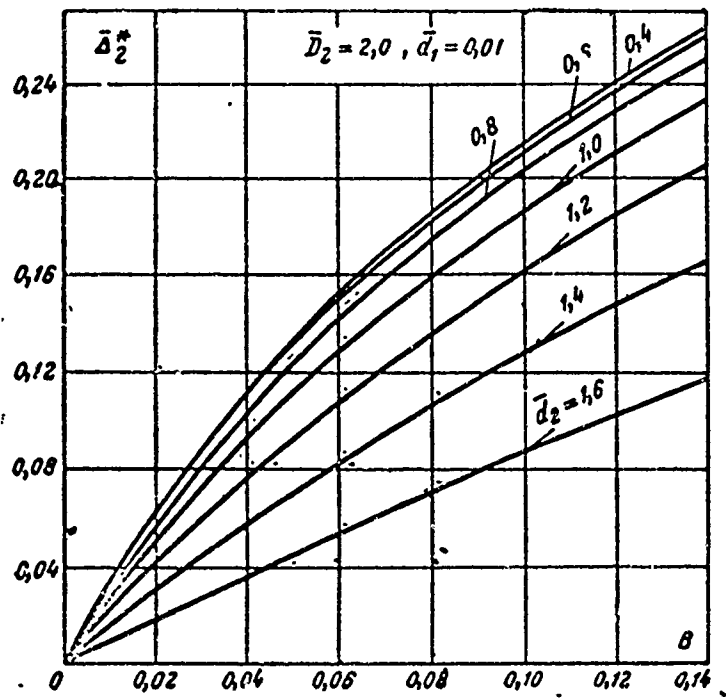






Reproduced from
best available copy.





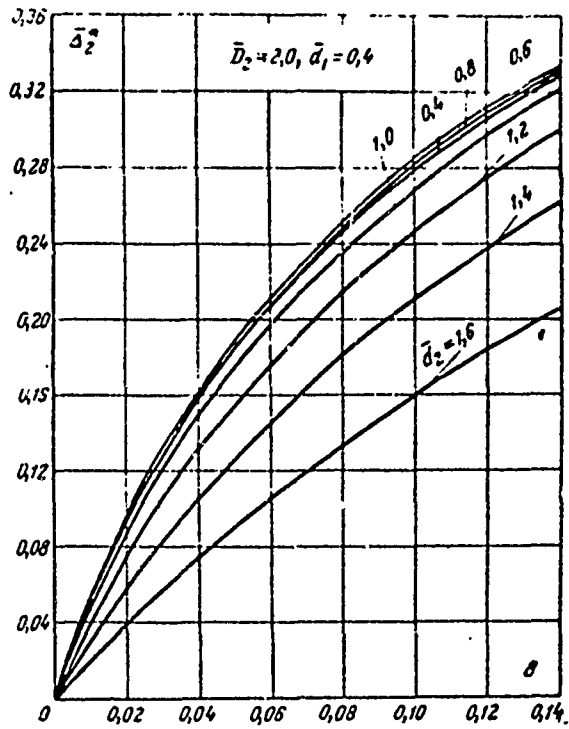
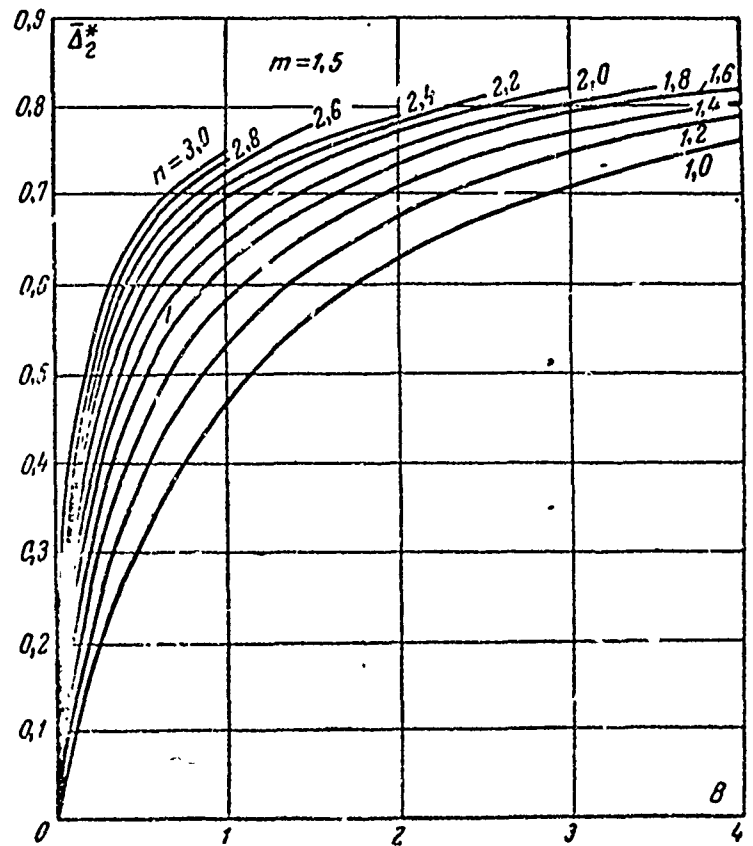


Fig. A-4. Nomograms
 for calculation of
 $\bar{\Delta}_2^*$ by formula
 (6-4).



BIBLIOGRAPHY

1. Абрамович С. Ф., Васильев Л. Г., Исследование кольцевых диффузоров судовых газотурбинных установок, «Судостроение», 1963, № 3.
2. Абрамович С. Ф., Самсонов Е. Ф., Исследование работы судовых турбин с диффузорами, «Судостроение», 1967, № 3.
3. Амелюшкин В. П., Уманский М. П., Влияние закрутки потока на эффективность криволинейного диффузора, «Энергомашинностроение», 1963, № 12.
4. Бай Шн-й, Турбулентное течение жидкостей и газов, Изд-во иностр. лит., 1962.
5. Бам-Зеликович Г. М., Расчет отрыва пограничного слоя, Изв. АН СССР, ОТН, 1954, № 12.
6. Бекнев В. С., Расчет осесимметричного патрубка с кольцевыми разделительными лопатками, «Теплоэнергетика», 1967, № 4.
7. Биндлер И. А., Исследование кольцевых диффузоров с криволинейной осью. Автореферат диссертации, 1948.
8. Богомазов Р. П., Дорфман Л. А., Из опыта исследования и отработки патрубков осевых турбомашин, «Энергомашинностроение», 1961, № 1.
9. Бушель А. Р., Исследование коротких радиальных и комбинированных диффузоров, «Промышленная аэродинамика», 1966, вып. 28.
10. Вирозуб П. Е., Дорфман Л. Ш., Об оптимальной форме диффузора, «Теплоэнергетика», 1962, № 6.
11. Винник П. Д., Уманский М. П., Черников В. А., Некоторые результаты аэродинамического исследования выходного патрубка транспортного двигателя, «Энергомашинностроение», 1959, № 4.
12. Волкова Л. П., Юделович М. Я., Потери на удар в ступенчатых трубах при сверхзвуковых отношениях давлений, Изв. АН СССР, ОТН, 1958, № 4.
13. Врублевская В. А., О влиянии начальной степени турбулентности потока на характеристики направляющих и рабочих решеток турбин, «Теплоэнергетика», 1960, № 2.
14. Врублевская В. А., К вопросу о влиянии турбулентности внешнего потока на турбулентный пограничный слой, Изв. вузов, «Энергетика», 1960, № 7.

15. Ведерников А. И., Труды ЦАГИ, 1926, вып. 21.
16. Герман Г., Сверхзвуковые диффузоры, Изд-во иностр. яз., 1961.
17. Гиневский А. С., О расчете гидравлического сопротивления каналов, ИФЖ, 1965, № 4.
18. Гиневский А. С., Изв. АН СССР, ОТН, 1956, № 3.
19. Гиневский А. С., Расчет потерь в расширяющихся и суживающихся каналах, сб. «Промышленная аэродинамика», 1956, вып. 7.
20. Голубев В. В., Труды по аэродинамике, Гостехиздат, 1957.
21. Головина Л. Г., Влияние геометрических и режимных параметров на характеристики конических диффузоров, Автореферат диссертации, МЭИ, 1967.
22. Гуревич Д. В., Экспериментальное исследование диффузорных выпускных трактов вертолетных ТВД, сб. «Силовые установки вертолетов», Оборонгиз, 1959.
23. Гукасова Е. А., Жуковский М. И., Завадовский А. М., Зыкина-Моложен Л. М., Скляр И. А., Тырышкин В. Г., Аэродинамическое совершенствование лопаточных аппаратов паровых и газовых турбин, Госэнергоиздат, 1960.
24. Гурженко Е. А., Об установившемся турбулентном течении в конических диффузорах с малым углом раскрытия, Труды ЦАГИ, 1, 1939, вып. 462.
- 24а. Гухман А. А., Гандельсман А. Ф., Кацнельсон Г. Г., Кадер Б. А., Науриц А. Н., Усанов В. В., О влиянии больших отрицательных градиентов давления на структуру турбулентного потока, сб. «Тепло- и массоперенос», т. I, изд-во «Энергия», 1968.
25. Дейч М. Е., Техническая газодинамика, Госэнергоиздат, 1961.
26. Дейч М. Е., Самойлович Г. С., Основы аэродинамики осевых турбомашин, Машигиз, 1959.
27. Дейч М. Е., Трояновский Б. М., Исследование и расчет ступеней осевых турбин, Машигиз, 1964.
28. Дейч М. Е., Зарянкин А. Е., Зацепин М. Ф., Результаты испытаний выхлопных патрубков турбомашин с кольцевыми диффузорами, «Теплоэнергетика», 1965, № 5.
29. Дейч М. Е., Зарянкин А. Е., Зацепин М. Ф., Исследование выхлопных патрубков с косо срезанными диффузорами, «Теплоэнергетика», 1964, № 12.
- 29а. Дейч М. Е., Лазарев Л. Я., Исследование перехода турбулентного пограничного слоя в ламинарный, ИФЖ, 1961, № 4.
30. Дейч М. Е., Филиппов Г. А., Исследование ступеней турбин с кольцевыми диффузорами, «Теплоэнергетика», 1963, № 10.
31. Демидов С. А., Исследование течения и определение потерь полного давления в круглых, плоских и кольцевых диффузорах, Техн. отчет № 118, Институт имени Баранова, 1960.
32. Дементьев М. А., Чертков А. К., Гидромеханическое исследование вариантов выхлопного патрубка паровой турбины, «Когитурбостроение», 1948, № 1.

33. Дорфман А. Ш., Сайковский М. И., Определение оптимальной формы диффузора с произвольной средней линией при отрывном течении, ИФЖ, 1963, № 12.
34. Дорфман А. Ш., Назарчук М. М., Польский Н. И., Сайковский М. И., Аэродинамика диффузоров и выхлопных патрубков турбомашин, Изд-во АН УССР, 1960.
35. Дорфман А. Ш., Назарчук М. М., Польский Н. И., Сайковский М. И., О расчете потерь в диффузорах, ИФЖ, 1965, № 4.
36. Дорфман А. Ш., Сайковский М. И., Диденко О. И., Степаненко А. П., Результаты аэродинамической обработки моделей патрубков газотурбинной установки ГТ-6-750, «Энергомашиностроение», 1965, № 2.
37. Дорфман А. Ш., К вопросу расчета потерь полного давления в диффузорных каналах, «Энергомашиностроение», 1966, № 8.
38. Дорфман А. Ш. и др., Влияние угла раскрытия на эффективность криволинейных кольцевых диффузоров, Изв. вузов, «Энергетика», 1967, № 8.
39. Дорфман А. Ш. и др., Расчет кольцевых диффузоров турбомашин и определение потерь в них, «Энергомашиностроение», 1968, № 5.
- 39а. Дьяконов Р. И., Кузьмичев Р. В., Дроконов А. М., Отработка конструкции выходного патрубка газовой турбины, «Энергетическое машиностроение», 1969, № 8.
40. Довжик С. А., Гиневский А. С., Экспериментальное исследование напорных патрубков стационарных турбомашин, Отчет № 130 ЦАГИ, 1955.
41. Довжик С. А., Морозов А. И., Исследование кольцевых диффузоров осевых турбомашин, сб. «Промышленная аэродинамика», 1961, вып. 20.
42. Зарянкин А. Е., Зацепин М. Ф., Результаты исследования конических и кольцевых диффузоров, Труды МЭИ, 1963, вып. 47.
43. Зарянкин А. Е., О вихревых течениях в плоских диффузорах, Труды МЭИ, 1963, вып. 47.
44. Зарянкин А. Е., О методике интегральных испытаний диффузоров и выхлопных патрубков, «Теплоэнергетика», 1962, № 3.
45. Зарянкин А. Е., К вопросу о расчете потерь в диффузорных элементах, ИФЖ, 1965, № 4.
46. Зарянкин А. Е., Зацепин М. Ф., Некоторые результаты обработки выхлопных патрубков турбин, Изв. вузов, «Энергетика», 1965, № 11.
47. Зарянкин А. Е., Кругленков А. А., Исследование выхлопных патрубков конденсационных паровых турбин, «Теплоэнергетика», 1963, № 2.
48. Зарянкин А. Е., Зацепин М. Ф., Результаты исследований конических и кольцевых диффузоров, Труды МЭИ, 1963, вып. 47.
49. Зарянкин А. Е., Шерстюк А. И., Радиально-осевые турбины малой мощности, Машиз, 1963.

50. Зарянкин А. Е., Зацекин М. Ф., Шах Р. К. Д., Влияние симметрических параметров на работу кольцевых осесимметричных диффузоров, «Теплоэнергетика», 1966, № 7.
51. Зарянкин А. Е., Головина Л. Г., Этт В. В., Влияние режимных параметров на характеристики конических диффузоров, «Теплоэнергетика», 1967, № 4.
52. Зарянкин А. Е., Головина Л. Г., Этт В. В., Исследование течения вблизи угловой точки, Сб. докладов научно-технической конференции МЭИ, секция энергомашиностроения, 1967.
53. Зарянкин А. Е., Дыскин Л. М., Этт В. В., О возможных путях снижения гидравлических сопротивлений выхлопных патрубков транспортных ГТУ, Сб. докладов научно-технической конференции МЭИ, секция энергомашиностроения, 1967.
54. Идельчик И. Е., Гидравлические сопротивления, Госэнергоиздат, 1954.
55. Идельчик И. Е., Аэродинамика потока и потери напора в диффузорах, сб. «Промашроаэродинамика», Госэнергоиздат, 1947.
56. Карлсон, Джонстон, Сейджи, Влияние формы стенки на режимы течения и характеристики плоских диффузоров, Труды американского общества инженеров-механиков (Trans of ASME) — (русский перевод), серия Д («Теоретические основы инженерных расчетов»), 1967, № 1.
57. Кириллов И. И., Теория турбомашин, Машгиз, 1964.
58. Кириллов И. И., Аэродинамика проточной части паровых и газовых турбин, Машгиз, 1958.
59. Кириллов И. И., Гоголев И. Г., Дьяконов Р. Н., Климов А. А., Аэродинамическое исследование выходного патрубка газовой турбины, Изв. вузов, «Энергетика», 1961, № 8.
60. Кондак Н. М., Исследование кольцевых поворотов для выхлопных патрубков паровых турбин, Автореферат диссертации, Киев, 1952.
61. Константинов Н. И., Экспериментальное исследование турбулентного пограничного слоя с положительным перепадом давления, Труды ЛПИ, 1958, № 198.
62. Кочин Н. Е., Кибель И. А., Розе И. В., Теоретическая гидромеханика, ч. I, Гостехтеориздат, 1955.
63. Куниц, Развитие турбулентного пограничного слоя в кольцевых диффузорах, Труды американского общества инженеров-механиков (Trans of ASME) (русский перевод), серия «Д» («Теоретические основы инженерных расчетов»), 1965, № 2.
64. Лаврентьев Л. М., Шабат Б. В., Методы теории функций комплексного переменного, Госфизматгиздат, 1965.
65. Ландау Л. Д., Лифшиц Е. М., Механика сплошных сред, Гостехтеориздат, 1954.
66. Ланков А. И., Инженерный журнал, 1962, т. II, вып. II; Инженерный журнал, 1964, т. IV, вып. III.
67. Либби, Баронти, Наполитано, Исследование несжимаемого турбулентного пограничного слоя с градиентом давления, «Ракетная техника и космонавтика» (AIAA Joun.) (русский перевод), 1964, т. 2, № 3.
68. Лойцянский Л. Г., Ламинарный пограничный слой, Госфизматгиздат, 1962.

69. Лойцянский Л. Г., Механика жидкости и газа, Гостехтеориздат, 1957.
70. Лойцянский Л. Г., Аэродинамика пограничного слоя, Гостехтеориздат, 1941.
71. Марков Н. М., Расчет аэродинамических характеристик плоской решетки профилей осевых турбомашин, Машгиз, 1952.
72. Мельников А. П., Основы теоретической аэродинамики, Гостехтеориздат, 1963.
73. Морозов Д. И., Щекалкин В. М., Результаты улучшения выхлопного патрубка газовой турбины, «Теплоэнергетика», 1964, № 1.
74. Морозов Д. И., О наилучшей форме диффузора выхлопного патрубка турбины, Изв. вузов, «Энергетика», 1966, № 11.
75. Морозов Д. И., Повышение эффективности выхлопных патрубков турбин, «Энергомашиностроение», 1965, № 5.
76. Мигай В. К., Исследование оребренных диффузоров, «Теплоэнергетика», 1962, № 10.
77. Мигай В. К., Повышение эффективности диффузоров путем установки поперечного оребрения, «Теплоэнергетика», 1961, № 4.
78. Мигай В. К., О повышении эффективности диффузорных течений с отрывом, Изв. АН СССР, «Механика и машиностроение», 1960, № 4.
79. Меллор Д. Л., Джипсон Д. М., Равновесные турбулентные пограничные слои, «Механика» (сб. переводов), 1967, № 2.
80. Мозес, Чэппел, Исследование пограничного слоя в диффузорах с частичным отрывом течения (Труды американского общества инженеров-механиков (Trans of ASME), (русский перевод), серия «Д» («Теоретические основы инженерных расчетов»), 1967, № 3.
81. Носовицкий А. И., Амелюшкин В. Н., Наумчик Б. В., Работа выходного патрубка паровой турбины, «Энергомашиностроение», 1968, № 5.
82. Овчинников О. Н., Влияние входного профиля скоростей на работу диффузора, Труды ЛПИ, 1955, № 176.
83. Орлов И. И., Продувка моделей входного патрубка осевого компрессора, «Вестник машиностроения», 1954, № 6.
84. Прандтль Л., Гидроаэромеханика, Изд-во иностр. лит., 1949.
85. Полоцкий Н. Д., Результаты исследования потока в плоских кривоосных диффузорах, Труды ВИНМ, 1962, вып. 31.
86. Повх Н. Л., Аэродинамический эксперимент в машиностроении, Машгиз, 1965.
87. Ротта Н. К., Турбулентный пограничный слой в несжимаемой жидкости, изд-во «Судостроение», 1967.
88. Рено, Джонстон, Клайн, Характеристики и расчет плоских диффузоров с прямой осью, Труды американского общества инженеров-механиков (Trans of ASME) (русский перевод), серия «Д» («Теоретические основы инженерных расчетов»), 1967, № 1.
89. Рено, Джонстон, Метод определения характеристик плоских безотрывных диффузоров, Труды американского общества инженеров-механиков (Trans. of ASME) (русский перевод), серия «Д» («Теоретические основы инженерных расчетов»), изд-во «Мир», 1967, № 3.

90. Романенко П. П., Харченко В. П., Влияние вдува газов в турбулентный пограничный слой с продольным градиентом давления на сопротивление трения, МТИФ, 1963, № 1.
91. Саги, Хановер, Джонстон, Конструкция и характеристика двумерных криволинейных диффузоров, Труды американского общества инженеров-механиков (Trans. of ASME) русский перевод), серия «Д» («Теоретические основы инженерных расчетов»), 1967, № 4.
92. Седов Л. П., Методы подобия и размерности в механике, Гостехтеориздат, 1957.
93. Слезкин Н. А., Динамика вязкой несжимаемой жидкости, Гостехтеориздат, 1955.
94. Сергеевко А. А., Грецов В. К., Переход турбулентного пограничного слоя в ламинарный, ДАН СССР, 1959, т. 125, № 4.
- 95а. Спэлдинг Л. Б., Некоторые приложения нового метода расчета турбулентного пограничного слоя, сб. «Тепло- и массообмен», т. 1, изд-во «Энергия», 1968.
95. Солодкин Е. Е., Гиневский А. С., К вопросу о влиянии начальной неравномерности потока на характеристики диффузорных каналов, сб. «Промышленная аэродинамика», 1959, вып. 12.
96. Соколовский Л. П., Исследование аэродинамики выходных патрубков турбин и компрессоров, «Энергомашиностроение», 1952, № 9.
97. Сциллард К. С., Исследование диффузоров аэродинамических труб больших скоростей, Технические заметки ЦАГИ, 1938, № 160.
98. Стрэтфорд, «Механика» (сб. переводов), 1959, № 6.
99. Тарг С. М., Основные задачи тес. в ламинарных течениях. Гостехтеориздат, 1951.
100. Таушканова В. Б., Испытания выхлопных патрубков мощных паровых турбин, Машигиз, 1960.
101. Чертков А. К., Исследование гидравлических сопротивлений турбинных выхлопных патрубков, Автореферат диссертации, Ленинград, 1947.
102. Уайтмен, Рено, Клайн, Влияние условий входа на характеристики двумерных дозвуковых диффузоров, Труды американского общества инженеров-механиков (Trans. of ASME), (русский перевод), серия «Е» («Техническая механика»), 1961, № 3.
103. Учанский М. П., Исследование осерадиальных диффузоров, «Энергомашиностроение», 1964, № 10.
104. Уманский М. П., Амелюшкин В. Н., Сопротивление диффузорных патрубков турбомашин при изменении втулочного отношения, «Энергомашиностроение», 1967, № 1.
105. Федяевский К. К., Колесников А. В., Смолянинова А. Н., К расчету турбулентного пограничного слоя с продольным градиентом давления, Труды ЦАГИ, 1967, вып. 1 088.
106. Фейл, Системы лопаток для дозвуковых диффузоров с очень большими углами расхождения, Труды американского общества инженеров-механиков (Trans. of ASME) (русский перевод), серия «Д» («Теоретические основы инженерных расчетов»), 1964, № 4.

107. Фокс, Клайн. Режимы течения в криволинейных дозвуковых диффузорах. Труды американского общества инженеров-механиков (Trans. of ASME), (русский перевод), серия «Е» («Техническая механика»), 1962, № 3.
108. Шерстюк А. Н., Расчет течений в элементах турбомашин, изд-во «Машиностроение», 1967.
109. Шерстюк А. Н., Приближенный метод расчета криволинейных каналов, «Теплоэнергетика», 1958, № 8.
110. Шлихтинг Г., Возникновение турбулентности, Изд-во иностр. лит., 1962; «Теплоэнергетика», 1958, № 8.
111. Шлихтинг Г., Теория пограничного слоя. Изд-во иностр. лит., 1956.
112. Сб. «Современное состояние аэродинамики больших скоростей», под ред. Л. Хоуэрга, Изд-во иностр. лит., 1955.
113. Ханин Г. А., Некоторые вопросы аэродинамического исследования вспомогательных элементов прочной части турбомашин, «Теплоэнергетика», 1955, № 1.
114. Albring W., Wasserkraftmaschinen, 3, Lehrbuch, TH, Dresden, 1967.
115. Böhm J., Conrad W., Die Geschwindigkeitsverteilung in Endquerschnitt von Turbinen — Abdampfstützen bei verschiedener Zuströmung, Konstruktion, 1961, v. 13, № 6.
116. Brown D., Performance of a perforated wall intake at a Mach number of 2,5, Canadian Aeronautical Journal, 1960, № 6.
117. Carrière, Pet Luynaest J., Recherches sur les Preses d'air Supersoniques, сб. «Jahrbuch der Wissenschaftlichen Gesellschaft für Luftfahrt», 1959.
118. Cockerill D. J., Markland E., A review of incompressible diffuser flow, Aircraft Engineering, 1963, № 10.
119. Crispin B., Einlauf Diffusoren für den Überschallwind, DVL Bericht, 1961, IV, № 144.
120. Van Devoestine R. V., Fox R. W., An experimental investigation on the effect of subsonic inlet Mach number on the performance of conical diffusers, International Journal of Mechanical Sciences, 1966, v. 8, № 12.
121. Dutton R. A., Goldsmith E. L., Some characteristics of rectangular multishock and isentropic external compression intakes at a Mach number of 2,9, ARC CP, 1965, № 630.
122. Doehoff A. E., Tetervin N., Determination of general relations for the behaviour of turbulent boundary layers, NACA Report 772, 1943.
123. Eschrich R., Experimentelle Untersuchungen von Kegeldiffusoren an Venturidüsen, Maschinenbautechnik, 1968, № 1.
124. Fururga Y., Sato T., Pressure recovery efficiency of short conical diffusers and re-entrant diffusers, Bull. of ASME, 1960, v. 3, XI, № 12.
125. Ferry A., Problems related to matching turbulent engine requirements to inlet performances as function of flight Mach number and angle of attack, Air Intake Problems in Supersonic Propulsion, 1958.

126. Gibrings J. C., Pressure measurements on three open nose air intakes at transonic speeds with an analysis of their drag characteristics, ARC CP, 1961, № 514.

127. Goldsmith E. L., The effect of internal contraction initial rate of subsonic diffusion and coil and centrebody shape on the pressure recovery of a conical centrebody intake at supersonic speeds, ARC RM, 1962, № 3204.

128. Griggs C. F., An investigation of two methods of suppressing shock oscillation ahead of conical centrebody intakes, ARC CP, 1962, № 605.

129. Gibson A. H., On the flow of water through pipes and passages having converging or diverging boundaries, Proc. Roy. Soc., Ser. A, 1910, v. 83.

130. Hackeschmidt M., Über den Entwurf ebener, gerader Diffusoren mit kurzer Baulänge, Maschinenbautechnik, 1964, № 10.

131. Hackeschmidt M., Vogelsang E., Versuche an Austrittsgehäusen mit neuartigen Diffusoren, Maschinenbautechnik, 1966, № 5.

132. Hausenblas H., Versuche an Abströmgehäusen thermischer Turbomaschinen, Konstruktion, 1963, v. 15, № 12.

133. Hibs M., Mesikruhove difuzory, Ploudeni, v lopatkových strojich Sbornik ustavu provyzkum stroju, 1958.

134. Imbach H. E., Beitrag zur Berechnung von rotationsymmetrischen turbulenten Diffusorströmungen, Brown Boveri Mitteilungen, 1964, Bd 51, № 12.

135. Jerie Jan., A method for describing the shape of inlet and outlet casings of turbomachinery, Prace Instytutu Maszyn Przeplywowych, 1965, № 22.

136. Jarie J., The effect of losses into the exhaust casing on the properties of the last stage of steamturbine, Prace Instytutu Maszyn Przeplywowych, 1963, № 14-16.

137. Johnston I. H. I., Effect of inlet conditions on the flow in annular diffusers, Aeronautical Research Council, current papers, 1954, № 178.

138. Kaufmann K., Grenzschichtbeeinflussung bei Diffusoren von Strömungsmaschinen, Voith Forschung und Konstruktionen, 1957, № 2.

139. Kmonicek W., Unterschallströmung in Kegeldiffusoren, Acta Technika, 1959, № 8.

140. Kmonicek W., Zlepseni cinnosti diffusoru jednodu chymi Zaschy, Strojnický Sbornik, 1956, № 13.

141. Kroll S., Bessay, Etude sur la récupération de l'énergie cinétique d'échappement dans les diffuseurs de turbine, Rev. Electr. Mécan., 1953, № 92.

142. Kline S. J., On the nature of stall, Trans. of ASME, S. D., 1959, № 9.

143. Kline S. J., Abbott D. E., Fox R. W., Optimum design of straight walled diffusers, Trans. of ASME, S. D., 1959, № 3.

144. Lange A. H., Lee R. E., Journ. of Aeron. Sci., 1952, v. 21, p. 58.

145. Liepe F., Wirkungsgrade von schlanken Kegeldiffusoren bei drallbehafteten Strömungen, Maschinenbautechnik, 1960, № 3.
146. Liepe F., Jahn K., Untere Wirkungsgrade von Kegeldiffusoren, Maschinenbautechnik, 1962, № 11.
147. Liepe F., Untersuchungen über der Verhalten von Drallströmungen in Kegeldiffusoren, Maschinenbautechnik, 1963, № 3.
148. Liepe F., Experimentelle Untersuchungen über den Einfluss des Dralles auf die Strömung in schlanken Kegeldiffusoren, Wissenschaft, Zeitschrift der TH, Dresden, 1962, v. 8, № 2.
149. Linneken H., Betrachtungen über Wirkungsgrade gasdurchströmter Diffusoren, Konstruktion, 1963, v. 15, № 7.
150. Littl B. H., Wilbur S. W., Performance and boundary layers data from 12° and 23° conical diffusers of area ratio 2.0 at Mach number up to choking and Reynolds numbers up to $2.5 \cdot 10^6$, NACA Rep. 1201, 1954.
151. Ludwig H., Tillman W., Investigation on the wall-shearing stress in turbulent boundary layers, NACA TM 1265, May 1950.
152. Neale M. C., Lamb P. S., Tests with a variable ramp intake having combined external/internal compression and a design Mach number of 2.2, ARC CP, 1965, № 805; Further tests a variable ramp intake having a design Mach number of 2.2, ARC CP, 1966, № 826.
153. Nippert H., Über den Strömung Verlust in gekrümmten Kanälen, Forschungsarbeiten auf d. Geb. d. Ing. Wes., 1929, H. 32G.
154. Peryez S., Der Einfluss des Diffusorwirkungsgrades auf den Austrittsverlust in Dampfturbinen, BWK, 1961, v. 13.
155. Prechter H., Gesichtspunkte zur Auslegung von Diffusoren unter Berücksichtigung neuerer Forschungsergebnisse, Der Maschinenmarkt, 1961, v. 13a, № 82.
156. Peters H., Energieumsetzungen in Querschnittweiterungen bei verschiedener Zulaufbedingungen, Ing. Arch., 1931, № 1; 1932, № 2.
157. Rippl E., Experimentelle Untersuchungen über Wirkungsgrade und Abreisverhalten von schlanken Kegeldiffusoren, Maschinenbautechnik, 1956, № 5.
158. Robertson I. M., Fraser H. R., Investigation of the boundary layer still in a conical diffuser, Trans. of ASME, 1961, v. 81, № 1.
159. Ross D., A physical approach to turbulent boundary layer problems, Trans. of ASME, 1966, v. 121, papers 2838.
160. Friedrich O., Ringleb, Two-dimensional flow with standing vortexes in diffusers, Trans. of ASME, S.D., 1960, № 4.
161. Simons P., Untersuchungen an Diffusoren für Überschallwindkanäle, Aerodynamisches Institut der Techn. Hochschule, Aachen, 1943.
162. Schlichting H., Berechnung der Strömung in rotations-symmetrischen Diffusoren mit Hilfe der Grenzschichttheorie, Flugwissenschaftl. Zeitschrift, 1961, № 5.
163. Schramm G., Ergebnisse aerodynamischer Untersuchungen der Ein- und Austrittsgchäuse von Gasturbinenanlagen, Maschinenbautechnik, 1962, № 8.

164. Stedtschlag, Die Strömung in Diffusoren verschiedener Querschnittsformen, Wiss. Z. Techn. Univ., Dresden, 1963, v. 12, № 1.
165. Sprenger H., Experimentelle Untersuchungen an geraden und gekrümmten Diffusoren, Mitteilungen aus der Institute für Aerodynamik der E. H., Zürich, 1959, № 27.
166. Sternberg J., U. S. Army, Bab. Reslab Aberdeen, Rep. 906, May 1954.
167. Seymour Lieblein, Loss and stall analysis of compressor cascades, Trans. of ASME, S. D., 1961, v. 81, № 3.
168. Wisniewski R. J., Journ of the Aerospace Sci., 1961, v. 28, № 3.
- 168a. Ba. Jasutoshi Senoo, The boundary laure on the end wall of a turbine nozzle cascade, Trans. of ASME, S. C., 1958, v. 80, № 8.
169. Wu J. H. T., On a two-dimensional perforated intake diffuser, Aerospace Engineering, 1962, v. 21, VII, № 7.